Tephrostratigraphy, magnetostratigraphy and geochronology of some early and middle Pleistocene deposits in New Zealand

Philip A. R. Shane

A thesis submitted for the degree of Doctor of Philosophy in Geology

Victoria University of Wellington

June 1993

ABSTRACT

Numerous early Pleistocene silicic tephras are exposed in long sedimentary sequences in the East Coast and Wanganui basin regions in southern North Island of New Zealand, some 150-250 km south of the Taupo Volcanic Zone. They provide time planes that can be correlated between different facies and basins. Individual tephras can often be distinguished on the basis of major and trace element glass chemistry, and Fe-Ti oxide composition. Approximately 51 different eruptive events may be recorded in the interval from ca. 1.7 Ma to 0.5 Ma. Early Pleistocene tephras in deep-sea sediments of the Southern Pacific Ocean at latitudes >60°S were previously considered to have been sourced in the TVZ. However, their alkalic compositions are compatible only with volcanoes of Western Antarctica and the Ross Sea region.

Most of the tephras examined here are reworked, and many have been emplaced as catastrophic flood deposits in overbank settings of braid plains in the East Coast region. Their mode of emplacement and the presence of ignimbrites in the sequences indicate early Pleistocene transport routes through the site of the present main Axial Ranges, and suggest substantial tectonic uplift in the last 0.8 Ma.

Long sequences spanning the Jaramillo Subchron (0.99-1.07 Ma) and older Matuyama Chron are recognised at Mangatewaiiti and Mangatewainui in the East Coast region, and Rewa Hill in the Rangitikei Valley. Numerical age control is provided by $^{40}Ar/^{39}Ar$ single crystal laser fusion ages from plagioclase in key tephra horizons. This new chronology indicates the tephras are nearly twice as old as several previous studies have suggested, thus requiring a major revision of the New Zealand Pleistocene stratigraphy.

By integrating isotopic, paleomagnetic and geochemical data, 3 widespread tephras can be correlated between basins of the East Coast and Wanganui: Pakihikura Tephra (ca. 1.6 Ma), Potaka Tephra (1.00 Ma), and Kaukatea Tephra (ca. 1 Ma). These tephras and others provide a chronological framework for much of the early Pleistocene in southern North Island. Potaka Tephra is particularly widespread, allowing correlation between marine strata of the Castlecliffian (local early Pleistocene stage) type section at the Wanganui coast, and marine strata elsewhere in the Wanganui basin, as well as with fluvial and lacustrine strata in the East Coast. The tephra occurs as an ignimbrite and as a catastrophic flood deposit in the East Coast and as a fallout ash in North Canterbury, South Island (ca. 600 km from source). Potaka Tephra (normal polarity) and Kaukatea Tephra (reversed polarity) bracket the top of the Jaramillo Subchron and constrain its age to ca. 1 Ma. This is in accord with the astronomical calibration of the Pleistocene geomagnetic time scale, but older than previous determinations using the 'chronogram' method on K-Ar data.

The precise source vents for the distal early Pleistocene tephras are uncertain, however their ages indicate they are coeval with dated proximal ignimbrite sheets from the Mangakino Caldera in the SW part of TVZ. The large number of distal tephras would imply a greater frequency of eruptions from this source than previously expected.

ACKNOWLEDGEMENTS

CONTENTS

LIST OF FIGURES

(f denotes facing page)

LIST OF TABLES

(f denotes facing page)

Chapter 1
INTRODUCTION

1.1 AIM OF THE INVESTIGATION

The aim of this investigation is to develop a stratigraphic framework for early-middle Pleistocene (2-0.5 Ma) sediments in basins of the southern North Island of New Zealand via tephro- and magneto- stratigraphy and isotopic ages. The basins contain an abundance of rhyolitic volcaniclastic sediments and primary tephras. Their character and the facies in which they are contained have implications for the tectonic, paleoclimatic and eruptive history of the central and southern North Island.

1.2 GEOLOGIC SETTING

The North Island of New Zealand has been at an active convergent plate boundary and has experienced regional tectonism and volcanism since the Miocene. Associated volcanism in the central North Island was initiated at least 1.6 Ma ago (Pringle et al. 1992), in the south western part of the Taupo Volcanic Zone (Fig. 1.1). The Taupo Volcanic Zone (TVZ) is a province of calc-alkaline volcanism, dominated by large rhyolitic calderas and associated ignimbrite deposits (Wilson et al. 1984). To the south and east of the TVZ, subsidence during the Pleistocene has resulted in the accumulation of thick volcaniclastic sedimentary sequences in a shallow marine back-arc basin (Wanganui basin) and mainly terrestrial fore-arc basins of the East Coast region (Fig. 1.1). Tectonism in the late Pleistocene has produced a linear belt of mountains (the Main Axial Ranges) which now separates the basins, and has uplifted and exposed the sedimentary sequences on land.

Being located in the mid latitudes of the Southern Hemisphere and at the edge of the Pacific basin, New Zealand contains both marine and terrestrial records of Pleistocene climatic fluctuations (e.g. Pillans 1992). Near continuous volcanism has produced deposits in proximal and distal settings relative to volcanic source, providing a means of correlation and isotopic chronology, while rapid subsidence rates and voluminous detritus supplies, typical of convergent plate boundaries, have produced high resolution records (e.g. Black 1992).

Pleistocene tephras are also common in deep-sea sediments from the outer shelf and abyssal floor of the Tasman Sea and Pacific Ocean around New Zealand (e.g. Watkins & Huang 1977). A few deep-sea tephras have been correlated to those exposed on land (e.g. Froggatt 1983; Froggatt et al. 1986; Nelson et al. 1986), and many others up to 5000 km distant in the Southern Ocean have been attributed to the TVZ (Kyle & Seward 1984, Seward et al. 1986) without precise correlatives being identified.
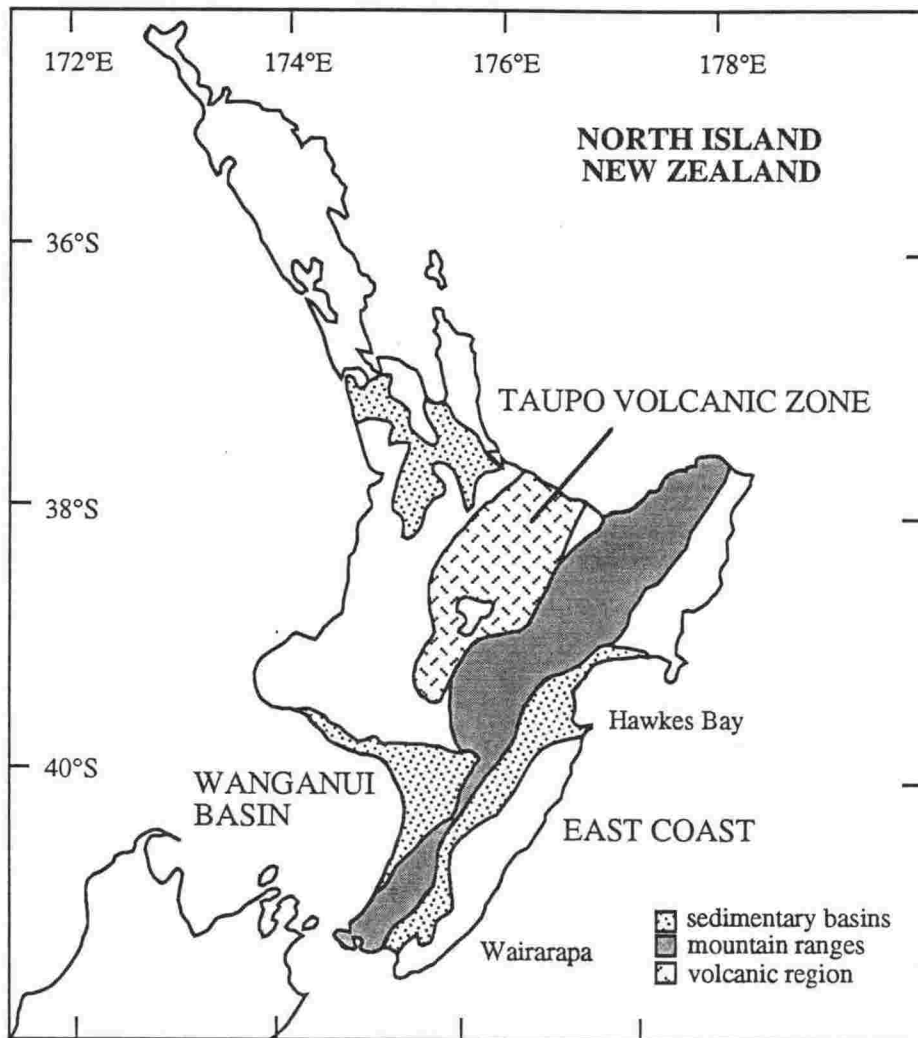
Fig. 1.1 Map showing the main Pleistocene physiographic features of the North Island of New Zealand.

1.3 QUATERNARY CHRONOLOGY OF THE NORTH ISLAND OF NEW ZEALAND

Much of the previous work on the classification and chronology of the Quaternary (particularly the early Pleistocene) of the North Island has focused on marine strata of the Wanganui basin. Local stages were defined on the basis of lithology and fossil assemblages (Table 1.1) from type sections at the cliffs along the Wanganui coast (Fleming 1953). This sequence consists of a series of unconformity-bound units, and recent workers have attributed them to high sealevel stands with the unconformities representing low stands (e.g. Beu & Edwards 1984; Pillans 1992). Numerical age control for the sequences has been limited due to the scarcity of isotopically datable materials. The recognition of bioevents: the disappearance of *Pseudoemiliana lacunosa* in the Castlecliffian and the appearance of *Geophyrocapsa sinuosa* in the Nukumaruan, became the primary age control points (Beu & Edwards 1984). On this basis, unconformity-bound formations were assigned to interglacial oxygen isotope stages and the unconformities to glacial periods. Such chronologies assume all cycles are preserved and identified. Subsequently, Turner & Kamp (1990) determined a magnetostratigraphy for the Castlecliffian part of the type sections and identified the Jaramillo Subchron and Brunhes-Matuyama boundary. Combining these data, several Plio-Pleistocene chronologies for New Zealand have been published including that depicted in Fig. 1.2. The assignment of formations to oxygen isotope stages resulted in the conclusion that an angular unconformity between the Castlecliffian and Nukumaruan represents as much as 0.5 Ma (Pillans 1992).

Table 1.1 New Zealand Quaternary chrono-stratigraphic stages (adapted from Pillans 1992).

Epoch	Series	Stage	Substage
Pleistocene	Wanganui	Haweran	
Pleistocene	Wanganui	Castlecliffian	Putikian
Pleistocene	Wanganui	Castlecliffian	Okehuan
Pliocene	Wanganui	Nukumaruan	Marahauan
Pliocene	Wanganui	Nukumaruan	Hautawan

Longer, more continuous Plio-Pleistocene sequences occur near the centre of the Wanganui basin. They are less fossiliferous, but contain many rhyolitic tephras, the most notable being the Rangitikei Valley. These sections became the focus of geochronology studies using fission-track ages determined on volcanic glass (Seward 1974; 1976). A series of ages
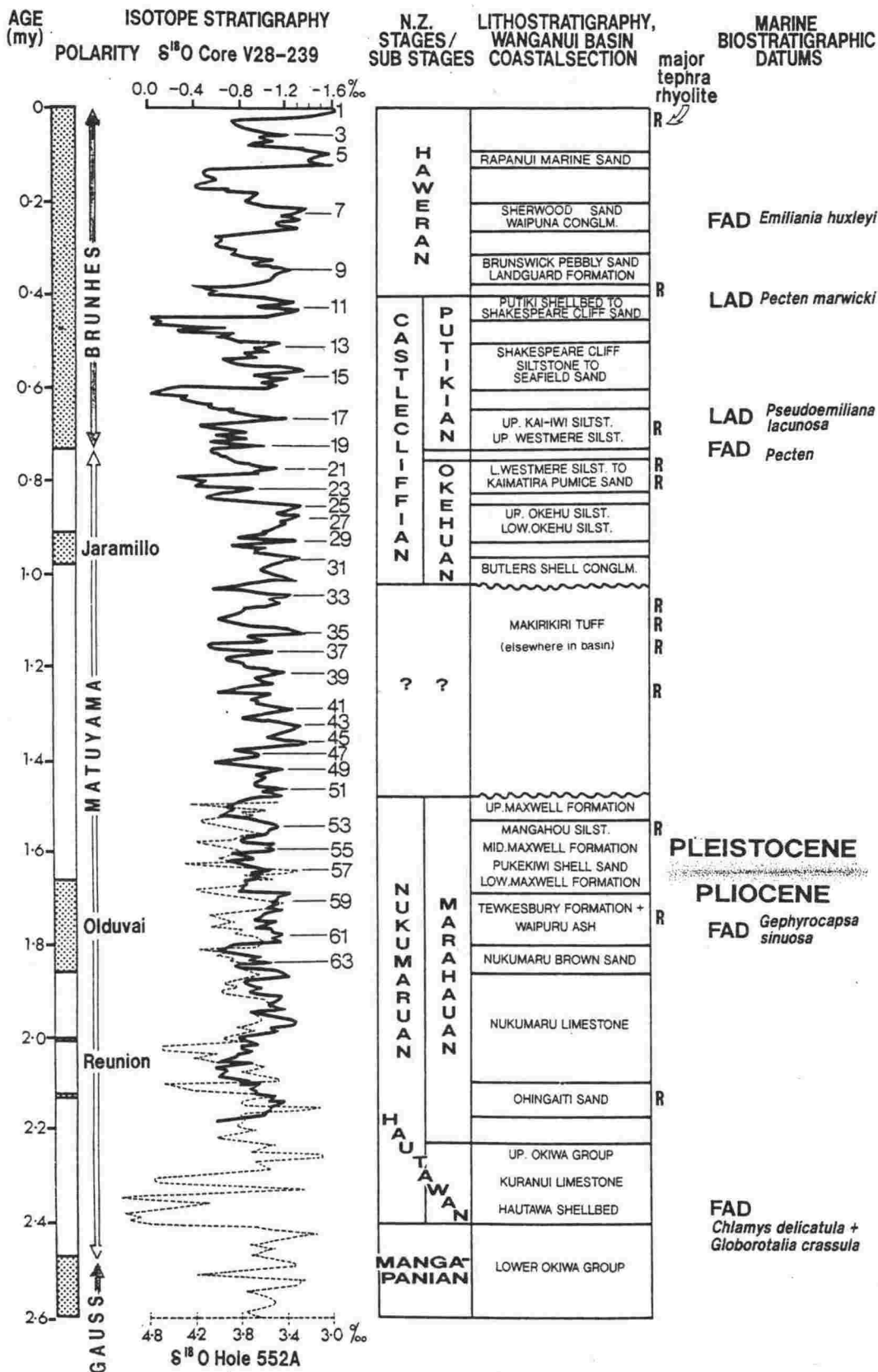
Fig. 1.2 Chronology of the Wanganui basin, based on the Pleistocene stage type sections at the coast (from Pillans 1992).

for tephras in the Rangitikei Valley were then used to estimate the age of local stage boundaries (Fig. 1.3). Several tephras in a marine/non-marine sequence at Cape Kidnappers in the East Coast region were also dated, and revealed a similar chronology (Seward 1975). Dated tephras were named and correlations within and between basins were proposed, mainly on the basis of age. With the realisation that fission-track ages on glass are affected by track annealing, zircon ages were determined for several tephras (Seward 1979).

In spite of this chronology, precise correlation between sections was hindered by the large error limits for the ages, the general lack of fossils in tephra-bearing sections, and the lack of tephras in the type sections at the Wanganui coast. Further, many long Pleistocene non-marine sequences in the East Coast region were largely unstudied, due to the lack of fossil datums, in spite of the large number of tephra horizons they contained (e.g. Lillie 1953). These sequences were simply assigned to the Castlecliffian because of their 'pumiceous' lithology. Apart from correlation based on radiometric ages, no other method of tephra correlation was available prior to the present study.

Geochemical studies of some of the tephras showed that many correlations on the basis of age were invalid (Froggatt 1983; Shane & Froggatt 1991). Subsequent paleomagnetic studies at the Cape Kidnappers section (Black 1992) and Ar/Ar age data for large silicic ignimbrites in the TVZ (Pringle et al. 1992) showed many of the fission-track ages (both glass and zircon) to be anomalously young. This is further supported by recent work on tephras in the Rangitikei Valley using the isothermal plateau fission-track technique (Alloway et al. 1993).

1.4 OBJECTIVES OF THE INVESTIGATION

Three major objectives are identified for developing a Pleistocene stratigraphic framework and chronology for the southern North Island:

1. Establish a tephrostratigraphy

Develop a tephrostratigraphic framework by recording the number and character of megascopic tephras in long sections of the early-middle Pleistocene in the Wanganui basin and East Coast regions. In particular, examine long non-marine sections in the East Coast, which contain abundant tephras but previously have received little attention. An *adjunct* to this is an investigation of the sedimentary facies in which the tephras are contained, and the mode of emplacement of the tephras themselves. This in turn has implications for the paleogeography and tectonic history of the southern North Island.

A complimentary study of the geochemistry of the glass and mineral phases in the tephras was undertaken for the purposes of characterisation and correlation. This included examining tephras in deep-sea cores from the Pacific and Southern Oceans, which have been attributed to New Zealand (e.g. Kyle & Seward 1984), to determine their composition and

	FT age (Ma)
Rangitawa	0.38 ± 0.04
Waiomio	0.45 ± 0.09
Waitapu	0.52 ± 0.08
Potaka	0.61 ± 0.06
Rewa	0.74 ± 0.09
Mangapipi	0.88 ± 0.13
Ridge	1.04 ± 0.15
Pakihikura	1.06 ± 0.16
Mangahou	1.26 ± 0.17
Ohingaiti	1.50 ± 0.21

Castlecliffian — Putikian — Okehuan

Nukumaruan

200 m

0
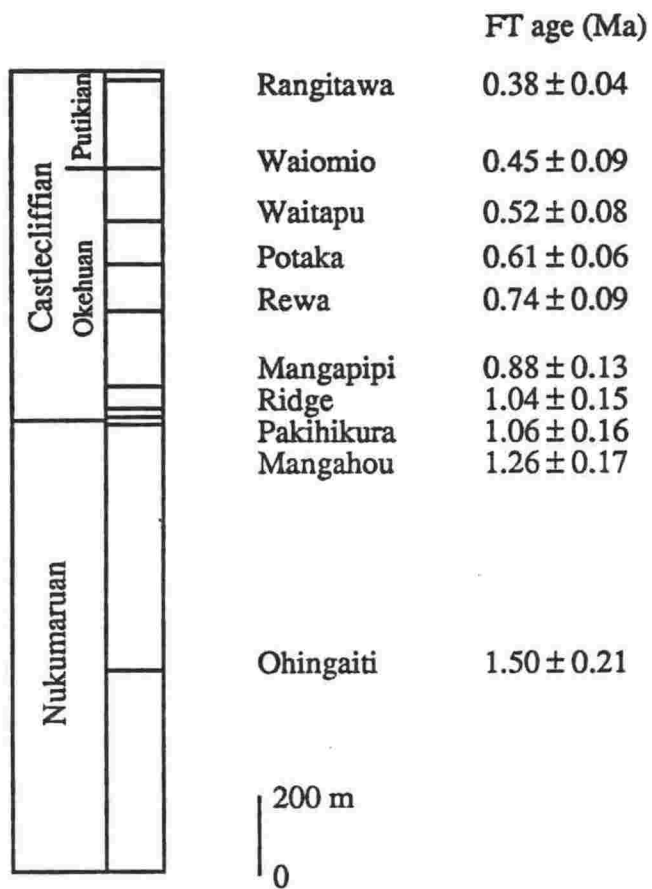
Fig. 1.3 Glass fission-track ages for tephras in the Rangitikei
Valley sequence (adapted from Seward 1974).

provenance, and their value to this tephrostratigraphic study. These studies may also provide insight to the nature and eruptive history of the TVZ.

2. *Establish a magnetostratigraphy*

A paleomagnetic study of long sections was undertaken to attempt to locate and identify major subchrons and reversal boundaries, including the Brunhes-Matuyama boundary, Jaramillo Subchron and Olduvai Subchron. By comparison to the Geomagnetic Time Scale (GMTS), this can provide a numerical chronology, and a means of correlation between sections and in particular, correlation to the Castlecliffian type section. Paleomagnetic polarity also provides an additional means of correlating tephra horizons.

3. *Obtain isotopic ages*

Crystals in the tephras provide a means to obtain high resolution $^{40}Ar/^{39}Ar$ ages for the sequences, using the Single Crystal Laser Fusion (SCLF) method. Such ages can be used as control points for magnetostratigraphy and as a check on previous age determinations by other methods. They are also important in tephra correlation studies. The geochronology of the tephras may also have implications for the eruptive history of the TVZ.

1.4.1 Wider implications

Ar/Ar dating of tephras in continuously deposited sedimentary sections in southern North Island provides an opportunity to calibrate the GMTS, which is based mainly on ages of discrete emplacement events such as domes or lava flows. Tephras in sedimentary sequences allow the position of the dated unit to be directly related to the chron or subchron it is contained. The traditional calibration of the Plio-Pleistocene GMTS is based on K/Ar whole rock ages of basalt (Mankinen & Dalrymple 1979). Alternative orbitally tuned chronologies from deep sea cores produce ages for reversal boundaries that are 5-7% older (e.g. Shackleton et al. 1990). High resolution ages from sedimentary sections may help resolve the discrepancy in the calibration alternatives (e.g. Tauxe et al. 1992).

Several studies have shown that climatic fluctuations have controlled the deposition of early Pleistocene sequences in New Zealand, both marine (e.g. Beu & Edwards 1984; Pillans 1992) and non-marine (Black 1992). These sequences are particularly thick (100 m+) and thus provide a high resolution record compared to that of typical continental deposits. However, direct investigation of paleoclimates with the use of fossil pollens and micro-organisms has not been widely applied to early Pleistocene sequences exposed onland in New Zealand. The development of a stratigraphic framework using tephras and paleomagnetism allows the correlation of marine to non-marine sediments and will greatly facilitate such paleoclimatic investigations. Isotopic ages of the tephras will provide a firm chronology.

Table 2.1 Published stratigraphic nomenclature and approximate formational equivalence for early Pleistocene strata, prior to this study.

NZ stages	Wanganui coast (Fleming 1953)	Rangitikei (Te Punga 1992)	Pohangina Valley (Carter 1972)	Cape Kidnappers (Kingma 1971)	Wakarara Range (Erdman & Kelsey 1992)	Southern Hawkes Bay (Lillie 1953)	Northern Wairarapa (Neef 1984)	Southern Wairarapa (Collen & Vella 1984)
early-middle Castlecliffian	Kai-iwi Group Okehu Group	Upper Rangitikei · Formation	Takapari Formation	Kidnappers Group	Poutaki Pumiceous Formation	Mangatarata Formation	Mangaohou Formation	Te Muna Formation
late Nukumaruan	Maxwell Group	Middle Rangitikei Formation	Konewa Formation		Okauawa Formation	Kumeroa Formation	Totaranui Formation	Hautotara Formation

Chapter 2
STRATIGRAPHY

2.1 DISTRIBUTION OF EARLY-MIDDLE PLEISTOCENE SEDIMENTS AND PREVIOUS STRATIGRAPHIC NOMENCLATURES

Early-middle Pleistocene sediments in the southern North Island of New Zealand have been classified and subdivided by various combinations of criteria including fossil assemblages, lithology, stratigraphic position and the presence of tephras, in different geographic regions. A summary of stratigraphic nomenclatures is shown in Table 2.1. The time interval of early-middle Pleistocene straddles the boundary of the New Zealand Nukumaruan and Castlecliffian stages, which are based mainly on marine biostratigraphy (Fleming 1953; Pillans 1992). In the Wanganui basin, sediments of this age form a nearly continuous, gently dipping sequence, which extends laterally from the Wanganui coast to the Ruahine Ranges. The sequence is thickest near the Rangitikei River, towards the centre of the basin, where Castlecliffian sediments are conformable with Nukumaruan sediments. The type sections for both stages are at the Wanganui coast, where the sequence is relatively thin and is entirely marine. At the coast, several groups, each comprising several formations, are defined on the basis of fossil assemblages and lithology. The contact between the Castlecliffian and Nukumaruan stages is an angular unconformity, making the precise definition of stage limits uncertain (Pillans 1992). Sediments eastward of the Rangitikei River become increasingly non-marine and contain abundant tephras. The association of thick tephras with Castlecliffian strata was noted by Te Punga (1952) and this has influenced the classification of strata in the absence of fossil data in the eastern Wanganui basin and east of the basin.

In the East Coast region, sedimentation in the early-middle Pleistocene was predominantly non-marine and a particularly long record of volcanism was recorded in the form of rhyolitic tephras. Therefore early workers notably Lillie (1953), Fleming (1953) and Kingma (1971), assigned strata to the Castlecliffian stage largely on the basis of lithology and the presence of tephras. In southern Hawkes Bay, Castlecliffian strata were referred to as Mangatarata Formation. These sediments are predominantly fluvial and lacustrine. They are thickest in the Dannevirke area, in particular at Mangatewaiiti Stream. In this region the strata are gently tilted and folded, and conformably overlie the Nukumaruan age, marine Kumeroa Formation (Lillie 1953). Further to the north, in the Ruataniwha plains area of Central Hawkes Bay, Mangatarata Formation is thinner and stratigraphic contacts are mainly obscured by tectonic deformation. At the Tukituki River, sequences are tectonically overturned. However, elsewhere Lillie (1953) has reported the deposition of Mangatarata Formation unconformably on early Cenozoic and older strata. The most northern, continuous exposure of early-middle Pleistocene strata is at Cape Kidnappers. This sequence differs from others in the East Coast
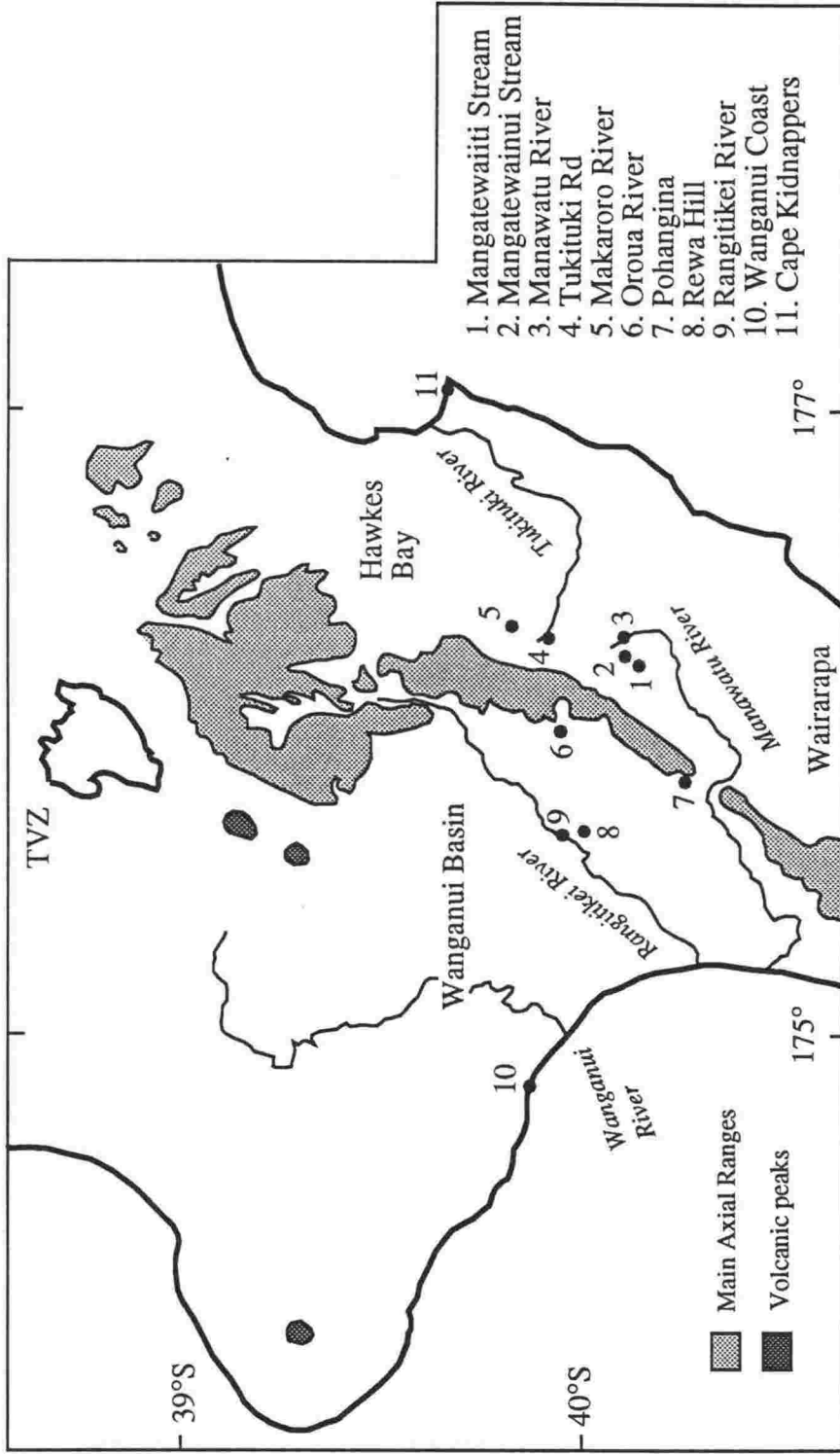
Fig. 2.1 Map showing the major physiography of the southern North Island and the location of the main stratigraphic sections examined.

region in having several estuarine units interbedded in a predominantly fluvial facies. The strata have been referred to as Kidnappers Group comprising several formations (Kingma 1971; Black 1992). A few macro-fossils, notably the genus *Pecten*, have been identified in the Kidnappers Group, and these fossils occur in the Castlecliffian of the Wanganui coast section indicating approximate equivalence.

2.2 MAJOR STRATIGRAPHIC SECTIONS

The major stratigraphic sections of early-middle Pleistocene strata examined are described in this chapter (Fig. 2.1). In addition other, short sequences and isolated exposures containing tephras were studied and are described in other chapters. The sedimentary facies and inferred depositional environments are summarised here. A more detailed explanation is given in Chapter 6. As lithological columns for Cape Kidnappers and the Wanganui coast have already been published, the columns are reproduced here and were not remeasured. Grid references for locations are those from the NZMS 260 map series.
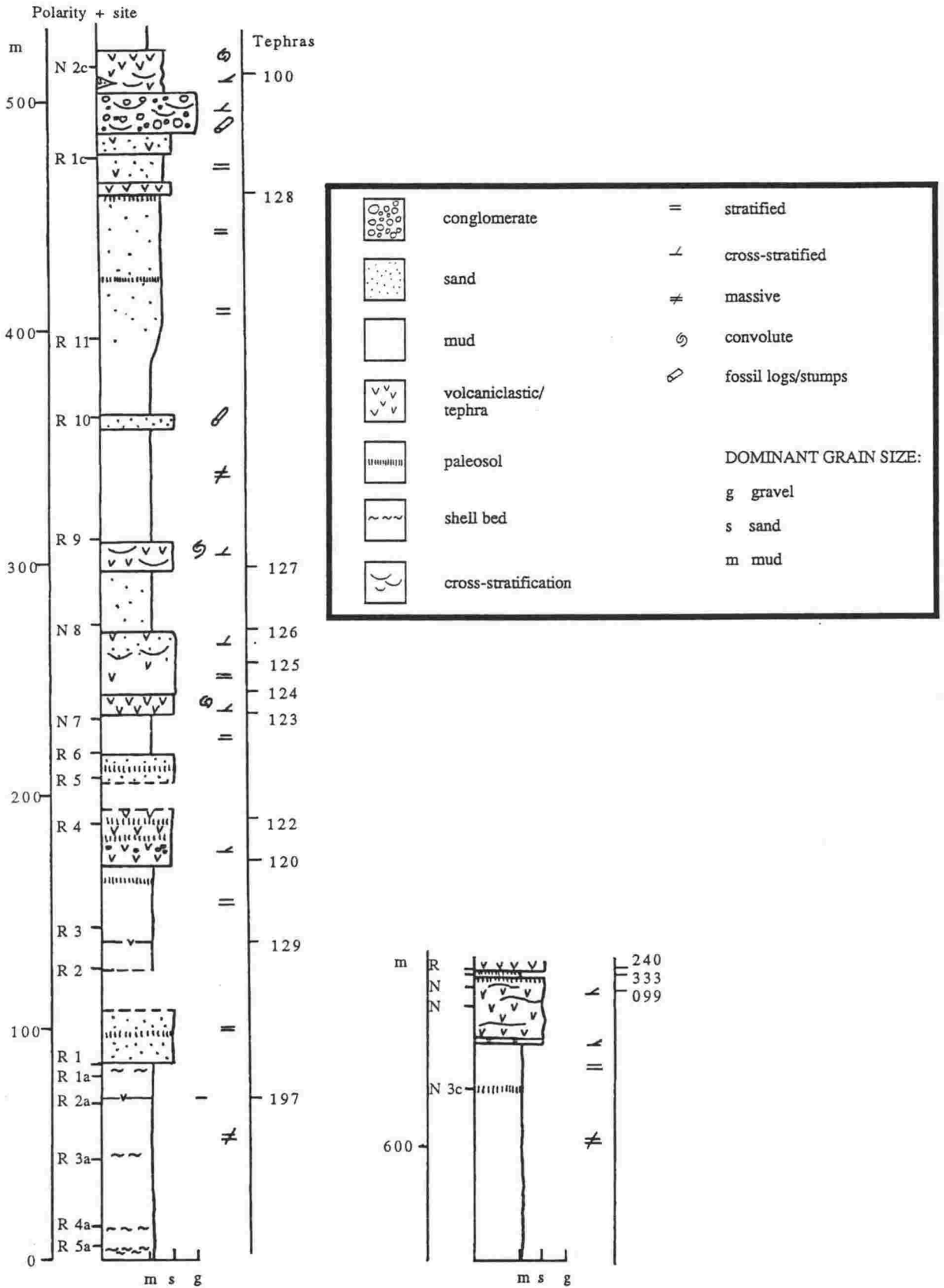
Fig. 2.2 Lithological column for Mangatewaiiti section

2.3 MANGATEWAIITI STREAM

top: U23/808172
base: U23/829139

Nearly 700 m of strata are exposed in Mangatewaiiti Stream, north of Dannevirke, from State Highway 2 to the railway bridge parallel to Matamau-Ormandville road. Lillie (1953) briefly described the section and mapped it as Castlecliffian Mangatarata Formation. The lower ca. 90 m of the section is exposed in Mangatewainui Stream and consists of entirely marine facies. This part is better defined as Nukumaruan Kumeroa Formation (Lillie 1953). The strata dip gently NW at 5-10° defining the broad limb of a syncline, the axis of which is located at the top of the section (parallel to SH 2).

Most of the strata are non-marine, being fluvial and lacustrine. The contact with marine strata in the lower part of the section is gradational and passes through estuarine sediments to fully marine shallow shelf facies. These latter facies are mainly massive sandy mudstone, but contain occasional shell beds (up to 1 m) with *Chlamys gemmulata* and *Neothyris sp*. The estuarine facies contain *Austrovenus* and *Mytilus*.

In the non-marine sequence, coarse grained sediments are mainly restricted to tuffaceous units, which often display cross-stratification and convolute bedding. Thick units also display very low angle cross-stratification and horizontal stratification with gradational bedding contacts, typical of scour and fill and hyperconcentrated flow deposits. Non-volcanic deposits are fine grained sandy mudstone and are mainly massive or finely laminated. Some massive mudstones contain the fresh water mollusc *Hyridella* and are diatomaceous. Lignites, paleosols and fossil logs are abundant, while conglomerate facies are rare. At least 13 megascopic tephras are exposed: all (except 197) within non-marine strata.

The quality of paleomagnetic remanence determination is variable in the section. Sites 2c, 3c and 4c display stable normal polarities and sites 1c, 5c, 6c and those in the lower 90 m of section, display stable reversed polarities. For the remainder of the sites no stable end-point is achieved during demagnetisation, but declinations change from normal to reversed and their initial negative inclinations decrease, suggesting an original reversed polarity.
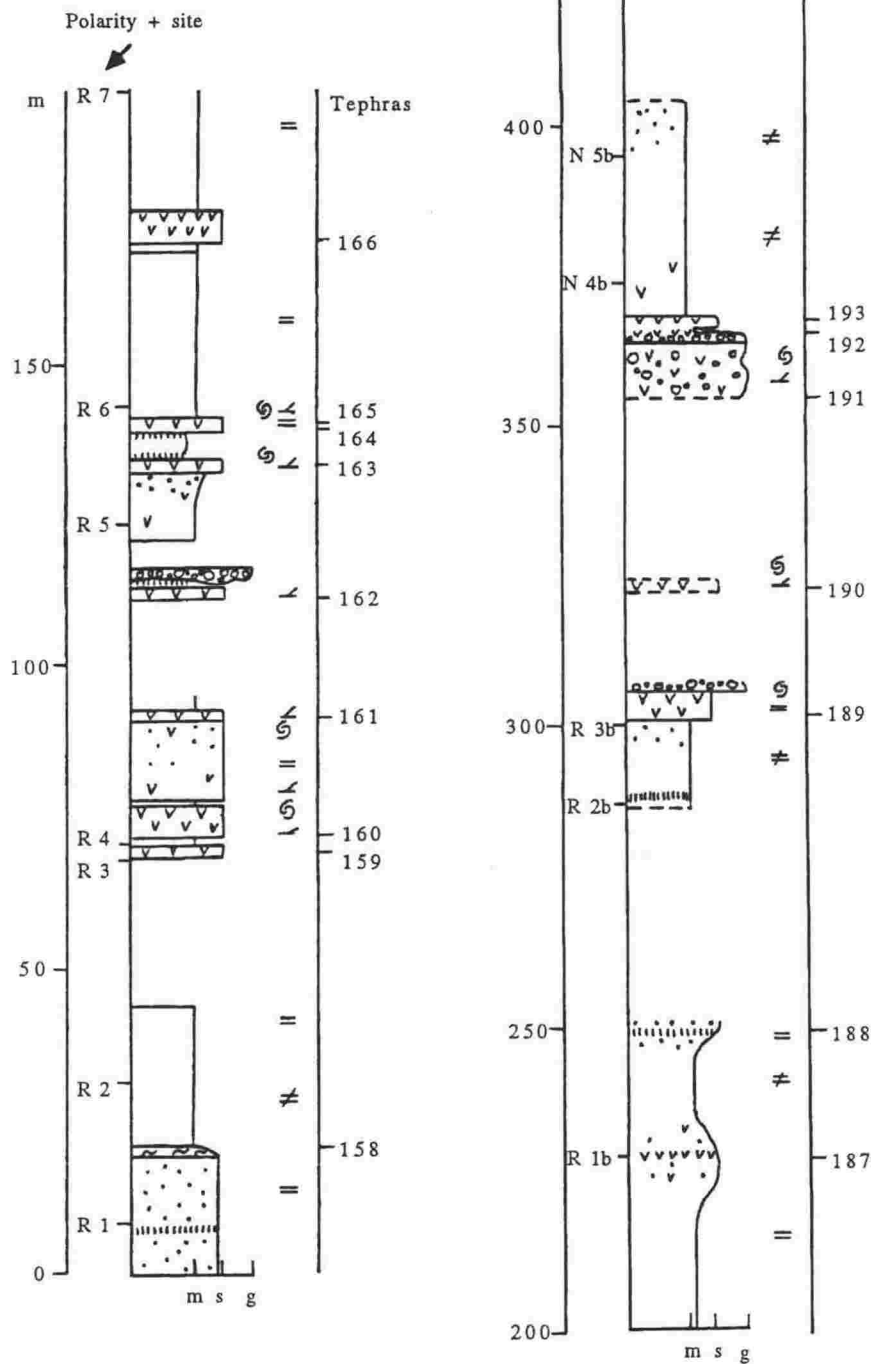
Fig. 2.3 Lithological column for Mangatewainui section

2.4 MANGATEWAINUI STREAM

top: U23/808185
base: U23/839165

Mangatewainui Stream, north of Dannevirke, exposes nearly 500 m of non-marine strata mapped as Castlecliffian Mangatarata Formation by Lillie (1953). The section extends from State Highway 2 to about 500 m down stream of the bridge on Blairgowie Road. It parallels the Mangatewaiiti section, about 2 km to the south-west and displays a similar sequence. The strata in Mangatewainui Stream dip gently to the NW at 5-10° and define the same syncline limb as the Mangatewaiiti section. The tops of both sections are terminated at the syncline axis.

The facies are typified by fine grained, poorly sorted sandy mudstones, either laminated or massive. Coarse grained facies are volcaniclastic, while conglomerate facies are rare. All lithologies are comparable to those described for Mangatewaiiti. At least 18 megascopic tephras are exposed, all of which occur in non-marine strata. Thicknesses range from < 1 cm to 20 m. Thick tephras display cross-stratification and convolute bedding indicative of rapidly deposited fluvial deposits.

Paleomagnetic remanence determination for this section is generally good. Sites 1c, 4b and 5b display stable normal polarities of high intensity. Sites 2, 5 and 7 display stable reversed remanences after the removal of weak overprints.
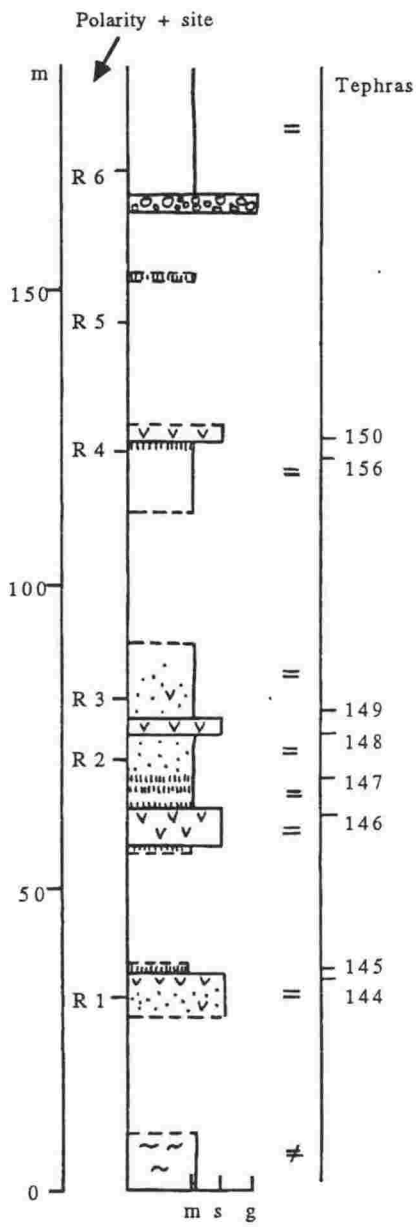
Fig. 2.4 Lithological column for Manawatu section

2.5 MANAWATU RIVER

top: U23/892193

base: U23/890199

Approximately 180 m of strata is exposed by the Manawatu River, down stream from the bridge on Kopua Road, north of Dannevirke. The steeply (ca. 90°) east-dipping strata are mapped as Castlecliffian Mangatarata Formation by Lillie (1953), and overlie fossiliferous Nukumaruan Kumeroa Formation. The contact between the formations is conformable and gradational. In this section, the Mangatarata Formation is non-fossiliferous and becomes increasingly carbonaceous up section. The dominant lithology is finely laminated and bedded sandy mudstone. Occasional lignite beds indicate subaerial settings in part, perhaps in a swampy overbank paleoenvironment.

Three relatively thick tephras (146, 148 and 150) are exposed along with several beds of very tuffaceous sediments. Remanence measurements from paleomagnetic samples were poor with most sites displaying unstable reversed declination directions, but negative inclinations during demagnetisation. The section is considered to be reversed by comparison with sample behaviour in other sections.

Fig. 2.5 Lithological column for Tukituki Road

2.6 TUKITUKI ROAD

top: U22/891420
base: U22/889421

A minimum of 52 m of non-marine sediments are exposed in a road cut along Tukituki Road, parallel to the Tukituki River, SW of Tikokino. Raub (1985) mapped the strata as Castlecliffian. The section is overturned and dips steeply (ca. 85°) to the west, forming part of a monocline that is exposed in Makaroro River to the north.

Sedimentary facies are dominated by massive, coarse (up to 7 cm clasts) greywacke conglomerate. Intercalated with these units is carbonaceous sandy mudstone and mudstone, both commonly finely laminated. The facies are comparable to those exposed in the Makaroro section. The sequence conformably overlies fossiliferous sandy mudstone containing *Austrovenus*. These sediments are mapped as Nukumaruan by Raub (1985). Three, thin megascopic tephras are exposed. No paleomagnetic samples were collected.
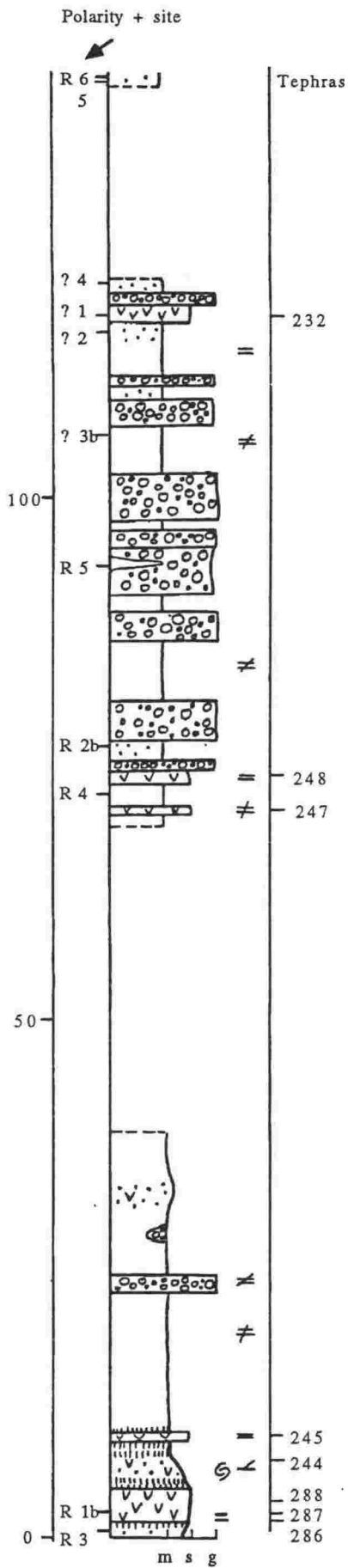
Fig. 2.6 Lithological column for Makaroro

2.7 MAKARORO RIVER

top: U22/923500
base: U22/920493

A sequence nearly 150 m thick occurs in the Makaroro River, east of Tikokino. Exposure is good, except near the middle of the section. The strata have been briefly referred to as Castlecliffian Mangatarata Formation by Raub (1985). The measured section represents a moderately east dipping (20-30°) monocline, which flattens to near horizontal at its crest where the lower part of the section is exposed. The base of the section is terminated by a fault against fossiliferous mudstone. This mudstone is mapped as Nukumaruan by Raub (1985).

The sequence is entirely non-marine, being dominated in its upper part by massive greywacke conglomerates, separated by thin, massive, carbonaceous sandy mudstone and mudstone. Paleosols and fine cross-stratified sands are common in the lower part. These facies are typical of a distal braid plain, however a few poorly sorted, reverse graded debris flow units occur near the top of the sequence.

Nine megascopic tephras occur in the measured section, most being characterised by coarse ash and fine lapilli textures, in comparison to finer tephras in other sections. Tephra 232 is a primary, non-welded ignimbrite containing flow oriented charred logs and crystal-enriched gas escape pipes. This unit consists of poorly sorted ash and lapilli, and overlies a subaerially weathered surface.

Remanence measurements of paleomagnetic samples collected are generally poor. Sites 1, 2, 3b and 4b display normal overprints acquired after tectonic tilting and retain no measurable primary remanence. Sites 3, 4, 2b and 5b display unstable reversed polarities.
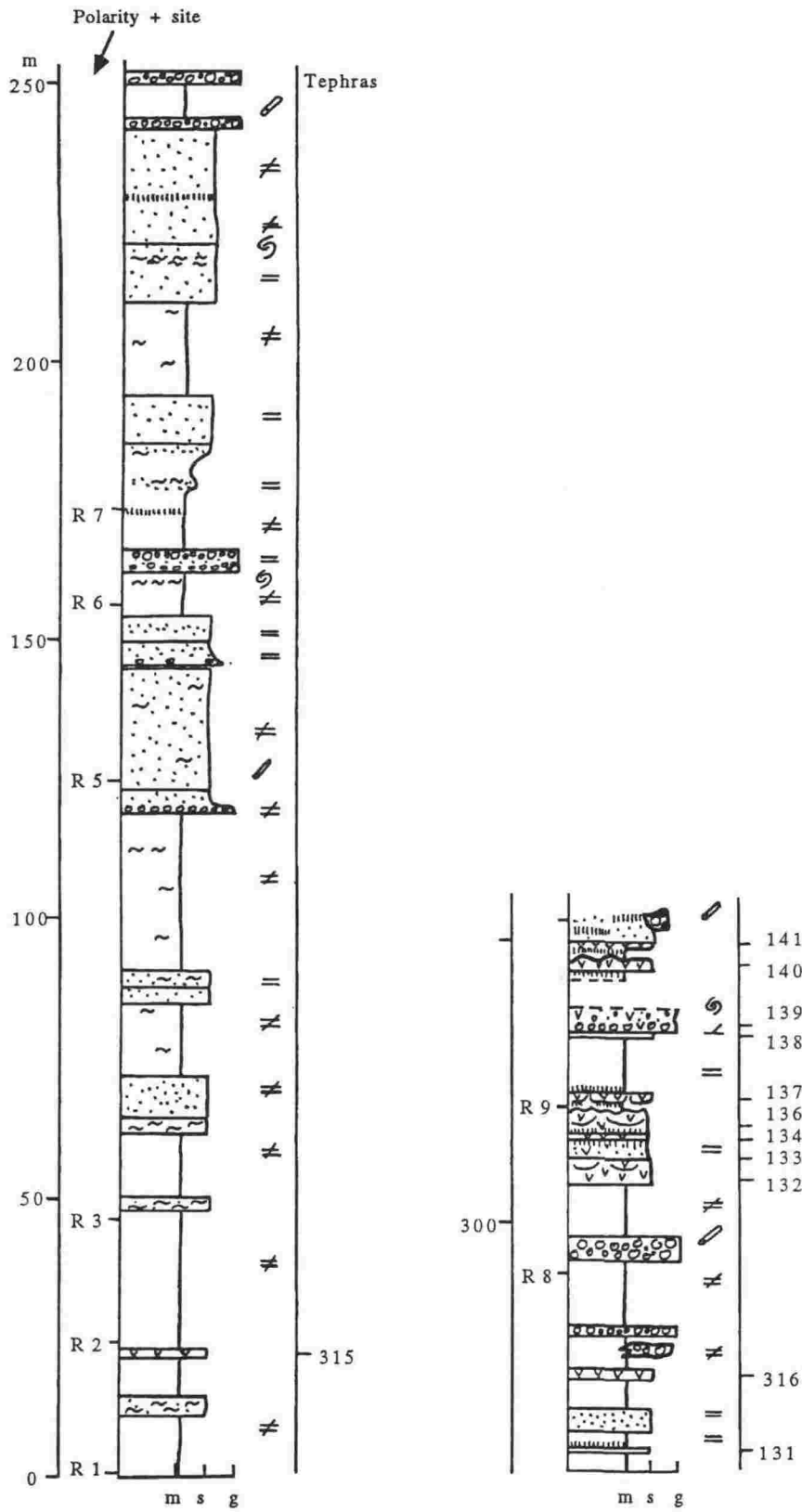
Fig. 2.7 Lithological column for Oroua section

2.8 OROUA RIVER

top: T22/625360
base: T22/617362

Over 350 m of strata was logged in the Oroua River, NE of Apiti. The strata has been previously referred to by Milne (1969), Seward (1976) and Maxwell (1988). These workers considered most of the sequence to be Nukumaruan, except for the upper non-marine part which was considered to be Castlecliffian. The strata examined is exposed on the western limb of a syncline and dips to the east. The dip is variable ranging from ca. 50° near the base of the section to near 90° for much of the middle section. The strata then flatten in dip to near 30° at the top.

The lower 240 m is mainly marine and records an overall regression from shelf facies sandy mudstones interbedded with shell beds to sands and muds containing the intertidal mollusc *Austrovenus*. The latter facies also contains rare lignites, logs and conglomerate beds. A short interval of massive, well sorted sands (presumably shore face facies) is overlain by non-marine massive, carbonaceous mudstone and greywacke conglomerate. This non-marine sequence is at least 110 m thick and contains several thick tephras.

A minimum of 12 megascopic tephras are recognised in the sequence, all of which are contained in non-marine strata except 315. The thick tephras have been fluvially emplaced being characterised by trough cross stratification. Most of the tephras are bound by lignites or paleosols suggesting episodic overbank deposition. The enclosing sediments also contain fossil logs and *in-situ* tree stumps.

Of the 9 paleomagnetic sites, only the upper 3 gave a clear magnetic remanence direction. These sites display normal overprints and a reversed primary direction. Sites 1 and 2 also show reversed polarity, but are relatively unstable. The remaining sites are unstable, but display reversed declinations.
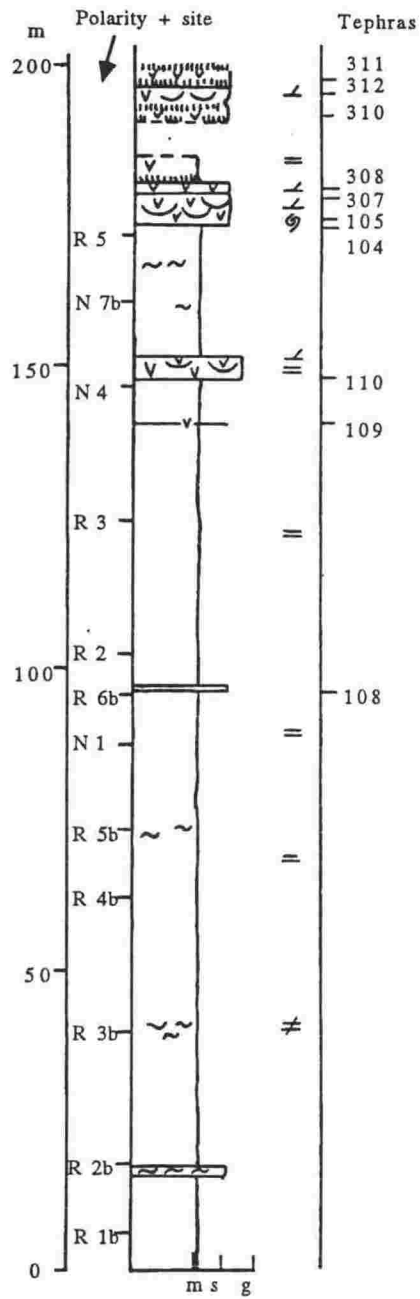
Fig. 2.8 Lithological column for Southern Pohangina section

2.9 SOUTHERN POHANGINA

top: T24/459993
base: T24/468990

192 m of strata were logged in a small, unnamed tributary to the Pohangina River, E of Ashhurst. The strata is mapped as Castlecliffian by Lillie (1953). An unknown thickness of sediments occurs beneath the logged section. Strata dips to the west at 20-30° and steepens near the top of the section to form a monoclinal flexure.

All of the section, except the top 10 m, is marine facies. The section records a regression. Fully marine shelf mudstones and sandstones are interbedded with shellbeds containing pectinids, including *Chlamys gemmulata*. These alternate with muddier sediments containing the intertidal mollusc *Austrovenus*. The top of the sequence contains well sorted sands and is tuffaceous. Lignites and paleosols are common in the top 10 m of the section. Tephras at this level are cross stratified and deposited on lignites suggestive of fluvial overbank sedimentation. Ten megascopic tephras are recognised and are contained within marine sediments, except 310, 311 and 312. The marine tephras 110, 307 and 308 are cross stratified and convolute bedded. They contain charcoal fragments and rip-up clasts of non-volcanic sediments.

Paleomagnetic remanences of the samples collected are generally good. Most sites display a high intensity reversed primary remanence, either with or without a weak normal overprint. Sites 1, 4 and 7b display a stable, high intensity normal polarity to high levels of demagnetisation.
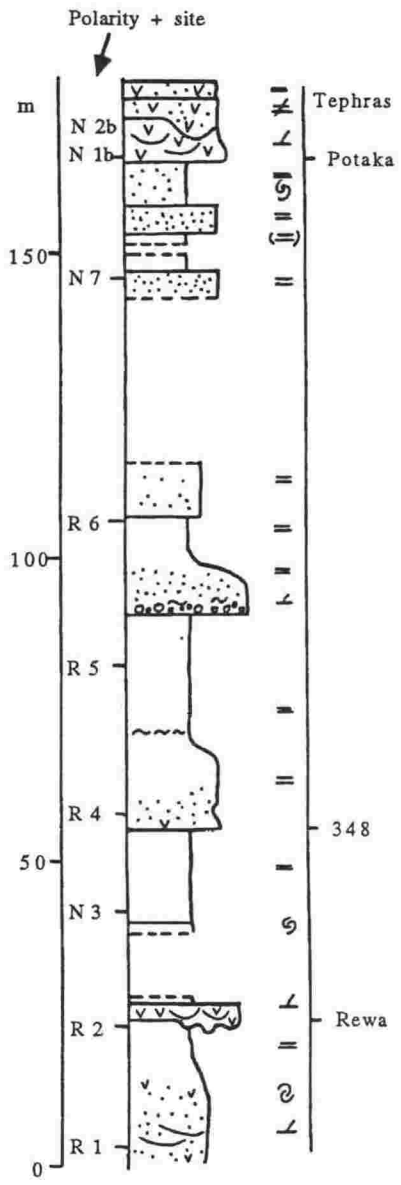
Fig. 2.9 Lithological column for Rewa Hill section

2.10 REWA HILL

top: T22/358309
base: T22/347318

Strata exposed along Highway 43 at Rewa Hill in the Rangitikei River Valley have been previously described by Te Punga (1952), who mapped them as Upper Rangitikei Formation of Castlecliffian age. Seward (1974; 1976) logged the section and determined fission-track ages for the megascopic tephras, as well as determining a magnetostratigraphy. Seward correlated the volcaniclastic sediments at Rewa Hill to the Kaimatira Pumice Sand at the Wanganui Coast, the type section for the Castlecliffian. The sequence logged is that containing the Rewa and Potaka tephras. Over 150 m of near-shore intertidal sediments are exposed, which dip 4° to the SSW.

Strata below Rewa tephra are generally coarse grained and display mega-ripples and mud drapes. Some sediments were deposited rapidly as they contain convolute bedding and de-watering features. At some horizons, rip-up clasts, up to 0.5 m in size, are present. Sediments between Rewa and Potaka tephras are generally finer grained and were deposited in quieter conditions. They consist of couplets of fine cross stratified sands, interbedded with laminated muds. Ripple cut surfaces, channels and mud drapes are common, suggestive of estuarine settings. A few units are sparsely fossiliferous.

Tuffaceous sediments are sparse throughout the section, expect at the level of Rewa and Potaka tephras. Remanent magnetism of most of the sites is multi-component in nature due to overprinting.

Polarity + site   Tephras

329   Mangapipi

330
328 — Pakihikura
327
m   326
331

R 7

400

R 6
R 5   291

R 4   ~ ~~   Vinegar Hill shell bed

200   R 3

? 2

325   Waipuru
R 1   ~ ~ ~   Waipuru shell bed

0   R 8
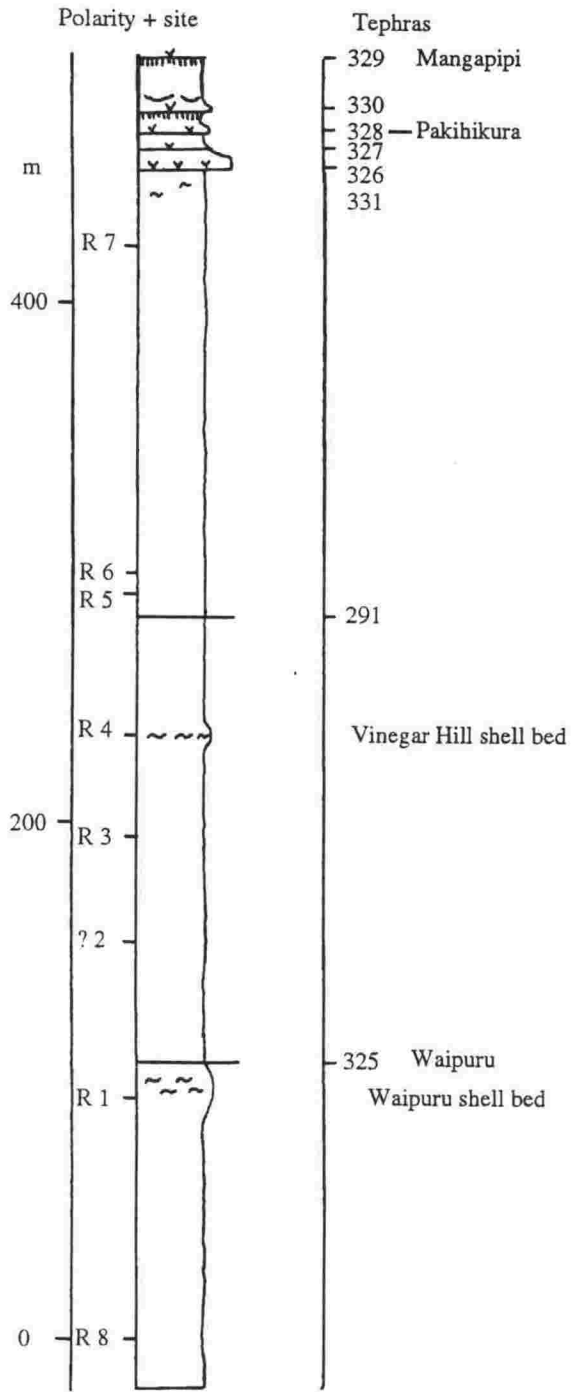
Fig. 2.10 Lithological column for Rangitikei River

2.11 RANGITIKEI RIVER

top: T22/354356
base: T22/374403

Strata exposed in the Rangitikei River, stratigraphically beneath the Rewa Hill section contain the megascopic tephras: Mangapipi, Pakihikura, Waipuru (named by Seward 1976) and several others. The strata are mainly marine, except for a short interval above Pakihikura tephra, where several lignites and paleosols are exposed. Te Punga (1952) considered the strata to be Nukumaruan in age and referred to them as Middle Rangitikei Formation. Seward et al. (1986) correlated the sequence to the Maxwell Group. The section was only logged at very low resolution and thicknesses estimated from aerial photos and maps. Tephra 291 was not located in the river sequence, but is exposed near by in a cut on Vinegar Hill Road (T22/351387). Its position in the sequence can be determined by structural projection down dip.

Paleomagnetic remanences of samples collected are poorly defined due to low intensity and multi-component magnetisation.
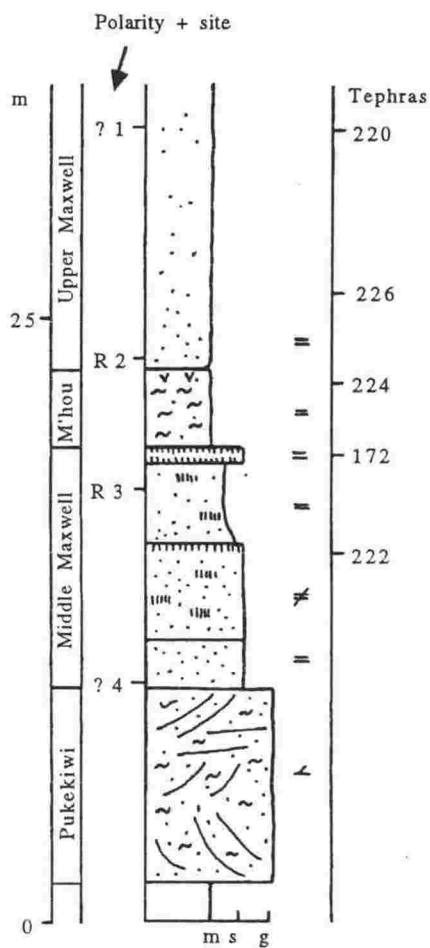
Fig. 2.11 Lithological column for part of the NukumaruanWanganui coast section

2.12 WANGANUI COAST (NUKUMARUAN TYPE SECTION)

R22/667472

The entire Nukumaruan type section exposed in cliffs along the Wanganui Coast (Fleming 1953) was examined for megascopic tephras. Only the upper interval of the sequence consisting of the Middle Maxwell, Mangahou Siltstone and Upper Maxwell Formations contained megascopic tephras and therefore were logged. Most of the section is exposed in the vicinity of Ototoka Stream. The lithologies of the formations have been described in detail by Fleming (1953) and Beu & Edwards (1984). The strata dip gently (2-3°) to the SE and are generally poorly exposed.

The Pukekiwi Formation consists of a coarse sandy shell grit and is cross-stratified. Mangahou Siltstone is also marine, containing a variety of mainly estuarine fossils (Fleming 1953), and consists of a tuffaceous sandy mudstone. A thin megascopic tephra occurs at the top of the unit (224). The Middle and Upper Maxwell Formations are non-marine, consisting of carbonaceous dune sands, paleosols and lignitic sandy mudstone. Volcanic glass occurs rarely as beds (e.g. 172) or as highly tuffaceous sediments and dispersed glass shards through most of of the Middle and Upper Maxwell Formations.

Paleomagnetic remanences of samples collected from 4 sites are unstable with highly erratic demagnetisation paths and weak intensities. However, sites 2 and 3 displayed the features of reversed polarity overprinted by one or more normal components.
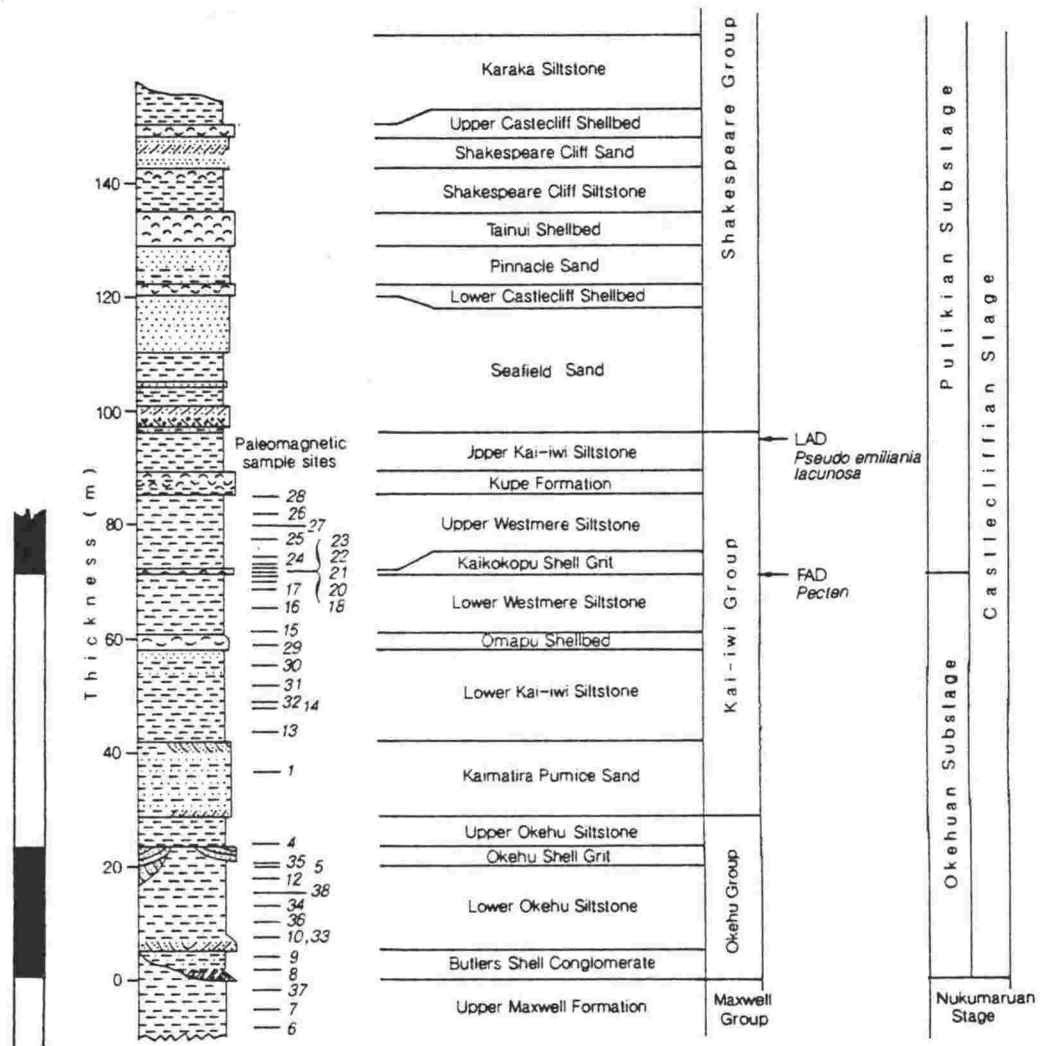
Fig. 2.12 Lithological column for the Castlecliffian type section exposed at the Wanganui coast (adapted from Turner & Kamp 1990)

2.13 WANGANUI COAST (CASTLECLIFFIAN TYPE SECTION)

Lithological columns for Castlecliffian strata exposed along the coast, have been presented by Fleming (1953), Beu & Edwards (1984) and Turner & Kamp (1990). The sequence was not re-logged in this study and the column presented here is adapted from Turner & Kamp (1990). This sequence represents the type section for the Castlecliffian. The strata are entirely marine and represent a series of unconformity bound units. One megascopic tephra (173) occurs and is referred to as Kaimatira Pumice Sand (Seward 1976). Magnetostratigraphy is presented by Turner & Kamp (1990).
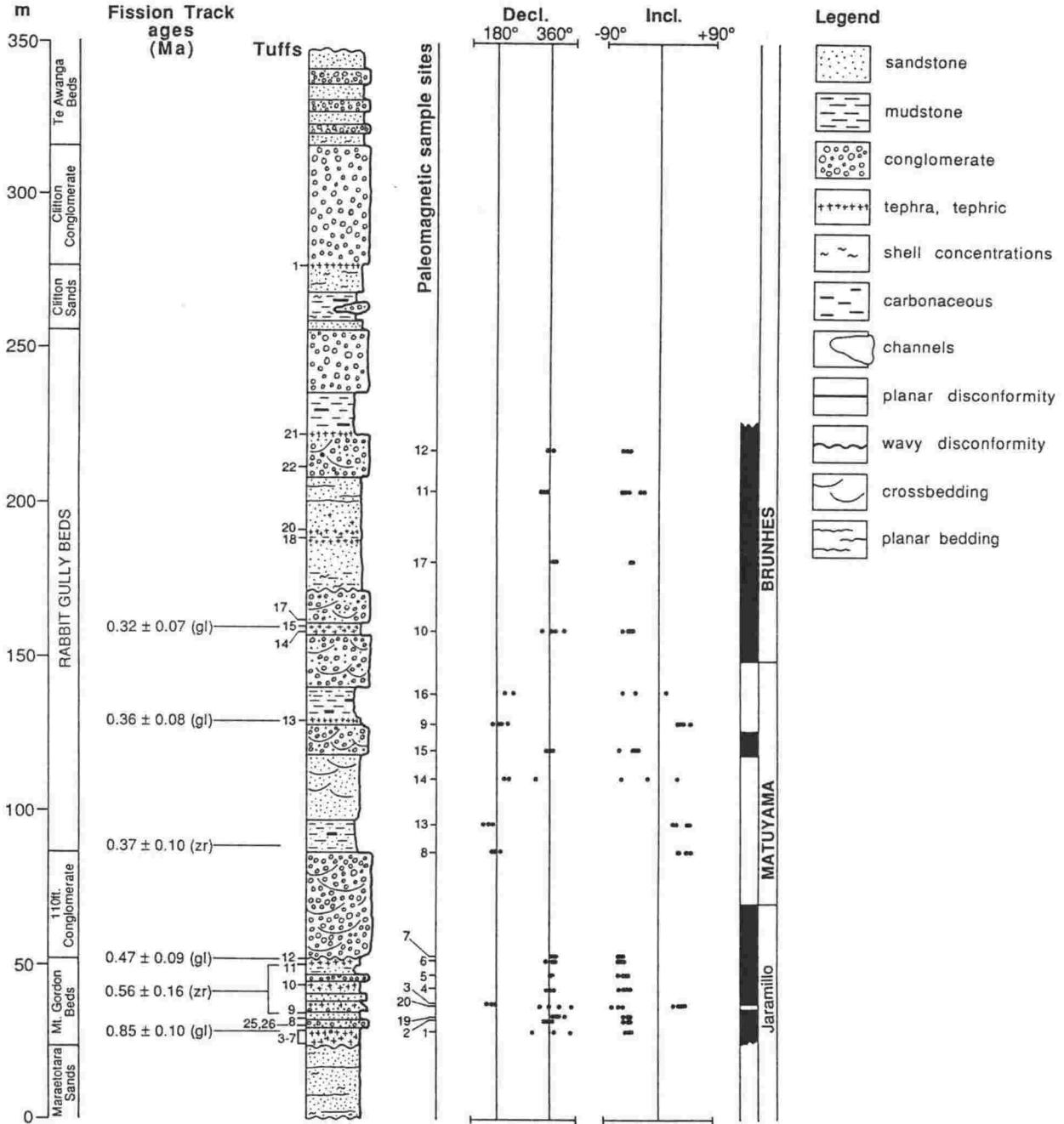
Fig. 2.13 Lithological column for Cape Kidnappers along with magneto-stratigraphy (from Black 1992).

2.14 CAPE KIDNAPPERS

Kamp (1990)

The sequence at Cape Kidnappers has been described in detail by Kingma (1971) and Black (1992), and therefore was not re-logged in this study. The column presented here is from Black (1992). The strata are considered Castlecliffian in age on the basis of macrofossils, in particular the presence of *Pecten*. Fission-track ages for some of the tephras have been reported by Seward (1975; 1979), and a revised chronology on the basis of magnetostratigraphy by Black (1992). The strata are classified as Kidnappers Group by Kingma (1971) and consist of several formations. Most of the strata is non-marine, being fluvial gravels, sands and muds, with abundant lignite layers. A few marine beds are intercalated and contain estuarine fossil assemblages.

At least 26 megascopic tephra layers (numbered 1-26) were recorded by Black (1992), many of which are reworked. Black divided the tephras into 6 major groups, each representing reworked events of a single eruption or a series of eruptions; A (3-5, 6, 7, 8, 26, 25); B (9, 11); C (13); D (14, 15) and E (18, 20, 21).
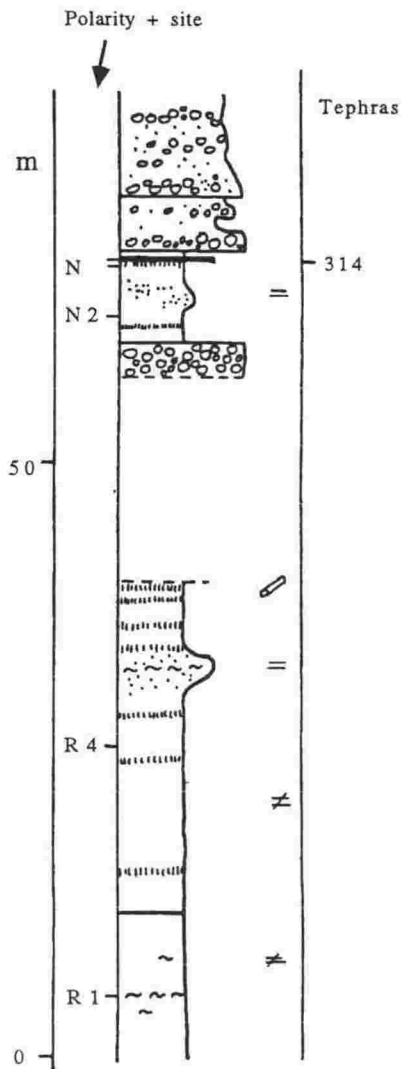
Fig. 2.14 Lithological column for Leader section

2.15 LEADER RIVER

top: O32/325420
base: O32/318423

Over 100 m of marine and non-marine Castlecliffian strata is exposed in the Leader River, North Canterbury. The lower part of the sequence consists of fossiliferous sandy mudstone, and contains the mollusc genus *Pecten*, indicating a Castlecliffian age. The remainder of the sequence consists of fluvial conglomerate and sandy mudstone, interbedded with lignites and paleosols. Fossil pollen, insecta and avifauna have been found in the non-marine sediments (G. Warren pers. comm. 1991). The section log is re-drawn from data of Warren (unpubl.) and field observations. One megascopic tephra occurs near the top of the section, and represents a fall out deposit (ca. 0.10 m thick). Paleomagnetic specimens from the top of the section display a stable normal polarity. Those from the lower part are strongly overprinted and appear to be of reversed polarity.

Chapter 3
MAGNETOSTRATIGRAPHY

3.1 INTRODUCTION

Previously, only limited attention has been paid to the magnetostratigraphy of New Zealand early-middle Pleistocene deposits. In an early study, Kennett et al. (1971) recognised the Olduvai Subchron in marine sediments of Nukumaruan age in southern Wairarapa. Seward (1974) presented data for Castlecliffian marine sediments at Rewa Hill near the Rangitikei River, and identified a paleomagnetic reversal in that section as the Brunhes-Matuyama, supported by using fission-track ages of interbedded tephras. This reversal boundary was also tentatively identified by Collen & Vella (1984) in southern Wairarapa. Seward et al. (1986) presented a magnetostratigraphy for most of the Cenozoic strata exposed in the Rangitikei River, beneath the Rewa Hill section, and identified the Olduvai Subchron as well as the Gauss and Gilbert Chrons. The Rewa Hill section and sequences in southern Wairarapa were re-examined by Shane & Froggatt (1991), who determined similar reversal patterns. The type section for the Castlecliffian stage exposed along the Wanganui coast was studied by Turner & Kamp (1990) who determined the position of the Brunhes-Matuyama boundary and the Jaramillo Subchron. A similar reversal stratigraphy was found by Black (1992) at the Cape Kidnappers section.

In other Pleistocene studies, Pillans & Wright (1990) determined a paleomagnetic record for a long loess core from the Wanganui Basin, representing the last 0.60 Ma. There have also been sparse publications on the paleomagnetism of Taupo Volcanic Zone ignimbrites and lavas, notably Cox (1971), who identified both reversed and normal Pleistocene units. In general paleomagnetic investigations in New Zealand have suffered from the lack of isotopic age data which would allow the precise correlation of sequences to the geomagnetic time scale.

In the present study, long Castlecliffian/Nukumaruan sections in the East Coast region and Wanganui Basin were sampled to develop a magnetostratigraphy in conjunction with isotopic age data for key tephras (see Chapter 7).

3.2 METHOD

Consolidated sediments were sampled by a portable motorised drill, while less consolidated sediments were cut by a knife and placed into plastic boxes which were oriented in the field. Specimens were transported and stored in magnetic shields. In the laboratory, the specimens were sequentially measured and demagnetised using a Molspin spinner magnetometer and a 2-spin axis alternating field demagnetiser. Noise limit for the magnetometer is about 0.03 mA/m. A pilot specimen from most sites was demagnetised in 5-10 mT steps in
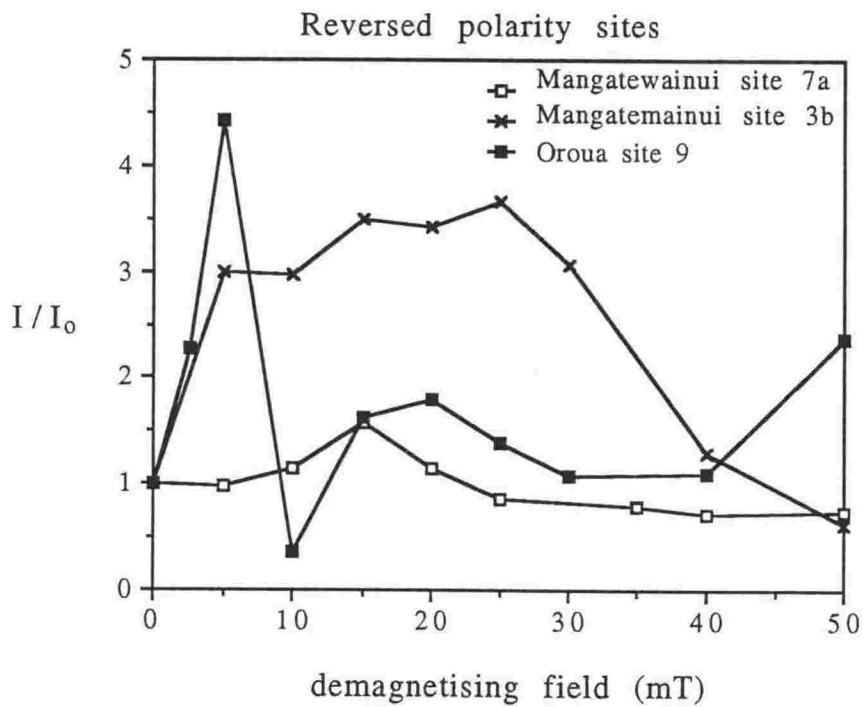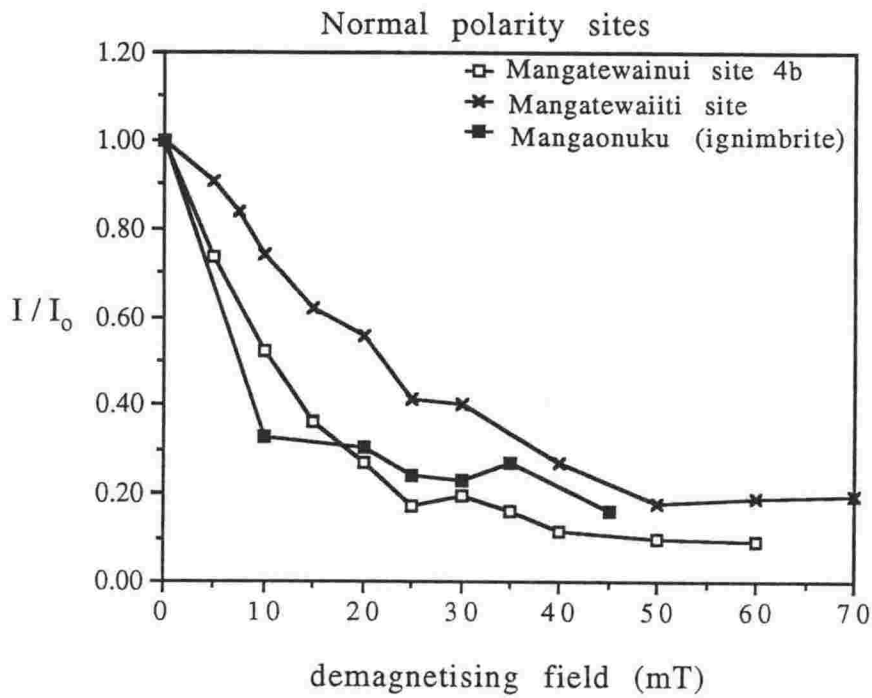
Fig. 3.1 Examples of specimen paleomagnetic intensity variations during demagnetisation.

fields in the range 0-70 mT, to test their behaviour. The remaining specimens were then demagnetised at optimum levels, usually involving 2 or 3 steps.

3.3 NATURE OF SPECIMEN MAGNETISATION

3.3.1 Natural Remanent Magnetisation and intensity

Specimens collected for paleomagnetic studies came from a variety of facies including unconsolidated to partly consolidated muds, sandy muds and tephras. For most of the sections, the specimens collected displayed a wide range in Natural Remanent Magnetisation (NRM) intensity and direction. NRM intensities may vary from ca. 0.05 to 60 mAm^{-1} with most specimens in the range 0.1-3.0 mAm^{-1}. The highest intensities are displayed by coarse grained sandy sediments and sediments with a high volcanogenic component. Glassy tephras, both fine and coarse, also display high NRM intensities. NRM directions are typically either normal or have negative inclinations (normal in Southern Hemisphere) regardless of their declinations. Inclinations are often low <40° for specimens with declinations in the range 090-270°, which is not consistent with a dipole field at the latitude of the site. This suggests magnetic overprinting of the original field.

The behaviour of specimen intensities during AF demagnetisation falls into two broad groups: (a) a decline in intensity with progressive demagnetisation; and (b) an initial increase in intensity followed by a decline with progressive demagnetisation (Fig. 3.1). The first group is typical of the progressive removal of a single component remanence and is commonly displayed by normal polarity specimens in this study. Median destructive fields are in the range 10-25 mT. The second group reflects the progressive removal of a low coercivity component of opposite polarity to another component of higher coercivity. This behaviour is commonly shown by reversed polarity specimens in the study. The behaviour of intensities during demagnetisation provided a simple indicator of the multiple component nature of the specimens and their polarity.

3.3.2 Specimens with single component magnetisation

Most normal polarity specimens show straight demagnetisation paths toward the origin of orthogonal component plots (Fig. 3.2), suggesting a single component NRM. A few displayed a very weak viscous overprint which is usually removed in 5-10 mT fields. These normal specimens produce site averages which differ within ca. 20° of declination with the present day field, thus the paleomagnetism is considered the primary depositional or post-depositional RM. Other specimens display a reversed NRM direction which follows a relatively straight path to the origin on component plots (Fig. 3.2). These specimens are considered to have a single component reversed primary magnetism. Some of the reversed specimens initially
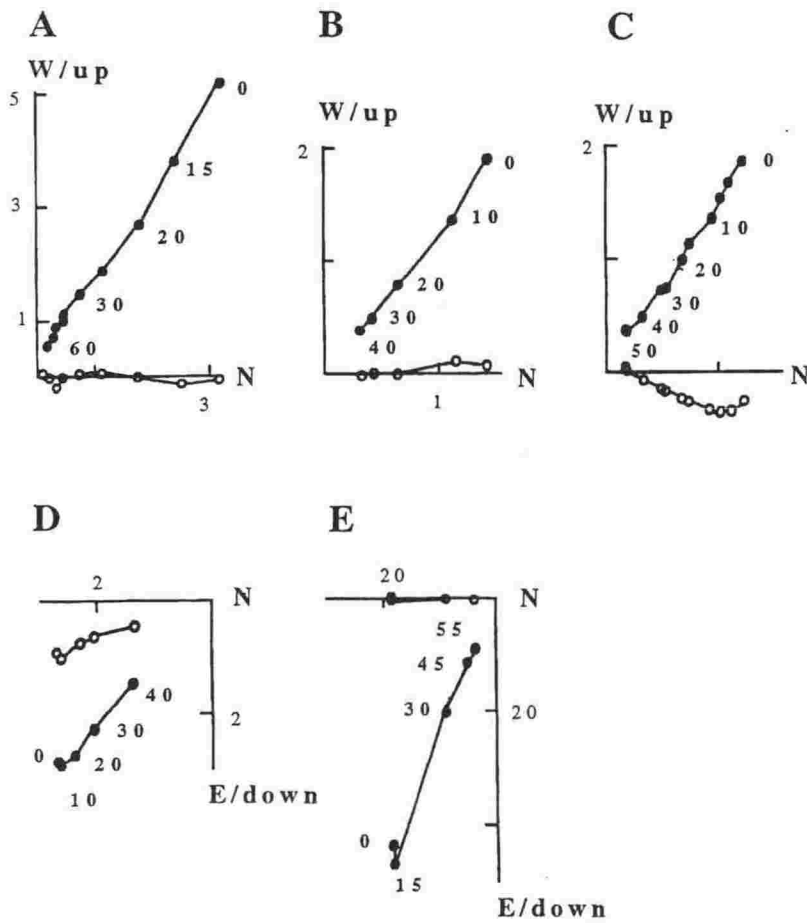
Fig. 3.2 Examples of demagnetisation behaviour of specimens with a single component magnetisation, plotted on orthogonal component diagrams. Solid dots represent the x and z components and open dots represent the x and y components.
A= Mangatewainui site 4; B= Mangatewainui site 1c; C= Mangatewaiiti site 1c; D= Mangatewaiiti site 2c; and E= tephra 291, Vinegar Hill Rd.

increase in intensity during demagnetisation which is accompanied with an increase in inclination. These specimens are considered to have a very weak normal overprint.

Specimens which are characterised by a single component magnetisation are not common and were collected mainly from near the tops of the Mangatewaiiti and Mangatewainui sections. Most specimens display multi-component magnetisation.

3.3.3 Specimens with two component magnetisation

Many specimens have NRM directions which differ greatly from directions expected from a dipole field. Demagnetisation reveals a magnetisation consisting of two components. These are shown by straight line segments of different direction on orthogonal component plots (Fig. 3.3). Specimens typically move away from the origin with the progressive removal of a low coercivity component which has an opposite direction to a higher coercivity component. The more viscous component is usually of normal polarity. A change in polarity is accompanied by a decline in intensity and forms a path toward the origin of the plot (Fig. 3.3). The higher coercivity component is typically reversed. This demagnetisation behaviour is interpreted as the removal of a secondary viscous overprint. The higher coercivity component is considered primary. The viscous overprints are typically removed in 10-25 mT fields.

Some of these specimens do not completely change to a reversed direction during demagnetisation (Fig. 3.3d). Typically, negative inclinations decrease and declinations move toward 180°, as in the early stages of demagnetisation of stable specimens. However, these unstable specimens do not move toward the origin on orthogonal component plots, although intensities may drop in an orderly fashion (Fig. 3.3d). By comparison to normally overprinted, reversed polarity specimens, these unstable specimens are also considered to have a reversed primary magnetisation. It is likely that the lower coercivity component partly overlaps the primary component spectrum, thus masking the primary polarity direction. This is confirmed by the fact that some specimens with 'masked' reversed polarity were collected from the same sites as specimens displaying a stable reversed polarity, reflecting differing degrees of overprinting. Specimens with this type of magnetisation are common from the Rangitikei, the lower part of Oroua and Mangatewaiiti, and Manawatu sections.

3.3.4 Specimens with multi-component magnetisation

Specimens displaying an erratic demagnetisation path or those consisting of 3 or more different segments on component plots, reflect multi-component magnetisation (Fig. 3.4). This type of behaviour was encountered in many of the sections examined. Typically the first component is of low coercivity and mainly eliminated in fields of 10-25 mT. This component is a modern viscous overprint of normal polarity. Its removal reveals a second higher coercivity
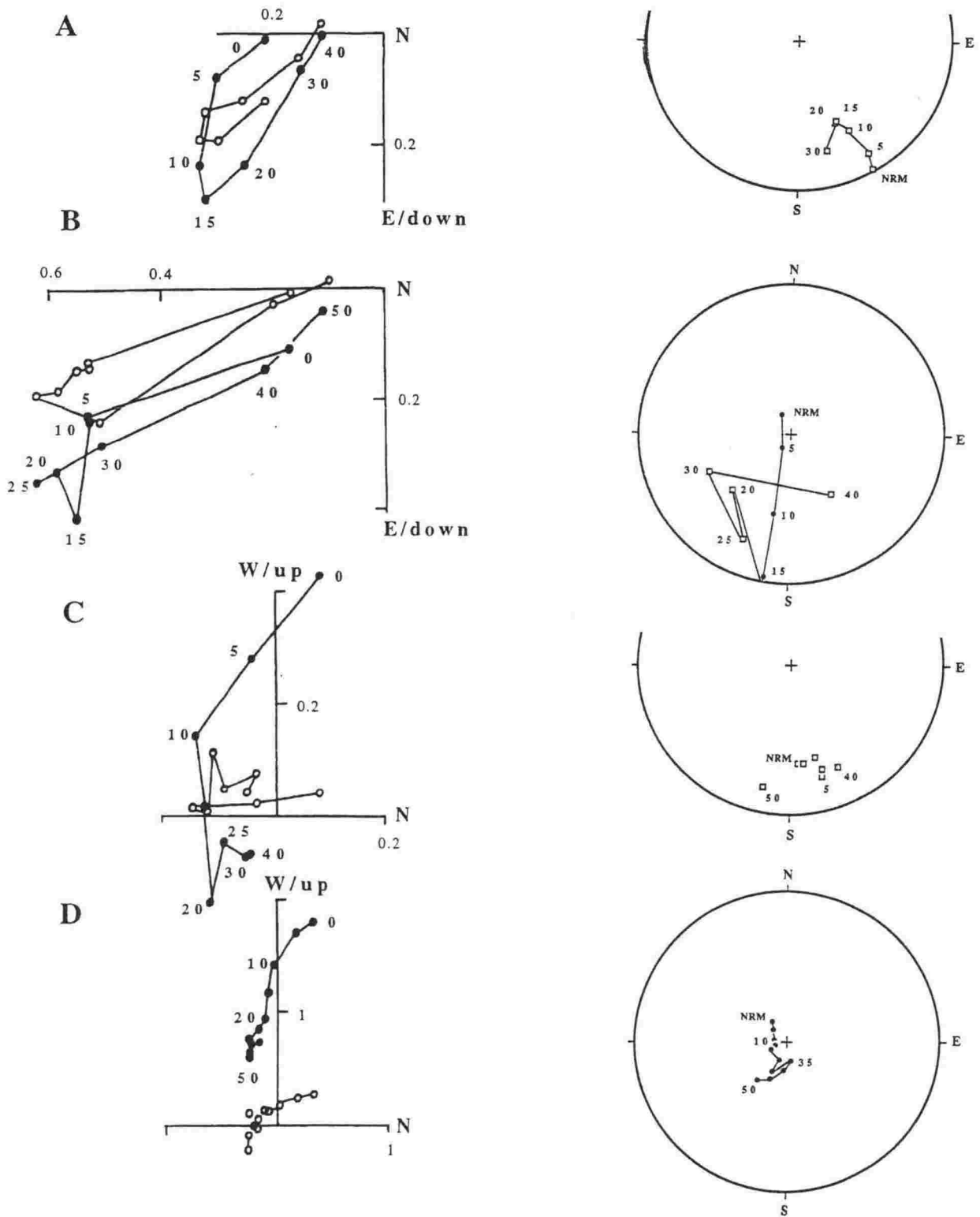
Fig. 3.3 Examples of demagnetisation behaviour of specimens with two major components of magnetisation shrown as orthogonal component plots (left) (symbols as in Fig. 3.2) and stereonet projections (right). Stereonet symbols: negative inclinations (dots) and positive inclinations (squares).
A= Mangatewaiiti site 2; B= Mangatewainui site 2b; C= Mangatewaiiti site 8a; D= Rewa Hill site 2.
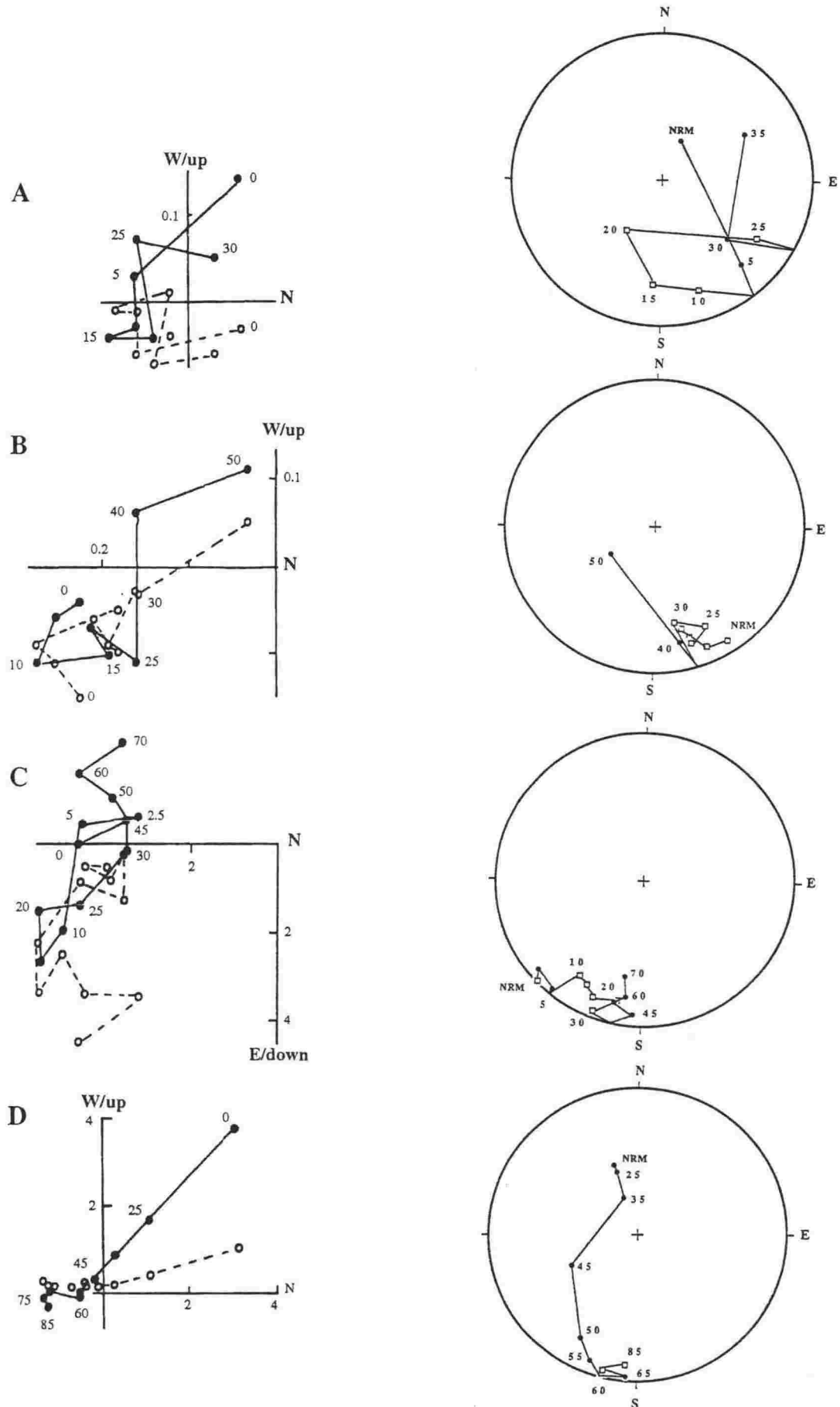
Fig. 3.4 Examples of demagnetisation behaviour of specimens with multi-component magnetisation, shown on orthogonal component plots (left) and stereonet projections (right). Symbols as in Fig. 3.2 and 3.3. A= Mangatewainui site 7; B= Pohangina site 2; C= Pakihikura tephra (Rewa Hill); D= Pohangina site 7b.

Sites 1, 2, 3B and 4B, Makaroro River

Fig. 3.5 Stereoplots of specimen magnetisation for sites near the top of the Makaroro section, showing the effects of tilt correction. Uncorrected measurements plot closer to that of the present day field suggesting their magnetisation is post tectonic.

component usually of reversed polarity which decays in fields of 20-40 mT. Intensities drop with progressive demagnetisation in this part of the spectrum. In fields >45 mT, intensities often increase again and directions become normal. This change represents a third very high coercivity component. In some cases, the very high coercivity component is of reversed polarity. Some specimens from the Pohangina section display a stable normal component in demagnetising fields of 0-50 mT, but show a second very high coercivity component in fields >60 mT of reversed polarity (Fig. 3.4d). By comparison to simply overprinted specimens, the intermediate coercivity component, revealed in the range of 20-50 mT fields, is considered to represent the primary depositional RM. High coercivity and high blocking temperature magnetic components has been reported by McGuire (1989) and Turner & Kamp (1990) in New Zealand mudstones. They are thought to be a result of chemical diagenesis. The polarity of this component reflects the timing of the chemical alteration. In most cases it is normal and thus is modern. The nature of the primary, intermediate coercivity component can be difficult to determine as this part of the coercivity spectrum is often overlapped by the other components.

3.3.5 Post-tectonic overprinting

Specimens from sites 1, 2, 3b and 4 near the top of the Makaroro section including an ignimbrite (S 232) display NRMs with an apparent intermediate direction or polarity when the tilting of strata is corrected for (Fig. 3.5). Orthogonal component plots reveal a straight demagnetisation path to the origin indicating an apparently single component magnetisation. The strata now dip at 22° to the east at a strike of 040°. If the effect of tilting is ignored, then the paleomagnetic directions are closer to that of the present day normal field. This implies the magnetisation represents a normal overprint acquired after tectonic tilting of the beds. No higher coercivity components are evident from demagnetisation and thus the original primary direction of magnetisation cannot be determined. Corrections for the tectonic tilt of bedding can provide insight into the timing of magnetic overprinting in the sections examined. In the case of the upper part of the Makaroro section the secondary nature of the magnetisation may not have otherwise been detected.

3.3.6 Assessment of site polarity

A severe degree of overprinting was encountered at most of the collection sites. As the success of isolating the primary depositional RM was variable due to the multi-component nature of the specimens, the RM directions for a particular site are often very scattered. This reflects the degree of overprint remaining after demagnetisation. Thus statistical measures of pole direction, such as Fisher statistics, provide little insight to the paleomagnetic field. However, the main purpose of the investigation was to determine the polarity of the sequences.

For this, the data provide much information, as the polarity of the specimens can often be readily determined from their behaviour during demagnetisation, even if the virtual geomagnetic pole is not adequately defined.

Various criteria have been proposed for determining the paleomagnetic polarity of a site (e.g. Hillhouse et al. 1986; Kodama 1979; Verosub 1981) with a bias toward reversed polarity specimens. As the Earth's magnetic field has been predominantly normal for the last 0.78 Ma (Brunhes Chron), viscous overprints are most likely to be of normal polarity. The early-middle Pleistocene sections examined here consist of thick conformable sequences with little evidence of unconformities due to uplift and exposure. Thus the sections have been deeply buried until uplift in the last ca. 0.5 Ma. As incising streams rapidly change their courses, most of the sediments have been exposed only since the Holocene and often in the last 10-100 years. Therefore overprinting can be assumed to be normal in most if not all cases. Thus specimens of reversed polarity or those that move toward a reversed direction during demagnetisation are most likely to reflect the magnetic field near the time of deposition.

Using this approach and considering the demagnetisation behaviour of each specimen, a site that contains at least one reversed polarity specimen is considered to be reversed (e.g. Verosub 1981). Similarly, a site characterised by specimens having reversed declinations (ca. 180°), but normal (negative) inclinations (a situation commonly encountered here), are best considered to be reversed as demagnetisation tests show a change toward reversed polarity. A similar classification of site polarity was used by Kodama (1979) for a severely overprinted sequence. Normal polarity sites are treated with additional caution due to like-polarity overprinting. Here a site is considered normal if all of the specimens display a stable normal magnetisation during demagnetisation. When specimen inclinations are close ($\pm 20°$) to that of the theoretical dipole field (ca. 60° for sites at 42°S latitude), the paleomagnetism is considered reliable. This can be further checked by correction for bedding tilt. The tilt correction should move the RM directions toward that of the dipole field if the the specimens' magnetisation is pre-tectonic.

3.3.7 Transitional paleomagnetic polarity

Intervals of intermediate or transitional polarity near reversal boundaries are interpreted as a record of the changing paleomagnetic field. They have been reported by Turner & Kamp (1990) in the Wanganui coast section, particularly near the Brunhes-Matuyama boundary. Sites classified as transitional are characterised by declinations in the range ca. 90-200°, and have negative (normal) inclinations (Turner & Kamp 1990). No stable sites with these characteristics have been found in the sections examined here. Some polarity directions of reversed specimens with normal overprints are similar to these transitional polarities, as the normal overprint is not completely removed. However, specimens in this study do not reach a stable end point, but
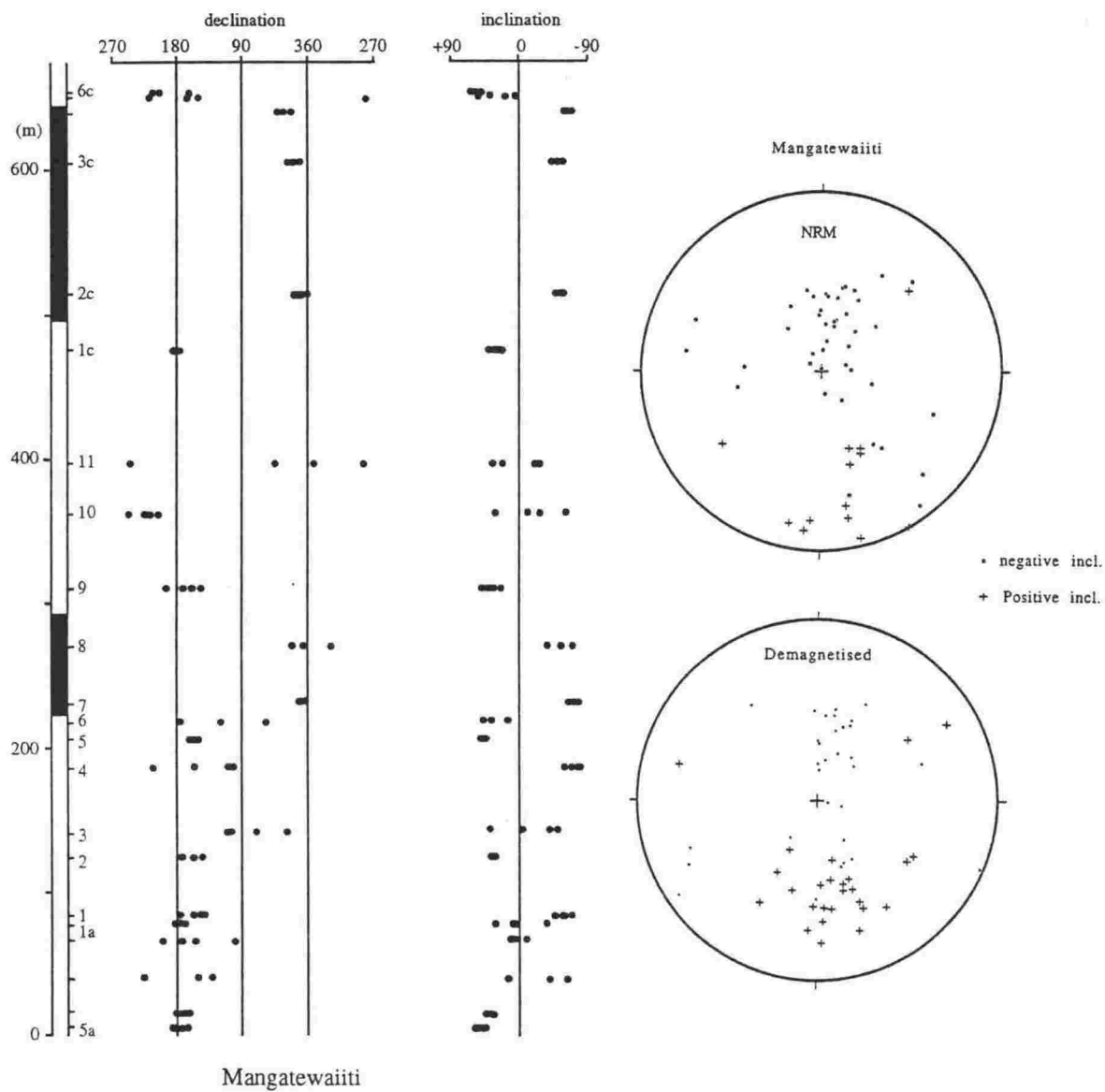
Fig. 3.6 Paleomagnetic specimen measurements for the Mangatewaiiti section. Each point represents a single measurement. At right: stereonet projections for the specimen directions.

move toward a reversed polarity. Therefore none of the sites examined here are considered to be transitional.

3.4 MAGNETOSTRATIGRAPHY OF STUDY SECTIONS

3.4.1 Correlation

The longer sections examined are dominated by reversed polarity sediments (Figs. 3.6, 3.7, 3.8). This was expected as previous paleontological, paleomagnetic and radiometric dating (Te Punga 1952; Lillie 1953; Kingma 1971; Seward 1974; Seward et al. 1986; Pillans 1992) have suggested the sequences are Plio-Pleistocene in age and thus should represent the Matuyama Reversed Chron [0.78-2.60 Ma on the basis of astronomical calculations (Shackleton et al. 1990)].

The longest sections representing the early-middle Pleistocene are exposed at Mangatewaiiti and Mangatewainui. These two parallel sections display similar specimen demagnetisation behaviour and a similar resulting reversal stratigraphy (Fig. 3.6, 3.7). Demagnetisation removed, with variable success, a normal viscous overprint to reveal a sequence of mainly reversed polarity at these sections. Most of the sites in the middle to lower part of the sections are characterised by declinations close to 180°, but either positive or negative inclinations or both. The lower ca. 90 m of the Mangatewaiiti section represents marine sediments of the Nukumaruan Kumeroa Formation (Lillie 1953). This part of the sequence is of reversed polarity. The remainder of the sequence is non-marine and represents the Castlecliffian Mangatarata Formation (Lillie 1953). Both the Mangatewaiiti and Mangatewainui sections have a normal interval near the top (Fig. 3.6, 3.7). Above this are reversed polarity sediments in a syncline axis which structurally terminates both sections, preventing further sampling. This normal interval is likely to be the Jaramillo Subchron (0.99-1.07 Ma, Shackleton et al. 1990), as this subchron has been located in other sections considered to be Castlecliffian in age (Turner & Kamp 1990; Black 1992). This is confirmed by isotopic ages for the interbedded tephras (Chapter 7). The lack of a long normal interval which could represent the Olduvai Subchron (1.77-1.79 Ma) in these sections suggests it could occur further below them or little deposition occurred during this interval.

A similar magnetostratigraphy was determined for the Rangitikei sequence exposed at Rewa Hill, between Rewa and Potaka tephras (Fig. 3.8). Seward (1974) also determined a similar reversal pattern for this section and interpreted the normal interval as the Brunhes Normal Chron (0-0.78 Ma), on the basis of fission track ages for the tephras. However, a recently determined Ar/Ar age of ca. 1 Ma for Potaka Tephra (Chapter 7), which occurs within the normal interval, indicates this interpretation is not possible and instead the interval represents the Jaramillo Subchron. Secondary normal overprinting is particularly severe at the
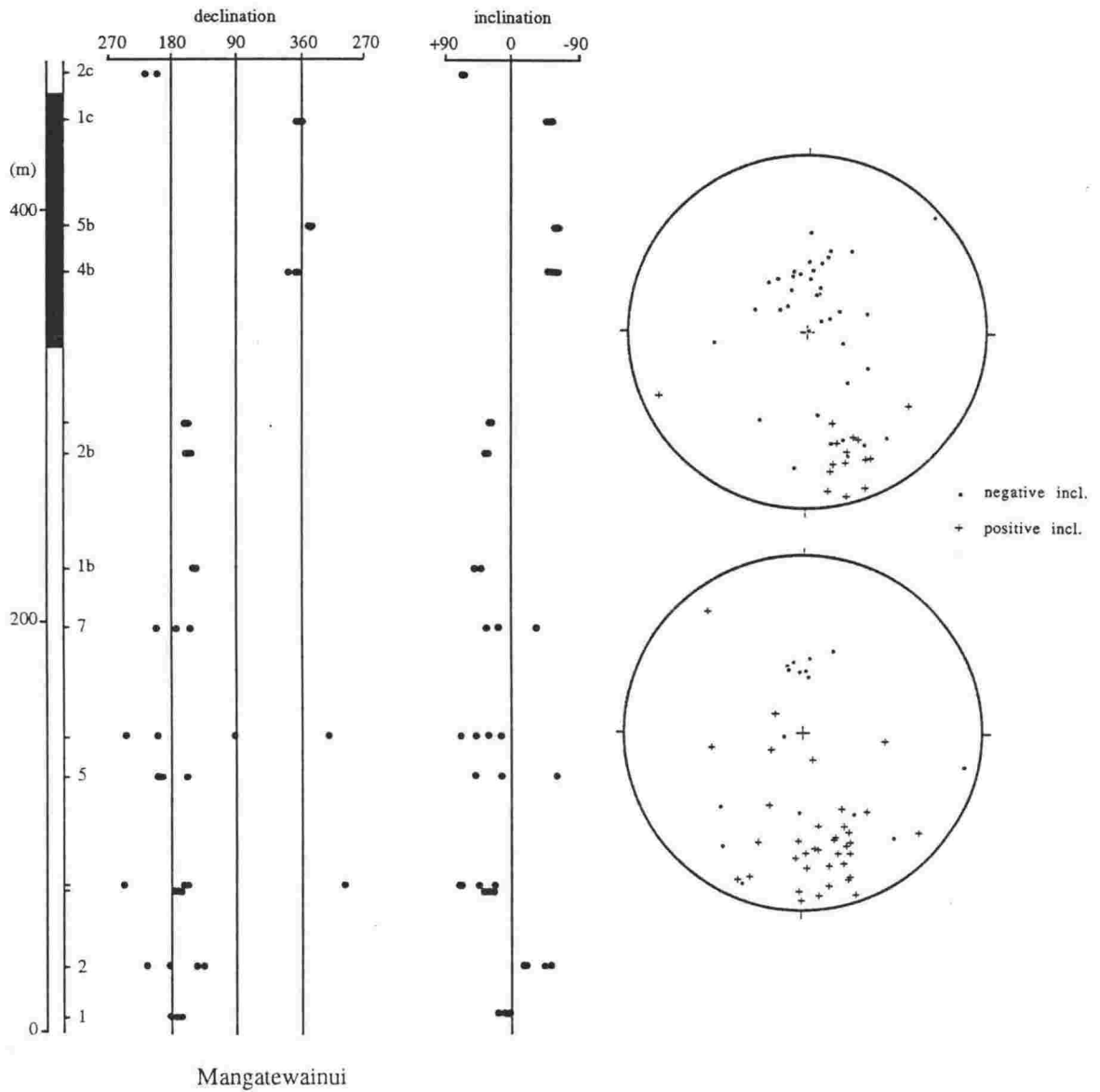
Fig. 3.7 Paleomagnetic specimen measurements for the Mangatewainui section.
Plotted as in Fig. 3.6.
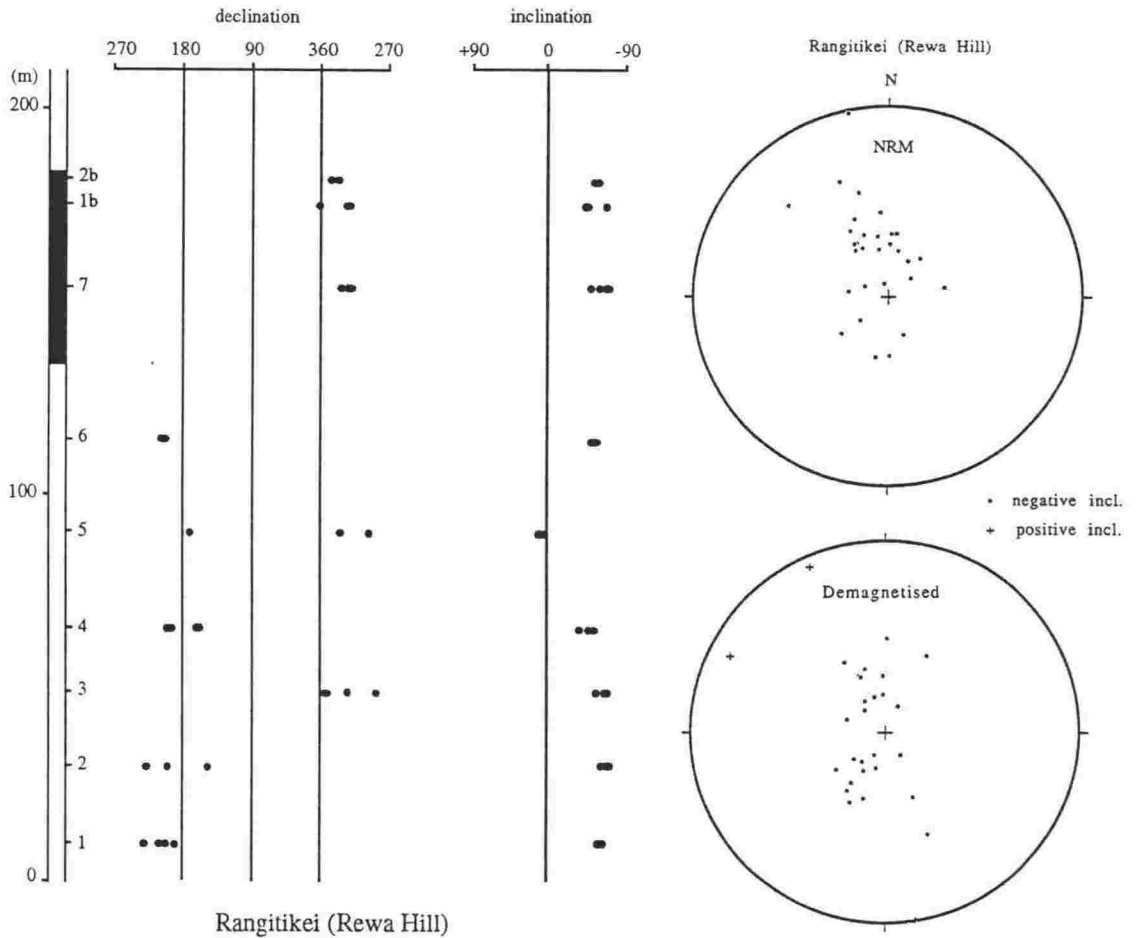
Fig. 3.8 Paleomagnetic specimen measurements for the Rewa Hill section.
Plotted as in Fig. 3.6.
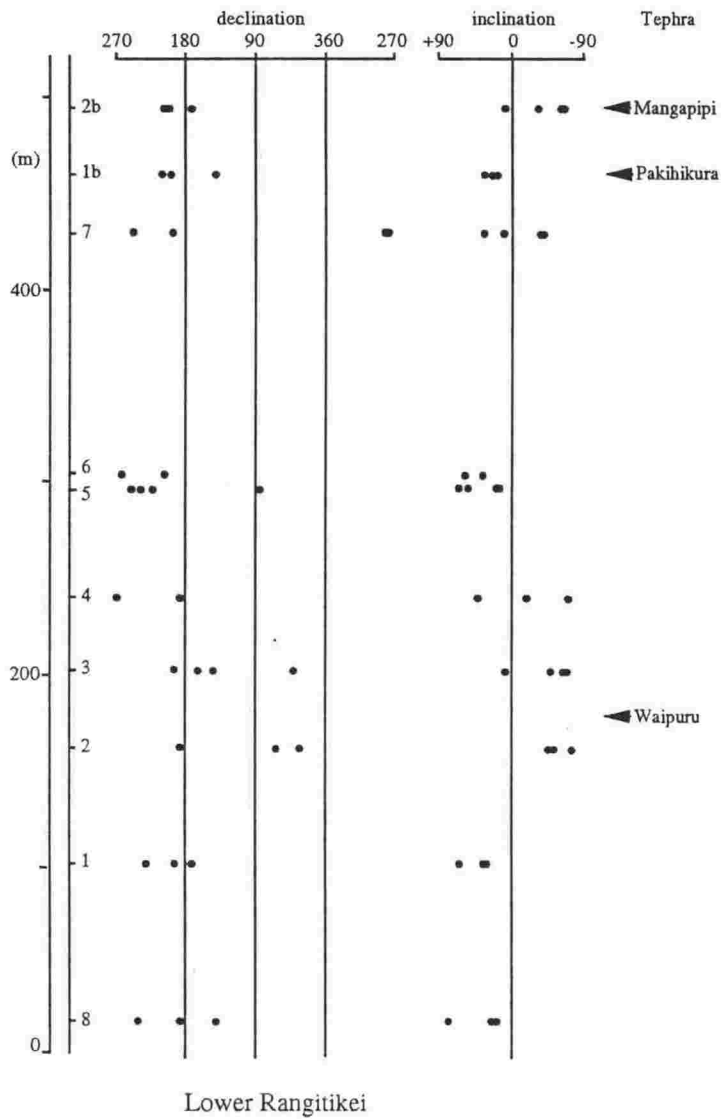
Fig. 3.9 Paleomagnetic specimen measurements for the Rangitikei River section. Plotted as in Fig. 3.6.

Rewa Hill section (Fig. 3.3d, 3.4d) and most of the reversed polarity sites are interpreted from declinations in the vicinity of 180° (Fig. 3.8), rather than their inclination alone. The reversed polarity is supported by an isotopic age of ca. 1.46 Ma for Rewa Pumice (Chapter 7).

Further samples were collected in the Rangitikei River below Rewa Hill sequence, which contains the Mangapipi, Pakihikura and Waipuru tephras (Fig. 3.9). Specimens from this part of the sequence displayed multi-component magnetisation of low intensity which hindered demagnetisation tests. As a result paleomagnetic directions are highly scattered. Each site, except site 2, has at least one specimen of reversed inclination. At the level of each of the tephras, sediments appear to be of reversed polarity. This is inconsistent with the results of Seward et al. (1986) who reported a long normal interval, interpreted to be the Olduvai Subchron, which contained the Waipuru Ash. Considering the normal overprinting and multi-component nature of the specimens' magnetisation, normal directions must be treated with extra caution. Further sampling is required to fully establish the magnetostratigraphy of the lower Rangitikei section.

Other sequences sampled including Oroua, Manawatu and Makaroro were found to be of mainly reversed polarity (Fig. 3.10, 3.11, 3.12). These sections can be correlated by the presence of Pakihikura Tephra in each of them (Chapter 8). They are interpreted as representing the same interval as the lower part Mangatewaiiti and Mangatewainui sections, i.e. Matuyama Chron, beneath the Jaramillo Subchron (>1 Ma). Strata exposed by a tributary to the Pohangina River, display two short normal intervals in a reversed polarity sequence (Fig. 3.13). Chronology for this section is lacking as the interbedded tephras have not been identified. However, the section records a marine regression to fluvial sediments with tephras at its top, similar to that of the Oroua section to the north. Thus the Pohangina section is considered to be relatively old. The normal polarity intervals could therefore represent the Olduvai or Reunion subchrons.

3.4.2 Implications

The thickness of strata considered to represent the Jaramillo Subchron at Mangatewaiiti and Mangatewainui is about 130 and 90 m, respectively. At Rewa Hill, the top of the subchron was not defined paleomagnetically, however its thickness can be estimated (ca. 50 m) by the position of the Potaka Tephra, which occurs at this boundary (Chapter 8). The Jaramillo Subchron represents the interval from 0.99 Ma to 1.07 Ma, a period of ca. 80 ka. This implies rapid average sedimentation rates of 1.6, 1.1 and 0.6 m/10^3 yr for the Mangatewaiiti, Mangatewainui and Rewa Hill sections, respectively. In the fluvial sequences, deposition is episodic and flood events can result in rapid vertical accretion. However, much of the Mangatewaiiti and Mangatewainui sections consist of fine grained lacustrine and swamp facies (Chapter 2) and thus a high constant sedimentation rate is implied. This high sedimentation rate
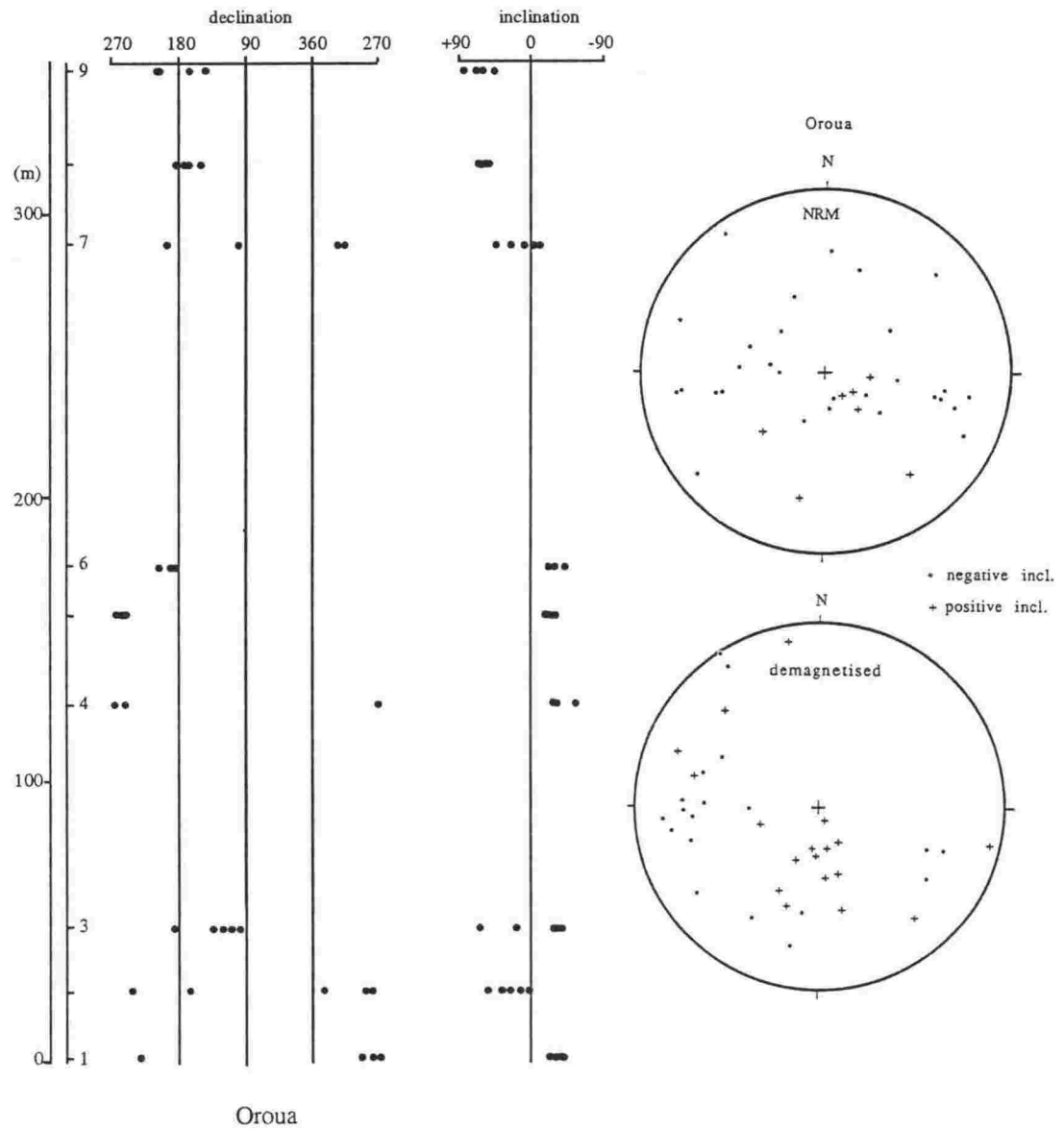
Fig. 3.10 Paleomagnetic specimen measurements for the Oroua section.
Plotted as in Fig. 3.6.
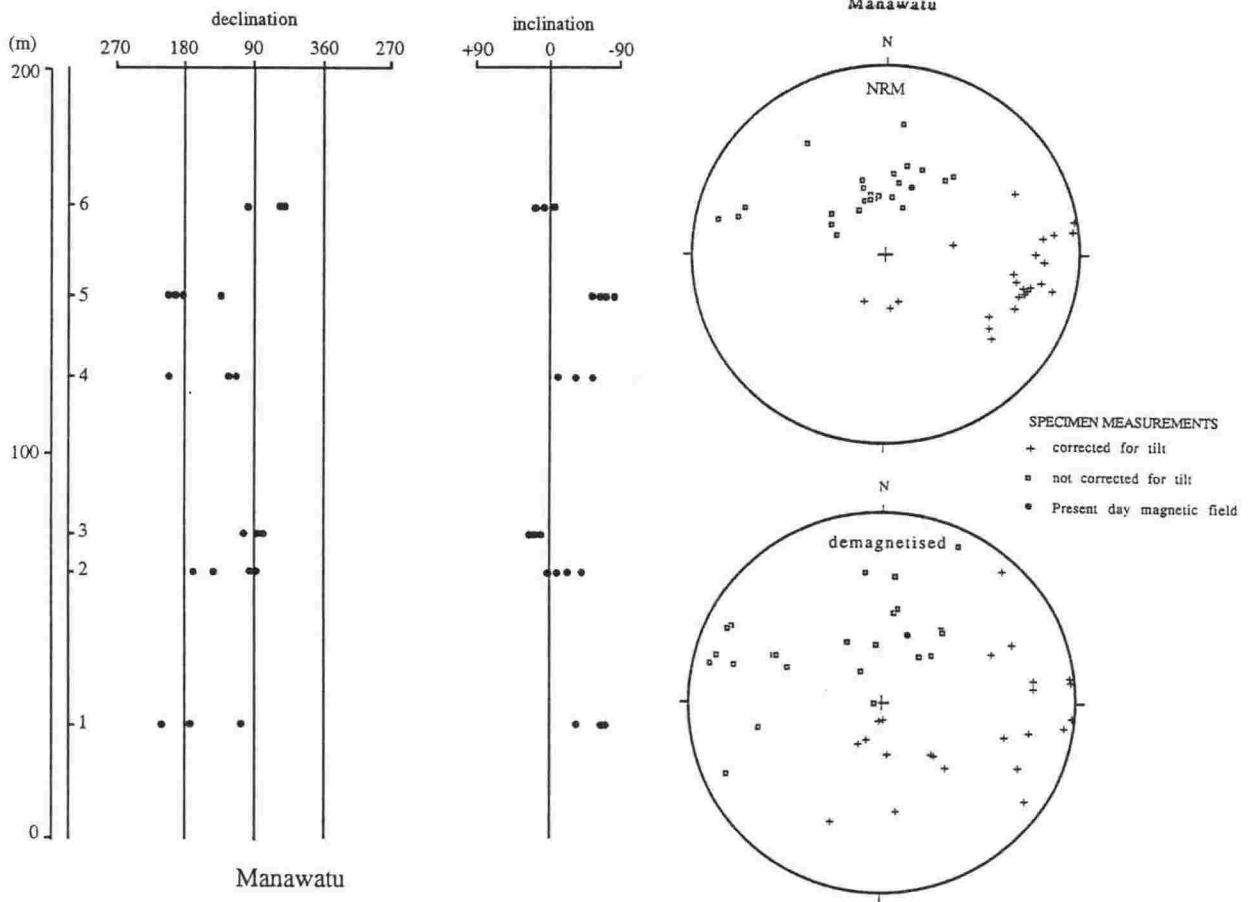
Fig. 3.11 Paleomagnetic specimen measurements for the Manawatu section.
Plotted as in Fig. 3.6.
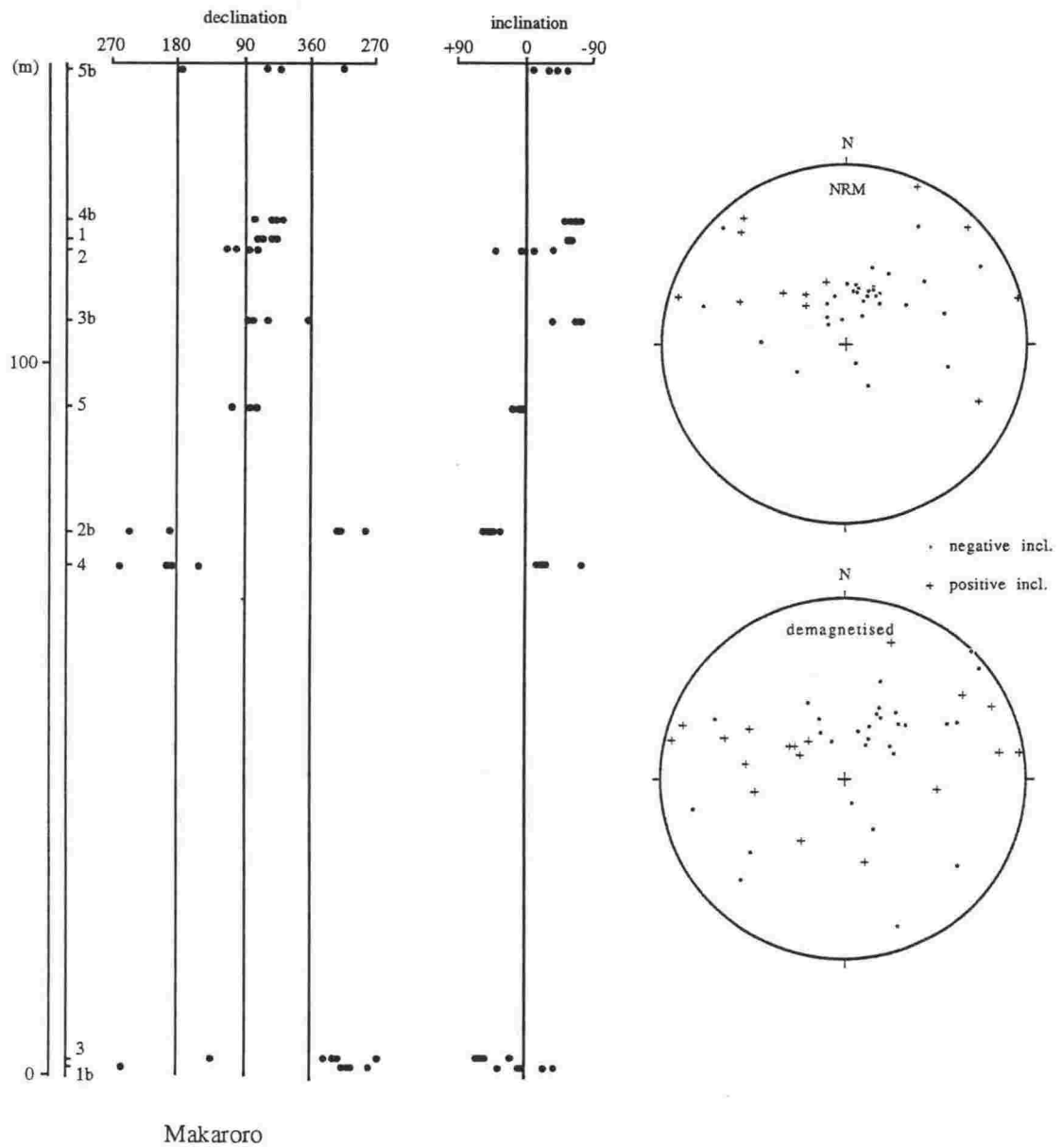
Fig. 3.12 Paleomagnetic specimen measurements for the Makaroro section.
Plotted as in Fig. 3.6.
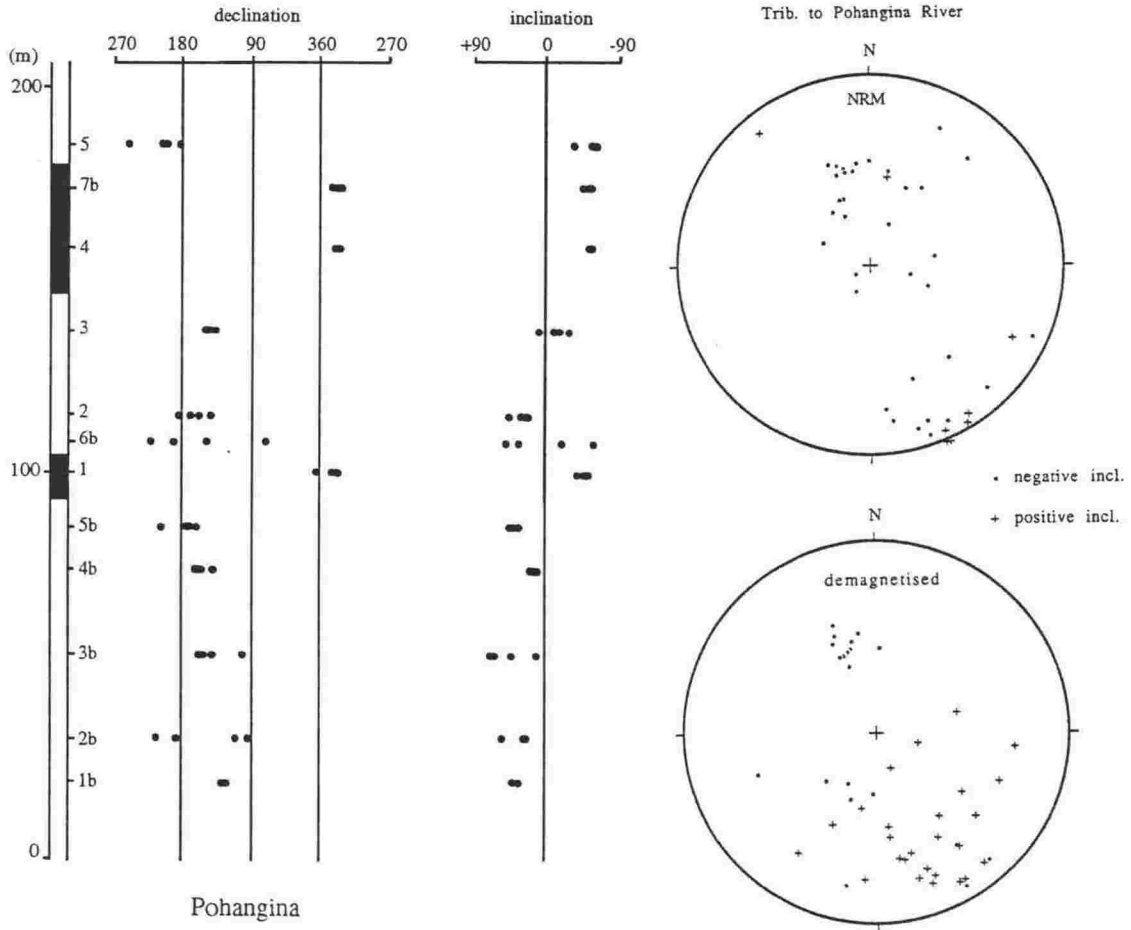
Fig. 3.13 Paleomagnetic specimen measurements for the Pohangina section.
Plotted as in Fig. 3.6.

in turn suggests rapid basin subsidence at ca. 1Ma in the East Coast and Wanganui basin regions. Kamp & Turner (1990) estimated a sedimentation rate of ca. 0.27 m/10^3 yr for the same interval at the Wanganui coast. This indicates that the sequences in the eastern Wanganui basin and East coast region are of higher resolution for the interval near the Jaramillo Subchron.

The Jaramillo Subchron occurs near the top of the Mangatarata Formation in the East Coast region and at the bottom of the Castlecliffian type section at the Wanganui coast. Therefore the subchron provides a means of direct correlation between the two regions. Also much of the Mangatarata Formation considered to be Castlecliffian by Lillie (1953) is stratigraphically older than that at the Castlecliffian type section. The sequences in the East Coast region are relatively continuous, lacking unconformities. Therefore they represent the time interval missing in the unconformity (Fleming 1953; Pillans 1992) between Castlecliffian and Nukumaruan strata at the Wanganui coast, which occurs directly beneath the Jaramillo Subchron.

3.5 CONCLUSIONS

1. Early Pleistocene sediments and tephras are characterised by two- and multi-component remanent magnetisation. The latter usually comprises of a low coercivity normal overprint, an intermediate coercivity primary magnetism, and a very high coercivity chemical overprint.

2. Due to overprinting, the polarity of most sites is inferred from specimen behaviour during demagnetisation, e.g. a directional shift from normal toward reversed, rather than a stable end point direction.

3. The Brunhes-Matuyama boundary, Jaramillo Subchron and a long interval of pre-Jaramillo Matuyama Chron are identified in Pleistocene sequences in the East Coast and Wanganui basins of New Zealand. They provide temporal constraints for the Pleistocene stratigraphy of New Zealand.

4. The Jaramillo Subchron has been recognised at the base of the Castlecliffian type section. A major interval of rhyolitic volcanism is recorded beneath the subchron, in more continuous sequences in the eastern Wanganui basin and East Coast which were previously considered to be temporally equivalent to the Castlecliffian type section.

Chapter 4
GEOCHEMISTRY OF TEPHRAS

4.1 INTRODUCTION

Commonly, volcanic glass weathers to clay in subaerial and river terrace settings over periods of 10^5 years. However, in subaqueous settings and when rapidly buried the glass phase in tephras is preserved in sediments as old as Miocene and Pliocene age in New Zealand (e.g. Nelson et al. 1986; Gosson 1986; Shane 1990). Early-middle Pleistocene tephras interbedded in fluvial and shallow marine sediments in Hawkes Bay and Wanganui Basin consist of fresh, unaltered glass shards and variable amounts of phenocrysts. Thus the tephras provide an opportunity to chemically characterise the eruptive events using a variety of techniques and materials. Such data can provide insight into volcanic source provinces and petrogenesis, as well as providing a means for the identification of individual events.

Westgate & Gorton (1981) have summarised the techniques and the potential of correlating distal silicic tephras, while Hildreth & Mahood (1986) have discussed the problems of correlating ignimbrites. In addition to stratigraphic and lithological studies, other techniques are often required to correctly identify a tephra where outcrops are sparse and many eruptive events are recorded. For tephras containing fresh, unaltered glass shards, the chemistry of the glass phase has long been a significant tool in correlation studies in North America (Smith & Westgate 1969; Sarna-Wojcicki et al. 1984; 1987; Izett et al. 1988; and many others); New Zealand (e.g. Froggatt 1983; Froggatt et al. 1986; Lowe 1988; Shane 1990; Black 1992) and elsewhere. The glass composition of a particular eruption reflects a number of factors including the original magma composition; the degree of crystallisation and crystal fractionation; the inter-reaction with other magma bodies and country rock; and the formation of physical and compositional gradients in the magma prior to eruption. As a result many tephras are chemically distinctive. Some studies have also focused on the chemistry of mineral phases for identification purposes, in particular Fe Ti-oxides (e.g. Kohn 1970; Westgate et al. 1977).

To assess the usefulness of glass and mineral phases in characterising early-middle Pleistocene tephras, electron microprobe and XRF analyses were performed. As many of the tephras were emplaced by fluvial processes, they contain detrital contaminants as well as xenocrystic and xenolithic components normally associated with explosive eruptives. Thus grain-specific techniques were used where possible.

4.2 MAJOR OXIDE GLASS COMPOSITIONS

4.2.1 Classification and types

All of the tephras examined consist predominantly of clear or milky white glass shards (>95% of the sample). Major oxide compositions were determined for 8-20 individual shards in

Table 4.1. Representative glass shard analyses of early Pleistocene tephras.

typical glasses

	305	287	196	261
SiO_2	74.62 (.30)	75.68 (.31)	76.46 (.30)	78.02 (.46)
Al_2O_3	13.51 (.14)	12.95 (.13)	12.83 (.12)	12.20 (.27)
TiO_2	0.17 (.03)	0.17 (.04)	0.16 (.05)	0.15 (.04)
FeO	2.15 (.07)	1.99 (.11)	1.52 (.10)	1.25 (.15)
MgO	0.12 (.04)	0.09 (.02)	0.12 (.03)	0.11 (.02)
CaO	1.07 (.04)	0.94 (.07)	0.94 (.05)	0.78 (.06)
Na_2O	4.57 (.09)	4.34 (.12)	4.29 (.20)	3.88 (.19)
K_2O	3.61 (.16)	3.64 (.15)	3.49 (.11)	3.45 (.18)
Cl	0.19 (.02)	0.18 (.04)	0.18 (.02)	0.16 (.02)
water	5.32 (1.40)	4.83 (1.19)	7.15 (1.15)	5.96 (1.17)
n	8	10	10	10
PI	0.85	0.85	0.84	0.83
Fe/Ca	2.01	2.12	1.62	1.60

high-Ca glasses

	315	134	301	335	148
SiO_2	75.07 (.64)	75.59 (.11)	75.72 (.33)	77.09 (.40)	78.02 (.30)
Al_2O_3	13.58 (.32)	13.94 (.07)	13.19 (.18)	12.68 (.12)	12.16 (.18)
TiO2	0.24 (.08)	0.15 (.03)	0.23 (.04)	0.15 (.06)	0.10 (.01)
FeO	1.72 (.22)	1.54 (.08)	1.68 (.13)	1.42 (.13)	1.25 (.17)
MgO	0.28 (.08)	0.33 (.08)	0.21 (.03)	0.11 (.03)	0.09 (.02)
CaO	1.54 (.10)	1.40 (.08)	1.52 (.06)	1.24 (.06)	1.27 (.02)
Na_2O	4.07 (.15)	3.93 (.10)	4.29 (.10)	3.79 (.18)	3.58 (.12)
K_2O	3.27 (.17)	2.98 (.12)	3.04 (.19)	3.34 (.18)	3.47 (.11)
Cl	0.23 (.05)	0.13 (.04)	0.20 (.03)	0.19 (.05)	0.13 (.03)
water	6.50 (1.18)	6.66 (1.22)	5.85 (1.04)	5.67 (1.08)	6.71 (2.25)
n	9	10	10	7	9
PI	0.75	0.70	0.79	0.78	0.79
Fe/Ca	1.12	1.10	1.11	1.15	0.98

high-K glasses

	172	131	291	304	190
SiO_2	74.76 (.21)	75.53 (.18)	76.62 (.16)	76.85 (.49)	77.52 (.46)
Al_2O_3	13.13 (.08)	12.76 (.11)	12.51 (.11)	12.43 (.20)	12.27 (.40)
TiO_2	0.16 (.02)	0.16 (.03)	0.23 (.03)	0.11 (.02)	0.13 (.03)
FeO	1.92 (.10)	1.80 (.08)	1.39 (.05)	1.44 (.06)	1.12 (.20)
MgO	0.11 (.02)	0.10 (.02)	0.17 (.03)	0.06 (.01)	0.11 (.01)
CaO	1.01 (.08)	0.85 (.05)	1.15 (.05)	0.70 (.05)	0.86 (.14)
Na_2O	3.73 (.15)	3.80 (.17)	3.13 (.09)	4.04 (.18)	3.64 (.12)
K_2O	4.95 (.09)	4.88 (.08)	4.59 (.12)	4.25 (.27)	4.11 (.24)
Cl	0.25 (.04)	0.14 (.03)	0.20 (.03)	0.22 (.03)	0.23 (.06)
water	5.21 (.92)	7.17 (.58)	5.15 (.68)	6.68 (1.62)	5.38 (1.71)
n	14	11	10	9	8
PI	0.88	0.91	0.81	0.90	0.85
Fe/Ca	1.90	2.12	1.21	2.06	1.30

Tephra sample numbers and locations as in Chapter 2 and Appendix 1. Analyses represent a mean and standard deviation of n shards determined by EMA. Water by difference. All Fe as FeO. PI=peralkaline index (molar Na_2O + K_2O/Al_2O_3).

each sample using an electron microprobe to test their homogeneity (Appendix 1). This discussion focuses on compositionally homogeneous tephras. Heterogeneous tephras, representing about half of the samples are discussed in Chapter 6. For homogeneous tephras the shard analyses are averaged to give a 'bulk' composition which represents the liquid phase of the magma at the time of eruption. This analytical approach avoids the possible compositional variation in bulk samples caused by crystal concentration or depletion due to magmatic and eruption processes, and subsequent eolian and subaqueous fractionation during emplacement of the tephras.

The mean glass compositions of the tephras are rhyolitic with SiO_2 contents in the range 72-78.5 wt. %, after recalculation to 100% on a volatile-free basis. All of the tephras classify as calc-alkaline rhyolites using the Total-Alkali-Silica scheme of La Bas et al. (1986). These glass compositions are consistent with the mafic mineral assemblages of the tephras (hypersthene, hornblende, biotite and augite) which are typical of rhyolites from the TVZ in North Island (Ewart 1966; Froggatt 1982). Representative early and middle Pleistocene tephra compositions are shown in Table 4.1. On variation diagrams (e.g. Fig 4.1a) the oxides of Al, Ti, Fe, Mg and Ca display a linear trend of decreasing abundance with increasing SiO_2 content in the glass. Na_2O shows less variation but is generally depleted in more silicic glasses, while Cl is generally invariant. K_2O displays incompatible trends, increasing with increasing SiO_2 contents.

Most tephras have Na/K>1, Fe/Ca>1.6 (mostly ca. 2) and Peralkaline Indices (PI) of ca. 0.84-0.87. These are referred to here as the 'typical group' as they are the most common. In addition, two separate compositional groups can be recognised on the basis of major oxides. Some tephras form a high-K trend on variation diagrams (Fig. 4.1) with K_2O contents in the range 3.8-5 wt. %. The highest K_2O contents occur in the less silicic glasses, which is the opposite trend to that observed in the 'typical glasses'. The high-K group of tephras have Na/K<1 and are generally more peralkaline (PI 0.84-0.91). Their Fe/Ca ratios and range in silica content are similar to that of 'typical glasses' (Table 4.1). These high-K tephras contain the mineral phase biotite, unlike most tephras, but otherwise show no petrographic or mineral chemistry differences. The high K_2O content of the glasses and its inverse trend with SiO_2 presumably reflects the crystallisation of biotite. A high-Ca group is also evident amongst the tephras examined (Fig 4.1). These tephras are characterised by Fe/Ca ratios close to unity, as opposed to 1.6-2.0 for 'typical glasses'. CaO contents for this group are >1.2 wt. %, K_2O contents are generally low, and Na/K ratios are greater than one (Table 4.1). Their PIs are generally the lowest (0.70-0.80) of the tephras examined. In silica content and petrography the high-Ca group show no differences from other tephras.

In the stratigraphic sections examined, there are no compositional trends in tephra composition in either space or time. For example, high-Ca tephras are found interbedded with tephras of 'typical' composition in the Oroua section (Fig. 4.2) and other sections.
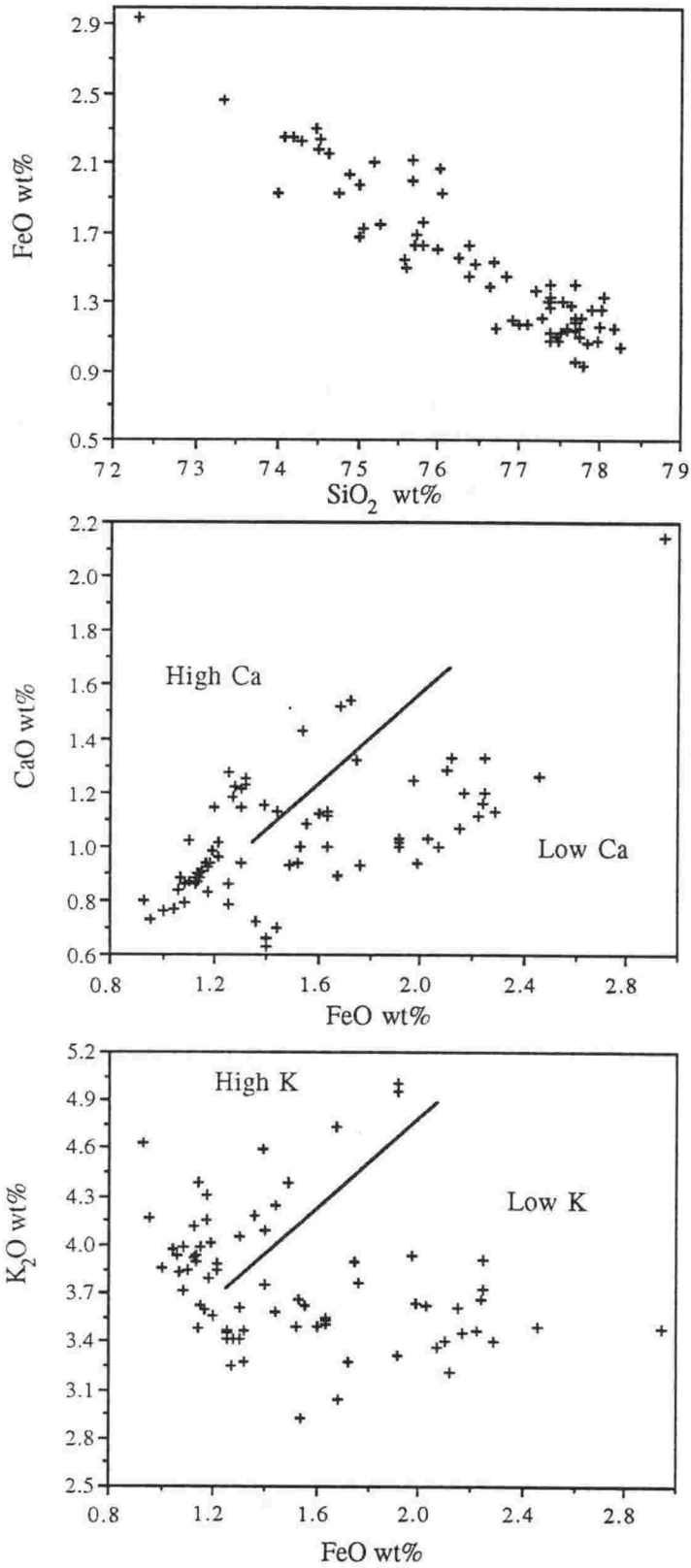
Fig. 4.1 Mean EMA composition of early Pleistocene tephras showing compositional trends.
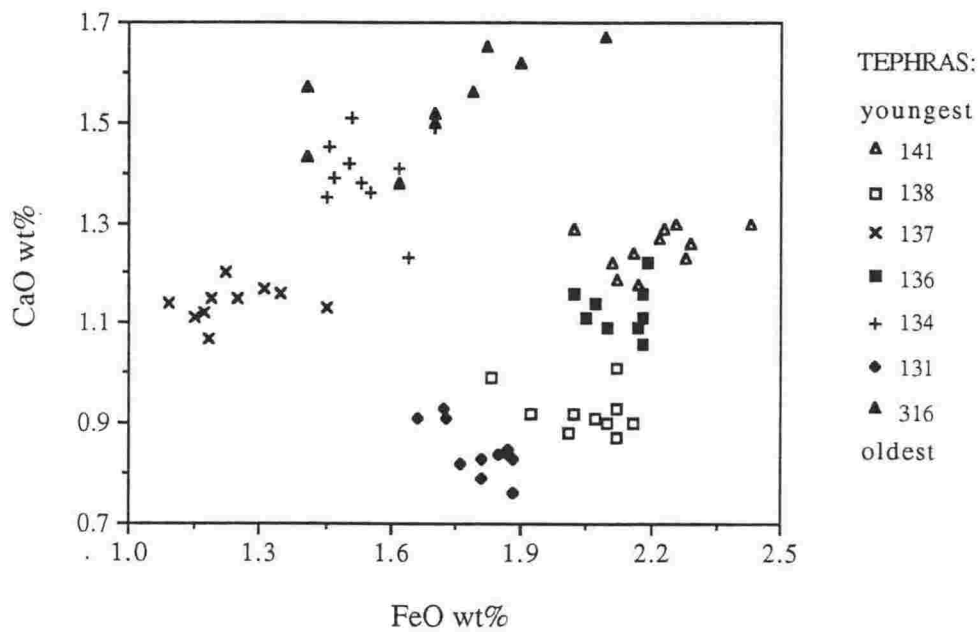
Fig. 4.2 Individual glass shard analyses of tephras from the Oroua section. The 7 tephras define two different compositional trends, but show no temporal trends.
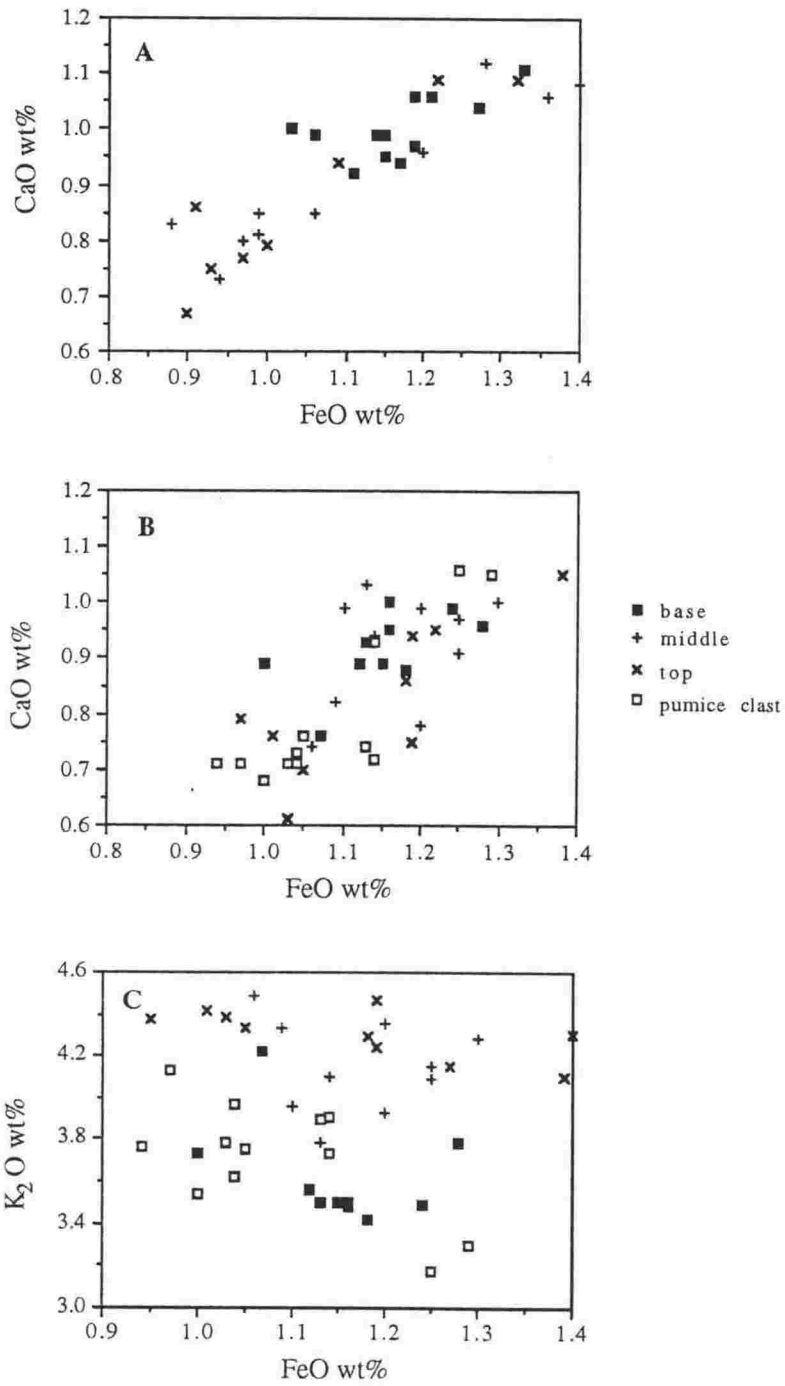
Fig. 4.3 Individual glass shard analyses of the Potaka ignimbrite showing a compositional trend, possibly due to zonation. A and C Cape Kidnappers exposure, B Mangaonuku stream exposure.

4.2.2 Characteristics and recognition of individual eruptive events

The compositional variation within a single eruptive event or tephra is generally minor. Variation in FeO of 0.15 wt. %, CaO of <0.10 wt. % and K_2O of <0.20 wt. % is typical for glass in most of the tephras examined, as determined by averaging individual shard analyses. A similar variability was found by Froggatt (1982; 1983) for late Pleistocene tephras from the TVZ. This degree of variation is comparable to that found in multiple analyses of glass standards which suggests it is due mainly to instrumental error.

Most stratigraphically different tephras display greater differences in their major oxide chemistry (when compared to each other) than would be explained by analytical error. Mean oxide compositions for different tephras fall in the range of 0.8-2.4 wt. % for FeO, 0.6-1.4 wt. % for CaO and 2.9-5.0 wt. % for K_2O, and thus provide a chemical basis for identification. The other oxides may also show significant differences in abundance, except Cl (Table 4.1). Within short stratigraphic intervals, for example the upper non-marine part of the Oroua section (Fig 4.2), the tephras can be recognised on the basis of just two oxides. However, in longer sequences such as Mangatewaiiti and Mangatewainui, the same glass composition may be found more than once, at different stratigraphic levels. Some tephras can be recognised in stratigraphic relation to other distinctive tephras, even if their own composition is not unique. The key to positive correlation in sequences of abundant tephras is the identification of two or more chemically distinctive tephras in the same stratigraphic order, such as the Potaka and Kaukatea Tephras in several sections (Chapter 8).

Of the tephras which have not been contaminated by post-eruption sedimentary mixing, there is little evidence of derivation from chemically zoned magma chambers. The same has been found for the latest Pleistocene eruptives (<0.50 ka) from the TVZ (Froggatt 1983; Dunbar et al. 1989b). Hildreth (1981) notes that zonation in large rhyolitic eruptives is common, if not the norm. Ubiquitous post-eruption welding of major Pleistocene ignimbrite sheets from the TVZ precludes the complete chemical characterisation of all units (section 4.2.3). Analyses of unwelded bases of large early Pleistocene ignimbrites such as Ongatiti and Ahuroa in the King Country (272 and 277 in Appendix 1) reveals chemical homogeneity, as has been found for younger ignimbrite sheets (Froggatt 1982). However, Hildreth & Mahood (1986) suggest sampling of such deposits and of distal deposits may characterise only a small part of the total magma body, and thus may not be representative.

The unwelded ignimbrite associated with the Potaka eruption (Chapter 8) provides another opportunity to sample both vertically and laterally through a large New Zealand ignimbrite. Analyses of glass shards do reveal a rather narrow compositional range which form linear trends on variation diagrams (Fig 4.3). This variation is however greater than that found in most early and middle Pleistocene tephras (e.g. Fig. 4.2). Matrix samples collected at the base of the flow unit at both Cape Kidnappers and Mangaonuku stream, are more FeO and CaO

rich than samples collected higher in the unit. Samples from the middle and upper parts are generally more K$_2$O rich than the base. Pumice clasts greater than 1 cm are rare in the ignimbrite. Those collected from near the top of the flow in the Mangaonuku site are generally more FeO and CaO deleted. However, a range of compositions are found at each horizon, suggesting mixing of any chemical stratification during emplacement. The compositional differences are accompanied with variation of ca. 1 wt. % SiO$_2$, suggesting the zonation is very minor.

4.2.3 Major oxide glass chemistry of early Pleistocene welded ignimbrites

In contrast to the tephras in distal settings discussed above, early Pleistocene proximal ignimbrites in the TVZ are nearly ubiquitously welded and have undergone vapour-phase alteration. As unwelded bases are generally difficult to find, pumice clasts were sampled from several moderately welded ignimbrites in the Taupo-King Country area in an attempt to chemically characterise them for correlation purposes. Ignimbrite A, Ongatiti, Ahuroa, Rocky Hill and Rangitaiki ignimbrites (Wilson 1986; Pringle et al. 1992) were examined. Typical EMA analyses are shown in Table 4.2. Compared to glasses in distal tephras (e.g. Appendix 1), these pumices are highly depleted in FeO (0.2-0.9 wt %, typically 0.3 wt %), Na$_2$O (2.5-3.6 wt %) and Cl, and contain variable amounts of K$_2$O. Others display very high K$_2$O contents (>5 wt %). These chemical features are typical of post depositional alteration due to vapour phase transport of mobile elements and ion-exchange during devitrification (e.g. Scott 1971; Hildreth & Mahood 1985). This alteration precludes the use of glass or bulk major oxide analyses of pumice clasts from many units for correlation or petrogenesis purposes.

Table 4.2 Six representative pumice clast glass compositions determined by EMA from welded ignimbrites in the TVZ. Analytical methods as in Table 4.1.

ignimbrite	SiO$_2$	Al$_2$O	TiO$_2$	FeO	MgO	CaO	Na$_2$O	K$_2$O	Cl	H$_2$O
Rangitaiki	77.98	12.21	0.22	0.82	0.06	0.67	2.64	5.24	0.16	2.49
Rocky Hill	78.69	12.60	0.16	0.29	0.00	1.01	3.53	3.63	0.10	7.38
	79.37	12.21	0.07	0.37	0.01	0.62	3.61	3.65	0.09	3.94
	79.29	12.14	0.12	0.27	0.00	0.88	3.61	3.59	0.10	4.63
Ongatiti	78.36	12.22	0.08	0.44	0.00	0.66	2.73	5.47	0.01	4.52
	77.80	12.50	0.06	0.92	0.00	0.66	2.68	5.36	0.03	5.38

4.3 TRACE ELEMENT GLASS CHEMISTRY

Abundances of 19 trace elements were determined by XRF on glass from tephras deemed to be homogeneous by electron microprobe analyses (Appendix 2). Of the elements
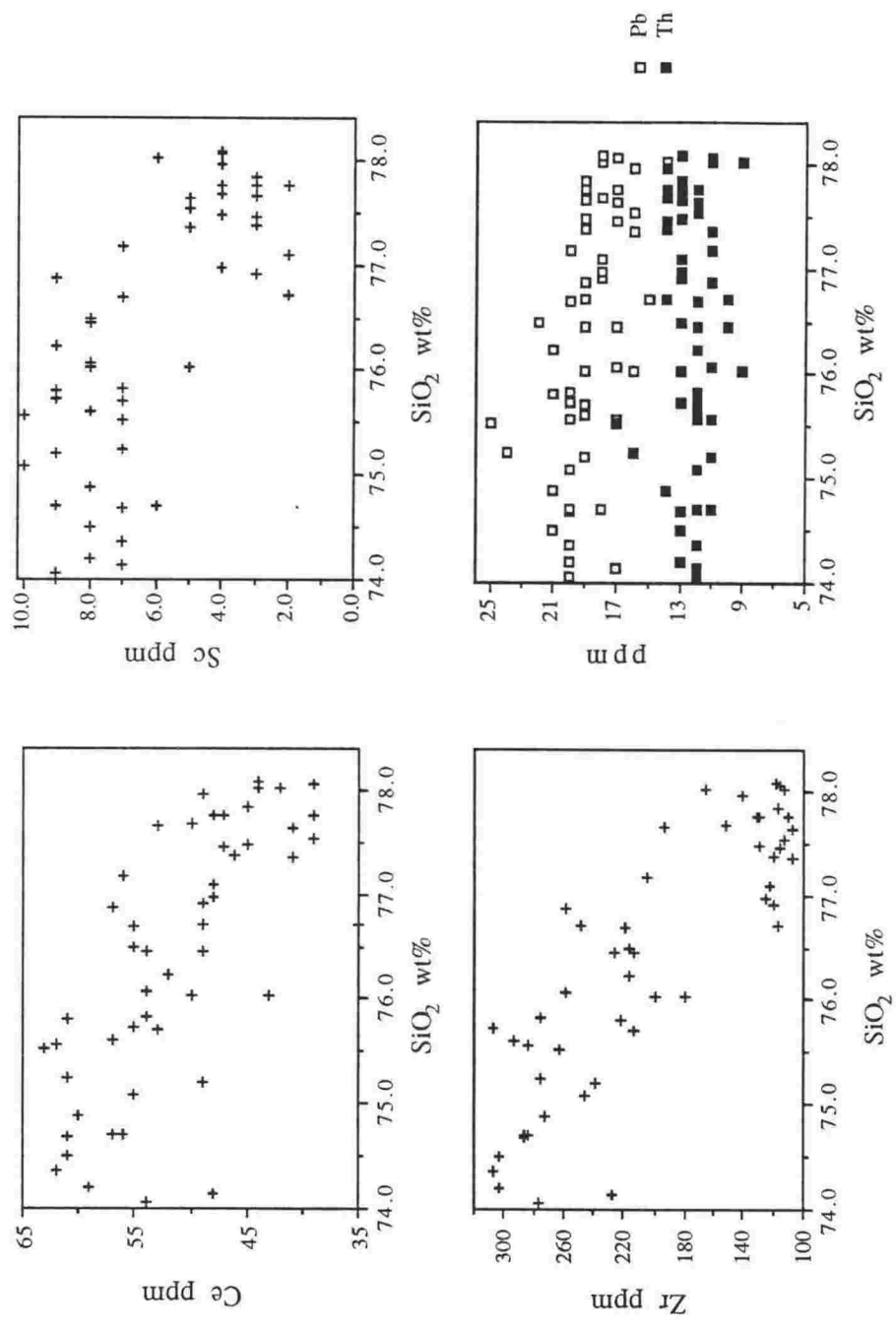
Fig. 4.4 Trace element composition of tephras determined by XRF, plotted against their mean SiO2 content determined by EMA.

determined, V, Cr, Ni and Cu were highly variable and in most cases close to or below detection limit. The most abundant trace elements in the tephras (>100 ppm) are Ba, Zr, Sr and Rb, with Ba (>500 ppm) by far the most abundant. The remaining elements are present in small quantities (<50 ppm). Most trace elements (i.e. La, Ce, Zn, Zr, Nb, Sc, Sr, Ga and Y) form broadly linear inverse trends when plotted against SiO_2 (Fig. 4.4), similar to that shown by most oxides. These trends, which are shown by both compatible and incompatible elements, may be due to the constant sum effect. Also, in highly silicic glasses elements such as Zr, La and Ce can be compatible, being fractionated into zircon. The elements Rb, Pb, Th, and U are generally invariant within the compositional range of tephras examined (Fig. 4.4).

To test the potential of trace elements in characterising individual eruptive events, known stratigraphic horizons were sampled from a wide aerial distribution. Six widespread tephras spanning a long time interval were selected: Taupo Pumice (ca. 1.8 ka), Kawakawa Tephra (ca. 22 ka), Rangitawa Tephra (0.33 Ma), Kaukatea tephra (1.0 Ma), Potaka tephra (1.0 Ma) and Pakihikura tephra (ca. 1.6 Ma). This allowed a range of factors to be assessed, including weathering due to time and local climate; lateral variation as a function of distance to source; and possible differences between flow phases and fallout phases. Each eruptive event could be distinguished from the others by a number of elements. Multiple analyses generally formed a tight cluster on variation diagrams (Fig. 4.5). Elements in high abundance (Zr, Y, Rb, Sr and Ba) are particularly useful in distinguishing between the eruptives. The tight clustering of multiple analyses suggest little alteration due to weathering has occurred and that these eruptives are generally homogeneous in trace element composition. The use of major and trace element compositions in distinguishing between eruptions is further examined in Chapter 5.

4.4 PHENOCRYST CHEMISTRY

4.4.1 Plagioclase

The most ubiquitous phenocryst phase in the early Pleistocene tephras is feldspar, representing 60-95% of the total mineral fraction. Nearly all feldspars are plagioclase with compositions in the range An2-73 and Or<10 (Fig. 4.6). Most classify as andesine or labradorite. Many individual plagioclase crystals are normally zoned with core-rim differences in An up to 15%. Core compositions within a tephra can show variation in An up to 40%. The more calcic labradorite and bytownite crystals found in some tephras are usually associated with intermediate whole rock compositions. Thus their presence in rhyolitic tephras could be due to detrital or xenocrystic contamination (Chapter 6; Froggatt & Rogers 1990).
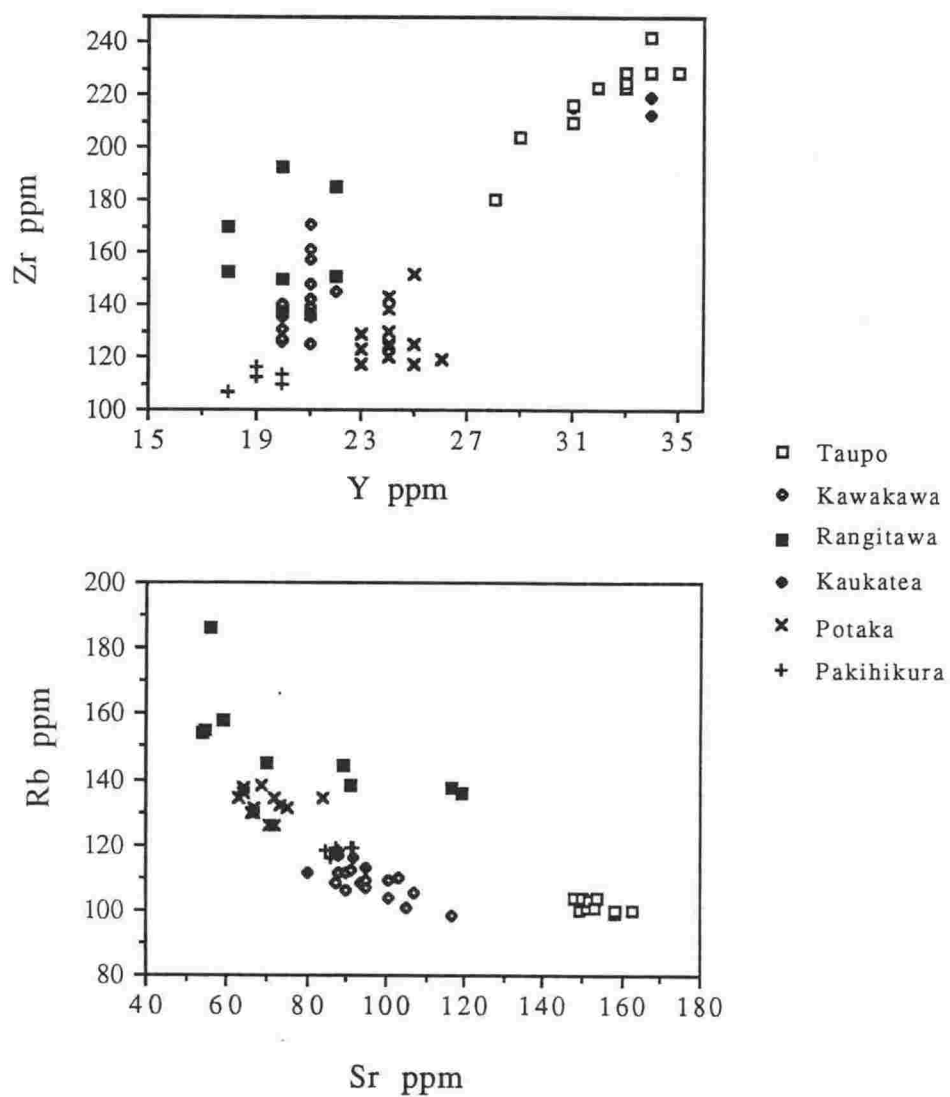
Fig. 4.5 Trace element composition of samples of six widespread tephras from the TVZ.
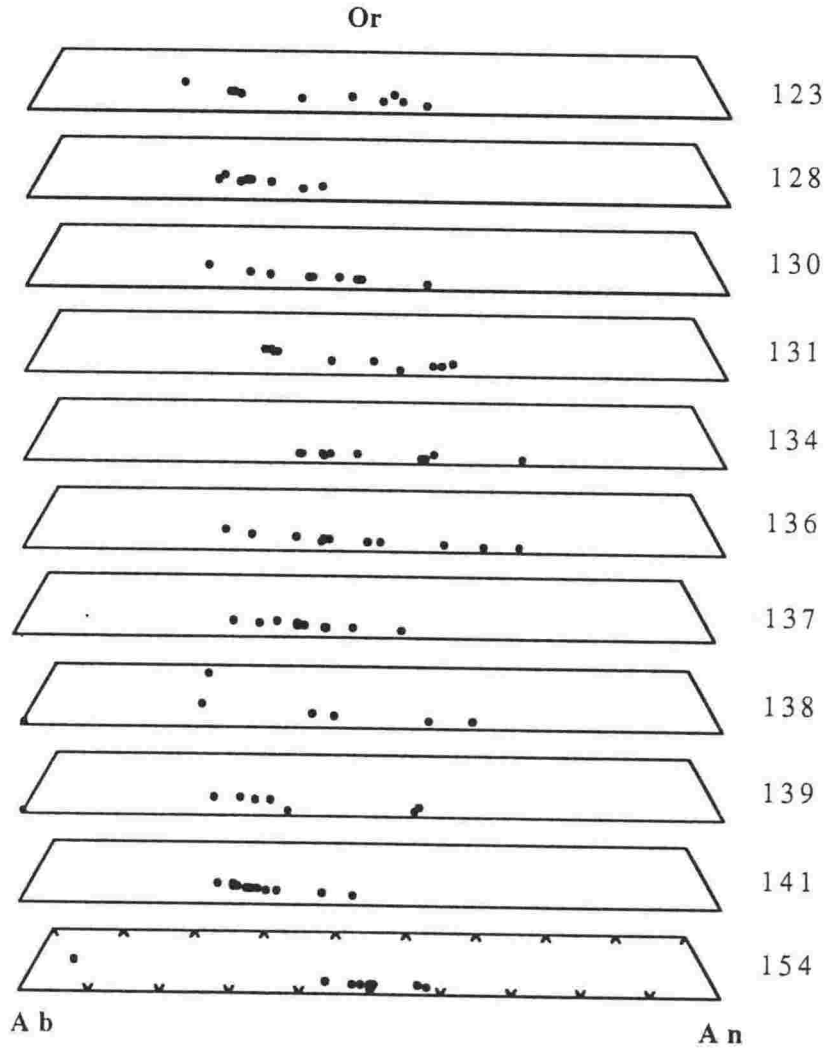
Fig. 4.6 Core compositions of feldspar crystals in early Pleistocene tephras plotted on part of a Or-Ab-An diagram.
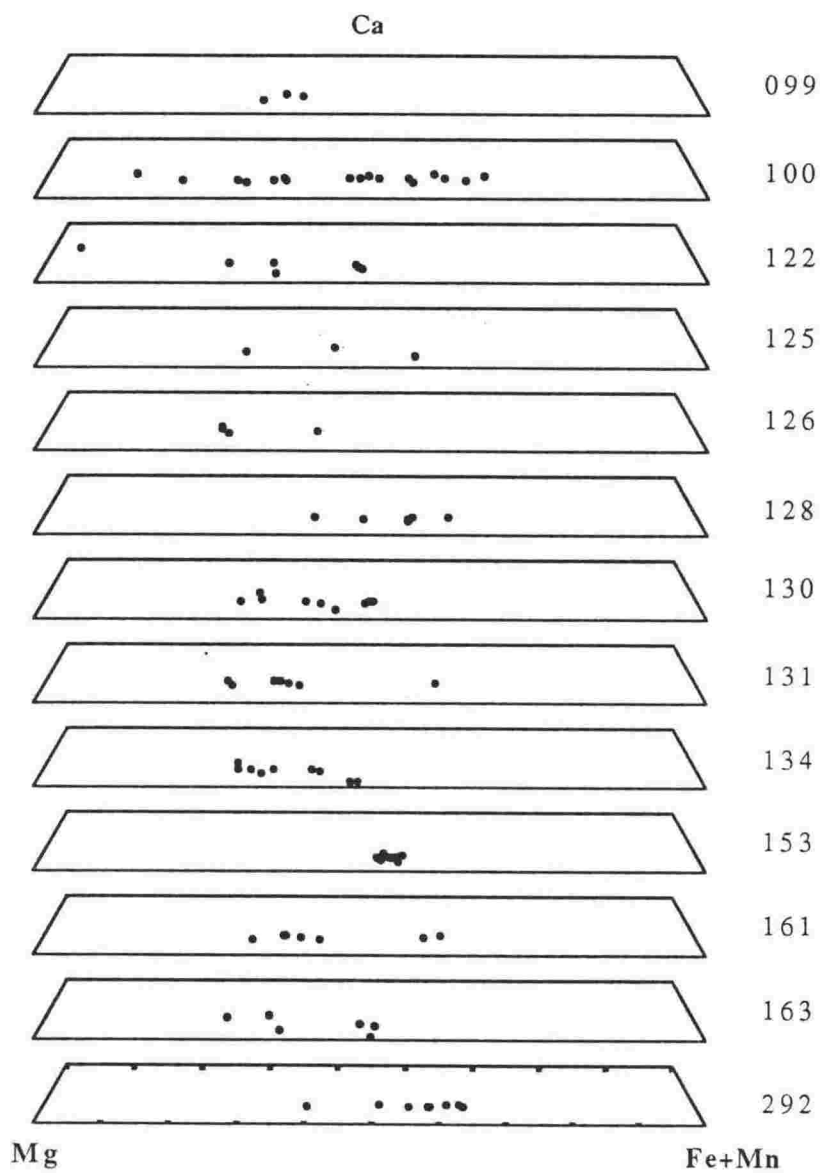
Fig. 4.7 Core compositions of orthopyroxene crystals in early Pleistocene tephras plotted on part of a Ca-Mg-Fe+Mn ternary diagram.

4.4.2 Pyroxene

Orthopyroxene is the most common ferromagnesian phenocryst phase in the early Pleistocene tephras. Microprobe analysis reveals a wide range of crystal compositions (En33-95) (Fig 4.7). Chemical zonation was not detected. Within a single tephra, En compositions may vary up to 60% and no relationship to glass compositions is evident. Most orthopyroxenes classify as hypersthene or ferrohypersthene, although some tephras also contain a significant group classifying as bronzite. This latter group is atypical of TVZ rhyolites and could be due to contamination from andesitic eruptives (Froggatt & Solloway 1986; Froggatt & Rogers 1990). The pyroxene compositional variation within a single tephra is greater than that between different tephras (Fig. 4.7) and are thus of little value in distinguishing individual eruptive events. The rarer clinopyroxene crystals in the tephras are unzoned augites which display a relatively narrow compositional range (Chapter 6).

4.4.3 Amphiboles

Amphiboles are the second most abundant ferromagnesian mineral phase in the tephras. Optically, all of the crystals observed are hornblende. This is confirmed by microprobe analysis (Fig. 4.8). Compositionally they classify as magnesio- and ferro-hornblendes and show no sign of zonation. The hornblendes show little chemical variation both within and between tephras. All are comparable to those found in other rhyolitic tephras (Froggatt 1982; Froggatt & Rogers 1990).

4.4.4 FeTi-oxides

Several workers have shown the potential of FeTi-oxides for correlating tephras and identifying source regions using both major oxides and trace elements (Kohn 1970; 1979; Lowe 1988). FeTi-oxides also provide insight to the chemical and physical heterogeneity of magma chambers (e.g. Hildreth 1981). These mineral phases are less common or absent in the early Pleistocene tephras examined here. Their absence is likely to be due to eolian and subsequent subaqueous sorting during transport.

In addition to FeO and TiO_2, which account for >90 wt. %, all of the crystals contain (in commonly decreasing order): Al_2O_3, MnO, MgO and SiO_2 in major oxide abundances (Appendix 3). The elements Zn, Cr, V and Co occur in trace amounts which are often at or below detection limit of the microprobe. These elements were not routinely analysed for. Nearly all FeTi-oxides are spinel phase titanomagnetites with ulvospinel in the range 25-53 mol %. A similar compositional range occurs in late Pleistocene rhyolitic tephras from the TVZ
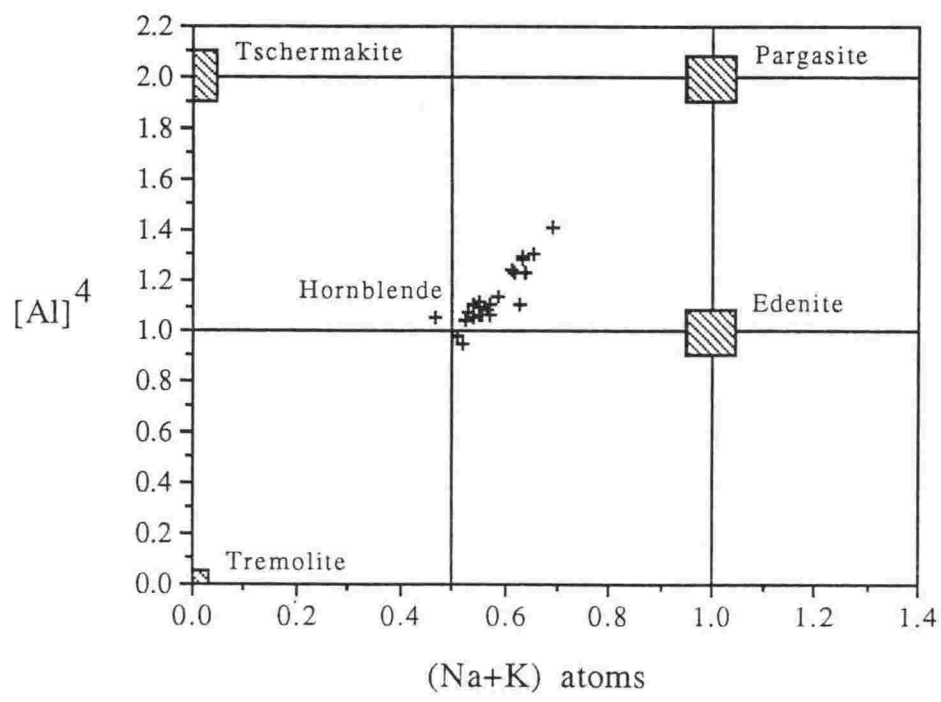
Fig. 4.8 Composition of hornblende crystals in early Pleistocene tephras.

(Froggatt 1982). Ilmenites were only encountered very rarely and thus were not characterised sufficiently for discussion.

Unlike the other phenocryst phases, the FeTi-oxide compositions are closely related to the coexisting glass phase in the tephras examined. The ulvospinel content shows a linear inverse trend with SiO_2 content in the glass (Fig. 4.9), while the total Fe content shows the opposite trend. Glasses high in FeO are accompanied with FeTi-oxides low in FeO, while glasses high in TiO_2 and MgO coexist with FeTi-oxides high in these elements (Fig. 4.9). Similar trends have been found by Froggatt (1982) and confirms the FeTi-oxides are co-magmatic rather than detrital. The compositional range of FeTi-oxides within individual tephras are generally narrow (Fig. 4.10; Appendix 3). This homogeneity is consistent with that of the co-existing glass and indicate homogeneous source magma bodies. Some tephras do however contain a few crystals which differ in composition to the main compositional group (Fig. 4.10). These could represent detrital or xenocrystic contaminants (e.g. Kohn 1979).

Most of the variation in the FeTi-oxides between different tephras is shown in the FeO and TiO_2 contents, which are often sufficient to distinguish different eruptive events (Fig. 4.10). However, the other elements such as Al_2O_3 and MnO, also display variation between tephras.

4.5 IMPLICATIONS FOR VOLCANIC SOURCE(S)

The volcanic source regions for the distal early Pleistocene tephras in the Wanganui and Hawkes Bay regions are uncertain. The sparse tephra exposures do not allow the construction of isopach maps which could shed light on vent locations. Similarly the tephra grain sizes is controlled by depositional processes, and show no systematic geographic trends. Chemically and mineralogically, the early Pleistocene tephras are similar to those of the latest Pleistocene and Holocene of the TVZ, in particular the Taupo and Okataina Volcanic Centres (Froggatt & Lowe 1990). As the early Pleistocene tephras are in the age range of ca. 2.0-0.5 Ma, the most likely source region in the TVZ is the Mangakino Volcanic Centre, which is known to have been active during this interval (Wilson et al. 1984; Wilson 1986; Pringle et al. 1992). The late stage of rhyolitic volcanism in the now extinct Coromandel Volcanic Zone (CVZ) also partly overlaps this time interval (Skinner 1986). There is no fundamental difference in the glass chemistry and mineralogy of eruptives known or assumed to have been derived from these two volcanic zones (Nelson et al. 1985; Gosson 1986; Shane 1989; Briggs & Fulton 1991), thus they cannot be distinguished on a compositional basis.

The precise correlation of the distal tephras to the large Mangakino-derived ignimbrite sheets in the King Country is hindered by widespread post-emplacement welding and vapour-phase alteration of the latter. Such alteration is known to change the original chemistry of the glass phase (e.g. Hildreth & Mahood 1985). Attempts to characterise glass in pumice clasts
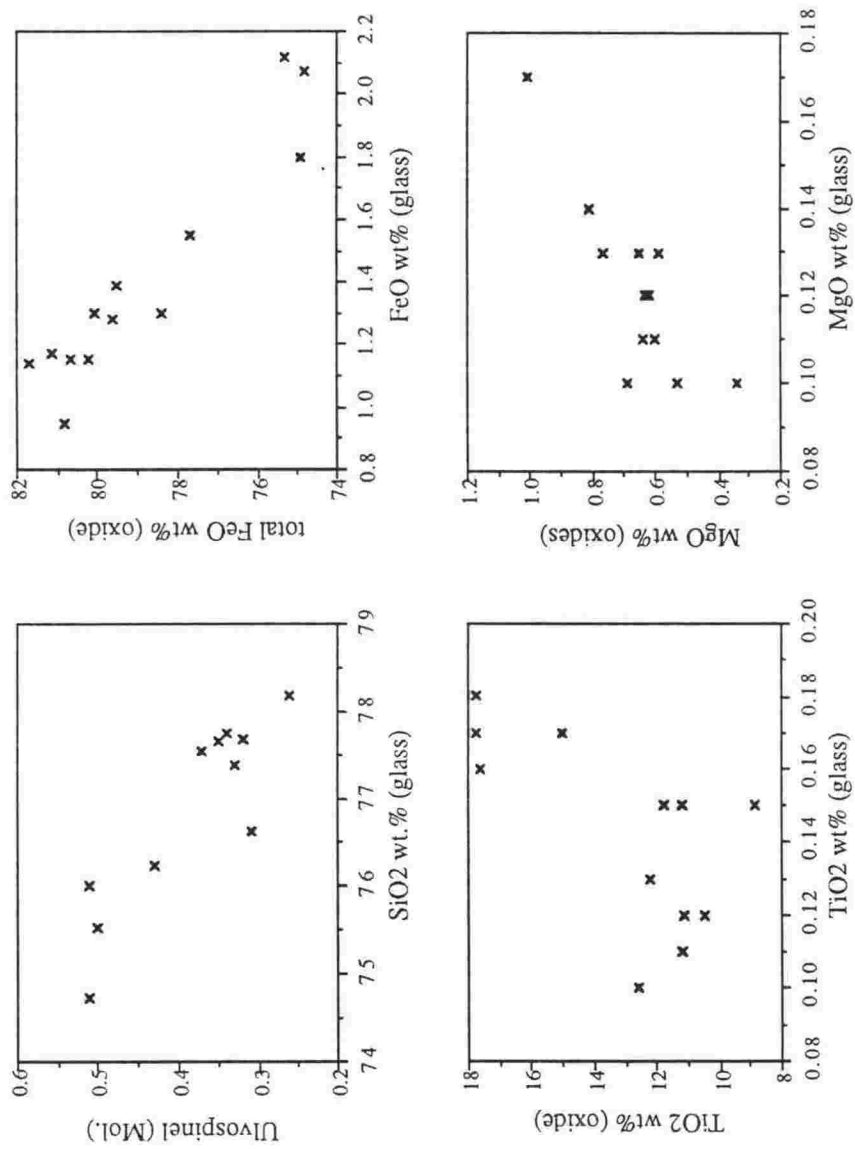
Fig. 4.9 Mean composition of FeTi-oxides plotted against the mean composition of co-existing glass in the tephra.
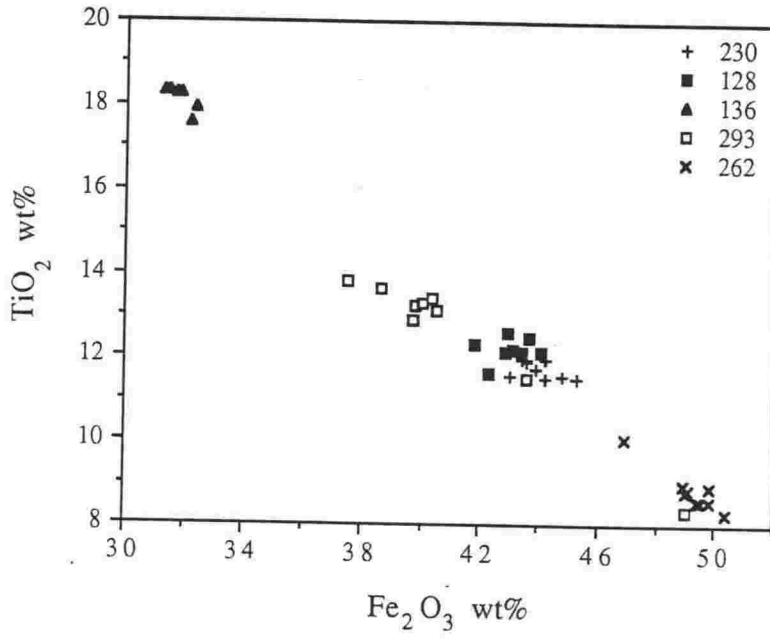
Fig. 4.10 FeTi-oxide compositions of 5 different tephras showing their potential for discrimination. Tephras 293 and 262 contain crystals that plot away from the main group and may be contaminants.

from welded ignimbrites in this study has resulted in analyses that are variable with very low FeO (<0.4 wt. %) and Na_2O (<2.0 wt. %) contents, and high K_2O (>5.0 wt. %) content (Table 4.2). This is typical of depletion and enrichment from vapour-phase alteration, and confirms the pervasive nature of this alteration.

The best eruptive record for the early Pleistocene interval is contained in the distal tephra sequences where the stratigraphic order is clear and the glass and mineral components are unaltered. The glass compositions from the distal tephras reveal several major affinities or groups, including a high-K group and a high-Ca group. The groups form diverging trends on variation diagrams (Fig. 4.1, 4.2). Tephras of different chemical affinities are often interpreted or shown to be sourced from different volcanic provinces (e.g. Izett 1981; Sarna-Wojcicki et al. 1984). Products of explosive volcanism in the last 22 ka in New Zealand can be grouped by their chemical affinities to different source regions (Froggatt 1982; Lowe 1988; Stokes & Lowe 1988; Stokes et al. 1992). By analogy, the compositional groups evident in the early Pleistocene tephras may also represent different source volcanoes. Such volcanoes may have been closely spaced within the Mangakino volcanic centre or separated, but now deeply buried by younger eruptives. These source volcanoes must have been active contemporaneously as tephras of different groups are interbedded in the same sequence (e.g. Fig. 4.2). No compositional trends, or appearances or disappearances of chemical types as a function of time are evident in the sequences examined. Thus as many as 3 different eruptive sources (representing the 3 major groups in Table 4.1) may have been active during the interval 2.0-0.5 Ma. This is not surprising as at least two major calderas (Taupo and Okataina) have been active in the last 50 ka (e.g. Froggatt & Lowe 1990).

4.6 CONCLUSIONS

1. Major and trace element compositions of glass in the tephras define linear trends on variation diagrams suggesting they are related by similar petrogenetic processes. The tephra compositions define diverging trends on variation diagrams allowing them to be subdivided into groups, including high-K glasses and high-Ca glasses. These groups may represent different volcanic provinces which were contemporaneously active during the early-middle Pleistocene.

2. Tephras in short stratigraphic intervals can be distinguished on the basis of their major oxide compositions, in some cases by as few as two oxides, e.g. FeO and CaO.

3. Trace element compositions also provide a means of distinguishing between tephras, if the glass is chemically homogeneous. The high abundance elements Zr, Ba, Sr and Rb are particularly distinctive.

4. Felsic and ferromagnesian phenocrysts display a wide range of compositions which do not serve to distinguish different eruptive events. However, they can provide an indication of contamination in a tephra by basic and intermediate volcanics.

5. FeTi-oxide major element compositions are closely related to the coexisting glass compositions in the tephras and thus have the potential for tephra correlation purposes.

6. Both glass and FeTi-oxide compositions suggest most the eruptives examined are homogeneous and provide no evidence for intensely zoned magma chambers. However a limited compositional zonation is found in the widespread Potaka Tephra.

Chapter 5
TEPHRA CORRELATION TECHNIQUES USING GEOCHEMICAL DATA

5.1 INTRODUCTION

With the advent of rapid analytical techniques, geochemical data have become increasingly important for tephra correlation studies. Early studies relied heavily on binary and ternary variation diagrams to display differences between tephras (e.g. Smith & Westgate 1969, Westgate & Gorton 1981), in particular the Fe-Ca-K ternary plot or a similar plot using an *ad hoc* selection of trace elements or REE. These plots proved useful for separating tephras from different source volcanoes or provinces. A few early studies employed numerical methods of comparison including coefficients based on ratios of element concentrations for pairs of samples and discriminant function analyses (Borchardt et al. 1971; Smith & Nash 1976). However, the widespread use of rigorous statistical criteria has developed slowly (Stokes et al.1992). As a result various criteria and different *ad hoc* selections of elements have been used in tephra correlations studies.

This chapter examines the different techniques commonly employed in tephra correlation studies using geochemical data and then assesses the relative value of major and trace element data for correlating tephras from the TVZ and western United States.

5.2 CLOSED DATASETS AND THE EFFECT ON COMPOSITIONAL TRENDS

In characterising volcanic rocks or glasses, geochemical data are thought to reflect petrogenetic processes which cause chemical trends or differences in suites of samples. However, most compositional data is expressed as % or ppm, and thus sum to a constant value (e.g. 100). This places a constraint on the statistical meaning of the data and the dataset is said to be closed (see Rock (1989), Woronow (1991) and Rollinson (1992) for a discussion of related problems). As a result elements with large absolute variance (e.g. SiO_2) will control many of the other elements (variables) by reducing the 'space' remaining for them with increasing abundance. This results in negative linear trends in binary variation diagrams: a feature seen in most of the oxides and trace elements in early Pleistocene tephras (see Chapter 4). On ternary diagrams, the dataset is doubly closed as the 3 components are further normalised to each other. Due to closure, each element does not represent an independent variable solely controlled by petrogenetic processes, and caution is required in deciding which variables are contributing to similarities or differences between samples.

In multi-variate analysis, the effects of closure can be minimised by a log-ratio transformation (e.g. Rock 1989; Woronow 1991) of the compositional data. This is further discussed below.

A

B

Legend:
- ▲ Taupo
- □ Kawakawa
- + Rangitawa
- △ Kaukatea
- ■ Potaka
- ✖ Pakihikura
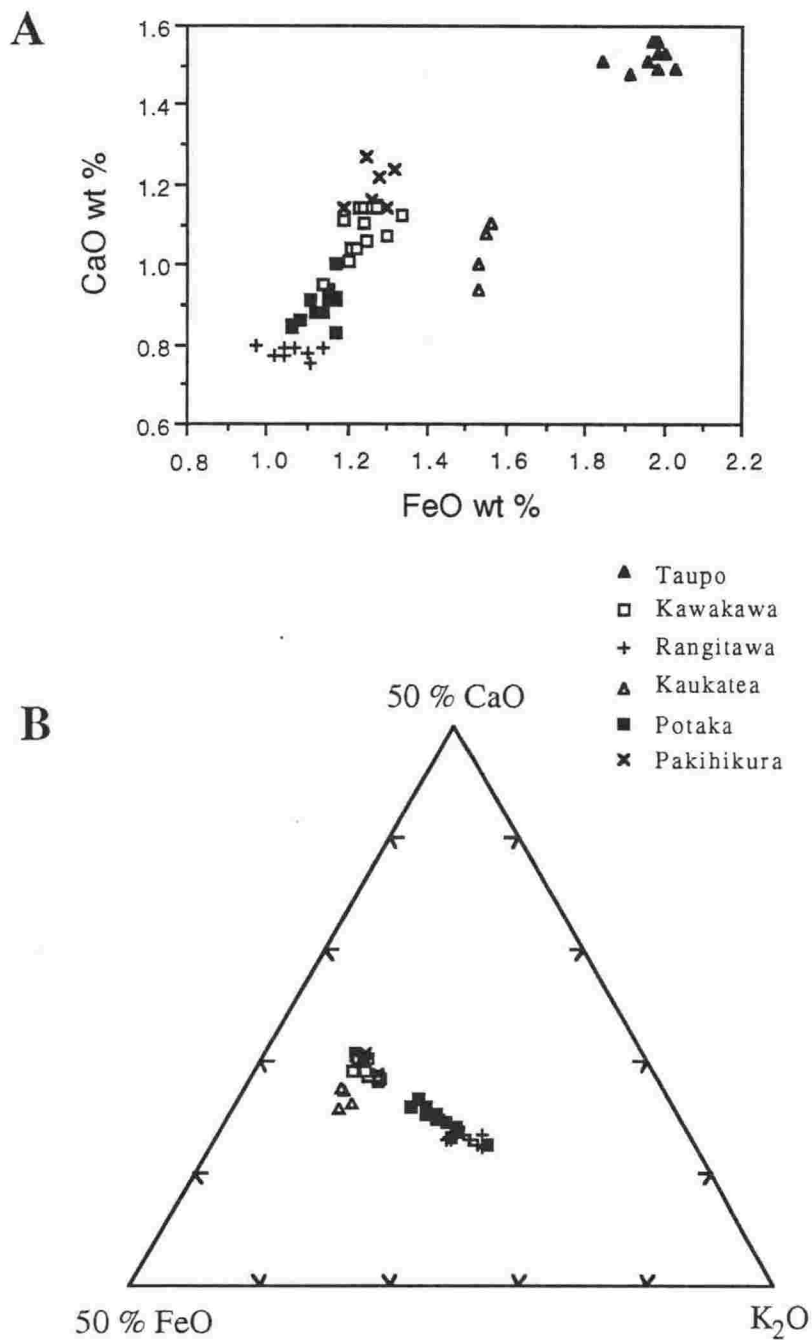
Fig. 5.1 Examples of the use of variation diagrams to display the mean glass composition of samples of different tephras.

5.3 GRAPHICAL METHODS

Stratigraphically different tephras can often be distinguished by plotting their oxide contents on variation diagrams, either binary or ternary (Fig. 5.1). A wide variety of oxides from EMA data or elements from XRF data can be used. For New Zealand Pleistocene tephras, pairs of FeO, CaO, K_2O, Rb, Sr and Ba in the glass phase, and Fe_2O_3 and TiO_2 in FeTi-oxides are particularly useful for such representations (see Chapter 4). Such plots give a visual presentation of separation, while correlative tephras commonly form a cluster. However such plots are limited to 2 or 3 different elements and do not use all of the compositional data available. In some cases sequences of stratigraphically different tephras cannot be distinguished. As some element contents in a sample are closely related to each other by common petrogenetic processes such as crystal fractionation, graphical separation shown by 2 or 3 elements is not necessarily the result of 2 or 3 independent variables. Graphical methods are also limited as they do not provide a numerical measure of separation of different samples. However graphs can show compositional trends and provide a simple means of presenting distinctive compositional differences within the limits imposed by a closed dataset.

5.4 SIMPLE NUMERICAL METHODS: SIMILARITY COEFFICIENT

A commonly used numerical measure of compositional similarity in tephra studies is the Similarity Coefficient SC (e.g. Borchardt et al. 1971; Sarna-Wojcicki et al. 1987). This method allows any number of different oxides and various types of data sets to be compared in a single calculation. It compares the composition of two samples by a mean ratio of each of their oxide contents and is defined as:

$$d_{(A,B)} = \left[\Sigma \, Ri/n \right]$$

where $d_{(A,B)}$ = SC between analyses of tephras A and B; i = element number; n = number of elements; $Ri = XiA/XiB$ or XiB/XiA, whichever is< 1.0; XiA = concentration of element i in sample A; XiB = concentration of element i in sample B.

An identical match in composition will produce a SC of 1.00. This is commonly not achieved for correlative samples due to natural compositional variability in the eruptive and to analytical error. Different workers (e.g. Smith & Nash 1976; Froggatt et al. 1986; Sarna-Wojcicki et al. 1987; Izett et al. 1988; Busacca et al. 1992; Kohn et al. 1992) have proposed different SC ranges to define whether a pair of samples are chemically similar to support correlation. In general SC values >0.90 are considered chemically similar, while SC values <0.90 are dissimilar and reflect different eruptives. The SC value calculated will depend on which elements are being compared, because each element may have different natural variability

Table 5.1 Similarity Coefficient matrices for the composition of correlative tephra samples.

Taupo EMA (Si, Al, Ti, Fe, Mg, Ca, Na, K)

	1	2	3	4	5	6	7	8	9
1	1	0.96	0.98	0.97	0.98	0.97	0.96	0.97	0.99
2		1	0.96	0.97	0.98	0.98	0.97	0.98	0.97
3			1	0.97	0.98	0.98	0.97	0.97	0.99
4				1	0.97	0.97	0.97	0.98	0.97
5					1	0.98	0.96	0.98	0.98
6						1	0.95	0.98	0.98
7							1	0.96	0.98
8								1	0.97
9									1

Taupo XRF (Sc, Ba, La, Ce, Zn, Zr, Nb, Ga, Pb, Rb, Sr, Th, Y)

	1	2	3	4	5	6	7	8	9
1	1	0.92	0.92	0.94	0.90	0.92	0.92	0.93	0.94
2		1	0.96	0.92	0.94	0.93	0.95	0.96	0.96
3			1	0.91	0.96	0.95	0.97	0.96	0.96
4				1	0.90	0.90	0.90	0.91	0.94
5					1	0.98	0.95	0.97	0.95
6						1	0.94	0.95	0.95
7							1	0.96	0.95
8								1	0.96
9									1

Kawakawa EMA (Si, Al, Ti, Fe, Mg, Ca, Na, K)

	1	2	3	4	5	6	7	8	9	10
1	1	0.98	0.96	0.93	0.93	0.92	0.95	0.96	0.95	0.95
2		1	0.95	0.94	0.93	0.91	0.94	0.97	0.95	0.94
3			1	0.96	0.96	0.95	0.96	0.95	0.96	0.96
4				1	0.96	0.95	0.96	0.96	0.97	0.96
5					1	0.98	0.98	0.95	0.96	0.98
6						1	0.97	0.93	0.95	0.96
7							1	0.95	0.97	0.99
8								1	0.97	0.96
9									1	0.96
10										1

Kawakawa XRF (Sc, Ba, La, Ce, Zn, Zr, Nb, Ga, Pb, Rb, Sr, Th, Y)

	1	2	3	4	5	6	7	8	9	10
1	1	0.93	0.93	0.94	0.96	0.94	0.95	0.92	0.93	0.94
2		1	0.95	0.93	0.95	0.93	0.92	0.91	0.92	0.92
3			1	0.96	0.95	0.96	0.94	0.94	0.95	0.94
4				1	0.95	0.95	0.91	0.92	0.93	0.93
5					1	0.96	0.95	0.93	0.94	0.92
6						1	0.96	0.96	0.95	0.92
7							1	0.94	0.93	0.93
8								1	0.93	0.92
9									1	0.92
10										1

in a sample and different analytical uncertainty. An additional problem with SC is that it is sensitive to the element abundance as well as the differences in abundance. For example, if Xi_A = 0.10 and Xi_B = 0.11, then their ratio is 0.91. If Xi_A = 0.11 and Xi_B = 0.12, then their ratio is 0.92. In both examples the compositional difference is 0.01, but the resulting SC is different.

Using EMA data, Sarna-Wojcicki et al. (1987) consider correlative tephra pairs to have SCs >0.95, based on the oxides of Si, Al, Fe, Ca, Na and K. The oxides of Ti and Mg, are also commonly determined in EMA, but are not included in SC calculations by Sarna-Wojcicki et al (1987) because of their greater analytical uncertainty. These oxides (TiO_2 and MgO) are used in other tephra studies (e.g. Froggatt et al. 1986; Kohn et al. 1992), as they can be distinctive in some tephras within their limits of uncertainty. Their analytical accuracy also depends on the instrument used to determine them. In these latter cases SCs for correlative tephras may be >0.92.

To test the range of SC values from different samples of the same eruptive unit produced by analytical techniques in this study, EMA and XRF data were obtained on multiple glass samples of two widespread tephras which can be conclusively identified by field character and stratigraphic position alone. These tephras were (1) Taupo Pumice (ca. 2 ka), which is stratigraphically the youngest large rhyolitic eruptive from the TVZ; and (2) Kawakawa Tephra (ca. 22 ka), a widespread eruptive found in a young loess unit throughout much of central New Zealand (Froggatt & Lowe 1990). Field samples were provided by P. Froggatt. SCs comparing 9 different Taupo Pumice samples using Si, Al, Ti, Fe, Mg, Ca, Na and K from EMA are in the range 0.95-0.99 with a mean of 0.97 ± 0.01. Of the 26 comparison pairs of different samples, all but one are >0.96 (Table 5.1). Comparisons of 10 different samples of Kawakawa Tephra produced SCs in the range 0.91-0.99 with a mean of 0.96 ± 0.02, from EMA data. Most are >0.93 (Table 5.1). Using the elements which could be accurately determined from XRF (Sc, Ba, La, Ce, Zn, Zr, Nb, Ga, Pb, Rb, Sr, Th and Y), the 9 samples of Taupo Pumice produced SCs in the range 0.90-0.97 with a mean of 0.94 ± 0.02 (Table 5.1). The same trace elements for the 10 Kawakawa Tephra samples produced SCs in the range 0.91-0.96 with a mean of 0.94 ± 0.01.

Although the mean SC for each data set is similar (0.94-0.97), SC for individual comparison pairs can vary widely, creating a problem in defining a SC value to accept or reject a correlation between a pair of samples. For EMA data, Taupo Pumice samples consistently produced higher SC values with a narrower range than for Kawakawa Tephra data. As well as possible greater natural variation in the Kawakawa eruptive, the concentration of several oxides including Ti, Mg, Fe and Ca in its glass are lower than in the Taupo Pumice glasses. Thus small absolute differences in the element ratios have a greater percentage affect in the resulting SCs for Kawakawa Tephra. This problem is particularly evident in the SC matrix produced from XRF data. The relatively low SCs for some Taupo Pumice pairs (0.90-0.93) compared

with those determined from EMA data, result from the low total concentration of Sc, Nb and Th (<11 ppm), which although determined accurately may vary by 1-2 ppm between samples.

As the mean SC in each of the data sets are similar while the ranges are not (Table 5.1), comparison of an unknown sample to a set of correlative samples is a more reliable method of assessing a possible correlation than comparison to a single known sample.

Allied to SC, are other numerical comparisons based on composition ratios of pairs of samples. Coefficient of Variation (Borchardt et al. 1971) is based on the mean and standard deviation of ratios calculated as in SC. RATIONAL (Sarna-Wojcicki et al. 1987) is based on the standard deviations of averages of ratios of element concentration. Both methods suffer from the problems outlined for SC. The advantages of each of these techniques are that they are simple to calculate, they include a wide variety of compositional data, and they can compare pairs of samples without the need for a reference set of samples (e.g. Stokes et al. 1992).

5.5 DISCRIMINANT FUNCTION ANALYSIS

5.5.1 Background

In the commonly used techniques discussed above, no statistical procedure is used to evaluate the relative significance of the different elements to discrimination. Discriminant Function Analysis (DFA) provides a means to assessing the discriminating power of different variables and a measure of the separation achieved by multi-variable datasets, such as the composition of tephras (Smith & Nash 1976; Stokes & Lowe 1988; Stokes et al. 1992). DFA determines a linear combination of variables (elements), in which one or more allows the discrimination between a number of groups (each consisting of samples of a particular tephra). Thus the procedure requires a reference set of known samples. The method used here is similar to that described by Stokes & Lowe (1988). In the first stage, a stepwise discriminant analysis determines which variables best discriminate the groups. Variables are added sequentially to improve the separation between groups. The order will depend on the variables already selected, and thus some may be later removed by the addition of others. The second stage is a canonical discriminant analysis using the variables selected in the stepwise procedure. This produces the highest possible multiple correlation within the groups (canonical variates) (Stokes & Lowe 1988). Software packages are available to run these procedures (Joyner 1985). A Mahalanobis squared distance statistic (D^2) is also calculated which provides a measure of the degree of separation achieved between the groups.

DFA in tephra studies have utilised various types of datasets, but the technique has not be widely applied. For example, Smith & Nash (1976) used a range of trace element analyses of glass in DFA to distinguish between tephras, and Beaudoin & King (1986) used major oxide data from titanomagnetites. In New Zealand, Stokes & Lowe (1988) were the first to use a log-

ratio transformation in DFA to avoid the effects of a closed dataset. They showed that latest Pleistocene tephras from 5 different source volcanoes could be distinguished by DFA using EMA data from glass shards. Stokes et al. (1992) used glass EMA data to distinguish between chemically similar tephras from common source volcanoes. However, previous studies have not attempted to test the relative discriminating power of major and trace elements, and their possible differences between different tectonovolcanic provinces.

In this investigation using DFA to evaluate different types of compositional data for New Zealand and western US tephras, P. Froggatt provided the samples of Taupo, Kawakawa and Rangitawa tephras, and ran the software on the computer.

5.5.2 Evaluation of volcanic glass compositional data by discriminant function analysis for the correlating widespread Quaternary silicic tephras in New Zealand and Western United States (a manuscript submitted to Quaternary Research).

Evaluation of volcanic glass compositional data by discriminant function analysis for correlating widespread Quaternary silicic tephras in New Zealand and Western United States

Philip A. R. Shane and Paul C. Froggatt

Research School of Earth Sciences, Victoria University of Wellington, P. O. Box 600, Wellington,

New Zealand

ABSTRACT Major, trace and rare earth element analyses of volcanic glass are used separately or in combination for correlating Quaternary tephras, often by graphical or simple comparative methods. We have taken a statistical approach using discriminant function analysis (DFA) to assess the relative discriminating power of the different elements in volcanic glasses from several tectonovolcanic provinces. We found that major oxides are powerful discriminating variables for widespread tephras from the Taupo Volcanic Zone in New Zealand and here they can be more discriminating than trace elements. A wide selection of tephras from the western United States can also be distinguished on major oxides alone, particularly those from Cascade Range volcanoes. For tephras from large intracontinental calderas, such as Long Valley or Yellowstone, REE and trace elements are more effective at discriminating than major oxides. However, tephras erupted from the Long Valley area can be distinguished on major oxide composition by DFA, in spite of their similar chemistry. The selection and relative significance of different elements for discriminating tephras depends on the total data set being compared, as well as the source volcano and the individual eruptive events. Caution must be exercised in the non-statistical selection of compositional data for characterising tephras: DFA is a more powerful and objective tool for the comparison of tephra chemistry.

INTRODUCTION

Widespread, silicic volcanic ashes (tephras) are the main recorders of the nature and frequency of large, catastrophic eruptions, which are often destructive rather than constructive at their vent location. The chemical characteristics of the tephra reflect the eruptive event and the tectonovolcanic province from which it originated. Frequent, large rhyolitic eruptions from volcanic regions such as Yellowstone (Christiansen and Blank, 1979) and Long Valley (Bailey et al., 1976) in the western United States, and Taupo Volcanic Zone (TVZ) in New Zealand (Wilson et al., 1984), have produced widespread Quaternary tephras. As well as providing information on petrogenetic processes, these tephras are an integral part of many interdisciplinary studies. Their correlation can provide a chronology and stratigraphic framework in volcanic and non-volcanic sequences.

Although multiple criteria are required to correlate a particular tephra, the abundance of various elements in the glass phase is one of the most diagnostic (e.g. Westgate and Gorton, 1981). However, often a rigorous statistical approach is not employed in (1) the selection of elements or oxides for use in correlation; (2) the determination of the relative importance of the different elements; (3) the consideration of variability of abundances both within and between tephras; and (4) the quantitative measure of overall difference between tephra compositions. Such factors vary between the tectonovolcanic provinces from which the tephras have been erupted and this has led to the *ad hoc* selection of elements for correlation. Discriminant function analysis (DFA) provides an approach to assess these factors, but has not been widely applied in tephrostratigraphic studies (e.g. Beaudoin and King, 1986). However, Stokes and Lowe (1988) demonstrated the efficacy of the method to discriminate between different source volcanoes in New Zealand using the major oxide composition of tephras, and investigated the significance of data pretreatment. Stokes *et al.* (1992) tested the performance of DFA to distinguish a number of chemically similar tephras, again using major oxide compositions.

Studies of large Quaternary eruptions from the TVZ in New Zealand have successfully correlated individual eruptive events using mainly major oxides in glass shards determined by electron microprobe analysis (EMA) (e.g. Froggatt, 1983; Froggatt *et al.*, 1986; Lowe, 1988; Shane and Froggatt, 1991). Many western US studies of tephras from large caldera-forming volcanoes (e.g. Yellowstone, Long Valley) have emphasised the value of trace elements and REEs determined from bulk glass separates (e.g Borchardt *et al.*, 1972; Westgate and Gorton, 1981; Sarna-Wojcicki *et al.*, 1984, 1987; Izett *et al.*, 1988). In these cases, major oxides alone were considered insufficient for correlation. The western US (excluding the Cascades volcanoes) and New Zealand TVZ volcanic regions represent fundamentally different tectonovolcanic provinces. The large western US calderas are intracontinental, being situated in areas undergoing extension (e.g. Izett, 1981). The TVZ in New Zealand is located at a convergent boundary between a thin continental plate and an oceanic plate (Cole, 1990). As a result, eruptives display different petrochemical and mineralogical characteristics.

In this paper we concentrate on the recognition of individual eruptive events and differences between tectonovolcanic provinces as revealed by DFA of glass compositions. Previously, little trace element data had been published for TVZ tephras and their relative importance in characterisation, in contrast to major oxides, was unknown. We have thus used DFA to assess their potential relative to major oxides. Samples were collected and analysed

using DFA on western US glass compositions taken from the literature to assess regional variations and to make a comparison with TVZ glasses.

THE PROBLEM OF CLOSURE AND THE LOG-RATIO TRANSFORMATION

Chemical analyses of rocks or glasses form a "closed" dataset: i.e. the data is constrained to a constant sum (100 %). It is inappropriate to use statistical procedures on closed data without first transforming the dataset (Rock, 1989; Woronow, 1991; Rollinson 1992), a problem first addressed in DFA of tephra compositions by Stokes and Lowe (1988). For the DFA study presented here, a further problem is the large magnitude range of the variables (elements or oxides), from 1 ppm to 80 wt % or a range of 10^7. In DFA, the variable with the greatest absolute and relative variance will have greatest influence on the outcome, thus SiO_2 and Al_2O_3 will overpower many of the trace elements. The log-ratio transformation (Aitchison, 1986) overcomes both these difficulties, removing closure and reducing the variables to one order of magnitude. In this study, major and trace element analyses were transformed separately and then merged using the transformation

$$Y_i = \log10(x_i/x_d),$$

where Y_i is the transformed variable of chemical element x_i in an analysis of d elements and where i lies between 1 and d-1. The choice of the divisor is arbitrary (e.g. Stokes *et al.*, 1992), but will result in small differences to the elements selected and the final discriminant functions, without affecting the overall discrimination. Examination of the pooled and within-sample variance of each element suggests the element with smallest variance will contribute least to the DFA. In this study, TiO_2 and La were chosen as divisors for the major and trace elements respectively, for their small variances and moderate abundances. It is also important that the dataset be multivariate-normal. Overall, the data used here have skewness values close to zero.

STATISTICAL METHODS

The use of DFA in tephrostratigraphic studies has been described by Beaudoin and King (1986), Stokes and Lowe (1988) and Stokes *et. al.* (1992). DFA determines a linear combination of variables (in this study, oxide or element abundances in glass). Variation of one or more of these variables allows the discrimination of a predetermined number of groups (eruptive events). To achieve this, a reference set of data (samples) is required for each of the groups. Using the SAS software package (Joyner, 1985) stepwise discriminant analysis (STEPDISC) selects variables that contribute significantly to the separation of the groups. Variables are added sequentially to improve the separation of the groups. In some cases this

may also involve removing previously entered variables where high correlation between the variables exists. DISCRIM determines a linear combination of the selected variables that results in high multiple correlation within the groups (see Stokes and Lowe, 1988). These discriminant functions can be used to determine the likelihood of classification of the samples into the groups as if they were unknowns or to classify unknown samples. Procedure CANDISC calculates discriminant scores which can be plotted graphically (e.g. Fig. 1). It also calculates the Mahalanobis distance statistic (D^2) which can be used as a measure of the separation of the groups.

TAUPO VOLCANIC ZONE TEPHRAS

Six relatively widespread TVZ tephras which could be confidently correlated on multiple, non-chemical criteria were selected to apply the DFA procedure: (1) Taupo Tephra, ca. 1850 yr B. P. (Froggatt and Lowe, 1990); (2) Kawakawa Tephra Formation, ca. 22 590 yr B. P. (Froggatt and Lowe, 1990); (3) Rangitawa Tephra (Kohn *et al.*, 1992) and associated proximal Whakamaru ignimbrites (ca. 0.35 myr) (Froggatt *et al.* 1986); (4) Kaukatea Ash (Seward, 1976; Shane and Froggatt, 1991), ca. 1 myr; (5) Potaka Pumice (Seward, 1976; Shane and Froggatt, 1991), ca. 1 myr; and (6) Pakihikura Pumice (Seward, 1976; Shane and Froggatt, 1991), ca. 1.5 - 2.0 myr. Ages for tephras 3-6 are based on $^{40}Ar/^{39}Ar$ single crystal isotopic data (Walter pers. comm. 1992). Tephras 1-3 can be recognised reliably on field character and stratigraphic position. The more distal exposures, and older tephras, require multiple criteria to correlate them including stratigraphic position, paleomagnetism and isotopic ages. Taupo Tephra and Kawakawa Tephra are known to have been erupted from Taupo Volcano in the TVZ. The source(s) for the remaining tephras is uncertain, but similar aged eruptives are known from the Mangakino Volcano (Wilson *et al.*, 1984).

A range of major oxides was determined by EMA on individual glass shards (Table 1), and trace elements by X-ray fluorescence (Table 2) for bulk glass separates, from each of the tephras.

DFA OF TAUPO VOLCANIC ZONE TEPHRAS

Because we obtained analyses on two different types of samples, we treat the data sets separately before attempting to combine them. Individual shard analyses can be treated as such or as a mean compositions, which is more commonly used in tephrostratigraphic studies. We initially performed DFA using four different data sets: (A) individual shard major oxides determined by EMA; (B) mean major oxide compositions for each tephra sample determined by EMA; (C) trace element analyses of each tephra sample determined by XRF; (D) combined mean major oxide and trace element compositions for each sample, i.e. a merger of data sets B

Table 1 Major oxide compositions of six New Zealand tephras determined by EMA. Analyses are recalculated to 100% and expressed as a mean and standard deviation of n shards. Water by difference. Analytical methods, see Froggatt (1983).

sample no.	SiO_2	Al_2O_3	TiO_2	FeO	MgO	CaO	Na_2O	K_2O	Cl	Water	n
Taupo											
78-16	75.11(.39)	13.03(.20)	0.29(.05)	2.03(.17)	0.29(.07)	1.49(.10)	4.76(.15)	2.87(.11)	0.14(.07)	4.44(2.99)	7
78-76	74.79(.25)	13.24(.09)	0.31(.04)	1.98(.13)	0.26(.03)	1.56(.12)	4.71(.20)	2.95(.09)	0.20(.04)	3.86(0.63)	8
79-11	75.20(.22)	13.20(.11)	0.29(.07)	1.96(.08)	0.30(.02)	1.51(.06)	4.58(.10)	2.80(.17)	0.15(.03)	1.83(0.70)	9
79-14	75.54(.37)	12.97(.37)	0.31(.07)	1.91(.10)	0.27(.05)	1.48(.07)	4.49(.17)	2.85(.28)	0.18(.02)	1.44(1.38)	7
79-29	74.97(.27)	13.08(.11)	0.30(.05)	2.00(.11)	0.29(.04)	1.53(.08)	4.71(.07)	2.96(.11)	0.17(.05)	2.94(0.41)	9
79-3	74.89(.21)	13.24(.12)	0.31(.06)	1.97(.11)	0.30(.04)	1.56(.04)	4.62(.13)	2.91(.09)	0.20(.04)	2.29(1.07)	10
79-41	75.13(.27)	13.35(.13)	0.28(.02)	1.84(.13)	0.26(.04)	1.51(.09)	4.60(.15)	2.84(.07)	0.17(.05)	2.19(0.55)	8
79-44	74.98(.31)	13.18(.19)	0.32(.11)	1.98(.13)	0.27(.05)	1.49(.11)	4.60(.18)	2.91(.11)	0.21(.06)	3.06(1.38)	10
79-51	75.10(.13)	13.18(.11)	0.29(.07)	1.98(.09)	0.29(.04)	1.53(.06)	4.64(.12)	2.79(.09)	0.19(.07)	2.26(1.26)	7
Kawakawa											
744	77.56(.45)	12.24(.21)	0.16(.05)	1.20(.17)	0.13(.03)	1.01(.22)	4.18(.20)	3.32(.42)	0.21(.04)	4.62(1.09)	9
50184	77.58(.23)	12.19(.12)	0.15(.05)	1.22(.10)	0.13(.03)	1.04(.09)	4.06(.15)	3.41(.10)	0.22(.05)	5.03(0.41)	10
50487	77.43(.31)	12.27(.12)	0.17(.03)	1.21(.11)	0.17(.03)	1.04(.08)	4.14(.12)	3.36(.13)	0.21(.03)	3.88(0.40)	10
50650	76.99(.43)	12.57(.19)	0.15(.03)	1.27(.21)	0.17(.03)	1.15(.13)	4.27(.16)	3.23(.29)	0.20(.13)	6.88(1.07)	10
50651	77.35(.46)	12.29(.28)	0.18(.06)	1.26(.19)	0.16(.04)	1.14(.12)	4.24(.16)	3.19(.15)	0.22(.05)	5.97(1.90)	10
50654	77.30(.48)	12.38(.22)	0.20(.04)	1.23(.09)	0.16(.06)	1.14(.09)	4.28(.15)	3.14(.19)	0.18(.06)	7.14(1.22)	9
50776	77.40(.37)	12.30(.25)	0.17(.03)	1.24(.17)	0.15(.03)	1.14(.12)	4.17(.12)	3.19(.18)	0.19(.03)	5.15(1.16)	10
50822	77.45(.44)	12.28(.37)	0.15(.05)	1.30(.18)	0.14(.02)	1.07(.10)	4.15(.18)	3.22(.21)	0.23(.07)	5.29(1.60)	10
50836	77.25(.41)	12.49(.23)	0.15(.03)	1.19(.13)	0.15(.04)	1.11(.15)	4.31(.12)	3.20(.25)	0.18(.04)	6.02(1.08)	10
KKT1	77.37(.45)	12.42(.32)	0.17(.07)	1.27(.20)	0.15(.04)	1.14(.09)	4.06(.23)	3.25(.10)	0.20(.04)	5.87(1.13)	8
KKT2	77.23(.42)	12.15(.24)	0.18(.04)	1.34(.19)	0.17(.06)	1.12(.15)	4.10(.22)	3.55(.34)	0.15(.05)	6.15(1.30)	9
KKT3	77.21(.33)	12.36(.24)	0.13(.05)	1.14(.16)	0.12(.05)	0.95(.29)	4.13(.21)	3.79(.49)	0.17(.06)	4.99(1.39)	9
KKT4	78.07(.22)	12.17(.13)	0.16(.04)	1.17(.13)	0.14(.03)	0.99(.06)	3.89(.17)	3.22(.12)	0.21(.03)	6.19(0.96)	10
KKT5	77.76(.24)	12.25(.12)	0.15(.06)	1.25(.12)	0.15(.04)	1.06(.08)	3.95(.09)	3.26(.15)	0.19(.04)	6.40(0.52)	10
Rangitawa											
50039	77.55(.27)	12.59(.16)	0.14(.03)	1.14(.06)	0.12(.07)	0.79(.03)	3.55(.18)	4.14(.16)	-	4.95(0.92)	10
50103	78.15(.32)	12.41(.19)	0.14(.04)	0.97(.10)	0.12(.03)	0.80(.06)	3.21(.31)	4.22(.14)	-	4.83(2.73)	20
50105	78.13(.72)	12.50(.35)	0.12(.03)	1.11(.08)	0.10(.04)	0.75(.04)	3.34(.39)	3.96(.22)	-	6.22(1.35)	10
50122	77.83(.40)	12.58(.29)	0.13(.04)	1.10(.10)	0.11(.03)	0.78(.04)	3.50(.09)	4.00(.20)	-	6.06(1.11)	10
50166	77.96(.25)	12.35(.13)	0.14(.04)	1.04(.08)	0.11(.04)	0.77(.05)	3.18(.26)	4.45(.10)	-	2.42(0.87)	20
50168	78.20(.33)	12.42(.13)	0.13(.05)	1.02(.10)	0.12(.03)	0.77(.09)	3.23(.24)	4.11(.18)	-	5.20(0.90)	16
50190	77.64(.27)	12.42(.10)	0.13(.02)	1.04(.07)	0.12(.01)	0.79(.05)	3.73(.11)	4.11(.18)	-	3.21(0.52)	11
50208	78.01(.25)	12.17(.11)	0.15(.02)	1.07(.07)	0.11(.03)	0.79(.03)	3.28(.15)	4.43(.17)	-	3.23(0.50)	10
Kaukatea											
9	76.01(.21)	12.89(.07)	0.20(.04)	1.56(.06)	0.15(.02)	1.10(.03)	4.30(.11)	3.62(.13)	0.17(.03)	5.98(0.95)	14
180	76.69(.21)	12.60(.07)	0.15(.04)	1.53(.09)	0.13(.04)	1.00(.06)	4.08(.20)	3.66(.18)	0.18(.02)	6.02(0.61)	10

196	76.46(.30)	12.83(.12)	0.16(.05)	1.53(.10)	0.12(.03)	0.94(.05)	4.29(.20)	3.49(.11)	0.18(.02)	7.15(1.15)	10
240	76.24(.26)	12.83(.12)	0.17(.02)	1.55(.07)	0.13(.03)	1.08(.03)	4.22(.13)	3.62(.10)	0.16(.02)	7.48(1.56)	10
Potaka											
3	77.34(.52)	12.36(.26)	0.12(.02)	1.17(.08)	0.13(.01)	1.00(.01)	3.82(.12)	3.85(.16)	0.22(.02)	7.02(1.08)	12
4	77.63(.30)	12.20(.21)	0.11(.04)	1.11(.19)	0.11(.03)	0.91(.14)	3.72(.11)	4.02(.23)	0.21(.05)	4.88(1.02)	10
5	77.81(.46)	12.10(.02)	0.12(.02)	1.06(.14)	0.11(.03)	0.85(.15)	3.68(.10)	4.10(.16)	0.23(.04)	5.43(0.86)	11
99	76.71(.30)	12.64(.11)	0.10(.03)	1.14(.17)	0.11(.03)	0.88(.16)	3.84(.16)	4.39(.02)	0.20(.02)	4.93(0.90)	10
173	77.67(.29)	12.23(.16)	0.11(.01)	1.15(.16)	0.11(.03)	0.94(.16)	3.55(.19)	4.05(.31)	0.23(.04)	6.09(2.28)	8
194	77.68(.21)	12.29(.12)	0.11(.03)	0.95(.07)	0.10(.03)	0.73(.06)	3.74(.07)	4.17(.08)	0.24(.02)	4.06(0.56)	10
230	77.75(.18)	12.28(.07)	0.15(.04)	1.15(.08)	0.12(.03)	0.91(.07)	3.79(.09)	3.62(.02)	0.23(.02)	5.99(0.70)	10
231	77.38(.20)	12.41(.06)	0.13(.04)	1.12(.15)	0.11(.02)	0.88(.13)	3.81(.07)	3.92(.20)	0.24(.02)	5.62(1.24)	10
232	77.47(.21)	12.32(.12)	0.13(.04)	1.08(.08)	0.10(.02)	0.86(.09)	3.78(.18)	3.98(.25)	0.25(.03)	7.04(1.04)	13
249	77.09(.25)	12.39(.11)	0.12(.04)	1.17(.08)	0.10(.02)	0.92(.10)	3.87(.15)	4.15(.22)	0.20(.02)	6.67(1.47)	10
250	76.98(.32)	12.47(.16)	0.12(.03)	1.17(.15)	0.11(.03)	0.83(.13)	3.80(.04)	4.31(.12)	0.23(.03)	5.77(1.04)	10
pot	77.43(.34)	12.29(.13)	0.12(.05)	1.17(.13)	0.11(.03)	0.91(.14)	3.84(.17)	3.91(.28)	0.23(.03)	5.00(0.93)	24
Pakihikura											
137	77.76(.28)	12.35(.11)	0.10(.04)	1.19(.17)	0.09(.02)	1.14(.03)	3.70(.15)	3.56(.14)	0.10(.03)	7.47(1.46)	11
148	78.02(.30)	12.16(.17)	0.10(.01)	1.25(.17)	0.09(.03)	1.27(.05)	3.58(.12)	3.47(.11)	0.13(.02)	6.71(0.90)	9
165	77.64(.22)	12.44(.13)	0.11(.04)	1.28(.14)	0.10(.01)	1.22(.06)	3.71(.09)	3.42(.13)	0.19(.06)	5.83(1.33)	12
182	78.05(.25)	12.07(.09)	0.09(.02)	1.32(.05)	0.10(.02)	1.24(.03)	3.54(.11)	3.47(.21)	0.14(.03)	6.02(0.57)	10
245	77.36(.36)	12.47(.36)	0.11(.03)	1.30(.16)	0.10(.03)	1.14(.05)	3.76(.09)	3.61(.12)	0.16(.02)	6.04(0.80)	8
293	77.53(.44)	12.43(.11)	0.10(.02)	1.30(.08)	0.10(.02)	1.21(.07)	3.75(.20)	3.42(.13)	0.15(.02)	7.22(1.46)	10

Table 2. Trace element compositions of six New Zealand tephras determined by XRF.

sample no.	Sc	Ba	La	Ce	Zn	Zr	Nb	Ga	Pb	Rb	Sr	Th	U	Y	As
Taupo
78-14	9	561	22	42	58	180	7	16	17	104	150	10	2	28	4
78-16	9	550	24	42	63	204	9	15	17	100	149	9	3	29	4
78-76	10	555	24	46	67	217	7	16	19	99	158	11	2	31	4
79-11	9	557	24	49	72	229	8	16	19	100	158	11	2	34	5
79-29	11	566	25	49	71	223	8	17	20	103	152	10	3	33	4
79-3	11	574	23	49	72	229	8	17	18	101	151	9	3	33	4
79-41	8	558	25	50	69	223	8	16	19	101	153	11	3	32	3
79-44	10	556	24	47	68	225	8	15	20	101	151	10	3	33	3
79-51	9	561	23	47	65	210	8	17	19	104	154	10	3	31	4
Kawakawa
50184	5	574	21	40	44	125	5	14	15	112	91	11	3	21	4
50487	6	570	21	38	44	135	7	14	15	110	103	11	3	21	4
50650	6	594	22	37	49	131	7	14	15	108	87	11	3	20	3
50651	5	575	21	42	48	142	7	14	14	106	90	11	2	21	3
50654	5	577	21	38	48	135	7	14	15	105	107	10	3	20	4
50744	5	588	23	40	45	145	7	13	14	111	88	10	2	22	3
50776	5	573	20	40	44	171	7	14	14	101	105	10	2	21	4
50822	5	557	21	37	40	140	7	15	15	98	117	10	3	20	3
50836	4	566	22	38	44	139	7	13	16	104	101	11	3	21	4
KKT1	6	568	22	36	41	157	6	13	14	107	95	10	3	21	4
KKT2	5	574	22	39	42	161	7	12	14	108	94	10	3	21	3
KKT3	5	575	22	40	43	148	8	13	14	111	90	11	2	21	3
KKT4	5	564	22	37	45	126	7	15	14	109	101	11	3	20	4
KKT5	6	568	22	37	42	127	8	13	14	109	95	10	3	20	4
Rangitawa
50039	5	793	24	44	36	137	7	14	18	154	54	16	3	20	5
50103	6	721	25	48	44	193	7	17	19	138	91	14	4	20	4
50105	5	798	22	40	33	170	7	14	17	145	70	15	3	18	3
50122	4	822	25	45	34	136	9	13	20	155	55	17	4	21	4
50166	5	839	24	42	34	150	7	13	19	158	59	16	4	20	4
50168	4	726	25	45	37	151	7	14	17	144	89	15	3	22	4
50190	4	802	23	40	34	153	7	15	23	137	117	14	2	18	4
50208	5	835	24	53	31	339	7	15	20	136	119	18	4	21	4
Kaukatea
9	7	654	25	46	50	302	11	14	21	113	95	12	4	29	4
180	7	673	27	55	58	219	10	14	20	111	80	12	3	34	5
196	8	682	26	54	63	213	11	16	19	117	88	12	4	34	4
240	9	712	24	52	48	216	10	13	21	116	92	12	3	31	4
Potaka
3	2	730	26	46	40	138	9	13	18	126	72	13	4	24	8
4	2	749	25	49	41	125	7	15	19	132	73	14	4	25	6
5	3	757	24	46	39	124	8	13	19	134	72	14	3	24	5
99	2	765	26	49	40	117	8	14	19	138	69	14	3	25	6
173	4	714	27	50	40	152	8	12	18	134	84	14	3	25	7
195	3	729	26	45	65	117	8	13	19	131	67	13	3	23	5
230	4	729	26	47	44	130	8	13	19	126	71	14	3	24	4
231	3	738	26	46	44	120	8	14	19	134	63	14	4	24	5
232	4	734	25	45	45	129	8	13	19	130	66	13	3	23	5
249	2	733	25	48	43	123	9	14	18	130	67	13	4	23	5
250	4	734	26	48	43	125	9	14	18	136	64	13	4	24	5
Pot	3	751	26	49	38	143	8	14	18	131	75	13	4	24	5
Pakihikura
137	3	766	23	39	38	110	5	15	17	119	87	12	3	20	5
148	6	790	23	44	43	113	6	14	18	119	91	11	3	20	4
165	5	802	24	41	39	107	5	14	17	119	92	12	3	18	5
182	4	715	21	39	45	116	7	14	17	116	86	11	2	19	5
245	5	734	22	41	39	107	6	13	16	118	85	11	3	18	5
293	5	740	21	39	37	112	5	13	16	118	88	12	3	19	6

and C. In (D) we combined data sets to assess the relative importance of major vs. trace elements, and used the mean major oxide composition as is analogous to the trace elements determined on bulk glass separates.

DFA (A) selected all oxides available showing that they all had a significant effect on the degree of separation of the tephras (Table 3). K_2O, CaO and Na_2O contributed the most to the variation. The first canonical discriminant function accounted for 69.8% of the variance, with the first three functions combined contributing 96%. Using this data set, the efficiency of classification ranges from 85-99% (Table 4), which although lower than other DFAs described below, indicates that the majority of individual shards are classified correctly. There is greater scatter in the single-shard EMA data, which decreases when means are used. (This is largely due to the 'Central Limit Theorem'; Rock, 1989).

DFA (B) also showed all oxides were significant in separating the tephras, with K_2O, CaO and FeO contributing the most (Table 3). As in (A) the first three canonical functions accounted for most of the variance (97%). Each tephra can be distinguished on plots of the first and second canonical variates (Fig. 1). D^2 values are significantly greater for (B) (Table 5), which in most cases are an order of magnitude greater than (A). All samples classify correctly in (B).

Most trace elements (DFA (C)) made a significant contribution to the separation of the tephras, except Zn, Ga, Th, U and As. In particular, Y and Sc were most significant, while Ba, Rb and Sr were also important (Table 3). Similar to the DFA using major oxides, the first trace element canonical discriminant function contributed 78% of the variance, while the first three functions combined accounted for 95%. Clear separation of different tephras are evident in canonical variate plots (Fig. 1) and D^2 values are large, being comparable to those in DFA (B) (Table 5). Correct classification of samples was achieved for each tephra (100%).

DFA (D) selected a combination of both major and trace elements as being significant in discrimination (Table 3). All major oxides were selected, in an order similar to (B), with K_2O and CaO contributing most to the variance. K_2O was subsequently removed in the 11th step of the selection process after other variables were added. The analyses also selected Y and Ba as being important. The selection order of the remaining trace elements varied from that of (C) and some elements selected previously (in C) did not contribute significantly (e.g. Ce, Nb). The first canonical function accounted for 81% of the variance. The combination of major oxides and trace elements resulted in a complete separation of the tephra groups (Fig. 1) and the correct classification of each sample. This DFA also produced the largest D^2 values between each of the tephras (Table 5), suggesting that the combined dataset has greater discriminating power than either major or trace element data alone.

Table 3. Stepwise discriminant analysis of variables significant in distinguishing between six widespread New Zealand tephras.

Step	Variable entered	Partial R^2	Wilks' Lambda $(\times 10^2)$
(A) Major element analyses of individual shards			
1	K_2O	0.645	35.50
2	CaO	0.722	9.86
3	Na_2O	0.475	5.17
4	FeO	0.394	3.13
5	SiO_2	0.314	2.15
6	Al_2O_3	0.422	1.25
7	MgO	0.194	1.00
(B) Mean major element analyses			
1	K_2O	0.948	5.22
2	CaO	0.915	0.44
3	FeO	0.749	0.11
4	Na_2O	0.699	0.03
5	MgO	0.559	0.02
6	SiO_2	0.513	0.01
7	Al_2O_3	0.418	0.00
(C) Trace element analyses			
1	Y	0.931	6.89
2	Sc	0.745	1.76
3	Ba	0.720	0.49
4	Rb	0.653	0.17
5	Sr	0.615	0.07
6	Zr	0.627	0.02
7	Pb	0.487	0.01
8	Nb	0.397	0.01
9	Ce	0.315	0.01
(D) Mean major and trace element analyses			
1	K_2O	0.948	52.16
2	CaO	0.915	0.44
3	Y	0.802	0.09
4	Ba	0.652	0.03
5	Sc	0.537	0.01
6	Na_2O	0.524	0.06
7	FeO	0.577	0.00
8	MgO	0.526	0.00
9	Sr	0.433	0.00
10	SiO_2	0.451	0.00
11	K_2O*	0.173	0.00
12	Al_2O_3	0.413	0.00
13	Zr	0.383	0.00
14	Pb	0.291	0.00
15	Rb	0.229	0.00

*removed in the step

Table 4. Classification efficiency for six New Zealand tephras determined by DFA using major oxide analyses of individual shards (DFA (A)).

	Taupo	Kawakawa	Rangitawa	Kaukatea	Potaka	Pakihikura
Taupo	98.63	1.37	0	0	0	0
Kawakawa	0	92.54	2.24	2.24	2.99	0
Mt Curl	0	0	90.29	0	9.71	0
Kaukatea	0	0	0	97.67	2.33	0
Potaka	0	4.76	9.52	0	84.76	0.95
Pakihikura	0	0	0	0	1.54	98.46

Table 5. Mahalanobis distance measures (D^2) for the six New Zealand tephras.

	Taupo	Kawakawa	Rangitawa	Kaukatea	Potaka	Pakihikura
(A) Major oxide analyses (individual shards)						
Taupo	0	45	91	24	71	61
Kawakawa		0	28	17	11	14
Mt Curl			0	31	8	25
Kaukatea				0	17	24
Potaka					0	13
Pakihikura						0
(B) Mean major oxides						
Taupo	0	195	391	111	312	321
Kawakawa		0	116	73	39	110
Mt Curl			0	142	41	142
Kaukatea				0	83	135
Potaka					0	97
Pakihikura						0
(C) Trace elements						
Taupo	0	135	427	59	272	336
Kawa kawa		0	112	114	53	80
Mt Curl			0	318	57	86
Kaukatea				0	170	336
Potaka					0	53
Pakihikura						0
(D) Mean major and trace elements						
Taupo	0	474	1461	313	1017	1017
Kawakawa		0	433	203	192	224
Mt Curl			0	617	104	280
Kaukatea				0	332	475
Potaka					0	143
Pakihikura						0
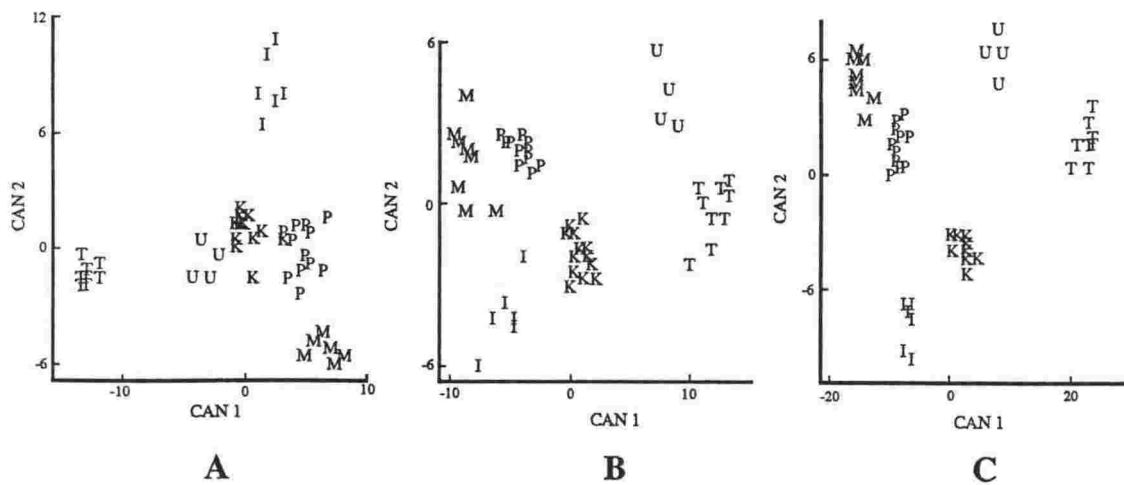
Fig. 1. Plots of the first and second canonical variates for DFA of TVZ tephras: (A) major oxides (DFA (B)); (B) trace elements (DFA (C)); and (C) combined major and trace elements (DFA (C)). Plots represent a two-dimensional view and do not reflect the total separation of the groups. T=Taupo; K=Kawakawa; M=Rangitawa; U=Kaukatea; P=Potaka; I=Pakihikura.
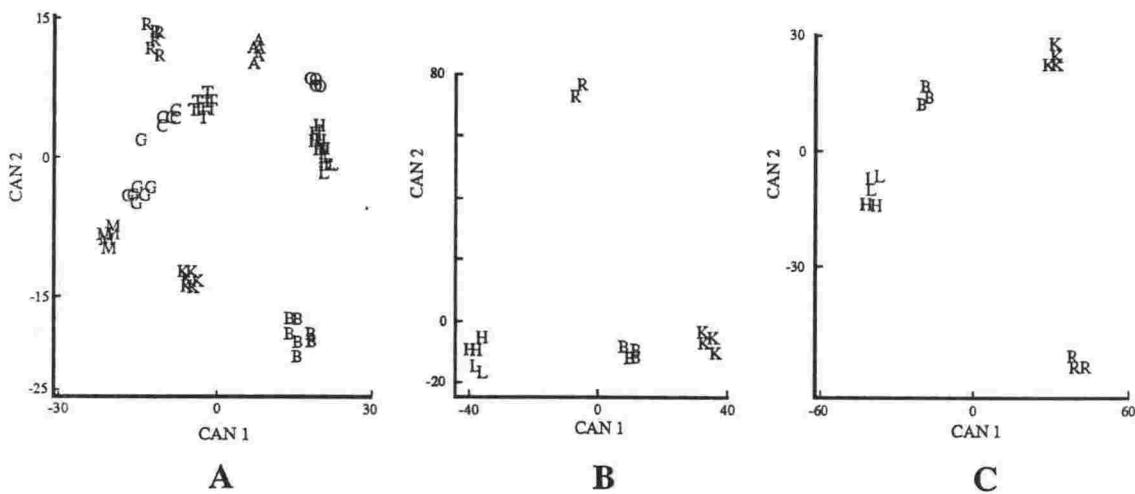
Fig. 2. Plots of the first and second canonical variates for DFA of western US tephras erupted from different volcanoes: (A) major oxides (DFA (E)); (B) trace elements (DFA (F)); and (C) combined major and trace elements (DFA (G)). Identifying symbols as in Table 8.
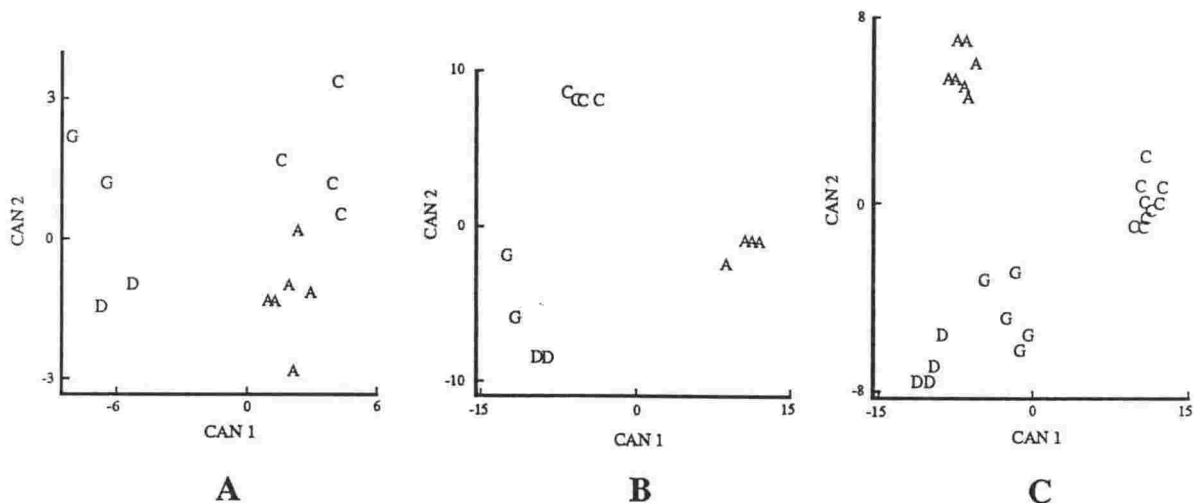
Fig. 3. Plots of the first and second canonical variates for DFA of tephras with close chemical affinity to Bishop ash, erupted from the Long Valley area: (A) major oxides (DFA (H)); (B) major oxides and REE (DFA (I)); and (C) REE (DFA (J)). A=Bishop; C=Bailey; D=Glass Mountain D; G=Glass Mountain G.

DFA OF WESTERN US TEPHRAS

Data and tephras

To perform DFA on late Cenozoic tephras from the western US, we obtained compositional data from the literature. Where possible we selected data determined by similar analytical methods and for the same elements as used in the DFA of TVZ tephras. As there is a great variety of data sets in the literature, some of which are incompatible, our DFA is considered only a reconnaisance to test the potential of the method. First, we selected 11 widespread tephras from different source regions with sufficiently large data sets (mainly EMA) to perform DFA. Secondly, we undertook DFA on a set of tephras from the same source volcano which are chemically similar (Table 6).

DFA of tephras from different source areas

Since much compatible EMA data is available in the literature, we could perform DFA (E) on all 11 tephras using the mean composition of the major oxides (Table 7). K_2O and CaO are most significant in distinguishing the tephras. The first three canonical functions accounted for 97% of the variance. Clear separation of the tephras is shown by the canonical variates (Fig. 2). Lava Creek B and Huckleberry Ridge, both erupted from Yellowstone, show the least separation ($D^2 = 16$); otherwise the distances between the groups are large ($D^2 > 181$, Table 8).

We were restricted to 5 tephras for DFA (F) using trace elements alone (where major oxides were also available for comparison): Huckleberry Ridge, Bishop, Lava Creek B, Rio Dell and Rockland. Of the elements that are available only 7 are selected (Table 7) with Sr and Rb producing most of the variance. Separation of the tephras is significantly greater than that achieved by the major oxides (Fig. 2, Table 8). The smallest separation was that between Lava Creek B and Huckleberry Ridge ($D^2 > 95$). For the same 5 tephras we then combined the major and trace element data sets (G) (Table 7). Eight elements or oxides were selected for the separation of the tephras. Again Sr and Rb produced most of the variance, with Sc, Y, Th and Nb also selected. K_2O and Fe_2O_3 are selected in the seventh and eighth steps, respectively, contributing a small amount of variance. In spite of a similar selection of elements to DFA (F) being used, the combined data set produced higher D^2 values in the range 101-9400 (Table 8).

In all three DFAs (E, F and G) the efficiency of classification was 100% for individual samples into their correct tephra group.

Table 6. Western US tephras and elements used in DFA.
Volcanic source regions: A= Aleutian arc; C=Cascade Range; L=Long Valley; Y=Yellowstone.

Tephra	Age	Source	Reference
Tephras used for interprovince comparison[a]			
Glacier Peak (Chiwawa Bed, B)	0.11 - 0.13 ka	C	Westgate & Evans (1978)
Trego Hot Springs	0.23 ka	C	Davis (1985)
Mt St Helens C (Marble Bluff Tephra)	0.35 ka	C	Davis (1985)
Olema Ash	0.55 - 0.75 ka	?	Sarna-Wojcicki et al. (1988)
Old Crow Tephra	0.15 myr	A	Westgate et al. (1985)
Rockland Tephra	0.4 myr	C	Sarna-Wojcicki et al. (1985)
Loleta ash	0.4 myr	C	Sarna-Wojcicki et al. (1987)
Lava Creek B	0.62 myr	Y	Sarna-Wojcicki et al. (1987)
Bishop ash	0.74 myr	L	Sarna-Wojcicki et al. (1987)
Rio Dell ash	1.2 - 1.5 myr	C	Sarna-Wojcicki et al. (1987)
Huckleberry Ridge ash	2.01 myr	Y	Sarna-Wojcicki et al. (1987)
Tephras used in intraprovince comparison[b]			
Bishop ash	0.74 myr	L	Sarna-Wojcicki et al. (1984)
Glass Mountain D	0.9 myr	L	Sarna-Wojcicki et al. (1984)
Glass Mountain G	1.0 myr	L	Sarna-Wojcicki et al. (1984)
Bailey Ash	1.2 myr	L	Sarna-Wojcicki et al. (1984)

Elements used in DFA:

[a]Sc, La, Ce, Zr, Nb, Rb, Sr, Th, U, SiO_2, Al_2O_3, TiO_2, Fe_2O_3, MgO, CaO, Na_2O, K_2O

[b]Sc, Zn, Rb, Cs, La, Ce, Nd, Sm, Eu, Tb, Dy, Yb, Lu, Hf, Ta, Th, U, SiO_2, Al_2O_3, TiO_2, Fe_2O_3, MgO, CaO, Na_2O, K_2O

Table 7. Stepwise discriminant analysis of variables significant in distinguishing between tephras from the Western US.

Step	Variable entered	Partial R^2	Wilks' Lambda $(\times 10^2)$
Interprovince comparison			
(E) Major oxides			
1	K_2O	0.975	25.46
2	CaO	0.984	0.04
3	Fe_2O_3	0.980	0.00
4	Al_2O_3	0.964	0.00
5	MgO	0.736	0.00
6	SiO_2	0.629	0.00
7	Na_2O	0.498	0.00
(F) Trace elements			
1	Sr	0.999	0.15
2	Rb	0.992	0.00
3	Sc	0.992	0.00
4	Nb	0.863	0.00
5	Y	0.660	0.00
6	Th	0.690	0.00
7	Zr	0.450	0.00
(G) Major oxides and trace elements			
1	Sr	0.998	0.17
2	Rb	0.992	0.00
3	Sc	0.992	0.00
4	Y	0.834	0.00
5	Th	0.698	0.00
6	Nb	0.701	0.00
7	K_2O	0.599	0.00
8	Fe_2O_3	0.565	0.00
Intraprovince comparison (Long Valley area)			
(H) Major oxides			
no variables selected as significant			
(I) Major oxides and REE			
1	Ta	0.871	12.94
2	Sc	0.914	1.11
3	Sm	0.953	0.05
4	Eu	0.650	0.02
5	Ce	0.602	0.01
(J) REE			
1	Ta	0.896	10.40
2	Sc	0.876	1.29
3	Th	0.635	0.50
4	Yb	0.663	0.16
5	Zn	0.404	0.09
6	Sm	0.428	0.05
7	Lu	0.335	0.04
8	Rb	0.293	0.03

Table 8. Mahalanobis distance measures (D^2) for Western US tephras.

Interprovince comparisons
(E) Major oxides

	G	T	M	O	C	K	A	L	B	R	H
G	0	254	186	1350	175	219	862	1374	1349	354	1270
T		0	577	492	154	365	205	661	1013	174	583
M			0	1870	592	377	1194	1883	1505	520	1818
O				0	986	1040	182	183	760	1000	199
C					0	436	607	1024	1419	355	880
K						0	862	904	545	775	904
A							0	444	1042	397	399
L								0	451	1360	16
B									0	1823	399
R										0	1233
H											0

(F) Trace elements

	K	L	B	R	H
K	0	5125	1757	8408	5283
L		0	3170	8915	95
B			0	7970	3015
R				0	7970
H					0

(G) Major oxides and trace elements

	K	L	B	R	H
K	0	6104	4685	6685	6537
L		0	4103	9400	101
B			0	8740	3784
R				0	8785
H					0

Intraprovince comparisons (Long Valley area)

(H) Major oxides

	A	D	G	C
A	0	60	92	11
D		0	12	97
G			0	118
C				0

(J) REE

	A	D	G	C
A	0	173	130	341
D		0	74	490
G			0	199
C				0

(I) Major oxides and REE

	A	D	G	C
A	0	457	534	351
D		0	40	297
G			0	201
C				0

Interprovince comparisons:
G=Glacier Peak, T=Trego Hot Springs, M=Mt St Helens C, O=Olema, C=Old Crow, K=Rockland, A=Loleta, L=Lava Creek, B=Bishop, R=Rio Dell, H=Huckleberry Ridge.

Intraprovince comparisons:
A=Bishop Ash, D=Glass Mountain D, G=Glass Mountain G, C=Bailey Ash.

DFA of tephras from a common source volcano

A series of eruptions including Bishop Ash (0.74 Ma), Glass Mountain D (0.90 Ma), Glass Mountain G (1.0 Ma) and Bailey Ash (1.2 Ma) are thought to have originated from the Long Valley caldera in southern California (Sarna-Wojcicki *et al.*, 1984; Izett *et al.*, 1988). These tephras are considered to be chemically identical on the basis of EMA data, but show small differences in REE contents. We have performed DFA on data from Sarna-Wojcicki *et al.*, (1984) for these tephras to test the discriminating power of the method using a range of major oxides and REEs. From EMA we tested SiO_2, Al_2O_3, Fe_2O_3, MgO, CaO, Na_2O and K_2O; and from INAA: Sc, Zn, Rb, Cs, La, Ce, Nd, Sm, Eu, Tb, Dy, Yb, Lu, Hf, Ta, Th and U.

In DFA (H), STEPDISC did not select any variables as being significant from major oxide data (Table 7), but this is dependent on the level of significance chosen (0.1). Thus, following the DFAs of the other tephras, we used all of the major oxides to test the potential for discrimination. Practically all of the variance (99.7%) was accounted for by the first two canonical functions. The resulting separation distance between each tephra is generally small (D^2 11-117, Table 8) indicating chemical similarity. Different fields for the tephras can be recognised using canonical variate plots (Fig. 3) in spite of much scatter, although we note the data set is very small. Next we performed DFA (I) using all elements available. Only five elements (Ta, Sc, Sm, Eu and Ce) contributed to the variance (Table 7). The resulting degree of separation was high (Fig. 3) with the first two canonical functions contributing 99.3% of the variance. D^2 values range from 40 for Glass Mountain D and Glass Mountain G, to 457 for Bishop Ash and Glass Mountain D.

As only trace or REEs were selected when all data was used, we attempted to improve the DFA classification for the Long Valley tephras by adding INAA data of samples for which no EMA data was available to increase the number of samples in each group. This DFA (J) selected 8 elements (Table 7) to distinguish the tephras, again with Ta and Sc contributing most of the variance. Although most of the resulting D^2 values are less than those of DFA (I), we consider this latter grouping of samples to be more representative of the variation between the tephras, as they represent a larger data set.

In each of the DFAs for the Long Valley tephras, the efficiency of classification of each sample into its correct group is 100% .

DISCUSSION

Selection and relative discriminating power of elements in TVZ glasses

The use of major oxide analyses of individual glass shards resulted in the lowest efficiency of classification of samples into their correct group and the smallest D^2 values, which are a measure of the distance between the groups (tephras). In particular, some shards of Potaka Pumice classified as Kawakawa Tephra and Rangitawa Tephra (Table 4). We suspect this is a result of real chemical heterogeneity within the Potaka Pumice samples, which would be detected by grain-specific analysis, but not in bulk glass separates or when shard compositions are meaned. On chemical variation diagrams, individual shards from Potaka Pumice plot as a linear trend. This is particularly evident in sequences of samples taken vertically through the ignimbrite phase, suggestive of chemical zonation in the magma chamber. The result is wider dispersion of the data in DFA. Such variation is most unusual in TVZ tephras (e.g. Froggatt, 1983; Dunbar et al., 1989). In spite of this natural variablity, DFA can classify individual shards with a better than 84% efficiency for these tephras, or better than 92% if Potaka Pumice is omitted. In all cases, if enough shard analyses are obtained (ca. 10) on each sample, the correct overall classification for the sample is achieved, a result similar to that of Stokes et al. (1992) who examined 18 tephras from the TVZ using a comparable type of data set.

Stokes et al., (1992) showed that D^2 values can be used as a proxy measure of the dissimilarity between different tephras. They obtained D^2 values <5 using individual shard analyses of the same oxides as used in this study, for 9 rhyolitic eruptions from Taupo Volcano in the past 22 ka period. The tephras we have studied were erupted over a time span of nearly 2 Ma and display significantly larger D^2 values (13-91) reflecting the greater chemical variation between tephras erupted over a longer period of time.

We prefer to use the mean of the individual shard analyses as this is a more statistically reliable measure of sample chemistry than individual shard analyses. It also provides a method of comparison with trace element analyses which are determined on bulk samples. Our DFA results using individual shard analyses show they do produce useful classifications, as demonstrated by Stokes et al., (1992), but D^2 values on the mean major oxide compositions are larger (39-391) than those produced using individual shard analyses, and efficiency of sample classification is 100% for each tephra. The use of trace elements alone in DFA can produce good separation between each of the TVZ tephras. D^2 values using these data are comparable to those produced by the mean major compositions (Table 5). Of the trace elements used in DFA, those of high abundance e.g. Ba, Y, Rb and Sr, contributed most to the variance. However, the separation between Pakihikura Pumice and four other tephras is greater using major oxides alone. Similarly, the separation between Taupo Tephra and three of the other

tephras is greater using major oxides. Thus the greatest separation achievable using either major or trace elements alone depends on which tephras are being compared, but neither dataset is markedly superior. Further, Stokes and Lowe (1988) found that the removal of the most distinctive tephra(s) in DFA can enhance separation of the more chemically similar tephras.

The greatest separation between the tephras in this study is achieved by combining the major oxide and trace element data sets. This results in D^2 values 2-3 times greater than those of the data sets used in isolation. Both sets of data contribute significantly to the separation of the tephras. While all major oxides are selected, only 7 of the 15 trace elements are used. Y and Ba are still important, but the selection and relative order of the other trace elements differ from using this data set in isolation. Beaudoin and King (1986) also found that the selection and order of variables (elements) in DFA is dependant on the whole data set used. Thus caution must be used when systematically excluding some variables.

In sum, DFA can distinguish each of the six New Zealand tephras using any of the data sets we have used. In each case, Taupo Tephra is the most easily distinguished tephra, while Rangitawa and Potaka Pumice are the most similar. Although samples were collected from localities with differing depositional environments, varied climatic factors and different stratigraphic positions within the eruptive units (both airfall and pyroclastic flow), DFA successfully classified each into its correct group (eruptive event) with a high probability. This suggests that any vertical or lateral compositional heterogeneity and subsequent diagenetic changes have not significantly distorted the chemical nature nor uniqueness of the eruptive events.

DFA of Western US tephras

The use of mean major oxide compositions allowed all 11 western US tephras to be readily distinguished with the exception of Lava Creek B from Huckleberry Ridge (Fig. 2, symbols L and H). In general, the D^2 distances of separation are comparable to or greater than those for TVZ tephras. Western US tephras separated by the shortest D^2 distance are those erupted from the same source area, e.g. Lava Creek B and Huckleberry Ridge from the Yellowstone area (D^2=16). Separations between tephras known or thought to be from the general region of the Cascade Range province, i.e. Glacier Peak, Mt St Helens, Trego Hot Springs, Rio Dell and Rockland, are in the moderate to high range (D^2 =150-600). These values reflect different source volcanoes but a common tectonovolcanic province. The greatest separations achievable by DFA are those between tephras from different tectonovolcanic provinces, e.g. Rockland (southern Cascades) and Bishop (Long Valley) (D^2=1823). Thus plots of canonical variates and Mahalanobis distance measures based on chemical data are potential methods for recognising source regions and quantifying differences between them. For example, Old Crow Tephra, widespread in central Alaska (Westgate *et al.*, 1985) is placed

closer to Cascade Range tephras by DFA, reflecting a convergent plate boundary source (possibly the Aleutian Arc).

Trace elements combined with major oxides improves the distinguishing power of DFA for western US tephras. The DFA procedure gives preference to trace elements and thus supports the approach of previous workers (e.g. Sarna-Wojcicki *et al.*, 1984, 1987). However, the degree of separation achieved between western US tephras is significantly greater than is possible for New Zealand TVZ tephras using a similar suite of elements (Tables 5,8). REEs are particularly powerful in distinguishing tephras from the same source volcano, as shown by the DFA of eruptives having a close chemical affinity to the Bishop Ash from Long Valley caldera. However, we obtained a comparable degree of separation by major oxides alone, for Taupo Tephra and Kawakawa Tephra, which also have a common source volcano (Taupo). Thus the distinguishing power of elements depends on multiple factors including the source volcano, tectonovolcanic province, and the particular eruption.

Tephras of close chemical affinity to Bishop Ash (Glass Mountain D and G, and Bailey Ash) are considered nearly identical in major oxide composition (Sarna-Wojcicki *et al.*, 1984). Previous studies have suggested that these and other tephras from a common source caldera can only be compositionally distinguished by their REE abundances. However, DFA allows each to be distinguished using major oxides (Fig. 3; Table 8), and thus DFA provides a higher resolving power than previous comparison techniques used. A similar conclusion was reached by Stokes *et al.*, (1992) for chemically similar tephras from the TVZ.

CONCLUSIONS

1. The unique classification of eruptive events based on samples collected vertically and laterally deposits of six widespread tephras from the TVZ, is achieved using major oxides, trace elements or a combination of both, by DFA. The combined data set provides the greatest discriminating power, but major oxides determined by EMA can be equally or more discriminating than trace elements determined by XRF, for some tephras from TVZ.

2. K_2O, CaO and Na_2O are important major oxides, while trace elements in high abundance, e.g. Ba, Y and Sr are important for discriminating TVZ tephras. However, the selection and relative order of significance of elements depends on the total data set and the tephras being compared. Thus caution must be exercised if elements are to be excluded from comparison studies.

3. DFA using major oxides determined by EMA clearly distinguish a range of tephras from the western US, especially those from the Cascade Range area. Tephras of close chemical affinity

(e.g. those erupted from the Long Valley area) can also be distinguished on EMA data using this technique.

4. Trace elements and REEs are the most discriminating variables in tephras from western US sources. However, a similar range of elements are less discriminating for TVZ tephras. REEs are particularly important in separating eruptions from long lived intracontinental calderas such as Long Valley.

5. Most of the chemical differences in glasses reflect seem to the tectonovolcanic province from which they originated. Thus DFA has the potential to classify source provinces as well as source volcanoes and individual eruptive events.

Chapter 6
DEPOSITIONAL PROCESSES AND SOURCES FOR EARLY PLEISTOCENE
TEPHRAS IN NEW ZEALAND AND THE SOUTHERN PACIFIC OCEAN

6.1 INTRODUCTION

This chapter discusses the depositional characteristics and source(s) for early Pleistocene tephras in the southern North Island of New Zealand and in deep-sea cores from the southern Pacific Ocean.

Widespread tephras in distal settings are commonly emplaced as fallout deposits from plinian eruptions. These tephras are typically fine ash, structure-less and systematically thin away from the source vent. In contrast, most early Pleistocene megascopic tephras in the southern North Island display current bedding and may be several metres thick up to 250 km from the closest volcanic source areas. There are few thin tephras that can be attributed to fallout emplacement recorded in the early Pleistocene sequences. The predominance of reworked, fluvially emplaced tephras has implications for the sedimentary transport routes and paleogeography of the central and southern North Island. The chemical characteristics of the tephras provide insight to the nature of volcanism in the TVZ and the depositional history of the tephras themselves. This investigation is presented as a paper in section 6.2.

Early Pleistocene tephras in deep-sea cores from the continental shelf and abyssal plains, up to 5000 km from New Zealand have been attributed to activity in the TVZ (Ninkovich 1968; Watkins & Huang 1977; Kyle & Seward 1984; Nelson et al. 1986). The most distal of these tephras occur in the Southern Ocean around Antarctica at latitudes higher than 60°S. Their similarity in age to fission-track dated tephras in the Wanganui basin and East Coast region, led Kyle & Seward (1984) to propose a source for them in the TVZ. The composition of these tephras is investigated and the implications for source(s) and emplacement mode is presented as a paper in section 6.3. A full compositional data set for the glasses is presented in Appendix 4.

Dispersed volcanic glasses are common in Miocene to Pleistocene deep-sea sediments on the Chatham Rise, east of the South Island. The nature and origin of these glasses is presented in Appendix 5, as part of a joint investigation with P. Barnes.

6.2 REMOBILISED SILICIC TUFFS IN MIDDLE PLEISTOCENE FLUVIAL SEDIMENTS,
SOUTHERN NORTH ISLAND, NEW ZEALAND

(reprinted from New Zealand Journal of Geology and Geophysics (1991) 43: 489-499)

Remobilised silicic tuffs in middle Pleistocene fluvial sediments, southern North Island, New Zealand

P. A. R. SHANE

Research School of Earth Sciences
Victoria University of Wellington
P. O. Box 600
Wellington, New Zealand

Abstract Fluvial and lacustrine sediments of middle Pleistocene age (lower Matuyama Reversed Chron and Jaramillo Subchron) contain numerous thick silicic tuffs that have been deposited in the central southern North Island of New Zealand, 100–200 km from their source in the Taupo Volcanic Zone (TVZ). Sedimentary facies indicate most of the tuffs have been transported and deposited subaqueously in a distal braid-plain environment. Individual emplacement events represent catastrophic floods involving vertical accretion up to 30 m. Sedimentation patterns reflect rapid volcaniclastic aggradation in response to volcanism, and intervening hiatuses. Over half of the tuffs examined are composed of reworked and mixed rhyolitic (SiO_2 72–79 wt%) eruptive products. In addition, most contain brown glasses (SiO_2 53–79 wt%) and minerals derived from a range of intermediate to silicic eruptives. Ages and characteristics of the tuffs indicate a major phase of volcanism before and during the Jaramillo Subchron, similar in chemical composition and reflecting common petrogenesis to late Pleistocene volcanism in the TVZ (i.e., frequent eruptions of voluminous, homogeneous rhyolites contemporaneous with subordinate intermediate eruptives). The emplacement of the tuffs in the East Coast region requires substantial transport routes through the present-day Main Axial Ranges and points to considerable uplift in the last c. 0.91 Ma.

INTRODUCTION

Pumiceous, lacustrine, and fluvial sediments of middle Pleistocene age in central North Island, New Zealand, occur as thick sequences on both sides of the Main Axial Ranges (Lillie 1953; Kingma 1971; Carter 1972). The sequences are tilted, folded, and intermittently exposed in Hawke's Bay, northern Wairarapa, and the western side of Wanganui Basin (Fig. 1). They contain a great proportion (20%) of coarse, partly

consolidated volcaniclastics (or tuffs) and have been deposited 100–200 km from the nearest volcanic source region, Taupo Volcanic Zone (TVZ; Cole 1979; Wilson et al. 1984).

Distal, rhyolitic volcaniclastic deposits in these sequences have been examined macroscopically to determine their mode of emplacement and facies characteristics, and microscopically to investigate the character and homogeneity of glass and mineral components. The TVZ has been active since c. 2.0 Ma (Wilson et al. 1984; Grindley et al. 1988), but much of the products are now deeply buried at the source regions and are not easily accessible except from drillholes. Therefore the chronology of distal tuffs and characteristics of their components provide an insight to timing and style of middle Pleistocene volcanism.

Many of the study sequences are now isolated from volcanic centres by ranges over 1000 m high; thus a study of tuff emplacement could also provide insight to paleoenvironment and tectonic history. In this study, several of the longest sections of middle Pleistocene volcaniclastic sediments have been examined and sampled, as well as other shorter sequences (Fig. 1).

STRATIGRAPHY AND CHRONOLOGY

The mainly nonmarine, pumiceous sediments examined here conformably overlie fossiliferous Nukumaruan (early Pleistocene) marine strata of the Kumeroa Fomation in Hawke's Bay and have been named Mangatarata Formation (Lillie 1953). In northern Hawke's Bay, the formation unconformably overlies Cretaceous and early Cenozoic strata in places. To the south, in northern Wairarapa, the Mangatarata Formation is considered to be the equivalent of the Mangahao Formation (Lillie 1953; Neef 1984). On the western side of the Main Axial Ranges, in the Pohangina River valley, sequences studied here are similar lithologically and stratigraphically to the Takapari Formation (Carter 1972). Fleming (1953) and Lillie (1953) considered these pumiceous sequences adjacent to the Main Axial Ranges to be equivalent to the Mangatarata Formation. The Takapari Formation conformably overlies Nukumaruan marine sediments of the Konewa Formation. All sections are unconformably overlain by late Pleistocene–Recent alluvial terrace conglomerate.

A middle–late Pleistocene age (Castlecliffian Stage) was assigned to the Mangatarata Formation (Lillie 1953) and to equivalent strata in central Hawke's Bay (Kingma 1971) mainly on the basis of stratigraphic position and the first significant appearance of pumice in the sediments which is considered to be indicative of the Castlecliffian. Carter (1972) and Neef (1984) considered the lower parts of the Takapari Formation and Mangahao Formation, respectively, could be at least partly late Nukumaruan.

As part of an ongoing study (Shane & Froggatt 1991), reconnaissance paleomagnetic samples and samples of all tuffs were collected from several of the longest sequences:
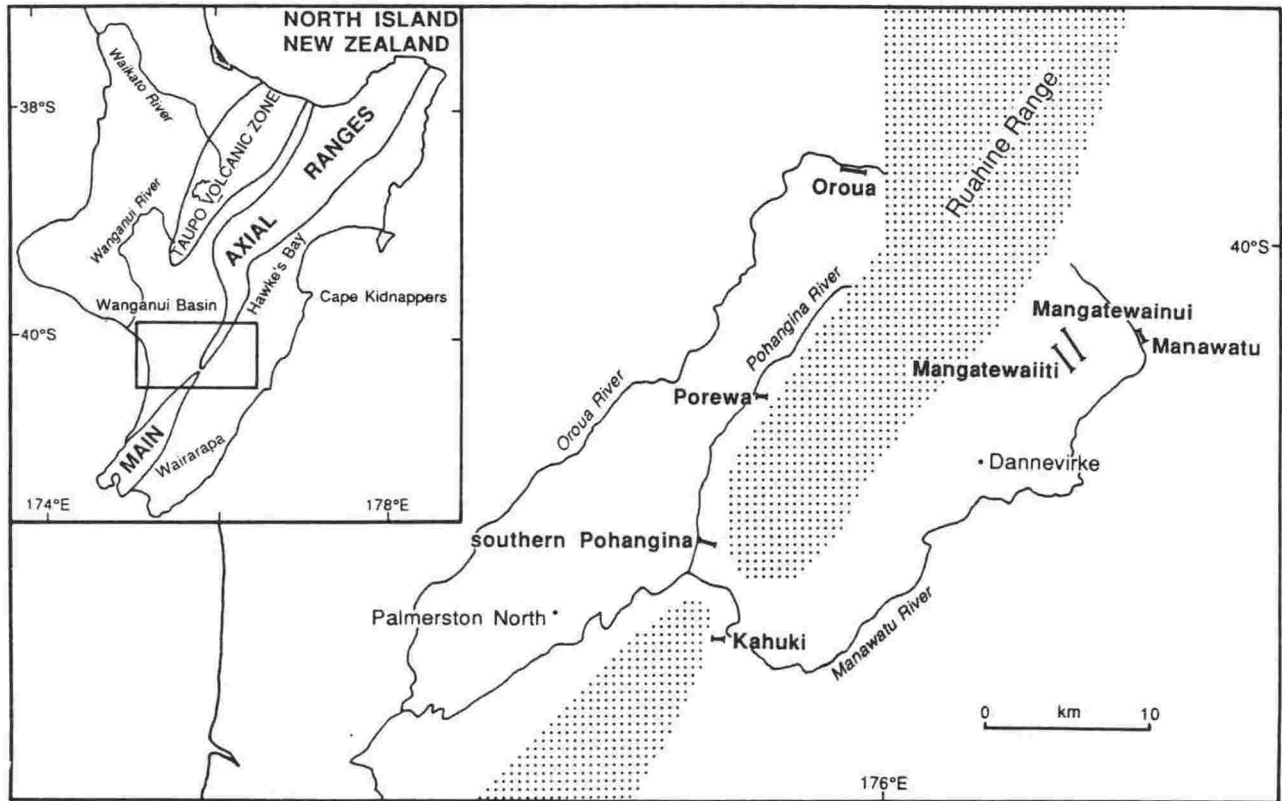
Fig. 1   Southern central North Island showing the location of middle Pleistocene sections examined in the study.

Oroua, Manawatu, Mangatewainui and Mangatewaiiti (Fig. 2). Between three and seven specimens per paleomagnetic site were demagnetised in alternating fields up to 40 mT and measured by a spinner magnetometer. Detailed results are to be presented elsewhere. In some parts of the sections (i.e., middle of Mangatewaiiti and lower half of Oroua) a stable end-point magnetic remanence was not reached in some specimens. Such specimens changed from a normal declination to a reversed declination during demagnetisation, but maintained a normal (negative) inclination, sometimes with decreasing value. This behaviour has been interpreted as incomplete removal of a normal viscous overprint from a reversed specimen (Shane & Froggatt 1991), thus the sites are considered reversed.

Magnetostratigraphy is summarised in Fig. 2. The normal interval near the top of the Mangatewaiiti section was interpreted as the Brunhes Normal Chron by Shane & Froggatt (1991). Subsequently an additional site was sampled at the top of the section and found to be reversed. In the nearby Mangatewainui section, a similar polarity sequence has been found, and a correlation between the sections can be made using the chemical and field characteristics of a tuff (Fig. 2). In light of this new data and a Castlecliffian age proposed by Lillie (1953), the normal interval is considered to be the Jaramillo Subchron (Shane in prep.). If this interpretation is correct, the short normal interval lower in the Mangatewaiiti section could represent the Cobb Mountain Subchron (1.10 Ma, Mankinen et al. 1978).

By glass chemistry and paleomagnetism, a tuff can be used to correlate between the Oroua, Manawatu, and Mangatewaiiti sections (Fig. 2). This tuff has identical glass chemistry to the

Pakihikura Pumice in the Wanganui Basin which occurs in sediments of reversed polarity (Shane & Froggatt 1991) and has been dated at c. 1.06 Ma (Seward 1979).

On the basis of magnetostratigraphy and tuff correlations, the stratigraphic interval studied here is considered to represent the Jaramillo Subchron (0.91–0.97 Ma) and a long part of the upper Matuyama Reversed Chron (pre 0.97 Ma).

NONVOLCANICLASTIC SEDIMENTS

In the Mangatewainui section (Fig. 1, 2), the lower 100 m of Mangatarata Formation, as defined by Lillie (1953), consists of mainly massive sandy mudstone with shellbeds of the intertidal mollusc *Austrovenus*. Above this interval only a few rare shellbeds occur and sediments are mostly nonmarine. This latter part of the formation is at least 600 m thick at the longest section (Mangatewaiiti). The dominant nonmarine lithology of the study sections (Fig. 3) is massive carbonaceous mudstone or finely laminated sandy mudstone in units up to c. 50 m thick. These units contain many peat and lignite beds with some leaf impressions. The common occurence of pinkish mudstone containing freshwater diatoms, and the rarer occurence of the freshwater mussel *Hydridella*, indicates a lacustrine depositional setting.

Monolithological, clast supported, greywacke conglomerate is a minor facies in most sections, but is more common in the Oroua section (Fig. 3). It is commonly cross bedded at a metre scale and displays imbrication. Clasts are generally <0.04 m in size. Conglomerates occur in units generally <3 m thick. These units often contain rip-up clasts of mudstone and fossil logs. Most conglomerates occur in channels and have a
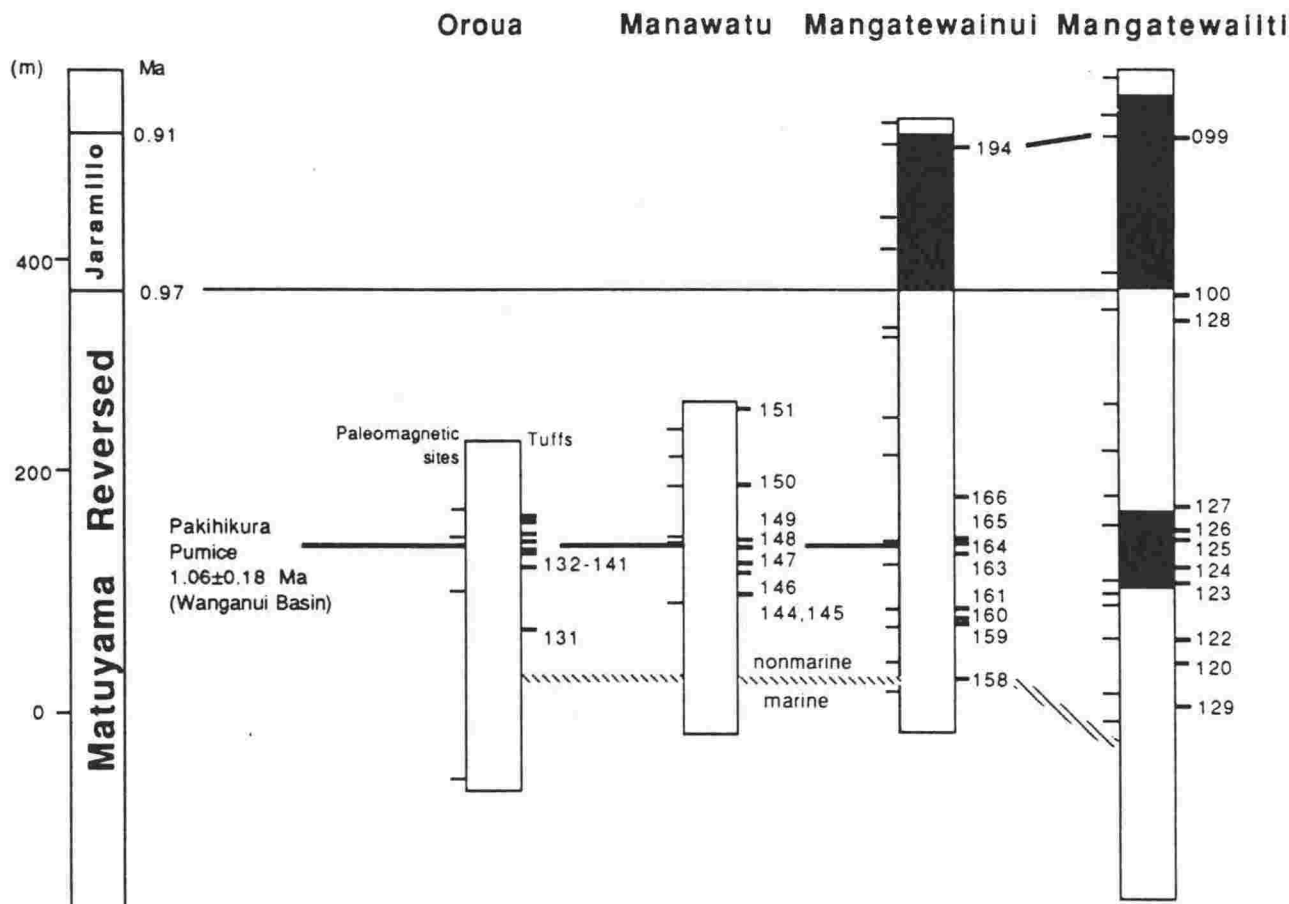
Fig. 2 Summary of magnetostratigraphy for sections of the Mangatarata Formation and Takapari Formation (Oroua). Numbers refer to megascopic tuffs. Lines show correlation between tuffs made on the basis of glass chemistry and magnetic polarity. Also shown is the top of the marine to nonmarine facies transition. Black = Normal, white = Reversed.

scoured base, indicative of fluvial channel deposits. Carbonaceous, trough cross bedded sands, sometimes pebbly and with an erosion base, are a common facies. They are also considered fluvial. Evidence for periodic subaerial exposure is common in the form of paleosols and in-situ tree stumps in many of the sequences.

VOLCANICLASTIC SEDIMENTS

Volcaniclastic sediments occur almost entirely as nonmarine facies. They consist of nearly pure vitric tuffs ranging in thickness from c. 0.05 to 30 m. Grain sizes are mainly coarse ash (<3 mm), but some tuffs contain lapilli pumice up to 70 mm in size. These thicknesses and grain sizes point to reworking of proximal deposits, rather than distal primary airfall in sites which are 100–200 km from the closest volcanoes (TVZ).

Sedimentary structures

The sedimentary structures displayed by the 51 megascopic tuff exposures (summarised in Table 1) are mostly indicative of subaqueous deposition. The majority display planar (horizontal) current bedding (millimetre to metre scale). Individual beds may be graded or nongraded. Some tuffs show sharp contacts between stratification while others, in particular

coarser deposits, display gradational interstratal contacts and may be crudely bedded. Small cross-stratified laminae may also occur. In some exposures, planar-beds display low (2–3°) dips over scoured surfaces and represent scour and fill deposits. Many planar-bedded tuffs display an erosion base and/or paleosol and thus represent overbank deposits.

Cross stratification (in 39% of tuffs, Table 1) range from millimetre-scale ripples to 1 m scale trough or planar cross beds. Often the entire range of cross stratification occurs in a single tuff, along with fine-grained massive beds, suggesting rapidly fluctuating paleocurrent intensities. A typical sequence is an erosion surface overlain by trough cross bedded pumice ash and lapilli with foresets on a 10–30 cm scale. These grade into smaller ripple stratification in a number of cycles and then into planar laminations with an increasing nonvolcanic component. The top of the sequence is typified by massive mudstone or sandstone with lignites or paleosols. Some tuffs have a massive or weakly laminated fine ash immediately above the erosion base. This may represent the initial airfall ash or reworked equivalent.

About 18% of the tuffs examined display synsedimentary deformation: convolute beds and/or water escape structures. These features are most common in cross-bedded, coarse tuffs. Sedimentary folds in a tuff in the Oroua section have amplitudes up to 2 m. Deformation on this scale points to rapid, subaqueous deposition of thick deposits.
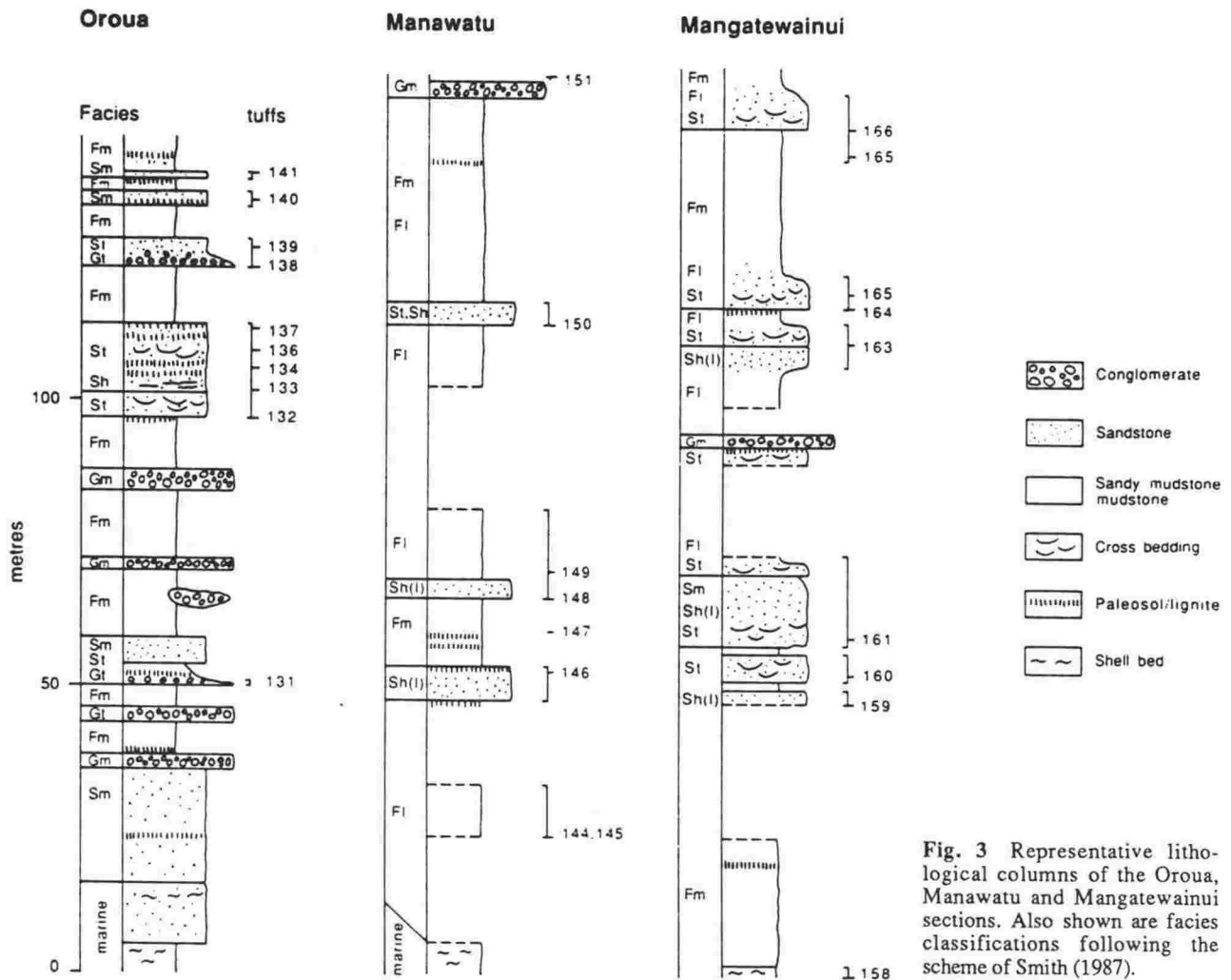
Fig. 3 Representative lithological columns of the Oroua, Manawatu and Mangatewainui sections. Also shown are facies classifications following the scheme of Smith (1987).

Table 1 Summary of sedimentary structures displayed by tuffs in middle Pleistocene sections examined. Numbers represent number of tuffs displaying those features in the section. Percentages are the total number of tuffs from all sections displaying those characteristics.

	1	2	3	4	5	6	7	%
Bedding:								
cross	11	2	1	3	1	2	–	39
horizontal	9	4	8	3	3	3	1	61
convolute	4	1	–	4	–	–	–	18
Massive	1	4	–	3	–	–	2	20
Graded	2	–	1	1	2	1	1	16
Lenses[a]	7	2	1	–	3	2	1	31
Other[b]	3	1	–	2	–	–	–	12
n	14	10	8	8	4	3	4	

1, Mangatewaiiti, bottom U23/828149, top U23/808172.
2, Oroua, T22/620363, T22/624360.
3, Manawatu, U23/890199, U23/892193.
4, Mangatewainui, U23/839165, U23/808185.
5, Southern Pohangina, T24/468990, T24/459992.
6, Kahuki, T24/474902, T24/481898.
7, Porewa, T23/561160, T23/556165.
(Grid references from the NZMS 260 map series).
a, Non-volcanic lenses or beds.
b, Fossil logs, tree stumps, rip-up clasts, intraformational conglomerate.
n, Total number of tuffs in the section.

Ten of the tuffs are massive. These beds are thin (<1.0 m) compared to the other tuffs. Some show little evidence of subaqueous transport and are thus possibly primary airfall deposits. However, a common association with paleosols may point to pedogenic destruction of sedimentary structures.

Other features displayed by the tuffs include rip-up clasts, fossil logs and tree stumps, nonvolcanic sand and gravel lenses, and fragments of charcoal. Some tuffs in the Mangatewaiiti and Oroua sections contain rip-up clasts of nonvolcanic mudstone and of previously deposited, laminated tuff. These clasts may be up to 0.15 m wide and usually occur near the base of the tuff. Two of the tuffs have basal intraformational breccia layers (<0.5 m thick) composed of rip-up clasts. Fossil logs range in size up to 0.20 m in width and 0.80 m long. This incorporated material points to high erosive power of the transporting currents. Other tuffs, especially at Oroua, are deposited directly over in-situ fossil tree stumps and display current bedding.

Relationship to paleosols and lignites

Twenty-two of the tuffs are in contact with either paleosols or lignites. Of these, 14 overlie such horizons. This common association indicates that tuff emplacement events often precede or follow significant hiatuses, which are marked by
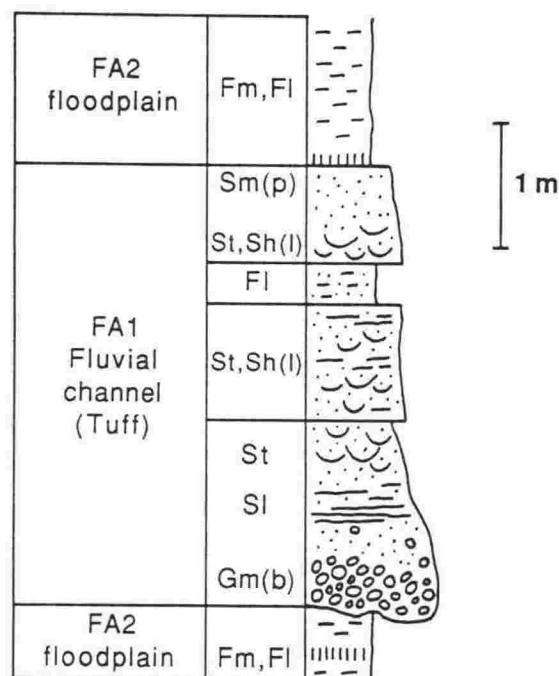
Fig. 4 A typical facies sequence for a middle Pleistocene tuff in the Mangatarata Formation. Symbols and facies as in Fig. 3.

Fig. 5 Field for individual clear-glass shard and brown glass shard analyses (crosses) plotted on a Total Alkali-Silica diagram (after Le Maitre 1986). O1, basaltic andesite; O2, andesite; O3, dacite; R, rhyolite.

the establishment of vegetation. Current bedding in the tuffs shows the association does not reflect airfall deposition and instead implies overbank deposition during floods. The close relationship of paleosols and lignites to tuffs points to the strong influence of volcaniclastic sedimentation in the fluvial system and suggests rapid aggradation or accretion occurs largely as a response to volcanic input.

Facies classification

Most of the tuff sequences can be classified readily as facies of a braided river system, using facies models of Miall (1978) as modified by Smith (1987) for volcaniclastic-dominated systems. Coarse, massive lapilli tuffs and cross or planar-bedded ash tuffs are Gm(b), St, or Sp facies representing channel deposits of bars or dunes, or lag. Very poorly sorted, matrix-supported deposits (e.g., debris flows) are rare or absent. Low-angle cross-stratified tuffs (Sl) are scour fills or antidunes deposited in a high-flow regime and at shallow depths (e.g., Smith 1988). Some planar-bedded tuffs are coarse and show graded interstratal contacts. They may be Sh(b) facies of hyperconcentrated flood flows (Smith 1987). Most planar (horizontal) bedded deposits are Sh(l) facies representing normal high-flow regimes (floods) or Fl facies (displaying laminations, ripples and convolute beds) indicative of waning floods or overbank deposits.

The typical tuff sequence (Fig. 4) is: Gm(b), St, and Sp grading up to Fl in a number of cycles and then into Fm (muddrapes) topped by a paleosol. The sequence reflects rapid deposition followed by rapid waning of paleocurrents. These sequences are typically 2–10 m thick and represent catastrophic flood events. Facies Fl and Fm may result either from a reduction in velocity (flood waning) or a channel shift due to rapid aggradation and lake or swamp development.
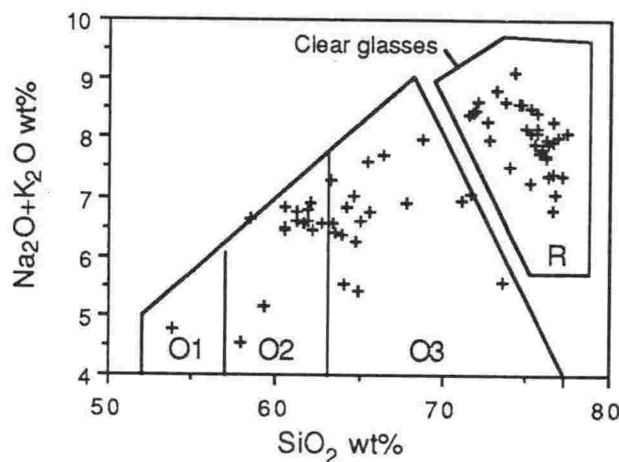
GLASS CHEMISTRY OF TUFFS

Composition

Over 500 glass shards were analysed by electron microprobe from tuffs in the study sections (for methods see Froggatt 1983). About 99% of glass shards within the tuffs are clear or colourless. These clear glasses have a silica content in the range of 72–79 wt% (recalculated on a water-free basis) and all have a calc-alkaline rhyolitic composition using the Total Alkali-Silica scheme of Le Maitre (1984) (Fig. 5). Although such schemes are based on whole-rock analyses, they still provide a framework for comparison, since glass represents the most voluminous component of the eruptions. Most tuffs also contain a small fraction (<1.0%) of highly magnetic brown glasses, some of which have nonrhyolitic compositions (see below).

All clear glass compositions are broadly similar, suggesting a common source. They are also similar to late Pleistocene tephras from the TVZ analysed by Froggatt (1983), Nelson et al. (1986), and Froggatt & Rogers (1990) suggesting a TVZ source.

Single clear-glass populations

Twenty-two of the 51 tuffs analysed consist of a discrete single glass population (Fig. 6A). Shard analyses from each tuff have low standard deviations when grouped: <0.04 wt% for TiO_2 and MgO and <0.15 wt% for FeO, indicating the tuffs are homogeneous (Froggatt 1983) and probably represent a single eruptive event. These discrete populations show no evidence of chemical zonation. Many display small differences in most oxide contents, thus in short stratigraphic intervals, tuffs can be distinguished, sometimes on the basis of just two oxides (e.g., FeO and CaO; Fig. 6A). It is not yet possible to determine the total number of eruptions recorded in the sections, because some tuff exposures are likely correlatives but have similar glass chemistry to more than one tuff in other sections. Also, some closely spaced, chemically similar tuffs within a section may be reworked deposits from the same eruption.
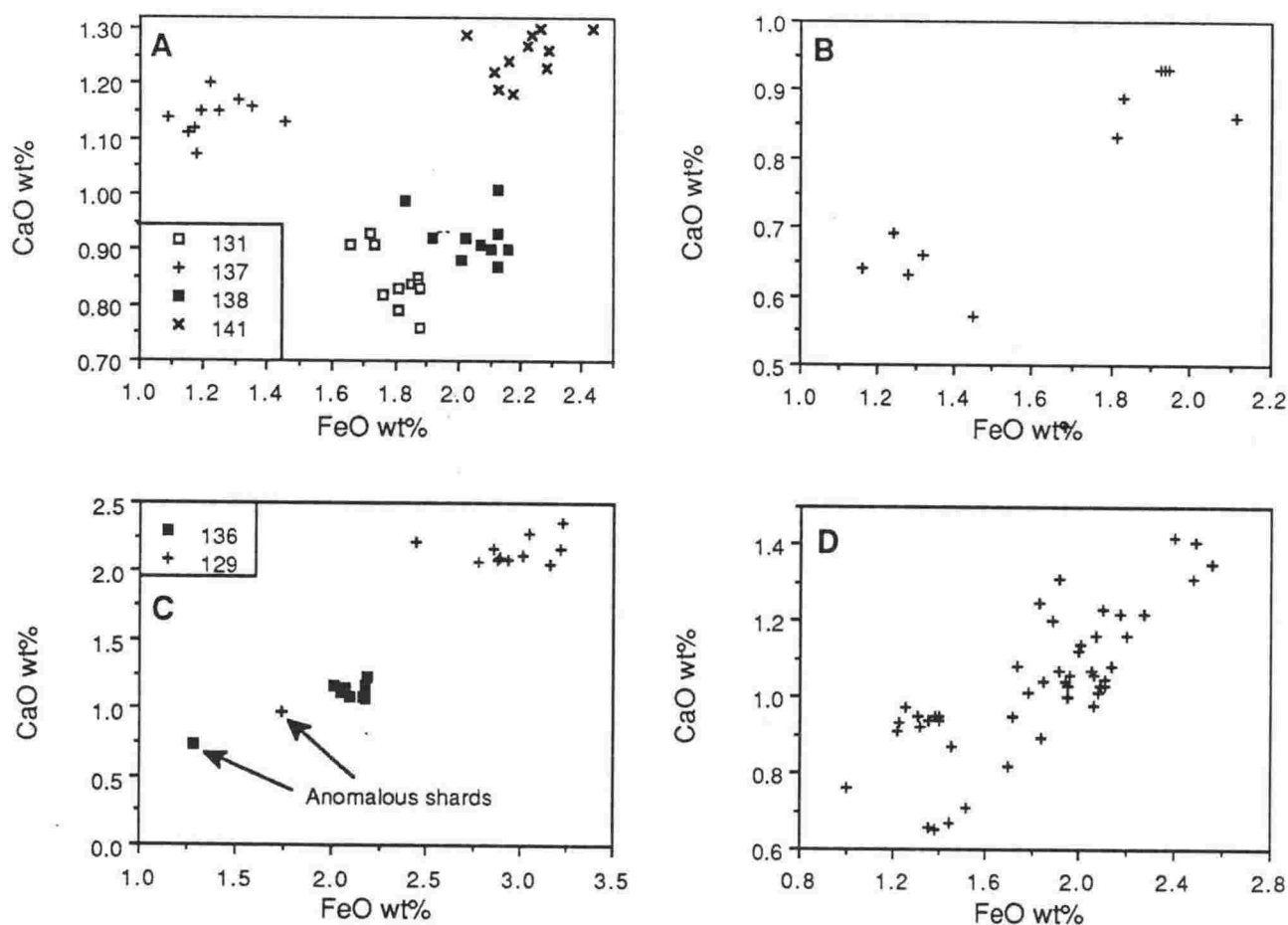
Fig. 6 Examples of analyses of individual shards from middle Pleistocene tuffs. A, Four tuffs (Oroua section) consisting of discrete single glass populations. In ascending stratigraphic order: 131, 137, 138 and 141. B, A tuff consisting of two different glass populations (132, Oroua section). C, Two tuffs containing anomalous shards in addition to a major group. D, A tuff consisting of a near-continuum of shard compositions (100, Mangatewaiiti section).

Multiple glass populations

Twenty-nine (57%) of the 51 tuffs analysed represent multiple populations with different chemical compositions, shown by variation diagrams (Fig. 6). Three broad classes occur: (1) two or more relatively discrete groups of shards, each representing a large proportion of the total sample (Fig. 6B); (2) a large discrete shard group representing c. 80% or more of the sample and one or several anomalous shard(s) with different composition(s) (Fig. 6C); and (3) a continuum of compositions with no discrete group(s) (Fig. 6D).

Interpretation

Multiple glass populations have been reported in New Zealand Pleistocene tuffs (Froggatt 1983; Shane & Froggatt 1991) and elsewhere (Cerling et al. 1978). They could arise from: (1) disruption of a chemically zoned magma chamber or magma mixing (e.g., Carey & Sigurdsson 1978); (2) accidental ejecta; or (3) sedimentary mixing of different volcanic products. The first option is not favoured because primary rhyolitic eruptives in TVZ are relatively homogeneous (Froggatt 1983; Dunbar et al. 1989a, b), while reworked tuffs display multiple glass populations. Accidental ejecta is also not a likely origin because it could not account for the large volumes of some subpopulations (e.g., 40% of the sample, Fig. 6B). Nor is it

likely to produce a near-continuum of compositions (e.g., Fig. 6D). Thus, sedimentary mixing is the most likely cause. This is supported by the abundance of evidence for fluvial remobilisation displayed by the tuffs. The rip-up clasts of tuff found in some deposits would provide a source for chemical heterogeneity since they are relatively cemented, suggesting deposition long before the emplacement event in which they are contained. Therefore, the rip-up clasts could represent a separate eruption.

Tuffs that consist of a large group of chemically homogeneous shards and one or several chemically distinct shards (Fig. 6C) are interpreted as the incorporation of a small volume of older eruptive product into a new emplacement deposit (the large group). The dominant population often differs from older tuffs in the sequence and could represent a new eruption. When no dominant glass population is present in a tuff (e.g., Fig. 6D), the relative ages of the compositions are uncertain. Such tuffs may represent reworking of several older deposits, unassociated with an influx of new volcaniclastic sediment.

Brown glasses

A small fraction (<1.0% of sample) of dark glass shards occurs in nearly all tuffs examined. The glasses range in colour from
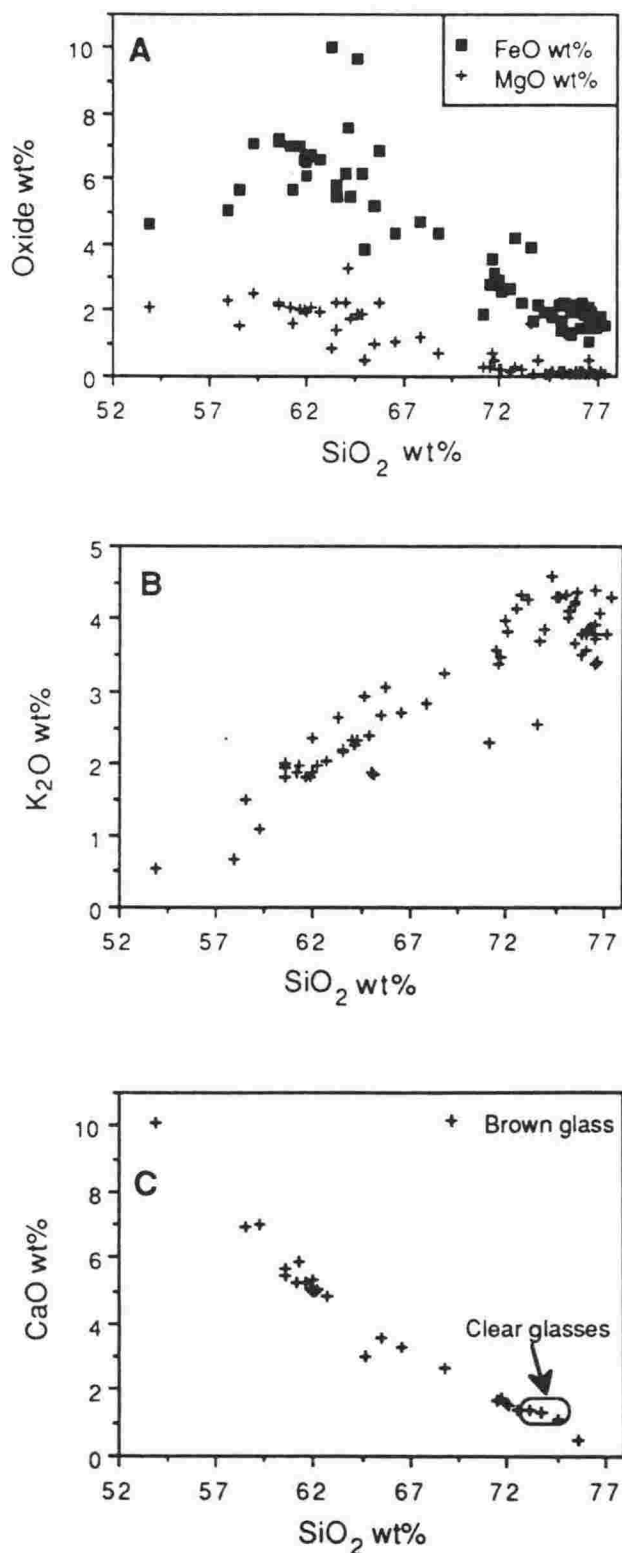
Fig. 7 A and B, Compositional range shown by brown glasses (n= 72). C, An example of the compositional diversity of brown and clear glasses within a single tuff (108, southern Pohangina section).

reddish brown to black, but are mostly brown. They have a high magnetic susceptibility compared to clear glasses, allowing easy separation. Other than colour, the brown glasses do not differ in physical appearance or morphology to the more common clear glasses. They display typical bubble wall or pumiceous morphologies and are generally dissimilar to obsidian. Of the 72 brown shard analyses obtained by electron microprobe, 53.5% are rhyolitic, 24% dacitic, 21% andesitic, and 1.5% basaltic andesite (Fig. 5). All are calc-alkaline. Typical analyses are given in Table 2. Most oxide contents in brown glasses show an inverse relationship to SiO_2 content, except K_2O, and form a single linear differentiation trend (Fig. 7). Within a tuff, a typical brown glass population may display a range of rhyolitic compositions extending beyond that of the clear glass population. In addition, a range of dacitic and andesitic compositions may be present (Fig. 7C).

Interpretation

The high chemical diversity displayed by brown glasses could arise from: (1) compositional gradients within a magma chamber (Hildreth 1981); (2) accidental ejecta; or (3) sedimentary mixing. As with multiple clear-glass populations, the first option is not favoured as an origin. Although magma chamber zonation is common (Hildreth 1981), there is little evidence for it in large rhyolitic eruptives in TVZ (Froggatt 1983; Wilson et al. 1984; Dunbar et al. 1989a, b). As well, zoning is not likely to result in the production of >90% rhyolite (clear glasses) leaving a small c.1% volume of basic and intermediate residue (brown glasses). Such an origin also could not explain why 53.5% of brown glasses are rhyolitic. Sedimentary mixing could be invoked to explain the presence of brown glasses, in particular dacitic and andesitic shards. An analogy to multiple clear-glass populations described above could be made. Froggatt & Rogers (1990) have reported examples of posteruption mixing of airfall rhyolitic and andesitic tephras in peat bogs.

As for highly magnetic, brown rhyolitic glasses in intimate association with weakly magnetic, clear rhyolitic glasses, the origin may involve accidental incorporation and differing thermal histories. Schlinger et al. (1986) have described highly magnetic, dark glasses mixed with clear glasses of identical composition. The dark glasses contain Fe-oxide microcrystals (20–100Å) which precipitate in already quenched glass shortly after eruption, and are dependent on cooling history. Accidental ejecta could go through a complex thermal history if ingested into a new pyroclastic flow. This would explain their presence, if the tuffs were derived from ignimbrites.

Brown glasses have been recognised in numerous marine tuffs of Miocene and Pliocene age in New Zealand (Gosson 1986; Shane 1989); however, their complete nature is still to be investigated.

MINERAL CHEMISTRY

Mineral phases in the tuffs generally represent only a small component (<5%). Most minerals have glassy jackets indicating a volcanogenic origin, but some are abraded and lack adhering glass. Plagioclase feldspar is the most abundant phase (c. 90% of minerals) and occurs in all tuffs, with minor amounts of quartz. Ferromagnesian phases and zircon are rare (<10% of minerals), while titanomagnetite is absent from all but c. 5% of the tuffs. The rarity of the latter probably reflects removal by hydraulic sorting.

CaSiO$_3$
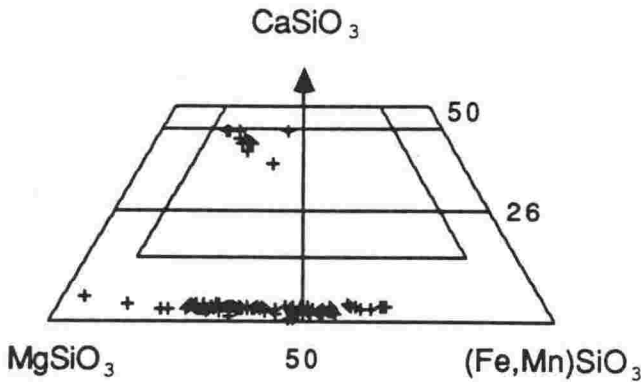
Fig. 8 Composition of pyroxenes (*n*= 98) from middle Pleistocene tuffs plotted on part of the Mg- Ca- (Mn,Fe) triangle.

Of the ferromagnesian phases, orthopyroxene occurs in all tuffs with mafic components and is nearly always the dominant phase. Green amphibole occurs in 80% of the tuffs and clinopyroxene in c. 50%. Biotite is present in c. 33% of the samples and is most abundant in tuffs whose glass chemistry is characterised by high K$_2$O content with the Na/K ratio <1.0. The mineral assemblages are typical of rhyolitic eruptives of the TVZ (Ewart 1966). The relative proportions of the phases are not detailed, because some phases show a high degree of dissolution, and hydraulic sorting has occurred.

Pyroxene chemistry

Ninety-eight pyroxene crystals from 12 tuffs were analysed using the electron microprobe (Fig. 8). No significant zoning was detected. Of the 86 orthopyroxenes analysed (En$_{33-95}$), most are hypersthene or ferrohypersthene. In addition, a small, but significant group (14%) of bronzite compositions and one enstatite occur. Individual tuffs display wide ranges (up to 60%) in En composition (Table 3), and variation within tuffs is usually greater than between tuffs. The 12 clinopyroxenes analysed are all augites and generally display a narrow range in composition (Fig. 8, Table 3).

Primary orthopyroxenes in rhyolitic tephras from TVZ, of similar glass composition to tuffs examined here, are hypersthene and ferrohypersthene (En$_{30-60}$). More Mg-rich phases (e.g., bronzite) in rhyolitic tephras have been attributed to andesitic contamination, either syneruption or posteruption (Ewart et al. 1975; Roxborgh 1976; Froggatt & Rogers 1990). A similar origin is proposed here for the occurence of Mg-rich pyroxenes, and is consistent with the presence of intermediate brown glasses. The small proportion of intermediate glasses relative to Mg-rich pyroxenes may reflect the rapid weathering of the former.

Amphibole chemistry

Only six amphibole crystals were analysed. All are calc-amphiboles and are either magnesio- or ferrohornblendes. Their compositions are typical of hornblendes from rhyolitic tephras (see Roxborgh 1976; Froggatt & Rogers 1990).

Table 2 Brown and clear-glass analyses from tuff S065 (Kahuki section) determined by electron microprobe (for method see Froggatt 1983). Analyses are recalculated to 100% on a water-free basis. Water by difference. All Fe as FeO. Clear-glass analyses represent mean and standard deviation. *n*, number of shards.

	Clear-glass	Brown glass				
	1	2	3	4	5	6
SiO$_2$	75.48 (0.17)	72.72	67.75	65.62	63.98	59.29
Al$_2$O$_3$	13.21 (0.08)	12.12	14.80	13.13	14.83	17.24
TiO$_2$	0.18 (0.03)	1.11	0.93	1.21	1.03	1.53
FeO	1.97 (0.14)	4.19	4.70	6.84	6.18	7.10
MgO	0.10 (0.02)	0.27	1.17	2.26	2.22	2.52
CaO	0.98 (0.04)	1.39	3.66	4.18	5.28	4.49
Na$_2$O	4.19 (0.13)	3.64	4.08	3.70	4.03	4.49
K$_2$O	3.74 (0.12)	4.34	2.84	3.06	2.34	1.97
Cl	0.17 (0.02)	0.23	0.06	0.00	0.10	0.17
Water	2.75 (0.82)	3.20	6.65	2.09	1.31	7.45
n	9	1	1	1	1	1

Table 3 Typical electron microprobe core analyses on pyroxene crystals from a middle Pleistocene tuff (S102, Mangatewaiiti).

	Orthopyroxene			Clinopyroxene	
SiO$_2$	48.83	50.86	53.30	52.17	52.85
Al$_2$O$_3$	0.44	3.63	0.96	2.46	1.59
TiO$_2$	0.18	0.36	0.13	0.47	0.47
FeO	33.33	21.67	18.88	8.02	9.54
MnO	1.52	0.54	0.46	0.25	0.38
MgO	12.35	20.92	24.41	14.57	14.40
CaO	1.50	1.38	1.21	21.23	20.78
Na$_2$O	–	–	–	0.37	0.29
K$_2$O	–	–	–	–	–
Total	98.16	99.36	99.35	99.54	100.30
Sum of cations on the basis of 6 (O):					
	4.00	4.00	4.01	4.00	4.00

Or
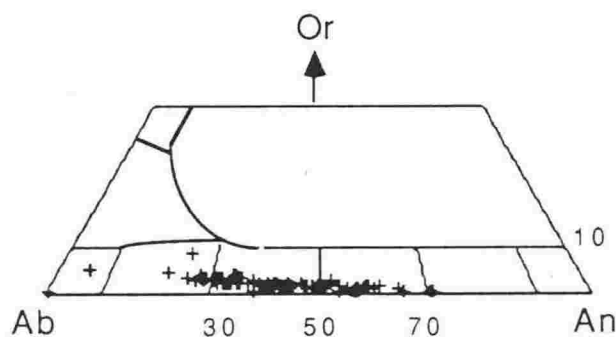
Fig. 9 Composition of plagioclases from middle Pleistocene tuffs plotted on an orthoclase, anorthite and albite (Or-An-Ab) ternary diagram.

Plagioclase chemistry

Some 126 plagioclase crystals from 11 tuffs were analysed. Core compositions range from An_{2-73} but most classify as either andesine or labradorite (Fig. 9). The crystals are mostly normally zoned. Individual crystals have ranges in An up to 15%, but usually <10%. Differences between crystal core compositions within a tuff are generally greater (typically An_{25-65}) (Table 4). Ewart & Taylor (1969) reported primary plagioclase compositions from TVZ as: rhyolitic (An_{28-46}), dacitic (An_{53}), and andesitic (An $_{68-81}$). Froggatt & Rogers (1990) have detected mixed plagioclase populations with some tephras containing a rhyolitic andesine group (An_{33-46}) and an andesitic labradorite (An_{55-72}) and bytownite (An_{78-81}) group.

Calcic plagioclases (labradorite and bytownite) in the tuffs examined here are also most likely contaminants from intermediate eruptives and could easily be explained as posteruption sedimentary mixing.

DISCUSSION

Paleoenvironment

Sections of the Mangatarata, Mangahao, and Takapari Formations examined show a transition from an estuarine setting to a lowland distal braid-plain with lakes, on both sides of the present-day Main Axial Ranges shortly before the Jaramillo Subchron (Fig. 2). This was accompanied by a major influx of volcaniclastic sediments, which contributed to sedimentary infilling and thus a change to nonmarine conditions. The same phase of volcanism is recorded throughout the Wanganui Basin to the west (Seward 1974). The similarity in

Table 4 Representative electron microprobe core analyses on plagioclase crystals from a middle Pleistocene tuff (S136, Oroua).

SiO_2	51.00	58.38	58.36	58.83	61.15
Al_2O_3	30.72	25.40	25.64	24.45	23.62
FeO	0.57	0.14	0.20	0.19	0.23
CaO	13.84	8.21	7.98	6.62	5.79
Na_2O	4.00	6.90	7.02	7.69	8.07
K_2O	0.14	0.28	0.41	0.46	0.54
Total	100.27	99.33	99.61	98.24	99.40
An%	65	39	38	31	28
Sum of cations based on 32 (O):					
	20.11	20.01	20.05	20.08	20.02

facies and timing of facies changes on both sides of the present ranges suggests that, shortly before and during the Jaramillo Subchron, the region (Fig. 1) behaved as a single basin or series of closely connected basins. This would require at least parts of the Main Axial Ranges to be absent or of low relief at that time.

The occurence of conglomerates (Fig. 3) and unconformities in late Cenozoic strata in Hawke's Bay indicates pulses of uplift and erosion extending from the Miocene to late Pleistocene (Lillie 1953; Kingma 1971). However, the middle Pleistocene greywacke conglomerates differ from those on late Pleistocene (last 0.1 Ma) terraces that unconformably overlie the former. Conglomerates in the study sequences are thin (<3 m) and generally have a maximum clast size of 40 mm, while those of the late Pleistocene can be up to 20 m thick with maximum clast sizes up to 500 mm. This implies greatly increased relief in the late Pleistocene. In addition, facies of the middle Pleistocene are typified by conformable sequences of predominantly fine grained fluviolacustrine sandstone and mudstone. Late Pleistocene facies are entirely coarse alluvium deposited on a series of uplifted terraces. The change in facies reflects a change in tectonic regime and greatly increased uplift. The presence of Nukumaruan limestone at high elevation in parts of the ranges confirms significant uplift in the last 1 Ma (Beu et al. 1981).

Middle Pleistocene tuffs in Hawke's Bay are thick (up to 30 m), coarse grained (up to 70 mm sized clasts), and contain charcoal, indicative of derivation from ignimbrites. Sedimentary structures indicate fluvial transport to sites up to 200 km from the nearest volcanic centres (TVZ). These features would require a paleorelief towards the East Coast of North Island from the TVZ and across the present Main Axial Ranges. The coarseness of pumice in the tuffs, and the presence of charcoal, which would not be expected to survive great distances in a coarse fluvial system, suggests derivation from proximal volcanic deposits. Therefore, ignimbrites travelled to catchment areas in the Hawke's Bay. This is confirmed by the presence of two middle Pleistocene (c. 0.91 and 0.70 Ma) ignimbrite flow units at Cape Kidnappers (Black 1990). Thus, substantial transport routes through the ranges were present at least as recently as middle Pleistocene.

In the last perhaps 0.50 Ma, the Main Axial Ranges have been a barrier to volcanic and volcaniclastic transport to the East Coast. At present, the main drainage routes from the TVZ are to the north via the Waikato River and to the southwest via the Wanganui and allied rivers. Large ignimbrite-producing eruptions (rock volumes >300 km³) have occured in the last 0.50 Ma (Wilson et al. 1984), however related flow units and reworked deposits of comparable size to those of the Mangatarata Formation are not present in Hawke's Bay. This suggests such eruptions where not capable of flowing over ranges in excess of 1700 m height and up to 50 km from calderas. Thus, Matuyama Reversed Chron eruptions were either significantly more violent than more recent eruptions, allowing transport over the ranges, or much of the uplift has been post c. 0.91 Ma.

Volcaniclastic sedimentation and comparison to other volcanic settings

Middle Pleistocene volcaniclastic sequences in North Island compare closely to distal (>100 km from source) Neogene facies surrounding the Cascade Range of North America, where sedimentation was largely in response to explosive

volcanism (Smith 1987, 1988). The Neogene Deschutes Formation in Oregon and the late Miocene Ellensburg Formation in Washington consist of poorly sorted debris flows, hyperconcentrated flows, and scour and fill deposits, which form an apron surrounding volcanoes close to source (<50 km) (Smith 1987, 1988). Further from source (>100 km), debris flows became increasingly dilute as normal fluvial braid-plain processes dominated and relief was more subdued. These latter facies are typified by trough cross bedded pumiceous sandstone and overbank sandstone and mudstone, often highly pedogenically altered. Planar laminated mudstone, considered lacustrine, is also common. In distal settings of the Ellensburg Formation, these sandstone and mudstone facies represent c. 50% and 40% of the sequences (Smith 1988). These distal facies are very similar to those of the Mangatarata and Takapari Formations (Fig. 3).

Smith (1988) noted inter-eruption facies are dominated by clast-supported conglomerates of normal fluvial bedloads, while syneruption facies are typified by sheets of pumiceous sandstones and debris flows bound by paleosols. The change in facies is a response to a massive influx of volcaniclastic sediment. This provides an analogy for the Mangatarata Formation where coarse ash and lapilli, often bound by paleosols, is interbedded with mainly fine grained lacustrine mudstone and occasional fluvial conglomerates.

Following the facies code of Smith (1987), tuffs represent Facies association 1 (fluvial channel deposits) typified by Gm, Sp, and Sh(l) facies (Fig. 4). The long, intervening, non-volcaniclastic mudstone/sandstone units represent Facies association 2 (floodplain deposits) dominated by Fm and Fl facies (Fig. 3, 4). These associations, along with the lack of debris flow and poorly sorted coarse facies, point to a more distal river setting relative to the volcanic source, which is consistent with their distance relative to the TVZ (Fig. 1).

Although distal volcaniclastic facies of the Mangatarata Formation were dominated by fluvial processes, the tuffs display primary sedimentary structures and secondary deformation which reflect periods of abnormal vertical accretion (10 m scale) and rapid deposition (Fig. 4). This led to rapid channel migration and deposition in overbank settings. Debris incorporated into the tuffs indicate highly erosive paleocurrents and high discharge rates. Thus, tuff-emplacement events are considered to represent catastrophic floods. The result is a pattern of sedimentation which is highly episodic, being marked by the alternation of tuffs with paleosols and lignites, reflecting the establishment of vegetation between periods of rapid volcaniclastic aggradation. A similar sedimentation pattern is recorded in the peripheral formations of the Cascade Range (Smith 1987, 1988). Therefore, volcanism had a major influence on the depositional system at least up to 100–200 km from volcanic centres.

The tuffs in the study sequences commonly consist of a dominant glass population (amongst other minor groups), which is different from that of the previous tuff in the sequence. This suggests many major tuff-emplacement events were associated with a new influx of pyroclastic material following an eruption, and supports the inference that rapid vertical accretion was in response to volcanism.

Volcanism

Compositional diversity displayed by the tuffs in this study provides insight to the nature of mid-Pleistocene volcanism in the TVZ. About 98% (by volume) of known late Pleistocene volcanics in the TVZ are calc-alkaline rhyolites, mainly in the form of ignimbrites (Cole 1979). This is comparable to the abundance of rhyolitic compositions (c. 99%) in middle Pleistocene tuffs and suggests volcanism during this period was dominated by explosive rhyolitic eruptions. The presence of basaltic andesite, andesitic and dacitic shards (Fig. 5), and of magnesian and calcic minerals in the tuffs (Fig. 8, 9) indicate intermediate volcanoes were active but subordinate in the same volcanic region during this period. The total chemical diversity shown by the tuffs (Fig. 5) is similar to that displayed by late Pleistocene lavas and tephra in the TVZ (e.g., Cole 1979) and point to a similar style in volcanism and petrogenesis.

Linear differentiation trends displayed by brown shard analyses (Fig. 7) show the compositions are controlled by similar petrogenic processes, consistent with a common source region. Clear glasses occur on the silicic end of such trends (e.g., Fig. 7C) and presumably reflect similar processes. No chemical trends as a function of time are evident in the tuff sequences, and individual tuffs show no evidence of chemical zonation (Fig. 6). This is also true of the latest period (last 50 ka) of rhyolitic volcanism in the TVZ (Dunbar et al. 1989b). Presumably a thin, weak crust in the TVZ precludes the formation of large, high-level magma chambers capable of significant magma evolution (Wilson et.al. 1984); instead, small, frequent eruptions of homogeneous magmas result.

Implications for tephrochronology

Many tephrochronological studies use chemical characterisation of tuffs for correlation purposes, and bulk samples or various components of tuffs for radiometric dating (for a summary see Westgate & Gorton 1981). It has been shown here that chemical heterogeneity within tuffs is common in fluvial and terrestrial settings. Over half the tuffs examined consist of multiple rhyolitic glass populations. Most tuffs also contain chemically diverse brown glasses. These features mean chemical characterisation using bulk samples of tuff are of little value because they do not represent a single eruption composition. Even when using grain-specific methods (e.g., microprobe), many shards must be analysed to fully characterise the deposits, some of which contain no volumetrically dominant chemical population of shards. Mineral assemblages in these tuffs are also chemically diverse and have been derived from a variety of intermediate and acidic eruptives. This imposes limitations on radiometric dating, and precludes the use of bulk samples.

Most of the tuffs in this study have been emplaced by fluvial processes, and their distribution is therefore limited to a single floodplain compared to airfall deposits which can mantle large areas. The eruptive events recorded in a sequence reflect the location of the catchment relative to the volcanic source. Therefore, different tuffs are found in different sections, and fewer correlations can be made than would be expected from airfall deposits.

assisted in various stages of the fieldwork. An Internal Research Grant from VUW supported part of the fieldwork.

REFERENCES

Black, T. M. 1990: Paleomagnetism and tephrostratigraphy of the Kidnappers Group, Hawkes Bay, New Zealand. Unpublished B.Sc. (Hons) project, lodged in the Library, Victoria University of Wellington.

Beu, A. G.; Browne, G. H.; Grant-Taylor, T. L. 1981: New *Chlamys delicatula* localities in the central North Island and uplift of the Ruahine Range. *New Zealand journal of geology and geophysics 24*: 127–132.

Carey, S. N.; Sigurdsson, H. 1978: Deep sea evidence for distribution of tephra from the mixed magma eruption of the soufriere on St. Vincent, 1902: ash turbidites and airfall. *Geology 6*: 271–274.

Carter, R. M. 1972: Wanganui strata of Komako District, Pohangina Valley, Ruahine Range, Manawatu. *Journal of the Royal Society of New Zealand 2*: 293–324.

Cerling, T. E.; Cerling, B. W.; Curtis, G. H.; Drake, R. E.; Brown, F. H. 1978: Correlation of reworked ash deposits; the KBS tuff, northern Kenya. *United States Geological Survey open file report 78–701*: 61–63.

Cole, J. W. 1979: Structure, petrology and genesis of Cenozoic volcanism, Taupo Volcanic Zone, New Zealand—a review. *New Zealand journal of geology and geophysics 22*: 631–657.

Dunbar, N. W.; Hervig, R. L.; Kyle, P. R. 1989a: Determinations of pre-eruptive H_2O, F and Cl contents of silicic magmas using melt inclusions, examples from Taupo Volcanic Center, New Zealand. *Bulletin of volcanology 51*: 177–185.

Dunbar, N. W.; Kyle, P. R.; Wilson, C. J. N. 1989b: Evidence for limited zonation in silicic magma systems, Taupo Volcanic Zone, New Zealand. *Geology 17*: 234–236.

Ewart, A. 1966: Review of mineralogy and chemistry of the acidic rocks of the Taupo Volcanic Zone, New Zealand. *Bulletin volcanologique 29*: 147–172.

Ewart A.; Taylor, S. R. 1969: Trace element geochemistry of the rhyolitic volcanic rocks, central North Island, New Zealand: phenocryst data. *Contributions to mineralogy and petrology 22*: 127–146.

Ewart A.; Hildreth, W.; Carmichael, I. S. E. 1975: Quaternary acid magma in New Zealand. *Contributions to mineralogy and petrology 51*: 1–27.

Fleming, C. A. 1953: The geology of Wanganui subdivision. *New Zealand Geological Survey bulletin 52*.

Froggatt, P. C. 1983: Toward a comprehensive Upper Quaternary tephra and ignimbrite stratigraphy of New Zealand using electron microprobe analysis of glass shards. *Quaternary research 19*: 188–200.

Froggatt, P. C.; Rogers, G. M. 1990: Tephrostratigraphy of high altitude peat bogs along the axial ranges, North Island, New Zealand. *New Zealand journal of geology and geophysics 33*: 111–125.

Gosson, G. J. 1986: Miocene and Pliocene silicic tuffs in marine sediments of the East Coast Basin, New Zealand. Unpublished Ph.D. thesis, lodged in the Library, Victoria University of Wellington.

Grindley, G. W.; Oliver, P. J.; Seward, D. 1988: Stratigraphy, geochronology and paleomagnetism of ignimbrites in the Matahana Basin, New Zealand. *Geological Society of New Zealand miscellaneous publication 41a*: 71.

Hildreth, W. 1981: Gradients in silicic magma chambers: Implications for lithospheric magmatism. *Journal of geophysical research 86*: 10153–10192.

Kingma, J. T. 1971: Geology of Te Aute subdivision. *New Zealand Geological Survey bulletin 70*.

Le Maitre, R. W. 1984: A proposal by the IUGS subcommission on the systematics of igneous rocks for a chemical classification of volcanic rocks based on the total alkali silica (TAS) diagram. *Australian journal of earth science 31*: 243–255.

Lillie, A. R. 1953: The geology of Dannevirke subdivision. *New Zealand Geological Survey bulletin 46*.

Mankinen, E. A.; Donnelly, J. M.; Gromme, C. S. 1978: Geomagnetic polarity event recorded at 1.1 m.y. B.P. on Cobb Mountain, Clear Lake volcanic field, California. *Geology 6*: 653–656.

Miall, A. D. 1978: Lithofacies types and vertical profile models in braided river deposits: a summary. *Canadian Society of Petroleum Geologists memoir 5*: 597–604.

Neef, G. 1984: Late Cenozoic and early Quaternary stratigraphy of the Eketahuna district (N153). *New Zealand Geological Survey bulletin 96*.

Nelson, C. S.; Froggatt, P. C.; Gosson, G. J. 1986: Nature, chemistry and origin of late Cenozoic megascopic tephras in Leg 90 cores from the southwest Pacific. *In*: Kennett, J. P. et al. *ed*. Initial reports of the Deep Sea Drilling Project 9. Washington, United States Government Printing Office. Pp. 1161–1173.

Roxborgh, H. J. 1976: Lake Taupo late Pleistocene tephras, a petrochemical study. Unpublished M.Sc. thesis, lodged in the Library, Victoria University of Wellington.

Schlinger, C. M.; Smith, R. M.; Veblen, D. R. 1986: Geologic origin of magnetic volcanic glasses in the KBS tuff. *Geology 14*: 959–962.

Seward, D. 1974: Age of New Zealand Pleistocene substages by fission track dating of glass shards from tephra horizons. *Earth and planetary science letters 24*: 242–248.

————1979: Comparison of zircon and glass fission track ages from tephra horizons. *Geology 7*: 470–482.

Shane, P. A. R. 1989: The characterisation and correlation of late Cenozoic tuffs, southeastern North Island, New Zealand. Unpublished M.Sc. thesis, lodged in the Library, Victoria University of Wellington.

Shane, P. A. R.; Froggatt, P. C. 1991: Glass chemistry, paleomagnetism and correlation of middle Pleistocene tuffs in southern North Island, New Zealand, and Western Pacific. *New Zealand journal of geology and geophysics 34*: 203–211.

Smith, G. A. 1987: The influence of explosive volcanism in fluvial sedimentation: The Deschutes Formation (Neogene) in Central Oregon. *Journal of sedimentary petrology 57*: 613–629.

————1988: Sedimentology of proximal to distal volcaniclastics dispersed across an active fold belt: Ellensburg Formation, Central Washington. *Sedimentology 35*: 953–977.

Westgate, J. A; Gorton, M. P. 1981: Correlation techniques in tephra studies. *In*: Self, S.; Sparks, R. S. J. *ed*. Tephra studies. Riedel, Dordrecht. Pp. 73–94.

Wilson, C. J.; Rogan, A. M.; Smith, I. E.; Northey, D. J.; Nairn, I. A.; Houghton, B. J. 1984: Caldera volcanoes of the Taupo Volcanic Zone, New Zealand. *Journal of geophysical research 89*: 8463–8484.

6.3 COMPOSITION OF WIDESPREAD VOLCANIC GLASS IN DEEP-SEA SEDIMENTS OF THE SOUTHERN PACIFIC OCEAN: AN ANTARCTIC SOURCE INFERRED

(reprinted from Bulletin of Volcanology (1992) 54: 595-601)

In this paper, P. Froggatt provided the samples, and the analyses of tephra zones F1, F2 and G.

Composition of widespread volcanic glass in deep-sea sediments of the Southern Pacific Ocean: an Antarctic source inferred

Philip AR Shane and Paul C Froggatt

Research School of Earth Sciences, Victoria University of Wellington, P. O. Box 600, Wellington, New Zealand

Abstract. Widespread Plio-Pleistocene (2.43–0.06 Ma) tephra zones recognised in deep-sea cores from high latitudes (>60°) in the Southern Pacific Ocean were thought to have originated from calc-alkaline rhyolitic eruptions in New Zealand, some 5000 km distant. Electron microprobe analyses of the glasses reveal a wide diversity of alkalic felsic compositions, as well as minor components of basic and intermediate glasses, incompatible with a New Zealand Neogene source but similar to contemporaneous eruptives from the Antarctic region. Most tephra zones are trachytic; seven zones are peralkaline rhyolite. The rhyolitic zones represent a deep-sea record of widespread silicic eruptions from continental Antarctica, possibly Marie Byrd Land. The extent of these rhyolitic zones suggest a greater frequency of large explosive eruptions in Antarctica than previously documented. The coarse grain size of some of the shards (up to 3 mm), their great distance from the closest sources (>1600 km for some cores), and the presence of nonvolcanic ice-rafted debris indicate some of the glasses, especially the more basic compositions, may have been ice-rafted, contrary to previous suggestions of a fallout origin.

Introduction

Hydraulic piston cores of sediments collected during cruises of the vessel *Eltanin* in the Southern Pacific (Fig. 1) contain numerous zones of volcanic glass dispersed in Plio-Pleistocene calcareous and siliceous abyssal oozes. Zones of higher glass concentration have been recognised and were correlated between cores over distances of ca. 4000 km (Huang et al. 1975). These Southern Pacific Tephra Zones (SPTZ) have been used in a variety of studies including paleoexplosivity and eruption column height calculations (Huang et al. 1973, 1975; Shaw et al. 1974; Huang and Watkins 1976).

Correspondence to: P Shane
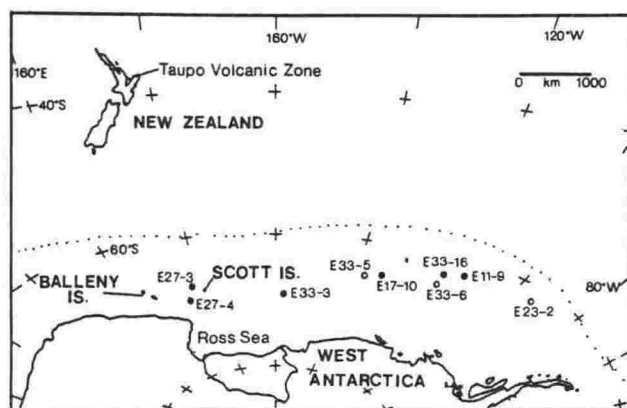
Fig. 1. Location of *Eltanin* cores containing Southern Pacific tephra zones. Core localities from which samples were examined (Table 1) are shown as *solid dots*. *Dotted line* represents the extent of ice sheets during the last glacial maximum (CLIMAP 1976)

Originally, the Balleny Islands had been considered the volcanic source, as the tephra zones appeared to decrease in thickness and grain size away from the islands. Later, Kyle and Seward (1984) proposed the Taupo Volcanic Zone in New Zealand as the source, on the basis of chronology and the composition of some of the tephra zones, which they considered to be calc-alkaline. New Zealand is the nearest region of explosive calc-alkaline eruptions in the Southern Pacific. Volcanoes of the Balleny Islands (Johnson et al. 1982) and Ross Sea and Western Antarctica (e.g Kyle 1990; LeMasurier 1990) are alkalic and dominated by intermediate and basic eruptives.

Previously little was known about the chemical nature of the glasses in the Southern Pacific. Huang et al. (1975) determined refractive indices of the glasses, which indicated they are highly silicic. Kyle and Seward (1984) presented ten shard analyses from three tephra zones and interpreted them to be calc-alkaline rhyolites on the basis of their low alkali contents. Froggatt et al. (1986) analysed shards from a young tephra zone (F) and showed many were phonolitic or trachytic. To fully

characterise the SPTZs, to test correlations between cores and to determine their source provenance, a more comprehensive analysis of glass shards was undertaken. Evidence presented here shows the Taupo Volcanic Zone in New Zealand can be ruled out: Antarctica and/or the Balleny Islands are more likely source areas for the tephra zones.

Samples and method

Thirty tephra zones in nine cores form the Southern Pacific Ocean have been recognised (Huang et al. 1975). Twenty-six samples from six cores, which have good magneto- and bio-stratigraphic age control, were selected from intervals where glass shards are most abundant (Table 1). Each sample is composed of dispersed glass shards in either fine terrigenous-glacial or siliceous ooze. They were sieved and magnetically separated to obtain shards greater than 60 µm, which is the most convenient size for electron microprobe analyses. The non-glassy components greater than 60 µm included siliceous and calcareous fossil fauna and flora, feldspar, quartz and igneous rock fragments. The free mineral phases are commonly euhedral but lack adhering glass; thus it is difficult to determine whether they represent primary volcanic phenocrysts. The high abundance of granitic rock fragments composed of feldspar and quartz suggests the free crystals may have a common detrital origin. Most of the terrigenous rock fragments are highly angular and up to 10 mm in size, and are probably ice-rafted debris. Foraminiferal assemblages were

Table 1. Southern Pacific Tephra Zones, ages and sample intervals from *Eltanin* cores containing glasses analysed in this study

Zone	Age	Depth in core (cm)					
		E27-3	E27-4	E11-9	E17-10	E33-3	E33-16
G	>0.06					0– 6	111
F2	0.38		158		204–206	92–94	
F1	0.44						
E4	0.87		622– 628				300
E3	0.98	602– 608					
E2	1.04	647– 653					
E1	1.09		812– 818				
D5	1.29		977– 983				
D2	1.56	870– 875					
C3	1.69	947– 953	1337–1343				
C2	1.76	997–1003		1162–1168			927–933
C1	1.84	1032–1038	1452–1458	1192–1198			947–953
B3	2.00	1122–1128					
B1	2.06	1152–1158					
A3	2.33	1292–1298					
A2	2.39			1512–1518			
A1	2.43	1347–1353					

Tephra zone name follows Huang et al. (1975)
Ages (Ma) determined from sedimentation rate based on paleomagnetism (Huang et al. 1975) and correlated for revised time scale following Kyle and Seward (1984)

Table 2. Standards, precision and detection limits for electron microprobe analyses (EMA) of glass in this study. EMA compositions represent a mean and standard deviation

	KN-18		VG-A99		
	EMA	1	EMA	2	DL
SiO_2	74.95(0.37)	74.60	50.80(0.30)	50.94	0.07
Al_2O_3	10.42(0.23)	10.53	12.28(0.25)	12.49	0.06
TiO_2	0.17(0.04)	0.18	4.15(0.12)	4.06	0.07
FeO	3.40(0.16)	3.45	13.23(0.31)	13.30	0.11
MgO	0.02(0.02)	0.01	5.03(0.12)	5.08	0.06
CaO	0.15(0.05)	0.15	9.19(0.20)	9.30	0.05
Na_2O	5.29(0.32)	5.68	2.81(0.14)	2.66	0.09
K_2O	4.45(0.14)	4.39	0.82(0.04)	0.82	0.05
Cl	0.31(0.05)	0.37	—	—	0.05
Total	99.15(0.51)	99.36	98.30(0.65)	98.65	
n	30		34		

KN-18: comenditic obsidian, Naivasha, Kenya
VG-A99: basaltic glass, Makaopuhi, Hawaii (USNM 113498/1)
1: analysis from Nielsen and Sigurdsson (1981)
2: analysis from Jarosewich et al. (1980)
DL, typical detection limit; n, number of analyses

Table 3. Electron microprobe analyses of glasses from SPTZs in *Eltanin* cores. Analyses are recalculated to 100%. Multiple analyses represent means and standard deviations. Shards are grouped to give an average composition of a particular tephra zone and do not imply they are products of a single eruption

	1	2	3	4	5	6	7	8
SiO_2	42.87	47.66	53.23	58.61	58.80	63.94 (3.42)	64.08 (2.33)	64.85 (0.44)
Al_2O_3	15.87	16.12	18.02	19.07	14.95	16.30 (0.82)	15.93 (1.02)	14.47 (0.36)
TiO_2	5.13	4.01	1.59	0.22	1.24	0.51 (0.18)	0.31 (0.09)	0.65 (0.10)
FeO	12.11	13.86	9.46	4.91	6.82	4.70 (0.99)	5.72 (0.65)	7.71 (0.44)
MgO	5.15	4.38	2.13	0.12	2.86	0.56 (0.07)	nd	0.26 (0.08)
CaO	12.01	9.27	5.84	1.03	6.06	2.62 (2.46)	1.21 (0.32)	1.34 (0.25)
Na_2O	4.82	3.28	6.16	10.37	5.30	6.28 (0.36)	7.57 (0.98)	5.81 (0.32)
K_2O	1.93	1.42	3.40	5.15	3.84	4.94 (0.59)	4.97 (0.11)	4.48 (0.12)
Cl	0.11	nd	0.17	0.52	0.13	0.29 (0.10)	0.21 (0.09)	0.13 (0.04)
Total	98.38	97.37	98.12	98.24	99.51	95.31 (2.49)	96.60 (0.90)	98.01 (0.99)
PI				1.17		0.96	1.12	1.02
n	1	1	1	1	1	8	9	4

	9	10	11	12	13	14	15
SiO_2	65.09 (0.43)	66.05 (0.95)	73.89	74.21	75.77 (2.02)	76.31 (0.71)	76.54 (0.80)
Al_2O_3	14.94 (0.13)	14.96 (0.33)	7.66	8.58	11.27 (0.73)	11.90 (0.51)	11.39 (0.74)
TiO_2	0.71 (0.05)	0.37 (0.03)	0.24	0.21	0.20 (0.10)	0.10 (0.20)	0.15 (0.06)
FeO	7.43 (0.35)	5.42 (0.32)	5.98	6.12	2.84 (1.17)	1.86 (0.19)	2.31 (0.68)
MgO	0.29 (0.04)	0.10 (0.04)	nd	0.06	nd	nd	0.06
CaO	1.25 (0.17)	1.50 (0.17)	0.11	0.28	0.26 (0.13)	0.22 (0.03)	0.25 (0.05)
Na_2O	5.37 (0.31)	6.07 (0.38)	7.47	5.98	5.04 (0.49)	4.84 (0.31)	4.71 (0.19)
K_2O	5.13 (0.16)	5.41 (0.13)	4.09	4.29	4.44 (0.24)	4.43 (0.33)	4.48 (0.21)
Cl	0.18 (0.06)	0.18 (0.02)	0.57	0.27	0.22 (0.08)	0.24 (0.06)	0.18 (0.03)
Total	98.70 (0.54)	96.40 (0.99)	94.59	95.55	94.90 (1.16)	95.25 (1.55)	95.21 (0.82)
PI	1.16	1.06	2.19	1.69	1.16	1.27	1.10
n	9	5	1	1	10	8	10

1, basanitic shard, E3, E27-3, *2,* basaltic shard, E2, E27-3, *3,* basaltic trachyandesite shard, E3, E27-3, *4,* phonolitic shard, B1, E27-3, *5,* trachyandesitic shard, E3, E27-3, *6,* trachytic shards, C3, E27-3, *7,* trachytic shards, D5, E27-4, *8,* trachytic shards, F2, E33-3, *9,* trachytic shards, G, E33-3, *10,* trachytic shards, D5, E27-4, *11,* rhyolitic shard, D5, E27-4, *12,* rhyolitic shard, D2, E27-3, *13,* rhyolitic shards, C1, E11-9, *14,* rhyolitic shards, C2, E33-16, *15,* rhyolitic shards, C1, E27-2; *nd,* not detected; *PI,* Peralkaline Index (molar $Na_2O + K_2O/Al_2O_3$); *n,* number of analyses

examined and consist almost entirely (>90%) of the sinistrally coiled planktonic species *Neogloboquadrina pachyderma* indicating cold water conditions.

About 75% of the glasses examined are colored, mainly reddish brown to black, but a few are grey or green. These colored glasses are highly vesicular or pumiceous. Maximum shard size is about 3 mm, but most are less than 300 µm. Colorless glasses are finer than colored glasses and have bubble-wall morphologies (cuspate remnants of vesicle walls). They are abundant only in ash zones C, E1 and F.

About ten shards from each sample were analysed using the JEOL 733 electron microprobe at the Analytical Facility of Victoria University, with a current of 8 nA at 15 kV and a 20-µm beam diameter to minimise the loss of Na. Glass standards and analytical detection limits are given in Table 2. All shards analysed were vitreous and isotropic, and no sign of alteration was evident in transmitted or reflected light. Totals are less than 100%, mainly due to hydration (e.g. Froggatt 1983). The compositions we obtained (Table 3) are typical of alkalic glasses and rocks analysed elsewhere (e.g. Bowden 1974; Palais et al. 1988), indicating no significant exchange of more mobile elements between the glasses and ocean water or sediments. A complete list of analyses is available from the authors on request.

Glass chemistry

A wide diversity of chemistries was found in the SPTZs (Fig. 2, Table 3), all of which are alkalic. Of the 235 shards analysed, 60% are rhyolitic, 34% trachytic and the rest are intermediate to basic alkalic compositions (Fig. 2). Tephra zones C1, C2, C3, E1, B3, F2 and G consist of mainly rhyolitic shards and together these zones contain 89% of rhyolitic shards analysed. The other 13 tephra zones examined contained few or no rhyolitic shards and are mainly trachytic. Thus rhyolites are not the most common type in the Southern Pacific (c.f. Huang et al. 1975). The more common trachytic glasses are dark-colored with Peralkaline Indices (PI) (molar $Na_2O + K_2O/Al_2O_3$) of 0.92–1.20 and SiO_2 contents in the range 58–69 wt %. Most compositions have Na/K ratios >1. Rhyolitic glasses display higher Na_2O and K_2O contents (>4.00 wt %) compared to calc-alkaline glasses of middle Pleistocene Taupo Volcanic Zone tephras (Fig. 2). The SPTZ rhyolites have higher PIs
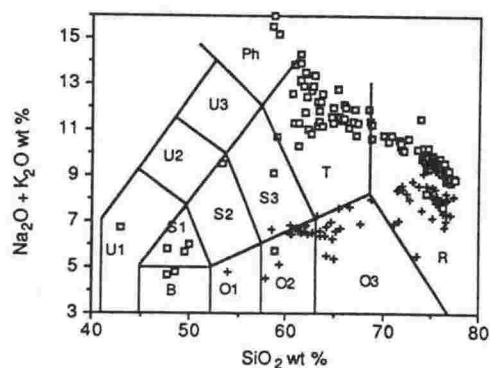
Fig. 2. Individual shard analyses from SPTZs (*squares*) plotted on a total alkali-silica diagram (after Le Bas et al. 1986). A representative range of contemporaneous Taupo Volcanic Zone (*TVZ*) glasses (*crosses*) is shown for comparison (from Shane 1991)
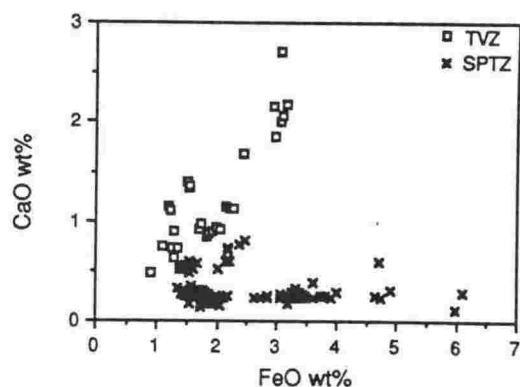
Fig. 3. SPTZ and representative Taupo Volcanic Zone (*TVZ*) rhyolitic glasses plotted on a FeO vs CaO diagram, showing clear separation and different trends of each type

Fig. 4A–C. Examples of the compositional diversity of glasses within SPTZs. *Lines* represent possible compositional trends. **A** Four different SPTZs. All shards in E4 and some of those in D2 define linear trends. Shards in B1 and D5 form groups or are heterogeneous. **B** Analyses of layers assigned to tephra zone C1 (Eltanin Ash) by Huang et al. (1975) in four cores. **C** Analyses of layers assigned to tephra zone F2 by Huang et al. (1975) in three cores

(0.93–2.19, mostly 1.20) than Taupo Volcanic Zone glasses (0.84–0.87) and are peralkaline. Glasses from the Southern Pacific display high FeO and very low CaO (< 0.4 wt %) and low MgO (< 0.05 wt %) contents compared to Taupo Volcanic Zone rhyolitic glasses (Fig. 3) and are similar to pantelleritic and comenditic glasses (e.g. Bowden 1974).

Most SPTZs display a great diversity in compositions, often with SiO_2 ranges > 15 wt % within a sample (Fig. 4). Fifteen of the 26 samples analysed have shards that plot in more than one compositional classification, using the scheme of Le Bas et al. (1986). The most common compositional range is trachyte to rhyolite, which was found in ten of the samples (e.g. Fig. 4A). A few samples contain a wider compositional range, including basaltic shards in addition to trachytic and rhyolitic shards. Linear compositional trends are evident in some of the SPTZs, but most also contain shards that plot away from such trends, either forming groups or being scattered (Fig. 4). A linear compositional trend could result from the eruption of a zoned magma chamber. However, groups of compositionally distinct shards and compositions that are scattered on variation diagrams probably represent different eruptions.

Mixing of different eruptive products could occur via bioturbation in sediments after deposition, especially in slow sedimentation environments such as the deep-sea. Different eruptive products could also be mixed by ice-rafting. Extended ice sheets around Antarctica during glacial periods (CLIMAP 1976) could receive fallout from several eruptions over a period of time and from different volcanoes as the ice sheets move. The ice sheets could then carry the tephra to *Eltanin* core sites and deposit it by melting. It is possible that both of these factors and magma zonation have contributed to the chemical diversity in the samples. If the SPTZs were em-

placed via ice-rafting, as we suggest below, then this mechanism would have been a very important factor controlling chemical diversity, especially for very heterogeneous tephra zones.

Between core correlations

Analysis of the glass shards allows us to test correlations of the tephra zones between cores. Tephra zone C has the highest abundance of glass in the Southern Pacific. This zone has been correlated between a number of cores and named the Eltanin Ash (Huang et al. 1975). Analyses of shards from layers correlated as this zone show chemical heterogeneity both within and between cores (Fig. 4B). Two compositional trends are evident in this tephra zone, possibly representing two different eruptions. In addition, a number of shards plot between these trends, especially in core E33-16, and may represent another eruptive event (Fig. 4B).

In two cores (E17-10 and E33-3), some shards from tephra zone F2 form diverging compositional trends, while shards assigned to F2 from a third core (E27-4) plot as groups away from these trends (Fig. 4C). Such chemical diversity implies multiple sources. Thus some of the SPTZs correlated between cores by Huang et al.(1975) do not represent single, instantaneous eruptions, but instead represent concentrations of tephra from multiple events. The chemical diversity of glass within a tephra zone and between zones of similar age limits the potential of these zones for widespread correlation.

Volcanic sources

The eruptive history of the Taupo Volcanic Zone in the last 0.5 Ma is reasonably well established, and compositions are well known (e.g. Cole 1979; Froggatt 1983; Wilson et al. 1984). However, the late Pliocene to middle Pleistocene silicic eruptive history has received less attention. Recently, glasses in numerous tephras ranging from 1.80 to 0.5 Ma in age, from localities 100 to 1000 km from source, have been analysed by electron microprobe (Froggatt 1983; Froggatt et al. 1986; Nelson et al. 1986; Shane and Froggatt 1991; Shane 1991). The tephras come from a variety of sedimentary environments, including deep-sea cores, and include all of those radiometrically dated and reported by Kyle and Seward (1984). Glasses from these tephras are high-SiO_2 calc-alkaline rhyolites, and <2.0% consist of calc-alkaline intermediate and basic compositions. Late Pleistocene lavas and ignimbrites of the Taupo Volcanic Zone display an identical compositional range (e.g Cole 1979). These compositions are distinctly different from those of the SPTZs (Fig. 3), which are alkalic, and indicate that the Taupo Volcanic Zone could not have been the source region.

Chemical analyses of rhyolitic glasses from the Southern Pacific reported by Kyle and Seward (1984) differ from those presented here (Table 3), particularly in their very low Na_2O contents (<1.6 wt %). This led to the interpretation that the glasses were calc-alkaline. However, such Na_2O values are atypical of rhyolites and may have resulted from volatilization of Na under the electron beam during analysis. We found a wider range of glass compositions (SiO_2 42–77 wt %) than Kyle and Seward (1984) (SiO_2 69–79 wt %), but this was probably due to the larger number of analyses we performed and the number of different zones we obtained the samples from.

The compositions of the SPTZs (Fig. 2) are similar to compositions reported from late Cenozoic alkalic volcanoes of the Balleny Islands, Scott Island, Ross Sea and Western Antarctica (LeMasurier and Thomson 1990). Rocks from the Balleny Islands are poorly dated, but are known to include basalt, trachybasalt and basanite, and those of the nearby Scott Island include mugearite and phonolite (Johnson et al. 1982). These volcanoes could have been sources for the non-rhyolitic glasses, especially in cores E27-3 and E27-4, which are less than 500 km distant (Fig. 1). Miocene to Recent eruptions of basanite, basalt, trachybasalt, phonolite and trachyte are known from numerous volcanoes in the McMurdo Volcanic Group in the Ross Sea region (Kyle 1990) and from Marie Byrd Land in Western Antarctica (LeMasurier 1990). Several of these volcanoes could have been sources. Glassy fallout tephra in the Byrd Ice Core in Western Antarctica are trachytic (Palais et al. 1988) and similar to the most common glasses in the SPTZs (Fig. 5). The Byrd Ice Core tephras are thought to be from Mt Takahe and range in age from 150 to 30 ka (Palais et al. 1988), which is in the age range of the youngest SPTZs (Table 1). The Byrd Ice Core is more than 350 km from the nearest source volcanoes, but this is still considerably less than the distance from the volcanoes to the *Eltanin* cores (>1500 km)

Large rhyolitic eruptions have not been documented from Antarctica; however, highly silicic lavas, including
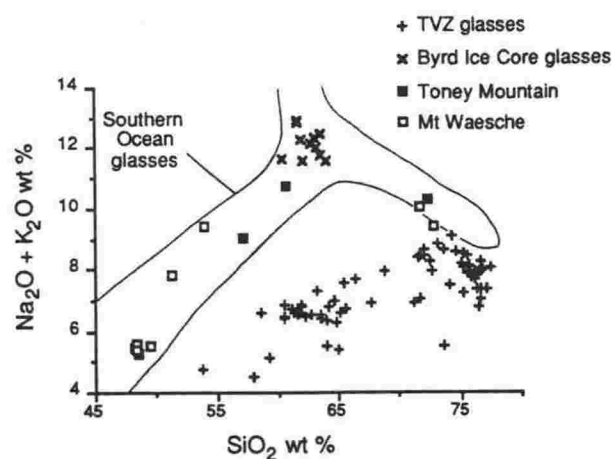
Fig. 5. Composition of SPTZ glasses compared to contemporaneous rocks and glasses from Antarctic volcanoes and the Taupo Volcanic Zone. Analyses for Toney Mountain from LeMasurier et al. (1990), Mt Waesche from LeMasurier and Kawachi (1990) and Byrd Ice Core from Palais et al. (1988)

pantellerite, comendite and alkali rhyolite, have been reported from several late Cenozoic stratovolcanoes in Marie Byrd Land. Compositions of these glassy rocks are characterised by low CaO (<0.5 wt %), high alkali and variable FeO contents (LeMasurier 1990), which is also typical of rhyolitic glasses in the SPTZs (Table 3, Fig. 3). Although radiometric dates are sparse, highly silicic eruptions in the last 2 Ma are known from at least two volcanoes: Tony Mountain (LeMasurier et al. 1990) and Mt Waesche (LeMasurier and Kawachi 1990). The compositions of rocks from these volcanoes match well with the compositional range of SPTZ glasses (Fig. 5), indicating they are possible sources.

Mode of emplacement

The wide distribution of tephra in the Southern Pacific requires exceptionally large explosive eruptions if all the material was emplaced as fallout. This seems highly unlikely for the basanite, basaltic and trachybasaltic glasses as these compositions are generally associated with low explosivity eruptions. Silicic plinian eruptions could distribute tephra this widely. There is evidence for explosive eruptions from silicic volcanoes in Marie Byrd Land (Palais et al. 1988; Kyle personal communication, 1991), but these volcanoes are generally thought to be ash poor (LeMasurier 1990), although there are few onland exposures to test this.

Some trachytic shards in SPTZs are coarse grained (up to 3 mm) in cores E33-16 and E9-11 considering the distance (>1500 km) to likely sources in Marie Byrd Land. Such shards are not likely to be emplaced via direct fallout at this distance (e.g. Fisher 1964). All the samples examined also contain coarse nonvolcanic debris interpreted as being ice-rafted, so it is possible that some or all of the glasses have been ice-rafted as well. The shards display sharp, bubble-wall morphologies and little evidence of abrasion, but this does not discount possible ice transport, as other documented ice-rafted glass shards also display primary morphologies (e.g. Ruddiman and Glover 1972). Much of the tephra in the SPTZs could have originated from fallout on to floating ice sheets rather than the incorporation of debris into basal ice flows during transport over land. Thus the shards could retain their primary morphologies. Surface ocean currents flow away from the Antarctic coast and Ross Sea in a northeasterly direction before reaching the Antarctic Convergence (Huang et al. 1975). These currents could transport icebergs containing tephra to *Eltanin* core sites in the Southern Pacific. Models for sea ice distribution during the last glacial maximum indicate the presence of ice sheets to latitudes in the vicinity of 60°S (CLIMAP 1976), lower than the latitudes of *Eltanin* core sites (Fig. 1). These ice sheets could have provided an additional mechanism for transport of debris, including tephra, during glacial periods.

Ice rafting has been proposed to explain the distribution of some dispersed tephra zones in the Northern Atlantic where they occur in glacial intervals of extensive sea-ice development (Ruddiman and Glover 1972). The

age of each SPTZ (Table 1) does not match uniquely to a glacial isotope stage; however, the chronology of the SPTZs is based on a small number of magnetic reversals and the assumption of constant sedimentation rates. Twenty-three tephra zones are identified in the Southern Pacific in the last 1.84 Ma with a fairly regular spacing of ca. 0.08 Ma. This compares to 30 glacial stages recognised for the same period (Williams et al. 1988) and leaves open the possibility of the tephra zones being glacially controlled.

Conclusions

Electron microprobe analyses of glasses from the Southern Pacific reveal many tephra zones are dominated by trachytic shards, similar in composition to those reported from Antarctic volcanoes. This is contrary to previous suggestions that the glasses are rhyolitic (e.g. Huang et al. 1975) and that they originated from the Taupo Volcanic Zone in New Zealand, some 5000 km distant (Kyle and Seward 1984). Seven rhyolitic tephra zones are recognised, dated between 2.00 and >0.06 Ma, but these have peralkaline (comendite) compositions and are dissimilar to Taupo Volcanic Zone calc-alkaline glasses. Large stratovolcanoes in Marie Byrd Land are the closest alkalic provinces known to have erupted rhyolitic magmas and therefore are the most likely sources. The deep-sea cores provide a record of explosive silicic eruptions from Antarctica not previously documented from studies on the continent.

Many of the SPTZs consist of several eruptive events, possibly mixed together by ice-rafting and bioturbation after deposition. Therefore, although tephra zones correlated between cores may represent the same or similar time intervals, they are not the products of single instantaneous eruptions (cf. Huang et al. 1975; Kyle and Seward 1984). The occurrence of tephra in deep-sea sediments and knowledge of their onshore source indicated here could provide insight to paleooceanic and sea-ice circulation in the Southern Pacific Ocean.

References

Bowden P (1974) Oversaturated Alkaline rocks: granites, pantellerites and comendites. In: Sorensen H (ed) The Alkaline rocks. London, Wiley, pp 109–123

CLIMAP project members (1976) The surface of the ice-age Earth. Science 191:1131–1137

Cole JW (1979) Structure, petrology, and genesis of Cenozoic volcanism, Taupo Volcanic Zone, New Zealand - A review. NZJ Geol Geophys 22:631–657

Fisher RV (1964) Maximum size, median diameter, and sorting of tephra. J Geophys Res 64:341–355

Froggatt PC (1983) Towards a comprehensive late Quaternary tephra and ignimbrite stratigraphy using electron microprobe analysis of glass shards. Quat Res 19:178–200

Froggatt PC, Nelson CS, Carter L, Griggs G, Black KP (1986) An exceptionally large late Quaternary eruption from New Zealand. Nature 319:578–582

Huang TC, Watkins ND (1976) Volcanic dust in deep-sea sediments: Relationships of microfeatures to explosivity estimates. Science 193:576–579

Huang TC, Watkins ND, Shaw DM, Kennett JP (1973) Atmospherically transported volcanic dust in South Pacific deep sea sedimentary cores at distances over 3000 km from the eruptive source. Earth Planet Sci Lett 20:119–124

Huang TC, Watkins ND, Shaw DW (1975) Atmospherically transported volcanic glass in deep-sea sediments: Volcanism in subantarctic latitudes of the South Pacific during late Pliocene and Pleistocene time. Geol Soc Am Bull 86:1305–1315

Jarosewich E, Nelen JA, Norberg JA (1980) Reference samples for electron microprobe analysis. Geostandards Newsletter 4:43–47

Johnson GL, Kyle PR, Vanney JR, Campsie J (1982) Geology of Scott and Balleny Islands, Ross Sea, Antarctica, and morphology of the adjacent seafloor. NZJ Geol Geophys 25:427–436

Kyle PR (1990) McMurdo Volcanic Group-Western Ross embayment Introduction. In: LeMasurier WE, Thomson JW (ed) Volcanoes of the Antarctic Plate and Southern Oceans. American Geophysical Union, Antarctic Research Series 48, pp 19–25

Kyle PR, Seward D (1984) Dispersed rhyolitic tephra from New Zealand in deep sea sediments of the Southern Ocean. Geology 12:487–490

La Bas MJ, Le Maitre RW, Streckeisen A, Zanettin B (1986) A chemical classification of volcanic rocks based on the total alkali-silica diagram. J Petrol 27:745–750

LeMasurier WE (1990) Marie Byrd Land-Summary. In: Le Masurier WE, Thomson JW (ed) Volcanoes of the Antarctic Plate and Southern Oceans. American Geophysical Union, Antarctic Research Series 48, pp 147–163

LeMasurier WE, Kawachi Y (1990) Mount Waesche. In: Le Masurier WE, Thomson JW (ed) Volcanoes of the Antarctic Plate and Southern Oceans. American Geophysical Union, Antarctic Research Series 48, pp 208–211

LeMasurier WE, Kawachi Y, Rex DC (1990) Toney Mountain. In: Le Masurier WE, Thomson JW (ed) Volcanoes of the Antarctic Plate and Southern Oceans. American Geophysical Union, Antarctic Research Series 48, pp 175–179

LeMasurier WE, Thomson JW (ed) (1990) Volcanoes of the Antarctic Plate and Southern Oceans. American Geophysical Union, Antarctic Research Series 48

Nelson CS, Froggatt PC, Gosson GJ (1986) Nature, chemistry and origin of late Cenozoic megascopic tephras in Leg 90 cores from the southwest Pacific. In: Kennett JP, Von der Borch CC et al. (ed) Initial reports of the Deep Sea Drilling Project, 90. Washington, United States Government Printing Office, pp 1161–1173

Nielsen CH, Sigurdsson H (1981) Quantitative methods for electron microprobe analysis of sodium in natural and synthetic glasses. Am Mineral 66:547–552

Palais JM, Kyle PR, McIntosh WC, Seward D (1988) Magmatic and phreatomagmatic volcanic activity at Mt. Takahe, West Antarctica, based on tephra layers in the Byrd Ice core and field observations at Mt. Takahe. J Vol Geoth Res 35:295–317

Ruddiman WF, Glover KL (1972) Vertical mixing of ice-rafted volcanic ash in North Atlantic sediment. Geol Soc Am Bull 83:2817–2836

Shane PAR (1991) Remobilised silicic tuffs in middle Pleistocene fluvial sediments, southern North Island, New Zealand. NZJ Geol Geophys 34:489–499

Shane PAR, Froggatt PC (1991) Glass chemistry, paleomagnetism and correlation of middle Pleistocene tuffs in southern North Island, New Zealand and Western Pacific. NZJ Geol Geophys 34:203–211

Shaw DM, Watkins ND, Huang TC (1974) Atmospherically transported volcanic glass in deep-sea sediments: theoretical considerations. J Geophys Res 7:3087–3084

Williams DF, Thunnel RC, Tappa E, Rio D, Raffi I (1988) Chronology of the Pleistocene oxygen isotope record: 0–1.88 m.y. B.P. Paleogeogr Paleoclimatol Paleoecol 64:221–240

Wilson CJN, Rogan AM, Smith IE, Northey DJ, Nairn IA, Houghton BF (1984) Caldera volcanoes of the Taupo Volcanic Zone, New Zealand. J Geophys Res 89:8463–8484

6.4 CONCLUSIONS

1. Many early Pleistocene tephras in southern North Island have been transported by fluvial systems and emplaced as catastrophic flood deposits. The sedimentation pattern in the East Coast region was typified by slow fluvial/lacustrine deposition and subaerial exposure, punctuated by rapid vertical accretion of volcaniclastic sediments following eruptions.

2. Reworked tephras in these depositional settings are commonly chemically heterogeneous, consisting of multiple populations of glass shards of different compositions. Such deposits probably arise during the post-eruption transport and erosion of new and pre-existing units in the proximal volcanic region.

3. Glass and mineral compositions of the tephras provide evidence for a variety of volcanic activity, ranging from calc-alkaline basaltic andesites to rhyolites, in the TVZ during the early Pleistocene.

4. The occurrence of coarse, fluvially transported volcaniclastic sediments and primary ignimbrites in the East Coast region implies early Pleistocene transport routes through the present day main Axial Ranges, and thus substantial tectonic uplift in the last 0.7 Ma.

5. Widespread volcanic glasses in deep-sea sediments of the Southern Pacific Ocean are peralkaline in composition, ranging from basalts and basanites through to comendites. Although previously attributed to activity in the TVZ, some 5000 km distant, their compositions are only compatible with sources in Western Antarctic and the Ross Sea region.

Chapter 7
ISOTOPIC AGES OF TEPHRAS

7.1 INTRODUCTION

Isotopic dating of early-middle Pleistocene tephras in New Zealand has been based almost entirely on the fission-track method using glass or zircons. Seward (1974) presented glass fission-track ages for a sequence of tephras in marine sediments of the Wanganui basin in the range ca. 1.50-0.30 Ma. These ages became a basis to estimate ages for local stage boundaries and the Plio-Pleistocene boundary in New Zealand (ca. 1.8 Ma). In the East Coast region, Seward (1975) presented several ages for tephras in the range ca. 1.0-0.3 Ma for the marine/non-marine sequence at Cape Kidnappers. Subsequently, track annealing in many of the glasses was identified. Zircons, which are not prone to annealing at ambient temperatures, were dated from several tephras as a check on previously determined ages (Seward 1979). Ironically, many of the zircon ages were in close agreement with the glass ages, in spite of the track annealing problems in the latter. Few attempts have been made to independently verify these ages. However, magnetostratigraphy for the sequence at Cape Kidnappers revealed that the ages (both glass and zircon) are anomalously young by as much as 50% (Black 1992). Similarly, fission-track ages determined using the isothermal plateau method, which corrects for annealing, are significantly older than the earlier ages determined for several tephras in the Wanganui basin (Alloway et al. 1993).

This study applies the $^{40}Ar/^{39}Ar$ single crystal laser fusion (SCLF) technique (York et al. 1981) to feldspars from key tephras in an attempt to obtain high resolution ages. The method involves the total fusion of individual crystals with the use of a continuous laser. The advantages of the method are: (1) it can date feldspars which are common in and easily extracted from the tephras; (2) analytical errors are typically much less than 10% over the age range being studied, and often less than 5%; and (3) an age distribution of single grains can be determined allowing contaminant and aberrant analyses to be omitted (e.g. Deino & Potts 1990). This is particularly significant as many of the tephras have been deposited by fluvial and nearshore processes. The SCLF method has been used successfully to date reworked silicic tephras in sedimentary sequences in East Africa which contain both detrital and xenocrystic contaminants (e.g. Deino & Potts 1990, Walter et al. 1991). Although the highest resolution ages have been obtained on high-K sanidine and anorthoclase, the SCLF method can also produce ages on other types of feldspar and hornblende.

Previously, the Ar/Ar SCLF method has not been applied to Pleistocene tephras in New Zealand. However, Pringle et al. (1992) have used a similar technique utilising mini-bulk feldspar separates from proximal ignimbrites in the TVZ, to obtain ages in the range 1.6-0.3 Ma. In the present study selected samples were dated using the SCLF method by R. C. Walter

Table 7.1 Tephra samples dated by the SCLF ^{40}Ar/^{39}Ar method

#	Tephra	Locality	Grid ref.	Stratigraphic context	Lithology
Potaka Tephra correlatives:					
293	(Potaka Pumice)	Rewa Hill	T22/357311	top Jaramillo	pumice clasts
173	(Kaimatira Pumice sand)	Wanganui coast	R22/729454	top Jaramillo	pumice clasts
194		Mangatewainui stream	U23/816188	top Jaramillo	pumice clasts
232		Makaroro	U23/922501		ignimbrite matrix
005	(Kidnappers A)*	Cape Kidnappers	W21/581655	top Jaramillo	ignimbrite matrix
others:					
262	Rabbit Gully Ignimbrite (Kidnappers D)*	Cape Kidnappers	W21/556650	near B/M	pumice clasts
009	Kidnappers B* (Kaukatea Tephra?)†	Cape Kidnappers	W21/581655	above Jaramillo	ash
128	un-named	Mangatewaiiti stream	U23/817166	below Jaramillo	ash
Rewa	Rewa Pumice	Rewa Hill	T22/348317	below Jaramillo	fine lapilli
Pak	Pakihikura Tephra†	Oroua River	T22/623362	above Olduvai?	ash
318	un-named	Oroua River	T22/623362	below Pak.	ash

*name as in Black (1992).
†likely correlative (see Chapter 8)

at the Institute for Human Origins in California, who irradiated the samples and collected the Ar/Ar data. The individual crystal analyses were supplied to P. C. Froggatt and the author. The presentation and interpretation of the data in this chapter is that of the author's.

7.2 SAMPLES AND THE $^{40}Ar/^{39}Ar$ METHOD

Tephras were selected for dating on the basis of their widespread geographic distribution and position relative to paleomagnetic reversal boundaries (Table 7.1). Several samples of Potaka Tephra were selected as this tephra is particularly widespread (Chapter 8) and occurs as a variety of different deposits including an ignimbrite and volcaniclastic sediments. The selection was restricted to relatively coarse grained tephras.

Tephra samples (pumice clasts where available) were crushed and sieved to obtain the size fraction >250 μ. Feldspars in this fraction were purified by a frantz magnetic separator and about 50 large, visually clear crystals were hand picked under a binocular microscope. Sanidine is rare in the tephras, thus plagioclase feldspar was used for dating. EMA indicates the crystals typically have K_2O contents <0.7 wt % and classify mainly as andesine. The crystals were sent to R. C. Walter (Institute of Humans Origins) for analysis. The samples were irradiated and Ar isotopic data obtained using standards and corrections similar to that described by Deino & Potts (1990) and Walter et al. (1991).

7.3 RESULTS

7.3.1 Ages

$^{40}Ar/^{39}Ar$ SCLF ages and weighted means for each sample are given in Table 7.2. The weighted mean is calculated using the inverse variance as a weighting factor and the deviation is then recalculated around the weighted mean (e.g. Deino & Potts 1990). The weighted mean is taken as the best estimate of the sample age considering the different analytical uncertainty associated with each crystal. Sample age spectra are plotted as histograms in Fig. 7.1 & 7.2. The histograms provide a visual representation which allows outliers or multiple populations to be identified. Such analyses may then be removed from the weighted mean calculation. The analyses which are determined on low-K plagioclase produce weighted uncertainties of <10% of the mean age, and is some cases <5% (Table 7.2). This degree of error is low compared to that produced by the fission-track method for New Zealand tephras of a similar age (e.g. Seward 1979; Alloway et al. 1993). However, the precision is not as good as that produced by the $^{40}Ar/^{39}Ar$ method using sanidine or anorthoclase which typically have errors as small as 2-3% (e.g. Walter et al. 1991). This greater uncertainty along with the relatively small number of

Table 7.2. ^{40}Ar/^{39}Ar SCLF analyses for New Zealand early Pleistocene tephras

sample	Ca/K	% Ar*	age	±
Potaka Tephra correlatives:				
SO 293	11.195	34.2	1.132	0.061
	12.130	*9.7*	*0.676*	*0.184*
	16.977	*94.6*	*1.715*	*0.233*
	11.216	61.2	1.209	0.146
	12.061	*14.2*	*0.677*	*0.130*
	13.899	53.8	0.942	0.107
	Avg/SD		1.059	0.435
	Wtd Mn/SD		**1.049**	**0.100**
SO 293†	18.801	40.2	1.217	0.031
	13.724	37.9	0.912	0.032
	13.188	44.8	0.967	0.032
	16.037	30.0	0.936	0.039
	19.543	26.2	0.912	0.041
	15.810	53.0	0.985	0.043
	12.469	34.7	1.003	0.034
	Avg/SD		0.990	0.106
	Wtd Mn/SD		**1.002**	**0.044**
173	12.781	80.0	1.106	0.106
	10.275	*47.3*	*0.886*	*0.079*
	10.911	*49.1*	*0.771*	*0.165*
	10.153	52.0	1.101	0.051
	11.149	46.6	0.991	0.117
	Avg/SD		0.971	0.144
	Wtd Mn/SD		**1.029**	**0.056**
194	9.166	65.9	1.303	0.175
	9.620	86.5	1.113	0.107
	10.062	*90.0*	*1.384*	*0.243*
	10.223	*36.2*	*0.691*	*0.195*
	11.232	*29.4*	*0.685*	*0.082*
	Avg/SD		1.035	0.342
	Wtd Mn/SD		**0.907**	**0.133**
232	*9.388*	*29.8*	*0.856*	*0.079*
	11.662	55.2	1.102	0.107
	11.670	60.1	0.992	0.071
	7.600	59.6	1.259	0.107
	7.980	59.5	1.240	0.072
	11.727	46.2	1.104	0.053
	Avg/SD		1.092	0.110
	Wtd Mn/SD		**1.084**	**0.059**
05	*11.912*	*30.0*	*0.862*	*0.038*
	17.851	27.8	1.084	0.058
	15.064	53.0	1.205	0.056
	14.886	52.9	1.063	0.047
	16.660	*37.8*	*1.305*	*0.073*
	14.479	*53.9*	*1.360*	*0.058*
	12.630	53.5	1.135	0.046
	14.498	40.1	1.029	0.064
	22.212	*34.5*	*0.877*	*0.081*
	14.406	62.3	1.041	0.049
	Avg/SD		1.096	0.163
	Wtd Mn/SD		**1.073**	**0.050**
Pooled Wtd Mn/SD (no outliers)			*1.001*	*0.011*

Others:				
262	12.688	31.1	0.736	0.034
	13.172	54.2	0.922	0.042
	13.591	42.1	0.903	0.042
	12.713	72.6	0.831	0.023
	12.738	57.0	0.828	0.034
	13.481	88.0	0.897	0.028
	13.350	78.8	1.042	0.032
	12.332	67.5	0.846	0.034
	12.162	62.0	1.074	0.036
	13.364	47.6	0.754	0.034
	Avg/SD		0.883	0.110
	Wtd Mn/SD		**0.877**	**0.034**
09	10.577	30.2	0.859	0.034
	11.866	47.0	0.924	0.048
	17.869	35.8	1.256	0.088
	15.753	*11.8*	*1.902*	*0.114*
	13.077	30.7	1.383	0.077
	16.959	*26.4*	*1.912*	*0.073*
	16.765	21.8	1.091	0.077
	14.336	49.6	1.262	0.075
	15.319	16.3	0.663	0.099
	11.349	23.4	1.436	0.125
	19.115	18.0	1.088	0.073
	Avg/SD		1.252	0.396
	Wtd Mn/SD		**1.098**	**0.105**
Wtd Mn/SD (no outliers)			*1.006*	*0.021*
Pak	7.526	29.4	1.068	0.093
	23.944	60.6	1.490	0.070
	16.826	27.8	0.799	0.082
	10.969	54.1	1.574	0.069
	11.864	51.0	1.214	0.047
	7.892	31.1	1.040	0.084
	15.702	48.6	1.852	0.099
	8.242	37.3	0.973	0.106
	11.609	13.0	0.576	0.115
	7.590	9.6	1.975	0.128
	Avg/SD		1.257	0.456
	Wtd Mn/SD		**1.260**	**0.114**
318	*24.654*	*33.7*	*0.915*	*0.078*
	26.934	43.2	1.441	0.109
	9.694	54.6	1.397	0.094
	12.847	66.6	1.591	0.104
	10.489	98.3	1.911	0.053
	12.237	81.3	1.753	0.057
	24.787	*24.5*	*0.722*	*0.092*
	12.457	43.8	1.485	0.070
	10.432	87.4	1.595	0.046
	Avg/SD		1.421	0.360
	Wtd Mn/SD		**1.535**	**0.118**
Wtd Mn/SD (no outliers)			*1.656*	*0.025*

† crystals >400 μ

Analyses in italics are contaminants or altered crystals (see text).

Mean ages presented as simple average of all crystals (plain text); weighted mean of all crystals (bold); and weighted mean excluding outliers (italics).

Fig. 7.1 Histograms showing age distributions for samples of Potaka Tephra.
Bin width = 0.025 Ma.

Fig. 7.2 Histograms showing Ar./Ar age distributions of early Pleistocene tephras. Bin width = 0.025 Ma.

analyses, results in less defined peaks in the age spectra of samples in this study (Fig. 7.1, 7.2).

Age data were obtained from 5 different exposures of tephra considered to be correlatives of the Potaka Tephra (Chapter 8). Although much scatter and weakly defined peaks are displayed by some of the age spectra, each sample produced a weighted mean close to 1.0 Ma and all ages overlap at 1 σ (Table 7.2). The coarse grain size split (>400 µm) from Rewa Hill (293) produced the age with the smallest associated error (1.002 ± 0.044 Ma) and forms a tight single peak in the age spectra (Fig. 7.1). Smaller crystals in the range 250-400 µm from the same exposure produce a very diffuse age spectra (Fig. 7.1) and a larger weighted uncertainty but identical age (1.049 ± 0.100 Ma). This suggests data from larger crystals have a greater analytical precision, but smaller crystals can produce a correct age (within error limits).

Crystals from Potaka Tephra samples display a wide range in %Ar* (radiogenic Ar) (Table 7.2). In samples 194 and 293 (250-400 µ), the %Ar* appears to display a positive correlation with crystal age (Fig. 7.3), i.e. younger aged crystals have low %Ar*. This trend is not evident in the other samples of Potaka Tephra, including the coarser fraction of 293. Such age and composition relationships have been reported by Deino & Potts (1990) who consider it to be the result of partial Ar loss in some crystals due to alteration. This may explain the secondary peak in the combined age spectra for Potaka Tephra (Fig.7.1) at about 0.7 Ma. Stratigraphic relationships suggest the age of Potaka Tephra is ca. 1 Ma (Chapter 8), which is in accord with the main distribution of Ar/Ar age data and the weighted means (Table 7.2), and indicates ages of ca. 0.7 Ma are anomalous. On the same stratigraphic basis, a single crystal with an age of ca. 1.7 Ma (Fig. 7.1) is also anomalous and possibly represents a detrital contaminant or xenocryst. Removing these anomalous or outlier analyses produces a pooled weighted mean of 1.001 ± 0.011 Ma for Potaka Tephra (Table 7.2).

Of the other samples analysed, the Rabbit Gully Ignimbrite (262), tephra 128 and Rewa Pumice all display single age populations and low errors in their age determination. Samples of each of these tephras are relatively coarse grained. Tephra 09 (correlative of Kaukatea Tephra) from Cape Kidnappers, produced an age with a large analytical error (1.098 ± 0.105 Ma) due partly to two crystals of ca. 1.9 Ma in age which are incompatible with the stratigraphic position of the tephra (above the Jaramillo). These crystals are presumably contaminants. A weighted mean of 1.006 ± 0.021 Ma is obtained if these two outiers are omitted (Table 7.2). The sample of Pakihikura Tephra and a tephra immediately below it (318) produced poor ages with much scatter (Fig. 7.2). In the case of Pakihikura Tephra, this may be partly due to the fine grain size. Both tephras display crystals with anomalously young ages (<1.0 Ma), incompatible with stratigraphy which indicates they are older than the Jaramillo Subchron and Rewa Pumice (ca. 1.4 Ma). These crystals display relatively low %Ar* compared to the other crystals in the samples and may have undergone alteration. If the two crystals <1.0 Ma are excluded from
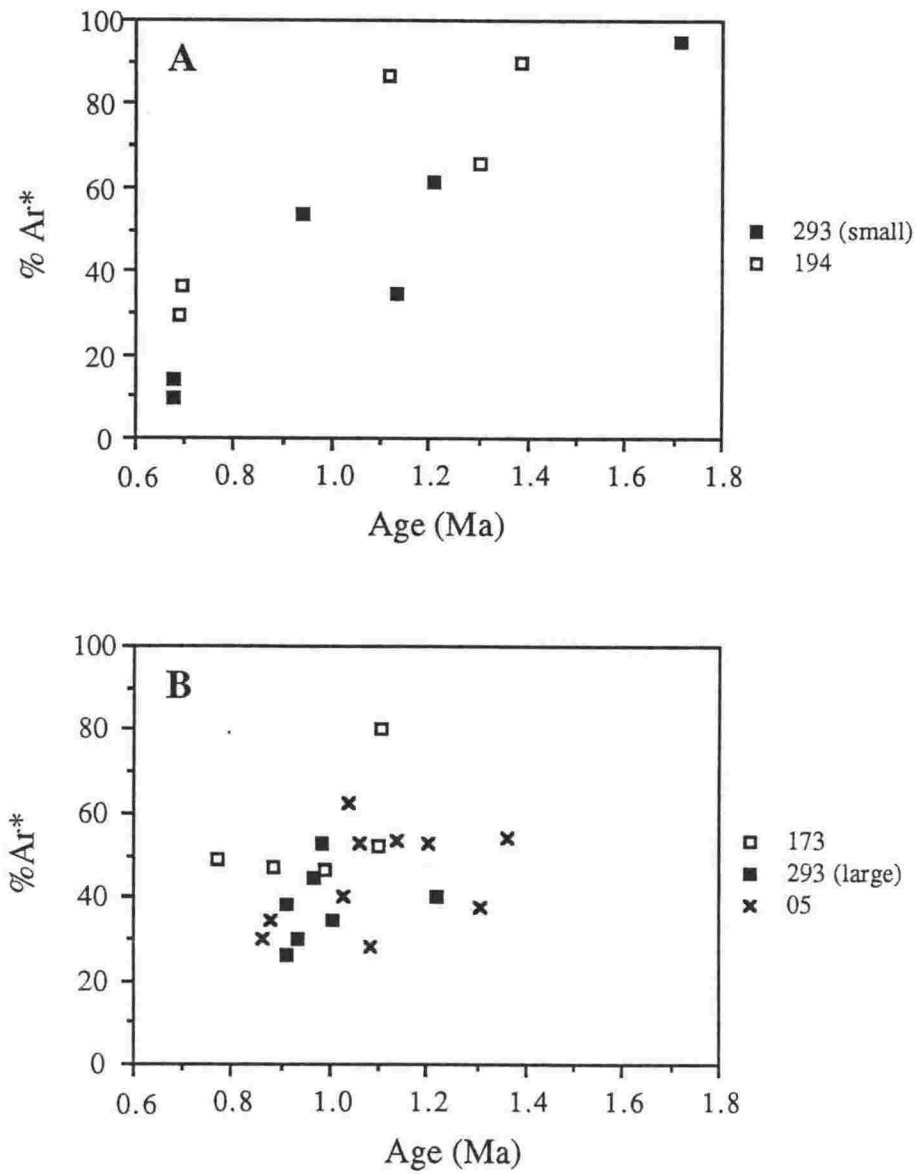
Fig. 7.3 Age of single feldspar crystals plotted against % Ar* (radiogenic) for samples of Potaka Tephra. (A) A positive correlation is evident in samples 293 and 194. (B) Samples that show no relationship between age and % Ar*.

tephra 318, then a peak at ca. 1.6 Ma is evident in the spectra (Fig. 7.2) with a weighted mean of 1.656 ± 0.025 Ma (Table 7.2). This is in accord with an isothermal plateau fission-track age of 1.63 ± 0.15 Ma for Pakihikura Tephra (Alloway et al. 1993).

7.3.2 Comparison to previously determined ages

The Ar/Ar SCLF ages are significantly older than ages determined by the fission-track method using both glass (un-corrected for track annealing) and zircon (Table 7.3). However they are consistent with the paleomagnetic polarity of the tephras. Alloway et al. (1993) determined an isothermal plateau glass fission-track age for Potaka Tephra of 1.05 ± 0.05 Ma which is corrected for the effects of track annealing. This is in good agreement with an Ar/Ar SCLF age of 1.002 ± 0.044 Ma determined on large crystals for the same tephra exposure. As suggested by Black (1992), the early fission track ages are only about half of their true age indicated by the Ar/Ar method. The cause of the anomaly in the zircon fission-track ages is uncertain, but it may be due to systematic under etching and/or errors in irradiation doses. As a result New Zealand Pleistocene chronologies based on these early ages must be significantly revised.

Table 7.3 Comparison of ^{40}Ar/^{39}Ar SCLF ages (Ma) with previously determined ages for early Pleistocene tephras in New Zealand. Fission-track ages from Seward (1974; 1975; 1979), except the isothermal plateau fission track (IPFT) age (Alloway et al. 1993).

Tephra	Glass fission-track	Zircon fission-track	IPFT	^{40}Ar/^{39}Ar SCLF	Polarity
262	0.32 ± 0.07			0.877 ± 0.034	R
09		0.56 ± 0.16		1.006 ± 0.021	R
05	0.85 ± 0.10			1.078 ± 0.050	N
Potaka (293)	0.61 ± 0.06	0.64 ± 0.18	1.05 ± 0.05	1.002 ± 0.044	N
Rewa	0.74 ± 0.09			1.429 ± 0.056	R

7.4 IMPLICATIONS FOR NEW ZEALAND STRATIGRAPHY AND THE AGE OF THE JARAMILLO SUBCHRON

7.4.1 Background on the calibration of the Geomagnetic Time Scale

The traditionally quoted age estimates for the Geomagnetic Time Scale (GMTS) are based mainly on K/Ar ages of basaltic bulk samples (e.g. Mankinen & Dalrymple 1979). These ages are from individual emplacement events such as lava flows and domes rather than from continuously deposited sedimentary sections. Statistical procedures are used to produce a best age estimate for a reversal boundary from isolated depositional units of known polarity, considering the accuracy of their ages: the chronogram method (Mankinen & Dalrymple 1979;
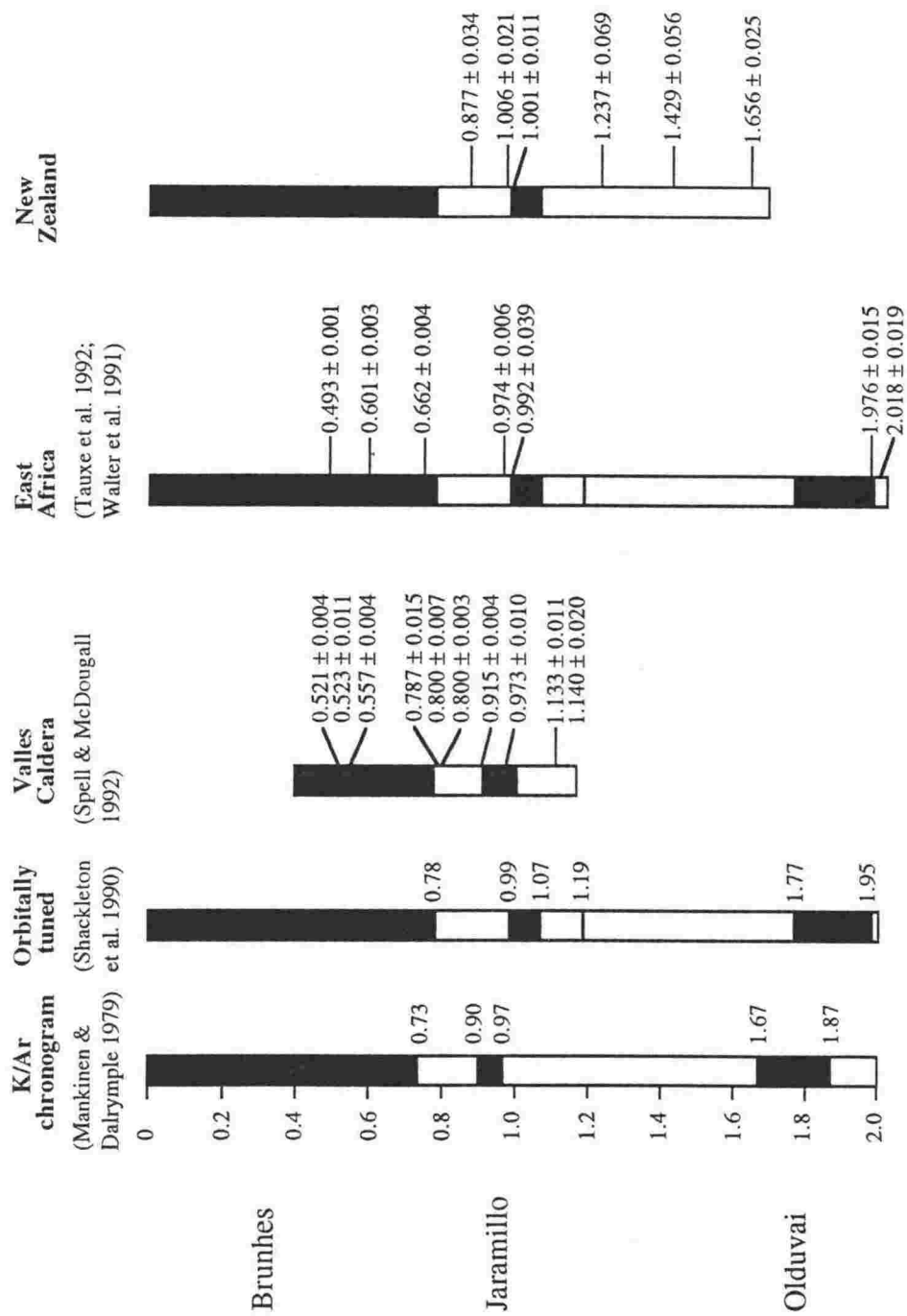
Fig. 7.4 Chronology of the GMTS compared to Ar/Ar ages from different sequences. Ages from Valles Caldera are from domes, and those from East Africa and New Zealand are from tephras in sedimentary sequences.

Tauxe et al. 1992). The calibrated GMTS for the Plio-Pleistocene is summarised in Fig. 7.4. Alternative ages for paleomagnetic reversals have been proposed on the basis of oxygen isotope stratigraphies from deep-sea cores by assuming particular orbital periodicities are reflected in the isotope cycles (e.g. Johnson 1979; Shackleton et al. 1990). These orbitally tuned stratigraphies consistently produce ages for reversal boundaries that are 5-7% older than those indicated by the K/Ar chronogram method (Fig. 7.4). For example, K/Ar data place the Brunhes-Matuyama boundary at ca. 0.73 Ma, while orbitally tuned chronologies place it at 0.78 Ma. More recently, deposits dated by several methods have confirmed an age of ca. 0.78 Ma for this reversal, including K/Ar and fission-track ages for the Bishop Tuff in California (Izett et al. 1988) and SCLF Ar/Ar ages on crystals from felsic rocks (e.g. Baksi et al. 1992, Spell & McDougall 1992).

High-resolution Ar/Ar ages have also provided support for other parts of the orbitally tuned calibration of the GMTS. For example, an age of ca. 0.99 Ma for the top of the Jaramillo Subchron (Deino & Potts 1990; Tauxe et al. 1992) and >1.98 Ma for the base of the Olduvai Subchron (Walter et al. 1991). These ages have been obtained on silicic tephras interbedded in continuously deposited terrestrial sequences in East Africa. This allows the position of the dated unit to be directly related to the subchron it which it is contained, unlike many dome and lava flow ages.

Spell & McDougall (1992) determined SCLF Ar/Ar ages for two domes in the Valles Caldera in New Mexico, from which the Jaramillo Subchron was originally defined. The ages, 0.915 ± 0.004 Ma (intermediate polarity) and 0.973 ± 0.010 Ma (normal polarity), are inconsistent with orbitally tuned chronology for the Jaramillo Subchron (0.99-1.07 Ma). The cause of this discrepancy is uncertain. It is possible that intermediate polarity dome may represent a short lived excursion rather than the top of the Jaramillo Subchron. Alternatively, either or both of the domes may have been erupted during the less well known, younger Kamikatsura Subchron (e.g. Champion et al. 1988). The stratigraphic order of intra-caldera domes can be more complex than that of continuously deposited sedimentary sequences and as the domes represent only short instants in time, their relationships to longer polarity intervals can be speculative.

As well as refining the calibration of the GMTS, the high-resolution ages from terrestrially deposited sequences provide independent support for orbitally tuned isotope and thus climatic chronologies which are almost exclusively deep marine records.

7.4.2 ^{40}Ar/^{39}Ar ages for New Zealand silicic tephras: implications for the age of the Jaramillo Subchron

(a manuscript submitted to Earth and Planetary Science Letters)

^{40}Ar/^{39}Ar ages for silicic tephras in New Zealand: implications for the age of the Jaramillo Subchron

Philip A. R. Shane[a], Robert C. Walter[b] and Paul C. Froggatt[a]

[a]Research School of Earth Sciences, Victoria University of Wellington, PO Box 600,Wellington, New Zealand

[b]Geochronology Center, Institute of Human Origins, 2453 Ridge Road, Berkeley, California 94709

ABSTRACT

Several ^{40}Ar/^{39}Ar ages have been obtained on low-K plagioclase from Pleistocene silicic tephras in New Zealand using the Single Crystal Laser Fusion method. This technique has allowed us to avoid detrital contaminants which are common in the tephras as they have been deposited in fluvial and coastal settings, and produce relatively high resolution ages for this time interval. Data from several sections of the widespread Potaka Tephra provide a mean age of 1.001 ± 0.011 Ma near the top of a normal polarity subchron, interpreted to be the Jaramillo. An age of 1.006 ± 0.021 Ma was obtained for a reversed polarity tephra, which overlies the Potaka Tephra. These tephras provide a temporal constraint for the transition from normal to reversed. These ages and others we have obtained are in accord with the orbitally tuned chronologies for the Jaramillo Subchron (0.99-1.07 Ma) determined from deep sea cores, and are older than expected from K/Ar data. The new ages for tephras also indicate that New Zealand Pleistocene sequences are significantly older than previously thought.

1. Introduction

We report on ^{40}Ar/^{39}Ar ages for several widespread silicic tephras that occur near paleomagnetic reversal boundaries in thick Pleistocene sequences in the North Island of New Zealand (Seward 1974; Shane & Froggatt 1991, Shane 1991, Pillans 1992). Such ages provide the potential for temporal constraints on climatic changes and eruptive records as well as the paleomagnetic reversals themselves.

The source region for these tephras is the Taupo Volcanic Zone (TVZ), some 150-300 km from where the tephras are exposed. The TVZ has produced many large (>300 km^3 of magma) silicic eruptions in the last 2 Ma (Wilson et al. 1984; Pringle et al. 1992), however the numerical age chronology is largely unknown in both proximal and distal sequences. Previous attempts to date the distal tephras have been based on the fission-track method using glass and zircon (Seward 1974; 1975; 1979). However the fission-track ages have been shown to be anomalously young from magnetostratigraphic and Ar/Ar studies (Pringle et al. 1992; Black 1992). In the distal settings, the prominent tephras are often reworked, having been emplaced as catastrophic flood deposits on fluvial braid plains (Shane 1991). Therefore grain-specific techniques are required to avoid detrital and xenocrystic contaminants in both chemical characterisation and isotopic dating. As low K$_2$O (< 0.7 wt%) plagioclase is the ubiquitous
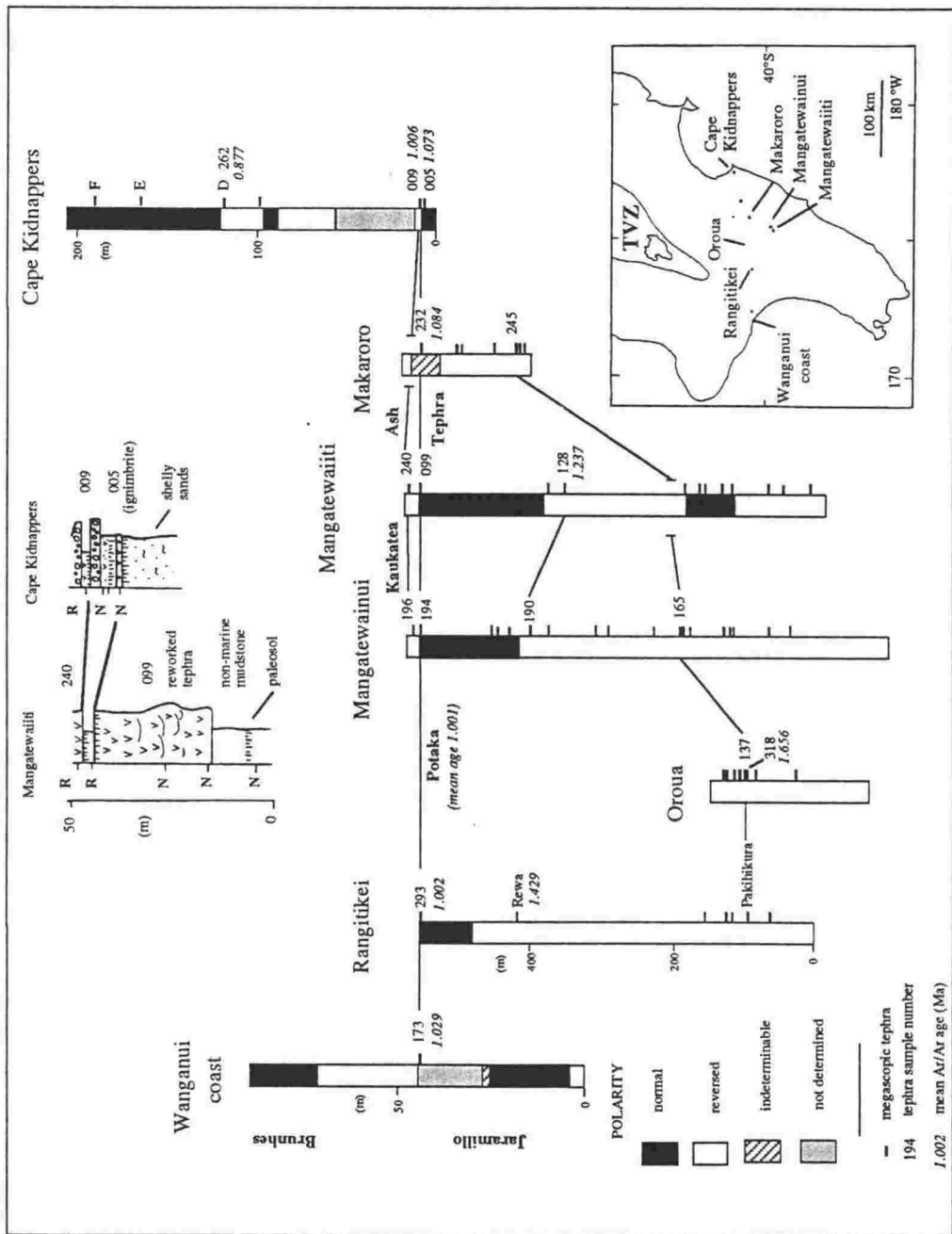
Fig. 1. Summary of the magnetostratigraphy, tephra correlations and Ar/Ar chronology for sections in the southern North Island of New Zealand. Magnetostratigraphy for Wanganui coast and Cape Kidnappers from Turner & Kamp (1990) and Black (1992) respectively. Inset at top shows the details of two sections displaying a normal to reversed paleomagnetic boundary above the Potaka Tephra, interpreted to be the top of the Jaramillo. N=normal site, R=reversed site.

mineral in these tephras, whereas sanidine is sparse or absent, a dating technique that can produce reliable ages on the former is required. We used the Single Crystal Laser Fusion (SCLF) method (e.g. Walter et al. 1991) to obtain several $^{40}Ar/^{39}Ar$ ages from key tephra localities.

We have established a Pleistocene stratigraphic framework using paleomagnetism, and the geochemistry and lithologic character of interbedded tephras, which allows correlation between sedimentary basins in the southern North Island of New Zealand (Fig. 1). Our Ar/Ar age data has implications for the chronology of the Jaramillo Subchron and New Zealand Pleistocene.

2. Tephrostratigraphy

We have recognised several important tephra horizons in basins of the East Coast and Wanganui regions (Fig. 1). The Potaka Tephra (Chapter 8) is particularly widespread in southern North Island. It represents a water-laid, coarse volcaniclastic unit which was deposited in an estuarine setting throughout much of the Wanganui basin. Originally referred to as Potaka Pumice in the Rangitikei Valley (Te Punga 1952), Seward (1976) correlated it to the Kaimatira Pumice Sand exposed along the Wanganui coast where it is contained within the type section for the New Zealand Castlecliffian Stage (early-middle Pleistocene) (Fleming 1953).

In East Coast sections (e.g. Mangatewaiiti and Mangatewainui), we have identified the Potaka Tephra as a thick (up to 30 m) catastrophic flood deposit which was emplaced on to a fluvial braidplain (Shane 1991; Chapter 8). Further north, the tephra represents a non-welded ignimbrite overlain by coarse remobilised volcaniclastics in the Mt Gordon Beds at Cape Kidnappers (Kidnappers A of Black (1992)). This ignimbrite can be traced inland some 40 km to a number of exposures including a thick fluvial sequence at Makaroro River (Fig. 1). At each exposure, the Potaka Tephra has a recognisable glass composition which differs from other interbedded tephras (Fig. 2).

At several sections (Fig. 1), we have found another tephra stratigraphically above Potaka Tephra, which displays a distinctively different glass composition (Fig. 2). We refer to this tephra as Kaukatea Ash, as it is compositionally similar to the tephra of this name in the Wanganui area (Seward 1976; Shane & Froggatt 1991). There, the Kaukatea Ash closely overlies the Kaimatira Pumice Sand (=Potaka Tephra). Thus we have a framework of two closely spaced, distinctive tephras in several sections. In addition, beneath these tephras we have identified a tephra, named Pakihikura Pumice in the Rangitikei Valley (Te Punga 1952), in several sections (Fig. 1,2) thus providing another stratigraphic control point.

A series of fluvially emplaced tephras occur above the Potaka Tephra in the Cape Kidnappers sequence and have been referred to as Kidnappers C, D, E and F (Black 1992). These tephras are closely tied to a magnetostratigraphy where reversals of the Brunhes-Matuyama and Jaramillo Subchron have been located (Fig. 1).
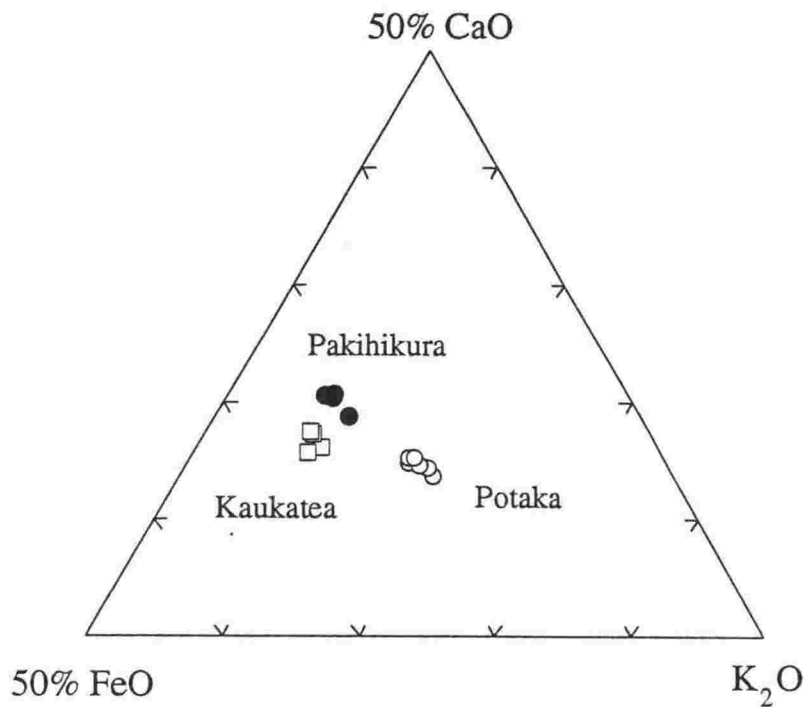
Fig. 2. Ternary plot of the normalised CaO, FeO and K2O contents of 3 widespread tephras used to correlate sections (Fig. 1). Each analysis represents a sample site and consists of a mean of 10-20 glass shard compositions determined by electron microprobe. Each tephra is chemically distinguishable as well as being recognised by lithologic character and stratigraphic position.

3. Magnetostratigraphy

Early fission-track ages and magnetostratigraphy (Seward 1974) placed the Potaka Tephra within the Brunhes Normal Chron. However, recent studies have shown tephras we consider to be correlatives of Potaka Tephra, to be overlain by reversed polarity strata at Cape Kidnappers (Black 1992) and Wanganui coast (Turner & Kamp 1990). Using alternating field demagnetisation techniques we have determined a normal polarity for several exposures of Potaka Tephra including the primary ignimbrite. In strata immediately above the Potaka Tephra, including the Kaukatea Ash, we obtained a stable reversed polarity (Fig 1). Thus we conclude from several sections that the Potaka Tephra occurs near the top of a short normal subchron representing the Jaramillo (Black 1992; Turner & Kamp 1990).

We consider the paleomagnetic transition from normal to reversed to occur a short distance above the Potaka Tephra. In the Mangatewaiiti section, a 10 cm paleosol with root structures is developed into the top of the tephra (Fig 1). Fluvially deposited sandy mudstone immediately overlies this paleosol and contains rare pumice clasts of identical chemistry to the Potaka Tephra. These sediments are reversely magnetised. As depositional rates are rapid in these sequences (Shane 1991) and the tephra shows no sign of discolouration, weathering or clay formation, we consider the paleosol to represent a relatively short time period, perhaps at the most a few thousand years by comparison with recently developed soils in the region. Also our studies of volcaniclastic sequences suggest that reworking of tephra up section, although common, is not prolonged on a scale of 10^4 years. Therefore, clasts of reworked Potaka Tephra in reversed polarity sediments indicate a close temporal spacing between the geomagnetic polarity transition and the eruptive event.

4. Ar/Ar ages

Individual plagioclase crystals were hand picked from crushed tephra samples and dated using the SCLF ^{40}Ar/^{39}Ar technique, similar to that described by Deino & Potts (1990). For each sample we obtained data on 5-10 individual crystals. Microprobe analyses of plagioclase from these tephras and others indicate most crystals are andesine or labradorite with K_2O contents <0.7 wt % (Shane 1991). Age data are presented as a weighted mean and standard deviation (e.g. Walter et al. 1991) (Table 1). For the combined mean age for Potaka samples, and for sample 318, we omitted anomalously young analyses with low radiogenic Ar which may result from alteration (Deino & Potts 1990), and old detrital or xenocrytic analyses. We tested the remaining analyses using chi-square statistics to check if they belonged to a single population.

5. Discussion

5.1 Implications for the age of the Jaramillo Subchron

Table 1. SCLF $^{40}Ar/^{39}Ar$ ages for Pleistocene tephras in New Zealand

sample	Tephra	Locality	Ca/K	$^{40}Ar/^{39}Ar$ age (Ma)	n
262	Kidnappers D (ignimbrite)	Cape Kidnappers	12.95	0.877 ± 0.034	10
009	Kaukatea Ash	Cape Kidnappers	14.82	1.006 ± 0.021	9
Potaka correlatives:					
293	Potaka Tephra	Rangitikei	12.91	1.049 ± 0.100	6
			15.37	1.002 ± 0.044	7*
173	Potaka Tephra	Wanganui coast	11.05	1.029 ± 0.056	5
194	Potaka Tephra	Mangatewainui	10.06	0.907 ± 0.133	5
232	Potaka Tephra (ignimbrite)	Makaroro	10.00	1.084 ± 0.059	6
005	Potaka Tephra (ignimbrite)	Cape Kidnappers	15.46	1.073 ± 0.050	10
Potaka pooled mean†				1.001 ± 0.011	21
128	un-named	Mangatewaiiti	7.37	1.237 ± 0.069	6
Rewa	Rewa Pumice	Rangitikei	11.46	1.429 ± 0.056	6
318	un-named	Oroua	16.06	1.656 ± 0.025	7

50

Analytical method similar to Deino and Potts (1990).
Ages represent a weighted mean and 1σ (e.g. Walter et al. 1991) determined on n crystals of plagioclase.

*rerun on large crystals >400 μm.
†anomalously young analyses with low radiogenic Ar and detrital contaminants omitted

Chronologies for the geomagnetic time scale are commonly based on the 'chronogram' method using K/Ar bulk sample age data on (mainly) basalts (e.g. Mankinen & Dalrymple 1979). Such age data are obtained from single emplacement events, lava flows and domes of known magnetic polarity, rather than from continuously deposited sedimentary records. Using this K/Ar data, the Jaramillo Subchron has been determined to represent the interval 0.91-0.97 Ma. Based on orbitally tuned stable isotope chronologies from deep-sea cores, Johnson (1982), Shackleton et al. (1990) and others have proposed that several Plio-Pleistocene paleomagnetic reversal boundaries are older (5-7%) than indicated by K/Ar ages. Subsequent Ar/Ar age data on high-K feldspars have provided independent support for the orbitally tuned chronologies (Walter et al. 1991; Tauxe et al. 1992; Baksi et al. 1992; Spell & McDougall 1992). However only a few isotopic ages have been determined from sedimentary sequences with defined paleomagnetic boundaries.

Shackleton et al. (1990) determined that the Jaramillo Subchron represented the interval 0.99-1.07 Ma based on astronomical calculations. This is in accord with an Ar/Ar single crystal fusion age of 0.992±0.039 Ma for a tephra at the top of the subchron in a sedimentary sequence of the Olorgesailie Formation in Kenya (Tauxe et al. 1992). However, Spell & McDougall (1992) have suggested an age of 0.915-1.010 Ma for the subchron using Ar/Ar data from two domes in the Valles Caldera, New Mexico, where the subchron was originally defined. Our data from rhyolitic tephras in New Zealand, support the orbitally tuned chronologies (Shackleton et al. 1990). An age of 1.00 Ma for the Potaka Tephra (normal polarity) at the top of the Jaramillo Subchron is in good agreement with an age of 0.99 Ma for the paleomagnetic transition. The chronology of Mankinen & Dalrymple (1979) or Spell & McDougall (1992), would place the tephra near the base of the subchron and thus be overlain by an interval of normal polarity: a situation incompatible with the sequences we have examined (Fig. 1). Similarly, an age of 1.006 ± 0.021 Ma for the reversed polarity Kaukatea Ash, above Potaka Tephra, constrains the timing of the normal to reversed transition at about 1 Ma. Although some of our Ar/Ar ages have larger errors (Table 1) than those reported for high-K feldspars [e.g. Walter et al. 1991), we can confidently place the tephras within a continuously deposited magnetostratigraphy (Fig. 1), which is consistent only with the astronomically derived age for the Jaramillo Subchron.

5.2 New Zealand Pleistocene chronologies

New Zealand has many long, high resolution records of the Pleistocene, both marine and non-marine, where the sedimentation is thought to be climatically controlled [e.g. Pillans 1992; Black 1992; Turner & Kamp 1990). Most of these sequences have little or no isotopic age control and chronologies are commonly based on the interpretation and number of climatic cycles. Our data for Kaimatira Pumice Sand (=Potaka Tephra) at the Wanganui coast provides an age constraint (ca. 1 Ma) for near the base of the Castlecliffian type section and confirms that

the lower part of the sequence represents the Jaramillo Subchron. Ages for tephras in the Cape Kidnappers sequence constrain the base at about 1 Ma, comparable to that of the Castlecliffian type section. An age of 0.877 ± 0.034 Ma for CK D tephra near the middle of the sequence, confirms the overlying paleomagnetic reversal (Black 1992) represents the Brunhes-Matuyama (0.78 Ma). These ages are consistent with magnetostratigraphy and further support the contention that early fission-track age determinations are anomalously young (Black 1992). Similarly our age data for Potaka Tephra and Rewa Pumice in the Rangitikei sequence, and sample 318 immediately below Pakihikura Pumice in the nearby Oroua section (Table 1) are nearly twice as old as previous age estimates for these tephras (Seward 1976; 1979). However, a recently determined isothermal plateau glass fission-track age for Potaka Tephra (1.05 ± 0.05 Ma) (Alloway et al. 1993) is in accord with our Ar/Ar data for the Rangitikei exposure. Thus previous chronologies must be treated with caution and significant revisions to the New Zealand Pleistocene stratigraphy are required. The recognition of key dated tephra horizons is critical to future studies as is shown here for the Potaka Tephra which marks a paleomagnetic reversal boundary as well as tying sequences to the local Stage type section.

The sections we have studied contain particularly long sequences of the Jaramillo Subchron. At Mangatewaiiti and Mangatewainui, this interval is about 150 and 120 m thick respectively, representing just 80 ka. Such sequences reflect the rapid subsidence and the voluminous supply of detritus at an active convergent plate boundary. The sections provide a yet unstudied high resolution record of paleomagnetic and climatic changes within the Jaramillo interval.

7.5 CONCLUSIONS

1. Early Pleistocene tephras may contain old detrital or xenocrystic contaminants and crystals with low Ar*, which produce anomalously young ages. The latter may be due to alteration. The Ar/Ar SCLF method allows these crystals to be recognised and omitted from age determinations.

2. Ar/Ar SCLF analyses of plagioclase provide high resolution ages for New Zealand tephras and indicate the tephras are up to twice as old as previously determined. This necessitates major revisions of New Zealand Pleistocene stratigraphy.

3. The Ar/Ar ages are in accord with magnetostratigraphy and with recently determined fission-track ages on glass using the isothermal plateau technique.

4. The widespread Potaka Tephra has an age of ca. 1 Ma. This age and the position of the tephra at the top of the Jaramillo Subchron provides support for the orbitally tuned calibration of the GMTS, which indicates the subchron represents the interval 0.99-1.07 Ma.

Chapter 8
STRATIGRAPHY AND CORRELATION OF KEY EARLY PLEISTOCENE
TEPHRAS

8.1 INTRODUCTION

In the years since early Pleistocene tephras were examined in the Rangitikei Valley and their potential for correlation recognised (e.g. Te Punga 1952; Fleming 1953), several studies have named particular horizons and attempted to identify them elsewhere in the Wanganui basin, East Coast basins, and in deep-sea cores (Lillie 1953; Seward 1975; 1976; Watkins & Huang 1977; Kyle & Seward 1984). The use of glass chemistry as a tool for correlation has invalidated many of these early correlations that were based mainly on age data (Froggatt 1983; Shane & Froggatt 1991).

The integrated use of glass chemistry, paleomagnetism and Ar/Ar ages in this study has allowed previous correlations to be refined and new ones made. Most of the named early Pleistocene tephras are named from exposures in the Wanganui basin (e.g. Seward 1976). Many of these tephras are not widespread in the southern North Island, and thus are only of local significance in dating. A greater frequency of tephras are recorded in the East Coast region, mainly in non-marine strata, and are previously un-named.

This chapter examines the character and distribution of tephras found to be widespread in the southern North Island and also discusses the status of some other less widespread tephras which have been previously studied or have been isotopically dated. Where a widespread tephra is correlated to a previously named exposure in the Wanganui basin, this name is used in this study, with minor corrections to eliminate grain size implications (after Froggatt & Lowe 1990).

8.2 PAKIHIKURA TEPHRA

8.2.1 Introduction and previous work

In the Rangitikei Valley, Te Punga (1952) used the name Pakihikura Pumice for a volcaniclastic sequence exposed in a bluff cut by the Pakihikura Stream. This unit was considered (Fleming 1953, Seward 1976) to be the equivalent of a sequence of tephras collectively called Makirikiri Tuff, which was traced throughout the entire Wanganui basin. Seward (1976) amended the definition of Pakihikura Pumice to represent the lowest tephra in a sequence exposed in a road cut of what is now Highway 43 (T22/362356), a short distance from the bluff described by Te Punga (1952). Fission-track ages of 1.06 ± 0.16 Ma (glass) and

Table 8.1. Glass composition of tephras considered correlatives of the Pakihikura Tephra.

	293	328	174a	174b	182	137	245	148	165
SiO_2	78.32(.45)	77.39(.24)	77.62(.19)	77.26(.83)	78.05(.25)	77.76(.28)	77.36(.36)	78.02(.30)	77.64(.22)
Al_2O_3	12.40(.15)	12.51(.11)	12.44(.13)	12.49(.04)	12.07(.09)	12.35(.11)	12.47(.36)	12.16(.17)	12.44(.13)
TiO_2	0.09(.02)	0.13(.03)	0.09(.03)	0.09(.03)	0.09(.02)	0.10(.04)	0.11(.03)	0.10(.01)	0.11(.04)
FeO	1.26(.07)	1.27(.09)	1.18(.06)	1.13(.42)	1.32(.05)	1.19(.17)	1.30(.16)	1.25(.17)	1.28(.14)
MgO	0.10(.02)	0.11(.03)	0.09(.02)	0.08	0.10(.02)	0.09(.02)	0.10(.03)	0.09(.03)	0.10(.01)
CaO	1.16(.09)	1.18(.09)	1.17(.11)	0.80(.19)	1.24(.03)	1.14(.03)	1.14(.05)	1.27(.05)	1.22(.06)
Na_2O	3.42(.25)	4.01(.12)	3.50(.10)	3.55(.29)	3.54(.11)	3.70(.15)	3.76(.09)	3.58(.12)	3.71(.09)
K_2O	3.20(.36)	3.25(.15)	3.75(.09)	4.53(.31)	3.47(.21)	3.56(.14)	3.61(.12)	3.47(.11)	3.42(.13)
Cl	0.17(.05)	0.16(.05)	0.18(.05)	0.15(.03)	0.14(.03)	0.10(.03)	0.16(.02)	0.13(.02)	0.19(.06)
H_2O	5.72(.79)	5.67(0.80)	6.33(.99)	7.05(1.93)	6.02(.57)	7.47(1.46)	6.04(.80)	6.71(.90)	5.83(1.33)
n	27	10	6	3	10	11	8	9	12
Sc	5				4	3	5	6	5
V	4				5	3	6	9	7
Cr	-				-	-	1	1	-
Ba	741				715	766	734	790	802
La	21				21	23	22	23	24
Ce	39				39	39	41	44	41
Ni	1				2	-	-	1	-
Cu	5				7	4	8	16	14
Zn	37				45	38	39	43	39
Zr	112				116	110	107	113	107
Nb	5				7	5	6	6	5
Ga	13				14	15	13	14	14
Pb	16				17	17	16	18	17
Rb	118				116	119	118	119	119
Sr	88				86	87	85	91	92
Th	12				11	12	11	11	12
U	3				2	3	3	3	3
Y	19				19	20	18	20	18
As	6				5	5	5	4	5

Tephra samples and locations as in Chapter 2 and Appendix 1:
293 Highway 43 T22/362356; **328** Pakihikura Stream T22/362356; **174** Smiths Rd N137/500954; **182** Turakina N137/864889; **137** Oroua T22/623362; **245** Makaroro River U22/921502; **148** Manawatu River U22/921502; **165** Mangatewainui stream U23/834174
174a and 174b represent compositionally different subgroups within the sample.

Major oxides determined by EMA on n shards in wt%. Trace elements (in ppm) determined by XRF on a single glass separate.

1.06 ± 0.18 Ma (zircon) (Seward 1979), and 1.26 ± 0.12 Ma (glass) (Boellstorff & Te Punga 1977) have been determined for this tephra.

Fleming (1953) considered the Makirikiri Tuff (and hence the Pakihikura Pumice) to be the partial lateral equivalent of the Butlers Shell Conglomerate, at the base of the Castlecliffian type section. Subsequently, the age of Pakihikura Pumice has been considered to provide temporal age control for the base of the Castlecliffian stage (Seward 1974; Boellstorff & Te Punga 1977). However, more recently, tephras of the Makirikiri Tuff are considered to be absent in the Castlecliffian type section (e.g. Pillans 1992) owing to the presence of a major unconformity at the base of the Butlers Shell Conglomerate.

Here the tephra exposed in the road cut of Highway 43 (Pakihikura Pumice of Seward 1976) is referred to as Pakihikura Tephra, as the unit is not characterised by a pumiceous lithology. The name Pakihikura follows the first published name given to the unit (Te Punga 1952). This tephra is not the lowest tephra in the sequence, but it does have a distinctive glass chemistry (Shane & Froggatt 1991) allowing it be correlated to other sequences (Table 8.1).

8.2.2 Stratigraphy

Lithological columns of sections containing Pakihikura Tephra are shown in Fig. 8.1. At the road cut of Highway 43 in the Rangitikei Valley, the Pakihikura Tephra consists of at least 1.5 m of trough cross-stratified ash with occasional pumice lapilli up to 5 cm in size. The unit displays a channel geometry, cut into volcaniclastic sediments deposited in an estuarine setting, as indicated by flaser bedding. Te Punga (1952) classified the strata as Upper Rangitikei Formation. The Pakihikura Tephra is recognised by field character and glass composition in a nearby bluff cut by the Pakihikura Stream, where it enters the Rangitikei River. There it is a 0.6 m massive ash interbedded with sandy sediments displaying flaser beds. In the western part of the Wanganui basin, the Pakihikura Tephra occurs in a road cut near the Turakina River, interbedded in fine, muddy marine sediments. The tephra is not recognised at the Wanganui coast or in volcaniclastic sequences along the Wanganui River. However, a tephra of similar glass chemistry occurs at a 1m thick current bedded unit in an isolated road cut of Smiths Road near Kai-iwi. This exposure is considered to be the base of the Makirikiri Tuff by Fleming (1953), however the lack of stratigraphic control makes the correlation tentative. In the eastern part of the Wanganui basin, the Pakihikura Tephra is exposed in the Oroua River, interbedded in a fluvial sequence. The tephra overlies a paleosol with *in situ* tree stumps and consists of 0.5-1.0 m of fine ash. Its base is massive, while the upper part is finely laminated and cross-stratified at its top. At Oroua, the tephra has been emplaced as an overbank deposit within a fluvial system. The sequence is now part of a tight, south plunging syncline.

Pakihikura Tephra is also found in the East Coast region, where it occurs in the lower part of the Mangatarata Formation. At Mangatewainui Stream, Manawatu River and Makaroro

Oroua   Rangitikei   Makaroro   Tukituki   Manawatu   Mangatewainui
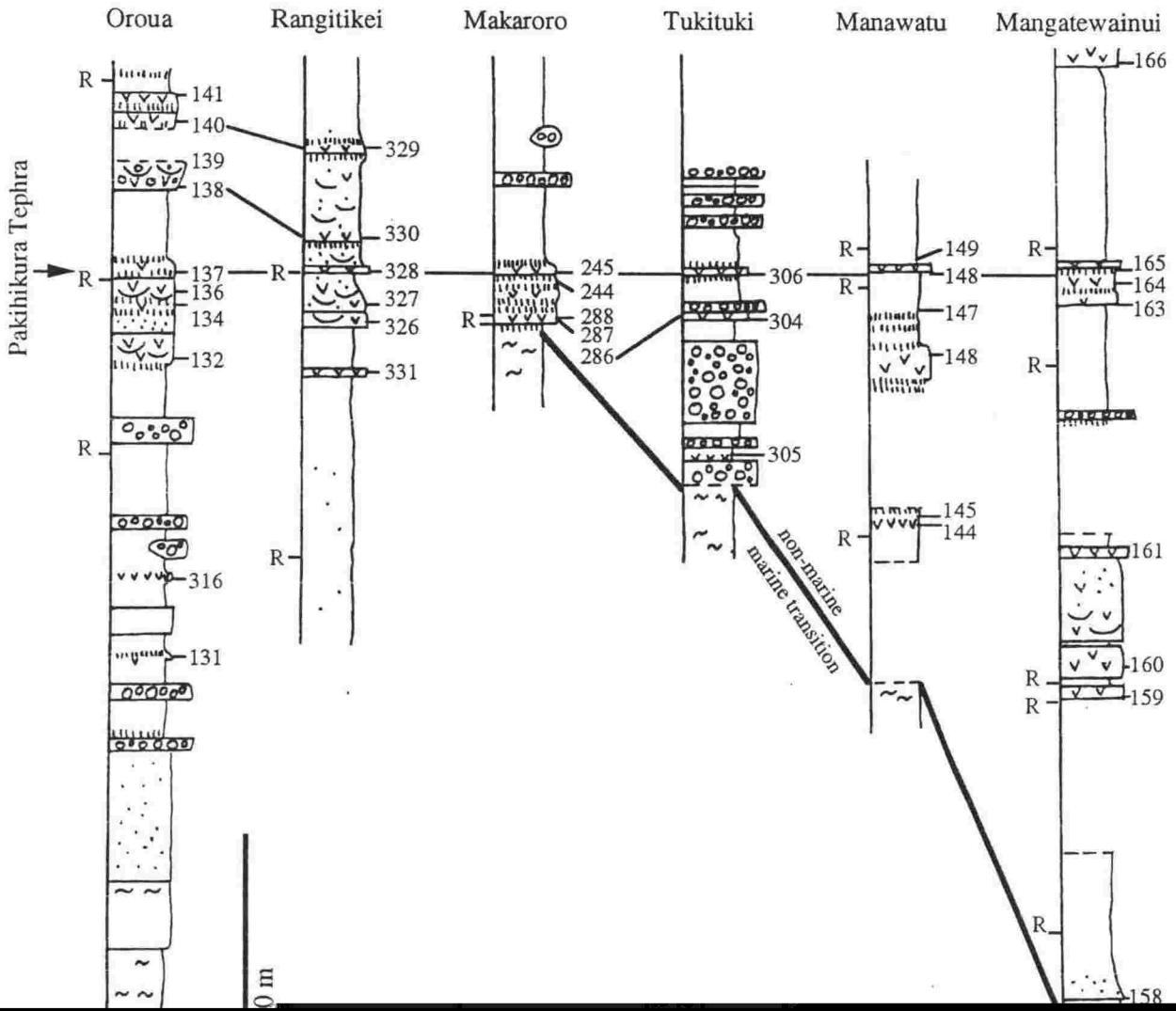
River it consists of a finely bedded ash 0.3-3.0 m thick interbedded in carbonaceous muddy sediments or volcaniclastic sediments, and usually overlying a paleosol or lignite bed. At Makaroro, the tephra occurs near the base of a volcaniclastic sequence defining a gently east dipping monocline.

8.2.3 Chemical characteristics

Pakihikura Tephra is found in a stratigraphic sequence with several other tephras (Fig. 8.1), but can be identified as it is chemically distinctive (Fig. 8.2). The tephra belongs to the high-Ca group of tephras (Chapter 4) and thus on variation diagrams it plots away from most of the other tephras in stratigraphic proximity (Fig. 8.2). In trace element composition, Pakihikura Tephra is characterised by relatively low abundances of many incompatible elements, such as La, Ce and Y (Fig. 8.3, Table 8.1), compared to other tephras.

Using EMA data, compositions of each of the Pakihikura Tephra correlatives can be compared using similarity coefficients (Borchardt et al. 1971). The resulting SC values of >0.94 suggest close chemical similarity for each of the correlatives (Table 8.2). Similarly, a selection of trace elements produce SC values >0.90 (mostly >0.94, Table 8.2).

Sample 174 from the Smiths Road exposure consists of two compositionally different glass shard groups (Table 8.1). The larger group is chemically similar to other Pakihikura Tephra correlatives. The presence of different glass types suggests depositional mixing of different eruptives.

8.2.4 Paleomagnetism and age

The Pakihikura Tephra and enclosing sediments are of reversed polarity (Table 8.3). At each of the sites sampled, the specimens display moderate to severe normal overprinting. As a result mean polarity directions are highly scattered reflecting differing degrees of success in removing the overprint. However in all cases, the specimens display a trend toward a reversed direction during demagnetisation.

The Pakihikura Tephra occurs beneath the Jaramillo Subchron in the Mangatewainui and Rewa Hill sections, in a long interval of reversed polarity strata and is therefore older than 1.07 Ma. Rewa Tephra occurs above Pakihikura Tephra at Rewa Hill, and has an Ar/Ar age of ca. 1.46 Ma (Chapter 7). As the Olduvai Subchron has not been identified in these sections, the Pakihikura Tephra may be younger than 1.77 Ma. Ar/Ar ages on plagioclase crystals from the Oroua exposure range from 0.574-1.975 Ma (Chapter 7); suggesting loss of Ar for the younger age determinations. Therefore, Pakihikura Tephra is considered to be in the age range 1.46-1.77 Ma, significantly older than indicated by previously published fission-track ages. An Ar/Ar age of 1.656 ± 0.025 Ma has been determined for tephra 318 (=136, Fig. 8.1), which
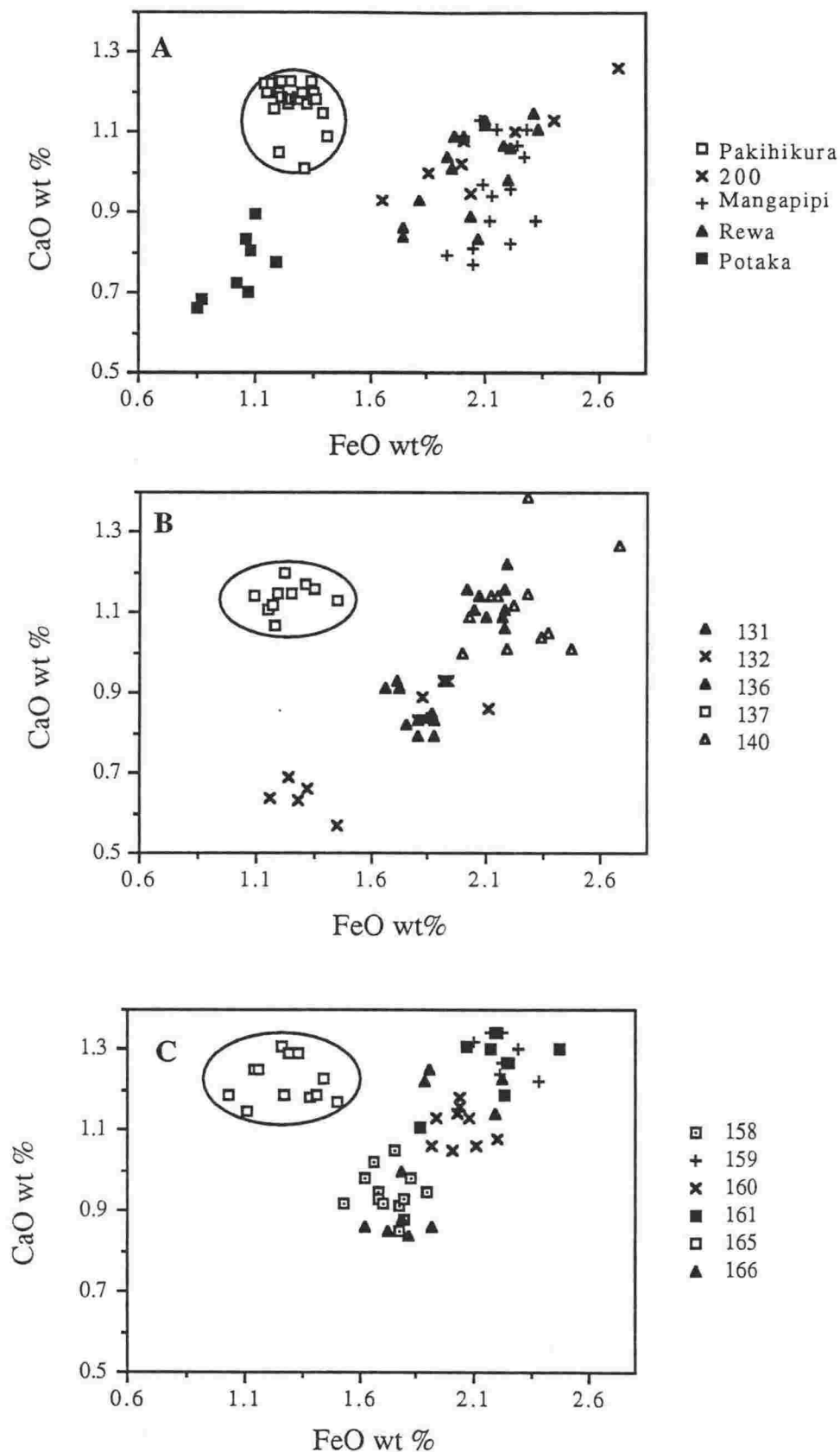
Fig 8.2. Glass composition of Pakihikura Tephra and other tephras in close stratigraphic proximity, determined by EMA. A Sequence along Highway 43, Rangitikei valley (data from Shane & Froggatt 1991). B Oroua River and C Mangatewainui stream. Pakihikura Tephra is circled in each case.
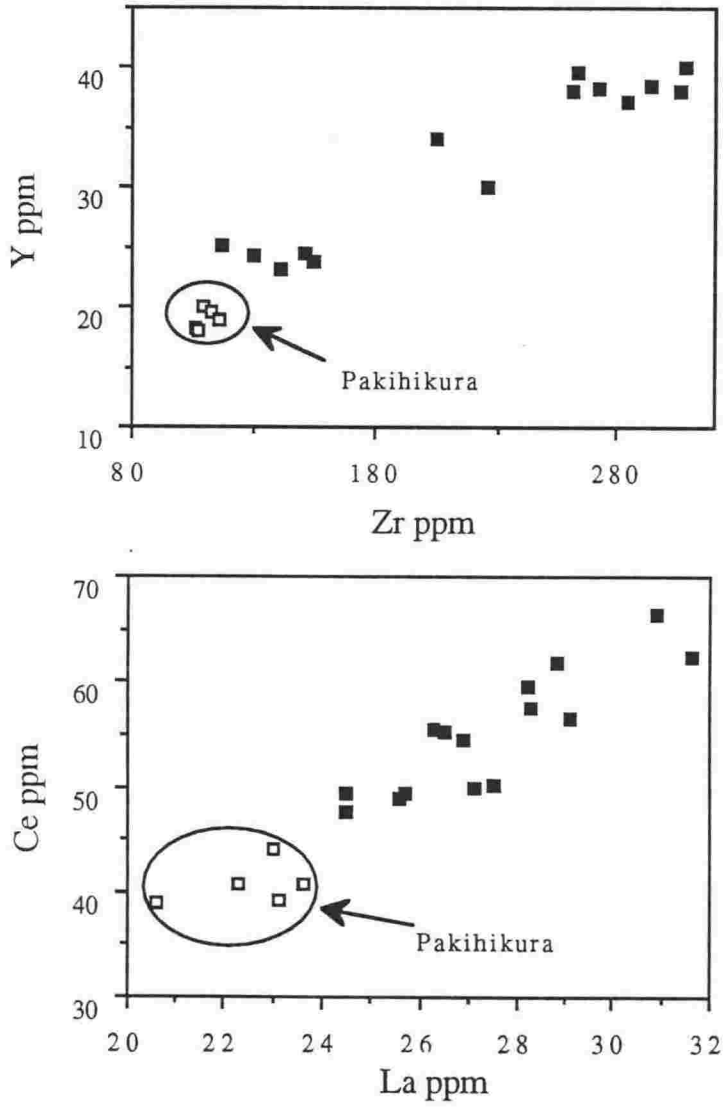
Fig 8.3. Trace element composition of Pakihikura Tephra correlatives compared to that of other early Pleistocene tephras in the sequences.

Table 8.2. Similarity Coefficients comparing tephras considered correlatives of the Pakihikura Tephra. Those for major and minor elements are calculated on Si, Al, Ti, Fe, Mg, Ca, Na and K. Those for trace elements are calculated on Ba, La, Ce, Zn, Zr, Nb, Rb, Sr and Y.

Major and minor elements:

	293	328	174	182	137	245	148	165
293	1	0.96	0.96	0.97	0.94	0.94	0.94	0.95
328		1	0.94	0.97	0.96	0.97	0.97	0.98
174			1	0.95	0.97	0.94	0.96	0.93
182				1	0.94	0.95	0.96	0.96
137					1	0.96	0.97	0.95
245						1	0.94	0.98
148							1	0.96
165								1

Trace elements:

	293	182	137	245	148	165
293	1	0.94	0.97	0.95	0.93	0.95
182		1	0.92	0.94	0.94	0.90
137			1	0.96	0.94	0.96
245				1	0.94	0.96
148					1	0.94
165						1

Table 8.3. Paleomagnetic data for Pakihikura Tephra and enclosing sediments

position	lithology	section	decl.	incl.	α_{95}	n
Pakihikura Tephra		Highway 43	175	29	17	3
+30m*	mudstone	Oroua	193	69	19	4
-0.2m	mudstone	Oroua	169	66	10	4
+3m	mudstone	Mangatewainui	254	78	85	4
-7m	mudstone	Makaroro	341	78	38	4
-17m	mudstone	Mangatewainui	192	52	19	3

* site distance above (+) or below (-) tephra

α_{95} = circle of 95% confidence, n= number of specimens.

occurs immediately below Pakihikura Tephra in the Oroua section. A recent isothermal plateau fission-track age on glass of 1.63 ± 0.15 Ma (Alloway et al. 1993) for the exposure in the Pakihikura Stream bluff is consistent with the stratigraphy presented here.

8.2.5 Implications

Te Punga (1952) suggested Pakihikura Tephra occurs at the base of the Castlecliffian stage as Nukumaruan macrofossils occur below it, but typical Castlecliffian species occur above it, in the Rangitikei valley. The age of the tephra (ca. 1.63 Ma) is considerably older than the base of the Castlecliffian type section (0.99-1.07 Ma), which occurs in the Jaramillo Subchron (Turner & Kamp 1990). As the base of the Castlecliffian type section is an angular unconformity, the Pakihikura Tephra could occur within the interval missing and thus Castlecliffian faunas referred to by Te Punga (1953) extend further back in time than that represented at the type section.

In the East Coast region, from Dannevirke to Makaroro River, the Pakihikura Tephra occurs above the transition of marine to non-marine facies (Fig. 8.1). This suggests the sea retreated from the region prior to ca. 1.63 Ma, significantly earlier than in the Wanganui basin. The transition occurs at a greater stratigraphic distance beneath the tephra in more southerly sections (Fig. 8.1), suggesting more rapid sedimentation rates and/or earlier marine regression in the south of the basin.

8.3 A WIDESPREAD EARLY PLEISTOCENE TEPHRA (POTAKA TEPHRA, 1 MA) IN NEW ZEALAND: CHARACTER, DISTRIBUTION AND IMPLICATIONS
(a manuscript submitted to New Zealand Journal of Geology & Geophysics)

Abstract At about 1 Ma, a large eruption in the Taupo Volcanic Zone of North Island, New Zealand produced an extensive silicic ignimbrite now found up to 200 km from source and a fall out ash up to 600 km distant. The eruptive, collectively referred to as Potaka Tephra, is an important marker horizon and temporal control point in many early Pleistocene sequences, which otherwise lack numerical age control. The tephra is identified at many localities using multiple criteria including lithology, mineralogy, glass and mineral chemistry, magnetostratigraphy and isotopic ages. It occurs near the top of the Jaramillo Subchron and is immediately overlain by a Normal to Reversed transition. Potaka Tephra is found in both marine and terrestrial facies, and on both major islands of New Zealand. Its identification allows correlation of (1) mid shelf, glacioeustatic cyclothems on the western side of North Island with fluvial and lacustrine facies on the eastern side of North Island and (2) the only known middle Pleistocene marine sequence in South Island with extensive sequences in North Island. Stratigraphic position and chronology suggest Potaka Tephra was erupted during

Table 8.4. Localities of Potaka Tephra

Site	Locality	Grid ref.	Thickness (m)	Deposit	Stratigraphic context
1	Rewa Hill, road cut on Highway 45	T22/357311	ca. 10	volcaniclastic	nearshore marine sediments, Upper Rangitikei Fm
2	Wanganui Coast, coastal cliffs	R22/729454	ca. 5	volcaniclastic	nearshore marine sediments, Kaimatira Pumice Sand, lower Kai-iwi Group
3	Kaimatira bluff, road cut on Highway 3	R22/890434	ca. 20	volcaniclastic	nearshore marine sediments Kaimatira Pumice Sand, lower Kai-iwi Group
4	Smiths/Makuhou Rd intersection, road cut	S22/137319	4	volcaniclastic	nearshore marine sediments
5	Cape Kidnappers, coastal cliffs	W21/581655	1.5 6	ignimbrite volcaniclastic	fluvial sediments overlying marine Maraetotara Fm, Kidnappers Tuff
6	Air Hill Station, road cut on Highway 50	V21/115603	3	ignimbrite	fluvial sediments
7	Kereru Rd, road cut in Gwavas Forest	V21/030631	3	ignimbrite	fluvial sediments
8	Mangaonuku stream, near Highway 50	U22/097592	4	ignimbrite	fluvial sediments
9	Makaroro River	U22/922501	1.5	ignimbrite	fluvial sediments, Mangatarata Fm.
10	Mangatewainui stream	U23/816188	25	volcaniclastic	fluvial sediments, Mangatarata Fm.
11	Mangatewaiiti stream	U23/807173	30	volcaniclastic	fluvial sediments, Mangatarata Fm
12	Leader River	O32/325414	0.10	fallout ash	fluvial sediments

Grid references are those of the NZMS 260 map series.

oxygen isotope stage 27. The distribution of Potaka Tephra indicates rapid uplift of the main Axial Ranges in central North Island and progradation of coast lines in the last 1 Ma.

8.3.1 Introduction

Numerous silicic tephras are interbedded in Pleistocene strata of the North Island of New Zealand. They have the potential to provide a numerical chronology and be a correlation tool for thick, high resolution Pleistocene sequences which are thought to be climatically controlled (e.g. Pillans 1992). Although the stratigraphy of eruptive events is well known for the last 50 ka (Froggatt & Lowe 1990), less is known about the tephras in the interval extending back to ca. 2 Ma (e.g. Seward 1976; Nelson et al. 1986; Shane & Froggatt 1991). This paper reports on a large, rhyolitic ignimbrite-producing eruption, which occurred about 1 Ma ago. The source vent is uncertain as the tephra has not been recognised in proximal areas of the Taupo Volcanic Zone (TVZ) (Wilson et al. 1984). However, ignimbrites of similar age are known from the Mangakino caldera (Wilson et al. 1984; Pringle at al. 1992). The widespread tephra has been previously referred to in many localities and by various names, including Potaka Pumice (Te Punga 1952), Kaimatira Pumice Sand (Fleming 1953) and Kidnappers Tuff (Kingma 1971). It is referred to here as Potaka Tephra. This name does not have grain size connotations and follows the first published name for the tephra (Te Punga 1952), for exposures in the Rangitikei Valley. A type locality has not been defined, but reference localities are described here, covering a range of tephra facies and depositional environments (Table 8.4).

The ignimbrite is identified some 200 km from possible source vents and the fallout ash up to 600 km. The eruptive is found in a variety of sedimentary facies, both marine and terrestrial, and on both major islands of New Zealand (Fig. 8.4). This paper demonstrates the correlation of the tephra between different exposures using stratigraphic, chemical and paleomagnetic methods, and discusses the significance of its distribution, age and magnetostratigraphic position to the New Zealand Pleistocene.

8.3.2 Distribution and character of Potaka Tephra

Potaka Tephra is widespread in the southern North Island. Localities of the tephra that have been identified and correlated by various criteria including glass chemistry (Table 8.4) are shown in Fig. 8.4. Lithological columns of key localities are shown in Fig. 8.5.

Rewa Hill

Approximately 10 m of stratified and cross stratified ash, lapilli and pumice blocks are exposed in a road cut at Rewa Hill, near the Rangitikei River (Fig. 8.4), within early to middle
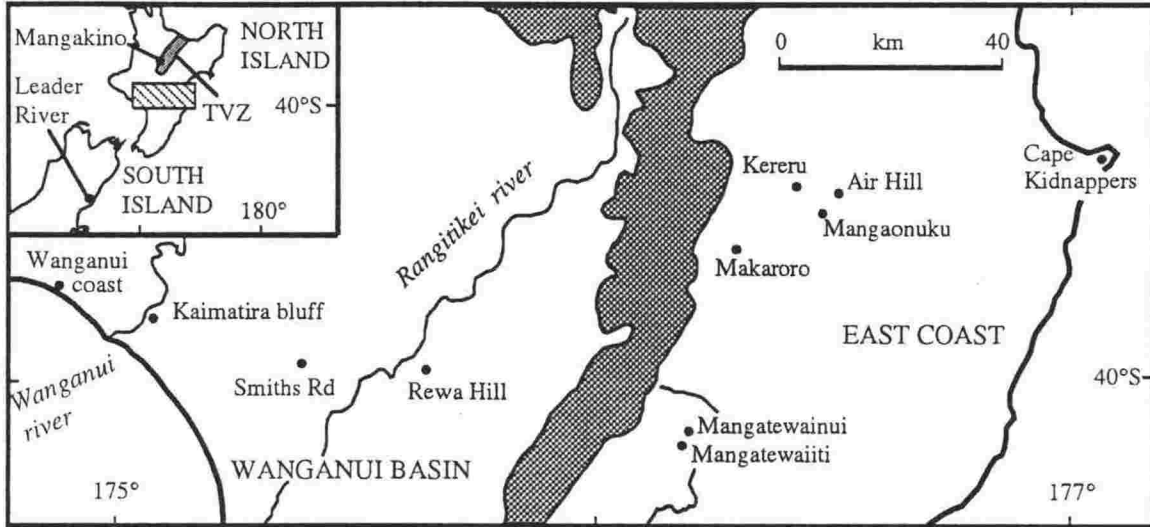
Fig. 8.4 Map of southern North Island showing localities of Potaka Tephra. Shaded area represents the main Axial Ranges.
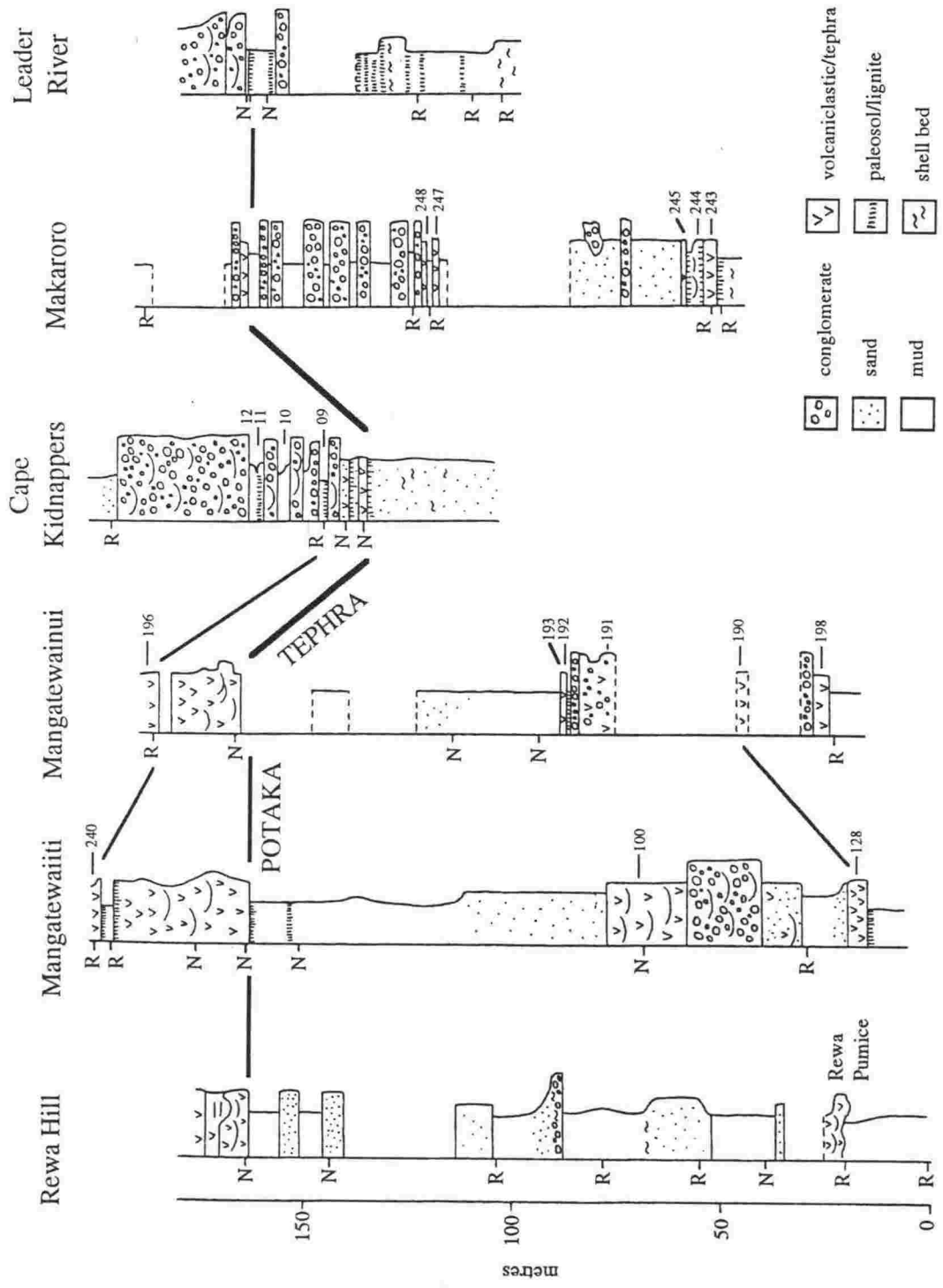
Fig. 8.5 Stratigraphic columns of key localities of Potaka Tephra. Numbers refer to megascopic tephras. Tephra correlation lines are based on multiple criteria including glass chemistry. Paleomagnetic sites shown as normal (N) or reversed (R). Leader River redrawn from data of G. Warren (pers. comm. 1993).

Pleistocene Upper Rangitikei Formation (Te Punga 1952), and has been referred to as Potaka Pumice (Seward 1976). Pumice blocks are conspicuously large (up to 10 cm in size) compared to other tephras in the section, and contain hornblende and biotite phenocrysts up to 2-3 mm long. The tephra overlies well sorted, stratified sands, with mud-drapes suggestive of an intertidal setting. Its base is an undulating ripple surface cut into the sands. The lowermost 0.5 m of the tephra unit consists of a laminated, cross stratified fine white ash which possibly represents reworked, initial fallout. This is overlain by several units of cross-stratified and current bedded ash and pumice, interbedded with non-volcaniclastic sands. Trough cross beds of 0.4-0.5 m amplitude, often bipolar directional, are the most common sedimentary structures in the tephra. Occasional rip-up clasts of mudstone and greywacke and fragments of charcoal also occur. Erosion surfaces and channels with up to 2 m relief occur near the top of the unit. The sedimentary structures are suggestive rapid of deposition and prolonged reworking in a near shore and/or estuarine environment.

Wanganui coast

The Potaka Tephra can be traced intermittently as a mappable formation, some 60 km west of the Rewa Hill section to near the Wanganui coast (Fig. 8.4). At these more westerly exposures, the coarse volcaniclastic formation has been referred to as Kaimatira Pumice Sand (Fleming 1953). Seward (1976) made the tentative correlation of Potaka Tephra to Kaimatira Pumice Sand and traced the unit through out much of the Wanganui basin. At Kaimatira bluff on the west bank of Wanganui River, the tephra consists of ca. 20 m of coarse, fossiliferous, cross stratified ash and lapilli overlain by stratified ashy sands. Fossil assemblages include intertidal and subtidal species (Fleming 1953). The whole unit unconformably overlies fossiliferous marine mudstone. The Potaka Tephra also outcrops at the Wanganui coast, type section for the early-middle Pleistocene Castlecliffian stage. There it represents a 5 m bed of pumice blocks (14 cm maximum size) in an ashy sand matrix with fragments of charcoal and other coarse fossiliferous debris.

Cape Kidnappers

On the East Coast of the North Island, the Potaka Tephra is found in non-marine facies (Fig. 8.5). At Cape Kidnappers (Fig. 8.4), the tephra has been referred to as Kidnapper Tuff (Kingma 1971) and Kidnappers-A (Black 1992). Its base is a 0.5-1.5 m unwelded ignimbrite which overlies a paleosol developed on eolian dune sands at the top of the Maraetotara Sands (Kingma 1971; Black 1992). An in situ, charred fossil tree stump protrudes into the base of the ignimbrite and charred, flow-oriented logs are contained in the top of the unit indicating high temperature emplacement. The base of the ignimbrite is weakly laminated and composed of fine

lapilli and lithic clasts. Most of the flow unit is massive, poorly sorted and almost entirely vitric. Maximum clast size is 2 cm. Immediately overlying this unit is ca. 6 m of cross stratified fluvial volcaniclastic sediments, consisting of graded and sorted ash and pumice. In contrast to the underlying ignimbrite, clast sizes reach 6 cm and are thus likely to have been derived from more proximal exposures of coarse ignimbrite. At least four depositional episodes are recorded in the volcaniclastic unit, each separated by a paleosol, suggesting prolonged reworking after the eruption. The episodic nature of the deposits suggests they may have resulted from floods. The Potaka Tephra unit is overlain by fluvial conglomerate and sands of the Mt Gordon Beds (Black 1992) at this section.

Other East Coast sections

The Potaka ignimbrite phase can be recognised at several exposures in the East Coast region, up to 50 km inland from Cape Kidnappers (Fig. 8.4). It is thickest (4 m) at Mangaonuku Stream, where it has been emplaced on to fluvial gravels. The most southerly exposure of ignimbrite examined, and thus most distal from source, occurs in the Makaroro River. There it is 1.5 m thick and occurs in a easterly tilted sequence of fluvial conglomerate and mudstone. The ignimbrite at Makaroro contains flow oriented charred logs, up to 1.5 m in length and 0.2 m wide. Some logs show evidence of in situ combustion which has formed crystal rich gas escape pipes. At this exposure, the ignimbrite has been emplaced on to a subaerially exposed surface. The ignimbrite is overlain by conglomerate and no associated volcaniclastic units are found above it.

Further south in the East coast region, at localities more distal to source, the Potaka Tephra is recognised in the predominantly fluvial and lacustrine Mangatarata Formation (Lillie 1953; Shane 1991) (Fig. 8.5). In the most southerly exposures (Mangatewaiiti and Mangatewainui) the tephra consists of up to 30 m of fluvially deposited cross stratified and laminated ash and lapilli. Pumice blocks are up to 15 cm in size and contain the characteristic large hornblende and biotite phenocrysts. The sequences is well exposed in the Mangatewaiiti Stream, where the tephra overlies lignitic mudstone, on a previously vegetated surface. Although multi-depositional, the tephra was emplaced rapidly as indicated by cross stratification, scour and fill structures, and convolute and deformation structures associated with dewatering during depositional compaction. Rip-up clasts of a variety of lithologies and charcoal also occur. The top of the tephra is marked by a paleosol with root structures. Rapid vertical accretion on a 30 m scale in an overbank setting implies the deposit represents a very large scale catastrophic flood event (e.g. Shane 1991).

Leader River

Table 8.5. Major oxide glass chemistry of Potaka Tephra correlatives determined by EMA.

Site		SiO$_2$	Al$_2$O$_3$	TiO$_2$	FeO	MgO	CaO	Na$_2$O	K$_2$O	Cl	Water	n
1	base	77.38(.31)	12.27(.13)	0.14(.05)	1.23(.08)	0.12(.02)	0.97(.08)	3.94(.14)	3.74(.14)	0.23(.04)	5.50(0.78)	15
	top	77.51(.39)	12.32(.13)	0.09(.02)	1.05(.13)	0.09(.04)	0.80(.14)	3.70(.19)	4.20(.21)	0.24(.02)	6.30(0.53)	9
2		77.67(.29)	12.23(.16)	0.11(.01)	1.15(.16)	0.11(.03)	0.94(.16)	3.55(.19)	4.05(.31)	0.23(.04)	6.09(2.28)	8
3		77.78(.27)	12.15(.10)	0.12(.03)	1.12(.18)	0.13(.02)	0.95(.11)	3.51(.16)	4.04(.12)	0.23(.02)	5.51(1.59)	9
4		78.07(.41)	12.04(.12)	0.13(.03)	1.02(.17)	0.11(.03)	0.89(.14)	3.49(.18)	4.13(.27)	0.23(.03)	5.53(1.35)	10
5	base	77.34(.52)	12.36(.26)	0.12(.02)	1.17(.08)	0.13(.01)	1.00(.01)	3.82(.12)	3.85(.16)	0.22(.02)	7.02(1.08)	12
	middle	77.63(.30)	12.20(.21)	0.11(.04)	1.11(.19)	0.11(.03)	0.91(.14)	3.72(.11)	4.02(.23)	0.21(.05)	4.88(1.02)	10
	top	77.81(.46)	12.10(.24)	0.12(.02)	1.06(.14)	0.11(.03)	0.85(.15)	3.68(.10)	4.10(.16)	0.23(.04)	5.43(0.86)	11
6		77.22(.58)	12.43(.43)	0.16(.05)	1.12(.22)	0.13(.03)	0.96(.16)	3.86(.16)	3.92(.20)	0.25(.06)	3.40(1.14)	10
7		77.05(.22)	12.33(.20)	0.14(.03)	1.24(.12)	0.14(.03)	0.95(.18)	3.89(.18)	4.00(.27)	0.25(.06)	4.08(0.99)	11
8	base	77.75(.18)	12.28(.07)	0.15(.04)	1.15(.08)	0.12(.03)	0.91(.07)	3.79(.09)	3.62(.24)	0.23(.02)	5.99(0.70)	10
	middle	77.09(.25)	12.39(.11)	0.12(.04)	1.17(.08)	0.10(.02)	0.92(.10)	3.87(.15)	4.15(.22)	0.20(.02)	6.67(1.47)	10
	top	76.98(.32)	12.47(.16)	0.12(.03)	1.17(.15)	0.11(.03)	0.83(.13)	3.80(.04)	4.31(.12)	0.23(.03)	5.77(1.04)	10
9		77.47(.21)	12.32(.12)	0.13(.04)	1.08(.08)	0.10(.02)	0.86(.09)	3.78(.18)	3.98(.25)	0.25(.03)	7.04(1.04)	13
10	base	76.92(.27)	12.49(.13)	0.16(.05)	1.19(.11)	0.12(.02)	0.98(.12)	3.90(.10)	4.01(.22)	0.23(.02)	6.54(0.73)	11
	top	77.68(.21)	12.29(.12)	0.11(.03)	0.95(.07)	0.10(.03)	0.73(.06)	3.74(.07)	4.17(.08)	0.24(.02)	4.06(0.56)	10
11		76.71(.30)	12.64(.11)	0.10(.03)	1.14(.17)	0.11(.03)	0.88(.16)	3.84(.16)	4.39(.02)	0.20(.02)	6.50(0.78)	10
12		77.71(.23)	12.21(.10)	0.14(.03)	1.18(.09)	0.11(.02)	0.94(.10)	3.70(.12)	3.79(.17)	0.24(.03)	5.05(0.90)	14

Site numbers and deposits sampled as in Table 1.

Analyses recalculated to 100% on a volatile-free basis and presented as a mean and standard deviation of n shard analyses. Determined by a Jeol 733 Superprobe using a 8 nA current at 15 kV and a 20 μm beam diameter. Method and standards as in Froggatt (1983).

The Potaka Tephra occurs as a thin (10 cm) pink-white, fallout ash in fluvial sediments exposed by the Leader River in North Canterbury, South Island (Fig. 8.4, 8.5). The tephra is interbedded with lignitic paleosols within a sequence of sandy mudstone alternating with conglomerate, which contain pollen, insecta and sub-fossil avifauna. Marine sediments beneath the sequence contain early Pleistocene (Castlecliffian) faunas (G. Warren pers. comm. 1991). The thickness of Potaka Tephra at this locality, some 600 km from source, is comparable to that of the widespread 22 ka Kawakawa Tephra found at localities in North Canterbury and elsewhere in the South Island (Kohn 1979; Campbell 1986). This thickness probably reflects both the initial fall out and subsequent local reworking, but does point to a very explosive eruption.

8.3.3 Glass chemistry

Petrographically, the Potaka Tephra is composed of clear glass shards (80-90%) and plagioclase crystals (10-15%). Both the ignimbrite and fallout ash are characterised by large green hornblende and biotite phenocrysts (>90% of mafic fraction), with minor components of hypersthene and Fe-Ti oxides.

The major oxide composition of glass shards from Potaka Tephra exposures were determined by Electron Microprobe Analysis (EMA) (Table 8.5). Mean glass shard analyses have a SiO_2 content of about 77 wt.% and a total alkali content of about 7.5 wt.%, indicative of a calc-alkaline rhyolite. The glass composition is broadly similar to those of middle and late Pleistocene tephras erupted from the TVZ (Froggatt 1983; Nelson et al. 1986; Shane & Froggatt 1991). The mean composition from each exposure is very similar within variation limits (Table 8.5), consistent with them representing a common eruption. If individual shard compositions are examined separately, a limited compositional zonation in the samples is evident (Fig. 8.6). Shards from different stratigraphic heights in the exposures form a linear trend on variation diagrams suggestive of pre-eruptive zonation in the magma chamber. However the trend with high FeO and CaO in the base of the unit is the reverse of most zoned eruptives, which are usually more silicic at the base (e.g. Hildreth 1981). This zonation is evident in exposures of fluvially deposited tephra as well as the ignimbrite phase. It is also found in the thin fallout ash at Leader River, some 600 km from source. This suggests the compositional variation is not the product of mixing of different eruptions, but reflects variation in the main eruptive phase. In the ignimbrite, shards of a variety of compositions are present at different stratigraphic heights suggesting thorough mechanical mixing during emplacement. However, samples from the base of the ignimbrite are generally dominated by shards of higher FeO and CaO contents (Fig. 8.6b) and Na/K ratios >1. Large pumice clasts from the top of the volcaniclastic units and matrix from the top of the ignimbrite are characterised by higher K_2O contents (Fig. 8.7). The segregation of compositions is most evident in the volcaniclastic
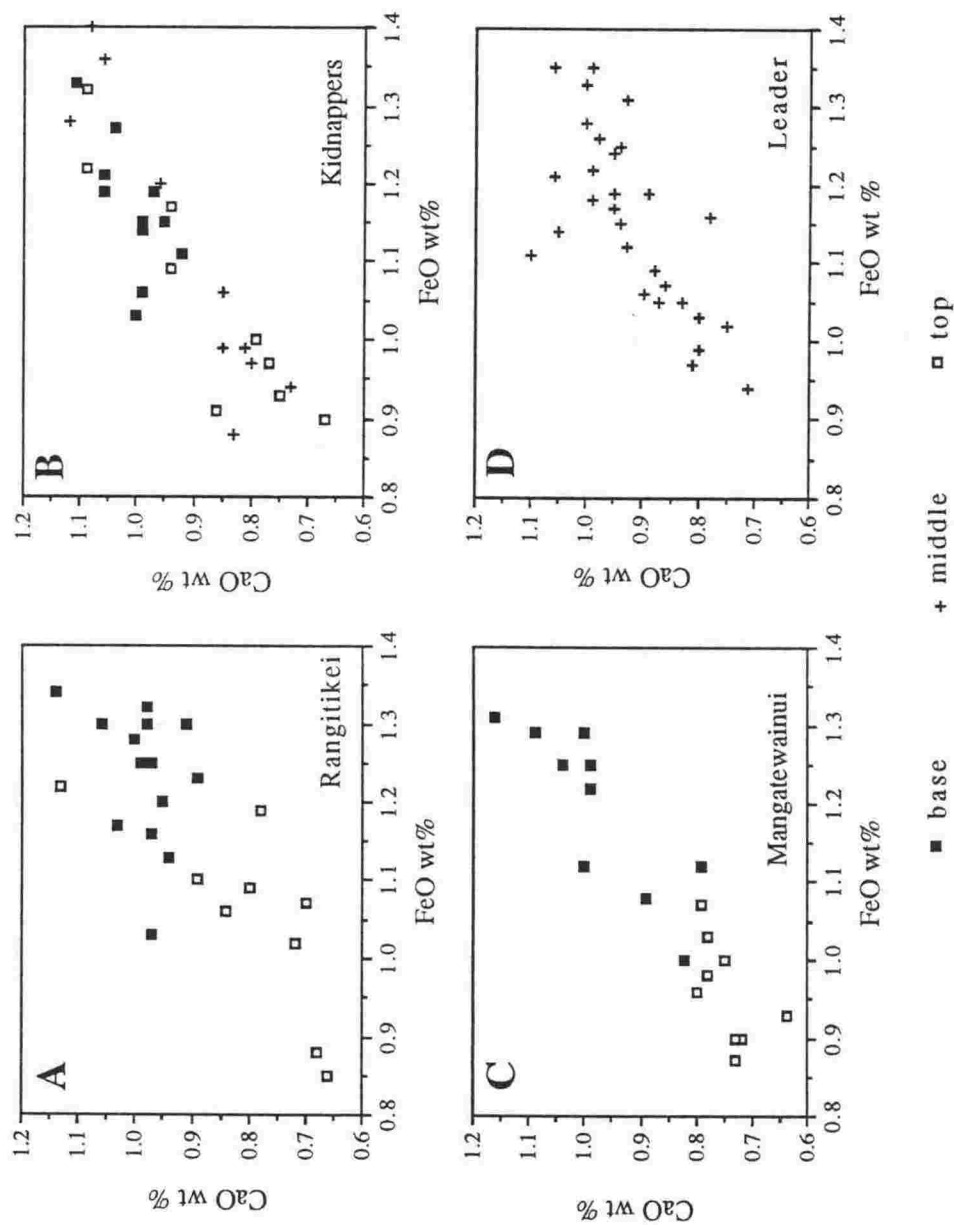
Fig. 8.6 Individual glass shard compositions determined by EMA from samples of Potaka Tephra.
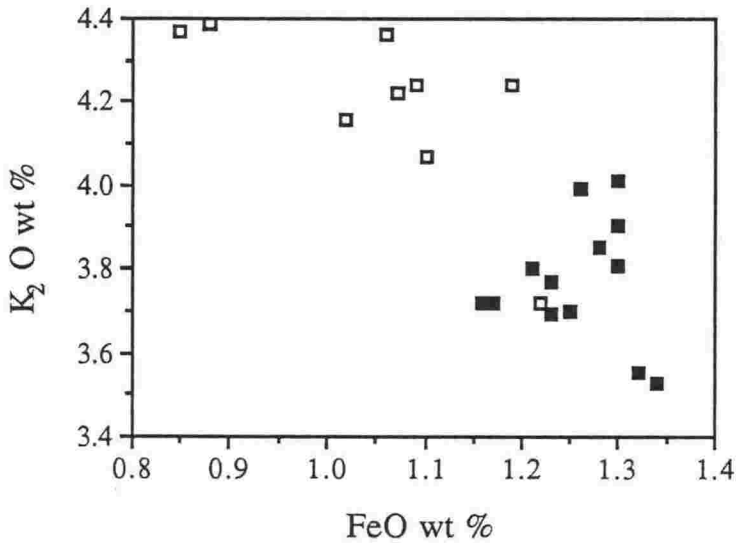
Fig. 8.7 Individual glass shard analyses of Potaka Tephra at the Rewa Hill section, showing variation in Fe and K contents.

Fig. 8.8 Glass shard analyses of different tephras in close stratigraphic proximity to Potaka Tephra at the Mangatewaiiti section. Tephra positions shown in Fig. 8.5.
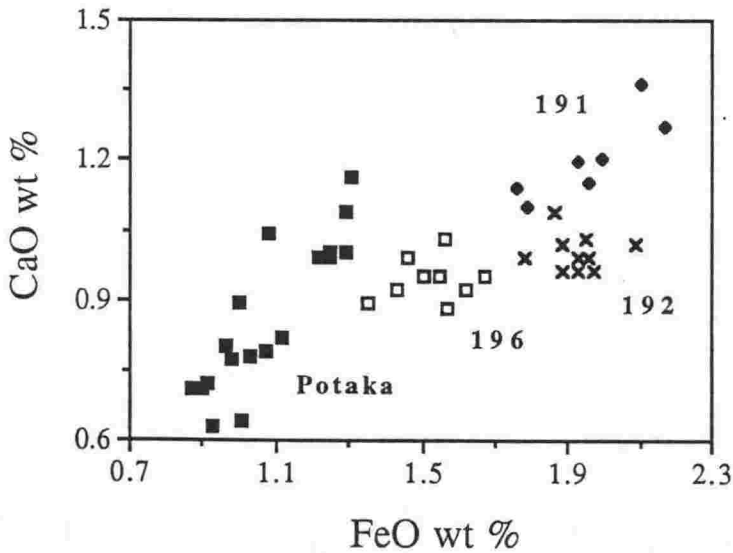
Table 8.6. Trace element analyses (ppm) of Potaka Tephra correlatives determined by XRF.

	1	2	4	5	6	8	9	10	11
Sc	3	4	4	2	4	3	4	3	2
V	7	9	6	6	6	6	10	8	7
Cr	-	2	-	-	-	-	1	4	-
Ba	751	714	730	745	748	732	734	729	765
La	26	27	26	25	25	25	25	26	26
Ce	49	50	49	47	49	48	45	45	49
Ni	-	3	1	-	-	-	-	-	-
Cu	10	22	11	10	4	5	6	12	16
Zn	38	40	38	40	41	43	45	41	40
Zr	143	152	141	129	119	126	129	117	117
Nb	8	8	8	8	8	9	8	8	8
Ga	14	12	14	14	14	14	13	13	14
Pb	18	18	16	19	18	18	19	19	19
Rb	131	134	138	131	137	130	130	131	138
Sr	75	84	63	72	64	68	66	67	69
Th	13	14	14	14	15	14	13	13	14
U	4	3	3	4	3	4	3	3	3
Y	24	25	23	24	26	24	23	23	25
As	5	7	5	6	5	5	5	5	6
n	2	1	1	3	1	3	1	1	1

Site numbers as in Table 8.4.
n= number of analyses.

deposits, which indicate the initial eruptive phase is more FeO and CaO rich (Fig. 8.6a, c). This chemical signature makes Potaka Tephra distinctive, as most New Zealand Pleistocene tephras are chemically homogeneous (e.g. Froggatt 1983; Shane & Froggatt 1991).

The Potaka Tephra can be easily distinguished from other tephras in close stratigraphic proximity, solely on the basis of major oxide composition (Fig. 8.8). Other tephras are also chemically distinctive, allowing correlation. They form tie lines above and below the Potaka Tephra horizon which produces a stratigraphic framework (e.g. Fig. 8.5). To further characterise different samples of the tephra, bulk separates of fresh glass were purified by electromagnetic methods and analysed by XRF for a number of trace elements (Table 8.6). Again the similarity in analyses of different samples is consistent with a single eruptive event. The compositional zonation in the eruptive (especially in major oxide contents) makes numerical comparisons of sample compositions of little value in correlation tests. However, discriminant function analyses of the compositional data indicates that each sample of Potaka Tephra be distinguished from samples of other widespread Pleistocene tephras (Shane & Froggatt unpubl. data).

8.3.4 Fe-Ti oxide chemistry

Fe-Ti oxide compositions are sensitive to the conditions of the magma at the time of eruption (e.g. temperature) and therefore have the potential for characterising a particular eruptive event. Fe-Ti oxides were extracted from several exposures of Potaka Tephra and their major oxide composition determined by EMA (Table 8.7). The spinel phase have ulvospinel in the range 31-34 mol. %. Crystals from the base of the tephra are generally higher in TiO_2 and lower in Fe_2O_3 content, compared to those from the top and from large pumice clasts (Fig. 8.9a). They form a compositional trend which is seen in both the ignimbrite and volcaniclastic deposits, and reflects the compositional trend in the co-existing glasses, suggestive of a zoned magma chamber. This distinctive zonation strongly supports the equivalence of different exposures. Insufficient ilmenite analyses were obtained to determine eruption temperatures. However, Potaka Tephra can be distinguished from other tephras in the sections on the basis of Fe-Ti oxide compositions (Fig. 8.9b).

8.3.5 Paleomagnetism

Oriented specimens were collected from several sections to determine the paleomagnetic polarity of the Potaka Tephra and the enclosing sediments. Cube-shaped specimens of fine ash were cut with a knife and placed in 6 cm^3 plastic boxes which were oriented in the field. Cores were drilled into the more consolidated enclosing sediments. Specimens were measured and demagnetised sequentially with a Molspin spinner magnetometer and in alternating fields of 0-

Table 8.7. Fe-Ti oxide compositions determined by EMA for correlatives of the Potaka Tephra.

	1	2	4	5	6	8	10
SiO2	0.08(.07)	0.15(.05)	-	0.12(.05)	0.11(.03)	0.09(.04)	0.11(.03)
Al2O3	1.42(.08)	1.51(.06)	1.43(.10)	1.45(.07)	1.49(.09)	1.44(.07)	1.42(.21)
TiO2	10.43(.50)	11.09(.07)	10.69(.52)	10.52(.40)	11.22(.67)	11.65(.45)	11.48(.74)
Fe2O3	46.00(1.24)	45.15(.27)	45.60(.62)	46.23(1.49)	44.99(1.29)	44.11(.98)	44.67(1.59)
FeO	39.17(.60)	40.02(.22)	39.28(.65)	39.68(.68)	40.02(.54)	40.68(.89)	40.44(.54)
MnO	0.46(.07)	0.54(.08)	0.49(.04)	0.45(.02)	0.59(.04)	0.45(.08)	0.48(.06)
MgO	0.57(.05)	0.60(.02)	0.57(.13)	0.60(.03)	0.59(.10)	0.58(.09)	0.60(.19)
CaO	-	0.02(.02)	-	-	0.02(.02)	0.01(.01)	0.01(.02)
Total	97.84(.92)	99.09(.34)	98.06(1.06)	98.80(.99)	99.05(.26)	98.84(.83)	99.21(.81)
% ulvosp.	0.31(.01)	0.32(.02)	0.32(.01)	0.31(.01)	0.33(.02)	0.34(.01)	0.32(.01)
n	18	7	9	4	7	27	7

Site numbers as in Table 8.4.
Analyses presented as means and standard deviations on n crystals and determined by a Jeol 733 Superprobe using a 12 nA current at 15 kV and a 2μm beam diameter.
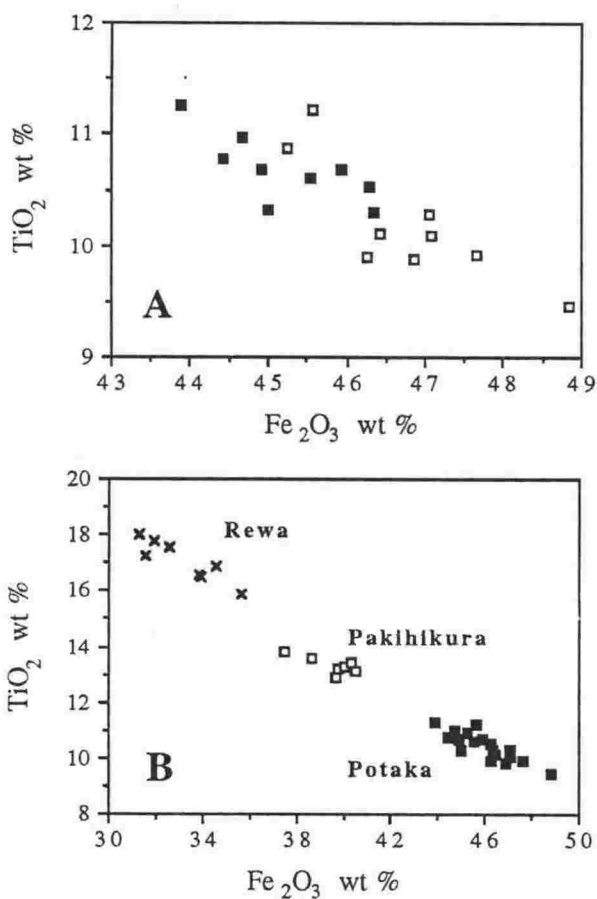
Fig. 8.9 (A) Composition of Fe-Ti oxide crystals determined by EMA from Potaka Tephra at the Rewa Hill section. Black boxes are crystals from the basal ash, open boxes are crystals from pumice clasts near the top of the tephra. (B) Composition of Fe-Ti oxide crystals from 3 different prominent tephras in the Rewa Hill section.

50 mT. Natural remanent magnetism intensities of the tephra are mainly in the range 0.2-3.0 mAm^{-1}, being greatest in the coarser grained specimens. Median destructive fields are typically 10-20 mT. Paleomagnetic site measurements of Potaka Tephra and sediments in close proximity to it (Table 8.8) show various degrees of directional scatter (α_{95}) reflecting the success of overprint removal and the ability of the sediments (often coarse grained) to hold a remanent magnetism. In sites with little scatter ($\alpha_{95}<13°$), specimens display relatively high stability during demagnetisation and usually a single component magnetism (Fig. 8.10a). Those with greater scatter ($>13°$), contain specimens with partial overprints which remain after demagnetisation. These specimens have a two- or multi-component magnetism (Fig. 8.10c). In most cases, a normal viscous overprint is removed or partially removed during demagnetisation in fields of 5-20 mT. In spite of the poorer site statistics, the polarity of these latter sites is determinable from their behaviour during demagnetisation.

Data from several sites reveal the Potaka Tephra is of normal polarity and that it overlies normal polarity sediments. Reversed polarity sediments occur above the tephra at several sites (Table 8.8). Therefore, Potaka Tephra is located close to a paleomagnetic transition. At the Mangatewaiiti section, where exposure allowed a site to be sampled just 20 cm above the tephra, it is shown to be immediately overlain by reversed polarity sediments. At this section, the top of Potaka Tephra is marked by a paleosol, which presumably represents the time of the paleomagnetic transition. A transition from normal to reversed at the top of the Potaka Tephra was also recorded by Black (1992) at the Cape Kidnappers section. A long normal interval of 130 and 90 m at Mangatewaiiti and Mangatewainui, respectively, occurs below the Potaka Tephra (Fig. 8.5). At each of these three localities the normal interval is considered to be the Jaramillo Subchron (Shane 1991; Black 1992). Turner & Kamp (1990) suggested the Kaimatira Pumice Sand occurs near the top of the Jaramillo Subchron at the Wanganui coast, but did not present the polarity of the tephra itself. Thus from several sections the Potaka Tephra is shown to occur near the top of a normal polarity subchron interpreted to be the Jaramillo.

8.3.6 Isotopic age

Several exposures of tephra, here considered to represent the Potaka Tephra, have been dated by the fission-track method. Using glass, this method has produced ages in the range 0.60-1.10 Ma (Table 8.9). The presence of reversed polarity sediments above the tephra indicates many of these ages are too young (also see Black 1992). Recently, plagioclase crystals from exposures at the Wanganui coast, Rewa Hill, Makaroro and Cape Kidnappers have yielded an age of ca. 1 Ma ($\pm5\%$) (Table 8.9), using the single crystal laser fusion method (R. C. Walter pers. comm. 1992). This age is in close agreement with an isothermal plateau fission-track age determined on glass of 1.05 ± 0.05 Ma from the Rewa Hill section (Alloway

Table 8.8 Paleomagnetic data for Potaka Tephra and enclosing sediments.

Site	deposit	Decl.	Incl.	α95	n	polarity
Potaka Tephra						
1	volcaniclastic	342	-62	12	5	N
4	volcaniclastic	348	-55	17	3	N
5	ignimbrite	323	-59	28	4	N
5	volcaniclastic	360	-54	13	4	N
8	ignimbrite	010	-58	21	3	N
10	volcaniclastic	008	-54	13	3	N
sediments below Potaka Tephra						
1	mudstone -14 m	335	-67	12	4	N
11	mudstone -10 m	020	-48	13	3	N
12	mudstone -5 m	013	-68	7	4	N
sediments above Potaka Tephra						
5	tephra +9 m	161	38	18	4	R
10	tephra +3 m	216	65	6	3	R
11	mudstone +0.2 m	171	42	45	3	R
11	tephra +2 m	197	62	21	3	R

Declination and inclination are a mean on n specimens. a95=radius of circle of 95% confidence.
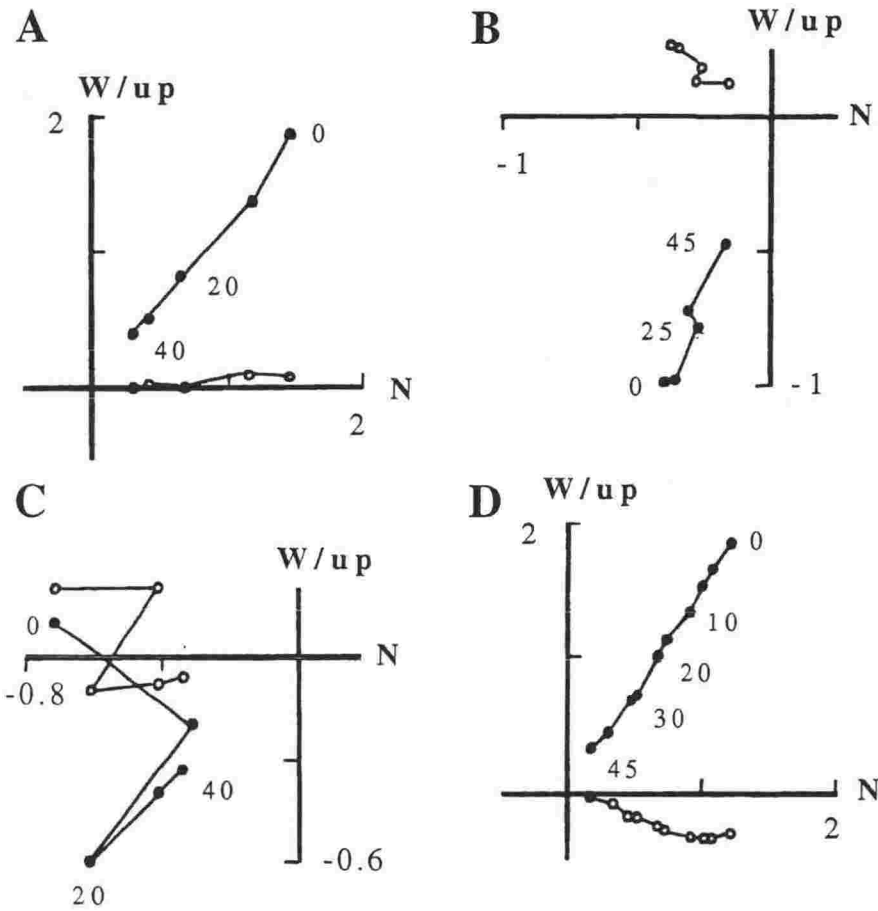
Fig. 8.10 Typical demagnetisation behaviour of tephras and sediments in sections containing Potaka Tephra, shown on orthogonal component plots. Individual AF steps are in mT. Horizontal components are shown as open dots. Unit axes in mA/m. (A) Potaka Tephra at Mangatewainui displaying a stable normal magnetisation. (B) A tephra 5 m above Potaka Tephra at Mangatewainui displaying a stable reversed magnetisation. (C) Mudstone 20 cm above Potaka Tephra at Mangatewaiiti showing reversed polarity and the removal of a viscous overprint. (D) Normal polarity mudstone beaneath Potaka Tephra at Mangatewaiiti.

Table 8.9. Age data for Potaka Tephra (Ma)

site	Fission-track	IPFT[g]	$^{40}Ar/^{39}Ar$[h]
1. Rewa Hill	0.61 ± 0.06[a] 0.64 ± 0.18[b]	1.05 ± 0.05	1.002 ± 0.044
2. Wanganui coast			1.029 ± 0.056
5. Cape Kidnappers	0.85 ± 0.10[c]		1.073 ± 0.050
9. Makaroro river			1.084 ± 0.059
10. Mangatewainui stream			0.907 ± 0.133
12. Leader River	0.63 ± 0.07[d] 0.76 ± 0.08[e] 0.76 ± 0.12[e] 0.77 ± 0.07[e] 0.97 ± 0.14[f] 1.11 ± 0.13[f]		

[a] glass age,Seward (1976)
[b] zircon age, Seward (1979)
[c] glass age, Seward (1975)
[d] glass age, D. Seward (G. Warren pers. comm. 1991)
[e] glass age, B. Kohn (G. Warren pers. comm. 1991)
[f] glass age, J. Boellstorf (G. Warren pers. comm. 1991)
[g] Isothermal plateau fission-track age on glass, Alloway et al. (1993)
[h]R. C. Walter pers. comm. (1992)

et al. 1993). Identical Ar/Ar ages were determined for the ignimbrite phase and the volcaniclastic sediments supporting their equivalence. The Ar/Ar ages are in accord with the magnetostratigraphy, which suggests the Potaka Tephra occurs within the Jaramillo Subchron (0.99-1.07 Ma, based on astronomical chronologies of Shackleton et al. (1990)). Details of the Ar/Ar data are to be presented elsewhere.

8.3.7 Discussion

Stratigraphic implications

Magnetostratigraphy for several new exposures of Potaka Tephra in the East Coast region and Ar/Ar ages indicates the tephra occurs in the Jaramillo Subchron and is significantly older than previous age estimates (ca. 0.60 Ma) (Seward 1974; Seward et al. 1986; Shane & Froggatt 1991). This means that sequences which contain the tephra and were previously thought to represent the Brunhes Chron (e.g. Rewa Hill sequence), instead represent the Jaramillo Subchron, an increase in age from younger than 0.78 Ma to the interval 0.99-1.07 Ma.

Traditionally, marine invertebrate macrofossils have been used to subdivide and classify Pleistocene strata in New Zealand (Fleming 1953; Beu et al. 1987; Pillans 1992). However, this has been hindered by the lack of widespread age-indicative bioevents, and does not allow correlation of non-marine strata. The widespread occurrence of Potaka Tephra shown here, provides a tie line between many Pleistocene sections of different sedimentary facies, both marine and non-marine, and in both major islands, over a distance of 600 km (Fig. 8.4). Thus it is a key marker horizon in the Pleistocene. For example, the Potaka Tephra directly correlates the base of the marine Kai-iwi Group (Fleming 1953) of the Castlecliffian type section at Wanganui coast to the lower part of the alternating marine/non-marine Kidnappers Group (Kingma 1971) at Cape Kidnappers, and to the top of the non-marine Mangatarata Formation (Lillie 1953) in the East Coast. This provides direct correlation between climatically controlled cyclothems deposited on a shelf (Wanganui coast, Beu & Edwards (1984)) with fluvial and lacustrine sequences deposited on land. Strata underlying the Potaka Tephra in the Leader River represent the only known early-middle Pleistocene (Castlecliffian) marine sediments in the South Island (G. Warren pers. comm. 1991). The occurrence of Potaka Tephra allows direct correlation of these sediments to the more extensive sequences in the North Island. Potaka Tephra gives an temporal control point of ca. 1 Ma to all of these sequences and indicates the position of the Jaramillo Subchron, in which it is contained. The tephra is also important as it occurs close to a paleomagnetic transition from normal to reversed (Fig. 8.5). Thus the position of Potaka Tephra adds substantial temporal control to the New Zealand early Pleistocene.

The presence of Potaka Tephra in sequences provides an opportunity to test the possible diachroneity of fossil bioevents. For example, first appearance of the marine mollusc

genus *Pecten*, occurs 30 m above the tephra and also above the Brunhes-Matuyama boundary (0.78 Ma) (Turner & Kamp 1990) at the Wanganui coast. However, at Cape Kidnappers, the genus occurs below the tephra in the Maraetotara Sands (Kingma 1971). It also occurs below the tephra in the Leader River on the eastern side of South Island (G. Warren pers. comm. 1991). Thus *Pecten* makes an appearance some 200-300 ka earlier in the East Coast region.

Potaka Tephra is contained within sequences of unconformity bounded cyclothems at the Wanganui coast and Rewa Hill. These cyclothems are considered to represent high sea level stands corresponding to odd numbered oxygen isotope stages (Beu & Edwards 1984; Pillans 1992). At periods of low sea level, the coast in the Wanganui area regresses several tens of kilometres offshore, exposing the shelf. During subsequent transgression, low stand sediments are eroded producing an unconformity. Therefore the presence of Potaka Tephra in shallow near-shore marine sediments suggests the eruption occurred during a high sea level stand. As the tephra occurs near the top of the Jaramillo Subchron, the eruption may correspond to oxygen isotope stage 27, using the chronology of Shackleton et al. (1990). This is consistent with the presence of reversed polarity sediments immediately above the tephra. If a period of normal polarity did occur after the deposition of the tephra, but was not preserved in the sequences examined, then the eruption may have occurred in stage 29.

Paleogeography

The correlation of the Potaka Tephra provides insight to the paleogeography of the southern North Island at ca. 1 Ma, as it demonstrates the temporal equivalence of different sequences. Its emplacement as an ignimbrite in the East Coast region, some 200 km from possible sources in the TVZ, requires lowland passageways though the area of the present Main Axial Ranges (Fig. 8.4) (Shane 1991; Black 1992). The ranges are now up to 1700 m in elevation and separate depositional basins from the TVZ. The presence of pumice clasts up to 15 cm in size in fluvially deposited Potaka Tephra at Mangatewaiiti and Mangatewainui (250 km distant from TVZ) suggest river transport from areas more proximal to the source volcano. These deposits were not derived from the distal ignimbrite, as it is fine grained with maximum clast sizes of just 2 cm. Thus river catchments drained to the East Coast region from TVZ (e.g. Shane 1991). Today, major river systems in the TVZ flow to the north and south. To the east, the Main Axial Ranges form a barrier. This points to substantial tectonic activity in the last 1 Ma in the central North Island and the formation of a linear mountain range which now separates the depositional basin into a East Coast region and the Wanganui basin.

The Potaka ignimbrite was emplaced over a distance of at least 50 km radially to the TVZ in the central East Coast region, i.e. it was not confined to a single valley. Its distribution and the associated facies, suggest much of the region was lowlands comprising of river braid plains and freshwater swamps and lakes. At the most easterly exposure, at Cape Kidnappers, the ignimbrite overlies dune sands on top of near shore sediments, and thus indicates the

Table 8.10 Geochemical data for Kaukatea Tephra

(A) Glass chemistry of correlatives of the Kaukatea Tephra

sample no.	180	196	240	9
SiO_2	76.69(.21)	76.46(.30)	76.24(.26)	76.01(.21)
Al_2O_3	12.60(.07)	12.83(.12)	12.83(.12)	12.89(.07)
TiO_2	0.15(.04)	0.16(.05)	0.17(.02)	0.20(.04)
FeO	1.53(.09)	1.53(.10)	1.55(.07)	1.56(.06)
MgO	0.13(.04)	0.12(.03)	0.13(.03)	0.15(.02)
CaO	1.00(.06)	0.94(.05)	1.08(.03)	1.10(.03)
Na_2O	4.08(.20)	4.29(.20)	4.22(.13)	4.30(.11)
K_2O	3.66(.18)	3.49(.11)	3.62(.10)	3.62(.13)
Cl	0.18(.02)	0.18(.02)	0.16(.02)	0.17(.03)
water	6.02(0.61)	7.15(1.15)	7.48(1.56)	5.98(0.95)
n	10	10	10	14
Sc	7	8	9	7
V	6	7	7	18
Cr	-	1	-	5
Ba	673	682	712	654
La	27	26	24	25
Ce	55	54	52	46
Ni	1	-	-	-
Cu	9	13	5	14
Zn	58	63	48	50
Zr	219	213	216	302
Nb	10	11	10	11
Ga	14	16	13	14
Pb	20	19	21	21
Rb	111	117	116	113
Sr	80	88	92	95
Th	12	12	12	12
U	3	4	3	4
Y	34	34	31	29
As	5	4	4	4

180=Longacre Road (S22/901424)
196=Mangatewainui (U23/817185)
240=Mangatewaiiti (U23/810172)
9=Cape Kidnappers (Black unpubl. data).
Major oxides in wt% (mean and standard deviation) determined by EMA on n shards. Water by difference. Trace elements in ppm determined on a single bulk glass separate by XRF.

(B) Similarity coefficients comparing the composition of tephras considered to be correlatives of Kaukatea Tephra.
Those for major oxides are based on Si, Al, Ti, Fe, Mg, Ca, Na and K. Those for trace elements are based on Ba, La, Ce, Zn, Zr, Nb, Rb, Sr and Y. *=without Zr due to likely zircon contamination in sample 9.
Major oxides:

	180	196	240	9
180	1	0.96	0.97	0.93
196		1	0.96	0.92
240			1	0.96
9				1

trace elements:

	180	196	240	9
180	1	0.95	0.93	0.90*
196		1	0.93	0.91*
240			1	0.94*
9				1

paleocoast line. The emplacement of the tephra on to paleosols with in situ tree stumps and the presence of logs in the ignimbrite, suggest the region was forested at the time of the eruption.

In contrast, the western side of the North Island (Wanganui basin) was a shallow marine shelf at 1 Ma. The Potaka Tephra was carried by rivers and deposited along at least 60 km of coast line, in an estuarine setting. The distribution of the tephra is tangential to the present coast line (Fig. 8.4), and up to 40 km inland from it, reflecting subsequent regression due mainly to tectonism. Overall, the distribution of Potaka Tephra suggests significantly gentler relief in much of the southern North Island at 1 Ma compared to the present.

The temporal position of Potaka Tephra (1 Ma) is also of interest as it occurs close to the change in the amplitude and frequency of climatic cycles as indicated by oxygen isotope chronologies, at about 0.90 Ma (Williams et al. 1988). Increased cycle amplitudes in the isotope records of the last 0.90 Ma coincides with a change in the cyclic nature of alternating fluvial conglomerate with mudstone and marine facies in the Cape Kidnappers, thought to be climatically controlled (Black 1992). Conglomerate units are thicker above the stratigraphic position of Potaka Tephra, perhaps reflecting more pronounced glaciations and devegetation in highland areas supplying the coarse detritus. This change to coarser and thicker conglomerate facies at this time is widespread in the East Coast region, occurring in the Makaroro section, and elsewhere. The coarse detritus supply may have also been enhanced by increased uplift of basement in the last 1 Ma. Further studies using climatic indicators such as pollen from sections containing Potaka Tephra may ultimately provide a very detailed environmental record of the early and middle Pleistocene.

8.4 KAUKATEA TEPHRA

8.4.1 Introduction

Kaukatea Ash is a name originally given by Seward (1976) to a 4 m thick fine ashy tephra exposed in the valley of Kaukatea Stream, near Wanganui. The tephra is contained in marine sediments of the Lower Kai-iwi Siltstone of the Kai-iwi Group, about 14 m above the Kaimatira Pumice Sand (=Potaka Tephra). Seward (1976) determined a fission-track glass age of 0.57 ± 0.08 Ma for the tephra. Here, the unit is referred to as Kaukatea Tephra to avoid the implication of grain-size. The tephra can be correlated to several other exposures by its major and trace element glass chemistry (Table 8.10), paleomagnetism and stratigraphic position above the Potaka Tephra.

8.4.2 Stratigraphic characteristics

The Kaukatea Tephra can be correlated via its stratigraphic position and chemistry to an exposure along Longacre Road (S180), near Kaukatea Stream. The Longacre Road site provides an easily accessible reference locality for the tephra. There, it consists of a 1 m thick, cross-stratified and laminated coarse ash, contained within shelly marine sands.

In the East Coast region, at Mangatewaiiti and Mangatewainui Streams, the Kaukatea Tephra correlative occurs 1.5-3.0 m above the Potaka Tephra. The sequence is well exposed in Mangatewaiiti stream, where the tephra (S240) is contained within fluvial sediments. Its base is irregular with a local relief of ca. 0.50 m on top of a paleosol with in situ tree stumps. The paleosol is developed on weakly stratified sandy mudstone. The lower 0.50 m of tephra is mainly massive and contains fossil plant fragments. Above the basal ash are two sets of desiccation cracks and gammate structures developed into the tephra, suggesting at least two periods of subaerial exposure and non-deposition. This is overlain by at least 1.5 m of horizontally laminated ash. In Mangatewainui Stream, the base and the top of the tephra (S196) is not exposed, but at least 3-4 m of finely laminated and bedded tephra occurs. At both these sections, the tephra has been emplaced by fluvial processes into an overbank setting. Deposition has involved at least 3 events, possibly floods. The finely laminated top of the tephra, composed of fine sand and silt sized particles suggest deposition into a still-standing body of water, such as a small lake. Such a feature is likely to be ephemeral, as the tephra represents the product of a rapid depositional event on a previously vegetated surface.

The Kaukatea Tephra also occurs at Cape Kidnappers. It is correlated to sample 9 (Kidnappers B) of Black (1992). This tephra (ca. 20 cm thick) is a hard, massive, coarse ash overlying a paleosol and contained within fluvial, cross-stratified sandy mudstone. The tephra occurs within the Mt Gordon Beds, above the Potaka Tephra. In total the Kaukatea Tephra can be correlated over a distance of about 150 km in the southern part of the North Island.

Each of the Kaukatea Tephra correlatives are chemically similar, with SCs in the range 0.92-0.97 for major oxides from EMA data and 0.90-0.95 for trace elements from XRF data (Table 8.10), supporting their equivalence.

8.4.3 Paleomagnetism and age

At Mangatewaiiti, Mangatewainui and Cape Kidnappers, specimens collected for paleomagnetic studies from the Kaukatea Tephra reveal a stable reversed polarity (Table 8.11). A weak, viscous normal component was partially removed in specimens from Mangatewaiiti and Cape Kidnappers. Differences in mean direction between sites probably reflects the degree of overprint remaining after demagnetisation rather than indicating any real difference in original field direction. Sandy mudstone beneath the tephra at Mangatewaiiti is of reversed polarity,

while the underlying Potaka Tephra is of normal polarity. Thus the Kaukatea Tephra occurs a short distance above a paleomagnetic reversal boundary, interpreted to be the top of the Jaramillo Subchron. This position is inconsistent with the fission-track age determined for the tephra (ca. 0.57 Ma) by Seward (1976). Ar/Ar age data from plagioclase in the Cape Kidnappers exposure give an age of ca. 1 Ma (Chapter 7).

Table 8.11 Paleomagnetic data for the Kaukatea Tephra

site	Decl.	Incl.	α95	n	Polarity
Mangatewaiiti	197	65	21	3	R
Mangatewainui	216	65	6	3	R
Cape Kidnappers	161	38	18	4	R

The position of Kaukatea Tephra makes it an important marker horizon which identifies the top of the Jaramillo Subchron, and can be found close to the widespread Potaka Tephra, thus producing a stratigraphic framework. Its occurrence indicates the equivalence of parts of the Kidnappers Group, Mangatarata Formation and Kai-iwi Group.

8.5 STATUS OF SOME OTHER TEPHRAS

8.5.1 Mangapipi Ash

Seward (1976) referred to several tephras exposed by the Mangapipi Stream, near Highway 43 in the Rangitikei valley (T22/355344), as Mangapipi Ash. These tephras occur stratigraphically between Pakihikura Tephra and Rewa Pumice. At least 4 tephra beds (20-100 cm) are exposed, separated by lignite layers and interbedded with carbonaceous mudstone. In respect to the lignite beds, this sequence differs from the rest in the Rangitikei valley which is mainly marine. The tephra exposure in Mangapipi Stream can be projected up dip to the top of a bluff cut by the Pakihikura Stream where it enters the Rangitikei River (T22/345355). There, two tephras (330 and 329), each overlying lignitic paleosols, are exposed 5 and 20 m respectively, above the Pakihikura Tephra (328) (Fig. 8.1). These tephras presumably represent part of the Mangapipi sequence. They can be correlated to a pair of tephras (138 and 140) exposed in the Oroua River, on the basis of glass chemistry and their stratigraphic position above Pakihikura Tephra (Fig. 8.1). Other than this occurrence at Oroua River, the distribution of Mangapipi Ash is unknown as several tephras, both above and below Pakihikura Tephra in the East Coast region, have similar glass chemistries and lack distinguishing lithologic characteristics. However, this does suggest a series of chemically similar eruptives at a similar stratigraphic level are widespread in the southern North Island.

Seward (1976) determined a fission-track age of 0.88 ± 0.13 Ma on glass from the upper most bed at Mangapipi Stream. Shane & Froggatt (1991) determined a reversed polarity for the enclosing mudstone. Stratigraphy determined here, indicates the tephras occur beneath the Jaramillo Subchron and close to the Pakihikura Tephra (ca. 1.63 Ma).

8.5.2 Rewa Pumice

Rewa Pumice (Seward 1976) is a 1.5m thick, coarse ash and lapilli unit, exposed by Highway 43 at Rewa Hill in the Rangitikei valley (T22/348317). In this sequence, Rewa Pumice is the next major volcaniclastic unit beneath Potaka Tephra. Rewa Pumice is current bedded and cross-stratified. It is enclosed in volcaniclastic sediments which display large mega-flaser beds and couplets of coarse sand and fine mud beds, suggestive of an intertidal paleoenvironment. The tephra has not been recognised in any of the other sections examined here.

Shane & Froggatt (1991) inferred a reversed magnetic polarity for sediments immediately underlying Rewa Pumice. Although the sequence is severely overprinted, the declination of specimens move toward 180° during demagnetisation and away from a normal polarity (Chapter 3). Seward (1976) determined a fission-track age of 0.74 ± 0.09 Ma on glass for the tephra. An Ar/Ar age of 1.429 ± 0.056 Ma on plagioclase was determined by the SCLF method (Chapter 7). This age is consistent with a reversed polarity for the tephra.

8.5.3 Un-named tephra in Mangatewaiiti Stream (128)

A tephra (128) with a coarse crystal rich base and consisting of ca. 0.5 m of horizontally stratified ash and fine lapilli is exposed in Mangatewaiiti Stream (U23/817166). The tephra overlies a lignitic paleosol developed on carbonaceous muddy sands. Above the basal ash bed, up to 3 m of fluvially reworked, laminated fine ash and sand is exposed. The crystal rich base may represent the initial fallout ash. The tephra can be correlated to another exposure (190) in Mangatewainui Stream to the NE, by its glass chemistry and magnetostratigraphic position. In Mangatewainui Stream, the tephra is a 2 m thick cross-stratified and convolute bedded coarse ash and fine lapilli unit, which is horizontally stratified at its top.

The tephra occurs a short distance beneath a normal polarity interval, interpreted to be the Jaramillo Subchron (0.99-1.07 Ma) in both sections (Chapters 2 and 3). An Ar/Ar SCLF age of 1.237 ± 0.069 Ma determined on plagioclase from the tephra at Mangatewaiiti is consistent with this magnetostratigraphic position.

8.5.4 Rabbit Gully Ignimbrite

A 20-50 cm thick, partially welded ignimbrite within the Rabbit Gully Beds (Kingma 1971) at Cape Kidnappers (Kidnappers D of Black 1992) (W21/556650) is informally referred to as the Rabbit Gully Ignimbrite. The ignimbrite overlies a thin (10 cm) ash bed and is overlain by redeposited volcaniclastic sediments, within beds of fluvially deposited conglomerate. The ignimbrite contains abundant pumice clasts (up to 4 cm in size), both dark and light coloured. These clasts are often flattened by post-depositional compaction and welding. Accidental ejecta and rounded greywacke pebbles ingested into the flow during emplacement are also common. Part of the ignimbrite exposure is disrupted: displaying a wavy base and pinching-out along strike. Ash beneath the unit displays convolute structures suggestive of subaqueous deposition and dewatering.

Although the ignimbrite has not been correlated to other sections, it is significant as it occurs close to the Brunhes-Matuyama boundary and has an Ar/Ar SCLF age of 0.877 ± 0.034 Ma (Chapter 7). This age provides temporal control to near the top of the sequence of abundant tephras in the early-middle Pleistocene in southern North Island, and to the Kidnappers Group. It also indicates that pyroclastic flows had lowland routes to the East Coast region from the TVZ, as recently as ca. 0.88 Ma.

8.6 CONCLUSIONS

1. Pakihikura (1.63 Ma), Potaka (1.00 Ma) and Kaukatea (ca. 1 Ma) are 3 widespread early Pleistocene tephras which can be correlated between basins of the Wanganui and East Coast regions on the basis of lithology, geochemistry, paleomagnetism and isotopic ages.

2. Potaka Tephra was emplaced as a pyroclastic flow up to 250 km from source into the East Coast region, and further as a catastrophic flood deposit. Associated fallout ash is found up to 600 km distant in the Leader River in north Canterbury.

3. Potaka Tephra and Kaukatea Tephra mark the top of the Jaramillo Subchron, and correlate the marine sequences of the Wanganui coast and Rangitikei valley, with fluvial and lacustrine sequences in the East Coast region.

Chapter 9
AN INTEGRATED TEPHRO- AND MAGNETO- STRATIGRAPHY FOR THE EARLY PLEISTOCENE, AND SOME IMPLICATIONS

9.1 CORRELATION

A stratigraphic framework has been developed using magnetostratigraphy and the geochemistry of tephras which allows correlation between the Wanganui basin and basins in the East Coast region (Fig. 9.1). Three particularly widespread tephra horizons are recognised: Kaukatea Tephra (ca. 1 Ma), Potaka Tephra (1 Ma) and Pakihikura Tephra (1.63 Ma). These provide time planes through different facies (both marine and non-marine) and between different basins. Non-marine sequences can now be tied directly to marine sequences where stage boundaries were originally defined, and in turn the non-marine sequences with abundant tephras can provide isotopic age control to the stages. As well, many other tephras are interbedded in these sequences (Fig. 9.1) and will provide further potential for correlation and age control. The Kaukatea Tephra and Potaka Tephra occur above and below, respectively, the top of the Jaramillo Subchron (ca. 0.99 Ma) and thus are important markers of this reversal boundary in the sequences. The age of the Pakihikura Tephra (1.63 Ma, Alloway et al. (1993)) suggests it occurs above the Olduvai Subchron (1.77-1.95 Ma) and thus explains the lack of a normal polarity interval in the lower parts of the sequences examined. As indicated by Alloway et al. (1993), the Pakihikura Tephra occurs close to the international Plio-Pleistocene boundary, defined as being a short distance above the top of the Olduvai.

Potaka Tephra occurs near the base of the Castlecliffian type section. It thus provides direct temporal control and is a marker horizon for the base of the stage, as defined at the Wanganui coast. Its occurrence in the East Coast region correlates the top of the Mangatarata Formation in the Dannevirke area, and the base of the Kidnappers Group at Cape Kidnappers, to the base of the Castlecliffian stage. Potaka Tephra is therefore particularly important to local stratigraphy due its widespread distribution in non-marine strata which typically lack bioevents. Based on the occurrence of Potaka Tephra at the top of the Mangatarata Formation, most of this formation is older than the Kidnappers Group. However, the two sequences overlap in time, as strata of Mangatarata Formation at Makaroro River overlie the Potaka Tephra. The Kidnappers Group represent the interval ca. 0.5-1 Ma (Black 1992). As Pakihikura Tephra (ca. 1.6 Ma) occurs in the lower part of the Mangatarata Formation, but the Olduvai Subchron is not recognised, this formation represents the interval from 1 Ma (Potaka Tephra at top) to ca. 1.6-1.7 Ma. Thus combined sequences in the East Coast region provide a high resolution record containing tephras, between 0.5 to 1.7 Ma. A similar continuous record is exposed in the Rangitikei Valley, although it contains fewer tephras.

Fig. 9.1 Summary of the tephro- and magnetostratigraphy for early Pleistocene sequences in southern North Island.
(note scale change for different sections)

The type sections for New Zealand Pleistocene stages (Castlecliffian and Nukumaruan) are separated by an unconformity of unknown duration (e.g. Pillans 1992). Although the Potaka Tephra occurs in the Castlecliffian part of the section, tephras in the top of the Nukumaruan part cannot be correlated to any of the prominent tephras elsewhere in the basin. This suggests that tephras in the sequence close to Pakihikura Tephra and below Potaka Tephra elsewhere (Fig. 9.1), may be included in the time interval of the unconformity. This would imply the interval from ca. 1 Ma to at least 1.7 Ma is missing from the Pleistocene stage type sections: a significant problem if stage classifications are to be used elsewhere.

9.2 IMPLICATIONS FOR BASIN DEVELOPMENT

The correlation and geochronology of the tephras provide insights to the history of sedimentation and paleogeography of the southern North Island. During the Pliocene fully marine conditions occurred throughout the Wanganui, Wairarapa and Hawkes Bay regions (e.g. Fleming 1953; Lillie 1953; Kingma 1971). In the Hawkes Bay region and the eastern side of the Wanganui basin (e.g. at Oroua), a gradational change from shallow marine to non-marine facies is recorded beneath the Pakihikura Tephra (Fig. 8.1). This transition probably reflected the sedimentary infilling of the basins from increased sediment influx, rather than tectonic induced regression, as there is a lack of significant disconformities or angular unconformities in the sequences. As the Pakihikura Tephra is dated at ca. 1.63 Ma, and the Olduvai Subchron (1.77-1.95 Ma) is not recorded in these sections, the marine to non-marine transition may have occurred at ca. 1.7 Ma. Further to the west, in the Wanganui basin, at Rangitikei and Turakina, the Pakihikura Tephra is contained within marine sediments, suggesting a paleocoast between these sites and the Oroua section. However, a brief change to non-marine conditions above the tephra at Rangitikei is recorded at the level of the Mangapipi Ash. In the East Coast region from Mangatewaiiti to Makaroro, a fluvial and lacustrine paleoenvironment persisted, un-interrupted at least until ca. 1 Ma (age of Potaka Tephra). This terrestrial paleoenvironment continued to ca. 0.5 Ma further north at Cape Kidnappers. There, marine conditions occurred before the eruption of Potaka Tephra, and 3 minor marine transgressions are recorded in the interval 1.0-0.5 Ma (Black 1992). These marine incursions at Cape Kidnappers probably reflected a setting close to the paleocoast, and a balance between subsidence and sedimentation allowing the preservation of glacioeustatic high sea level stands.

Early Pleistocene conglomerates are rare in sections in the Dannevirke area and in the Wanganui basin at Rangitikei and further west. However, beds of fine greywacke conglomerates occur near the level of Pakihikura Tephra at the Tukituki and Oroua sections (Chapter 2). Thus local Mesozoic greywacke basement was exposed close to the site of the present main Axial Ranges at ca. 1.6 Ma. Conglomerates become more common in the sequences of the East Coast at the level of Potaka Tephra and above (<1 Ma). This increase in

coarse detritus may reflect increased tectonic uplift in the area of the main Axial Ranges and/or more pronounced erosion due to devegetation linked to climatic cooling (e.g. Black 1992). Major fluvial and pyroclastic transport routes from the TVZ to the East Coast and through the main Axial Ranges, persisted to at least as recently as 0.8 Ma, as evidenced by the emplacement of the Rabbit Gully ignimbrite at Cape Kidnappers. Therefore much uplift must have taken place in the last 0.8 Ma.

In contrast to the late Pleistocene and Holocene tectonic regime of uplift and terrace formation in the East Coast and Wanganui basin regions, subsidence dominated from before 1.7 Ma to at least 0.5 Ma. The isotopic ages of the early Pleistocene tephras allow average sediment accumulation rates to be estimated (Table 9.1) and indicate deposition was rapid (> 0.4 m/10^3 yr). The actual sedimentation rates are highly variable as both flood deposits and paleosols are present in the sections. However, the average accumulation rates reflect the rate of basin subsidence for these time intervals. Accumulation rates are fast at sites distal to the present location of the Main Axial Ranges, e.g. at Cape Kidnappers and Rangitikei, and slow at Makaroro, the section closest to the ranges (Table 9.1).

Table 9.1. Average sediment accumulation rates for stratigraphic intervals between tephras with isotopic ages (Pot= Potaka, Pak= Pakihikura)

section	tephras	time interval (Ma)	thickness (m)	accumulation rate (m/10^3 yr)
Cape Kidnappers	Pot-Rabbit Gully	1.00-0.88	127	1.03
Mangatewainui	128-Pot	1.24-1.00	124	0.52
	Pak-128	1.63-1.24	177.5	0.46
Mangatewaiiti	128-Pot	1.24-1.00	165	0.69
Makaroro	Pak-Pot	1.63-1.00	107	0.17
Rewa Hill	Rewa-Pot	1.43-1.00	139	0.32
	Pak-Rewa	1.63-1.43	250	1.03

9.3 ERUPTIVE CHRONOLOGY

The onset of frequent volcanism recorded in sequences of the southern North Island, i.e. the first appearance of abundant tephras, occurs a short distance below the Pakihikura Tephra (ca. 1.6 Ma) (Fig. 9.1). This is equivalent to the age of the oldest ignimbrite thought to have been erupted from the Mangakino Caldera: Ignimbrite A (1.603 ± 0.022 Ma) (Pringle et al. 1992). Thus the distal tephra sequences may be a record of the onset of volcanism in the SW part of the TVZ. Prior to this, large scale rhyolitic volcanism is known to have occurred in the more distant Coromandel region (Skinner 1986) and this may explain the sparse occurrence of tephras below the tephra sequence at the level of Pakihikura Tephra. Exposures of an ignimbrite

Table 9.2. Number of tephras, their character and possible eruptive events in the main sections examined in this study.

| section | glass composition | | correlatives | unique eruptive events† |
	homogeneous#	mixed@		
Mangatewaiiti	9	3	3	6
Mangatewainui	13	3	3	10
Oroua	8	3	3	5
Rewa Hill/Rangitikei	9	2	4	5
Makaroro	7	1	3	4
Tukituki	3	0	2	1
Manawatu	2	6	1	1
Pohangina	7	3	0	7
Cape Kidnappers*	7	-	2	5
correlatives in more than one section				7
TOTAL				51

\# consist of a single or dominant compositional population of shards
@ consist of a multiple compositional populations of shards or are reworked layers
†calculated by subtracting correlatives from the tephras with homogeneous glasses
* Cape Kidnappers tephras represent groups associated with a particular eruption

referred to as Rocky Hill by Pringle et al. (1992) have yielded an age of 0.955 ± 0.025 Ma, and this ignimbrite is considered to be the youngest erupted from the Mangakino Caldera (e.g. Wilson et al. 1984, Wilson 1986). This age is close to that of the Potaka Tephra (ca. 1 Ma), and thus the distal sequences in the East Coast region may be a relatively complete eruptive record of the Mangakino Caldera.

In spite of the temporal similarity between the distal tephras and Mangakino ignimbrites, precise correlations are not yet possible due to geochemical alteration of the ignimbrites. Also, some of the distal tephras may be unrecognised in the Mangakino area as unwelded ignimbrites and fallout ash are generally poorly preserved there (e.g. Wilson 1986).

9.4 NUMBER AND FREQUENCY OF ERUPTIVE EVENTS RECORDED IN DISTAL SEQUENCES

The complete eruptive record of the TVZ for the early-middle Pleistocene is difficult to precisely determine for several reasons including: (1) small and less explosive eruptions may not be recorded in distal sequences; (2) the sequences are not completely exposed; (3) the chronology for some sequences is uncertain; (4) many tephras are chemically similar and occur stratigraphically close, making correlation uncertain; (5) many tephras have been reworked to produce new stratigraphic horizons in the same sequence; and (6) the differing preservation potential of various sedimentary facies.

To assess the number of different eruptive events in the study sections, the glass chemistry and stratigraphic position of each tephra were examined. Different eruptive events are identified as tephras having unique geochemistry and/or stratigraphic position. Further, the tephra must have a homogeneous glass composition or contain a distinctive dominant glass population, to be considered to represent an eruptive event. Therefore tephras consisting of multiple glass populations of different compositions are excluded and considered to represent the products of depositional reworking. A summary of tephras in the major sections classified according to this scheme is summarised in Table 9.2. For Cape Kidnappers, 7 different tephra groups are recorded following Black (1992). Each group is considered to represent multiple reworking events of an initial eruption. In all of the sections examined, correlatives of 7 different tephras can be found in more than one section (see Fig. 9.1). This leaves a total of 51 different tephra horizons. This number is tentative due to the factors outlined above. In particular, further correlations may be possible with additional chronological control.

The time interval represented by the sections extends from about 0.5 Ma (the top of the Cape Kidnappers section) to about 1.77 Ma, on the assumption that the Olduvai Subchron (1.77-1.95 Ma) is not present in any of the sections (Fig. 9.2). Many tephras are present in only one section and thus multiple sections of the same time interval provide a better record. Most of the sections represent the interval from 1 Ma to 1.77 Ma, excluding Cape Kidnappers
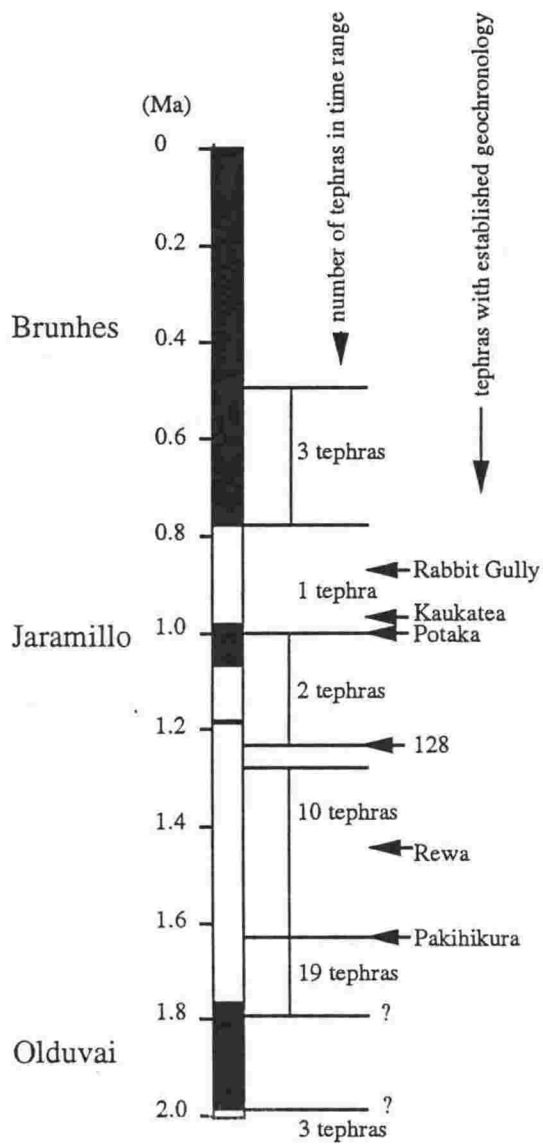
Fig. 9.2 A summary of the approximate stratigraphic distribution of the 44 different eruptive events exposed in the main study sections (see Table 9.2), excluding the Pohangina section where the chronology is uncertain.

and the Pohangina section (see Chapter 3). In this interval of ca. 0.77 Ma, 39 different tephras were found. This gives an average frequency of 1 event per 20 ka. A more conservative estimate of frequency can be obtained from the two long, closely spaced, parallel sections of Mangatewaiiti and Mangatewainui. Correlation between the sections is well constrained, thus avoiding the possible multiple counting of tephras that may be correlatives. These two sections contain 19 different tephras in an age range of 0.77 Ma at an average frequency of 1 per 40.5 ka. However, the distribution of tephras in this time interval is not uniform as most eruptive events are recorded at the level of Pakihikura Tephra (1.63 Ma) or immediately below it (Fig. 9.2).

REFERENCES

Aitchison, J. 1986: The statistical analysis of compositional data. Chapman and Hall, London.

Alloway, B. V.; Pillans, B. J.; Sandhu, A. S.; Westgate, J. A. 1993: Revision of the marine chronology in the Wanganui Basin, New Zealand, based on the isothermal plateau fission-track dating of tephra horizons. *Sedimentary geology 82*: 299-310.

Bailey, R. A.; Dalrymple, G. A.; Lanphere, M. A. 1976: Volcanism, structure, and geochronology of the Long Valley caldera, Mono County, California. *Journal of geophysical research 81*: 725-744.

Baksi, A. K.; Hsu, V.; McWilliams, M. O.; Farrar, E. 1992: ^{40}Ar/^{39}Ar dating of the Brunhes Matuyama geomagnetic field reversal. *Science 256*: 356-357.

Beaudoin, A. B.; King, R. H. 1986: Using discriminant function analysis to identify Holocene tephras based on magnetite composition: A case study from the Sunwapta Pass area, Jasper National Park. *Canadian journal of earth sciences 23*: 804-812.

Beu, A. G.; Browne, G. H.; Grant-Taylor, T. L. 1981: New *Chlamys delicatula* localities in the central North Island and uplift of the Ruahine Range. *New Zealand journal of geology and geophysics 24:* 127-132.

Beu, A. G.; Edwards, A. R. 1984: New Zealand Pleistocene and late Pliocene glacio-eustatic cycles. *Paleogeography, paleoclimatology, paleoecology 46*: 119-142.

Beu, A. G.; Edwards, A. R.; Pillans, B. J. 1987: A review of New Zealand Pleistocene stratigraphy, with emphasis on the marine rocks. *In*: Itihara , M.; Kamei, T. *ed* Proceedings of the first international colloquium on Quaternary stratigraphy of Asia and Pacific area, Osaka, 1986. Pp. 250-269.

Black, T. M. 1990: Paleomagnetism and tephrostratigraphy of the Kidnappers Group, Hawkes Bay, New Zealand. Unpublished B.Sc(Hons) project, lodged in the library, Victoria University of Wellington.

Black, T. M. 1992: Chronology of the Middle Pleistocene Kidnappers Group, New Zealand and correlation to global oxygen isotope stratigraphy. *Earth and planetary science letters 109*: 573-584

Boellstorff, J. D.; Te Punga, M. T. 1977: Fission-Track ages and correlation of middle and lower Pleistocene sequences from Nebraska and New Zealand. *New Zealand journal of geology and geophysics 20*: 47-58.

Borchardt, G. A.; Havard, M. E.; Schmitt, R. A. 1971: Correlation of volcanic ash deposits by activation analysis of glass separates. *Quaternary research 1*: 247-260.

Bowden, P. 1974: Oversaturated Alkaline rocks: granites, pantellerites and comendites. *In*: Sorensen, H. *ed* . The Alkaline rocks. London, Wiley. Pp 109-123.

Briggs, R. M.; Fulton, B. W. J. 1990: Volcanism, structure and petrology of the Whiritoa-Whangamata coastal section, Coromandel Volcanic Zone, New Zealand: facies model evidence for the Tunaiti caldera. *New Zealand journal of geology and geophysics 33*: 623-633.

Busacca, A. J.; Nelstead, K. T.; McDonald, E. V.; Purser, M. D. 1992: Correlation of distal tephra layers in loess in the channeled scabland and Palouse of Washington State. *Quaternary research 37*: 281-303.

Campbell, I. B. 1986: New occurrences and distribution of Kawakawa Tephra in South Island, New Zealand. *New Zealand journal of geology and geophysics 29*: 425-435.

Carey, S. N.; Sigurdsson, H. 1978: Deep sea evidence for distribution of tephra from the mixed magma eruption of the soufriere on St. Vincent, 1902: ash turbidites and airfall. *Geology 6*: 271-274.

Carter, R. M. 1972: Wanganui strata of Komako District, Pohangina Valley, Ruahine Range, Manawatu. *Journal of the Royal Society of New Zealand 2:* 293-324

Cerling, T. E.; Cerling, B. W.; Curtis, G. H.; Drake, R. E.; Brown, F. H. 1978: Correlation of reworked ash deposits; the KBS tuff, northern Kenya. *United States Geological Survey open file report 78-701:* 61-63.

Champion, D. E.; Lanphere, M. A.; Kuntz, M. A. 1988: Evidence for a new geomagnetic reversal from lava flows in Idaho: discussion of short polarity reversals in the Brunhes and late Matuyama Polarity Chrons. *Journal of geophysical research 93*: 11667-11680.

Christiansen, R. L.; Blank, H. R. 1972: Volcanic stratigraphy of the Quaternary rhyolite plateau in Yellowstone National Park. *U. S. Geological Survey professional paper 729-B.* 18 p.

CLIMAP project members 1976: The surface of the ice-age Earth. *Science 191*: 1131-1137

Cole, J. W. 1979: Structure, petrology and genesis of Cenozoic volcanism, Taupo Volcanic Zone, New Zealand- a review. *New Zealand journal of geology and geophysics 22:* 631-657.

Cole, J. W. 1990: Structural control and origin of volcanism in the Taupo volcanic zone, New Zealand. *Bulletin of volcanology 52*: 445-459.

Collen, J. D.; Vella, P. 1984: Hautotara, Te Muna and Ahiaruhe Formations, middle to late Pleistocene, Wairarapa, New Zealand. *Journal of the Royal Society of New Zealand 14*: 297-317.

Cox, A. 1971: Remanent magnetization an susceptibility of late Cenozoic rocks from New Zealand. *New Zealand journal of geology and geophysics 14*: 192-207.

Davis, J. O. 1985: Correlation of late Quaternary tephra layers in a long Pluvial sequence near Summer Lake, Oregon. *Quaternary research 23*: 38-53.

Deino, A.; Potts, R. 1990: Single-crystal $^{40}Ar/^{39}Ar$ dating of the Olorgesailie Formation, southern Kenya rift. *Journal of geophysical research 95*: 8453-8470.

Dunbar, N. W.; Hervig, R. L.; Kyle, P. R. 1989a: Determinations of pre-eruptive H_2O, F and Cl contents of silicic magmas using melt inclusions, examples from Taupo Volcanic Center, New Zealand. *Bulletin of volcanology 51:* 177-185.

Dunbar, N. W.; Kyle, P. R.; Wilson, C. J. N. 1989b: Evidence for limited zonation in silicic magma systems, Taupo Volcanic Zone, New Zealand. *Geology 17:* 234-236.

Erdman, C. F.; Kelsey, H. M. 1992: Pliocene and Pleistocene stratigraphy and tectonics, Ohara Depression and Wakarara Range, North Island, New Zealand. *New Zealand journal of geology and geophysics 35*: 177-192.

Ewart, A. 1966: Review of mineralogy and chemistry of the acidic rocks of the Taupo Volcanic Zone, New Zealand. *Bulletin volcanologique 29:* 147-172.

Ewart A.; Hildreth, W.; Carmichael, I. S. E. 1975: Quaternary acid magma in New Zealand. *Contributions to mineralogy and petrology 51*: 1-27.

Ewart A.; Taylor, S. R. 1969: Trace element geochemistry of the rhyolitic volcanic rocks, Central North Island, New Zealand: phenocryst data. *Contributions to mineralogy and petrology 22:* 127-146.

Fisher, R. V. 1964: Maximum size, median diameter, and sorting of tephra. *Journal of geophysical research 64*: 341-355.

Fleming, C. A. 1953: The geology of Wanganui subdivision. *New Zealand Geological Survey bulletin 52.*

Froggatt, P. C. 1982: A study of some aspects of the volcanic history of the Lake Taupo area, North Island, New Zealand. Unpublished PhD thesis, lodged in the library, Victoria University of Wellington.

Froggatt, P. C. 1983: Toward a comprehensive Upper Quaternary tephra and ignimbrite stratigraphy of New Zealand using electron microprobe analysis of glass shards. *Quaternary research 19:* 188-200.

Froggatt, P. C.; Nelson, C. S.; Carter, L.; Griggs, G.; Black, K. P. 1986: An exceptionally large late Quaternary eruption from New Zealand. *Nature 319*: 578-582

Froggatt, P. C.; Lowe, D. J. 1990: A review of late Quaternary silicic and some other tephra formations from New Zealand: their stratigraphy, nomenclature, distribution, volume and age. *New Zealand journal of geology and geophysics 33*: 89-109.

Froggatt, P. C.; Rogers, G. M. 1990: Tephrostratigraphy of high altitude peat bogs along the axial ranges, North Island, New Zealand. *New Zealand journal of geology and geophysics 33*: 111-125.

Froggatt, P. C.; Solloway, G. J. 1986: Correlation of Pananetu Tephra to Karapiti Tephra, Central North Island, New Zealand. *New Zealand journal of geology and geophysics 29*: 303-315.

Gosson, G. J. 1986: Miocene and Pliocene silicic tuffs in marine sediments of the East Coast Basin, New Zealand. Unpublished PhD thesis, lodged in the library, Victoria University of Wellington.

Grindley, G. W.; Oliver, P. J.; Seward, D. 1988: Stratigraphy, geochronology and paleomagnetism of ignimbrites in the Matahana Basin, New Zealand. *Geological Society of New Zealand miscellaneous publication 41a:* 71.

Hildreth, W. 1981: Gradients in silicic magma chambers: Implications for lithospheric magmatism. *Journal of geophysical research 86*:10153-10192.

Hildreth, W.; Mahood, G. 1985: Correlation of ash-flow tuffs. *Geological Society of America bulletin 96:* 968-974.

Hillhouse, J. W.; Cerling, T. E.; Brown, F. H. 1986: Magnetostratigraphy of the Koobi Fora Formation, Lake Turkana, Kenya. *Journal of geophysical research 91:* 11581-11595.

Huang, T. C; Watkins, N. D. 1976: Volcanic dust in deep-sea sediments; Relationships of microfeatures to explosivity estimates. *Science 193:* 576-579.

Huang, T. C.; Watkins, N. D.; Shaw, D. M.; Kennett, J. P.; 1973: Atmospherically transported volcanic dust in South Pacific deep sea sedimentary cores at distances over 3000 km from the eruptive source. *Earth and planetary science letters 20:* 119-124.

Huang T. C.; Watkins, N. D.; Shaw, D. W. 1975 Atmospherically transported volcanic glass in deep-sea sediments: Volcanism in sub-antarctic latitudes of the South Pacific during late Pliocene and Pleistocene time. *Geological Society of America bulletin 86:* 1305-1315.

Izett, G. A. 1981: Volcanic ash beds: recorders of Upper Cenozoic silicic pyroclastic volcanism in the Western United States. *Journal of geophysical research 86:* 10200-10222.

Izett, G. A.; Obradovich, J. D.; Mehnert, H. H. 1988: The Bishop ash bed (middle Pleistocene) and some older (Pliocene and Pleistocene) chemically and mineralogically similar ash beds in California, Nevada and Utah. *United States Geological Suvey bulletin 1675.* 36 p.

Jarosewich, E.; Nelen, J. A.; Norberg, J. A. 1980: Reference samples for electron microprobe analysis. *Geostandards newsletter 4:* 43-47.

Johnson, G. L.; Kyle, P. R.; Vanney, J. R.; Campsie, J. 1982: Geology of Scott and Balleny Islands, Ross Sea, Antarctica, and morphology of the adjacent seafloor. *New Zealand journal of geology and geophysics 25:* 427-436.

Johnson, R. G. 1982: Brunhes-Matuyama magnetic reversal dated at 790,000 yr B.P. by marine-astronomical correlations. *Quaternary research 17:* 135-147.

* Joyner, S. P. 1985: "SAS User's Guide: Statistics", Version 5.0 *ed.* SAS Institute, Cary, NC.

Kennett, J. P.; Watkins, N. D.; Vella, P. 1971: Paleomagnetic chronology of Pliocene to early Pleistocene climates and the Plio-Pleistocene boundary in New Zealand. *Science 171:* 276-279.

Kingma, J. T. 1971: Geology of Te Aute subdivision. *New Zealand Geological Survey bulletin 70.*

Kodama, K. P. 1979: New paleomagnetic results from the Rio Dell Formation, California. *Geophysical research letters 6:* 253-256.

Kohn, B. P. 1970: Identification of New Zealand tephra layers by emission spectrographic analysis of their titanomagnetites. *Lithos 3:* 361-368

Kohn, B. P. 1979: Identification and significance of a late Pleistocene tephra in Canterbury District, South Island, New Zealand. *Quaternary research 11:* 78-92.

Kohn, B. P.; Pillans, B.; McGlone, M. S. 1992: Zircon fission track age for middle Pleistocene Rangitawa Tephra, New Zealand: stratigraphic and paleoclimatic significance. *Paleogeography, paleoclimatology, paleoecology 95:* 73-94.

* Kamp, P. J. J. 1990: Kidnappers Group (middle Pleistocene), Hawke Bay. *Geological Society of New Zealand miscellaneous publication 50B:* 105-118.

Kyle, P. R. 1990: McMurdo Volcanic Group-Western Ross embayment Introduction. *In*:: LeMasurier, W. E.; Thomson, J. W. *ed.* Volcanoes of the Antarctic Plate and Southern Oceans. American Geophysical Union. *Antarctic research series 48*: 19-25

Kyle, P. R.; Seward, D. 1984: Dispersed rhyolitic tephra from New Zealand in deep sea sediments of the Southern Ocean. *Geology 12*: 487-490.

Le Maitre, R. W. 1984: A proposal by the IUGS subcommission on the systematics of igneous rocks for a chemical classification of volcanic rocks based on the total alkali silica (TAS) diagram. *Australian journal of earth science 31*: 243-255.

La Bas, M. J.; Le Maitre, R. W.; Streckeisen, A.; Zanettin, B. 1986: A chemical classification of volcanic rocks based on the total alkali-silica diagram. *Journal of petrology 27*: 745-750.

LeMasurier, W. E. 1990: Marie Byrd Land-Summary. *In*: LeMasurier, W. E.; Thomson, J. W. *ed.* Volcanoes of the Antarctic Plate and Southern Oceans. American Geophysical Union. *Antarctic research series 48*: 147-163.

LeMasurier, W. E.; Kawachi, Y. 1990: Mount Waesche. *In*: LeMasurier, W. E.; Thomson, J. W. *ed.* Volcanoes of the Antarctic Plate and Southern Oceans. American Geophysical Union. *Antarctic research series 48*: 208-211.

LeMasurier, W. E.; Kawachi, Y.; Rex, D. C. 1990: Toney Mountain. *In*: LeMasurier, W. E.; Thomson, J. W. *ed.* Volcanoes of the Antarctic Plate and Southern Oceans. American Geophysical Union. *Antarctic research series 48*: 175-179.

LeMasurier, W. E.; Thomson, J. W. 1990: *ed.* Volcanoes of the Antarctic Plate and Southern Oceans. American Geophysical Union. *Antarctic research series 48*.

Lillie, A. R. 1953: The geology of Dannevirke subdivision. *New Zealand Geological Survey bulletin 46*

Lowe, D. J. 1988: Stratigraphy, age, composition, and correlation of late Quaternary tephras interbedded with organic sediments in Waikato lakes, North Island, New Zealand. *New Zealand journal of geology and geophysics 31*: 125-165.

Mankinen, E. A.; Donnelly, J. M.; Gromme, C. S. 1978: Geomagnetic polarity event recorded at 1.1 m. y. B. P. on Cobb Mountain, Clear Lake volcanic field, California. *Geology 6*: 653-656.

Mankinen, E. A.; Dalrymple, G. B. 1979: Revised geomagnetic polarity time scale for the interval 0-5 m.y. B.P. *Journal of geophysical research 84*: 615-626.

Maxwell, F. A. 1988: Late Plio-Pleistocene sedimentation near Apiti, and implications for the uplift of the Ruahine Ranges, northeast Manawatu, New Zealand. Unpublished BSc(Hons) thesis, lodged in the library, Victoria University of Wellington.

Miall, A. D. 1978: Lithofacies types and vertical profile models in braided river deposits: a summary. *Canadian Society of Petroleum Geologists memoir 5:* 597-604.

Milne, J. D. G. 1969: The geology and soils of the Apiti district.Unpublished MSc thesis, lodged in the library, Victoria University of Wellington.

McGuire, D. M. 1989: Paleomagnetic stratigraphy and magnetic properties of Pliocene strata, Turakina River, North Island, New Zealand. Unpublished PhD thesis, lodged in the library, Victoria University of Wellington.

Neef, G. 1984: Late Cenozoic and early Quaternary stratigraphy of the Eketahuna district (N153). *New Zealand Geological Survey bulletin 96.*

Nelson, C. S.; Froggatt, P. C.; Gosson, G. J. 1986: Nature, chemistry and origin of late Cenozoic megascopic tephras in Leg 90 cores from the southwest Pacific. *In* : Kennett, J. P. et al., *ed.* Initial Reports of the Deep Sea Drilling Project 90, Washington, United States Government Printing Office. pp 1161-1173.

Nielsen, C. H.; Sigurdsson, H. 1981: Quantitative methods for electron microprobe analysis of sodium in natural and synthetic glasses. *American mineralogist 66*: 547-552.

Ninkovich, D. 1968: Pleistocene volcanic eruptions in New Zealand recorded in deep sea sediments. *Earth and planetary science letters 4*: 89-102.

Palais, J. M.; Kyle, P. R.; McIntosh, W. C.; Seward, D. 1988: Magmatic and phreatomagmatic volcanic activity at Mt. Takahe, West Antarctica, based on tephra layers in the Byrd Ice core and field observations at Mt. Takahe. *Journal of volcanology and geothermal research 35*: 295-317.

Palmer, K. 1990: XRF analyses of granitoids and associated rocks, St. Johns Range, South Victoria Land, Antarctica. Research School of Earth Sciences geology board of studies publication 5, Victoria University of Wellington. 23 p.

Pillans, B. 1992: New Zealand Quaternary stratigraphy: An overview. *Quaternary science reviews 10*: 405-418.

Pillans, B.; Wright, I. 1990: 500,000 yr paleomagnetic record from New Zealand loess. *Quaternary research 33*: 178-187.

Pringle, M. S.; McWilliams, M.; Houghton, B. F.; Lanphere, M. A.; and Wilson, C. J. N. 1992: $^{40}Ar/^{39}Ar$ dating of Quaternary feldspar: examples from the Taupo Volcanic Zone, New Zealand. *Geology 20*: 531-534.

Raub, M. L. 1985: The neotectonic evolution of the Wakarara area, Southern Hawkes Bay, New Zealand. Unpublished M.Phil thesis, lodged in the library, University of Auckland.

Rock, N. M. S. 1989: Numerical Geology. Springer-Verlag, Berlin. 427 p.

Rollinson, H. R. 1992: Another look at the constant sum problem in geochemistry. *Mineralogical magazine 56*: 469-475.

Roxborgh, H. J. 1976: Lake Taupo late Pleistocene tephras, a petrochemical study. Unpublished MSc thesis, lodged in the library, Victoria University of Wellington.

Ruddiman, W. F.; Glover, K. L. 1972: Vertical mixing of ice-rafted volcanic ash in North Atlantic sediment. *Geological Society of America bulletin 83*: 2817-2836.

Sarna-Wojcicki, A. M.; Bowman, H. R.; Meyer, C. E.; Russell, P. C.; Woodward, M. J.; McCoy, G.; Rowe, J. J.; Baedecker, P. A.; Asaro, F.; Michael, H. 1984: Chemical analyses, correlations, and ages of Upper Pliocene and Pleistocene ash layers of east-central and southern California. *United States Geological Survey professional paper 1293*. 40 p.

Sarna-Wojcicki, A. M.; Meyer, C. E.; Bowman, H. R.; Hall, N. T.; Russell, P. C.; Woodward, M. J.; Slate, J. L. 1985: Correlation of Rockland ash bed, a 400, 000 year-old stratigraphic marker in northern California and western Nevada, and implications for middle Pleistocene paleogeography of central California. *Quaternary research 23*: 236-257.

Sarna-Wojcicki, A. M.; Morrison, S. D.; Meyer, C. E.; Hillhouse, J. W. 1987: Correlations of Upper Cenozoic tephra layers between sediments of the Western United States and Eastern Pacific Ocean and comparison with biostratigraphic and magnetostratigraphic age data. *Geological Society of America bulletin 98*: 207-223.

Sarna-Wojcicki, A. M.; Meyer, C. E.; Adam, D. P.; Sims, J. D. 1988: Correlations and age estimates of ash beds in upper Pleistocene sediments of Clear Lake, California. *Geological Society of America special paper 214*: 141-150.

Schlinger, C. M.; Smith, R. M.; Veblen, D. R. 1986: Geologic origin of magnetic volcanic glasses in the KBS tuff. *Geology 14:* 959-962.

Scott, K. B. 1971: Alkali exchange during devitrification and hydration of glasses in ignimbrite cooling units. *Journal of geology 79*: 100-110.

Seward, D. 1974: Age of New Zealand Pleistocene substages by fission track dating of glass shards from tephra horizons. *Earth and planetary science letters 24:* 242-248.

Seward, D. 1975: Fission-track ages of some tephras from Cape Kidnappers, Hawke's Bay, New Zealand. *New Zealand journal of geology and geophysics 18*: 507-510.

Seward, D. 1976: Tephrostratigraphy of the marine sediments in Wanganui Basin, North Island, New Zealand. *New Zealand journal of geology and geophysics 19*: 9-20.

Seward, D. 1979: Comparison of zircon and glass fission track ages from tephra horizons. *Geology 7:* 470-482.

Seward, D.; Christoffel, D. A.; Lienert, B. 1986: Magnetic polarity stratigraphy of a Plio-Pleistocene sequence of North Island, New Zealand. *Earth and planetary science letters 80*: 353-360.

Shackleton, N. J.; Berger, A.; Peltier, W. R. 1990: An alternative astronomical calibration of the lower Pleistocene timescale based on ODP site 677. *Transactions of the Royal Society of Edinburgh: Earth Sciences 81*: 251-261.

Shane, P. A. R. 1989: The characterisation and correlation of late Cenozoic tuffs, southeastern North Island, New Zealand. Unpublished MSc thesis, lodged in the library, Victoria University of Wellington.

Shane, P. A. R. 1990: Correlation of some Pliocene tuffs in southern Wairarapa, New Zealand, and comparison with biostratigraphic and magnetostratigraphic data. *New Zealand journal of geology and geophysics 33*: 349-354.

Shane, P. A. R. 1991: Remobilised silicic tuffs in middle Pleistocene fluvial sediments, southern North Island, New Zealand. *New Zealand journal of geology and geophysics 34*: 489-499.

Shane, P. A. R.; Froggatt, P .C. 1991: Glass chemistry, paleomagnetism and correlation of middle Pleistocene tuffs in southern North Island, New Zealand and Western Pacific. *New Zealand journal of geology and geophysics 34:* 203-211.

Shaw, D. M.; Watkins, N. D.; Huang, T. C. 1974: Atmospherically transported volcanic glass in deep-sea sediments: Theoretical considerations. *Journal of geophysical research 7*: 3087-3084.

Skinner, D. N. 1986: Neogene volcanism in the Hauraki Volcanic region. *Royal Society of New Zealand bulletin 23*: 21-47.

Smith, D. G. W.; Westgate, J. A. 1969: Electron probe technique for characterising pyroclastic deposits. *Earth and planetary science letters 5*: 313-319.

Smith, G. A. 1987: The influence of explosive volcanism in fluvial sedimentation: The Deschutes Formation (Neogene) in Central Oregon. *Journal of sedimentary petrology 57*: 613-629.

Smith, G. A. 1988: Sedimentology of proximal to distal volcaniclastics dispersed across an active fold belt: Ellensburg Formation, Central Washington. *Sedimentology 35:* 953-977.

Smith, R. P.; Nash, W. P. 1976: Chemical correlation of volcanic ash deposits in the Salt Lake Group, Utah, Idaho and Nevada. *Journal of sedimentary petrology 46*: 930-939.

Spell, T. L.; McDougall, I. 1992: Revisions to the age of the Brunhes-Matuyama Boundary and the Pleistocene geomagnetic polarity timescale. *Geophysical research letters 19*: 1181-1184.

Stokes, S.; Lowe, D. J. 1988: Discriminant function analysis of late Quaternary Tephras from five volcanoes in New Zealand using glass shard major element chemistry. *Quaternary research 30*: 270-283.

Stokes, S.; Lowe, D. J.; Froggatt, P. C. 1992: Discriminant function analysis and correlation of late Quaternary tephra deposits from Taupo and Okataina volcanoes, New Zealand, using glass shard major element compositions. *Quaternary international 13/14*: 103-120.

Tauxe, L.; Deino, A. D.; Behrensmeyer, A. K.; Potts, R. 1992: Pinning down the Brunhes/Matuyama and upper Jaramillo boundaries: a reconciliation of orbital and isotopic time scales. *Earth and planetary science letters 109*: 561-572.

Te Punga, M. T. 1952: The geology of the Rangitikei Valley. *New Zealand Geological Survey memoir 8.*

Turner, G. M.; Kamp, P. J. J. 1990: Paleomagnetic location of the Jaramillo Subchron and the Matuyama-Brunhes transition in the Castlecliffian stratotype section, Wanganui Basin, New Zealand. *Earth and planetary science letters 100*: 42-50.

Verosub, K. L. 1981: The interrelationship between magnetostratigraphy and tephrochronology. *In* : Self, S.; Sparks. R. S. J. *ed.* Tephra Studies. Reidel, Dordrecht.Pp. 65-72.

Walter, R. C.; Manega, P.C.; Hay, R. L.; Drake, R. E.; Curtis, G. H. 1991: Laser-fusion ^{40}Ar/^{39}Ar dating of Bed I, Olduvai Gorge, Tanzania . *Nature 354*: 145-149.

Watkins, N. D.; Huang, T. C. 1977: Tephras in abyssal sediments east of the North Island, New Zealand: chronology, paleowind velocity, and paleoexplosivity. *New Zealand journal of geology and geophysics 20*: 179-198.

Westgate, J. A.; Christiansen, E. A.; Boellstorff, J. D. 1977: Wascana Creek Ash (middle Pleistocene) in southern Saskatchewan: characterisation, source, fission track age, paleomagnetism and stratigraphic significance. *Canadian journal of earth sciences 14*: 357-374.

Westgate, J. A.; Evans, M. E. 1978: Compositional variability of Glacier Peak Tephra and its stratigraphic significance. *Canadian journal of earth sciences 15*: 1554-1567.

Westgate, J. A.; Gorton, M. P. 1981: Correlation techniques in tephra studies. *In* : Self, S.; Sparks. R. S. J. *ed.* Tephra Studies. Reidel, Dordrecht.Pp. 73-94.

Westgate, J. A.; Walter, R. C.; Pearce, G. W.; Gorton, M. P. 1985: Distribution, stratigraphy, petrochemistry, and paleomagnetism of the late Pleistocene Old Crow tephra in Alaska and the Yukon. *Canadian journal of earth sciences 22*: 893-906.

Williams, D. F.; Thunell, R. C.; Tappa, E.; Rio, D.; and Raffi, I. 1988: Chronology of the Pleistocene Oxygen isotope record: 0-1.88 m.y. B.P. *Paleogeography, paleoclimatology, paleoecology 64*: 221-240.

Wilson, C. J. N. 1986: Reconnaissance stratigraphy and volcanology of ignimbrites from Mangakino Volcano. *Royal Society of New Zealand bulletin 23*: 179-193.

Wilson, C. J. N.; Rogan, A. M.; Smith, I. E.; Northey, D. J.; Nairn, I. A.; Houghton, B. J. 1984: Caldera volcanoes of the Taupo Volcanic Zone, New Zealand. *Journal of geophysical research 89:* 8463-8484.

Woronow, A. 1991: Enigmas and solutions in the analyses of compositional data. *Journal of geological education 39*: 299-302.

York, D.; Hall, C. M.; Yanse, Y.; Hanes, J. A.; Kenyon, J. 1981: ^{40}Ar/^{39}Ar dating of terrestrial minerals with a continuous laser. *Geophysical research letters 8*: 1136-1138.

Appendix 1

ELECTRON MICROPROBE ANALYSES OF GLASS SHARDS IN EARLY PLEISTOCENE TEPHRAS

Technique

Samples of ash or pumice clasts were crushed and wet sieved to obtain the 60-250 μ size fraction. Glass in this fraction was purified with the use of a frantz magnetic separator, mounted in epoxy resin and polished. Individual glass shards were analysed by a Jeol 733 Superprobe at the Analytical Facility at Victoria University using a procedure similar to that described by Froggatt (1983). Operating conditions included a current of 8 nA at 15 kV and a 20 μ beam diameter. Analytical standards were measured frequently for monitoring and calibration. Typical standard analyses obtained in the period spanning 1990 to 1993 and detection limits are as follows:

	KN-18		VG-A99		
	EMA	1	EMA	2	DL
SiO_2	74.95(.37)	74.60	50.80(.30)	50.94	0.07
Al_2O_3	10.42(.23)	10.53	12.28(.25)	12.49	0.06
TiO_2	0.17(.04)	0.18	4.15(.12)	4.06	0.07
FeO	3.40(.16)	3.45	13.23(.31)	13.30	0.11
MgO	0.02(.02)	0.01	5.03(.12)	5.08	0.06
CaO	0.15(.05)	0.15	9.19(.20)	9.30	0.05
Na_2O	5.29(.32)	5.68	2.81(.14)	2.66	0.09
K_2O	4.45(.14)	4.39	0.82(.04)	0.82	0.05
Cl	0.31(.05)	0.37	-	-	0.05
Total	99.15(.51)	99.36	98.30(.65)	98.65	
n	30		34		

KN-18: comenditic obsidian, Naivasha, Kenya.
VG-A99: basaltic glass, Makaopuhi, Hawaii (USNM 113498/1)
1: analysis from Nielsen and Sigurdsson (1981)
2: analysis from Jarosewich et al. (1980).
DL= typical detection limit; n= number of analyses.

Analyses of the early Pleistocene glasses are recalculated to 100% on a volatile-free basis with the difference being expressed as water, due almost entirely to hydration (e.g. Froggatt 1983). In this appendix each analysis represents a single shard with the mean and standard deviation shown on the last two lines of the analyses columns. Where shards of different composition are recognised, they are presented separately from the main population.

SiO$_2$	Al$_2$O$_3$	TiO$_2$	FeO	MgO	CaO	Na$_2$O	K$_2$O	Cl	water

120 Mangatewaiiti Sm U23/825150-817163

SiO$_2$	Al$_2$O$_3$	TiO$_2$	FeO	MgO	CaO	Na$_2$O	K$_2$O	Cl	water
75.38	12.99	0.14	2	0.07	1.04	4.4	3.83	0.16	5.44
75.15	12.94	0.18	1.97	0.14	0.99	3.69	4.86	0.23	3
75.33	12.89	0.17	2.07	0.14	0.97	4.58	3.63	0.22	5.61
75.14	12.91	0.21	2.02	0.1	1.09	4.54	3.79	0.2	6.36
76.25	12.35	0.13	1.85	0.08	0.89	4.04	4.22	0.19	7.11
75.56	12.72	0.19	2.09	0.12	1.11	4.35	3.62	0.23	3.06
75.8	12.55	0.23	1.78	0.08	0.9	4.32	4.16	0.17	5.27
76.21	12.32	0.14	1.85	0.09	0.86	4.19	4.13	0.21	4.74
76.04	12.68	0.16	1.69	0.1	0.84	4.07	4.27	0.25	6.45
75.61	12.79	0.17	1.89	0.11	0.98	4.24	4.02	0.21	5.06
0.44	0.26	0.03	0.16	0.04	0.11	0.25	0.35	0.03	1.41
73.3	13.73	0.33	2.38	0.29	1.71	4.63	3.34	0.27	4.3
73.6	13.78	0.17	2.42	0.35	1.62	4.53	3.37	0.16	5.69
73.44	13.68	0.28	2.45	0.32	1.74	4.44	3.45	0.21	4.94
76.37	12.51	0.12	1.47	0.06	0.81	4.21	4.18	0.27	5.15

122 Mangatewaiiti Sm U23/825150-817163

SiO$_2$	Al$_2$O$_3$	TiO$_2$	FeO	MgO	CaO	Na$_2$O	K$_2$O	Cl	water
74.45	13.4	0.25	1.97	0.15	1.24	4.33	3.99	0.23	6.67
74.68	13.11	0.23	2.01	0.22	1.16	4.37	3.92	0.3	5.94
74.63	13.07	0.24	2.51	0.14	1.07	4.51	3.67	0.17	5.89
74.53	13.24	0.23	2.24	0.17	1.08	4.68	3.58	0.24	5.64
74.02	13.4	0.21	2.36	0.21	1.09	4.74	3.71	0.26	5.2
75.03	12.79	0	2.07	0.32	1.11	4.58	3.78	0.33	8.13
74.41	13	0.24	2.28	0.21	1.15	4.66	3.71	0.33	9.48
77.11	12.13	0.06	1.45	0.14	1.09	3.49	4.28	0.25	4.36
74.86	13.02	0.18	2.11	0.2	1.12	4.42	3.83	0.26	6.41
0.95	0.41	0.1	0.32	0.06	0.06	0.4	0.23	0.05	1.66

123 Mangatewaiiti Sm U23/825150-817163

SiO$_2$	Al$_2$O$_3$	TiO$_2$	FeO	MgO	CaO	Na$_2$O	K$_2$O	Cl	water
74.58	13.28	0.24	2.29	0.09	0.92	4.72	3.68	0.19	6.87
75.43	12.83	0.1	2.11	0.09	1.06	4.63	3.72	0.13	6.21
76.08	12.23	0.21	2.07	0.08	0.79	4.41	3.78	0.24	5.41
76.15	12.72	0.11	1.89	0.11	0.91	4.26	3.62	0.23	5.73
76.02	12.44	0.14	2.05	0.17	0.86	4.41	3.62	0.28	5.06
75.91	12.51	0.09	2.14	0.15	0.8	4.32	3.78	0.28	4.88
76.55	12.14	0.16	2	0.09	0.83	4.42	3.76	0.15	5.8
76.66	12.1	0.22	1.78	0.08	0.82	4.36	3.72	0.25	5.87
76.28	12.34	0.24	2.01	0.11	0.86	4.4	3.55	0.22	5.41
75.96	12.51	0.17	2.04	0.11	0.87	4.44	3.69	0.22	5.69
0.63	0.38	0.06	0.15	0.03	0.08	0.15	0.08	0.05	0.6
77.28	12.31	0.11	1.42	0	0.56	3.97	4.13	0.22	5.82

124 Mangatewaiiti Sm U23/825150-817163

SiO$_2$	Al$_2$O$_3$	TiO$_2$	FeO	MgO	CaO	Na$_2$O	K$_2$O	Cl	water
75.89	12.75	0.16	2.04	0.1	0.92	4.35	3.85	0.04	5.26
76.08	12.84	0.15	1.53	0.06	1	4.32	3.77	0.24	5.37
75.86	12.57	0.2	1.89	0.1	0.88	4.42	3.81	0.27	4.53
76.05	12.67	0.15	2.27	0.14	1.05	3.53	3.95	0.18	6.58
74.67	13.13	0.21	2.22	0.1	1.03	4.67	3.82	0.16	5.71
77.46	12.33	0.06	1.22	0.07	1.11	3.63	3.91	0.2	5.91
77.22	12.81	0.1	0.8	0.1	0.7	3.53	4.72	0.12	7.21
75.1	13.39	0.16	1.84	0.15	1.2	4.39	3.58	0.18	5.99
77.53	11.84	0.15	1.38	0.05	0.68	3.97	4.17	0.23	5.26
77.53	12.19	0.1	1.3	0.1	0.68	3.99	3.84	0.26	6.35
77.42	12.7	0.09	1.02	0.12	0.92	3.62	3.89	0.22	5.9
77.57	12.36	0.04	0.97	0.06	0.9	3.61	4.32	0.16	5.59
77.78	12.3	0.08	1.07	0.08	1.05	3.72	3.72	0.18	5.48
77.81	12.26	0.05	1.11	0.1	1.14	3.61	3.91	0.11	5.56
76.71	12.58	0.12	1.48	0.1	0.95	3.95	3.95	0.18	5.76
1.07	0.4	0.05	0.49	0.03	0.17	0.4	0.29	0.06	0.65

125 Mangatewaiiti Sm U23/825150-817163

SiO$_2$	Al$_2$O$_3$	TiO$_2$	FeO	MgO	CaO	Na$_2$O	K$_2$O	Cl	water
75.45	12.63	0.19	2.22	0.29	1.87	4.1	3.08	0.17	6.28
75.31	12.81	0.14	1.97	0.13	1.03	4.71	3.66	0.23	5.18
75.47	12.87	0.15	2.12	0.16	0.99	4.5	3.81	0.09	7.88
75.62	12.63	0.23	1.82	0.16	1.07	4.29	3.85	0.33	7.84
74.59	13.28	0.21	2.04	0.17	1.16	4.69	3.63	0.24	6.76
75.94	12.24	0.21	2.08	0.12	0.89	4.48	3.77	0.26	4.77
74.74	13.19	0.21	2.12	0.19	1.12	4.49	3.74	0.19	6.27
75.3	12.81	0.19	2.05	0.17	1.16	4.47	3.65	0.22	6.43
0.48	0.36	0.03	0.13	0.06	0.32	0.21	0.26	0.08	1.19
77.8	11.85	0.11	1.07	0.11	0.69	3.86	4.35	0.18	5.42
77.63	11.99	0	1.22	0.08	0.6	3.96	4.29	0.23	7.27

126 Mangatewaiiti Sm U23/825150-817163

SiO$_2$	Al$_2$O$_3$	TiO$_2$	FeO	MgO	CaO	Na$_2$O	K$_2$O	Cl	water
78.26	12.16	0.13	1.16	0.05	1.13	3.88	3.1	0.14	5.99
78.49	12.1	0.14	0.79	0.14	1.09	3.46	3.52	0.28	6.26
77.92	11.97	0.1	1.41	0.05	1.1	3.75	3.49	0.2	3.82
78.1	12	0.14	1.21	0.09	1.2	3.82	3.29	0.16	4.76
78.36	11.71	0.05	1.22	0.11	1.26	3.7	3.43	0.16	2.13
77.23	12.42	0.05	1.23	0.09	0.86	3.5	4.4	0.2	5.18
78.4	11.92	0.11	1.22	0.07	1.09	3.49	3.53	0.17	3.06
78.03	11.94	0.06	1.34	0.05	1.16	3.74	3.53	0.14	2.88
78.07	12.18	0.08	1.25	0.06	1.12	3.75	3.31	0.17	3.77
78.1	12.04	0.1	1.2	0.08	1.11	3.68	3.51	0.18	4.21
0.38	0.2	0.04	0.17	0.03	0.11	0.15	0.36	0.04	1.43
76	12.61	0.22	1.62	0.07	0.94	4.26	4.11	0.18	6
75.14	12.99	0.15	2.28	0.14	1.13	4.17	3.82	0.16	8.19

127 Mangatewaiiti Sm U23/825150-817163

SiO$_2$	Al$_2$O$_3$	TiO$_2$	FeO	MgO	CaO	Na$_2$O	K$_2$O	Cl	water
75.51	12.69	0.18	1.97	0.11	1.11	4.51	3.73	0.19	5.8
76.21	12.55	0.14	1.85	0.07	0.86	4.45	3.79	0.13	6.17
75.96	12.78	0.19	1.94	0.05	0.96	4.24	3.67	0.21	5.63
76.95	12.13	0.14	1.5	0.09	0.74	4.07	4.18	0.2	5.15
75.91	12.74	0.13	1.92	0.07	1.01	4.28	3.8	0.15	4.63
75.92	12.4	0.13	2.11	0.13	1	4.26	3.84	0.2	7.12
77.18	12.25	0	1.6	0.07	0.76	3.82	4.05	0.25	5.72
76.35	12.43	0.15	1.93	0.09	0.97	4.07	3.82	0.19	5.15
76.25	12.5	0.13	1.85	0.09	0.93	4.21	3.86	0.19	5.67
* 0.56	0.24	0.06	0.2	0.03	0.13	0.22	0.17	0.04	0.76
77.9	12.16	0.09	1	0	0.96	3.55	4.18	0.16	5.06
78.19	11.88	0.11	1.04	0.11	1.14	3.6	3.82	0.12	5.06
77.91	12.33	0	1.01	0.08	0.86	3.25	4.39	0.17	5.36

128 Mangatewaiiti Sm U23/825150-817163

SiO$_2$	Al$_2$O$_3$	TiO$_2$	FeO	MgO	CaO	Na$_2$O	K$_2$O	Cl	water
77.28	12.15	0.11	1.19	0.12	0.85	3.88	4.13	0.29	6.16
77.53	11.9	0.11	1.31	0.11	0.87	3.65	4.2	0.33	5.05
77.83	11.59	0.14	1.14	0.15	0.99	3.7	4.21	0.27	6.69
77.83	11.54	0.12	1.35	0.08	0.83	3.69	4.28	0.28	8.72
77.69	11.77	0.15	1.35	0.12	0.84	3.77	4.04	0.27	7.28
78.02	11.36	0.15	1.27	0.12	0.93	3.73	4.13	0.29	8.86
77.18	11.75	0.11	1.35	0.13	0.83	3.85	4.47	0.32	8.79
77.81	11.59	0.15	1.22	0.16	0.87	3.61	4.29	0.31	5.55
77.65	11.75	0.11	1.38	0.15	0.97	3.73	4.12	0.27	5.78
77.65	11.71	0.13	1.28	0.13	0.89	3.73	4.21	0.29	6.99
0.27	0.23	0.02	0.08	0.02	0.06	0.09	0.13	0.02	1.5

129 Mangatewaiiti Sm U23/825150-817163

SiO$_2$	Al$_2$O$_3$	TiO$_2$	FeO	MgO	CaO	Na$_2$O	K$_2$O	Cl	water
72.19	13.43	0.52	3.21	0.48	2.16	4.28	3.53	0.19	5.68
73.2	13.89	0.56	2.44	0.38	2.22	3.89	3.31	0.11	5.98
72.22	13.58	0.52	3.16	0.51	2.05	4.27	3.46	0.24	7.24
72.7	13.7	0.55	2.87	0.49	2.09	4.05	3.34	0.21	4.86
72.31	13.72	0.47	2.77	0.49	2.07	4.35	3.57	0.25	6.65
72.64	13.55	0.44	2.93	0.46	2.08	4.1	3.56	0.24	7.25
72.26	13.77	0.56	3.01	0.47	2.11	3.95	3.58	0.29	10.08
72.58	13.43	0.49	2.88	0.44	2.1	4.19	3.56	0.34	10.88
72.05	13.63	0.45	3.04	0.49	2.27	4.37	3.38	0.32	8.88
71.82	13.97	0.53	2.85	0.48	2.17	4.42	3.53	0.22	5.72
71.41	13.98	0.51	3.23	0.65	2.35	4.19	3.43	0.25	12.32
72.31	13.7	0.51	2.94	0.49	2.15	4.19	3.48	0.24	7.78
0.48	0.19	0.04	0.23	0.06	0.09	0.17	0.1	0.06	2.43
76.22	12.46	0.13	1.74	0	0.97	3.7	4.56	0.22	6.48

130 Whitby R27/684095

SiO$_2$	Al$_2$O$_3$	TiO$_2$	FeO	MgO	CaO	Na$_2$O	K$_2$O	Cl	water
75.62	13.26	0.24	1.88	0.15	0.87	4.9	2.97	0.11	9.4
76.4	13.01	0.25	1.68	0.15	0.89	4.57	3.21	0.08	8.18
76.52	12.75	0.3	1.53	0.17	0.9	4.79	2.95	0.09	7.47
75.69	12.98	0.18	1.9	0.16	0.89	4.96	3.16	0.09	6.83
75.69	13.15	0.21	1.8	0.15	0.94	4.96	3.01	0.09	7.39
76.1	13.09	0.23	1.65	0.17	0.96	4.74	2.97	0.1	7.95
76.13	12.96	0.2	1.71	0.16	0.88	4.82	3.01	0.13	6.36
76.49	12.79	0.21	1.62	0.2	0.91	4.7	2.98	0.11	8.67
76.02	13.15	0.22	1.58	0.14	0.95	4.76	3.04	0.14	8.2
76.07	13.02	0.23	1.71	0.16	0.91	4.8	3.03	0.1	7.83
0.35	0.17	0.03	0.13	0.02	0.03	0.13	0.09	0.02	0.93

131 Oroua River T22/622362

SiO$_2$	Al$_2$O$_3$	TiO$_2$	FeO	MgO	CaO	Na$_2$O	K$_2$O	Cl	water
75.33	12.78	0.18	1.88	0.1	0.76	4.06	4.91	0.1	6.63
75.15	13.03	0.17	1.81	0.07	0.79	4.03	4.84	0.1	7.92
75.36	12.66	0.2	1.87	0.07	0.85	3.94	4.87	0.2	7.95
75.64	12.57	0.19	1.72	0.1	0.93	3.91	4.79	0.14	6.92
75.6	12.77	0.15	1.85	0.09	0.84	3.75	4.81	0.15	6.15
75.49	12.75	0.11	1.87	0.12	0.84	3.64	5.03	0.15	7.18
75.6	12.72	0.16	1.88	0.08	0.83	3.76	4.83	0.15	7.06
75.62	12.76	0.13	1.76	0.14	0.82	3.68	4.95	0.14	6.85
75.74	12.71	0.15	1.81	0.11	0.83	3.52	4.99	0.14	6.83
75.53	12.84	0.21	1.66	0.1	0.91	3.82	4.8	0.13	7.91
75.74	12.73	0.13	1.73	0.12	0.91	3.67	4.87	0.1	7.45
75.53	12.76	0.16	1.8	0.1	0.85	3.8	4.88	0.14	7.17
0.18	0.11	0.03	0.08	0.02	0.05	0.17	0.08	0.03	0.58

132 Oroua River T22/623364

SiO$_2$	Al$_2$O$_3$	TiO$_2$	FeO	MgO	CaO	Na$_2$O	K$_2$O	Cl	water
75.92	13.13	0.17	1.94	0.1	0.93	4.55	3.13	0.14	9.22
75.91	12.87	0.15	1.92	0.12	0.93	3.88	4.23	0.14	9.27
75.96	12.84	0.15	1.83	0.07	0.89	4.4	3.77	0.09	8.33
76.04	12.93	0.09	1.81	0.1	0.83	4.22	3.92	0.16	7.5
74.82	12.62	0.19	2.11	0.08	0.86	4.09	4.1	0.13	5.64
75.92	12.76	0.16	1.93	0.09	0.93	4.47	3.65	0.09	7.23
75.76	12.86	0.15	1.92	0.09	0.9	4.27	3.8	0.13	7.87
0.46	0.17	0.03	0.11	0.02	0.04	0.25	0.39	0.03	1.38
77.2	12.3	0.13	1.32	0.06	0.66	3.99	4.25	0.1	6.72

77.32	12.43	0.12	1.16	0.1	0.64	3.66	4.57	0.13	7.45
77.44	12.25	0.12	1.28	0.06	0.63	3.55	4.75	0.12	7.51
77.29	12.17	0.11	1.45	0.05	0.57	3.83	4.42	0.11	7.02
77.56	11.99	0.11	1.24	0.06	0.69	3.74	4.5	0.12	10.35
77.36	12.23	0.12	1.29	0.07	0.64	3.75	4.5	0.12	7.81
0.14	0.16	0.01	0.11	0.02	0.04	0.17	0.18	0.01	1.46

133 Oroua River T22/623364

75.23	13.13	0.11	1.94	0.12	1.03	4.52	3.81	0.12	8.31
76.42	12.59	0.16	1.63	0.06	0.75	4.2	4.07	0.1	6.99
76.26	13.03	0.12	1.79	0.08	0.85	4.32	3.64	0	7.34
75.52	13.22	0.15	1.95	0.09	0.87	4.73	3.35	0.12	8.39
75.18	13.32	0.15	1.88	0.13	1.01	4.84	3.35	0.14	7.5
76.38	12.76	0.12	1.73	0.08	0.71	4.47	3.71	0.11	7.61
75.44	13.37	0.18	1.96	0.08	0.88	4.77	3.41	0	10.07
75.8	13.01	0.14	1.85	0.09	0.87	4.52	3.65	0.09	8.03
0.49	0.27	0.03	0.11	0.02	0.1	0.22	0.24	0.05	0.93
76.89	12.5	0.07	1.39	0.07	0.58	3.87	4.51	0.13	8.56
77.2	12.38	0.11	1.4	0.05	0.66	3.99	4.06	0.14	7.98
77.34	12.14	0.12	1.17	0.07	0.69	3.81	4.63	0.11	8.39
77.28	12.68	0.11	1.04	0.11	0.98	3.81	3.93	0.08	7.28
77.18	12.43	0.1	1.25	0.08	0.73	3.87	4.28	0.12	8.05
0.2	0.23	0.02	0.18	0.03	0.17	0.08	0.34	0.03	0.57

134 Oroua River T22/624364

75.42	13.98	0.13	1.7	0.34	1.49	3.95	2.85	0.14	9.85
75.77	13.91	0.12	1.5	0.35	1.42	3.91	2.85	0.17	5.94
75.6	14.05	0.21	1.62	0.37	1.41	3.72	2.86	0.16	5.91
75.59	13.88	0.17	1.51	0.3	1.51	3.89	2.97	0.18	5.88
75.61	13.86	0.12	1.46	0.36	1.45	4.05	2.98	0.12	6.66
75.52	14	0.13	1.53	0.37	1.38	4.03	2.89	0.15	6.63
75.5	13.91	0.13	1.45	0.36	1.35	4.04	3.11	0.16	7.16
75.52	14.01	0.18	1.64	0.32	1.23	3.99	3.04	0.06	6.8
75.69	13.88	0.17	1.47	0.28	1.39	3.85	3.17	0.1	6
75.72	13.91	0.13	1.55	0.28	1.36	3.88	3.08	0.09	5.8
75.59	13.94	0.15	1.54	0.33	1.4	3.93	2.98	0.13	6.66
0.11	0.07	0.03	0.08	0.04	0.08	0.1	0.12	0.04	1.22

136 Oroua River T22/624364

74.54	13.62	0.19	2.18	0.11	1.06	4.46	3.67	0.16	7.65
74.63	13.52	0.16	2.05	0.1	1.11	4.62	3.7	0.11	7.37
74.78	13.51	0.21	2.02	0.11	1.16	4.65	3.5	0.07	8.27
74.95	13.5	0.21	2.07	0.16	1.14	3.99	3.86	0.12	7.58
74.7	13.53	0.11	2.19	0.11	1.22	4.32	3.75	0.09	8.99
75.02	13.29	0.12	2.17	0.09	1.09	4.6	3.57	0.06	7.16
74.54	13.54	0.13	2.18	0.1	1.16	4.62	3.63	0.11	7.95
74.79	13.44	0.2	2.1	0.16	1.09	4.4	3.69	0.13	8.41
74.73	13.29	0.11	2.18	0.16	1.11	4.47	3.79	0.15	8.51
74.35	13.45	0.17	2.19	0.11	1.22	4.66	3.75	0.11	6.28
74.74	13.49	0.17	2.12	0.12	1.13	4.46	3.67	0.11	7.92
0.2	0.11	0.04	0.07	0.03	0.05	0.21	0.11	0.03	0.78
76.95	12.63	0.17	1.29	0.08	0.74	3.85	4.18	0.12	6.74

137 Oroua River T22/624364

77.9	12.23	0.06	1.25	0.08	1.15	3.86	3.36	0.11	6.96
77.71	12.24	0.08	1.45	0.11	1.13	3.8	3.43	0.05	8.17
78.3	12.31	0.11	0.79	0.09	1.16	3.55	3.61	0.08	8.86
77.95	12.16	0.1	1.22	0.13	1.2	3.6	3.51	0.13	6.9
77.53	12.31	0.1	1.35	0.09	1.16	3.64	3.78	0.13	10.14
77.23	12.36	0.2	1.31	0.09	1.17	3.84	3.7	0.09	4.61
77.72	12.46	0.11	1.18	0.09	1.07	3.76	3.51	0.12	6.56
77.69	12.38	0.1	1.19	0.07	1.15	3.77	3.55	0.11	6.37
77.91	12.38	0.11	1.09	0.11	1.14	3.74	3.41	0.11	8.14
77.52	12.54	0.13	1.17	0.09	1.12	3.8	3.54	0.1	7.4
77.89	12.47	0.07	1.15	0.1	1.11	3.37	3.78	0.07	8.09
77.76	12.35	0.11	1.2	0.1	1.14	3.7	3.56	0.1	7.47
0.28	0.11	0.04	0.17	0.02	0.03	0.15	0.14	0.03	1.46

138 Oroua River T22/623362

74.37	13.7	0.15	2.12	0.1	0.87	5.07	3.53	0.09	9.53
74.61	13.69	0.2	2.02	0.12	0.92	4.91	3.56	0.09	9.11
75.09	13.55	0.14	2.01	0.09	0.88	4.57	3.55	0.12	9.89
74.97	13.43	0.15	2.07	0.07	0.91	4.84	3.45	0.1	5.91
75.11	13.6	0.14	2.12	0.12	0.93	4.82	3.19	0.09	9.47
74.9	13.37	0.15	2.12	0.12	1.01	4.86	3.35	0.13	6.15
75.45	13.25	0.13	1.92	0.09	0.92	4.77	3.39	0.1	6.2
74.54	13.57	0.19	2.16	0.1	0.9	5.01	3.44	0.1	8.39
74.64	13.54	0.12	2.1	0.11	0.9	4.91	3.59	0.09	9.58
75.15	13.34	0.2	1.83	0.06	0.99	4.83	3.53	0.06	5.4
74.88	13.5	0.16	2.05	0.1	0.92	4.86	3.46	0.1	7.96
0.33	0.15	0.03	0.1	0.02	0.04	0.14	0.12	0.02	1.82

139 Oroua River T22/623362

74.84	13.58	0.13	2.18	0.08	0.95	4.7	3.46	0.08	9.23
75.12	13.53	0.16	1.74	0.09	0.95	4.7	3.61	0.11	6.64
74.59	13.49	0.17	2.19	0.08	0.96	4.99	3.46	0.06	7.35
75.22	13.34	0.15	1.81	0.07	0.99	4.52	3.8	0.1	6.65
74.62	13.72	0.12	2	0.08	0.9	4.99	3.56	0.1	7.8

75.19	13.31	0.14	1.89	0.12	0.91	4.9	3.46	0.08	5.83
75.53	13.17	0.11	1.96	0.06	0.78	4.64	3.66	0.1	6.45
75.24	13.41	0.13	1.94	0.08	0.83	5.07	3.22	0.07	5.84
75.22	13.07	0.16	1.98	0.06	1.01	4.72	3.61	0.17	3.91
75.09	13.34	0.13	2.09	0.13	1.09	4.3	3.67	0.16	5.82
75.36	13.13	0.19	2.02	0.13	0.89	4.38	3.72	0.18	6.26
75.09	13.37	0.14	1.98	0.09	0.93	4.72	3.57	0.11	6.53
0.29	0.2	0.02	0.14	0.03	0.09	0.25	0.16	0.04	1.34

140 Oroua River T22/623360

74.84	13.45	0.21	2.03	0.15	1.09	4.77	3.39	0.07	7.98
74.08	13.77	0.15	2.47	0.15	1.01	5.12	3.13	0.1	9.32
73.95	13.7	0.22	2.22	0.1	1.12	5.11	3.49	0.09	9.48
74.26	13.87	0.18	2.15	0.17	1.14	4.82	3.31	0.1	7.01
74.86	13.43	0.23	2	0.1	1	4.91	3.33	0.13	8.43
74.43	13.81	0.2	2.19	0.12	1.01	4.7	3.41	0.12	10.88
73.39	14.31	0.18	2.68	0.14	1.27	4.63	3.28	0.12	10.01
74.3	13.65	0.24	2.35	0.15	1.04	4.74	3.46	0.08	7.13
74.68	13.59	0.25	2.37	0.09	1.05	4.43	3.43	0.12	8.74
74.6	13.4	0.18	2.12	0.13	1.14	4.68	3.58	0.18	4.12
74.07	13.63	0.2	2.28	0.13	1.39	4.88	3.26	0.16	6.01
74.84	13.16	0.16	2.28	0.11	1.15	4.76	3.35	0.2	4.97
74.36	13.65	0.2	2.26	0.13	1.12	4.8	3.37	0.12	7.84
0.44	0.29	0.03	0.19	0.02	0.12	0.19	0.12	0.04	2.06

141 Oroua River T22/623360

74.3	13.42	0.34	2.17	0.11	1.18	4.34	4.02	0.12	9.86
75.01	13.35	0.14	2.02	0.13	1.29	4.47	3.39	0.21	8.25
74.06	13.36	0.24	2.29	0.33	1.26	4.45	3.62	0.39	7.12
74.14	13.51	0.24	2.28	0.15	1.23	4.83	3.7	0.06	9.16
74.42	13.46	0.24	2.17	0.15	1.18	4.32	3.76	0.28	6.12
75.41	12.84	0.18	1.95	0.13	0.94	4.37	3.97	0.21	6.53
75.18	13.26	0.17	2.11	0.15	1.22	4.37	3.59	0.09	8.09
74.43	13.56	0.22	2.12	0.19	1.19	4.49	3.86	0.15	9.59
73.93	13.31	0.22	2.43	0.15	1.3	4.68	3.78	0.19	6.63
74.33	13.49	0.24	2.26	0.15	1.3	4.47	3.75	0.16	7.13
74.8	13.33	0.17	2.16	0.16	1.24	4.48	3.49	0.18	7.04
74.42	13.75	0.19	2.23	0.11	1.29	4.01	3.82	0.19	8.79
74.18	13.61	0.26	2.22	0.13	1.27	4.57	3.59	0.16	8.95
74.51	13.4	0.22	2.19	0.16	1.22	4.45	3.72	0.18	7.94
0.45	0.22	0.05	0.12	0.06	0.1	0.19	0.18	0.08	1.26

142 Oroua River T23/542257

74.49	13.54	0.12	2.24	0.12	0.97	4.93	3.49	0.1	7.27
74.94	13.39	0.11	2.12	0.08	1.23	4.93	3.11	0.09	9.11
75.68	13.22	0.12	1.99	0.13	1.05	4.66	3.04	0.12	7.09
75.25	13.03	0.17	2.15	0.14	1.16	4.75	3.24	0.11	7.44
75.9	13.17	0.13	1.96	0.12	1.1	4.61	2.9	0.11	7.54
75.56	13.19	0.18	1.95	0.09	0.99	4.63	3.31	0.11	9.07
75.52	13.14	0.16	2.11	0.12	1.17	4.63	3.04	0.1	7.18
75.25	13.24	0.17	2.12	0.14	1.11	4.57	3.27	0.13	6.43
75.32	13.24	0.15	2.08	0.12	1.1	4.71	3.18	0.11	7.64
0.45	0.16	0.03	0.1	0.02	0.09	0.14	0.19	0.01	0.95
77.11	12.51	0.13	1.3	0.07	0.72	3.85	4.18	0.14	5.2
77.25	12.54	0.08	1.36	0.08	0.74	3.9	3.94	0.11	9.7
72.98	14.07	0.36	2.97	0.38	1.86	4.73	2.54	0.11	7.62

144 Manawatu River U23/890199-892193

75.13	13.25	0.1	1.7	0.08	1.03	4.37	4.14	0.2	8.92
76.37	13.96	0.05	0.83	0.1	0.97	3.23	4.34	0.15	7.31
75.23	13.55	0.21	1.91	0.15	1.21	4.08	3.48	0.18	10.69
75.58	13.59	0.12	1.48	0.11	1.07	3.89	3.99	0.18	8.97
0.69	0.36	0.08	0.57	0.04	0.12	0.59	0.45	0.03	1.69

145 Manawatu River U23/890199-892193

75.14	13.1	0.19	1.98	0.16	1.28	4.04	3.94	0.15	7.19
75.23	13.1	0.18	1.76	0.13	1.16	4.25	4.03	0.16	8.91
75.19	13.19	0.22	1.8	0.14	1.27	4.16	3.9	0.13	7.25
74.75	13.4	0.18	2	0.08	1.21	4.31	3.86	0.21	9.93
74.7	13.04	0.16	2.29	0.16	1.27	4.27	3.93	0.2	10.33
75	13.17	0.19	1.97	0.13	1.24	4.21	3.93	0.17	8.72
0.26	0.14	0.02	0.21	0.03	0.05	0.11	0.06	0.03	1.47
78.05	12.3	0.1	0.73	0.06	0.72	3.14	4.9	0.1	7.21
76.02	12.85	0.11	1.53	0	0.93	4.13	4.26	0.18	9.85

146 Manawatu River U23/890199-892193

75.2	12.73	0.14	2.02	0.06	1.07	4.25	4.31	0.22	7.24
74.82	13	0.18	2.07	0.08	1.24	4.4	4.02	0.2	9.52
76.17	12.82	0.18	1.84	0.07	0.96	4	3.8	0.16	4.35
75.48	12.83	0.22	1.99	0.07	1.16	3.96	4.09	0.2	5.76
73.84	13.88	0.24	2.06	0.2	1.27	4.6	3.71	0.19	9.43
77.38	12.5	0.12	1.01	0.1	1.12	3.78	3.83	0.17	9.49
77.04	12.46	0.11	1.29	0.07	1.18	3.7	4.01	0.14	8.8
77.82	12.39	0.1	0.94	0.11	1.21	3.53	3.87	0.12	8.51
76.73	12.3	0.07	1.43	0.07	0.76	4.18	4.29	0.18	8.95
77.84	12.24	0.12	0.78	0.08	1.1	3.56	4.12	0.17	7.81
77.47	12.15	0.15	1.42	0.06	0.74	3.75	4.05	0.21	5.37

77.3	12.18	0.08	1.4	0.1	0.75	3.95	4.1	0.23	4.49
77.87	12.51	0.1	1.01	0.09	1.12	3.47	3.79	0.14	7.18
77.42	12.4	0.13	1.05	0.07	1.16	3.72	3.88	0.16	8.87
77.37	12.5	0.1	1.1	0.11	1.12	3.63	3.92	0.14	9.13
76.65	12.59	0.14	1.43	0.09	1.06	3.9	3.99	0.18	7.66
1.26	0.43	0.05	0.46	0.03	0.18	0.34	0.18	0.03	1.84

147 Manawatu River U23/890199-892193

76.24	12.15	0.08	1.8	0.07	0.78	4.51	4.19	0.2	8.56
75.19	13.34	0.21	1.49	0.08	0.98	4.47	4.1	0.14	8.93
74.95	13.11	0.24	1.88	0.11	1.2	4.46	3.81	0.24	8.13
76.94	12.24	0.08	1.25	0.34	1.22	3.72	3.9	0.32	5.38
77.62	12.27	0.1	0.89	0.06	1	3.48	4.55	0.13	6.66
77.19	12.26	0.1	1.41	0.05	0.91	3.96	4	0.12	9.02
78	12.53	0.1	1.03	0.06	1.1	3.34	3.76	0.18	6.53
77.97	12.32	0.1	1	0.12	1.13	3.44	3.78	0.15	6.92
77.49	12.54	0.08	0.86	0.07	0.85	3.87	4.27	0.12	10.36
77.03	12.29	0.13	1.48	0.07	0.87	3.92	4.08	0.21	8.06
77.31	12.4	0.07	0.94	0.07	1.13	3.55	4.42	0.12	9.57
77.79	12.18	0.08	1.04	0.09	1.06	3.54	4.13	0.16	8.55
76.98	12.47	0.11	1.26	0.1	1.02	3.86	4.08	0.17	8.06
1.02	0.38	0.05	0.35	0.08	0.14	0.42	0.25	0.06	1.43

148 Manawatu River U23/890199-892193

78.35	11.85	0.1	1.24	0.06	1.2	3.59	3.45	0.16	5.77
77.67	12.03	0.09	1.44	0.12	1.28	3.7	3.58	0.09	4.64
77.91	12	0.09	1.36	0.1	1.27	3.58	3.63	0.16	4.81
78.17	12.24	0.1	1.19	0.13	1.24	3.45	3.44	0.14	5.18
77.83	12.14	0.08	1.33	0.08	1.28	3.74	3.42	0.11	7.79
77.94	12.22	0.11	1.24	0.07	1.3	3.57	3.43	0.11	4.14
77.58	12.3	0.1	1.33	0.07	1.32	3.67	3.58	0.16	9.99
78.34	12.29	0.1	1.3	0.09	1.2	3.38	3.27	0.11	8.67
78.35	12.35	0.1	0.83	0.09	1.32	3.51	3.41	0.12	9.38
78.02	12.16	0.1	1.25	0.09	1.27	3.58	3.47	0.13	6.71
0.3	0.17	0.01	0.17	0.02	0.05	0.12	0.11	0.03	2.25

149 Manawatu River U23/890199-892193

78.09	12.04	0.1	1.22	0.1	1.26	3.63	3.43	0.14	5.66
78.76	11.88	0.06	1.17	0	1.16	3.52	3.33	0.12	7.56
76.65	12.73	0.17	1.5	0.08	0.89	4.04	3.8	0.14	9.37
77.31	12.59	0.08	1.3	0.08	1.24	3.79	3.49	0.13	8.52
76.75	12.91	0.12	1.21	0.08	1.24	3.84	3.7	0.15	9.62
77.51	12.43	0.11	1.28	0.07	1.16	3.76	3.55	0.14	8.15
0.9	0.45	0.04	0.13	0.04	0.15	0.2	0.19	0.01	1.61
74.94	13.33	0.19	1.97	0.11	1.26	4.41	3.61	0.19	9.31
73.37	14.83	0.18	2.12	0.33	2.33	3.82	2.83	0.18	7.76
75.04	13.39	0.13	1.79	0.1	1.15	4.37	3.86	0.16	9.02
77.86	12.37	0	0.85	0.07	0.74	3.35	4.66	0.1	5.61

150 Manawatu River U23/890199-892193

75.17	13.32	0.13	1.97	0.11	1.04	4.58	3.49	0.19	6.39
74.55	13.51	0.19	2.16	0	1.14	4.41	3.8	0.24	9.89

151 Manawatu River U23/890199-892193

75.72	13.16	0.16	1.39	0.15	1.24	4.1	3.88	0.18	8.08
77.09	12.55	0.16	1.22	0.09	0.93	3.73	4.02	0.21	7.72
76.11	13.05	0.2	1.51	0.17	1.33	3.85	3.59	0.19	6.64
75.76	12.87	0.21	1.64	0.18	1.4	4.06	3.63	0.24	4.98
75.07	13.33	0.2	1.68	0.19	1.4	4.25	3.64	0.23	7.27
75.44	13.26	0.2	1.64	0.18	1.31	4.2	3.58	0.19	9.96
76.67	12.79	0.19	1.36	0.16	1.22	3.52	3.92	0.17	5.86
76.26	12.95	0.23	1.45	0.13	1.19	3.9	3.73	0.2	5.79
76.02	13	0.19	1.49	0.16	1.25	3.95	3.75	0.2	7.04
0.66	0.26	0.02	0.16	0.03	0.15	0.25	0.17	0.02	1.58
76.63	12.88	0.15	1.17	0.14	1.08	3.89	3.88	0.18	8.68
76.89	12.75	0.15	1.18	0.12	1.08	3.89	3.76	0.19	8.41

152 Porewa Sm T23/562159

74.22	13.59	0.19	2.27	0.1	1.22	4.5	3.79	0.13	5.6
74.72	13.47	0.18	2.18	0.14	1.16	4.45	3.66	0.16	8.86
73.67	13.88	0.2	2.28	0.15	1.24	4.67	3.75	0.17	10.49
74.6	13.48	0.13	2.26	0.15	1.22	4.24	3.78	0.2	7.86
74.14	13.64	0.17	2.28	0.15	1.23	4.35	3.85	0.17	7.91
73.77	13.78	0.22	2.36	0.18	1.17	4.49	3.84	0.2	10.06
73.82	13.7	0.25	2.28	0.13	1.19	4.75	3.69	0.19	7.53
74.04	13.39	0.12	2.21	0.13	1.21	4.76	3.63	0.2	8.28
74.81	13.33	0.21	2.11	0.17	1.17	4.44	3.57	0.18	5.9
74.2	13.58	0.19	2.25	0.14	1.2	4.52	3.73	0.18	8.05
0.42	0.18	0.04	0.07	0.02	0.03	0.18	0.1	0.02	1.65

153 Porewa Sm T23/557165

77.96	12.02	0.14	1.06	0.07	0.78	3.6	4.09	0.27	4.22
77.54	12.16	0.09	1.26	0.13	0.98	3.92	3.7	0.23	6.15
77.55	12.42	0.15	1.09	0.08	0.94	3.77	3.82	0.19	5.21
77.55	12.11	0.16	1.23	0.11	0.96	3.71	3.92	0.26	6.24
77.46	12.3	0.12	1.24	0.14	0.96	3.82	3.72	0.24	7.53
77.5	12.24	0.13	1.27	0.13	0.95	3.77	3.84	0.16	7.54
77.39	12.3	0.08	1.2	0.08	1.02	3.73	4.08	0.12	5.85
77.22	12.21	0.14	1.23	0.15	1.02	3.69	4.14	0.2	5.95
77.6	12.22	0.12	1.21	0.11	0.98	3.73	3.82	0.2	6.15
0.34	0.16	0.05	0.07	0.03	0.07	0.15	0.23	0.04	1.66
78.05	12.11	0.14	0.91	0.12	0.83	3.26	4.34	0.24	3.9
78.04	12.15	0.12	0.93	0.06	0.81	3.55	4.09	0.23	5.46
77.58	12.23	0.1	0.94	0.08	0.8	3.7	4.32	0.25	7.68
77.89	12.16	0.12	0.93	0.09	0.81	3.5	4.25	0.24	5.68
0.27	0.06	0.02	0.02	0.03	0.02	0.22	0.14	0.01	1.9

154 Porewa Sm T23/557165

76.48	12.64	0.16	1.47	0.14	0.92	3.99	4.03	0.17	9.73
76.17	12.45	0.19	1.48	0.09	1.08	3.84	4.57	0.14	6.17
76.46	12.8	0.11	1.64	0.07	1.02	3.93	3.82	0.16	7.86
76.44	12.66	0.1	1.66	0.11	1.01	3.96	3.92	0.15	5.8
76.59	12.62	0.13	1.54	0.1	1.02	3.83	3.94	0.22	8.98
76.44	12.68	0.13	1.58	0.09	0.88	4.17	3.9	0.13	9.14
76.25	12.79	0.12	1.72	0.1	1.26	3.87	3.78	0.12	4.6
77.63	12.06	0.13	1.48	0.1	0.94	3.7	3.87	0.19	4.66
76.64	12.69	0.13	1.67	0.08	1.08	3.86	3.73	0.13	4.33
75.92	12.95	0.13	1.66	0.09	1.04	4.14	3.91	0.16	8.28
76.5	12.63	0.13	1.59	0.1	1.03	3.93	3.95	0.16	6.96
0.45	0.24	0.03	0.09	0.02	0.11	0.14	0.23	0.03	2.08

155 Porewa Sm T23/557165

75.73	12.86	0.15	1.75	0.16	1.06	4.4	3.7	0.18	5.75
75.62	12.97	0.17	1.7	0.13	1.08	4.3	3.81	0.22	8.13
76.28	12.78	0	1.73	0.09	1.16	4.18	3.48	0.2	5.76
75.92	12.99	0.15	1.73	0.17	1.08	4.11	3.65	0.19	7.68
75.62	13.21	0.18	1.65	0.12	1.07	4.17	3.8	0.18	7.25
76.86	12.39	0.14	1.45	0.1	1.05	3.9	3.91	0.21	7.61
75.48	13.03	0.22	1.58	0.14	1.31	4.29	3.73	0.21	8.69
76.21	12.65	0.14	1.96	0.14	1.09	4.33	3.33	0.16	4.81
75.28	13.02	0.15	1.96	0.1	1.02	4.73	3.58	0.16	8.82
76.23	12.84	0.21	1.61	0.14	1.07	4.06	3.67	0.17	6.23
75.92	12.87	0.15	1.71	0.14	1.1	4.25	3.67	0.19	7.07
0.47	0.23	0.06	0.16	0.03	0.08	0.22	0.17	0.02	1.37
77.48	12.54	0.11	1.02	0.07	0.7	3.37	4.49	0.21	9.18
77.43	12.43	0.11	1.16	0.15	0.96	3.57	3.97	0.21	8.63

156 Manawatu River U23/890199-892193

75.1	13.26	0.14	1.84	0.09	0.88	4.44	4.19	0.16	9.73
75.25	13.25	0.11	1.8	0.09	1.02	4.34	4.04	0.12	6.64
75.06	13.21	0.19	2.15	0.17	1.15	4.52	3.35	0.21	3.94
74.03	13.7	0.21	2.35	0.09	1.13	4.86	3.45	0.19	9.24
74.46	13.4	0.22	2.19	0.13	1.19	4.46	3.72	0.23	7.63
75	13.19	0.18	2.24	0.09	1.13	4.16	3.86	0.15	7.44
75.05	13.18	0.15	2.12	0.09	1.16	4.53	3.51	0.21	6.97
75.99	12.82	0.1	1.59	0.09	0.78	4.41	4.05	0.19	7.38
74.99	13.25	0.16	2.04	0.11	1.06	4.47	3.77	0.18	7.37
0.57	0.24	0.04	0.26	0.03	0.15	0.2	0.31	0.04	1.76
77.09	12.83	0.13	1.08	0.11	1.06	3.5	4.1	0.1	9.49

158 Mangatewainui Sm U23/838166-827178

75.15	13.1	0.07	1.9	0.06	0.95	4.27	4.37	0.2	3.18
74.9	13.32	0.16	1.83	0.06	0.98	4.31	4.21	0.24	3.59
75.31	13.13	0.12	1.66	0.06	1.02	4.1	4.3	0.3	5.19
75.28	13.06	0.09	1.62	0.11	0.98	4.35	4.25	0.25	5.01
75.63	13.02	0.17	1.7	0.07	0.92	4.05	4.26	0.24	5.79
74.89	13.4	0.17	1.68	0.07	0.95	4.18	4.49	0.24	5.83
75.78	13.01	0.13	1.78	0.07	0.85	4.12	4.07	0.2	4.5
75.13	12.91	0.15	1.8	0.06	0.93	4.18	4.63	0.21	4.39
75.66	12.87	0.14	1.68	0.06	0.93	4.16	4.27	0.23	4.28
75.25	13.26	0.11	1.53	0.09	0.92	4.12	4.49	0.23	6.29
75.07	13.25	0.08	1.78	0.07	0.91	4.24	4.35	0.24	5.71
75.26	13.23	0.16	1.76	0.06	1.05	4.22	4.1	0.2	6.45
74.99	13.24	0.07	1.8	0.06	0.88	4.36	4.34	0.25	4.99
75.25	13.14	0.12	1.73	0.07	0.94	4.2	4.32	0.23	5.02
0.28	0.16	0.04	0.1	0.01	0.05	0.1	0.16	0.03	1

159 Mangatewainui Sm U23/838166-827178

73.74	13.77	0.28	2.21	0.16	1.24	4.43	3.96	0.21	6.91
73.74	13.54	0.2	2.44	0.19	1.46	4.36	3.86	0.22	4.35
73.65	13.71	0.2	2.2	0.17	1.47	4.39	4	0.22	4.71
74.67	13.21	0.24	2.17	0.2	1.34	4.18	3.84	0.16	4.59
73.93	13.99	0.21	2.22	0.14	1.34	4.23	3.76	0.18	5.38
74.13	13.51	0.22	2.29	0.16	1.3	4.24	3.95	0.2	5.5
74.89	12.99	0.21	2.22	0.14	1.27	4.17	3.95	0.18	4.45
73.74	13.8	0.22	2.38	0.15	1.22	4.29	4.02	0.19	7.39
74.2	13.6	0.19	2.1	0.2	1.32	4.31	3.88	0.2	5.75
74.08	13.57	0.22	2.25	0.17	1.33	4.29	3.91	0.2	5.45
0.42	0.29	0.03	0.1	0.02	0.08	0.09	0.08	0.02	1.03

160 Mangatewainui Sm U23/838166-827178

74.48	13.54	0.14	2.03	0.11	1.14	4.62	3.76	0.18	6.12
74.64	13.36	0.12	2.04	0.08	1.18	4.68	3.7	0.21	4.86

74.93	13.34	0.18	1.94	0.1	1.13	4.41	3.76	0.22	5.84
74.7	13.62	0.16	1.92	0.14	1.06	4.61	3.61	0.19	5.7
74.38	13.62	0.22	2.11	0.12	1.06	4.7	3.66	0.13	5.98
74.95	13.28	0.14	2.08	0.07	1.13	4.39	3.78	0.18	4.4
74.97	13.45	0.18	2.04	0.11	1.16	3.37	4.4	0.31	9.86
74.48	13.5	0.1	2.2	0.13	1.08	4.53	3.75	0.23	4.47
74.7	13.47	0.19	2.01	0.12	1.05	4.54	3.73	0.19	4.71
74.69	13.46	0.16	2.04	0.11	1.11	4.43	3.79	0.2	5.77
0.22	0.12	0.04	0.08	0.02	0.05	0.41	0.23	0.05	1.67

161 Mangatewainui Sm U23/838166-827178

73.76	13.73	0.2	2.47	0.18	1.3	4.51	3.65	0.21	4.29
73.74	13.68	0.24	2.25	0.22	1.27	4.62	3.66	0.31	5.82
74.37	13.52	0.19	2.07	0.2	1.31	4.67	3.45	0.22	4.71
74.63	13.58	0.19	1.87	0.16	1.11	4.44	3.81	0.21	5.71
74.54	13.42	0.18	2.23	0.11	1.19	4.36	3.76	0.2	5.09
73.87	13.82	0.22	2.4	0.27	1.49	4.22	3.57	0.14	4.52
74.3	13.6	0.19	1.83	0.26	1.93	3.93	3.76	0.19	5.91
74.29	13.6	0.21	2.2	0.17	1.34	4.34	3.64	0.21	6.39
74.04	13.85	0.24	2.17	0.17	1.3	4.41	3.62	0.22	3.54
74.17	13.64	0.21	2.17	0.19	1.36	4.39	3.66	0.21	5.11
0.33	0.14	0.02	0.21	0.05	0.24	0.22	0.11	0.04	0.92

163 Mangatewainui Sm U23/838166-827178

77.05	12.7	0.1	0.95	0.05	0.99	3.73	4.4	0.13	7.01
75.44	12.94	0.12	2	0.07	1.04	4.29	3.92	0.18	3.6
76.13	12.79	0.12	1.53	0.07	0.73	4.14	4.34	0.21	8.77
76.49	12.74	0.1	1.48	0.07	0.8	4.18	4.03	0.19	8.33
75.33	13	0.11	1.95	0.11	1.25	4.43	3.55	0.25	4.31
75.44	12.94	0.18	1.94	0.07	0.97	4.4	3.84	0.23	4.7
75.82	13.04	0.14	1.91	0.08	1.02	4.02	3.78	0.19	6.89
77.23	12.55	0.08	1.13	0.11	1.21	3.56	3.95	0.18	4.89
77.44	12.73	0.08	1.16	0.07	1.11	3.51	3.77	0.13	3.39
76.65	12.69	0.07	1.49	0.06	0.77	3.93	4.18	0.22	5.06
75.46	13.05	0.15	1.93	0.13	1.03	4.35	3.67	0.23	6.14
76.23	12.83	0.11	1.59	0.08	0.99	4.05	3.95	0.19	5.74
0.79	0.17	0.03	0.38	0.02	0.17	0.33	0.27	0.04	1.83

164 Mangatewainui Sm U23/838166-827178

75.24	13.02	0.18	2.08	0.09	1.15	4.21	3.84	0.18	4.47
73.99	13.8	0.24	2.41	0.14	1.32	4.45	3.47	0.21	7.36
74.29	13.62	0.12	2.29	0.1	1.29	4.38	3.74	0.16	7.18
74.34	13.63	0.17	2.24	0.16	1.29	4.43	3.59	0.15	5.06
74.01	14.04	0.18	2.24	0.18	1.2	4.44	3.53	0.19	5.62
74.57	13.79	0.16	2.33	0.12	1.15	4.21	3.49	0.18	7.32
74.25	13.92	0.18	2.15	0.14	1.18	4.48	3.54	0.16	5.33
74.38	13.69	0.18	2.25	0.13	1.23	4.37	3.6	0.18	6.05
0.43	0.33	0.04	0.11	0.03	0.07	0.11	0.14	0.02	1.21

77.11	12.65	0.12	1.11	0.13	1.02	3.65	4.11	0.11	6.01
75.46	13.24	0.11	1.64	0	0.86	4.44	4.11	0.15	5.37
74.1	13.78	0.13	1.85	0.07	0.94	4.81	4.18	0.14	9.15
76.3	12.59	0.13	1.72	0	0.88	4.16	4	0.23	3.39
76.99	12.57	0	0.91	0.05	0.75	3.63	4.98	0.12	5.11

165 Mangatewainui Sm U23/838166-827178

77.87	12.38	0.09	1.11	0.09	1.15	3.66	3.53	0.11	4.03
77.92	12.22	0.09	1.29	0.12	1.29	3.69	3.24	0.15	6.17
77.72	12.32	0.1	1.41	0.1	1.19	3.66	3.34	0.15	4.42
77.86	12.61	0.1	1.14	0.1	1.25	3.67	3.47	0	4.94
77.59	12.44	0.07	1.26	0.11	1.31	3.69	3.35	0.17	6.38
77.91	12.29	0.1	1.44	0	1.23	3.83	3.3	0	4.16
77.56	12.46	0.19	1.03	0.12	1.19	3.59	3.6	0.25	5.64
77.66	12.62	0.1	1.33	0.1	1.29	3.87	3.23	0	7.26
77.42	12.63	0.11	1.16	0.11	1.25	3.78	3.38	0.15	7.78
77.44	12.37	0.11	1.38	0.08	1.18	3.68	3.56	0.21	6.97
77.38	12.45	0.1	1.5	0.08	1.17	3.8	3.45	0.17	4.9
77.33	12.48	0.11	1.27	0.1	1.19	3.64	3.58	0.3	7.26
77.64	12.44	0.11	1.28	0.09	1.22	3.71	3.42	0.14	5.83
0.22	0.13	0.03	0.14	0.03	0.05	0.09	0.13	0.1	1.33

166 Mangatewainui Sm U23/838166-827178

74.85	13.47	0.22	1.89	0.22	1.22	4.24	3.6	0.28	4.85
75.38	13.23	0.16	1.82	0.07	0.84	4.56	3.79	0.14	5.32
75.79	13.16	0.2	1.62	0.11	0.86	4.28	3.72	0.27	5.34
75.76	12.94	0.18	1.92	0.12	0.86	4.24	3.76	0.21	6.44
75.45	13.36	0.16	1.91	0.12	1.25	4.25	3.46	0.19	3.86
76	13.02	0.22	1.79	0.08	0.88	4.07	3.69	0.24	4.96
75.79	12.86	0.2	1.79	0.07	1	4.44	3.66	0.2	4.89
76.82	12.82	0.15	1.9	0.08	1	4.34	3.68	0.21	5.28
76.21	12.92	0.15	1.73	0.1	0.85	4.07	3.89	0.19	5.63
75.78	13.09	0.18	1.82	0.11	0.97	4.28	3.69	0.21	5.17
0.55	0.23	0.03	0.1	0.05	0.16	0.16	0.12	0.04	0.69

74.4	13.52	0.25	2.22	0.12	1.23	4.64	3.46	0.16	6.87
74.77	13.46	0.21	2.19	0.15	1.14	4.42	3.35	0.31	5.75

172 Wanganui coast R22/667472

74.76	13.16	0.15	1.96	0.11	1.05	3.77	4.78	0.27	5.74
74.46	13.18	0.16	1.97	0.14	0.97	3.94	4.92	0.26	6.63

74.72	13.08	0.15	2.09	0.09	1	3.7	4.92	0.25	5.1
74.48	13.13	0.15	1.85	0.11	1.13	3.96	4.94	0.24	5.66
74.48	13.25	0.23	1.95	0.13	1	3.87	4.88	0.21	4.31
74.82	13.22	0.15	1.89	0.13	1.02	3.82	4.88	0.22	6.11
74.66	13.17	0.17	1.95	0.1	0.99	3.81	5	0.24	5.47
74.73	13.06	0.17	1.99	0.08	0.99	3.76	4.95	0.27	4.13
74.65	13.1	0.16	1.96	0.09	1.08	3.79	4.95	0.22	3.72
74.82	12.97	0.16	2.02	0.09	1.05	3.57	5.05	0.27	4.1
74.97	13.09	0.13	1.87	0.09	0.99	3.7	4.89	0.27	5.13
74.8	13.08	0.14	1.92	0.1	1.1	3.61	4.94	0.31	4.64
75.08	13.07	0.18	1.81	0.11	0.99	3.54	5.04	0.18	5.69
75.17	13.2	0.13	1.68	0.11	0.78	3.44	5.15	0.34	6.46
74.76	13.13	0.16	1.92	0.11	1.01	3.73	4.95	0.25	5.21
0.21	0.08	0.02	0.1	0.02	0.08	0.15	0.09	0.04	0.92

173 Kaimatira Pumice, Handley Rd R22/729454

77.65	12.24	0.12	1.24	0.14	1.09	3.6	3.91	0	11.22
77.64	12.02	0.1	1.32	0.12	0.99	3.8	3.75	0.25	5.44
77.63	12.23	0.11	1.07	0.1	0.77	3.47	4.32	0.3	5.76
77.7	12.12	0.13	0.98	0.07	0.8	3.54	4.43	0.24	4.01
77.03	12.56	0.13	1.37	0.15	1.13	3.72	3.75	0.16	7.02
77.88	12.29	0.11	0.91	0.1	0.69	3.44	4.48	0.21	4.45
78	12.24	0.11	1.14	0.13	1.05	3.19	3.94	0.2	5.98
77.87	12.11	0.11	1.16	0.08	1	3.66	3.8	0.22	4.81
77.68	12.23	0.12	1.15	0.11	0.94	3.55	4.05	0.2	6.09
0.29	0.16	0.01	0.16	0.03	0.16	0.19	0.31	0.09	2.28

174 Makirikiri Tuff, Smiths Rd/State Highway 3 R22/765483

77.82	12.37	0.06	1.14	0.08	1.21	3.49	3.69	0.14	6.96
77.72	12.4	0.09	1.11	0.09	1.05	3.53	3.87	0.16	5.9
77.57	12.34	0.07	1.29	0.12	1.14	3.68	3.65	0.15	5.17
77.64	12.51	0.08	1.21	0.1	1.1	3.44	3.75	0.16	5.87
77.27	12.5	0.13	1.17	0.08	1.37	3.37	3.84	0.27	8.32
77.69	12.52	0.09	1.2	0.07	1.11	3.51	3.7	0.18	5.74
77.62	12.44	0.09	1.19	0.09	1.16	3.5	3.75	0.18	6.33
0.19	0.08	0.02	0.06	0.02	0.11	0.1	0.09	0.05	1.14

77.72	12.47	0.06	0.9	0	1	3.47	4.22	0.15	6.72
77.76	12.47	0	0.87	0	0.61	3.32	4.85	0.13	5.31
76.3	12.53	0.11	1.62	0.08	0.79	3.87	4.51	0.19	9.13
75.58	12.81	0.13	2.18	0.11	1.09	4.21	3.71	0.18	5.81

175 Makirikiri Tuff, Wanganui Riv. R22/884474

75.68	12.72	0.13	2	0.1	1.02	4	4.12	0.23	5.82
75.95	12.76	0.19	1.93	0.07	0.98	4.11	3.8	0.2	6.22
75.69	12.87	0.15	2.08	0.08	1.07	4.34	3.49	0.23	7.69
75.91	12.88	0.16	2	0.07	0.96	4.1	3.75	0.16	8.12
75.66	12.92	0.12	1.97	0.06	1.05	4.22	3.76	0.24	6.7
75.32	12.86	0.21	1.97	0.12	0.96	4.54	3.82	0.19	5.58
75.96	12.84	0.15	1.82	0.08	0.92	4.22	3.78	0.23	6.96
75.8	12.82	0.16	1.87	0.11	1	4.33	3.7	0.2	6.43
75.99	12.63	0.2	1.85	0.1	0.99	4.31	3.7	0.23	7.14
75.77	12.81	0.16	1.94	0.09	0.99	4.24	3.77	0.21	6.74
0.21	0.09	0.03	0.08	0.02	0.05	0.16	0.16	0.03	0.83

77.18	12.14	0.13	1.38	0.06	0.7	3.54	4.67	0.2	6.59
77.31	12.06	0.11	1.5	0.11	0.66	3.74	4.35	0.17	5.57

176 Makirikiri Tuff, Wanganui Riv. R22/884474

75.77	12.88	0.14	1.7	0.07	1	3.87	4.32	0.24	4.44
76.33	12.48	0.15	1.45	0.06	0.87	3.63	4.85	0.18	5.22
75.53	13.21	0.13	1.92	0.08	1.05	3.53	4.32	0.23	4.79
75.68	12.89	0.12	1.73	0.08	0.93	4	4.44	0.22	4.66
75.39	12.94	0.08	1.75	0.12	0.95	4.24	4.31	0.22	4.47
75.66	13.01	0.08	1.67	0.08	0.93	4.14	4.29	0.23	7.03
75.66	12.75	0.22	1.88	0.12	0.91	3.55	4.7	0.21	6.36
75.72	12.88	0.13	1.73	0.09	0.95	3.85	4.46	0.22	5.28
0.3	0.23	0.05	0.15	0.02	0.06	0.29	0.22	0.02	1.02

74.13	13.44	0.24	2.44	0.15	1.3	4.31	3.82	0.18	7.34
74.21	13.25	0.24	2.5	0.14	1.34	3.99	4.06	0.26	9.1
74.64	13.17	0.18	2.37	0.15	1.34	4.43	3.49	0.22	6.3

177 Kaimatira Pumice, Kaimatira Bluff R22/890434

78.04	12.14	0.17	1.05	0.1	1.03	3.4	3.87	0.2	4.69
77.68	12.04	0.1	1.36	0.13	0.82	3.67	3.94	0.25	8.97
77.29	12.22	0.13	1.27	0.11	0.88	3.74	4.11	0.25	4.31
77.64	12.16	0.13	1.23	0.12	0.96	3.42	4.13	0.22	6.23
78.15	11.98	0.13	1.22	0.13	0.99	3.42	4.05	0.2	4.67
78.03	12.16	0.1	0.99	0.13	0.78	3.63	3.95	0.24	5.73
77.65	12.24	0.11	0.96	0.15	1.1	3.52	4.06	0.21	6.58
77.89	12.08	0.16	0.79	0.1	0.96	3.57	4.26	0.2	3.79
77.68	12.3	0.09	1.19	0.17	1.07	3.24	4	0.26	4.65
77.78	12.15	0.12	1.12	0.13	0.95	3.51	4.04	0.23	5.51
0.27	0.1	0.03	0.18	0.02	0.11	0.16	0.12	0.02	1.59

76.05	12.89	0.23	1.68	0.13	1.16	4.12	3.56	0.18	8.81
76.26	12.74	0.13	1.78	0.16	1.19	4.07	3.47	0.19	6.22
75.72	12.93	0.14	1.76	0.14	1.21	4.22	3.68	0.2	6.79

178 Makirikiri Tuff, Wanganui Riv. S22/909463

75.48	13.1	0.12	2.19	0.09	1.14	4.14	3.54	0.2	6.05
75.27	12.99	0.15	2.13	0.09	1.13	3.94	4.11	0.19	6.29
75.52	12.99	0.16	2.04	0.07	1.04	4.39	3.57	0.21	6.2
75.27	12.87	0.15	2.34	0.1	1.16	4.27	3.59	0.25	8.61
74.96	13.21	0.23	1.94	0.13	1.12	4.28	3.95	0.17	8.17
75.23	13.06	0.15	2.12	0.1	0.97	4.47	3.84	0.16	7.07
75.29	12.92	0.13	2.1	0.14	1.04	4.19	4.03	0.17	4.9
75.64	12.93	0.17	2	0.12	1.05	4.36	3.59	0.15	6.41
75.15	12.93	0.16	2.16	0.1	1.11	4.2	4	0.19	6.44
75.31	13	0.16	2.11	0.1	1.08	4.25	3.8	0.19	6.68
0.21	0.11	0.03	0.12	0.02	0.06	0.16	0.23	0.03	1.13

179 Makirikiri Tuff, Wanganui Riv. S22/909463

75.35	13.08	0.19	2.1	0.09	1.32	4.27	3.44	0.16	4.82
75.8	12.79	0.15	2.11	0.12	1.33	4.15	3.33	0.22	5.15
75.83	12.89	0.19	2.09	0.15	1.23	4.01	3.35	0.26	6.99
75.6	13.09	0.1	1.99	0.17	1.32	4.3	3.22	0.21	6.92
75.09	13.19	0.15	2.23	0.14	1.25	4.19	3.55	0.21	8.64
75.91	13.02	0.14	1.86	0.14	1.31	4.15	3.25	0.22	8.84
75.62	12.89	0.17	1.91	0.18	1.27	4.37	3.37	0.22	6.25
75.6	12.99	0.16	2.04	0.14	1.29	4.21	3.36	0.21	6.8
0.29	0.14	0.03	0.13	0.03	0.04	0.12	0.11	0.03	1.56

78.11	12.13	0.12	0.92	0	0.63	3.2	4.64	0.24	5.05

180 Kaukatea Ash, Longace Rd S22/901424

76.9	12.61	0.07	1.48	0.13	1.02	4.24	3.4	0.16	6.47
76.49	12.66	0.22	1.49	0.15	0.97	4.12	3.71	0.18	5.44
76.43	12.61	0.16	1.62	0.1	0.94	4.07	3.83	0.23	5.72
76.89	12.46	0.15	1.38	0.19	1.16	3.65	3.92	0.18	7.18
76.57	12.7	0.16	1.62	0.12	0.96	4.13	3.59	0.16	5.49
76.51	12.55	0.18	1.62	0.08	1.02	4.05	3.83	0.16	5.7
76.55	12.66	0.17	1.54	0.14	0.96	4.26	3.54	0.18	5.24
76.95	12.57	0.13	1.53	0.13	1.04	3.87	3.77	0.15	6.51
76.96	12.6	0.11	1.38	0.07	0.97	4.1	3.61	0.19	6.1
76.61	12.62	0.14	1.6	0.18	0.98	4.31	3.39	0.16	6.37
76.69	12.6	0.15	1.53	0.13	1	4.08	3.66	0.18	6.02
0.21	0.07	0.04	0.09	0.04	0.06	0.2	0.18	0.02	0.61

182 Pakihikura Pumice, Turakina Valley Rd S22/113409

77.9	12.16	0.07	1.25	0.06	1.25	3.62	3.57	0.11	6.28
78.04	12.14	0.07	1.29	0.12	1.2	3.52	3.5	0.11	5.72
78.07	12.05	0.12	1.32	0.1	1.27	3.5	3.54	0.13	6.4
77.93	11.95	0.11	1.3	0.12	1.29	3.68	3.48	0.15	5.19
77.99	12.05	0.07	1.38	0.12	1.22	3.53	3.5	0.15	5.55
77.84	11.93	0.11	1.4	0.09	1.26	3.53	3.7	0.15	6.4
78.08	12.01	0.09	1.33	0.09	1.24	3.66	3.39	0.12	5.91
77.91	12.18	0.09	1.26	0.1	1.23	3.56	3.69	0.17	5.89
78.71	12.18	0.08	1.29	0.11	1.21	3.29	2.96	0.17	7.22
78.03	12.08	0.11	1.36	0.1	1.28	3.55	3.4	0.19	5.66
78.05	12.07	0.09	1.32	0.1	1.25	3.54	3.47	0.15	6.02
0.25	0.09	0.02	0.05	0.02	0.03	0.11	0.21	0.03	0.57

183 Turakina Valley Rd S22/104405

74.79	13.3	0.16	2.17	0.13	1.21	4.59	3.46	0.19	5.59
74.89	13.19	0.21	1.97	0.11	1.19	4.58	3.64	0.21	6.96
74.78	13.37	0.2	2.21	0.12	1.08	4.51	3.57	0.15	6.91
74.64	13.33	0.22	2.14	0.14	1.18	4.72	3.43	0.21	7.51
74.62	13.37	0.22	2.29	0.14	1.23	4.51	3.4	0.24	6.4
74.92	13.13	0.17	2.13	0.07	1.04	4.57	3.77	0.2	6.47
74.74	13.33	0.15	2.34	0.15	1.13	4.3	3.71	0.16	6.21
74.46	13.37	0.2	2.33	0.1	1.14	4.61	3.57	0.23	6.75
74.6	13.4	0.21	2.24	0.18	1.26	4.68	3.24	0.2	7.84
74.53	13.41	0.17	2.13	0.11	1.26	4.46	3.68	0.24	8.53
74.7	13.32	0.19	2.2	0.13	1.17	4.55	3.55	0.2	6.92
0.15	0.09	0.03	0.11	0.03	0.07	0.12	0.16	0.03	0.85

184 Turakina Valley Rd S22/104405

74.65	13.21	0.09	2.29	0.08	1.13	4.38	3.97	0.22	7.01
75.67	12.99	0.21	1.94	0.07	1.03	4.02	3.87	0.19	6.11
75.71	12.86	0.14	2	0.12	0.96	3.88	4.15	0.2	4.87
75.17	13.1	0.17	2.15	0.09	1.06	4.26	3.77	0.23	6.95
74.9	13.14	0.22	2.1	0.11	1.12	4.36	3.86	0.19	5.13
74.99	13.14	0.16	2.15	0.1	1.04	4.54	3.68	0.19	7.09
75.18	13.07	0.17	2.11	0.1	1.06	4.24	3.88	0.2	6.19
0.43	0.13	0.05	0.12	0.02	0.06	0.25	0.16	0.02	0.99

77.23	12.28	0.08	1.37	0	0.91	3.86	4.03	0.23	4.46
77.75	12.09	0.11	1.04	0	0.87	3.66	4.28	0.2	4.14
76.74	12.43	0.11	1.45	0	0.81	3.72	4.52	0.22	9.08
77.75	12.09	0.11	1.04	0	0.87	3.66	4.28	0.2	4.14
77.23	12.28	0.08	1.37	0	0.91	3.86	4.03	0.23	4.46
77.34	12.23	0.1	1.25	0	0.87	3.75	4.23	0.22	5.26
0.42	0.15	0.02	0.2	0	0.04	0.1	0.21	0.02	2.14

185 Potaka Tephra (matrix), Smiths/Makuhou Rds S22/137319

78.21	12.04	0	0.89	0	0.72	3.57	4.31	0.26	5.39
78.31	11.91	0.14	1.21	0.15	0.91	3.31	3.9	0.18	4.1
78.11	12.08	0.11	0.88	0	0.81	3.44	4.58	0	5.84

77.2	12.27	0.17	1.34	0.08	1.18	3.5	4.04	0.22	8.48
78.19	11.94	0.12	1.01	0.12	1.01	3.69	3.72	0.21	5.7
78.04	11.98	0.1	0.99	0	0.78	3.47	4.4	0.25	6.27
78.69	12.09	0.1	0.78	0	0.84	3.15	4.19	0.16	4.63
78.12	11.9	0.15	1.06	0.08	0.97	3.54	3.96	0.22	5.29
77.78	12.15	0.13	1.01	0.07	0.79	3.74	4.06	0.26	4.05

185 Potaka Tephra (clasts), Smiths/Makuhou Rds S22/137319

77.74	12.35	0.1	0.9	0	1.05	3.56	4.09	0.22	7.6
77.73	12.13	0.15	0.84	0.13	1	3.75	4	0.27	6.09
78.07	11.95	0	0.99	0	0.87	3.28	4.52	0.32	8.42
78.11	11.88	0.15	0.89	0.14	1.13	3.6	3.84	0.27	6.3
78.15	11.8	0.08	0.97	0.13	0.75	3.75	4.17	0.19	5.6
78.05	11.86	0	0.99	0.09	0.77	3.62	4.4	0.23	4.94
77.9	11.92	0.19	1.09	0.19	1.02	3.67	3.76	0.27	4.44

189 Mangatewainui Sm U23/827178-817185

75.72	13.14	0.19	1.63	0.18	1.21	4.12	3.64	0.18	6.47
76.52	12.94	0.16	1.36	0.1	1.08	3.93	3.73	0.18	7.3
76.44	12.9	0.14	1.34	0.16	1.1	4.02	3.66	0.22	6.31
76.17	12.87	0.17	1.58	0.19	1.16	4.01	3.64	0.19	6.99
76.59	12.78	0.16	1.35	0.12	1.17	4.03	3.57	0.24	6.54
76.88	12.75	0.1	1.2	0.15	1.14	3.88	3.69	0.2	6.82
76.1	13.09	0.16	1.61	0.19	1.13	4.13	3.34	0.25	7.42
76.62	13.01	0.11	1.45	0.14	1.04	3.92	3.48	0.24	7.4
76.38	12.94	0.15	1.44	0.15	1.13	4.01	3.59	0.21	6.91
0.37	0.14	0.03	0.15	0.04	0.05	0.09	0.13	0.03	0.44

190 Mangatewainui Sm U23/827178-817185

76.61	12.94	0.15	1.22	0.13	1.07	3.8	3.81	0.26	8.69
77.7	12.39	0.11	0.86	0.11	0.59	3.65	4.48	0.11	5.84
77.91	12.1	0.13	1.23	0.12	0.79	3.51	3.93	0.27	4.37
77.64	12.06	0.12	1.18	0.09	0.84	3.55	4.23	0.27	4.62
77.78	11.97	0.07	1.27	0.11	0.91	3.59	4.04	0.26	3.62
77.85	12.06	0.14	1.19	0.1	0.87	3.55	4.01	0.23	3.93
77.69	11.87	0.14	1.28	0.08	0.9	3.82	3.96	0.26	5.03
77	12.78	0.18	0.76	0.1	0.93	3.61	4.44	0.18	6.95
77.52	12.27	0.13	1.12	0.11	0.86	3.64	4.11	0.23	5.38
0.46	0.4	0.03	0.2	0.01	0.14	0.12	0.24	0.06	1.71

191 Mangatewainui Sm U23/827178-817185

71.26	14.33	0.67	3.25	0.66	2.52	4.54	2.64	0.14	5.54
74.91	13.32	0.26	2.17	0.19	1.27	4.64	3.06	0.17	5.59
75.03	13.11	0.25	2.33	0.19	1.33	4.45	3.1	0.2	6.97
76.23	12.74	0.16	1.79	0.08	1.1	4.32	3.37	0.21	4.62
73.09	13.75	0.45	2.58	0.42	1.87	4.46	3.23	0.16	6.43
75.35	13.09	0.15	1.96	0.12	1.15	4.49	3.46	0.22	6.11
75.13	13.32	0.16	2.1	0.11	1.36	4.46	3.19	0.16	6.83
75.92	12.88	0.18	1.76	0.12	1.14	4.43	3.41	0.16	5.61
72.33	14.19	0.45	2.9	0.57	2.28	4.5	2.65	0.14	5.06
74.36	13.42	0.3	2.32	0.17	1.56	4.48	3.12	0.17	5.86
1.72	0.56	0.18	0.51	0.22	0.53	0.09	0.3	0.03	0.79

192 Mangatewainui Sm U23/827178-817185

75.8	12.78	0.21	2.09	0.1	1.02	4.36	3.41	0.22	4.37
76.26	12.63	0.15	1.93	0.12	0.96	4.57	3.21	0.18	5.11
76.1	12.64	0.18	1.78	0.07	0.99	4.63	3.36	0.24	5.39
76.22	12.69	0.13	1.88	0.11	1.02	4.59	3.15	0.21	6.62
75.95	12.55	0.23	1.86	0.11	1.09	4.86	3.14	0.22	7.39
75.86	12.95	0.14	1.97	0.08	0.96	4.5	3.35	0.2	4.07
76.37	12.6	0.17	1.93	0.14	0.99	4.45	3.2	0.15	6.04
76.05	12.64	0.11	1.95	0.11	1.03	4.49	3.43	0.19	5.79
76.13	12.61	0.17	1.88	0.15	0.96	4.54	3.35	0.21	3.92
75.74	12.74	0.2	1.96	0.11	0.99	4.56	3.48	0.21	3.79
76.05	12.68	0.17	1.92	0.11	1	4.56	3.31	0.2	5.25
0.21	0.11	0.04	0.08	0.02	0.04	0.13	0.12	0.03	1.22

193 Mangatewainui Sm U23/827178-817185

76.74	12.54	0.13	1.56	0.14	1.09	4.33	3.28	0.18	5.85
76.43	12.88	0.15	1.6	0.06	0.97	4.43	3.27	0.19	7.54
75.84	13.07	0.19	1.83	0.18	1.26	4.24	3.23	0.15	7.21
76.15	12.88	0.17	1.77	0.13	1.09	4.25	3.42	0.16	6.01
75.76	13.19	0.2	1.8	0.15	1.33	4.51	2.9	0.16	6.55
74.85	13.72	0.31	1.66	0.2	1.61	4.54	2.97	0.15	5.96
76.23	12.81	0.16	1.86	0.08	1.01	4.46	3.23	0.15	5.88
73.63	14.07	0.28	2.2	0.35	1.69	4.66	2.97	0.15	5.83
76.45	12.93	0.16	1.61	0.13	1.01	4.28	3.27	0.16	6.5
75.3	13.37	0.15	1.78	0.16	1.34	4.57	3.19	0.15	5.63
75.74	13.15	0.19	1.77	0.16	1.24	4.43	3.17	0.16	6.3
0.93	0.46	0.06	0.18	0.09	0.25	0.15	0.17	0.02	0.64

194 (=195, clasts) Mangatewainui Sm U23/827178-817185

77.41	12.29	0.1	1.03	0.11	0.78	3.79	4.26	0.23	3.63
77.63	12.31	0.16	0.96	0.06	0.8	3.66	4.21	0.22	4.03
77.8	12.21	0.1	0.87	0.1	0.71	3.75	4.21	0.24	3.59
77.67	12.31	0.14	0.93	0.06	0.63	3.78	4.27	0.23	3.87
77.26	12.52	0.12	0.9	0.11	0.71	3.9	4.25	0.24	4.84
77.96	12.11	0.1	0.98	0.09	0.77	3.73	4.03	0.23	3.28
77.64	12.23	0.08	1.07	0.15	0.79	3.72	4.08	0.24	4.74

77.79	12.23	0.15	0.91	0.08	0.72	3.68	4.14	0.29	4.81
77.8	12.27	0.06	1.01	0.07	0.76	3.67	4.14	0.23	3.76
77.83	12.45	0.06	0.89	0.13	0.64	3.69	4.09	0.24	4.06
77.68	12.29	0.11	0.95	0.1	0.73	3.74	4.17	0.24	4.06
0.21	0.12	0.03	0.07	0.03	0.06	0.07	0.08	0.02	0.56

195 (=194, matrix) Mangatewainui Sm U23/827178-817185

78.28	11.84	0.12	0.95	0.13	0.72	3.67	4.08	0.21	5.42
77.15	12.47	0.09	1.01	0.13	0.64	3.97	4.3	0.23	6.38
77.9	12.19	0.11	1.16	0.1	0.92	3.8	3.62	0.2	6.27
78.06	11.89	0.1	1.1	0.07	1.01	3.69	3.84	0.23	3.82
78.21	11.71	0.11	1.07	0.1	0.91	3.89	3.73	0.28	6.42
77.74	12.24	0.11	0.87	0.06	0.68	3.79	4.26	0.25	6.21
77.67	12.36	0.06	1.01	0.09	0.8	3.77	3.97	0.28	6.05
77.87	12.15	0.11	1.02	0.06	0.81	3.69	4.08	0.21	6.16
77.87	12.23	0.14	1.23	0.09	0.9	3.64	3.67	0.24	7.61
77.69	12.21	0.11	1.12	0.06	1.04	3.79	3.77	0.21	5.56
77.84	12.13	0.1	1.06	0.09	0.84	3.77	3.93	0.23	5.99
0.32	0.24	0.02	0.1	0.02	0.13	0.1	0.25	0.03	0.96

196 Mangatewainui Sm U23/827178-817185

76.33	12.93	0.12	1.67	0.16	0.95	4.32	3.33	0.2	7.6
75.95	12.87	0.12	1.62	0.1	0.92	4.53	3.68	0.22	8.58
76.48	12.78	0.18	1.57	0.14	0.88	4.36	3.42	0.19	6.67
76.7	12.83	0.14	1.35	0.15	0.89	4.22	3.59	0.15	6.4
76.46	12.77	0.2	1.55	0.11	0.95	4.39	3.41	0.17	5.8
76.33	12.92	0.17	1.5	0.08	0.95	4.37	3.49	0.21	6.14
76.77	12.56	0.15	1.43	0.14	0.92	4.28	3.58	0.17	9.11
76.9	12.91	0.26	1.46	0.09	0.99	3.82	3.4	0.17	6.37
76.21	12.89	0.13	1.56	0.13	1.03	4.34	3.55	0.16	7.66
76.46	12.83	0.16	1.52	0.12	0.94	4.29	3.49	0.18	7.15
0.3	0.12	0.05	0.1	0.03	0.05	0.2	0.11	0.02	1.15

197 Mangatewainui Sm U23/828147

73.71	13.28	0.53	2.46	0.31	1.69	3.94	3.88	0.2	5.74
73.82	13.17	0.44	2.43	0.33	1.76	3.89	3.98	0.19	6.42
71.98	14.34	0.56	2.36	0.4	2.36	4.03	3.72	0.24	8.99
74.04	13.2	0.5	2.26	0.35	1.63	3.87	4.01	0.14	7.28
72.79	13.63	0.47	2.8	0.37	1.74	3.95	4.06	0.18	8.7
73.54	13.26	0.59	2.44	0.4	1.7	3.81	4.01	0.23	5.81
73.95	13.35	0.54	2.23	0.32	1.67	3.75	4.03	0.17	6.34
73.41	13.46	0.52	2.43	0.35	1.79	3.89	3.96	0.19	7.04
0.75	0.42	0.05	0.19	0.04	0.26	0.09	0.12	0.04	1.33

198 State Highway 45 T22/512335

75.74	13.19	0.14	1.86	0.12	1.04	4.63	3.28	0	8.57
75.66	12.83	0.15	2	0.13	1.09	4.41	3.55	0.19	4.02
75.72	12.93	0.2	2.04	0.14	1.08	4.42	3.3	0.17	5.93
76.09	12.72	0.12	1.65	0.07	0.88	4.39	3.87	0.21	5.48
75.17	13.25	0.23	2.05	0.16	1.26	4.33	3.39	0.17	6.18
74.33	13.49	0.21	2.46	0.22	1.34	4.66	3.13	0.16	7.73
76.19	12.79	0.14	1.72	0.06	0.91	4.47	3.53	0.18	7.43
75.65	12.88	0.16	1.77	0.07	0.8	4.52	3.91	0.24	8.28
72.71	14.15	0.35	2.79	0.35	2.02	4.61	2.88	0.14	6.33
72.43	14.17	0.37	3.09	0.47	1.98	4.53	2.81	0.15	7.06
74.97	13.24	0.21	2.14	0.18	1.24	4.5	3.37	0.16	6.7
1.37	0.54	0.09	0.48	0.13	0.43	0.11	0.37	0.06	1.39

199 Cheltenham/Hunterville Rd T22/357315

75.06	11.67	0.1	1.19	0.09	0.79	3.48	3.7	0.23	3.72
74.97	11.62	0.12	1.17	0.1	0.92	3.4	3.9	0.19	3.6
75.09	11.69	0.07	0.85	0.08	0.68	3.45	3.99	0.22	3.89
73.42	11.33	0.09	0.79	0.08	0.81	3.5	3.72	0.2	6.06
74.15	11.71	0.11	1.01	0.06	0.66	3.54	3.91	0.27	4.59
73.54	11.59	0.1	0.95	0.06	0.68	3.59	4.02	0.23	5.23
74.79	11.71	0.08	0.9	0.07	0.69	3.53	3.81	0.27	4.19
74.68	11.63	0.12	1.14	0.12	0.89	3.42	3.75	0.23	4.01
74.05	11.76	0.11	1.02	0.1	0.76	3.54	3.95	0.22	4.48
74.42	11.63	0.1	1	0.08	0.76	3.49	3.86	0.23	4.42
0.65	0.13	0.02	0.14	0.02	0.1	0.06	0.12	0.03	0.79

200 Ridge Ash, Cheltenham/Hunterville Rd T22/358353

74.87	13.25	0.16	2	0.13	1.02	4.44	3.93	0.21	5.43
75.81	12.94	0.09	1.86	0.07	1	4.4	3.59	0.25	6.29
74.96	13.27	0.17	2.04	0.1	0.95	4.56	3.73	0.22	5.66
75.9	12.94	0.14	1.65	0.11	0.93	4.15	3.97	0.21	6.28
74.25	13.53	0.17	2.4	0.17	1.13	4.53	3.61	0.21	5.16
74.47	13.5	0.17	2.23	0.12	1.1	4.71	3.5	0.2	6.86
73.5	13.87	0.23	2.68	0.17	1.26	4.37	3.75	0.17	7.18
74.67	13.46	0.14	2.01	0.12	1.08	4.6	3.65	0.26	7.76
74.8	13.35	0.16	2.11	0.12	1.06	4.47	3.72	0.22	6.33
0.79	0.31	0.04	0.32	0.03	0.11	0.17	0.17	0.03	0.9

220 Wanganui Coast R22/674470

75.09	12.74	0.16	2.01	0.1	0.91	3.95	4.77	0.26	7.01
74.3	13.18	0.25	2.32	0.12	1.37	4.68	3.61	0.18	6.37
73.82	13.19	0.26	2.52	0.2	1.41	4.76	3.59	0.24	8.74
75.6	13.35	0.11	1.58	0.11	1.14	4.54	3.58	0	9.42
74.55	13.43	0.21	1.83	0.23	1.36	3.9	4.29	0.21	8.17
75.45	13.04	0.14	1.54	0.09	1	3.67	4.93	0.11	3.33
74.8	13.16	0.19	1.97	0.14	1.2	4.25	4.13	0.17	7.17
0.7	0.24	0.06	0.4	0.06	0.21	0.46	0.62	0.1	2.19

222 Wanganui Coast R22/674470

73.94	13.74	0.2	1.95	0.1	0.99	3.95	4.86	0.28	6.01
74.37	13.52	0.15	1.86	0.11	0.92	3.96	4.86	0.27	5.5
73.44	13.92	0.14	2.08	0.08	1.08	3.83	5.15	0.27	7.64
74.74	13.34	0.17	1.83	0.08	1.14	3.74	4.76	0.2	3.65
73.99	13.47	0.18	2	0.13	0.97	4.08	4.97	0.21	5.75
73.43	13.85	0.13	1.87	0.12	1.07	4.12	5.16	0.25	8.1
74.62	13.5	0.16	1.84	0.11	0.98	3.6	4.97	0.23	4.91
73.55	13.76	0.15	1.95	0.07	1.08	3.96	5.22	0.27	7.32
74.01	13.64	0.16	1.92	0.1	1.03	3.91	5	0.25	6.11
0.52	0.21	0.02	0.09	0.02	0.07	0.18	0.17	0.03	1.5

224 Wanganui Coast R22/674470

75.78	13.02	0.14	1.33	0.07	0.76	4.03	4.64	0.23	5.75
75.32	13.21	0.16	1.42	0.06	0.82	3.71	5.04	0.25	7.3
75.54	13.16	0.06	1.42	0.08	0.8	3.8	4.88	0.25	5.86
74.31	13.37	0.22	1.98	0.13	0.97	3.88	4.95	0.2	8.14
74.41	13.6	0.12	1.6	0.08	0.94	4.19	4.84	0.23	7.58
75.23	13.04	0.22	1.74	0.07	0.87	3.81	4.76	0.26	5.95
74.39	13.22	0.26	1.95	0.1	0.93	4.11	4.81	0.23	8.59
75.23	13.15	0.18	1.71	0.07	0.84	4.11	4.49	0.22	5.77
74.68	13.46	0.14	1.86	0.1	0.99	4.19	4.34	0.24	6.49
75.26	13.12	0.16	1.71	0.11	0.97	3.84	4.58	0.26	6.52
75.01	13.23	0.17	1.67	0.09	0.89	3.97	4.73	0.24	6.8
0.52	0.19	0.06	0.23	0.02	0.08	0.18	0.22	0.02	1.04

226 Wanganui Coast R22/668472

74.21	13.82	0.31	1.62	0.18	1.15	4.04	4.42	0.25	6.2
74.14	13.53	0.25	2.41	0.18	1.19	4.5	3.62	0.18	6.46
75.54	12.79	0.18	1.88	0.07	0.87	3.92	4.49	0.25	5.81
74.21	13.27	0.26	2.08	0.11	0.89	4.02	4.93	0.22	8.99
73.47	13.68	0.25	1.96	0.11	0.94	3.87	5.45	0.27	6.74
74.04	13.56	0.19	2.36	0.16	1.22	4.63	3.61	0.22	6.35
73.55	13.72	0.26	2.53	0.15	1.2	4.68	3.68	0.23	7.95
73.83	13.47	0.18	2.57	0.12	1.23	4.72	3.69	0.19	5.74
74.26	13.54	0.2	1.82	0.07	0.95	3.93	4.98	0.25	5.33
74.14	13.49	0.23	2.14	0.13	1.07	4.26	4.32	0.23	6.62
0.6	0.3	0.04	0.34	0.04	0.15	0.37	0.7	0.03	1.16

230 (ignimbrite, base), Mangaonuku Sm U22/097592

77.83	12.34	0.14	1.12	0.15	0.89	3.78	3.56	0.2	5.29
77.75	12.2	0.21	1.16	0.09	0.95	3.9	3.5	0.24	6.65
77.9	12.12	0.11	1.24	0.13	0.99	3.82	3.49	0.21	4.8
77.34	12.35	0.21	1.28	0.12	0.96	3.73	3.78	0.23	5.91
77.87	12.25	0.14	1.18	0.14	0.88	3.88	3.42	0.25	6.12
77.84	12.3	0.14	1	0.15	0.89	3.74	3.73	0.22	5.32
77.8	12.24	0.19	1.15	0.15	0.89	3.82	3.5	0.26	5.82
77.93	12.29	0.14	1.13	0.12	0.93	3.75	3.5	0.22	7.02
77.7	12.36	0.12	1.16	0.11	1	3.88	3.48	0.21	6.52
77.59	12.32	0.13	1.07	0.06	0.76	3.59	4.22	0.26	6.43
77.75	12.28	0.15	1.15	0.12	0.91	3.79	3.62	0.23	5.99
0.18	0.07	0.04	0.08	0.03	0.07	0.09	0.24	0.02	0.7

231 (ignimbrite), Mangaonuku Sm U22/087574

77.49	12.36	0.09	1.01	0.1	0.87	3.79	4.06	0.24	5.49
77.31	12.43	0.15	1.33	0.13	0.88	3.86	3.7	0.22	4.87
77.38	12.45	0.11	1.02	0.14	0.71	3.78	4.18	0.24	4.57
77.08	12.48	0.21	1.26	0.11	1.09	3.84	3.7	0.24	4.83
77.59	12.45	0.15	1.08	0.08	0.75	3.71	3.98	0.22	5.12
77.44	12.46	0.12	1.12	0.09	0.9	3.75	3.9	0.22	5.62
77.32	12.44	0.14	0.99	0.08	0.79	3.79	4.18	0.28	6.44
77.28	12.33	0.17	1.24	0.13	1.06	3.86	3.69	0.25	4.53
77.76	12.33	0.09	0.88	0.12	0.74	3.76	4.1	0.22	8.68
77.18	12.34	0.12	1.3	0.11	0.97	3.94	3.76	0.27	6
77.38	12.41	0.13	1.12	0.11	0.88	3.81	3.92	0.24	5.62
0.2	0.06	0.04	0.15	0.02	0.13	0.07	0.2	0.02	1.24

232 (ignimbrite), Makaroro River U22/922501

77.75	12.31	0.06	1.02	0.12	0.78	3.45	4.29	0.22	5.97
77.24	12.43	0.15	1.1	0.09	1	3.98	3.77	0.26	6.26
77.46	12.52	0.13	0.97	0.09	0.77	3.72	4.11	0.24	7.53
77.21	12.48	0.13	1.06	0.1	0.8	4.01	3.92	0.3	6.2
77.23	12.44	0.13	1.22	0.11	0.87	4.03	3.68	0.3	8.36
77.17	12.46	0.16	1.05	0.09	0.79	3.72	4.29	0.26	8.3
77.54	12.29	0.16	1.06	0.11	0.76	3.6	4.24	0.25	8.67
77.48	12.43	0.12	0.96	0.08	0.83	3.53	4.33	0.25	7.4
77.65	12.23	0.1	1.04	0.12	0.79	3.77	4.1	0.22	7.15
77.44	12.18	0.16	1.13	0.13	1.04	3.82	3.82	0.28	6.24
77.54	12.3	0.2	1.06	0.13	0.89	3.67	4.24	0.24	7.79
77.83	12.19	0.1	1.11	0.07	0.94	3.86	3.73	0.19	5.85
77.59	12.25	0.16	1.22	0.1	0.94	3.71	3.86	0.19	5.84
77.47	12.35	0.13	1.08	0.1	0.86	3.78	3.98	0.25	7.04
0.21	0.12	0.04	0.08	0.02	0.09	0.18	0.25	0.03	1.04

233 Makaroro River U22/920492

77.28	12.41	0.16	1.34	0.11	1.1	3.92	3.47	0.21	4.83
77.45	12.36	0.18	1.08	0.15	1.04	3.75	3.79	0.22	4.43
77.58	12.33	0.16	1.21	0.07	0.94	3.76	3.69	0.25	5.14
77.9	12.3	0.06	0.88	0.1	0.6	3.84	4.07	0.25	6.59
77.43	12.45	0.06	0.98	0.1	0.74	3.7	4.29	0.24	6.85
77.51	12.23	0.16	1.22	0.12	0.93	4.02	3.58	0.24	7.15
77.58	12.34	0.09	0.84	0.09	0.58	4	4.24	0.25	8.43
77.68	12.2	0.13	1.05	0.12	1.02	3.99	3.63	0.19	5.79
77.34	12.45	0.12	0.93	0.13	0.76	3.91	4.13	0.24	6.48
76.73	12.63	0.15	1.46	0.06	1.02	4.07	3.67	0.21	6.8
77.45	12.37	0.13	1.1	0.1	0.87	3.9	3.85	0.23	6.25
0.98	0.18	0.04	0.2	0.02	0.18	0.11	0.26	0.02	1.21

234 Makaroro River U22/926488

76.09	12.89	0.17	1.55	0.15	1.11	4.46	3.44	0.14	7.03
75.6	13.16	0.23	1.71	0.17	1.1	4.3	3.52	0.2	7.77
76.25	12.93	0.17	1.6	0.15	1.14	4.17	3.41	0.17	6.45
75.75	13.11	0.12	1.59	0.16	1.11	4.3	3.64	0.23	7.07
75.43	13.13	0.22	1.72	0.16	1.12	4.4	3.62	0.19	6.54
75.84	13.07	0.2	1.54	0.14	1.08	4.46	3.48	0.18	6.08
75.53	13.01	0.26	1.67	0.2	1.13	4.29	3.71	0.22	7.74
75.49	13.07	0.23	1.78	0.16	1.11	4.26	3.68	0.21	5.46
76.38	12.87	0.16	1.52	0.17	1.1	4.37	3.27	0.17	6.34
75.82	13.03	0.2	1.63	0.16	1.11	4.34	3.53	0.19	6.72
0.35	0.11	0.04	0.09	0.02	0.02	0.1	0.14	0.03	0.76

235 Kiwitea Sm T22/478357

75.61	13.12	0.06	1.56	0.1	0.79	3.88	4.63	0.26	7.03
74.73	13.52	0.21	1.98	0.13	1.05	4.23	3.98	0.17	7.6
75.19	13.29	0.19	1.85	0.11	0.94	4.41	3.82	0.19	7.53
75.38	13.4	0.19	1.64	0.19	1.48	3.62	3.88	0.22	6.62
75.4	13.2	0.25	1.72	0.19	1.54	3.57	3.91	0.22	7.65
75.01	13.46	0.21	1.91	0.26	1.65	3.71	3.62	0.17	7.38
75.17	13.3	0.24	1.67	0.21	1.64	3.91	3.65	0.22	7.85
75.37	13.21	0.23	1.79	0.18	1.47	3.93	3.66	0.15	7.66
75.68	13.21	0.22	1.6	0.16	1.37	3.58	3.98	0.2	8.77
75.28	13.3	0.2	1.75	0.17	1.32	3.87	3.9	0.2	7.57
0.29	0.13	0.05	0.15	0.05	0.32	0.29	0.31	0.03	0.59

236 Kiwitea Sm T22/478357

74.24	13.68	0.28	1.98	0.2	1.17	4.53	3.73	0.2	7.73
74.84	13.3	0.22	1.99	0.14	1.02	4.67	3.57	0.26	6.06
75.23	13.47	0.2	1.69	0.2	1.37	4.01	3.66	0.17	9.65
76.09	12.99	0.15	1.72	0.11	1.12	3.87	3.77	0.19	8.75
74.67	13.54	0.18	1.88	0.15	1.14	4.18	4.1	0.15	6.54
73.85	13.81	0.3	2.08	0.16	1.16	4.64	3.86	0.15	8.53
74.74	13.46	0.16	2.08	0.12	1	4.45	3.78	0.2	6.92
74.75	13.36	0.17	2.3	0.15	1.38	3.97	3.76	0.15	8.29
74.4	13.65	0.19	2.03	0.11	1.1	4.5	3.8	0.21	7.42
74.64	13.45	0.21	2.13	0.12	1.03	4.22	4	0.22	8.45
74.74	13.47	0.21	1.99	0.15	1.15	4.3	3.8	0.19	7.83
0.6	0.23	0.05	0.18	0.03	0.13	0.29	0.15	0.03	1.11

238 Kiwitea Sm T22/478357

76.17	13.69	0.14	1.47	0.35	1.63	3.58	2.82	0.16	4.75
75.96	12.73	0.15	1.66	0.2	1.14	4.14	3.98	0.05	4.08
76.84	12.27	0.12	1.5	0.1	0.76	3.99	4.24	0.19	4.45
76.5	12.52	0.16	1.48	0.1	0.68	4.11	4.21	0.25	7.16
76.09	13.61	0.17	1.42	0.23	1.17	3.82	3.37	0.12	9.62
77.4	12.07	0.2	1.37	0.07	0.92	3.98	3.79	0.19	3.75
74.4	14.62	0.16	1.77	0.37	1.61	3.87	3.08	0.11	8.87
76.4	12.5	0.12	1.53	0.05	0.7	4.25	4.23	0.21	8.56
77.1	12.32	0.08	1.4	0.09	0.71	4	4.04	0.23	4.57
75.36	13.9	0.17	1.63	0.34	1.64	3.94	2.88	0.14	5.11
76.22	13.02	0.15	1.52	0.19	1.1	3.97	3.67	0.16	6.09
0.87	0.86	0.03	0.13	0.12	0.4	0.19	0.57	0.06	2.23

239 Mangatewaiiti Sm U23/809172

77.21	12.62	0.09	1.02	0.1	0.57	3.48	4.67	0.24	8.16
76.93	12.51	0.08	1.11	0.16	0.96	3.77	4.26	0.22	7.76
76.37	12.74	0.12	1.25	0.09	0.98	3.89	4.36	0.2	8.82
76.5	12.61	0.08	1.11	0.12	0.98	3.88	4.49	0.23	9.52
76.47	12.85	0.15	1.18	0.14	1.11	3.79	4.12	0.18	7.34
76.93	12.56	0.13	1.09	0.06	0.84	3.95	4.24	0.19	6.39
76.93	12.71	0.08	0.93	0.08	0.72	3.9	4.46	0.2	8.44
76.49	12.48	0.12	1.51	0.15	1	3.82	4.24	0.19	6.17
76.89	12.6	0.12	0.97	0.11	0.86	3.79	4.51	0.17	7.03
76.39	12.68	0.08	1.21	0.08	0.75	4.09	4.53	0.21	9.2
76.71	12.64	0.1	1.14	0.11	0.88	3.84	4.39	0.2	7.88
0.3	0.11	0.03	0.17	0.03	0.16	0.16	0.17	0.02	1.15

240 Mangatewaiiti Sm U23/810172

76.39	12.81	0.15	1.65	0.08	1.03	4.21	3.51	0.16	8.84
76.4	12.7	0.17	1.5	0.13	1.03	4.22	3.72	0.13	6.71
75.82	12.98	0.18	1.6	0.17	1.05	4.41	3.61	0.18	9.54
76.2	12.89	0.17	1.54	0.13	1.07	4.08	3.75	0.17	9.91
75.85	13	0.22	1.63	0.11	1.09	4.32	3.63	0.16	8
76.26	12.82	0.16	1.57	0.16	1.1	4.07	3.69	0.16	5.71
76.27	12.75	0.22	1.6	0.15	1.1	4.08	3.68	0.16	7.04

76.21	12.94	0.15	1.44	0.12	1.11	4.22	3.67	0.14	7.41
76.25	12.82	0.15	1.53	0.13	1.12	4.4	3.43	0.17	6.14
76.71	12.64	0.17	1.45	0.13	1.09	4.17	3.51	0.13	5.48
76.24	12.83	0.17	1.55	0.13	1.08	4.22	3.62	0.16	7.48
0.26	0.12	0.02	0.07	0.03	0.03	0.13	0.1	0.02	1.56

241 (=194, base), Mangatewainui Sm U23/821185

76.68	12.67	0.15	1.31	0.14	1.16	3.86	3.8	0.22	5.72
76.72	12.61	0.15	1.29	0.15	1.09	3.86	3.91	0.22	5.69
76.74	12.56	0.18	1.29	0.14	1	3.92	3.92	0.26	6.67
76.88	12.49	0.12	1.25	0.16	0.99	3.99	3.89	0.24	6.17
77.26	12.36	0.23	1.22	0.09	0.99	3.74	3.86	0.26	6.39
77.15	12.3	0.21	1.12	0.12	1	4.03	3.87	0.2	7.38
76.9	12.5	0.17	1.25	0.13	1.04	3.9	3.88	0.23	6.41
77.28	12.36	0.07	1.08	0.11	0.89	3.83	4.18	0.2	7.95
77.14	12.45	0.12	1	0.1	0.82	3.85	4.31	0.22	6
76.48	12.65	0.15	1.12	0.11	0.79	4.05	4.43	0.22	7
76.97	12.48	0.12	1.07	0.1	0.84	3.91	4.3	0.21	6.8
76.92	12.49	0.16	1.19	0.12	0.98	3.9	4.01	0.23	6.54
0.27	0.13	0.05	0.11	0.02	0.12	0.1	0.1	0.02	0.73

242 (=196, base), Mangatewainui U23/818184

76.01	12.89	0.2	1.67	0.13	0.94	4.37	3.62	0.16	7.83
75.22	13.27	0.19	1.69	0.12	0.99	4.89	3.49	0.13	8.54
76.07	13.02	0.21	1.55	0.1	1.06	4.42	3.38	0.19	9.47
75.48	13.04	0.17	1.67	0.15	0.98	4.73	3.62	0.15	8.13
75.7	13.01	0.15	1.59	0.09	1	4.7	3.64	0.12	8.82
75.7	13.06	0.18	1.6	0.12	1.02	4.66	3.5	0.17	9.14
75.7	13.05	0.18	1.63	0.12	1	4.63	3.54	0.15	8.66
0.32	0.13	0.02	0.06	0.02	0.04	0.2	0.1	0.02	0.62

243 Makaroro River U22/919503

74.77	13.3	0.15	2.19	0.1	0.93	4.7	3.69	0.18	7.56
74.37	13.56	0.13	2.12	0.13	1.09	4.69	3.7	0.21	7.91
76.1	12.64	0.06	1.47	0.07	0.7	3.99	4.78	0.19	9.09
74.31	13.41	0.17	2.16	0.1	0.96	4.7	3.98	0.22	9.5
74.46	13.4	0.19	2.26	0.12	0.99	4.47	3.92	0.21	9.86
76.52	12.51	0.05	1.56	0.05	0.66	4.22	4.22	0.2	8.71
74.46	13.41	0.18	2.26	0.13	1.12	4.63	3.64	0.19	8.17
76.21	12.56	0.11	1.53	0.07	0.7	4.37	4.22	0.25	8.79
74.43	13.25	0.14	2.21	0.12	1	4.8	3.85	0.2	7.22
75.7	12.69	0.14	1.71	0.07	0.79	4.16	4.52	0.22	8.39
76.33	12.34	0.06	1.6	0.06	0.69	4.27	4.45	0.22	8.41
75.24	13.01	0.12	1.91	0.09	0.88	4.45	4.09	0.21	8.51
0.92	0.45	0.05	0.33	0.03	0.17	0.27	0.38	0.02	0.8

244 Makaroro River U22/919502

76.86	12.86	0.08	1.02	0.07	0.89	3.67	4.45	0.1	8.17
76.37	12.53	0.15	1.67	0.06	0.77	4.35	3.92	0.18	7.58
76.98	12.32	0.07	1.42	0.06	0.68	4.16	4.22	0.07	6.55
76.93	12.4	0.14	1.37	0.06	0.57	3.75	4.51	0.26	7.51
74.71	13.16	0.15	2.17	0.11	1.03	4.73	3.75	0.18	6.15
75.41	12.84	0.14	2.08	0.06	0.93	4.51	3.87	0.17	5.22
75.04	13.16	0.15	2.01	0.11	1	4.68	3.66	0.19	6.06
77.13	12.71	0.08	1.06	0.09	1.05	3.7	4.02	0.17	6.75
76.18	12.75	0.12	1.6	0.08	0.87	4.19	4.05	0.17	6.75
0.97	0.32	0.04	0.45	0.02	0.17	0.44	0.31	0.06	0.96

245 Makaroro River U22/919502

76.76	13.23	0.08	1.04	0.1	1.12	3.8	3.74	0.15	9.15
77.56	12.12	0.13	1.49	0.1	1.23	3.7	3.51	0.18	7.36
77.44	12.57	0.09	1.17	0.07	1.09	3.69	3.76	0.13	6.77
77.64	12.43	0.11	1.19	0.14	1.16	3.63	3.57	0.14	8.64
77.32	12.55	0.09	1.36	0.1	1.21	3.73	3.54	0.13	6.05
76.99	12.49	0.13	1.38	0.12	1.13	3.89	3.71	0.16	5.31
77.2	12.39	0.14	1.47	0.09	1.09	3.85	3.59	0.19	5.64
77.36	12.48	0.11	1.3	0.1	1.14	3.76	3.61	0.16	8.01
77.36	12.47	0.11	1.3	0.1	1.14	3.76	3.61	0.15	7.3
0.35	0.34	0.03	0.15	0.02	0.05	0.08	0.11	0.02	1.44

247 Makaroro River U22/922500

75.2	13.19	0.17	1.99	0.16	1.25	4.46	3.41	0.18	5.74
75.12	13.13	0.15	2	0.13	1.28	4.54	3.5	0.16	5.9
75.34	13.06	0.14	2.08	0.13	1.3	4.17	3.58	0.19	6.92
75.23	13.14	0.19	2.16	0.11	1.14	4.29	3.53	0.21	8.95
75.01	13.28	0.12	2.17	0.15	1.29	4.38	3.39	0.2	8.39
74.94	13.16	0.15	2.18	0.14	1.33	4.65	3.23	0.24	6.44
75.38	13.16	0.12	2.11	0.1	1.29	4.25	3.35	0.24	7.6
75.25	13.14	0.11	2.18	0.1	1.35	4.39	3.29	0.2	8.72
75.34	13.23	0.17	2	0.09	1.26	4.29	3.44	0.18	6.58
75.2	13.17	0.15	2.1	0.12	1.28	4.38	3.41	0.2	7.25
0.15	0.06	0.03	0.08	0.03	0.06	0.15	0.11	0.03	1.21

248 Makaroro River U22/922500

75.34	12.91	0.23	1.99	0.07	1.1	4.49	3.74	0.13	8.52
77	12.3	0.12	1.43	0.07	0.65	4.36	3.9	0.17	7.96
75.29	13.03	0.18	1.99	0.07	0.98	4.76	3.53	0.18	7.82
75.09	12.95	0.16	2.15	0.12	1.05	4.79	3.5	0.16	8.98
75.55	12.93	0.27	1.95	0.1	0.92	4.78	3.32	0.17	8.54

123

75.66	12.81	0.2	2.07	0.12	1.02	4.61	3.36	0.16	6.54
75.58	12.85	0.2	1.95	0.09	0.96	4.67	3.54	0.17	7.87
0.66	0.25	0.05	0.24	0.03	0.15	0.19	0.21	0.02	0.93

249 (=230, ignimbrite middle), Mangaonuku Sm U22/097592

76.97	12.31	0.17	1.25	0.08	0.91	3.93	4.15	0.24	6.28
76.88	12.46	0.13	1.2	0.11	0.99	4.12	3.93	0.19	8.14
76.94	12.57	0.11	1.06	0.11	0.74	3.8	4.49	0.18	7.42
77.16	12.35	0.09	1.09	0.09	0.82	3.86	4.33	0.23	5.67
77.23	12.38	0.16	1.14	0.11	0.94	3.77	4.1	0.18	6.34
77.25	12.42	0.06	1.1	0.12	0.99	3.94	3.96	0.17	5.01
77.33	12.27	0.16	1.13	0.09	1.03	4.04	3.78	0.19	6.31
77.37	12.24	0.15	1.25	0.1	0.97	3.65	4.09	0.19	5.45
76.55	12.54	0.08	1.3	0.11	1	3.92	4.28	0.22	9.97
77.18	12.36	0.14	1.2	0.13	0.78	3.67	4.36	0.19	6.13
77.09	12.39	0.12	1.17	0.1	0.92	3.87	4.15	0.2	6.67
0.25	0.11	0.04	0.08	0.02	0.1	0.15	0.22	0.02	1.47

250 (=230, ignimbrite top), Mangaonuku Sm U22/097592

77.51	12.34	0.09	1.03	0.06	0.62	3.79	4.39	0.17	4.02
77.53	12.21	0.06	1.05	0.06	0.7	3.79	4.34	0.27	4.43
76.93	12.43	0.14	1.18	0.14	0.86	3.81	4.29	0.21	6.12
76.93	12.48	0.13	1.27	0.08	0.95	3.76	4.15	0.26	6.82
76.87	12.58	0.12	1.01	0.13	0.78	3.87	4.42	0.23	5.82
76.69	12.47	0.16	1.39	0.13	0.84	3.83	4.3	0.2	6.13
76.98	12.28	0.16	1.39	0.13	1.05	3.71	4.1	0.21	4.73
76.69	12.64	0.14	1.19	0.14	0.94	3.78	4.24	0.24	6.63
77.11	12.54	0.09	0.97	0.1	0.79	3.83	4.38	0.21	5.89
76.6	12.7	0.09	1.19	0.11	0.75	3.82	4.49	0.26	7.09
76.98	12.47	0.12	1.17	0.11	0.83	3.8	4.31	0.23	5.77
0.32	0.16	0.03	0.15	0.03	0.13	0.04	0.12	0.03	1.04

251 Waipawa River U22/903467

75.19	13.19	0.22	2.12	0.13	1.23	4.57	3.21	0.14	7.44
75.34	13.16	0.16	2.35	0.11	1.22	4.28	3.2	0.18	7.22
75.77	12.86	0.19	1.85	0.07	1.09	4.35	3.62	0.21	8.55
74.8	13.23	0.19	2.41	0.08	1.2	4.55	3.36	0.17	7.21
75.55	13.15	0.15	1.93	0.13	1.27	4.41	3.23	0.18	6.93
74.98	13.15	0.18	2.18	0.15	1.21	4.65	3.3	0.2	9.11
75.44	13.02	0.16	1.99	0.12	1.05	4.53	3.51	0.17	7.92
74.37	13.95	0.19	1.76	0.27	1.57	4.17	3.6	0.13	5.98
74.23	13.87	0.24	1.8	0.27	1.52	4.27	3.68	0.13	5.59
75.08	13.29	0.19	2.04	0.15	1.26	4.42	3.41	0.17	7.33
0.53	0.37	0.03	0.24	0.07	0.17	0.16	0.19	0.03	1.12

252 Waipawa River U22/903465

76.26	12.92	0.1	1.57	0.05	0.94	4.34	3.64	0.18	6.49
76.11	12.91	0.07	1.71	0.05	0.88	4.24	3.84	0.19	5.22
76.16	12.94	0.14	1.67	0.14	0.89	4.14	3.76	0.17	5.74
75.48	13.15	0.14	1.84	0.05	0.97	4.41	3.8	0.14	5.61
75.22	13.04	0.09	1.93	0.12	0.9	4.57	3.91	0.22	6.39
75.81	13.05	0.13	1.81	0.06	0.93	4.42	3.62	0.18	8.26
75.57	13.02	0.15	1.78	0.09	0.98	4.43	3.82	0.16	7.69
75.8	13	0.12	1.76	0.08	0.93	4.37	3.77	0.18	6.49
0.39	0.09	0.03	0.12	0.04	0.04	0.14	0.11	0.02	1.12

253 Waipawa River U22/903465

75.39	13.08	0.16	1.99	0.17	0.97	4.67	3.37	0.21	7.3
75.15	13.07	0.26	2.18	0.07	0.98	4.51	3.6	0.19	8.34
75.05	13.05	0.25	2.13	0.11	1.01	4.78	3.49	0.13	6.95
75.39	13.03	0.19	2.03	0.13	0.97	4.57	3.52	0.19	8.26
77.67	12.15	0.06	1.19	0.06	0.58	4.08	3.99	0.21	5.92
76.18	12.98	0.14	1.9	0.06	0.94	4.33	3.31	0.16	6.42
75.73	12.76	0.15	2.12	0.14	0.99	4.64	3.32	0.15	6.65
77.24	12.19	0.09	1.41	0.08	0.56	4.18	4.03	0.24	9.34
76.51	12.54	0.09	1.53	0.05	0.65	4.03	4.4	0.21	7.13
76.03	12.76	0.15	1.83	0.1	0.85	4.42	3.67	0.19	7.37
0.94	0.38	0.07	0.36	0.04	0.19	0.28	0.38	0.03	1.08

254 Wapawa River U22/908464

76.46	12.55	0.11	1.76	0.1	0.96	4.41	3.44	0.21	6.88
75.89	12.81	0.21	1.9	0.1	1	4.44	3.5	0.17	5.61
76.75	12.62	0.18	1.62	0.1	0.96	4.27	3.31	0.19	6.95
77.14	12.4	0.1	1.51	0.13	0.93	4.28	3.32	0.18	6.15
76.87	12.46	0.15	1.64	0.1	0.95	4.33	3.38	0.13	6.18
76.62	12.51	0.15	1.66	0.1	0.97	4.2	3.59	0.2	7.9
76.34	12.65	0.18	1.69	0.16	1.01	4.31	3.47	0.19	6.55
76.99	12.47	0.17	1.63	0.11	0.92	4.28	3.23	0.2	8.08
74.88	13.36	0.33	2.04	0.27	1.55	4.36	3.06	0.16	5.87
76.08	12.81	0.26	1.82	0.16	0.86	4.35	3.47	0.18	5.15
76.4	12.66	0.18	1.73	0.13	1.01	4.32	3.38	0.18	6.53
0.67	0.28	0.07	0.15	0.05	0.19	0.07	0.15	0.02	0.94

255 Waipawa River U22/919467

76.3	12.87	0.21	1.56	0.18	1.29	4.19	3.21	0.17	7.96
76.36	12.59	0.18	1.74	0.12	0.99	4.25	3.59	0.19	6.66
76.52	12.58	0.2	1.67	0.21	1.14	3.86	3.63	0.18	6.45
76.42	12.69	0.21	1.76	0.12	1.25	4.13	3.21	0.2	6.62
77.06	12.38	0.17	1.44	0.15	1.05	4.06	3.52	0.17	5.73

76.18	12.85	0.16	1.64	0.12	1.02	4.2	3.63	0.2	8.06
76.48	12.78	0.16	1.42	0.17	1.18	3.99	3.57	0.25	7.17
76.53	12.63	0.21	1.73	0.19	1.25	3.88	3.38	0.21	8.24
75.46	13.1	0.2	1.71	0.16	0.99	4.37	3.81	0.19	8.34
76.37	12.72	0.19	1.63	0.16	1.13	4.1	3.51	0.2	7.25
0.42	0.21	0.02	0.13	0.03	0.12	0.17	0.2	0.02	0.94

257 (ignimbrite) State Highway 50 V21/115603

77.29	12.56	0.16	1.03	0.15	0.99	3.72	3.78	0.32	4.57
77.75	11.75	0.21	1.21	0.14	0.99	3.81	3.94	0.2	4.5
77.33	12.06	0.21	1.02	0.11	0.93	3.9	4.12	0.32	3.13
76.49	12.07	0.15	1.38	0.36	1.29	3.86	3.8	0.61	4.58
77.63	12.36	0.17	0.53	0.08	0.99	3.76	4.21	0.29	5.73
76.38	12.52	0.13	1.48	0.13	0.7	4.23	4.2	0.23	2.86
76.35	13.09	0.16	1.21	0.19	1.04	3.79	3.93	0.24	4.84
77.56	12.85	0.09	0.85	0.15	0.85	3.82	3.55	0.31	1.79
77.9	12.2	0.22	0.84	0.08	0.8	3.75	4	0.19	2.19
77.17	12.41	0.12	1.29	0.1	1.02	3.83	3.86	0.2	3.29
77.18	12.39	0.16	1.09	0.15	0.96	3.85	3.94	0.29	3.75
0.58	0.4	0.04	0.29	0.08	0.16	0.15	0.2	0.12	1.28

261 Cape Kidnappers W21/557650

78.11	12.04	0.13	1.29	0.13	0.77	3.79	3.57	0.17	6.68
78.26	11.94	0.15	1.35	0.13	0.68	3.88	3.49	0.13	5.09
78.37	12.04	0.23	1.32	0.09	0.73	3.58	3.49	0.16	4.95
78.23	11.96	0.21	1.08	0.08	0.73	3.89	3.65	0.17	4.05
77.76	12.42	0.15	1.26	0.07	0.82	4.08	3.28	0.16	6.11
78.1	12.56	0.15	1.07	0.14	0.88	3.8	3.13	0.17	6.77
77.93	12.08	0.13	1.41	0.13	0.74	3.69	3.73	0.16	8.25
77.17	12.58	0.11	1.42	0.11	0.81	4.18	3.47	0.16	5.68
77.45	12.47	0.18	1.34	0.1	0.85	4.12	3.32	0.17	5.53
78.78	11.94	0.12	0.98	0.13	0.76	3.78	3.38	0.13	6.45
78.02	12.2	0.15	1.25	0.11	0.78	3.88	3.45	0.16	5.96
0.46	0.27	0.04	0.15	0.02	0.06	0.19	0.18	0.02	1.17

262 Rabbit Gully ignimbrite, Cape Kidnappers W21/556650

78	12.21	0.11	1.17	0.2	0.92	3.79	3.42	0.17	5.85
78.91	12.05	0.14	1	0.13	0.86	3.58	3.16	0.18	5.03
78.35	12.2	0.18	1.25	0.15	0.91	3.53	3.31	0.13	5.14
77.65	12.51	0.09	1.31	0.12	0.9	4.02	3.28	0.11	3.04
78.77	11.98	0.16	1.05	0.13	0.88	3.73	3.18	0.14	5.32
78.05	12.07	0.16	1.14	0.18	0.87	3.62	3.75	0.17	4.98
78.13	12.09	0.16	1.17	0.1	0.91	3.64	3.67	0.15	5.6
77.81	12.16	0.2	1.15	0.12	0.91	3.66	3.81	0.17	5.84
78	12.17	0.14	1.05	0.14	0.93	3.6	3.79	0.18	6.74
78.18	12.16	0.15	1.14	0.14	0.9	3.69	3.48	0.16	5.28
0.42	0.15	0.03	0.1	0.03	0.02	0.15	0.27	0.02	1

268 Mananui Ignimbrite S18/066704

77.65	12	0.19	0.98	0.11	0.78	3.36	4.71	0.23	3.14
77.63	11.99	0.15	0.97	0.14	0.82	3.36	4.68	0.25	2.54
77.98	12.13	0.1	0.92	0.11	0.76	3.36	4.42	0.22	3.44
77.78	11.91	0.13	1.06	0.11	0.89	3.35	4.54	0.23	3.35
77.67	11.87	0.13	0.96	0.14	0.83	3.5	4.65	0.25	2.44
78.02	11.95	0.1	0.88	0.13	0.79	3.31	4.69	0.13	2.02
77.88	12.14	0.09	0.77	0.08	0.75	3.36	4.69	0.24	2.2
77.8	12	0.13	0.93	0.12	0.8	3.37	4.63	0.22	2.73
0.16	0.1	0.03	0.09	0.02	0.05	0.06	0.11	0.04	0.57

271 Ongatiti Ignimbrite S17/098843

77.57	12.39	0.2	1.28	0.1	0.85	3.8	3.62	0.19	4.62
77.94	12.36	0.1	1.3	0.09	0.91	3.77	3.36	0.17	3.59
77.99	12.48	0.12	1.22	0.13	0.86	3.73	3.26	0.22	4.57
78.13	12.27	0.18	1.26	0.08	0.85	3.67	3.4	0.16	4.78
77.72	12.38	0.1	1.22	0.13	0.84	3.9	3.51	0.2	4.3
78.12	12.29	0.09	1.18	0.16	0.81	3.73	3.42	0.21	4.04
77.59	12.53	0.17	1.23	0.09	0.85	3.64	3.64	0.24	5.22
77.8	12.39	0.17	1.18	0.12	0.86	3.79	3.47	0.21	3.78
77.82	12.5	0.18	1.32	0.09	0.93	3.77	3.24	0.15	4
78.25	12.25	0.14	1.35	0.09	0.87	3.61	3.27	0.17	3.75
77.89	12.38	0.14	1.25	0.11	0.86	3.74	3.42	0.19	4.27
0.23	0.1	0.04	0.06	0.02	0.03	0.09	0.14	0.03	0.52

272 Ongatiti Ignimbrite S17/098843

76.97	12.14	0.12	1.45	0.14	1.03	3.6	4.23	0.33	5.21
77.46	11.96	0.2	1.25	0.13	0.9	3.61	4.19	0.29	4.55
77.22	12.17	0.18	1.39	0.12	0.97	3.57	4.07	0.3	4.51
77.56	12.08	0.16	1.28	0.1	1.02	3.5	3.95	0.36	4.53
77.58	12.21	0.17	1.25	0.11	0.94	3.56	3.91	0.26	3.46
77.5	12.21	0.08	1.26	0.1	0.91	3.67	3.98	0.29	3.7
77.35	12.11	0.1	1.27	0.1	0.99	3.83	3.97	0.28	3.95
77.42	12.16	0.12	1.32	0.1	0.85	3.61	4.12	0.28	3.72
77.28	12.19	0.16	1.27	0.06	0.92	3.72	4.11	0.29	4.41
77.49	12.03	0.18	1.3	0.17	0.89	3.7	3.94	0.29	4.65
77.38	12.13	0.15	1.3	0.11	0.94	3.64	4.05	0.3	4.27
0.19	0.08	0.04	0.07	0.03	0.06	0.1	0.11	0.03	0.54

273 Ignimbrite A S17/092013

75.24	13.04	0.12	1.99	0.07	0.97	3.56	4.8	0.21	4.85

77.17	12.07	0.05	1.37	0.06	0.73	3.4	4.85	0.28	4.59
77.05	12.13	0.13	1.38	0.06	0.64	3.52	4.81	0.27	5.28
76.39	12.52	0.09	1.63	0.05	0.76	3.42	4.85	0.28	4.09
75.97	12.65	0.14	1.66	0.06	0.71	3.61	4.92	0.29	5.46
76.82	12.31	0.11	1.45	0.07	0.69	3.37	4.89	0.28	4.16
76.21	12.65	0.13	1.64	0.07	0.9	3.24	4.91	0.24	3.68
77.47	12.15	0.13	1.24	0.07	0.74	3.18	4.77	0.24	4.48
76.4	13.23	0.11	1.6	0.11	0.97	3.44	3.88	0.27	5.79
76.09	12.73	0.13	1.49	0.06	0.78	3.49	4.96	0.26	3.52
77.38	12.21	0.09	1.37	0.06	0.69	3.13	4.77	0.3	4.03
76.13	12.58	0.09	1.6	0.09	0.86	3.44	4.94	0.27	3.66
74.97	13.11	0.2	2.07	0.1	1.1	3.46	4.69	0.3	3.55
76.09	12.76	0.06	1.48	0.05	0.88	3.45	4.94	0.29	4
76.38	12.58	0.11	1.57	0.07	0.82	3.41	4.79	0.27	4.37
0.74	0.37	0.04	0.23	0.02	0.13	0.14	0.27	0.03	0.74

277 Ahuroa Ignimbrite (clear glass) S17/897655

77.85	12.07	0.07	1.39	0.07	0.2	4.37	3.86	0.13	9.16
77.49	11.96	0.24	1.53	0.05	0.74	4.31	3.44	0.23	5.5
77.72	11.96	0.06	1.45	0.1	0.74	4.32	3.27	0.37	4.46
77.11	12.3	0.07	1.48	0.05	0.69	4.38	3.67	0.25	7.91
77.04	12.23	0	1.73	0	0.61	4.61	3.78	0	9.49
77.41	12.24	0.11	1.45	0.06	0.62	4.24	3.64	0.25	9.36
77.44	12.13	0.09	1.51	0.06	0.6	4.37	3.61	0.21	7.65
0.32	0.15	0.08	0.12	0.03	0.21	0.13	0.22	0.13	2.17

277 Ahuroa Ignimbrite (brown glass) S17/897655

76.08	12.5	0.22	2.12	0.12	1.02	4.47	3.26	0.22	3.49
76.19	12.59	0.14	2.02	0.1	0.99	4.42	3.35	0.19	3.39
76.66	12.4	0.13	2.03	0.08	0.95	4.37	3.18	0.2	3.22
76.57	12.39	0.17	2.01	0.09	0.95	4.36	3.29	0.18	3.9
76.4	12.6	0.15	1.89	0.09	0.96	4.4	3.3	0.21	2.76
76.3	12.33	0.18	2.02	0.09	1.07	4.37	3.42	0.23	2.87
76.45	12.5	0.22	2.04	0.08	0.89	4.31	3.28	0.22	2.66
76.55	12.55	0.14	1.98	0.13	0.95	4.19	3.29	0.19	2.26
76.12	12.56	0.2	2.05	0.07	0.97	4.49	3.35	0.2	2.73
75.37	13.02	0.17	2.06	0.07	0.97	4.73	3.43	0.17	5.02
75.58	12.7	0.2	2.16	0.11	1.13	4.48	3.48	0.16	3.56
74.95	12.97	0.18	2.3	0.12	1.12	4.54	3.63	0.19	5.31
75	13.03	0.24	2.2	0.11	1.02	4.69	3.53	0.18	6.47
76.02	12.63	0.18	2.07	0.1	1	4.45	3.37	0.19	3.66
0.59	0.24	0.03	0.11	0.02	0.07	0.15	0.12	0.02	1.23

278 Ignimbrite D (airfall ash) S17/897655

77.71	11.89	0.13	1.32	0.05	0.58	4.22	3.87	0.23	5.27
77.56	11.93	0.09	1.46	0.05	0.61	4.24	3.87	0.19	6.04
77.67	11.92	0.06	1.37	0.05	0.62	4.14	3.89	0.26	5.42
77.36	12.06	0.09	1.46	0.05	0.71	4.27	3.77	0.21	4.76
77.66	12.03	0.09	1.31	0.06	0.68	4.26	3.64	0.27	4.54
77.81	11.87	0.06	1.38	0.06	0.63	4.26	3.65	0.26	5.21
78.02	11.7	0.12	1.45	0.07	0.62	4.13	3.66	0.23	3.52
77.69	11.93	0.1	1.4	0.06	0.63	4.2	3.75	0.23	4.98
0.22	0.1	0.03	0.09	0.01	0.06	0.09	0.11	0.03	0.7

75.33	12.71	0.23	2.27	0.12	1.11	4.54	3.63	0.05	3.95
75.28	12.8	0.23	2.19	0.09	1.07	4.51	3.59	0.25	5.63
75.21	12.91	0.18	2.08	0.1	1.06	4.61	3.68	0.16	4.79
75.27	12.81	0.21	2.18	0.1	1.08	4.55	3.64	0.15	4.79
0.06	0.1	0.03	0.1	0.02	0.03	0.05	0.05	0.1	0.84

279 Ignimbrite D (ignimbrite) T17/897655

77.37	12.01	0.15	1.43	0.08	0.68	4.32	3.78	0.19	7.39
77.37	12.03	0.1	1.41	0.08	0.59	4.24	3.91	0.26	2.91
77.86	11.78	0.08	1.43	0.07	0.64	4.11	3.82	0.21	3.57
77.59	11.97	0.08	1.49	0.06	0.61	4.26	3.72	0.22	2.87
77.91	11.72	0.11	1.37	0.06	0.6	4.23	3.74	0.25	5.39
76.27	12.48	0.21	1.87	0.11	1.02	4.34	3.55	0.14	4.25
76.04	12.46	0.2	1.99	0.15	1.03	4.38	3.56	0.19	3.97
78.61	11.79	0.06	1.39	0.06	0.26	4.04	3.59	0.19	3.94
77.42	12.01	0.13	1.55	0.06	0.69	4.31	3.63	0.21	5.71
77.93	11.98	0.12	1.38	0.08	0.57	4.27	3.45	0.23	4.83
76.29	12.61	0.21	2.1	0.12	0.97	4.09	3.45	0.16	3.83
77.92	12	0.07	1.37	0.06	0.59	4.17	3.62	0.2	4.58
77.38	12.07	0.13	1.57	0.08	0.69	4.23	3.65	0.2	4.44
0.79	0.29	0.05	0.26	0.03	0.22	0.11	0.14	0.04	1.27

280 Ongatiti Ignimbrite (clast) S16/198218

78.21	12.01	0.14	0.88	0.08	0.78	3.61	4.04	0.25	5.17
78.04	11.92	0.15	1.11	0.1	0.8	3.66	3.93	0.29	2.41
78.09	11.84	0.09	1.3	0.13	0.78	3.55	3.91	0.31	2.42
78.23	11.84	0.15	1.15	0.06	0.75	3.59	3.99	0.23	2.12
78.7	11.85	0.15	0.84	0.06	0.7	3.52	3.89	0.28	3.13
78.3	11.83	0.14	0.94	0.05	0.8	3.55	4.05	0.34	3.01
78.26	11.88	0.14	1.04	0.08	0.77	3.58	3.97	0.28	3.04
0.24	0.07	0.02	0.18	0.03	0.04	0.05	0.07	0.04	1.11

281 Rocky Hill

74.98	13.18	0.22	2.27	0.16	1.38	4.5	3.06	0.25	7.84
76.34	13	0.18	1.96	0.13	1.4	3.71	3.1	0.19	5.4

75.71	12.95	0.23	2.1	0.14	1.32	4.17	3.2	0.18	5.91
75.92	12.95	0.17	2.08	0.11	1.27	4.1	3.19	0.19	7.35
75.64	12.89	0.21	2.09	0.14	1.39	4.13	3.32	0.2	5.64
75.68	13.06	0.17	2.13	0.15	1.27	4.27	3.03	0.23	6.3
76.01	12.94	0.17	2.17	0.15	1.3	3.72	3.34	0.2	6.6
75.52	12.78	0.23	2.24	0.22	1.32	4.14	3.37	0.19	7
75.22	13.28	0.11	2.01	0.13	1.3	4.44	3.3	0.22	8.27
75.67	13	0.19	2.12	0.15	1.33	4.13	3.21	0.21	6.7
0.41	0.15	0.04	0.1	0.03	0.05	0.27	0.13	0.02	0.99

282 Rocky Hill

77.11	12.31	0.09	1.41	0.13	1.14	3.81	3.81	0.2	3.33
77.73	12.09	0.13	1.18	0.13	1.01	3.69	3.77	0.28	4.14
77.64	12.19	0.14	1.23	0.1	0.93	3.7	3.83	0.23	3.4
78.01	11.96	0.13	0.97	0.07	0.81	3.66	4.16	0.22	3.68
77.79	12.13	0.1	1.15	0.09	0.71	3.66	4.11	0.26	3.8
77.4	12.19	0.18	1.28	0.17	1.13	3.68	3.73	0.25	4.01
77.36	12.23	0.17	1.27	0.08	1.02	3.8	3.85	0.22	3.94
78.08	12.02	0.14	1.19	0.11	0.95	3.56	3.72	0.23	4.03
77.61	12.14	0.14	1.25	0.09	0.99	3.7	3.83	0.25	2.95
77.83	12.06	0.12	1.28	0.09	1.1	3.45	3.81	0.25	3.79
78.03	12.15	0.11	0.93	0.08	0.81	3.63	4.04	0.23	3.18
77.67	12.05	0.09	1.35	0.1	0.95	3.68	3.85	0.25	4.17
77.69	12.13	0.13	1.21	0.11	0.96	3.67	3.88	0.24	3.7
0.29	0.1	0.03	0.14	0.03	0.13	0.1	0.15	0.02	0.4

286 Makaroro River U22/919503

75.37	13.04	0.23	1.99	0.06	0.91	4.51	3.68	0.19	5.75
75.94	12.89	0.2	1.77	0.12	0.96	4.38	3.51	0.23	3.93
77.47	12.23	0.08	1.3	0.06	0.69	3.92	4.05	0.19	4.68
77.24	12.14	0.15	1.54	0.07	0.68	3.71	4.27	0.2	7.98
77.63	12.05	0.08	1.43	0.06	0.66	3.79	4.1	0.2	4.29
77.1	12.26	0.08	1.46	0.09	0.6	4.03	4.16	0.21	4.67
77.43	12.13	0.09	1.51	0.11	0.68	3.99	3.84	0.21	4.12
77	12.61	0.11	1.26	0.05	0.65	3.79	4.36	0.17	6.83
77.31	12.27	0.14	1.44	0.05	0.69	3.81	4.1	0.2	4.34
77.9	12.06	0.13	1.29	0.05	0.63	3.84	3.88	0.23	4.29
77.38	12.22	0.11	1.4	0.07	0.66	3.86	4.09	0.2	5.15
0.29	0.18	0.03	0.11	0.02	0.03	0.11	0.18	0.02	1.44

287 Makaroro River U22/919503

75.76	12.9	0.1	1.84	0.09	0.94	4.41	3.75	0.19	4.58
75.4	13.02	0.11	2.08	0.1	0.86	4.53	3.72	0.18	4.23
76.1	12.84	0.24	1.97	0.06	0.91	4.2	3.49	0.18	4.59
75.64	13	0.22	2.04	0.09	0.94	4.2	3.7	0.16	4.61
75.19	12.99	0.17	2.17	0.12	0.98	4.19	3.92	0.27	8.09
75.86	12.87	0.17	1.99	0.07	1.05	4.31	3.52	0.16	4.17
76.14	12.7	0.18	1.98	0.09	0.86	4.41	3.45	0.2	4.33
75.36	13.15	0.2	2.13	0.07	1.04	4.37	3.55	0.14	4.97
75.57	12.98	0.19	1.91	0.09	0.91	4.47	3.74	0.16	3.94
75.83	13.04	0.16	1.84	0.09	0.96	4.29	3.59	0.2	4.79
75.68	12.95	0.17	1.99	0.09	0.94	4.34	3.64	0.18	4.83
0.31	0.13	0.04	0.11	0.02	0.07	0.12	0.15	0.04	1.19

288 Makaroro River U22/919503

77.89	12.46	0.13	1.08	0.07	1.07	3.45	3.69	0.16	3.7
77.86	12.37	0.09	1.02	0.12	1.04	3.57	3.82	0.1	3.28
77.41	12.58	0.07	1.16	0.07	1.02	3.34	4.2	0.15	4.07
77.1	12.82	0.11	1.18	0.1	1	3.67	3.87	0.16	5.88
78.39	12.3	0.09	0.97	0.09	0.98	3.45	3.59	0.14	4.71
77.37	12.68	0.11	1.11	0.11	1.04	3.43	3.97	0.19	5.21
77.66	12.57	0.09	0.98	0.08	0.88	3.36	4.25	0.13	4.1
77.69	12.47	0.07	1.11	0.1	1.14	3.47	3.82	0.12	4.65
77.83	12.37	0.1	1.13	0.12	1.07	3.48	3.75	0.15	3.47
78.05	12.41	0.07	1.24	0.07	1.01	3.43	3.58	0.14	4.84
77.73	12.5	0.1	1.1	0.1	1.02	3.46	3.85	0.14	4.39
0.37	0.16	0.02	0.09	0.02	0.07	0.1	0.23	0.02	0.82

289 (=230, clasts) Mangaonuku Sm U22/919503

78.72	12.14	0.11	0.94	0.08	0.71	3.53	3.76	0	8.84
78.26	12.43	0.11	1.04	0.08	0.73	3.67	3.62	0.06	3.59
77.86	12.35	0.21	1.14	0.14	0.93	3.5	3.73	0.13	4.41
78.15	12.4	0.14	1.03	0.07	0.71	3.55	3.78	0.19	4.4
77.91	12.46	0.14	1.25	0.11	1.06	3.76	3.17	0.15	4
78.22	12.38	0.08	1.05	0.09	0.76	3.42	3.75	0.26	7.53
77.67	12.48	0.13	1.04	0.06	0.71	3.75	3.97	0.19	4.73
77.9	12.39	0.07	1.13	0.1	0.74	3.51	3.9	0.27	7.8
78.47	12.32	0.11	1	0.08	0.68	3.68	3.54	0.11	3.63
77.45	12.63	0.11	1.14	0.11	0.72	3.75	3.91	0.19	6.06
77.53	12.44	0.11	0.97	0.09	0.71	3.88	4.13	0.16	6.74
77.56	12.65	0.21	1.29	0.11	1.05	3.68	3.3	0.15	5.14
77.97	12.42	0.13	1.08	0.09	0.79	3.64	3.71	0.16	5.57
0.4	0.13	0.04	0.11	0.02	0.14	0.14	0.27	0.08	1.78

291 Vineager Hill Rd T22/351387

76.58	12.57	0.23	1.36	0.15	1.06	3.22	4.63	0.2	5.63
76.47	12.58	0.21	1.36	0.18	1.15	3.2	4.65	0.2	5.31
76.66	12.49	0.22	1.37	0.14	1.18	3.1	4.68	0.16	5.35
76.31	12.63	0.25	1.4	0.15	1.2	3.3	4.53	0.23	6.7
76.92	12.36	0.21	1.4	0.18	1.21	3.14	4.39	0.2	4.26

76.65	12.44	0.27	1.48	0.18	1.17	3.17	4.46	0.18	4.93
76.57	12.59	0.23	1.37	0.21	1.16	3.05	4.57	0.25	4.87
76.58	12.63	0.23	1.35	0.15	1.12	2.97	4.82	0.16	5.09
76.79	12.43	0.27	1.36	0.17	1.12	3.08	4.59	0.19	4.44
76.68	12.36	0.19	1.47	0.23	1.18	3.11	4.58	0.2	4.9
76.62	12.51	0.23	1.39	0.17	1.15	3.13	4.59	0.2	5.15
0.16	0.11	0.03	0.05	0.03	0.05	0.09	0.12	0.03	0.68

292 Cheltenham-Hunterville Rd T22/351387

74.29	13.48	0.22	2.38	0.14	1.12	4.45	3.72	0.19	5.64
74.39	13.75	0.19	2.2	0.14	1.17	4.34	3.64	0.18	4.89
74.76	13.23	0.15	2.25	0.11	1.25	4.36	3.65	0.25	5.43
74.47	13.67	0.24	2.27	0.13	1.1	4.15	3.82	0.15	5.44
74.41	13.63	0.21	2.22	0.11	1.21	4.56	3.48	0.17	6.25
74.28	13.73	0.21	2.11	0.18	1.12	4.51	3.67	0.19	6.13
74.94	13.28	0.23	2.2	0.2	1.15	4.37	3.48	0.15	5.71
74.53	13.52	0.2	2.24	0.13	1.16	4.37	3.66	0.18	5.64
0.51	0.23	0.04	0.13	0.04	0.09	0.2	0.12	0.03	0.46

77.54	12.22	0.07	1.25	0.08	0.72	3.85	4.06	0.21	4.14
77.13	12.44	0.17	1.31	0.06	0.64	3.79	4.26	0.2	3.37
77.32	12.25	0.15	1.4	0.06	0.72	3.78	4.17	0.15	2.12
76.82	12.49	0.18	1.47	0.06	0.79	3.79	4.21	0.18	2.64
77.2	12.35	0.14	1.36	0.07	0.72	3.8	4.18	0.19	3.07
0.31	0.14	0.05	0.1	0.01	0.06	0.03	0.09	0.02	0.88

293 Pakihikura Pumice, Cheltenham-Hunterville Rd T22/362357

78.39	12.31	0.08	1.24	0.09	1.17	3.39	3.15	0.16	5.13
77.22	12.53	0.14	1.29	0.13	1.27	3.7	3.53	0.19	8.21
77.1	12.64	0.11	1.44	0.1	1.24	3.82	3.4	0.14	8.42
77.59	12.48	0.12	1.25	0.09	1.19	3.71	3.45	0.13	7.24
77.88	12.4	0.11	1.28	0.11	1.12	3.58	3.37	0.15	4.82
76.93	12.51	0.09	1.3	0.13	1.28	4.15	3.46	0.15	8.45
77.86	12.37	0.1	1.17	0.12	1.13	3.61	3.52	0.13	6.04
77.23	12.25	0.11	1.44	0.1	1.31	3.87	3.5	0.19	9.14
77.66	12.39	0.08	1.31	0.11	1.15	3.88	3.26	0.16	7.46
77.44	12.43	0.08	1.32	0.08	1.2	3.76	3.58	0.13	7.33
77.53	12.43	0.1	1.3	0.1	1.21	3.75	3.42	0.15	7.22
0.44	0.11	0.02	0.08	0.02	0.07	0.2	0.13	0.02	1.46

294 Kai-iwi/Brunswick Rd R22/778503

75.95	12.7	0.23	1.49	0.18	1.17	3.12	4.93	0.25	4.55
75.36	12.63	0.16	1.98	0.15	1.22	3.48	4.86	0.18	4.14
76.39	12.31	0.24	1.7	0.17	0.98	3.26	4.76	0.21	4.11
75.8	12.86	0.19	1.46	0.23	1.17	3.28	4.66	0.34	5.01
76.82	12.18	0.16	1.44	0.18	1.11	3.11	4.79	0.22	4
76.44	12.51	0.26	1.52	0.17	1.21	3.11	4.53	0.22	4.65
75.67	12.57	0.21	1.78	0.18	1.19	3.28	4.93	0.22	3.97
75.84	12.58	0.22	1.76	0.13	1.26	3.06	4.9	0.24	3.36
76.07	12.65	0.16	1.63	0.2	0.99	3.22	4.85	0.24	3.33
76.04	12.71	0.09	1.59	0.19	1.17	3.03	4.96	0.21	3.07
76.04	12.57	0.19	1.64	0.18	1.15	3.2	4.82	0.23	4.02
0.42	0.2	0.05	0.17	0.03	0.09	0.14	0.14	0.04	0.62

295 Matahina Ignimbrite (base)

77.26	12.41	0.14	1.12	0.14	0.85	4.04	3.86	0.17	4.66
78.01	12.31	0.1	1.09	0.06	0.95	3.69	3.58	0.19	3.09
76.59	13.27	0.14	1.1	0.14	0.9	4.38	3.94	0.19	8.8
77.56	12.47	0.11	1.06	0.1	0.91	3.86	3.7	0.21	3.63
76.87	12.56	0.14	1.08	0.12	0.96	3.97	4.15	0.15	7.27
77.73	12.44	0.12	1.07	0.1	0.83	3.74	3.79	0.17	4.58
77.05	12.51	0.1	1.18	0.11	0.85	3.97	4.05	0.18	6.4
77.31	12.62	0.12	0.93	0.11	0.91	4	3.8	0.2	5.45
77.62	12.35	0.16	1.12	0.12	0.86	3.82	3.72	0.21	2.79
77.79	12.42	0.1	1	0.12	0.8	3.84	3.75	0.19	3.7
77.38	12.54	0.12	1.07	0.11	0.88	3.91	3.83	0.18	5.04
0.45	0.27	0.02	0.07	0.02	0.05	0.15	0.17	0.02	1.95

297 ash below Matahina Ignimbrite

78.23	12.47	0.13	1.04	0.11	0.84	3.45	3.64	0.16	6.19
77.81	12.54	0.12	1.24	0.11	1.09	3.58	3.36	0.15	5.77
77.73	12.39	0.09	1.08	0.11	0.81	3.6	4.01	0.17	4.97
77.82	12.56	0.11	1.13	0.11	0.82	3.58	3.73	0.16	5.92
78.25	12.22	0.07	1.12	0.09	0.87	3.56	3.65	0.18	4.4
78.4	12.14	0.14	1.44	0.15	1.37	3.18	3.06	0.14	3.99
77.94	12.58	0.11	1.05	0.08	0.77	3.61	3.67	0.22	8.19
77.84	12.29	0.14	1.37	0.23	1.21	3.57	3.17	0.18	5.58
77.97	12.41	0.08	0.98	0.09	0.76	3.69	3.85	0.17	4.3
77.98	12.53	0.08	1.15	0.09	0.83	3.3	3.91	0.13	5.04
78	12.41	0.11	1.16	0.12	0.94	3.51	3.6	0.16	5.44
0.22	0.15	0.02	0.15	0.04	0.21	0.16	0.31	0.03	1.22

298 (ignimbrite), McCoy Rd

77.55	12.4	0.1	1.11	0.08	0.75	3.61	4.15	0.26	4.6
77.85	12.07	0.14	1.07	0.08	0.97	3.61	3.98	0.23	3.84
77.57	12.28	0.07	1.22	0.14	0.95	3.68	3.87	0.22	4.7
77.3	12.2	0.13	1.29	0.15	1	3.85	3.85	0.22	3.45
77.36	12.21	0.1	1.25	0.1	0.96	3.78	4.07	0.2	3.9
77.57	12.18	0.12	1.24	0.14	1.06	3.65	3.8	0.23	4.56
77.84	12.27	0.09	1.02	0.07	0.8	3.63	4.14	0.2	4.48

77.86	12.09	0.14	1.19	0.09	1	3.67	3.84	0.11	3.82
77.49	12.43	0.1	1.02	0.07	0.83	3.88	4.03	0.2	5.56
77.4	12.54	0.09	1.11	0.06	0.78	3.68	4.05	0.26	5.22
77.58	12.27	0.11	1.15	0.1	0.91	3.7	3.98	0.21	4.41
0.21	0.15	0.02	0.1	0.03	0.11	0.1	0.13	0.04	0.67

299 (lapilli), McCoy Rd

77.45	12.51	0.11	1.01	0.07	0.81	3.62	4.28	0.21	5.64
77.48	12.24	0.13	1.1	0.14	0.82	3.71	4.12	0.24	4.66
78.2	12.24	0.15	1.05	0.08	0.76	3.47	3.89	0.21	5.59
77.74	12.25	0.16	1.19	0.08	0.94	3.68	3.76	0.2	4.24
77.95	12.35	0.1	1.03	0.1	0.72	3.45	4.05	0.26	6.97
77.37	12.25	0.14	1.31	0.09	0.98	3.68	3.96	0.21	5.24
77.56	12.39	0.15	1.02	0.09	0.82	3.67	4.14	0.17	4.57
77.96	12.14	0.14	1.14	0.09	0.9	3.64	3.75	0.23	4.55
77.66	12.24	0.18	1.26	0.1	1.01	3.69	3.65	0.22	4.73
77.49	12.2	0.17	1.16	0.15	1	3.88	3.73	0.24	5.55
77.69	12.28	0.14	1.13	0.1	0.87	3.65	3.93	0.22	5.17
0.27	0.1	0.03	0.1	0.02	0.1	0.12	0.21	0.03	0.81

301 Mangataura Sm U22/919483

76.01	13.15	0.21	1.62	0.17	1.54	4.13	3.01	0.16	5.03
76.01	12.93	0.22	1.49	0.2	1.5	4.25	3.21	0.19	4.77
75.85	13.18	0.23	1.64	0.2	1.42	4.34	2.94	0.22	5.43
75.91	13.09	0.25	1.76	0.23	1.48	4.2	2.88	0.21	5.19
75.69	13.16	0.32	1.47	0.2	1.5	4.37	3.08	0.21	6.18
75.07	13.47	0.2	1.83	0.24	1.6	4.49	2.91	0.2	6.98
75.61	13.34	0.26	1.68	0.23	1.63	4.27	3.34	0.24	7.55
75.3	13.47	0.2	1.82	0.22	1.55	4.31	3.31	0.18	7.17
75.72	13.02	0.21	1.84	0.22	1.46	4.29	2.9	0.25	5.06
76.07	13.12	0.18	1.65	0.15	1.55	4.28	2.82	0.17	5.1
75.72	13.19	0.23	1.68	0.21	1.52	4.29	3.04	0.2	5.85
0.33	0.18	0.04	0.13	0.03	0.06	0.1	0.19	0.03	1.04

302 Mangataura Sm U22/921480

76.41	12.52	0.24	1.41	0.13	1.11	4.08	3.88	0.22	6.4
77.06	12.47	0.11	1.18	0.08	0.88	3.91	4.2	0.23	7.06
76.7	12.53	0.16	1.28	0.13	1.1	3.95	3.9	0.22	5.83
77.38	12.23	0.16	1.21	0.12	1.14	3.88	3.62	0.28	3.66
77.54	12.28	0.09	1.04	0.1	0.85	3.44	4.42	0.24	6.11
77.29	12.26	0.14	1.21	0.15	1.01	3.72	3.94	0.26	4.4
77.23	12.39	0.14	1.21	0.09	1.04	3.87	3.83	0.21	3.87
77.88	12.15	0.08	1.27	0.11	0.94	3.79	3.48	0.29	4.3
77.56	12.29	0.12	1.08	0.13	0.97	3.91	3.73	0.23	4.71
77.78	12.41	0.11	1.14	0.13	1.08	3.71	3.51	0.23	7.34
77.28	12.35	0.13	1.21	0.12	1.01	3.83	3.85	0.24	5.37
0.46	0.13	0.04	0.1	0.02	0.1	0.17	0.29	0.03	1.34

303 Mangataura Sm U22/921480

75.92	12.95	0.33	1.61	0.16	1.18	4.2	3.49	0.17	4.86
76.06	13	0.18	1.54	0.16	1.04	4.32	3.47	0.22	5.25
75.81	12.88	0.22	1.65	0.15	1.12	4.26	3.71	0.2	4.43
76.04	12.94	0.17	1.64	0.14	1.03	4.37	3.49	0.2	4.84
75.66	13.08	0.2	1.55	0.17	1.16	4.41	3.55	0.2	7.29
75.79	13	0.26	1.76	0.15	1.15	4.23	3.49	0.17	6.48
76.07	13.03	0.16	1.55	0.18	1.18	4.18	3.45	0.21	4.93
76.19	12.91	0.21	1.68	0.14	1.08	4.14	3.48	0.18	5.22
76.41	12.89	0.23	1.44	0.18	1.1	4.28	3.31	0.18	5.1
75.99	12.97	0.22	1.6	0.16	1.12	4.27	3.49	0.19	5.38
0.23	0.07	0.05	0.09	0.02	0.06	0.09	0.11	0.02	0.91

304 Tukituki Rd U22/891421

76.39	12.64	0.11	1.4	0.09	0.63	4.11	4.39	0.23	7.47
76.69	12.49	0.12	1.46	0.07	0.74	4.05	4.19	0.21	6.61
77.03	12.44	0.15	1.47	0.05	0.66	3.8	4.18	0.24	6.4
76.28	12.54	0.1	1.49	0.07	0.72	3.72	4.88	0.22	9.46
76.5	12.6	0.09	1.42	0.07	0.74	4.22	4.25	0.18	7.76
77.71	12.06	0.11	1.49	0.06	0.64	4.17	4.2	0.23	5.97
76.53	12.6	0.11	1.3	0.06	0.76	4.24	4.2	0.23	7.57
77.33	12.22	0.1	1.49	0.05	0.69	3.95	4.02	0.15	4.19
77.16	12.25	0.09	1.42	0.05	0.72	4.14	3.93	0.26	4.72
76.85	12.43	0.11	1.44	0.06	0.7	4.04	4.25	0.22	6.68
0.49	0.2	0.02	0.06	0.01	0.05	0.18	0.27	0.03	1.62

305 Tukituki Rd U22/891421

74.54	13.63	0.16	2.17	0.1	1.11	4.48	3.59	0.2	6.52
74.61	13.62	0.15	2.1	0.07	1.07	4.6	3.58	0.19	5.09
74.36	13.62	0.21	2.18	0.11	1.03	4.62	3.7	0.2	7.75
74.62	13.48	0.16	2.18	0.17	1.05	4.63	3.51	0.2	4.04
74.92	13.31	0.19	2.2	0.08	1.02	4.38	3.75	0.16	3.51
75.2	13.28	0.2	2	0.16	1.04	4.65	3.29	0.17	4.37
74.43	13.56	0.12	2.2	0.17	1.07	4.63	3.65	0.19	6.03
74.31	13.55	0.19	2.16	0.11	1.13	4.56	3.8	0.2	5.25
74.62	13.51	0.17	2.15	0.12	1.07	4.57	3.61	0.19	5.32
0.3	0.14	0.03	0.07	0.04	0.04	0.09	0.16	0.02	1.4

306 Tukituki Rd U22/891421

77.16	12.49	0.14	1.37	0.08	1.34	3.86	3.36	0.2	5.68
77.3	12.62	0.15	1.28	0.07	1.23	3.8	3.38	0.16	6.52

77.12 12.83 0.1 1.34 0.1 1.24 3.87 3.21 0.19 5.4
76.97 12.54 0.15 1.35 0.08 1.28 3.98 3.49 0.17 5.22
77.69 12.38 0.07 1.36 0.1 1.19 3.8 3.28 0.16 4.74
77.4 12.51 0.12 1.26 0.1 1.3 3.99 3.14 0.17 6.41
77.34 12.65 0.09 1.35 0.11 1.19 3.63 3.47 0.2 7.9
77.86 12.39 0.1 1.27 0.07 1.22 3.93 3.04 0.14 3.79
77.79 12.37 0.13 1.28 0.07 1.16 3.96 3.15 0.08 4.37
77.25 12.6 0.08 1.32 0.12 1.19 3.94 3.3 0.2 4.9
77.39 12.54 0.11 1.32 0.09 1.23 3.88 3.28 0.17 5.49
0.3 0.15 0.03 0.04 0.02 0.06 0.11 0.15 0.04 1.2

307 trib. to Pohangina River T24/459993

74.12 13.68 0.19 2.28 0.11 1.24 4.49 3.69 0.21 5.06
74.25 13.48 0.24 2.3 0.12 1.28 4.31 3.79 0.26 4.36
74.02 13.46 0.18 2.36 0.13 1.3 4.85 3.52 0.2 3.3
74.49 13.33 0.13 2.24 0.13 1.28 4.64 3.56 0.19 3.7
73.64 13.73 0.19 2.29 0.16 1.19 4.63 3.98 0.18 6.25
73.15 14 0.16 2.29 0.14 1.23 4.83 3.99 0.19 7.67
73.94 13.61 0.18 2.29 0.13 1.25 4.62 3.75 0.21 5.06
0.48 0.24 0.04 0.04 0.02 0.04 0.21 0.2 0.03 1.65

76.59 12.44 0.13 1.35 0.06 0.69 4.11 4.45 0.19
76.55 12.42 0.11 1.45 0.06 0.69 4.03 4.54 0.19
74.77 13.38 0.09 1.89 0.13 0.93 4.55 4.06 0.21
75.43 13.02 0.12 1.74 0.1 0.99 4.34 4.05 0.22

308 trib. to Pohangina River T24/459993

74.18 13.57 0.13 2.2 0.14 1.18 4.77 3.61 0.21 5.66
75.4 12.92 0.16 1.94 0.11 1 4.32 3.9 0.23 2.38
75.12 12.87 0.14 2.07 0.08 1.03 4.37 4.13 0.17 2.76
76.92 12.7 0.11 0.82 0.09 0.72 3.62 4.97 0.18 6.43
75.01 13.25 0.19 1.92 0.08 0.93 4.56 3.81 0.25 8.95
76.27 12.69 0.11 1.51 0.07 0.67 4.34 4.15 0.21 8.54
76.18 12.84 0.1 1.49 0.08 0.82 4.24 4.08 0.18 3.77
74.43 13.59 0.15 2.18 0.1 1.1 4.68 3.6 0.17 5.72
77.16 12.75 0.1 1.06 0.08 1.07 3.71 3.94 0.14 3.75
74.77 13.37 0.16 1.91 0.13 1.01 4.65 3.65 0.34 6.07
75.55 13.05 0.14 1.71 0.1 0.95 4.33 3.99 0.21 5.4
1.03 0.36 0.03 0.48 0.02 0.17 0.39 0.4 0.06 2.25

309 trib. to Pohangina River T24/459993

76.04 12.85 0.11 1.30 0.07 0.82 4.19 4.43 0.20
76.18 13.09 0.10 1.17 0.10 1.17 3.92 4.15 0.15
74.92 13.32 0.13 2.05 0.11 0.98 4.51 3.75 0.23
77.15 12.55 0.08 1.28 0.06 0.71 4.00 4.03 0.18
74.85 13.23 0.08 1.83 0.17 1.16 4.54 3.90 0.23

310 trib. to Pohangina River T24/459994

75.70 13.06 0.17 1.77 0.09 0.89 4.27 3.86 0.19 6.73
74.13 13.51 0.25 2.26 0.18 1.31 4.62 3.53 0.21 4.54

311 trib. to Pohangina River T24/459994

74.81 13.35 0.15 2.27 0.16 1.14 4.6 3.31 0.21 4.55
74.39 13.44 0.16 2.4 0.13 1.09 4.85 3.37 0.21 4.86
74.7 13.32 0.2 2.28 0.14 1.14 4.69 3.34 0.18 3.4
74.2 13.59 0.15 2.29 0.12 1.11 4.77 3.54 0.23 6.02
74.37 13.46 0.2 2.45 0.14 1.08 4.73 3.4 0.18 4.96
74.37 13.49 0.16 2.2 0.08 1.16 4.94 3.4 0.21 4.4
74.64 13.4 0.16 2.16 0.12 1.23 4.67 3.41 0.22 4.7
74.69 13.38 0.17 2.21 0.15 1.1 4.7 3.41 0.2 4.32
74.2 13.53 0.14 2.3 0.17 1.09 4.87 3.5 0.19 4.68
74.24 13.41 0.12 2.35 0.11 1.18 4.94 3.45 0.22 4.87
74.46 13.44 0.16 2.29 0.13 1.13 4.78 3.41 0.2 4.68
0.23 0.08 0.03 0.09 0.03 0.05 0.12 0.07 0.02 0.65

312 trib. to Pohangina River T24/459994

75.36 13.11 0.15 1.93 0.07 0.89 4.36 3.93 0.19 4.84
74.58 13.24 0.23 2.19 0.15 1.11 4.55 3.76 0.18 4.01
75.07 13.16 0.16 2.12 0.1 1.02 4.35 3.84 0.18 2.55
74.64 13.31 0.11 2.05 0.15 0.96 4.64 3.98 0.17 4.27
74.66 13.53 0.17 2.2 0.09 1.1 4.53 3.54 0.19 6.37
74.11 13.36 0.2 2.24 0.14 1.18 4.88 3.68 0.21 2.81
74.59 13.34 0.17 2.16 0.15 1.07 4.77 3.55 0.2 4.52
74.72 13.29 0.17 2.13 0.12 1.05 4.58 3.75 0.19 4.2
0.4 0.14 0.04 0.11 0.03 0.1 0.2 0.17 0.01 1.29

77.36 12.34 0.06 1.31 0.06 0.95 3.97 3.85 0.16 4.26
77.74 12.32 0.06 1.12 0.13 0.92 3.56 4.08 0.12 4.69

313 trib. to Leader River, N. Canterbury

77.09 12.29 0.13 1.25 0.15 0.94 3.90 3.97 0.27 7.42
77.39 12.27 0.16 1.35 0.14 1.06 3.81 3.57 0.26 4.15
77.45 12.27 0.16 1.31 0.12 0.93 3.76 3.79 0.22 6.04
77.63 12.24 0.13 1.14 0.12 1.05 3.72 3.73 0.25 4.5
77.76 12.21 0.13 1.09 0.07 0.88 3.90 3.72 0.23 4.99
77.93 12.17 0.12 0.97 0.06 0.81 3.87 3.83 0.23 5.5
77.75 12.24 0.12 1.19 0.09 0.89 3.83 3.66 0.23 4.74
77.88 12.21 0.07 1.15 0.05 0.94 3.79 3.68 0.22 5.76
77.56 12.36 0.08 1.02 0.06 0.75 3.69 4.20 0.29 7.49

77.87 12.31 0.15 0.94 0.06 0.71 3.61 4.08 0.26 4.68
77.51 12.37 0.11 1.07 0.08 0.86 3.70 4.11 0.19 5.37
77.21 12.36 0.15 1.33 0.09 1.00 3.68 3.95 0.23 4.93
77.48 12.20 0.17 1.22 0.13 0.99 3.64 3.91 0.27 4.05
77.51 12.34 0.13 1.05 0.07 0.83 3.72 4.04 0.33 8.33
77.70 12.18 0.09 1.03 0.09 0.80 3.65 4.22 0.25 6.4
77.58 12.31 0.16 1.06 0.09 0.90 3.71 3.98 0.20 6.9
77.58 12.27 0.13 1.13 0.09 0.90 3.75 3.90 0.25 5.70
0.23 0.07 0.03 0.13 0.03 0.10 0.09 0.20 0.03 1.29

314 Leader River, N. Canterbury

77.91 12.2 0.09 1.05 0.12 0.87 3.68 3.82 0.26 4.66
77.51 12.29 0.17 1.21 0.1 1.06 3.79 3.66 0.21 5.3
77.1 12.37 0.21 1.18 0.11 0.99 4.01 3.73 0.3 8.16
77.57 12.29 0.16 1.17 0.12 0.95 3.73 3.79 0.23 4.85
77.72 11.99 0.14 1.28 0.14 1 3.69 3.79 0.26 4.4
77.59 12.26 0.17 1.19 0.1 0.95 3.86 3.65 0.24 6.75
77.7 12.21 0.14 1.26 0.08 0.98 3.64 3.77 0.22 4.74
77.74 12.06 0.14 1.11 0.15 1.1 3.61 3.82 0.27 5.08
77.77 12.16 0.09 1.24 0.09 0.95 3.54 3.91 0.24 4.59
77.57 12.17 0.14 1.2 0.12 0.75 3.58 4.21 0.26 5.28
77.8 12.14 0.12 1.16 0.12 0.78 3.65 4 0.22 5.53
78.09 12.27 0.12 0.99 0.11 0.8 3.68 3.74 0.2 3.8
77.87 12.18 0.1 1.35 0.09 0.99 3.66 3.53 0.22 3.64
77.84 12.29 0.18 1.12 0.16 0.93 3.6 3.67 0.21 3.93
77.7 12.21 0.14 1.18 0.11 0.94 3.7 3.79 0.24 5.05
0.23 0.1 0.03 0.09 0.02 0.1 0.12 0.17 0.03 1.2

315 Oroua River T22/617362

74.76 13.86 0.21 1.82 0.23 1.65 3.84 3.44 0.22 7.79
75.71 13.14 0.27 1.41 0.28 1.57 4.08 3.34 0.2 5.72
75.57 13.38 0.23 1.7 0.21 1.52 3.92 3.24 0.25 5.8
75.77 13.46 0.17 1.62 0.32 1.38 4.07 3.03 0.2 5.54
74.44 13.9 0.39 1.79 0.28 1.56 3.96 3.36 0.31 5.62
74.09 13.96 0.3 2.09 0.3 1.67 4.34 3.02 0.24 8.94
75.75 13.15 0.19 1.41 0.49 1.43 4.14 3.2 0.28 5.7
74.89 13.51 0.3 1.7 0.25 1.5 4.16 3.52 0.17 6.6
74.68 13.86 0.13 1.9 0.21 1.62 4.14 3.29 0.18 6.75
75.07 13.58 0.24 1.72 0.28 1.54 4.07 3.27 0.23 6.5
0.64 0.32 0.08 0.22 0.08 0.1 0.15 0.17 0.05 1.18

75.8 13.4 0.08 1.19 0.08 0.92 3.72 4.67 0.15 5.65

316 Oroua River T22/622363

73.36 14.14 0.22 2.47 0.13 1.3 4.73 3.43 0.24 7.52
73.16 14.25 0.29 2.74 0.16 1.14 4.69 3.42 0.16 7.6
73.24 14.15 0.18 2.65 0.21 1.21 4.67 3.48 0.21 6.63
73.41 13.98 0.19 2.41 0.25 1.29 4.75 3.55 0.17 6.28
73.29 14.14 0.26 2.56 0.14 1.21 4.61 3.55 0.24 7.38
73.16 14.13 0.18 2.4 0.21 1.37 4.88 3.42 0.25 7.83
73.32 14.03 0.23 2.43 0.23 1.15 4.69 3.37 0.53 5.53
73.74 14.07 0.22 2.42 0.17 1.3 4.49 3.41 0.18 7.82
73.49 14.11 0.25 2.03 0.11 1.37 4.54 3.88 0.21 5.34
73.35 14.11 0.23 2.46 0.18 1.26 4.67 3.5 0.24 6.88
0.18 0.08 0.04 0.2 0.05 0.09 0.12 0.16 0.11 0.97

74.43 13.36 0.15 1.97 0.11 0.96 4.21 4.53 0.25 7.74

320 Makirikiri Tuff, Mangatipona Rd S22/099424

74.84 13.54 0.2 2.15 0.14 0.94 4.71 3.3 0.16 6.78
76.66 12.92 0.16 1.46 0.1 0.63 3.75 4.11 0.22 6.47
74.44 13.73 0.2 2.26 0.08 0.94 4.72 3.37 0.26 6.73
75.3 13.33 0.26 1.82 0.11 0.97 4.16 3.92 0.13 7.35
76.45 12.49 0.22 1.62 0.08 0.7 4.36 3.84 0.23 5.09
76.91 12.82 0.15 1.27 0.2 1.13 3.66 3.68 0.17 6.03
75.18 13.32 0.13 1.78 0.1 1 4.33 4.01 0.17 6.06
76.67 13.1 0.12 1.23 0.15 1.28 3.67 3.63 0.18 5.67
74.57 13.53 0.13 2.37 0.09 1.02 4.63 3.43 0.24 7.1
75.67 13.2 0.17 1.77 0.12 0.96 4.22 3.7 0.2 6.36
0.99 0.4 0.05 0.42 0.04 0.2 0.44 0.29 0.04 0.72

323 Makirikiri Tuff, Wanganui River T22/363390

74.94 13.25 0.22 1.97 0.16 0.85 4.88 3.5 0.22 5.99
74.73 13.54 0.16 2.3 0.12 0.98 4.57 3.4 0.21 4.75
74.75 13.14 0.32 2.19 0.18 1.06 4.81 3.35 0.21 4.98
74.55 13.4 0.24 2.14 0.1 1.02 4.61 3.7 0.21 5.29
74.74 13.34 0.23 2.15 0.14 0.98 4.72 3.49 0.21 5.25
0.16 0.17 0.07 0.14 0.04 0.09 0.15 0.15 0.01 0.54

324 Makirikiri Tuff, Wanganui River T22/363390

75.23 13.14 0.22 2.1 0.14 0.99 4.3 3.65 0.23 4.7
74.49 13.52 0.24 2.08 0.1 1.05 4.61 3.7 0.2 3.54
74.56 13.44 0.17 2.26 0.09 0.97 4.59 3.7 0.22 3.96
74.93 13.41 0.27 2.03 0.11 0.87 4.49 3.64 0.23 2.78
75.18 13.12 0.25 1.98 0.11 1.14 4.35 3.61 0.26 3.16
75.16 13.04 0.17 2.19 0.11 1 4.6 3.47 0.26 3.71
75.1 13.06 0.18 2.1 0.08 0.99 4.59 3.71 0.21 3.11
74.44 13.28 0.18 2.27 0.15 1.07 4.63 3.77 0.19 2.96
74.89 13.25 0.21 2.13 0.11 1.01 4.52 3.66 0.22 3.49
0.33 0.19 0.04 0.1 0.02 0.08 0.13 0.09 0.03 0.63

325 Waipuru Ash, Rangitikei River T22/363390

75.61	13.85	0.15	1.27	0.11	0.85	3.46	4.55	0.16	7.3
75.44	13.74	0.17	1.59	0.1	0.85	3.36	4.57	0.18	6.76
75.48	13.62	0.15	1.62	0.16	0.95	3.46	4.39	0.17	6.1
75.56	13.65	0.15	1.46	0.15	0.92	3.65	4.36	0.2	6.26
75.22	13.85	0.12	1.47	0.19	0.9	3.72	4.36	0.17	6.25
75.57	13.57	0.12	1.45	0.07	1.01	3.84	4.16	0.21	5.98
75.63	13.46	0.09	1.52	0.13	0.94	3.39	4.67	0.18	7.87
75.85	13.44	0.15	1.44	0.11	0.96	3.64	4.2	0.22	7.71
75.82	13.54	0.15	1.52	0.09	1	3.68	4.05	0.16	5.94
75.87	13.42	0.15	1.57	0.14	0.93	3.37	4.53	0.16	5.26
75.61	13.61	0.14	1.49	0.12	0.93	3.56	4.38	0.18	6.54
0.2	0.16	0.02	0.1	0.04	0.05	0.17	0.2	0.02	0.85

326 Rangitikei River T22/354355

75.11	13.13	0.17	1.86	0.17	0.94	4.5	3.87	0.25	2.47
74.6	13.28	0.27	1.98	0.22	1.02	4.15	4.13	0.38	2.89
76.25	13.49	0.14	1.52	0.08	0.71	4.28	3.96	0.22	5.24
76.39	12.71	0.11	1.45	0.06	0.66	4.07	4.36	0.2	5.24
74.44	13.83	0.29	1.8	0.15	1.05	4.32	3.84	0.27	4.9
75.96	13.03	0.12	1.47	0.09	0.63	4.3	4.3	0.17	6.09
76.28	12.83	0.1	1.48	0.04	0.69	4.1	4.28	0.2	6.01
75.73	13.23	0.11	1.7	0.09	0.72	4.16	3.99	0.26	7.28
76.34	12.94	0.15	1.4	0.16	0.75	4.35	3.81	0.14	5.47
74.75	13.63	0.2	1.74	0.15	0.9	4.72	3.63	0.26	8.24
75.58	13.21	0.16	1.64	0.12	0.81	4.3	4.02	0.24	5.38
0.78	0.36	0.07	0.2	0.06	0.16	0.2	0.24	0.07	1.75

327 Rangitikei River T22/354355

74.64	13.48	0.18	2.22	0.18	1.12	4.61	3.34	0.21	5.22
74.55	13.62	0.21	2.4	0.18	1.1	4.38	3.39	0.15	3.01
74.42	13.64	0.19	2.09	0.2	1.26	4.65	3.36	0.19	4.87
74.17	13.79	0.17	2.11	0.11	1.24	4.44	3.79	0.19	6.11
74.62	13.39	0.14	2.24	0.2	1.17	4.46	3.64	0.17	4.03
74.75	13.59	0.22	2.15	0.17	1.18	4.44	3.33	0.18	4.38
74.38	13.71	0.15	2	0.17	1.12	4.81	3.5	0.17	5.19
74.56	13.52	0.21	2.22	0.12	1.21	4.46	3.45	0.25	6.33
74.29	13.62	0.17	2.07	0.19	1.37	4.77	3.27	0.26	6.09
74.49	13.6	0.18	2.17	0.17	1.2	4.56	3.45	0.2	5.03
0.18	0.12	0.03	0.12	0.03	0.09	0.16	0.17	0.04	1.09

328 Pakihikura Pumice, Rangitikei River T22/354355

77.37	12.46	0.11	1.32	0.09	1.14	4.04	3.36	0.2	5.11
77.97	12.36	0.14	1.21	0.11	1.24	3.8	2.99	0.2	5.21
77.39	12.64	0.09	1.4	0.13	1.04	4.15	3	0.16	4.8
77.5	12.52	0.11	1.2	0.11	1.13	3.96	3.33	0.14	6.68
77.34	12.63	0.15	1.35	0.1	1.11	3.92	3.32	0.09	5.94
77.01	12.65	0.13	1.23	0.17	1.18	4.05	3.33	0.24	7.13
77.3	12.43	0.18	1.32	0.1	1.11	3.89	3.44	0.23	4.69
77.32	12.43	0.15	1.37	0.08	1.26	4	3.28	0.11	5.55
77.25	12.4	0.14	1.2	0.07	1.36	4.16	3.29	0.13	6.38
77.44	12.58	0.11	1.13	0.11	1.2	4.14	3.19	0.11	5.23
77.39	12.51	0.13	1.27	0.11	1.18	4.01	3.25	0.16	5.67
0.24	0.11	0.03	0.09	0.03	0.09	0.12	0.15	0.05	0.8

329 Rangitikei River T22/354355

74.32	13.49	0.2	2.37	0.16	1.03	4.72	3.54	0.19	3.86
74.26	13.6	0.2	2.25	0.19	1.13	4.9	3.31	0.18	4.9
74.05	13.47	0.22	2.27	0.17	1.07	4.88	3.65	0.21	4.78
74.29	13.56	0.22	2.06	0.2	1.12	4.74	3.6	0.22	3.89
74.67	13.48	0.24	2.17	0.15	1.11	4.45	3.56	0.17	5.92
74.3	13.51	0.16	2.39	0.19	1.19	4.74	3.31	0.21	5.49
74.49	13.63	0.18	2.11	0.16	1.1	4.8	3.3	0.23	5.26
74.01	13.82	0.24	2.17	0.19	1.11	4.71	3.51	0.23	5.7
74.3	13.57	0.21	2.22	0.17	1.11	4.74	3.47	0.21	4.98
0.21	0.12	0.03	0.12	0.02	0.04	0.14	0.14	0.02	0.78
75.6	13.14	0.17	1.8	0.15	0.94	4.33	3.6	0.26	6.26
75.8	13.27	0.18	1.65	0.13	0.87	4.53	3.68	0	6.19

330 Rangitikei River T22/354355

74.68	13.3	0.21	2.11	0.14	0.97	4.69	3.75	0.17	4.28
74.99	13.47	0.11	1.79	0.07	0.98	4.57	3.82	0.19	6.51
74.9	13.11	0.17	1.95	0.13	1	4.87	3.74	0.15	4.4
74.54	13.05	0.22	2.26	0.19	1.11	4.78	3.68	0.18	4.41
74.74	13.33	0.17	1.98	0.13	1.06	4.69	3.72	0.22	4.33
74.83	13.13	0.1	2.23	0.06	1.08	4.88	3.55	0.15	3.53
74.8	13.27	0.15	1.98	0.2	1.06	4.86	3.51	0.16	5.23
75.47	13.03	0.2	1.96	0.05	0.95	4.82	3.29	0.24	3.76
74.87	13.21	0.16	2.03	0.12	1.03	4.77	3.63	0.18	4.56
0.28	0.15	0.04	0.16	0.06	0.06	0.11	0.17	0.03	0.94
74.7	13.4	0.24	2.34	0.18	1.27	4.54	3.13	0.2	3.82

331 Pakihikura Sm T22/359355

76.64	12.15	0.09	1.68	0.08	0.66	4.11	4.4	0.2	4.68
76.11	12.75	0.14	1.92	0.11	0.97	4.22	3.58	0.22	6.53
75.92	12.69	0.21	2.02	0.08	0.72	3.72	4.47	0.19	3.93

75.42	12.95	0.24	1.98	0.14	1	4.38	3.7	0.2	4.05
75.82	13.01	0.07	1.87	0.12	1.05	4.37	3.56	0.14	5.72
76.32	12.86	0.28	1.87	0.1	0.99	4.26	3.2	0.18	5.86
75.58	12.85	0.18	1.9	0.12	1.04	4.49	3.68	0.16	3.26
77	12.21	0.15	1.61	0.1	0.7	4.09	3.94	0.21	4.02
76.1	12.69	0.17	1.86	0.11	0.89	4.2	3.82	0.19	4.76
0.53	0.33	0.07	0.14	0.02	0.17	0.24	0.43	0.03	1.15

333 Mangatewaiiti Sm U23/810172

77.76	12.1	0.2	1	0.13	0.84	3.78	3.93	0.26	4.13
77.92	11.93	0.15	0.89	0.17	0.83	3.8	4.11	0.2	3.5
77.39	11.97	0.16	1.22	0.2	1.14	4.16	3.51	0.26	4.92
77.11	12.45	0.11	1.09	0.13	0.83	4.07	4	0.21	4.08
78.01	11.91	0.1	1.15	0.11	0.82	3.84	3.85	0.22	3.58
77.43	12.35	0.19	1.04	0.13	0.8	3.79	4.11	0.18	4.44
77.06	12.54	0.16	1.4	0.08	1.1	3.65	3.79	0.2	2.42
76.59	12.81	0.28	1.24	0.12	0.97	3.81	3.89	0.3	3.77
76.46	13.03	0.17	1.34	0.18	1.09	3.73	3.77	0.23	5.09
77.3	12.34	0.17	1.15	0.14	0.93	3.85	3.89	0.23	3.99
0.55	0.4	0.05	0.16	0.04	0.14	0.16	0.19	0.04	0.81
75.09	13.56	0.23	1.58	0.16	1.16	4.59	3.39	0.22	5.7

334 Mangatewaiiti Sm U23/808172

77.55	12.39	0.11	1.32	0.19	1.07	3.75	3.46	0.17	5.26
76.73	13.56	0.19	0.87	0.07	0.86	3.48	4.02	0.22	4.42
77.68	12	0.19	1.04	0.08	0.88	3.56	4.35	0.23	7.06
76.45	13.39	0.13	1.08	0.15	1.08	3.64	3.92	0.16	4.58
77.77	12.13	0.17	1.09	0.15	1.11	3.72	3.68	0.18	5.16
76.89	12.64	0.23	1.28	0.15	1.09	3.78	3.72	0.23	3.17
76.93	12.53	0.22	1.39	0.12	1	3.93	3.64	0.26	5.1
77.14	12.46	0.14	1.38	0.2	1.01	4.12	3.36	0.19	5.72
77.37	12.16	0.27	1.2	0.19	1.07	3.63	4	0.14	6.14
77.55	12.53	0.13	1.1	0.19	1.08	3.7	3.52	0.21	3.44
77.21	12.58	0.18	1.17	0.15	1.02	3.73	3.77	0.2	5.01
0.45	0.52	0.05	0.17	0.05	0.09	0.18	0.3	0.04	1.18

335 Leader River, N. Canterbury

77.67	12.67	0.24	0.99	0.07	1.06	3.6	3.47	0.25	4.84
78.28	11.91	0.13	1.2	0.12	0.99	3.62	3.5	0.25	6.2
78.24	11.93	0.08	1.04	0.12	0.82	3.5	3.88	0.38	4.81
77.68	12.58	0.21	1.17	0.08	0.94	3.76	3.38	0.2	5.23
78.07	11.75	0.16	1.23	0.12	1.02	4.01	3.34	0.29	7.07
77.57	12.56	0.11	1.19	0.1	1.05	3.89	3.32	0.2	6.44
77.45	11.88	0.21	1.2	0.09	0.73	3.94	4.26	0.23	4.91
77.84	12.11	0.19	1.26	0.14	0.88	3.89	3.47	0.25	4.25
76.72	13.02	0.21	1.1	0.12	1.07	3.82	3.67	0.25	3.87
77.72	12.27	0.17	1.15	0.11	0.95	3.78	3.59	0.26	5.29
0.48	0.45	0.05	0.09	0.02	0.12	0.17	0.31	0.05	1.06

336 Duff Rd U21/011644

77.48	12.56	0.07	1.14	0.11	1.25	3.74	3.49	0.2	5.16
77.76	12.64	0.16	1.34	0.11	1.13	3.6	3.1	0.16	5.21
77.16	12.82	0.1	1.4	0.07	1.18	3.46	3.62	0.19	6.11
76.95	12.64	0.18	1.38	0.07	1.23	3.84	3.42	0.31	5.96
76.88	12.67	0.07	1.55	0.15	1.33	3.85	3.32	0.19	6.66
76.39	12.93	0.24	1.54	0.08	1.26	3.91	3.44	0.19	7.37
76.82	12.59	0.19	1.53	0.14	1.28	4.08	3.21	0.15	5.64
77.09	12.68	0.15	1.42	0.11	1.24	3.79	3.34	0.19	5.67
0.4	0.12	0.06	0.13	0.03	0.06	0.18	0.18	0.05	1.08

Appendix 2

TRACE ELEMENT ANALYSES OF EARLY PLEISTOCENE TEPHRAS

Samples of ash or pumice were crushed and wet sieved to obtain the 60-250 μ size fraction. Glass was purified with the use of a frantz magnetic separator. Powders for analytical purposes were obtained by milling in a TEMA tungsten carbide swing mill for 60 s. Four g of powder was pressed into boric acid backed pellets and analysed using a Philips PW1404 automatic sequential x-ray spectrometer at the Analytical Facility of Victoria University. The procedure, operating conditions and detection limits are described by Palmer (1990). Analyses in ppm.

ID	Sc	V	Cr	Ba	La	Ce	Ni	Cu	Zn	Zr	Nb	Ga	Pb	Rb	Sr	Th	U	Y	As
128	3	8	0	763	27	53	0	14	45	194	9	15	19	130	76	13	4	32	7
130	8	8	0	678	26	54	0	15	56	258	9	15	17	104	100	11	3	37	4
131	7	5	0	770	32	63	1	12	52	263	11	16	25	159	67	17	5	40	12
134	2	9	0	614	22	39	5	16	79	115	6	15	17	101	161	11	3	15	3
136	6	8	0	770	28	57	0	10	70	284	11	17	20	118	102	12	3	37	6
137	3	3	0	766	23	39	0	4	38	110	5	15	17	119	87	12	3	20	5
138	8	9	1	889	28	60	1	10	67	272	12	16	21	120	90	14	4	38	6
139	10	18	4	833	27	55	4	15	65	246	10	16	20	116	120	12	3	35	5
140	7	6	0	776	29	62	0	11	66	307	11	16	20	118	94	12	3	40	6
141	8	5	0	859	29	61	0	15	69	303	11	16	21	120	96	13	3	40	6
148	6	9	1	790	23	44	1	16	43	113	6	14	18	119	91	11	3	20	4
151	5	9	0	746	26	50	3	12	46	180	8	15	19	119	93	13	3	27	5
152	8	5	0	786	30	59	0	19	67	303	11	18	20	120	89	13	4	40	6
154	8	19	5	653	27	55	2	9	56	216	10	16	22	135	100	13	4	30	5
158	7	9	0	742	33	61	0	16	56	275	10	16	24	143	92	16	4	38	11
159	9	17	4	708	27	54	2	21	52	276	10	18	20	122	138	12	4	33	13
160	7	8	0	745	30	61	1	11	69	287	11	16	20	122	85	13	3	39	8
161	7	20	7	681	24	48	4	17	60	227	10	16	17	113	154	12	3	27	7
165	5	7	0	802	24	41	0	14	39	107	5	14	17	119	92	12	3	18	5
166	10	7	0	786	29	62	0	12	72	283	10	17	20	116	95	12	4	40	6
173	4	9	2	714	27	50	3	22	40	152	8	12	18	134	84	14	3	25	7
180	7	6	0	673	27	55	1	9	58	219	10	14	20	111	80	12	3	34	5
182	4	5	0	715	21	39	2	7	45	116	7	14	17	116	86	11	2	19	5
183	9	9	2	723	27	56	0	11	72	286	11	15	18	109	98	11	3	38	7
185	4	19	5	718	25	44	1	8	45	118	9	14	18	129	81	13	4	24	5
185	4	6	0	730	26	49	1	11	38	141	8	14	16	138	63	14	3	23	5
192	8	22	9	666	21	43	3	15	56	199	8	16	16	99	167	9	2	26	2
195	3	8	4	729	26	45	0	12	65	117	8	13	19	131	67	13	3	23	5
196	8	7	1	682	26	54	0	13	63	213	11	16	19	117	88	12	4	34	4
230	4	6	0	729	26	47	0	6	44	130	8	13	19	126	71	14	3	24	4
231	3	7	1	738	26	46	0	6	44	120	8	14	19	134	63	14	4	24	5
232	4	10	1	734	25	45	0	6	45	129	8	13	19	130	66	13	3	23	5
233	3	6	0	746	26	47	0	4	43	115	7	14	17	132	64	14	4	24	6
234	7	8	1	705	26	54	0	7	55	275	11	15	20	119	81	12	3	31	4
239	2	7	0	765	26	49	0	16	40	117	8	14	19	138	69	14	3	25	6
240	9	7	0	712	24	52	0	5	48	216	10	13	21	116	92	12	3	31	4
241	3	7	2	739	25	49	1	8	43	119	9	13	18	131	68	13	3	23	4
242	7	6	0	694	26	53	0	7	56	213	11	14	19	115	75	12	3	34	4
243	10	17	1	749	29	57	0	8	67	364	10	17	20	120	87	12	3	36	6
245	5	6	1	734	22	41	0	8	39	107	6	13	16	118	85	11	3	18	5
247	9	7	0	700	28	49	0	9	63	239	9	15	19	105	103	11	3	35	6
249	2	7	0	733	25	48	0	6	43	123	9	14	18	130	67	13	4	23	5
250	4	5	0	734	26	48	0	4	43	125	9	14	18	136	64	13	4	24	5
252	9	5	2	729	31	61	0	15	62	222	12	15	21	110	69	12	4	37	5
257	4	6	0	748	25	49	0	4	41	119	8	14	18	137	64	15	3	26	5
293	5	4	0	741	21	39	1	5	37	112	5	13	16	118	88	12	3	19	6
Rewa	8	11	2	655	25	49	1	8	57	226	9	15	17	100	142	10	4	30	5
Pot a	4	7	0	760	28	51	0	14	37	154	8	15	17	135	78	13	4	24	5
Pot b	2	6	0	742	25	48	0	6	39	131	8	13	19	127	72	13	3	24	6

Sample ID as in Appendix 1
Rewa= Rewa Pumice, Rewa Hill; Pot a= Potaka Tephra top and Pot b= Potaka Tephra base, Rewa Hill.

Appendix 3

FE-TI OXIDE ANALYSES OF EARLY PLEISTOCENE TEPHRAS

EMA method as in Appendix 1, except for a 12 nA current at 15 kV and 2 μ beam diameter. Analyses represent individual crystals. Mean and standard deviation in bold.
total Fe as FeO, * analytical total, † total for Fe expressed as Fe_2O_3 and FeO, ulvo = ulvospinel

SiO_2	Al_2O_3	TiO_2	FeO#	MnO	MgO	CaO	total*	Fe_2O_3	FeO	total†	ulvo
128											
0.12	1.42	12.18	79.84	0.38	0.66	0	94.6	43.13	41.04	98.92	0.35
0.08	1.3	12.45	80.91	0.53	0.52	0	95.8	43.63	41.67	100.2	0.35
0.07	1.25	12.11	79.98	0.31	0.64	0	94.36	43.42	40.91	98.71	0.35
0.06	1.31	12.29	78.09	0.37	0.59	0.02	92.73	41.77	40.51	96.91	0.36
0.14	1.42	11.63	77.8	0.34	0.67	0.03	92.02	42.32	39.72	96.27	0.35
0.07	1.35	12.61	80.26	0.42	0.62	0	95.33	42.97	41.6	99.64	0.36
0.08	1.31	12.11	79.18	0.37	0.7	0	93.75	42.9	40.57	98.05	0.35
0.08	1.49	12.15	80.89	0.38	0.76	0	95.73	44.1	41.2	100.2	0.35
0.09	**1.36**	**12.19**	**79.62**	**0.39**	**0.65**	**0.01**	**94.29**	**43.03**	**40.90**	**98.60**	**0.35**
0.03	**0.08**	**0.29**	**1.18**	**0.07**	**0.07**	**0.01**	**1.38**	**0.73**	**0.64**	**1.45**	**0.00**
131											
0.16	1.37	18.09	75.24	0.64	0.59	0.19	96.27	32.07	46.38	99.48	0.52
0.14	1.51	18.55	75.53	0.45	0.59	0	96.78	31.32	47.35	99.91	0.53
0.14	1.3	18.24	75.26	0.62	0.49	0.03	96.08	31.67	46.76	99.25	0.52

0.07	1.47	11.57	80.83	0.41	0.67	0	95.01	44.78	40.54	99.52	0.33
0.07	1.43	11.56	78.68	0.42	0.52	0	92.69	43.02	39.97	96.99	0.34
0.13	1.47	11.99	80.27	0.33	0.63	0	94.83	43.59	41.05	99.2	0.35
0.06	1.46	11.52	80.03	0.4	0.64	0	94.11	44.22	40.24	98.54	0.33
0.12	1.51	11.88	80.07	0.35	0.62	0	94.55	43.57	40.86	98.92	0.34
0.18	1.53	11.96	80.09	0.41	0.63	0	94.81	43.42	41.02	99.15	0.35
0.09	**1.46**	**11.74**	**80.22**	**0.42**	**0.62**	**0.00**	**94.56**	**44.00**	**40.63**	**98.97**	**0.34**
0.05	**0.04**	**0.20**	**0.73**	**0.07**	**0.05**	**0.00**	**0.82**	**0.71**	**0.37**	**0.87**	**0.01**

231

0.12	1.23	9.92	81.24	0.79	0.42	0.43	94.14	47.67	38.34	98.93	0.29
0.19	1.43	10.9	79.92	0.55	0.61	0	93.58	44.82	39.59	98.09	0.32
0.14	1.48	10.66	79.82	0.64	0.63	0.02	93.39	45.24	39.11	97.92	
0.14	1.38	10.54	81.22	0.57	0.54	0.02	94.42	46.32	39.54	99.05	0.31
0.17	1.41	10.53	81.1	0.49	0.52	0.06	94.26	46.13	39.59	98.9	0.31
0.11	1.51	11.06	80.65	0.59	0.64	0.01	94.57	45.32	39.87	99.1	0.32
0.17	1.31	9.99	81.61	0.8	0.38	0.03	94.27	47.29	39.06	99.04	0.29
0.15	**1.39**	**10.51**	**80.79**	**0.63**	**0.53**	**0.08**	**94.09**	**46.11**	**39.30**	**98.72**	**0.31**
0.03	**0.10**	**0.43**	**0.69**	**0.12**	**0.10**	**0.15**	**0.44**	**1.07**	**0.51**	**0.49**	**0.01**

240

0.11	1.41	14.31	78.42	0.48	0.69	0	95.43	39.39	42.92	99.39	0.41
0.14	1.49	14.75	78.72	0.57	0.65	0.07	96.39	39	43.63	100.3	0.42
0.08	1.59	15.61	75.5	0.5	0.8	0.06	94.13	35.64	43.43	97.7	0.45
0.1	1.45	14.62	77.81	0.47	0.74	0	95.2	38.56	43.11	99.05	0.42
0.07	1.65	15.42	77.64	0.52	0.8	0.02	96.1	37.46	43.93	99.86	0.44
0.1	1.47	14.49	77.12	0.47	0.75	0.04	94.44	38.27	42.69	98.27	0.42
0.1	1.65	15.31	78.05	0.51	0.83	0	96.45	37.87	43.98	100.2	0.43
0.05	1.58	15.51	77.82	0.47	0.88	0	96.31	37.59	44	100.1	0.44
0.08	1.57	14.78	77.83	0.49	0.77	0.02	95.55	38.39	43.29	99.41	0.42
0.09	**1.54**	**14.98**	**77.66**	**0.50**	**0.77**	**0.02**	**95.56**	**38.02**	**43.44**	**99.37**	**0.43**
0.03	**0.09**	**0.49**	**0.93**	**0.03**	**0.07**	**0.03**	**0.85**	**1.09**	**0.48**	**0.90**	**0.01**

249

0.07	1.41	11.59	80.13	0.47	0.59	0	94.28	44.2	40.36	98.69	0.33
0.05	1.35	11.09	80.56	0.42	0.47	0	93.96	45.05	40.02	98.45	0.32
0.07	1.52	12.25	80.39	0.53	0.64	0.02	95.41	43.58	41.17	99.79	0.35
0.08	1.39	11.7	80.04	0.42	0.63	0.04	94.3	44.03	40.42	98.71	0.34
0.12	1.54	12.03	80.87	0.61	0.59	0	95.75	44.11	41.18	100.2	0.34
0.11	1.44	12.25	80.92	0.35	0.53	0	95.6	43.65	41.65	99.97	0.35
0.1	1.47	11.48	80.4	0.44	0.6	0	94.49	44.45	44.4	98.94	0.33
0	1.4	11.89	78.71	0.41	0.52	0.02	92.95	42.76	40.24	97.23	0.35
0.08	**1.44**	**11.79**	**80.25**	**0.46**	**0.57**	**0.01**	**94.59**	**43.98**	**41.18**	**99.00**	**0.34**
0.04	**0.07**	**0.40**	**0.70**	**0.08**	**0.06**	**0.02**	**0.95**	**0.68**	**1.42**	**0.97**	**0.01**

250

0.14	1.46	12.17	80.33	0.38	0.62	0	95.11	43.39	41.28	99.45	0.35
0.04	1.34	11.26	79.95	0.34	0.49	0	93.4	44.36	40.03	97.87	0.33
0.09	1.37	11.71	79.66	0.59	0.37	0.04	93.84	43.51	40.51	98.19	0.34
0.09	1.36	10.89	81.15	0.41	0.49	0.03	94.41	45.73	40.01	99	0.32
0.07	1.38	11.63	79.34	0.56	0.61	0.02	93.59	43.69	40.03	97.99	0.34
0.16	1.44	11.89	79.21	0.43	0.68	0	93.81	43.02	40.5	98.11	0.35
0.08	1.27	10.59	81.78	0.64	0.36	0	94.73	46.6	39.85	99.37	0.31
0.13	1.26	10.61	80.99	0.52	0.41	0	93.91	45.91	39.68	98.52	0.31
0.07	1.49	12.2	78.79	0.47	0.63	0.02	93.68	42.42	40.62	97.92	0.35
0.16	1.5	11.67	80.63	0.42	0.74	0	95.13	44.41	40.67	99.67	0.34
0.10	**1.39**	**11.46**	**80.18**	**0.48**	**0.54**	**0.01**	**94.16**	**44.30**	**40.32**	**98.61**	**0.33**
0.04	**0.08**	**0.60**	**0.96**	**0.10**	**0.13**	**0.02**	**0.64**	**1.37**	**0.48**	**0.70**	**0.02**

257

0.14	1.44	10.98	81.06	0.64	0.53	0.02	94.79	45.63	40.01	99.38	0.32
0.13	1.44	10.51	81.29	0.58	0.59	0	94.54	46.46	39.49	99.19	0.3
0.11	1.58	12	79.57	0.6	0.69	0	94.55	43.34	40.61	98.9	0.35
0.08	1.49	11.36	80.61	0.55	0.64	0	94.73	44.92	40.19	99.23	0.33
0.13	1.45	10.49	80.76	0.66	0.55	0	94.03	46.09	39.29	98.66	0.31
0.09	1.64	12.19	79.56	0.54	0.73	0.1	94.85	43.16	40.74	99.18	0.35
0.07	1.37	11.02	80.76	0.59	0.43	0	94.25	45.32	39.79	98.79	0.32
0.11	**1.49**	**11.22**	**80.52**	**0.59**	**0.59**	**0.02**	**94.53**	**44.99**	**40.02**	**99.05**	**0.33**
0.03	**0.09**	**0.67**	**0.69**	**0.04**	**0.10**	**0.04**	**0.30**	**1.29**	**0.54**	**0.26**	**0.02**

262

0.02	1.58	8.84	81.41	0.46	0.81	0	93.12	49.09	37.24	98.04	0.25

0.04	1.48	8.57	81.89	0.53	0.77	0	93.28	49.82	37.06	98.27	0.25
0.16	1.44	8.78	81.25	0.6	0.85	0	93.09	49.04	37.13	97.99	0.26
0.09	1.51	8.9	82.46	0.52	0.85	0.01	94.33	49.8	37.65	99.32	0.26
0.16	1.52	8.55	81.54	0.52	0.81	0	93.11	49.4	37.09	98.05	0.25
0.13	1.51	8.31	82.17	0.67	0.8	0	93.58	50.35	36.87	98.63	0.24
0.11	1.58	10.06	80.91	0.51	0.72	0.06	93.94	46.91	38.7	98.65	0.29
0.09	1.49	8.98	81.52	0.44	0.79	0.02	93.32	48.9	37.52	98.22	0.26
0.11	1.44	8.58	81.61	0.45	0.82	0	93.02	49.51	37.06	97.97	0.25
0.08	1.43	8.58	81.92	0.43	0.83	0	93.26	49.79	37.12	98.26	0.25
0.10	**1.50**	**8.82**	**81.67**	**0.51**	**0.81**	**0.01**	**93.41**	**49.26**	**37.34**	**98.34**	**0.26**
0.05	**0.05**	**0.48**	**0.45**	**0.08**	**0.04**	**0.02**	**0.43**	**0.94**	**0.53**	**0.42**	**0.01**

272

0.12	1.32	10.79	80.8	0.49	0.62	0.01	94.14	45.78	39.6	98.72	0.31
0.07	1.37	11.35	79.3	0.41	0.57	0.02	93.08	43.87	39.83	97.69	0.33
0.07	1.37	11.01	80.27	0.51	0.62	0.01	93.85	45.17	39.63	98.37	0.32
0.05	1.35	11.24	79.33	0.46	0.65	0	93.09	44.21	39.55	97.51	0.33
0	1.38	11.01	80.6	0.48	0.57	0	94.04	45.44	39.71	98.59	0.32
0.04	1.33	11.2	79.74	0.47	0.77	0	93.55	44.76	39.47	98.03	0.32
0.12	1.5	11.34	80.91	0.54	0.71	0	95.13	45.18	40.25	99.65	0.33
0.18	1.3	11.43	79.35	0.4	0.57	0	93.23	43.62	40.11	97.6	0.34
0.08	**1.37**	**11.17**	**80.04**	**0.47**	**0.64**	**0.01**	**93.76**	**44.75**	**39.77**	**98.27**	**0.33**
0.06	**0.06**	**0.22**	**0.69**	**0.05**	**0.07**	**0.01**	**0.69**	**0.78**	**0.28**	**0.72**	**0.01**

277

0.05	1.31	18.29	74.34	0.75	0.51	0	95.34	31.24	46.33	98.48	0.52
0.11	1.28	18.33	74.96	0.77	0.52	0	95.98	31.5	46.62	99.14	0.52
0.16	1.35	17.66	75.2	0.8	0.46	0	95.63	32.4	46.64	98.88	0.51
0.14	1.33	18.7	74.64	0.82	0.54	0	96.18	30.77	46.95	99.25	0.53
0.12	1.34	18.63	75.55	0.83	0.54	0.03	97.02	31.6	47.11	100.2	0.53
0.08	1.38	18.34	72.33	0.77	0.55	0	93.45	29.59	45.7	96.42	0.54
0.14	1.57	17.98	74.08	0.59	0.55	0	94.9	31.02	46.16	98.01	0.52
0.08	1.36	18.44	75.45	0.87	0.51	0.01	96.71	31.8	46.83	99.9	0.52
0.11	**1.37**	**18.30**	**74.57**	**0.78**	**0.52**	**0.01**	**95.65**	**31.24**	**46.54**	**98.79**	**0.52**
0.04	**0.09**	**0.34**	**1.04**	**0.08**	**0.03**	**0.01**	**1.13**	**0.83**	**0.46**	**1.19**	**0.01**

0.06	2.36	13.1	76.76	0.52	2.02	0	94.81	41.13	39.75	98.94	0.37

279

0.21	1.33	18.53	72.7	0.79	0.5	0	94.06	29.36	46.28	97	0.54
0.06	1.34	18.39	73.49	0.73	0.43	0	94.44	30.25	46.27	97.47	0.53
0.12	1.33	18.58	74.63	0.82	0.41	0	95.89	30.79	46.93	98.97	0.53
0.29	1.34	18.82	72.68	0.79	0.47	0	94.41	28.77	46.79	97.27	0.55
0.17	**1.34**	**18.58**	**73.38**	**0.78**	**0.45**	**0.00**	**94.70**	**29.79**	**46.57**	**97.68**	**0.54**
0.10	**0.01**	**0.18**	**0.92**	**0.04**	**0.04**	**0.00**	**0.81**	**0.90**	**0.34**	**0.88**	**0.01**

0.16	2.03	12.91	77.14	0.29	1.01	0	93.53	40.16	41	97.55	0.38

282

0.1	1.54	10.11	80.18	0.41	0.58	0	92.93	46.03	38.77	97.53	0.3
0.14	1.42	10.56	80.49	0.41	0.56	0.03	93.61	45.65	39.41	98.18	0.31
0.09	1.62	11.11	80.25	0.51	0.63	0	94.21	44.86	39.88	98.71	0.32
0.07	1.35	10.12	80.92	0.49	0.56	0.04	93.54	46.78	38.82	98.24	0.29
0.07	1.5	10.93	79.07	0.52	0.67	0	92.77	44.39	39.13	97.21	0.32
0.1	1.45	10.61	81.49	0.41	0.52	0	94.57	46.3	39.83	99.22	0.31
0.12	1.43	10.62	80	0.51	0.64	0.02	93.34	45.41	39.14	97.89	0.31
0.08	1.47	10.63	80.44	0.44	0.64	0.02	93.71	45.72	39.3	98.3	0.31
0.1	1.5	10.98	80.55	0.4	0.64	0.04	94.21	45.28	39.8	98.76	0.32
0.04	1.38	10.68	80.31	0.53	0.55	0.04	93.53	45.63	39.25	98.11	0.31
0.09	**1.47**	**10.64**	**80.37**	**0.46**	**0.60**	**0.02**	**93.64**	**45.61**	**39.33**	**98.22**	**0.31**
0.03	**0.08**	**0.33**	**0.62**	**0.05**	**0.05**	**0.02**	**0.57**	**0.69**	**0.40**	**0.59**	**0.01**

289

0.07	1.58	11.02	78.99	0.48	0.6	0.01	92.75	44.03	39.38	97.16	0.32
0.12	1.33	10.41	80.63	0.53	0.52	0	93.55	46.04	39.2	98.15	0.31
0.1	1.55	10.88	79.78	0.59	0.61	0.02	93.53	44.89	39.39	98.03	0.32
0.09	1.66	11.89	77.04	0.55	0.73	0.04	92	41.62	39.59	96.17	0.35
0.11	1.5	10.68	80.39	0.51	0.64	0.03	93.86	45.61	39.35	98.43	0.31
0.07	1.33	10.23	81.4	0.61	0.4	0.01	94.06	46.85	39.25	98.73	0.3
0.05	1.6	10.75	79.86	0.44	0.57	0.01	93.28	45.01	39.36	97.77	0.31
0.02	1.36	10.13	80.72	0.44	0.48	0	93.15	46.53	38.86	97.61	0.29
0.08	**1.49**	**10.75**	**79.85**	**0.52**	**0.57**	**0.02**	**93.27**	**45.07**	**39.30**	**97.76**	**0.31**

0.03	0.13	0.56	1.35	0.06	0.10	0.01	0.66	1.67	0.21	0.80	0.02

291

0.18	1.95	10.88	79.04	0.35	1.03	0	93.43	44.35	39.14	97.87	0.32
0.16	1.87	10.64	79.98	0.53	1	0	94.18	45.54	39.01	98.74	0.31
0.17	1.81	10.52	79.67	0.5	0.98	0	93.64	45.43	38.79	98.2	0.31
0.27	1.74	10.47	79.32	0.49	1.01	0.04	93.33	45.17	38.68	97.87	0.31
0.20	1.84	10.63	79.50	0.47	1.01	0.01	93.65	45.12	38.91	98.17	0.31
0.05	0.09	0.18	0.41	0.08	0.02	0.02	0.38	0.54	0.21	0.41	0.01

293

0.17	1.57	13.4	79.05	0.42	0.32	0	94.95	40.33	42.76	98.97	0.39
0.14	1.62	13.6	77.2	0.42	0.29	0	93.26	38.68	42.4	97.15	0.4
0.1	1.57	12.86	76.93	0.48	0.34	0.04	92.33	39.71	41.2	96.3	0.38
0.17	1.72	13.8	76.01	0.41	0.36	0	92.47	37.51	42.26	96.23	0.41
0.11	1.61	11.52	79.74	0.39	0.46	0.01	93.86	43.6	40.52	98.21	0.34
0.13	1.56	13.23	77.83	0.41	0.38	0	93.54	39.79	42.03	97.52	0.38
0.12	1.46	13.29	78.23	0.43	0.34	0.03	93.89	40.04	42.17	97.93	0.39
0.14	1.61	13.11	78.61	0.41	0.36	0.04	94.27	40.51	42.16	98.34	0.38
0.13	1.46	8.35	81.63	0.52	0.19	0	92.3	49.01	37.53	97.2	0.25
0.13	1.58	12.57	78.36	0.43	0.34	0.01	93.43	41.02	41.45	97.54	0.37
0.02	0.08	1.71	1.67	0.04	0.07	0.02	0.93	3.41	1.62	0.92	0.05

295

0.09	1.54	11.06	80.07	0.65	0.51	0	93.92	44.78	39.77	98.41	0.32
0.08	1.42	10.61	81.54	0.69	0.56	0	94.91	46.65	39.57	99.57	0.3
0.17	1.42	10.68	80.97	0.62	0.39	0	94.24	45.7	39.85	98.83	0.31
0.1	1.41	10.51	81.28	0.58	0.51	0	94.39	46.41	39.52	99.04	0.3
0.26	1.33	10.59	80.34	0.63	0.49	0.05	93.68	45.42	39.47	98.24	0.32
0.18	1.57	10.86	80.96	0.63	0.58	0	94.78	45.61	39.92	99.35	0.32
0.11	1.43	10.37	81.28	0.73	0.48	0	94.4	46.64	39.31	99.07	0.3
0.11	1.45	10.7	82.27	0.64	0.5	0	95.66	46.88	40.09	100.4	0.31
0.16	1.49	10.01	81.1	0.76	0.56	0	94.07	47	38.81	98.79	0.29
0.16	1.6	10.67	80.57	0.58	0.47	0.01	94.06	45.41	39.71	98.6	0.31
0.14	1.47	10.61	81.04	0.65	0.51	0.01	94.41	46.05	39.60	99.03	0.31
0.05	0.08	0.28	0.63	0.06	0.05	0.02	0.58	0.76	0.36	0.62	0.01

Potaka Tephra, Rewa Hill

0.12	1.42	10.52	81.24	0.47	0.55	0	94.31	46.3	39.58	98.96	0.31
0.06	1.5	10.29	80.68	0.5	0.59	0.02	93.64	46.35	38.98	98.28	0.3
0.09	1.42	10.68	79.69	0.31	0.58	0	92.77	44.91	39.28	97.27	0.31
0.07	1.48	11.26	79.11	0.45	0.63	0	93	43.88	39.63	97.4	0.33
0.2	1.45	10.6	80.62	0.42	0.55	0	93.85	45.54	39.65	98.4	0.31
0.1	1.46	10.31	79.01	0.43	0.61	0	91.91	44.99	38.53	96.43	0.31
0.12	1.38	10.77	79.07	0.4	0.61	0.03	92.39	44.43	39.09	96.83	0.32
0.14	1.46	10.68	81.22	0.39	0.53	0	94.41	45.93	39.89	99.02	0.31
0.12	1.52	10.97	79.89	0.38	0.63	0	93.51	44.68	39.68	97.99	0.32

Potaka ignimbrite, Cape Kidnappers

0.14	1.42	10.65	80.98	0.57	0.64	0	94.41	46.08	39.52	99.03	0.31
0.06	1.37	10.56	81.36	0.62	0.53	0	94.5	46.55	39.47	99.16	0.3
0.26	1.5	10.5	80.73	0.66	0.61	0	94.25	45.88	39.86	98.86	0.31
0.13	1.41	10.39	81.6	0.44	0.61	0.02	94.6	46.8	39.49	99.29	0.3
0.14	1.37	10.25	82.21	0.62	0.52	0	95.11	47.44	39.52	99.86	0.31
0.21	1.4	10.52	81.12	0.52	0.63	0.02	94.42	46.22	39.53	99.05	0.31
0.09	1.49	10.75	80.37	0.64	0.61	0	93.94	45.57	39.37	98.52	0.31
0.1	1.45	10.49	80.73	0.58	0.58	0	93.93	46.1	39.25	98.55	0.31
0.18	1.4	10.96	80.51	0.48	0.55	0.02	94.1	45.1	39.93	98.62	0.32
0.13	1.47	10.23	80.82	0.46	0.6	0.96	94.68	47.29	38.27	99.42	0.3
0.09	1.54	10.74	79.56	0.43	0.62	0	92.99	44.81	39.24	97.48	0.31
0.07	1.38	10.14	82.2	0.43	0.61	0.04	94.87	47.72	39.26	99.67	0.29
0.1	1.45	10.29	80.45	0.55	0.63	0.01	93.47	46.2	38.88	98.1	0.3
0.14	1.34	10.59	81.16	0.56	0.53	0.02	94.34	46.21	39.97	98.97	0.31
0.16	1.26	9.32	82.07	0.72	0.4	0	93.92	48.53	38.41	98.78	0.27
0.09	1.38	10	80.56	0.61	0.54	0	93.16	46.69	38.55	97.83	0.29
0.14	1.25	10.03	81.49	0.75	0.38	0.02	94.06	47.19	39.02	98.79	0.29
0.09	1.47	10.57	81.51	0.64	0.5	0.02	94.8	46.53	39.65	99.47	0.3
0.17	1.48	10.56	81.35	0.61	0.61	0	94.78	46.39	39.61	99.43	0.31
0.16	1.44	10.65	80.67	0.7	0.56	0	94.18	45.81	39.45	98.77	0.31
0.1	1.52	11.01	80.24	0.57	0.6	0	94.04	45.04	39.72	98.55	0.32
0.13	1.42	10.44	81.03	0.58	0.56	0.05	94.22	46.39	39.33	98.87	0.30
0.05	0.08	0.37	0.68	0.09	0.07	0.21	0.54	0.91	0.47	0.59	0.01

Appendix 4

COMPOSITION OF GLASS SHARDS FROM THE SOUTHERN OCEAN

This appendix contains the composition of glass shards from deep-sea sediments sampled in Eltanin cores collected from the Southern Ocean (see section 6.3). P. Froggatt analysed samples E17/10-206, E27/4-158, E33/16-111, E33/16-300, E33/3-006 and E33/3-94. Analytical methods as in Appendix 1. Sample identifications = Eltanin cruise/core number-depth (cm) from top of core.

E27/3-608

SiO2	Al2O3	TiO2	FeO	MgO	CaO	Na2O	K2O	Cl	Water
66.99	15.25	0.32	4.39	0	0.96	6.65	5.27	0.16	3.29
63.56	14.19	0.61	7.76	0.1	1.4	7.13	5.11	0.15	3.45
58.8	14.95	1.24	6.82	2.86	6.06	5.3	3.84	0.13	0.49
48.55	24.7	2	5.68	1.82	12.41	3.87	0.9	0.06	0.73
42.87	15.87	5.13	12.11	5.15	12.01	4.82	1.93	0.11	1.66
61.33	16.86	0.41	7.44	0.11	2.41	6.96	4.37	0.1	0.07
63.35	14.45	0.73	7.69	0.21	1.61	6.84	5.01	0.1	0.17
53.23	18.02	1.59	9.46	2.13	5.84	6.16	3.4	0.17	1.88
63.26	14.16	0.61	7.99	0.15	1.43	7.29	4.96	0.14	0.1

E27/3-653

SiO2	Al2O3	TiO2	FeO	MgO	CaO	Na2O	K2O	Cl	Water
60.57	16.33	0.42	7.65	0.17	2.1	7.45	5.15	0.16	1.93
47.74	15.23	3.72	14.49	4.66	8.39	3.9	1.88	0	2.61
60.85	17.41	0.94	6.05	0.81	2.48	6.67	4.65	0.15	4.46
63.63	16.31	0.21	5.52	0	1.46	7.17	5.43	0.28	2.62
65.06	19.42	0.09	1.47	0	1.93	7.55	4.48	0	0.09
49.47	22.16	2.52	8.22	2.29	9.17	4.41	1.23	0	1.83
61.88	14.37	0.77	8.53	0.44	1.98	7.33	4.47	0.23	3.77
64.66	15.22	0.48	6.16	0	1.73	6.17	5.43	0.16	3.79
47.66	16.12	4.01	13.86	4.38	9.27	3.28	1.42	0	2.63
49.85	16.61	3.34	12.26	4.21	7.59	4.05	1.98	0.1	1.73

E27/3-875

SiO2	Al2O3	TiO2	FeO	MgO	CaO	Na2O	K2O	Cl	Water
70.55	15.14	0.17	2.38	0.14	0.77	5.28	5.3	0.28	4.01
70.09	15.28	0.18	2.47	0.09	0.8	5.38	5.42	0.29	5.08
68.87	12.53	0.45	5.91	0	0.81	6.28	4.97	0.18	4.07
58.65	19.74	0.08	4.17	0.07	0.99	10.74	5.23	0.33	3.32
59.17	19.35	0.13	4.59	0.08	1.15	9.44	5.76	0.32	2.71
74.21	8.58	0.21	6.12	0.06	0.28	5.98	4.29	0.26	4.45
68.79	15.83	0.32	2.67	0.2	1.19	5.3	5.39	0.33	8.46
61.26	17.67	0.63	6.65	0.82	2.44	7.16	3.15	0.22	0.7
64.84	14.04	0.59	7.4	0.07	1.65	5.97	5.37	0.06	4.07
74.54	13.16	0.21	2.31	0.14	1.2	4.59	3.65	0.21	5.08

E27/3-953

SiO2	Al2O3	TiO2	FeO	MgO	CaO	Na2O	K2O	Cl	Water
60.26	21.19	0.51	2.38	0.54	6.3	6.8	1.96	0.06	0.43
65.29	19.34	0.11	1.18	0.07	1.66	7.55	4.71	0.09	0.14
62.31	16.93	0.65	5.79	0.64	2.37	6.55	4.49	0.28	2.89
63.25	16.82	0.57	5.09	0.55	2.1	6.49	4.73	0.39	8.76
63.69	16.81	0.58	4.98	0.53	1.95	6.38	4.83	0.25	3.97
59.01	15.87	0.5	4.69	0.46	8.51	6.23	4.49	0.24	5.14
63.4	16.8	0.6	5.13	0.52	1.92	6.69	4.69	0.26	2.68
68.53	14.91	0.25	3.34	0	0.95	6.01	5.9	0.1	1.74
62.61	16.95	0.73	5.52	0.63	2.31	6.37	4.51	0.38	7.74
68.71	15.32	0.23	3.04	0.15	0.81	5.55	5.82	0.39	4.61

E27/3-1003

SiO2	Al2O3	TiO2	FeO	MgO	CaO	Na2O	K2O	Cl	Water
75.55	10.8	0.22	3.29	0	0.22	4.97	4.78	0.17	4.25
75.72	10.71	0.22	3.44	0	0.26	4.93	4.25	0.19	5.14
75.48	11.13	0.22	3.3	0	0.23	4.97	4.51	0.14	6.35
75.2	10.78	0.28	3.6	0	0.23	5.09	4.68	0.15	4.24
72.58	11.34	0.26	4.63	0	0.25	6.24	4.4	0.29	4.7
62.73	13.51	0.57	8.86	0.11	1.1	8.23	4.69	0.2	0.21
75.68	10.72	0.24	3.42	0	0.22	4.94	4.55	0.23	4.87
75.68	10.73	0.16	3.45	0.06	0.24	5.07	4.45	0.16	4.71
76.4	10.61	0.17	3.19	0	0.18	4.66	4.6	0.18	5.41
75.73	10.63	0.23	3.49	0	0.24	5.02	4.49	0.17	4.37

E27/3-1038

SiO2	Al2O3	TiO2	FeO	MgO	CaO	Na2O	K2O	Cl	Water
76.6	10.88	0.16	2.84	0.06	0.23	4.74	4.32	0.16	5.16
75.58	12.83	0.09	1.58	0	0.34	5.01	4.38	0.2	4.97
75.8	10.74	0.27	3.26	0	0.29	4.62	4.88	0.13	3.51
77.49	11.25	0.16	2	0	0.18	4.45	4.42	0.2	5.9
76.71	10.9	0.18	2.72	0	0.23	4.77	4.34	0.16	3.24
76.91	11.28	0.1	2.11	0	0.22	4.6	4.52	0.25	4.74
75.71	12.65	0.1	1.43	0	0.27	5.03	4.6	0.21	5.45
75.64	10.91	0.18	3.34	0	0.33	4.68	4.76	0.16	5.08
77.5	11.09	0.14	1.99	0	0.2	4.7	4.23	0.17	4.86
77.42	11.38	0.09	1.86	0	0.2	4.48	4.39	0.17	4.99

E27/3-1128

SiO2	Al2O3	TiO2	FeO	MgO	CaO	Na2O	K2O	Cl	Water
76.83	11.85	0.11	1.68	0	0.3	4.48	4.52	0.24	5.14
76.71	11.83	0.12	1.79	0	0.28	4.46	4.65	0.17	4.7
77.04	11.67	0.08	1.78	0	0.27	4.19	4.74	0.21	5.12
76.7	12.17	0.08	1.75	0	0.31	4.34	4.46	0.2	4.98
76.76	11.85	0.11	1.75	0.06	0.28	4.46	4.5	0.22	4.99
76.91	11.84	0.17	1.61	0	0.23	4.44	4.63	0.17	4.5
77.03	11.66	0.08	1.71	0	0.24	4.45	4.61	0.21	4.14
76.34	12.73	0.22	1.37	0.22	1.32	4.07	3.61	0.14	4.31
76.7	11.88	0.1	1.73	0	0.27	4.58	4.55	0.18	3.81

E27/3-1158

SiO2	Al2O3	TiO2	FeO	MgO	CaO	Na2O	K2O	Cl	Water
61.86	18.06	0.6	4.38	0.49	1.63	7.95	5.27	0.22	2.66
61.91	18.03	0.55	4.21	0.34	1.29	8.03	5.43	0.2	1.13
58.61	19.07	0.22	4.91	0.12	1.03	10.37	5.15	0.52	1.76
61.48	18.16	0.32	4.51	0.21	1.17	8.41	5.51	0.23	1.31

SiO2	Al2O3	TiO2	FeO	MgO	CaO	Na2O	K2O	Cl	Water
73.66	10.43	0.24	4.89	0	0.3	5.7	4.5	0.28	6
62.58	17.57	0.43	4.68	0.28	1.43	7.91	4.81	0.3	4.34
61.57	17.75	0.54	4.97	0.44	1.58	7.66	5.26	0.24	4.13
74.18	10.22	0.28	4.74	0	0.23	5.66	4.46	0.23	5.61
60.84	17.93	0.38	5.05	0.33	1.26	8.25	5.59	0.38	5.4
62.89	14.69	0.52	7.18	0.09	1	8.68	4.75	0.19	2.81

E27/4-628

SiO2	Al2O3	TiO2	FeO	MgO	CaO	Na2O	K2O	Cl	Water
66.4	14.79	0.39	5.45	0	1.68	5.74	5.38	0.17	4.4
65.76	14.99	0.38	5.56	0.07	1.58	5.92	5.54	0.19	0.96
71.88	14.37	0.19	2.2	0.11	0.59	5.07	5.27	0.32	3.09
67.39	14.59	0.37	4.87	0	1.24	6	5.36	0.18	4.32
71.91	14.26	0.15	2.16	0.05	0.6	4.68	5.79	0.39	8.48
72.03	14.37	0.1	2.16	0.07	0.71	5.24	4.99	0.32	4.22
65.9	14.97	0.4	5.41	0.13	1.52	5.99	5.53	0.15	0
72.14	14.34	0.23	2.16	0.08	0.61	5.02	5.08	0.33	3.99
64.78	15.48	0.32	5.83	0	1.45	6.72	5.24	0.19	3.38
72.06	14.51	0.11	2.14	0.07	0.59	5.02	5.19	0.31	3.52

E27/4-818

SiO2	Al2O3	TiO2	FeO	MgO	CaO	Na2O	K2O	Cl	Water
74.68	13.41	0.09	1.56	0	0.57	4.41	5.02	0.26	4.47
74.52	13.53	0.07	1.59	0	0.51	4.2	5.26	0.32	5.17
74.86	13.47	0.08	1.44	0.06	0.52	4.22	5.17	0.18	5.38
74.65	13.35	0.09	1.53	0.06	0.6	4.42	4.99	0.32	4.94
74.68	13.47	0.19	1.49	0	0.52	4.28	5.04	0.33	6.28
74.47	13.54	0.14	1.53	0.05	0.55	4.37	5.1	0.25	6.95
74.38	13.3	0.14	1.54	0.05	0.48	4.4	5.45	0.25	8.15
74.39	13.25	0.13	1.67	0.06	0.57	4.43	5.23	0.27	7.14
74.89	13.36	0.1	1.46	0	0.56	4.18	5.23	0.21	5.57
74.96	13.29	0.08	1.38	0	0.51	4.34	5.18	0.25	5.15

E27/4-983

SiO2	Al2O3	TiO2	FeO	MgO	CaO	Na2O	K2O	Cl	Water
73.89	7.66	0.24	5.98	0	0.11	7.47	4.09	0.57	6.41
62.08	16.87	0.29	6.43	0.08	1.67	7.5	4.95	0.12	2.03
65.44	14.77	0.39	6.36	0	1.26	6.63	4.95	0.19	6.7
61.91	16.72	0.25	6.07	0	1.34	8.4	5.15	0.15	1.62
67.23	14.3	0.52	5.69	0	1.26	6	4.83	0.17	5.47
66.03	15.42	0.28	5.12	0	0.75	7.23	4.79	0.39	3.45
65.99	15.91	0.26	4.42	0	1.08	7.11	5.01	0.23	2.91
61.45	16.76	0.22	5.92	0	1.1	9.29	5.01	0.25	4.53
65.24	15.47	0.25	5.07	0	0.81	7.87	4.96	0.33	4.27
61.38	17.19	0.29	6.15	0	1.65	8.11	5.04	0.19	2.34

E27/4-1343

SiO2	Al2O3	TiO2	FeO	MgO	CaO	Na2O	K2O	Cl	Water
75.35	10.9	0.23	3.38	0	0.28	5.21	4.44	0.2	4.78
75.7	11.07	0.2	3.08	0	0.23	4.98	4.59	0.16	4.58
75.19	11.19	0.23	3.08	0	0.27	5.24	4.67	0.13	4.22
76.03	11.08	0.18	2.86	0	0.25	4.83	4.65	0.13	4.93
75.49	11.13	0.21	3.17	0	0.23	5.13	4.47	0.18	7.36
75.79	11.07	0.16	3.14	0	0.25	4.91	4.57	0.12	6.71
66.93	13.56	0.47	6.24	0	1.26	6.43	5	0.11	6.48
74.13	13.79	0.14	1.36	0	0.55	4.47	5.33	0.23	7.55
75.1	11.2	0.21	3.29	0	0.25	5.07	4.72	0.15	6.82
75.45	11.01	0.2	3.33	0	0.26	5.17	4.41	0.16	6.63

E27/4-1458

SiO2	Al2O3	TiO2	FeO	MgO	CaO	Na2O	K2O	Cl	Water
75.95	12.82	0	1.42	0	0.27	4.96	4.37	0.21	4.14
75.6	10.87	0.24	3.26	0	0.29	4.95	4.65	0.14	3.16
77.03	11.15	0.16	1.99	0	0.19	4.7	4.58	0.21	2.96
76.13	12.73	0.13	1.41	0	0.26	4.91	4.24	0.19	4.76
71.69	14.81	0.13	2.02	0	0.52	5.83	4.79	0.22	4.1
75.9	12.88	0.11	1.35	0	0.32	4.88	4.38	0.19	5.68
75.9	12.79	0.06	1.55	0	0.24	4.86	4.43	0.16	5.27
77.03	11.39	0.14	2.03	0	0.16	4.58	4.44	0.24	3.32
75.97	12.81	0.07	1.46	0	0.25	4.56	4.73	0.15	4.08
75.53	13.02	0.09	1.43	0	0.31	5.06	4.38	0.17	6.41

E33/16-933

SiO2	Al2O3	TiO2	FeO	MgO	CaO	Na2O	K2O	Cl	Water
76.52	11.89	0.07	1.8	0	0.18	4.9	4.33	0.3	7.82
75.99	12.29	0.08	1.65	0	0.31	4.19	5.3	0.18	5.08
74.79	10.61	0.26	4	0	0.29	5.33	4.51	0.23	6.68
76.46	11.7	0.16	2.04	0	0.22	4.51	4.7	0.22	4.22
76.39	11.82	0.11	1.59	0.05	0.29	4.26	5.33	0.16	6.2
75.95	12	0.1	1.74	0	0.14	5.14	4.65	0.28	7.43
76.74	11.69	0.19	1.99	0	0.25	4.28	4.72	0.15	6.3
76.47	11.81	0.12	1.86	0	0.26	4.28	4.96	0.25	2.5
76.19	11.82	0.1	1.76	0	0.21	4.66	4.92	0.34	6.29
77.13	11.62	0.11	1.72	0	0.17	4.65	4.29	0.3	4.16

E33/16-953

SiO2	Al2O3	TiO2	FeO	MgO	CaO	Na2O	K2O	Cl	Water
76.52	11.87	0.13	1.84	0	0.21	4.85	4.32	0.28	3
75.98	12.13	0.09	1.83	0	0.25	5.01	4.4	0.31	7.54
76.84	11.82	0.08	1.73	0	0.24	4.77	4.25	0.26	4.01
74.67	13.04	0.07	1.55	0	0.18	5.11	5.16	0.22	3.34
76.55	11.77	0.1	1.94	0	0.21	5	4.15	0.28	5.63
76.53	11.51	0.09	2.17	0	0.25	4.72	4.58	0.16	4.39
76.87	11.58	0.14	2.04	0	0.23	4.16	4.81	0.18	3.91
76.49	11.49	0.11	1.8	0	0.21	5.07	4.54	0.3	6.14

E11/9-1168

75.09	10.82	0.26	3.61	0.06	0.39	4.89	4.75	0.13	4.38
77.06	11.28	0.19	2.07	0	0.22	4.62	4.34	0.22	3.91
75.69	10.74	0.18	3.36	0	0.22	5.2	4.44	0.18	3.25
76.89	11.73	0.12	1.93	0	0.22	4.29	4.31	0.2	4.89
70.6	15.4	0.18	2.16	0.05	0.73	5.65	4.98	0.24	4.7
76.54	11.13	0.2	2.62	0	0.23	4.39	4.75	0.14	4.98
76.61	11.73	0.07	1.95	0	0.2	4.81	4.42	0.22	3.9
75.32	10.94	0.25	3.34	0	0.28	5.05	4.69	0.12	2.83
76.68	11.63	0.11	1.75	0	0.2	4.84	4.21	0.29	4.97
75.77	10.67	0.22	3.35	0	0.26	5.14	4.41	0.18	5.04

E11/9-1198

75.37	10.4	0.23	3.91	0	0.22	5.26	4.44	0.18	4.89
75.28	10.37	0.31	3.74	0	0.24	5.21	4.66	0.2	6.83
75.46	10.54	0.23	3.8	0	0.24	5.4	4.15	0.18	4.43
76.86	11.5	0.11	1.91	0	0.17	4.64	4.56	0.26	6.19
76.57	11.51	0.11	1.95	0	0.18	4.94	4.38	0.36	6.12
77.05	11.63	0.16	2.01	0	0.23	4.48	4.26	0.19	5.06
70.86	12.58	0.35	4.7	0	0.59	5.95	4.87	0.09	3.73
77.65	11.21	0.08	1.73	0	0.24	4.42	4.45	0.23	3.36
76.8	11.69	0	1.84	0	0.19	5.03	4.16	0.29	5.33

analyst: P. Froggatt

E17/10-206

75.68	13.01	0.18	2	0	0.45	3.74	4.56	0.39	4.3
76.65	12.54	0.1	1.97	0	0.14	3.57	4.72	0.31	3.33
76.35	12.58	0.17	1.99	0	0.39	3.62	4.58	0.33	3.39
76.7	12.74	0.18	2.02	0	0.33	3.45	4.38	0.21	4.23
76.2	12.69	0.08	2.18	0	0.43	3.54	4.59	0.3	3.62
76.72	12.45	0	2	0	0.25	3.65	4.6	0.33	4.69
76.64	12.76	0.2	1.67	0	0.34	3.75	4.43	0.22	3.57
76.85	12.78	0	1.39	0	0.57	3.95	4.39	0.09	6.31
76.2	12.96	0.09	1.9	0	0.48	3.49	4.44	0.44	4.45
44.57	13.63	5.51	15.23	5.75	10.94	3.04	1.25	0.07	1.93
64.13	14.55	0.39	6.99	0	0.87	8.01	4.74	0.31	0
56.24	19.77	1.39	5.7	1.08	2.18	7.84	5.68	0.13	0.46
65.12	15.16	0.86	6.31	0.45	1.18	5.94	4.91	0.07	1.45
59.25	16.34	1.24	7.79	1.2	3.45	5.69	4.93	0.1	0.09
70.38	13.05	0.43	5	0	0.58	5.51	4.78	0.27	2.33
54.14	18.85	1.6	6.41	1.76	4.03	7.57	5.56	0.07	0.26
65.28	12.74	1	8.27	0.45	1.41	6.01	4.79	0.07	0.59
70.45	13.98	0.31	4.92	0	0.72	4.7	4.7	0.23	2.58
68.75	14.2	0.33	5.24	0	0.75	5.72	4.82	0.19	2.27
66.43	15.53	0.44	5.22	0	1.87	6.14	4.25	0.11	2.8

E27/4-158

68.26	15.79	0.29	3.39	0.17	1.07	4.94	5.85	0.25	2.22
68.8	12.45	0.69	7.4	0.09	0.88	4.75	4.77	0.17	1.9
68.8	16.05	0.43	3.28	0	1.07	4.71	5.66	0	4.39
68.79	12.02	0.57	7.76	0.19	0.88	4.88	4.75	0.15	0.48
69.13	15.84	0.38	3.12	0.19	0.97	4.6	5.61	0.18	4.04
68.26	15.67	0.37	3.89	0.2	0.96	4.73	5.76	0.16	1.96
67.76	13.49	0.68	6.68	0.18	0.95	5.35	4.82	0.1	0.56
69.98	16.01	0.34	2.19	0.18	1.01	4.51	5.56	0.22	4.72
68.98	15.98	0.28	3.24	0.27	0.92	4.71	5.44	0.2	2.94

E33/16-111

76.31	12.73	0.14	1.96	0	0.36	3.78	4.32	0.38	3.8
76.78	12.5	0.07	2.11	0	0.34	3.38	4.46	0.35	5.37
76.74	12.47	0.14	2.02	0	0.32	3.69	4.5	0.13	5.23
76.29	12.53	0.15	2.04	0	0.4	3.72	4.49	0.37	5.89
76.29	12.35	0	2.15	0	0.42	3.62	4.75	0.4	3.41
75.53	12.46	0.17	2.75	0	0.42	3.52	4.68	0.48	3.35
76.7	12.37	0.21	2.19	0	0.28	3.58	4.4	0.25	5.13
76.62	12.38	0	2.16	0	0.44	3.41	4.69	0.32	4.89
76.14	12.51	0	2.13	0.13	0.43	3.48	4.6	0.59	4.57
65.55	14.25	1.31	7.19	0.61	1.58	4.7	4.64	0.19	2.92

E33/16-300

65.56	13.45	1.13	8.06	0.51	1.28	5.01	4.9	0.1	0.33
74.67	12.18	0.24	4.24	0	0.46	3.76	4.31	0.14	4.95
66.85	13.35	0.75	7.35	0.23	1.07	5.26	4.98	0.16	2.27
53.47	14.13	2.51	11.11	2.19	5.12	7.52	3.84	0.12	2.52
62.16	16.26	0.22	6.88	0	0.97	8.25	4.96	0.29	0.26
62.19	15.63	0.68	7.9	0.45	2.76	5.04	5.3	0.06	0
71.91	14.71	0.2	2.57	0.08	0.66	4.19	5.32	0.37	4.46
65.52	16.2	0.33	5.28	0.09	1.26	5.67	5.42	0.23	2.63
67.37	13.49	0.69	6.92	0.23	1.11	5.23	4.86	0.11	2.68
65.38	16.21	0.28	5.4	0.13	1.26	5.42	5.62	0.31	0.49

E33/3-006

64.76	15.54	0.71	7.24	0.32	1.35	5.6	5.26	0.22	1.14
65.02	14.57	0.68	7.39	0.28	1.31	5.52	5.02	0.2	0.97
66.01	14.55	0	7	0.32	1.39	5.21	5.32	0.19	2.37
64.54	14.5	0.78	8.2	0.35	0.94	5.14	5.4	0.15	0.55
65.17	14.73	0.7	7.26	0.28	1.12	5.55	4.93	0.26	1.39
65.2	14.77	0.66	7.25	0.26	1.39	5.25	5.05	0.17	1.82
65.02	14.52	0.67	7.7	0.2	1.14	5.66	5.06	0.04	1.15
64.75	14.68	0.77	7.58	0.25	1.12	5.66	5.01	0.19	0.92
65.33	14.87	0.75	7.29	0.29	1.46	4.73	5.12	0.15	1.41

E33/3-94

64.71	14.69	0.77	7.5	0.22	1.3	5.73	5	0.07	1.73
65.07	14.63	0.66	7.4	0.36	1.36	5.63	4.72	0.17	2.36
75.62	12.83	0.15	2.26	0	0.46	3.64	4.72	0.32	5.88
65.32	13.93	0.64	7.56	0.21	1.04	6.28	4.86	0.15	0.66
76.44	12.67	0.07	2.1	0	0.43	3.26	4.65	0.37	5.55
64.31	14.63	0.53	8.36	0	1.66	5.58	4.79	0.13	3.22
75.72	12.64	0.11	2.1	0	0.44	3.93	4.71	0.35	3.96
75.66	12.71	0.13	1.8	0	0.45	4.08	4.78	0.4	5.35
76.06	12.69	0.13	1.94	0.06	0.42	3.63	4.68	0.38	4.79

Appendix 5

SUPPORTING PAPER

Late Neogene unconformity-bounded tuffaceous sequences: northwestern Chatham Rise, New Zealand.
P. M. Barnes and P. A. R. Shane

In this paper, P Shane provided the EMA compositions and interpretations related to tephra correlations, source and mode of emplacement.

Late Neogene unconformity-bounded tuffaceous sequences: northwestern Chatham Rise, New Zealand

PHILIP M. BARNES

New Zealand Oceanographic Institute
National Institute of Water and Atmospheric Research Ltd.
P. O. Box 14 901, Kilbirnie
Wellington, New Zealand

and

Department of Geology
University of Canterbury
Private Bag
Christchurch, New Zealand

PHILIP A. R. SHANE

Research School of Earth Sciences
Victoria University of Wellington
P. O. Box 600
Wellington, New Zealand

Abstract Unconformity-bounded, late Miocene to Recent sedimentary sequences produced by fluctuating paleoceanographic conditions on the northwestern Chatham Rise have been sampled in a series of piston-cores from exposures at wide, mid-bathyal, oblique to slope, current-scour channels and from submarine canyons at the head of the adjacent Hikurangi Trough. The biostratigraphic framework for these mostly hemipelagic sequences is based on foraminiferan and nannofossil dating of the cores. Volcanic glass-rich horizons (tephra), with glass shards of calc-alkaline rhyolitic composition, occur commonly in late Opoitian to Haweran (late Pliocene – late Pleistocene) sediments. Although the physical oceanography and sedimentary processes of the region are unfavourable for preserving megascopic tephra, five chemically and stratigraphically distinct tuffaceous horizons are recorded in Pleistocene cores, implying at least five discrete eruptions. Two late Pleistocene tuffaceous horizons are correlated tentatively with Layer E (c. 0.27 Ma) and Layer D (= Mt Curl Tephra; c. 0.35 Ma) in several southwestern Pacific deep-sea cores. Other tuffaceous horizons contain two or more chemical populations of glass shards that have been mixed and reworked by extensive bioturbation and current winnowing, during periods of very slow sedimentation. Distances of 460–600 km between the core sites and source vents in the Coromandel Volcanic Zone (early Pliocene) and Taupo Volcanic Zone (Pleistocene) imply very explosive eruptions.

Keywords late Neogene; sedimentary sequences; seismic reflection; currents; cores; biostratigraphy; glass chemistry; rhyolitic tephra; Chatham Rise

INTRODUCTION

The gently dipping (1–6°) northwest slope of the Chatham Rise extends for 80 km from Mernoo Bank on the rise crest to the southern part of the Hikurangi Channel about 60 km off the northeastern South Island coast (Fig. 1). The region lies within the broad zone of deformation associated with the New Zealand plate boundary, and is undergoing extensional faulting, which resumed in the late Neogene after a period of Paleogene and early Neogene quiescence (Lewis et al. 1986; Wood et al. 1989). The slope lies north of Mernoo Saddle— the 580 m deep depression between the Chatham Rise and the South Island—and has been the site of a complex, Pliocene– Pleistocene sedimentation history, involving the waxing and waning of regional-scale, mid-bathyal currents sweeping obliquely across the slope (Barnes 1992). High-resolution seismic profiles and piston cores reveal that numerous, unconformity-bounded, Pliocene–Pleistocene sequences on the slope are the result of alternating, climatically influenced episodes of current erosion, with sediment drift aggradation and hemipelagic sedimentation. The cores were obtained from a number of stratigraphically different sequences exposed at the seabed in areas of late Quaternary current scour.

Volcanic ash (tephra) is common in Pliocene–Pleistocene deep-sea sediments elsewhere in the Southwest Pacific, at sites up to 1100 km east and southeast of volcanic centres in central New Zealand (Ninkovich 1968; Watkins & Huang 1977; Froggatt et al. 1986). Tephras have been correlated between cores, and with tephras exposed onshore in New Zealand, by integrating magnetostratigraphy, fission-track ages, and chemical finger-printing (Watkins & Huang 1977; Froggatt 1983; Froggatt et al. 1986; Shane & Froggatt 1991). The cores of Pliocene–Pleistocene sediments from the northwest Chatham Rise slope also contain a significant amount of volcanic glass in tuffaceous horizons.

This paper briefly outlines the late Neogene sequence architecture of the northwestern Chatham Rise slope, and presents the biostratigraphy and sedimentology of the cores. We also present here the chemistry of various glass-rich (tuffaceous) horizons and identify the likely source region of the eruptions. We discuss the sedimentary aspects of volcanic glass accumulation and reworking in this deep-sea, current-swept environment, and attempt to correlate tuffaceous horizons (within the biostratigraphic framework) with tephra in other deep-sea cores and with onland sequences nearer the source.

DEEP-SEA PLIOCENE–PLEISTOCENE SEQUENCES: PRODUCTS OF ALTERNATING CURRENT SCOUR AND DEPOSITION

The regional, late Quaternary sedimentary processes of the northwestern Chatham Rise slope and southern Hikurangi Trough have been examined by 3.5 kHz echocharacter mapping (Barnes 1992). The Hikurangi Trough is a sink for
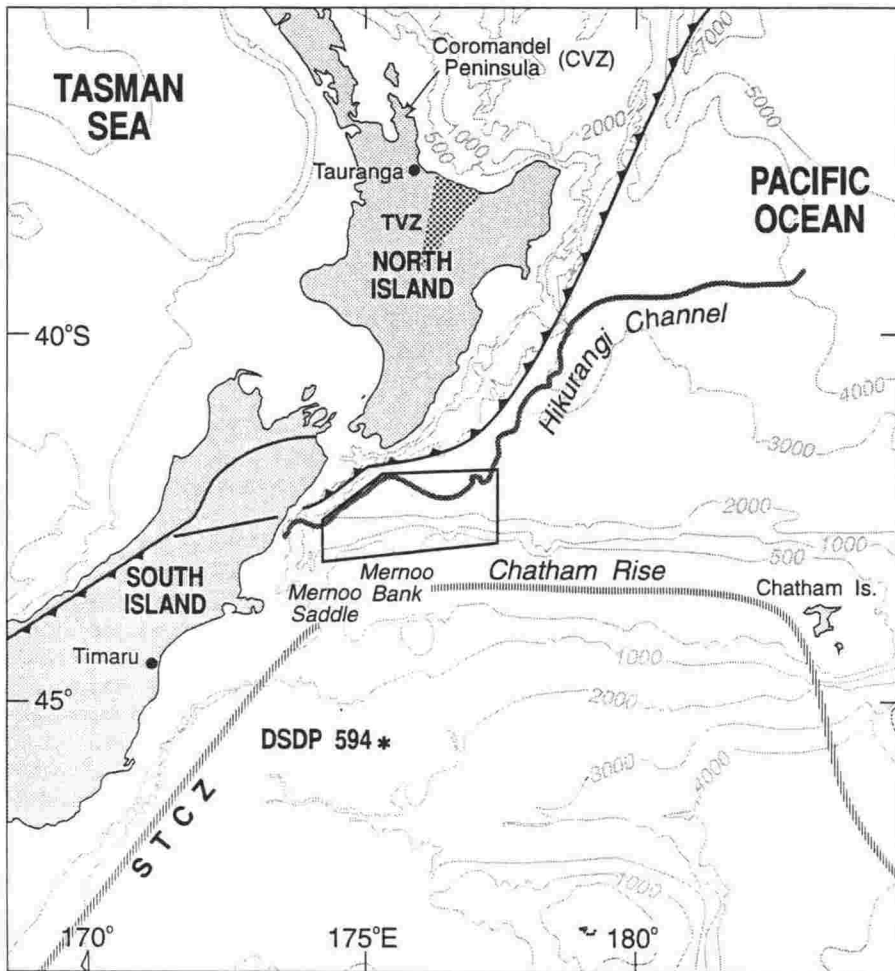
Fig. 1 Regional physiography and location of the study area. TVZ, Taupo Volcanic Zone; CVZ, Coromandel Volcanic Zone; STCZ, Subtropical Convergence Zone. The bold line with teeth marks the plate-boundary deformation front of the offshore Hikurangi margin and onshore Alpine Fault.

voluminous turbidite deposits. The turbidites have been channelled through canyons on the north Canterbury continental slope and in eastern Cook Strait, and fed into the Hikurangi Channel in the axis of the trough (Fig. 2) (Lewis 1980; Herzer 1981; Carter et al. 1982; Barnes 1992).

On the North Chatham Slope north of Mernoo Saddle, there are four associations of echotypes representing different late Quaternary sedimentary processes (Fig. 2). These include: (1) large, elongate areas of current-scoured and winnowed seafloor; (2) several coalescing sediment drifts between and downslope of current-scoured areas; (3) several steep, irregular areas of the lower slope east of the sediment drifts, resulting from combined alongslope current activity and downslope mass-wasting processes; and (4) areas of predominantly hemipelagic sedimentation on the mid and upper slope. The mid-bathyal currents are inferred to be predominantly Antarctic Intermediate Water (AIW) that rises south of the Chatham Rise, becomes entrained within the Subtropical Convergence Zone, flows northward through Mernoo Saddle, and then diverges down and across the North Chatham Slope. The flows and associated seabed erosion are thought to have been intensified during periods of lower glacio-eustatic sea level (Barnes 1992).

From high-resolution seismic-reflection profiles, 12 mappable sedimentary sequences (c. 10–40 m thick) above a regional early Pliocene onlap surface (L) are recognised (Fig. 2, 3). The sequence boundaries are represented by

erosional unconformities and onlapping seismic reflectors. Sequences are referred to as numbers 1 to 13, and their boundaries by letters A–L and LM. Most of the sequences are exposed at the seafloor in areas of late Quaternary current scour (Fig. 2). It is this favourable exposure that enabled several sequences to be sampled using conventional piston-coring equipment.

Stratigraphically below surface L there is a downslope-thickening sequence of strong, parallel to downslope diverging reflectors overlying a mid–lower slope wedge of weaker reflectors (Fig. 3A). The boundary (LM) between these two sequences, shown below to be of late Miocene age, is exposed in the axis of Pukaki Canyon close to the position of core S871 (Fig. 2). A packet of strong, parallel reflectors below this lower wedge has been traced in airgun profiles to the Canterbury shelf, where it represents the Oligocene Amuri Limestone (Lewis et al. 1986; Wood et al. 1989).

The Cenozoic sequences on the slope are characteristic of the Chatham Rise, thickening downslope and being erosionally truncated on the rise crest, which has experienced a long history of erosion and nondeposition (Cullen 1980; Wood et al. 1989).

CORING AND LABORATORY METHODS

Fifteen cores from the northwest Chatham Rise slope were collected in 1988 and 1989 using a modified Kullenberg
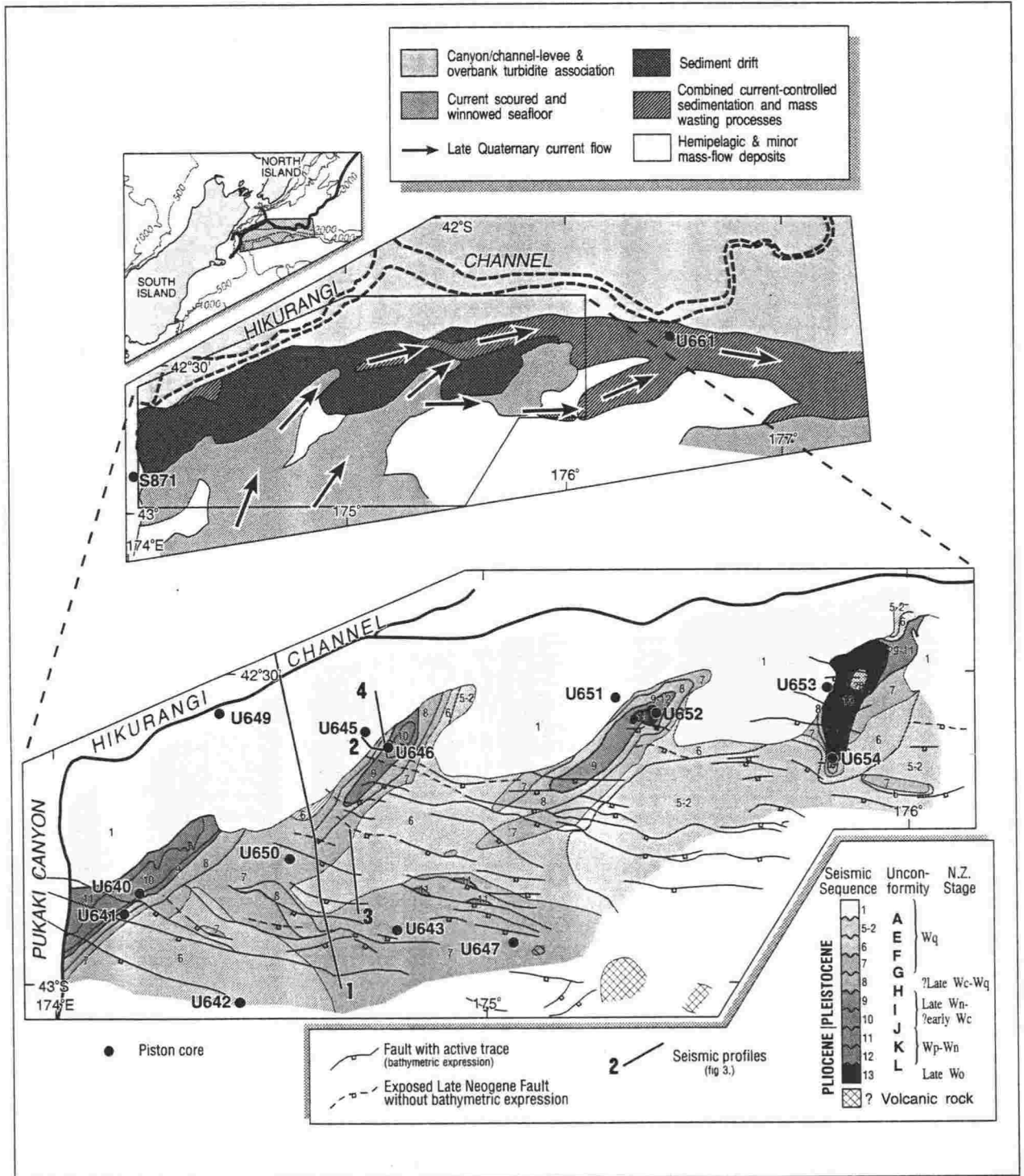
Fig. 2 Regional late Quaternary sedimentary processes of the northwestern Chatham Slope and southern Hikurangi Trough, with geological map of exposed seismic sequences and active faults in areas of seafloor erosion. Positions of piston cores examined in this study are indicated. New Zealand stage symbols: Wo, Opoitian; Wp, Waipipian; Wn, Nukumaruan; Wc, Castlecliffian; Wq, Haweran.

piston corer on R.V. *Rapuhia*. Sampling sites were chosen after shipboard interpretation of seismic profiles, and they lie in water depths ranging from 411 to 2830 m (Fig. 2). The cores are 69 mm in diameter and they range from 1.1 to 3.2 m long. A Shipek Grab sample was collected also from each site. At site S871, only a sample from the core head was recovered.

In the laboratory, cores were split, photographed, and described wet. One-half was retained for reference. Slices of representative lithologies were X-ray radiographed for examination of fine-scale sedimentary structure, and 38 samples (2–4 representative samples from each core) were taken for grainsize and carbonate analyses. Grainsize was
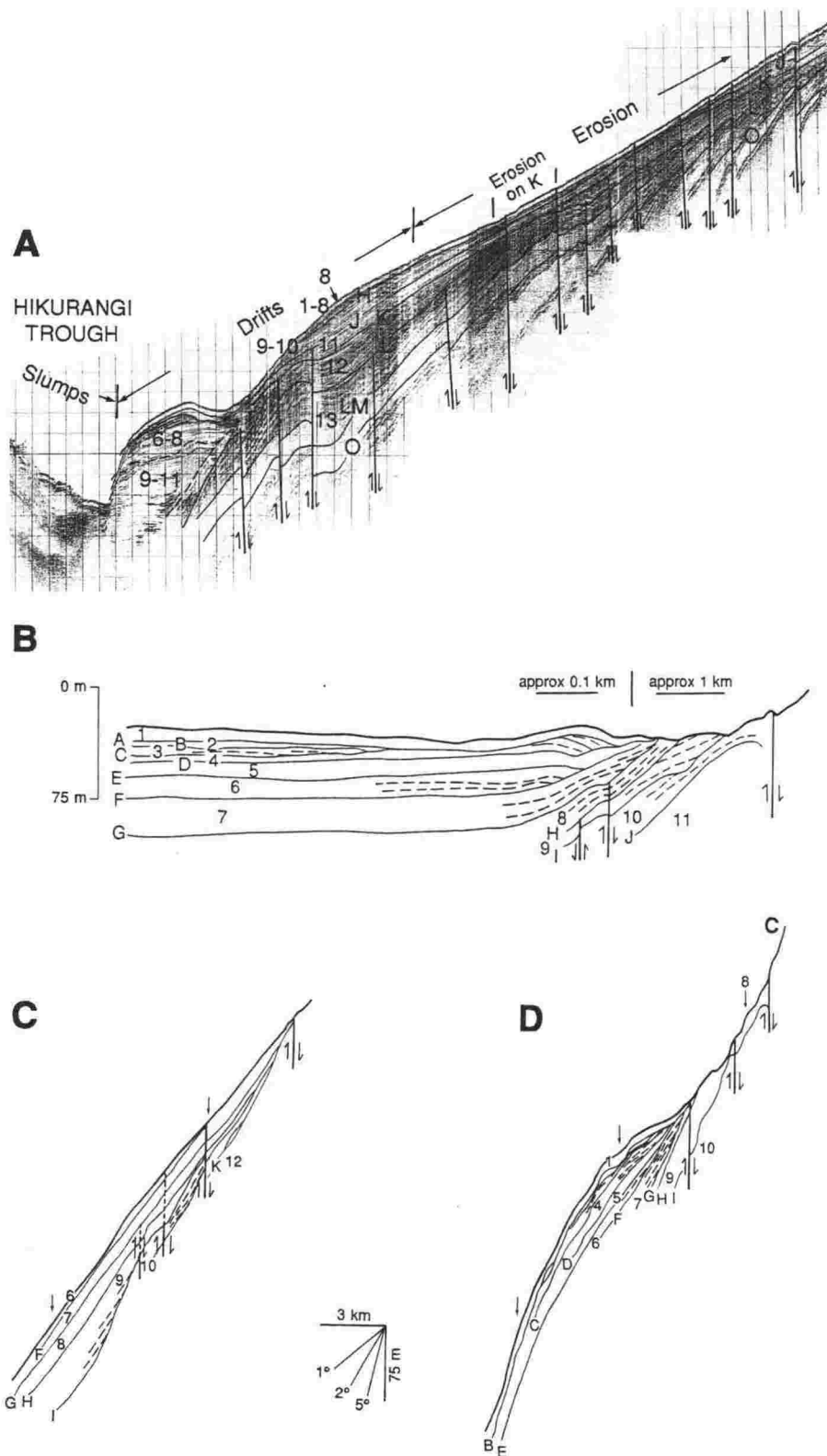
Fig. 3 Examples of seismic profiles of the northwest Chatham Slope showing seismic sequences, faults, and major sedimentary features. Positions of profiles are plotted in Fig. 2, and stratigraphy is summarised in Fig. 7. **A**, Airgun profile 1; **B**, Interpreted 3.5 kHz profile 2. **C**, Interpreted 3.5 kHz profile 3. **D**, Interpreted 3.5 kHz profile 4.

determined by the pipette method, and CaCO₃ by vacuum gasometric analysis. In addition, sand fractions were extracted from all cores at 100–300 mm intervals and examined so that microscopic tuffaceous horizons could be identified for analysis. For comparisons with relevant tephras in other deep-sea cores and nearer the source, the glass chemistry of shards

from 25 tuffaceous horizons in 8 cores was analysed by a Jeol 733 electron microprobe. Methods and standards for the Jeol 733 are described by Froggatt (1983). For microprobe operating conditions we used an 8 nA current at 15 kV and a 20 μm beam diameter. To determine ages, the foraminiferal fauna of 12 cores were analysed, along with the calcareous

nannofossil flora of 6 cores. The foraminifera microfossil data are archived on New Zealand Fossil Record File (SE42174/f1, f3–8; SE42175/f3–6; SE42176/f2–3). An attempt was made to establish a magnetostratigraphy of the cores using a Molspin Spinner Magnetometer. However, the natural remnant magnetisation intensities of pilot samples from five cores were too low to provide reliable data after stepwise cleaning by standard alternating field methods.

SEQUENCE LITHOLOGIES

Lithological characteristics

Cores are shown in Fig. 4–6, and their sequence stratigraphy appears in Fig. 7. Cores were recovered from the crests of lower slope sediment drifts (U645, U651, U653); from areas of mid-bathyal current erosion (U640–U643, U646, U650, U652, U654, U661) and turbidity current erosion (U649, S871); and from winnowed seafloor on the upper slope of Mernoo Bank (U647).

The cores typically consist of unconsolidated to well compacted, greyish olive to greyish green mud with minor amounts of sand (Fig. 4, 5). Different cores have different proportions of terrigenous detritus and planktic microfossils. Sand fractions consist of variable amounts of glauconite, clear glass shards, foraminifers, radiolarians, iron sulphides, and terrigenous detritals.

For ease of description, we recognise four lithofacies on the basis of texture and sedimentary structure, that are independent of age: (1) homogeneous mud; (2) laminated sandy mud; (3) mottled silts and muddy sands; and (4) carbonate sandy muds and muddy sands. In addition, cemented horizons characterise some buried erosion surfaces. Contacts between facies are mostly gradational but some are sharp.

Homogeneous muds

These are the finest grained and most abundant sediments, representing 73% of total core recovered. Even in carefully cleaned core splits, they appear to be almost completely structureless, greyish olive, light olive grey or dusky yellow green muds (Fig. 5A–B, 5D, 5F). However, X-ray radiographs show that they are not always homogeneous (Fig. 6A). The texture is predominantly clay with slightly less silt and very minor sand (1–6% sand), although a few samples analysed are almost pure silt (>80% silt), and one is a muddy sand (61% sand). Carbonate content is moderately low (5–20%). Bioturbation is thorough, destroying primary sedimentary structure. Pyrite-filled polychaete worm tubes may be abundant (Fig. 6A), and some consolidated samples are bored where they are exposed at the seabed by erosion (Fig. 5D).

Laminated sandy muds

Greyish olive or light olive grey sandy muds occur in three cores from eroded sequences (U642, sequence 6; U643, sequence 7; U661), forming 8% of total core recovered. The texture and structure is gradational with homogeneous mud and with stratified sections of mottled silts and muddy sand facies. The laminations are subtle, but clear in X-ray radiographs, and are defined by discontinous concentrations of silt and sand with intervening mud (Fig. 5C, 6B). Pyrite-filled worm tubes may be common, but bioturbation has been insufficient to destroy primary sedimentary structures.

Mottled silts and muddy sands

These occur in six cores (U640, U642, U643, U650, U652, U654) from various, eroded, Pliocene–Pleistocene sequences in gradational contact with both homogeneous and laminated muds (Fig. 4). The texture is very heterogeneous and comprises pockets, lenses, and irregular layers of muddy sand, silt, and mud, commonly producing a crude horizontal stratification (Fig. 5A–C, 6C). In 11 samples analysed, sand fractions range 1–62%, silt 19–38%, and clay 10–58%. Carbonate content is low (c. 5%). The high glauconite content of sandy horizons produces a greyish olive green or dark greenish grey colour.

Carbonate sandy mud and muddy sand

Carbonate sediments characterise one core (U647) from 411 m water depth upslope from the strongly eroded seafloor north of Mernoo Saddle (Fig. 2, 4). The core is from an irregular seabed morphology close to an area of exposed rocks which are thought to be volcanic (Barnes 1992). The high carbonate content of 40–59% results from an abundance of dispersed shelf and slope shell fragments, typically 1–5 mm long, including the gastropods *Bathypoma parengonius*, *Cominella alertae*, *Scaphander otagoensis*, and *Uberella vitrea*, the bivalve *Sacella bellula*, the scaphopod *Dentalium zelandicum*, and fragments of echinoderm plates. The greyish olive sediment is relatively coarse grained (37–63% sand) and faintly stratified, although fine-scale lamination is absent.

Cemented horizons

Cemented horizons up to 70 mm thick occur within two cores (U652, U653) at sequence boundaries (Fig. 4, 5F). In both cores, the cemented horizons are gradational with underlying, compacted or well-consolidated Pliocene mud and muddy sand. They represent late Quaternary erosion surfaces now buried by soft, homogeneous mud of the topmost sequence. The horizons are interpreted to represent in-situ submarine cementation and hardground formation on a current-swept seafloor.

SEDIMENTARY PROCESSES

The sedimentary processes of the region are discussed by Barnes (1992), who integrated both the sediment lithologies and their high-resolution seismic characteristics. Homogeneous mud characterises cores of seismic sequence 1 as well as large intervals of other Pliocene–Pleistocene cores from eroded sequences further upslope (Fig. 2, 4).

The cores from older, Pliocene–Pleistocene sequences from upslope of the drifts contain homogeneous muds in association with other less common deposits. These sequences exhibit the characteristics of hemipelagic deposition including bioturbation, mixed terrigenous and biogenic compositions, fine grainsize, and inferred slow sedimentation (e.g., Doyle et al. 1979). They are inferred to have accumulated during periods of diminished and localised current activity. The presence and absence of lamination in the muds is largely a function of the degree of bioturbation. The glauconitic sandy horizons in the mottled silts and muddy sands are inferred to have been redeposited in mass flows from the upper slopes of Mernoo Bank where carbonate and authigenic aprons exist (McDougall 1982), although textures of these deposits are not typical of turbidites (Walker & Mutti 1973). Reworking of the
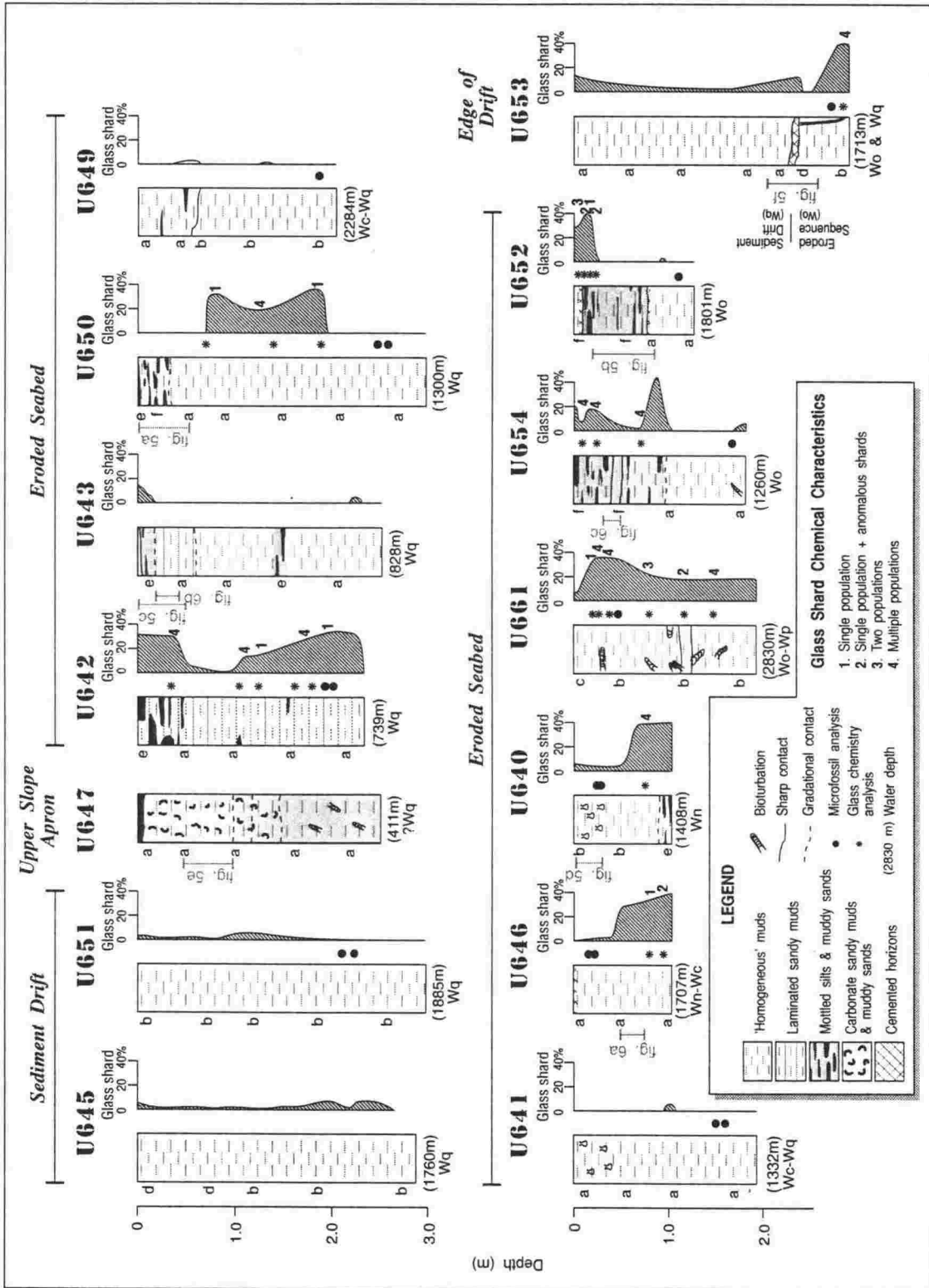
Fig. 4 Sedimentary lithofacies, relative volcanic glass distribution, and glass shard chemical population characteristics in cores from the north Chatham Slope. Cores are grouped according to New Zealand Stage ages (Wo, Opoitian; Wp, Waipipian; Wn, Nukumaruan; Wc, Castlecliffian; Wq, Haweran; see summary in Fig. 7). Major sedimentary environments are indicated, along with sample positions analysed for biostratigraphy and glass chemistry. Glass shard percentages are concentrations in the sand fractions. Sediment colour codes: a, 10Y4/2 greyish olive; b, 5Y5/2 light olive grey; c, 5Y7/2 yellowish grey; d, 5GY3/2 greyish olive green; e, 5GY5/2 dusky yellow green; f, 5GY4/1 dark greenish grey.
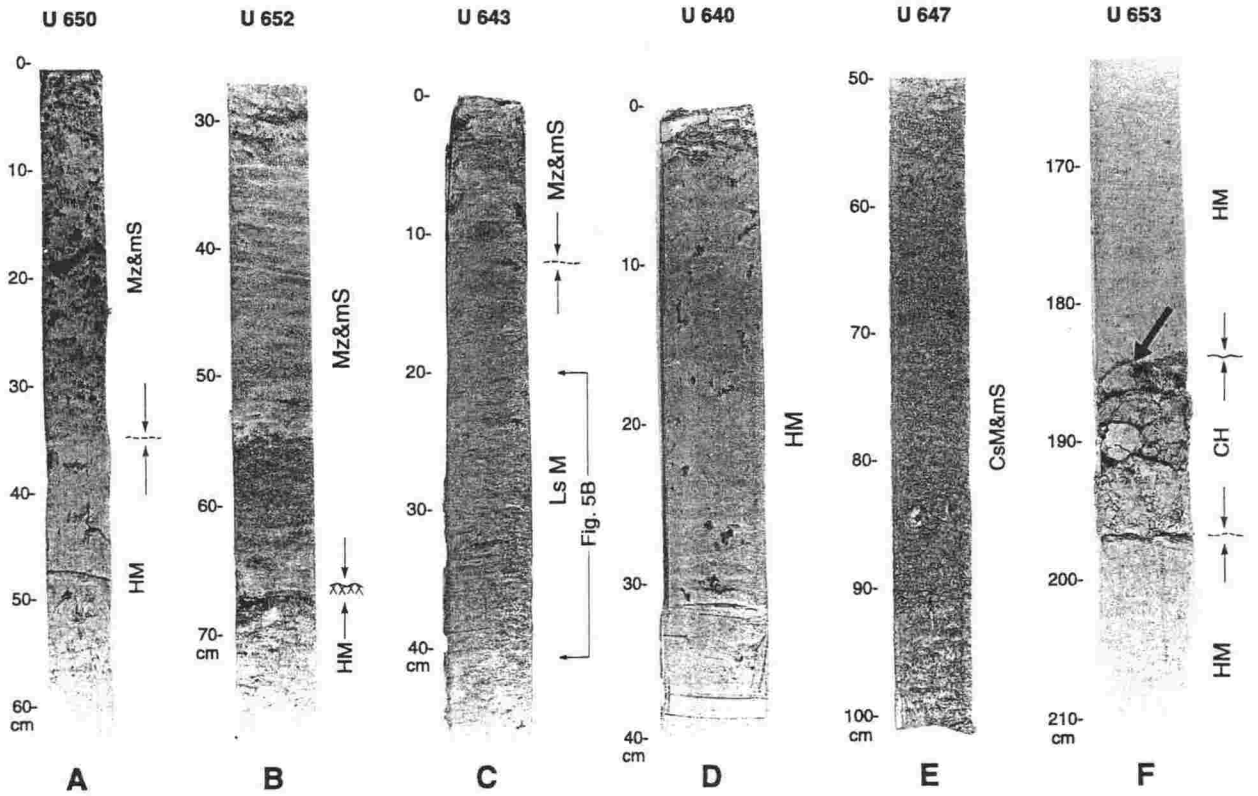
Fig. 5 Examples of lithofacies in cores. Positions of illustrated sections are shown on core logs in Fig. 4 by dotted lines. HM, homogeneous mud; Mz & mS, mottled silt and muddy sand; LsM, laminated sandy mud; CsM & mS, carbonate sandy mud and muddy sand; CH, cemented horizons.

Fig. 6 X-ray radiographs of 10 mm thick slices of cores illustrating the three main lithofacies. Large, irregular white areas are fractures in the core slices. A, Early Pleistocene, bioturbated, homogeneous mud with abundant sulphide-filled worm tubes. B, Late Pleistocene, laminated sandy mud with discontinuous stratification. C, Early Pliocene, mottled silts and sandy muds. See Fig. 4 for section positions marked by dotted lines.
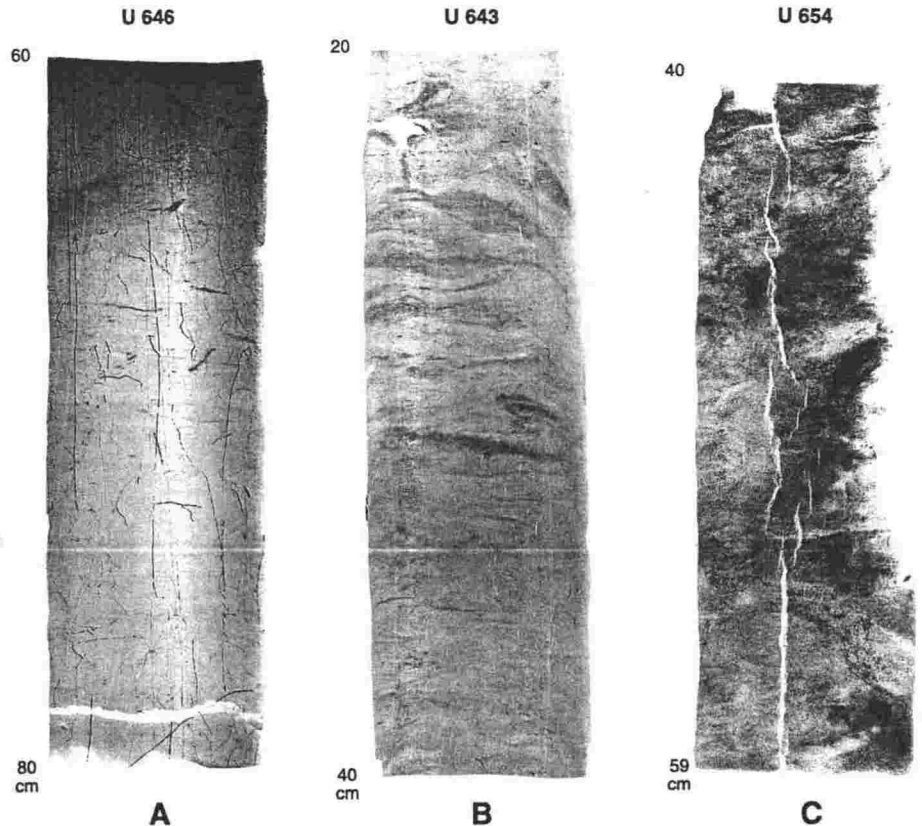
Fig. 7 Summary of late Neogene stratigraphy on the northwest Chatham Rise. Seismic sequences and reflection termination characteristics are indicated, along with the piston core stratigraphic positions, key microfossil datums, and tentative tephra correlations. Dashed vertical lines from cores indicate uncertainty in seismic correlation resulting from faulting near the core site. O, onlapping reflectors; T, truncation followed by onlap; C, conformable. Cores have sampled only small parts of sequences, hence, the ages of sequence boundaries are not well constrained.
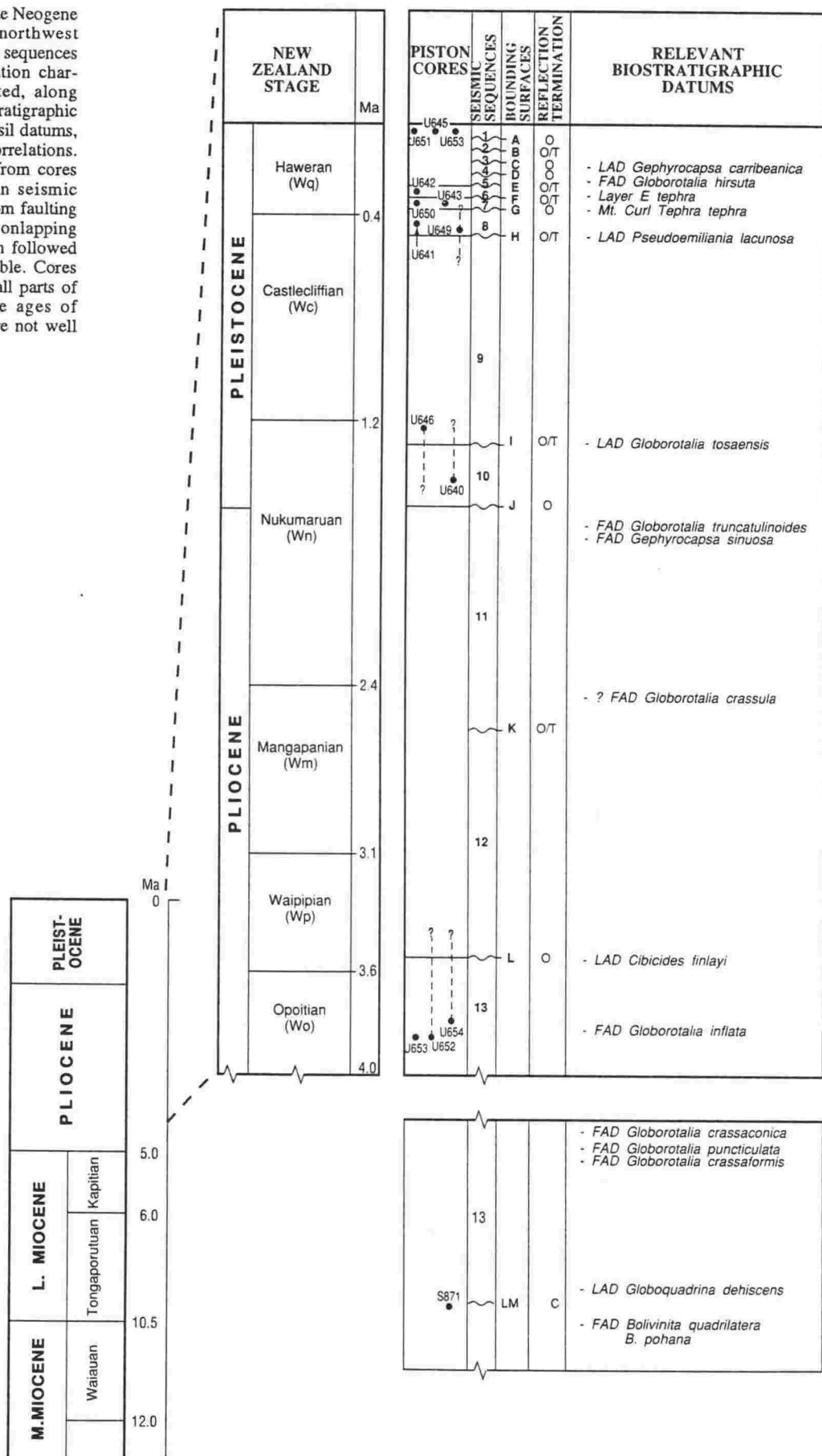
deposits by weak bottom currents, incapable of seismically expressed seabed scour and drift sedimentation, is evident by the association of sandy mottles, discontinous lamination, and homogeneous texture (e.g., Gonthier et al. 1984). Reworking and dissolution of calcareous microfauna and volcanic glass in these deposits is described below.

The homogeneous cores from the crests of sediment drifts may be comparable to the muddy contourite facies described from Northern Hemisphere deep-water sediment drifts (e.g., Stow & Holbrook 1984; Gonthier et al. 1984).

BIOSTRATIGRAPHY

The biostratigraphic ages of cores are compatible with the younging demonstrated by seismic stratigraphy (Fig. 7). Sequences are discussed below in order of decreasing age.

Reflector LM (S871)

Core S871 from the axis of Pukaki Canyon (Fig. 2) was positioned very close to reflector LM, the base of the strongly reflective sequence 13 on airgun profiles (Fig. 3). The sample contains *Bolivinita quadrilatera* and *B. pohana* (first occurrence (FO) at the base of, and in, the early Tongaporutuan Stage, respectively; Edwards 1987; Hornibrook et al. 1989). It also contains *Globoquadrina dehiscens* (last occurrence (LO) at 9.2 Ma; Wright et al. 1985) and *Globorotalia miotumida* (sinistral), which also indicate an early Tongaporutuan (late Miocene) age of 10.5–9.2 Ma.

Sequence 13 (U653, U652, U654)

Three cores recovered samples from stratigraphic positions close to the top of sequence 13. Each core contains *Globorotalia puncticulata* s.s., *G. crassaformis*, and *G. crassaconica*, taxa which first appear in the early Opoitian Stage (early Pliocene, 5.0–3.6 Ma; Hornibrook 1982; Edwards 1987; Edwards et al. 1988), together with early Pliocene, Opoitian–Waipipian Stage *G. subconomiozea* (Scott et al. 1990). Core U654 also contains more advanced *Globorotalia inflata* morphotypes and *G. puncticuloides?*, and may be a slightly younger sample than U653 and U652. However, it also contains *Cibicides finlayi* so it is not younger than Opoitian (Hornibrook et al. 1989). Thus, sequence 13 is inferred to extend (Fig. 7) from early Tongaporutuan (10.5–9.2 Ma) up to the late Opoitian – early Waipipian (c. 4.0–3.5 Ma, late Miocene – late early Pliocene).

Although the seismic stratigraphy of the easternmost core site (U661) is not established, the sample contains *Globorotalia crassaconica*, *G. subconomiozea*, sinistral forms of *G. crassaformis* and advanced *G. puncticulata*, along with *G. inflata*. It is inferred to be late Opoitian–Waipipian in age.

Sequences 12–11

No cores were recovered from sequences 12 and 11, so the precise ages of the sequences and their boundaries K and J are uncertain. The sequences fall within the period between early Waipipian and late Nukumaruan (c. 3.6–1.4 Ma).

Sequence 10 (U640)

Core U640 is inferred to be mid–late Nukumaruan (late Pliocene – early Pleistocene, 2.4–1.2 Ma) age (Fig. 7). It contains well-developed specimens of *Globorotalia crassacarina* and *G. puncticuloides*, atypical specimens of *G. crassula*, and specimens of the nannofossils *Gephyrocapsa*

sinuosa (FO in mid Nukumaruan; Edwards 1987) and *Gephyrocapsa oceanica* group. *Globorotalia crassaformis* (thought to terminate in the Nukumaruan; Scott et al. 1990) does not occur in the sample. Reworked late Eocene–Miocene nannofossils are present in small numbers.

Sequence 9 (U646)

Core U646, positioned to sample sequence 9, contains *Globorotalia crassula*, *G. puncticuloides*, *G. crassacarina*, and *G. truncatulinoides tosaensis* (well developed in the mid–late Nukumaruan; Scott et al. 1990), along with specimens of *Gephyrocapsa oceanica* group, *G. sinuosa*, and *Pseudoemiliania lacunosa*. Its age is inferred to be mid–late Nukumaruan Stage. Small numbers of reworked late Eocene–Miocene nannofossils occur.

Sequence 8 (U641, ?U649)

Specimens of both *Globorotalia truncatulinoides* and *G. crassacarina* occur in U641, which was positioned to sample sequence 8, indicating a late Castlecliffian age for the sequence. Approximately 90% of *G. truncatulinoides* in core U649 have a keel developed on the last chamber, which suggests that the sample lies close to the transition to *G. truncatulinoides truncatulinoides*, thought to occur in the Castlecliffian Stage (1.2–0.4 Ma) in the New Zealand region (Scott et al. 1990). The samples do not contain *Pseudoemiliania lacunosa* (LO at 0.46 Ma, late Castlecliffian; Edwards 1987) or *Gephyrocapsa carribeanica*, although the absence of the latter may be due to postdepositional dissolution of the species rather than deposition occurring after its extinction at 0.2 Ma (Edwards 1987). Thus, sequence 8 is inferred to be late Castlecliffian or earliest Haweran (mid–late Pleistocene) age. Very minor reworking of Miocene nannofossils is recorded.

Sequence 7 (U650, U643)

Over 80% of specimens of *Globorotalia truncatulinoides* are keeled in core U650, and *Pseudoemiliania lacunosa* is absent. These indicators, together with the seismic stratigraphic position of the sequence and the possible presence of Mt Curl Tephra in core U650 (see below), suggest a Haweran (late Pleistocene, <0.4 Ma) age for sequence 7 (Fig. 7). It is inferred that the overlying unconformity F is close to c. 0.3 Ma. If so, *Gephyrocapsa carribeanica* is unexpectedly absent from U650, but this is inferred to be due to the substantial degree of corrosion resulting in reduced nannofossil content and low diversity in the sample. Minor amounts of reworked, mainly Oligocene nannofossils occur.

Sequence 6 (U642)

The presence of *Globorotalia truncatulinoides* (nearly all keeled), and the absence of *Pseudoemiliania lacunosa*, *G. crassacarina*, and the late Quaternary entrant *Globorotalia hirsuta*, together with the seismic stratigraphic position of the sequence and tentative correlation with a 0.27 Ma deep-sea tephra, layer E (see below), suggests an early–mid Haweran age for core U642. The absence of *Gephyrocapsa carribeanica* may not be reliable due to sample corrosion.

Sequences 5–2

No cores were recovered from sequences 5–2; however, they are constrained by enveloping sequences to a late Haweran (late Pleistocene) age.
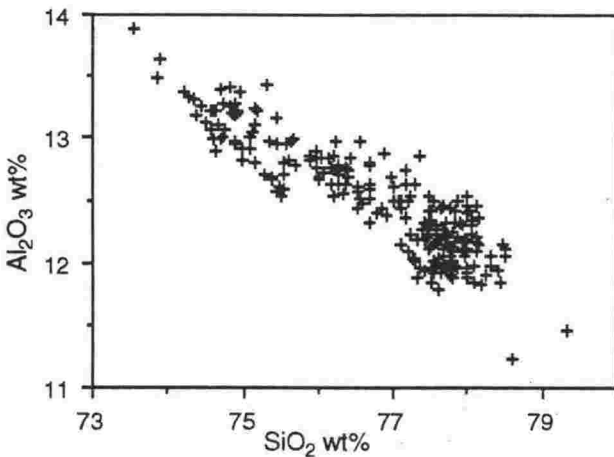
Fig. 8 Compositional range displayed by 230 glass shards from Chatham Rise cores.

Sequence 1 (U651, U645, U653)

One of three cores from sequence 1 was examined for microfossil content. A clear late Quaternary age for core U651 is indicated by the presence of *Emiliania huxleyi* and *Globorotalia hirsuta* (FO 0.27 Ma and 0.23 Ma, respectively; Edwards 1987), and the absence of *Pseudoemiliania lacunosa* and *Gephyrocapsa carribeanica*. This sequence is inferred to be largely post-last glacial in age, based on an interpretation that it represents a recent phase of reduced current activity. Reworked Oligocene nannofossils include excellently preserved specimens of *Chiasmolithus altus*, suggesting a nearby source.

VOLCANIC GLASS

Concentration and mineralogy

Megascopic tephra layers were not recognised in any core, but dispersed, clear, volcanic glass shards represent a dominant component of the sand fraction in many samples (Fig. 4). In some tuffaceous horizons, we also found sparse, euhedral, ferromagnesian crystals, some of which have adhering glass indicating a volcanogenic origin. Hypersthene and green hornblende are identified, consistent with the rhyolitic composition for the glasses from electron microprobe analysis.

Considerable amounts of glass occur in eight cores of late Opoitian to mid–late Haweran (late early Pliocene – late Pleistocene) age (Fig. 4). We have analysed those horizons in

Table 1 Electron microprobe analyses of glass shards in cores from the Chatham Rise. Analyses are recalculated to 100% on a volatile free basis and presented as a mean and standard deviation (in parentheses). Water by difference. n = number of shards analysed.

	642/31A	642/31B	642/103	642/131	642/161	642/181	650/91	650/181	650/210
SiO_2	77.74 (.21)	78.19 (.25)	77.42 (.97)	78.04 (.25)	77.98 (.55)	78.02 (.02)	77.64 (.32)	78.01 (.33)	77.31 (.79)
Al_2O_3	12.34 (.12)	12.35 (.17)	12.44 (.42)	12.17 (.16)	12.20 (.14)	12.21 (.11)	11.92 (.11)	11.92 (.06)	12.03 (.25)
TiO_2	0.17 (.05)	0.11 (.01)	0.17 (.09)	0.15 (.03)	0.13 (.05)	0.13 (.03)	0.15 (.04)	0.13 (.04)	0.15 (.05)
FeO	1.43 (.10)	1.14 (.06)	1.41 (.35)	1.26 (.14)	1.41 (.42)	1.11 (.10)	1.03 (.12)	0.93 (.18)	0.98 (.05)
MgO	0.14 (.02)	0.11 (.03)	0.16 (.05)	0.12 (.02)	0.11 (.03)	0.12 (.04)	0.12 (.03)	0.10 (.03)	0.13 (.03)
CaO	1.11 (.11)	1.02 (.13)	1.15 (.12)	1.07 (.05)	1.07 (.06)	1.08 (.08)	0.84 (.10)	0.79 (.23)	1.11 (.61)
Na_2O	3.95 (.08)	3.88 (.16)	3.93 (.12)	3.92 (.08)	3.82 (.07)	3.87 (.09)	3.60 (.08)	3.56 (.09)	3.55 (.15)
K_2O	3.00 (.12)	3.07 (.09)	3.16 (.12)	3.08 (.09)	3.09 (.13)	3.24 (.11)	4.47 (.22)	4.32 (.34)	4.47 (.11)
Cl	0.18 (.04)	0.17 (.04)	0.19 (.06)	0.20 (.04)	0.19 (.05)	0.22 (.06)	0.24 (.08)	0.24 (.04)	0.27 (.02)
H_2O	5.85 (.99)	5.70 (.97)	6.29 (.98)	4.70 (.99)	5.95 (2.06)	5.61 (1.14)	4.04 (.94)	6.10 (2.45)	4.36 (1.36)
n	8	3	8	10	8	10	10	6	7

	646/91	646/111	640/82	654/03	654/21	654/77	652/04	652/11	652/20
SiO_2	76.19 (.20)	76.20 (.46)	77.19 (.90)	77.60 (.19)	76.69 (.72)	77.10 (.38)	75.71 (1.18)	75.22 (.49)	75.02 (.38)
Al_2O_3	12.75 (.12)	12.81 (.17)	12.31 (.35)	12.27 (.17)	12.57 (.26)	12.68 (.19)	12.88 (.52)	13.02 (.25)	12.98 (.21)
TiO_2	0.24 (.06)	0.23 (.06)	0.15 (.05)	0.14 (.02)	0.16 (.05)	0.14 (.03)	0.15 (.04)	0.15 (.04)	0.17 (.03)
FeO	1.76 (.07)	1.67 (.20)	1.24 (.28)	1.24 (.18)	1.43 (.25)	1.35 (.19)	1.58 (.52)	1.84 (.25)	1.85 (.13)
MgO	0.16 (.02)	0.16 (.04)	0.12 (.04)	0.13 (.04)	0.13 (.03)	0.15 (.03)	0.12 (.03)	0.09 (.02)	0.11 (.02)
CaO	1.04 (.07)	1.09 (.11)	0.98 (.19)	1.08 (.11)	0.98 (.13)	1.36 (.08)	1.01 (.12)	0.92 (.13)	0.92 (.06)
Na_2O	4.39 (.09)	4.29 (.15)	4.06 (.28)	3.95 (.20)	4.23 (.23)	4.04 (.15)	4.20 (.34)	4.22 (.22)	4.07 (.14)
K_2O	3.23 (.07)	3.34 (.13)	3.75 (.26)	3.44 (.52)	3.62 (.10)	3.02 (.09)	4.07 (.36)	4.37 (.40)	4.62 (.23)
Cl	0.24 (.09)	0.20 (.05)	0.21 (.04)	0.21 (.03)	0.21 (.05)	0.18 (.06)	0.28 (.04)	0.23 (.05)	0.27 (.04)
H_2O	6.19 (1.56)	5.45 (.95)	5.53 (1.18)	5.79 (1.84)	6.14 (1.43)	7.90 (.88)	8.18 (1.15)	6.15 (1.12)	6.15 (.88)
n	7	10	10	10	10	9	9	10	10

	652/23	661/21	661/33	661/41	661/76	661/103	661/131	661/133	
SiO_2	74.99 (.44)	77.57 (.12)	76.65 (1.16)	77.03 (1.25)	76.36 (1.50)	75.74 (1.24)	75.35 (1.32)	76.65 (1.16)	
Al_2O_3	12.91 (.28)	12.06 (.11)	12.44 (.49)	12.31 (.43)	12.62 (.50)	12.90 (.47)	12.94 (.44)	12.44 (.49)	
TiO_2	0.18 (.05)	0.12 (.03)	0.17 (.07)	0.15 (.08)	0.20 (.09)	0.23 (.08)	0.27 (.09)	0.17 (.07)	
FeO	1.95 (.21)	1.23 (.09)	1.47 (.38)	1.53 (.52)	1.70 (.54)	1.79 (.35)	1.93 (.33)	1.47 (.38)	
MgO	0.10 (.02)	0.10 (.01)	0.13 (.06)	0.13 (.07)	0.21 (.12)	0.20 (.09)	0.27 (.06)	0.13 (.06)	
CaO	0.97 (.14)	0.96 (.03)	1.08 (.25)	1.09 (.23)	1.21 (.37)	1.57 (.25)	1.58 (.28)	1.08 (.25)	
Na_2O	4.10 (.19)	3.91 (.12)	4.08 (.24)	3.98 (.21)	4.13 (.23)	4.15 (.23)	4.23 (.15)	4.08 (.24)	
K_2O	4.56 (.38)	3.83 (.04)	3.79 (.38)	3.58 (.25)	3.50 (.37)	3.27 (.34)	3.30 (.17)	3.79 (.38)	
Cl	0.24 (.03)	0.23 (.02)	0.22 (.05)	0.20 (.03)	0.18 (.05)	0.15 (.05)	0.16 (.03)	0.22 (.05)	
H_2O	6.13 (1.28)	3.91 (.95)	3.99 (.67)	4.64 (1.01)	4.05 (.54)	5.73 (1.48)	6.03 (.03)	3.99 (.67)	
n	10	10	8	8	10	12	9	8	

Sample names = U core number/depth from top in centimetres.
Analyses with large standard deviations (e.g., FeO >0.15 wt%, TiO_2 and MgO >0.04 wt%) represent the means of two or more compositional populations within the sample (e.g., Fig. 9).
Sample 642/31 has been separated into two glass populations (A and B).
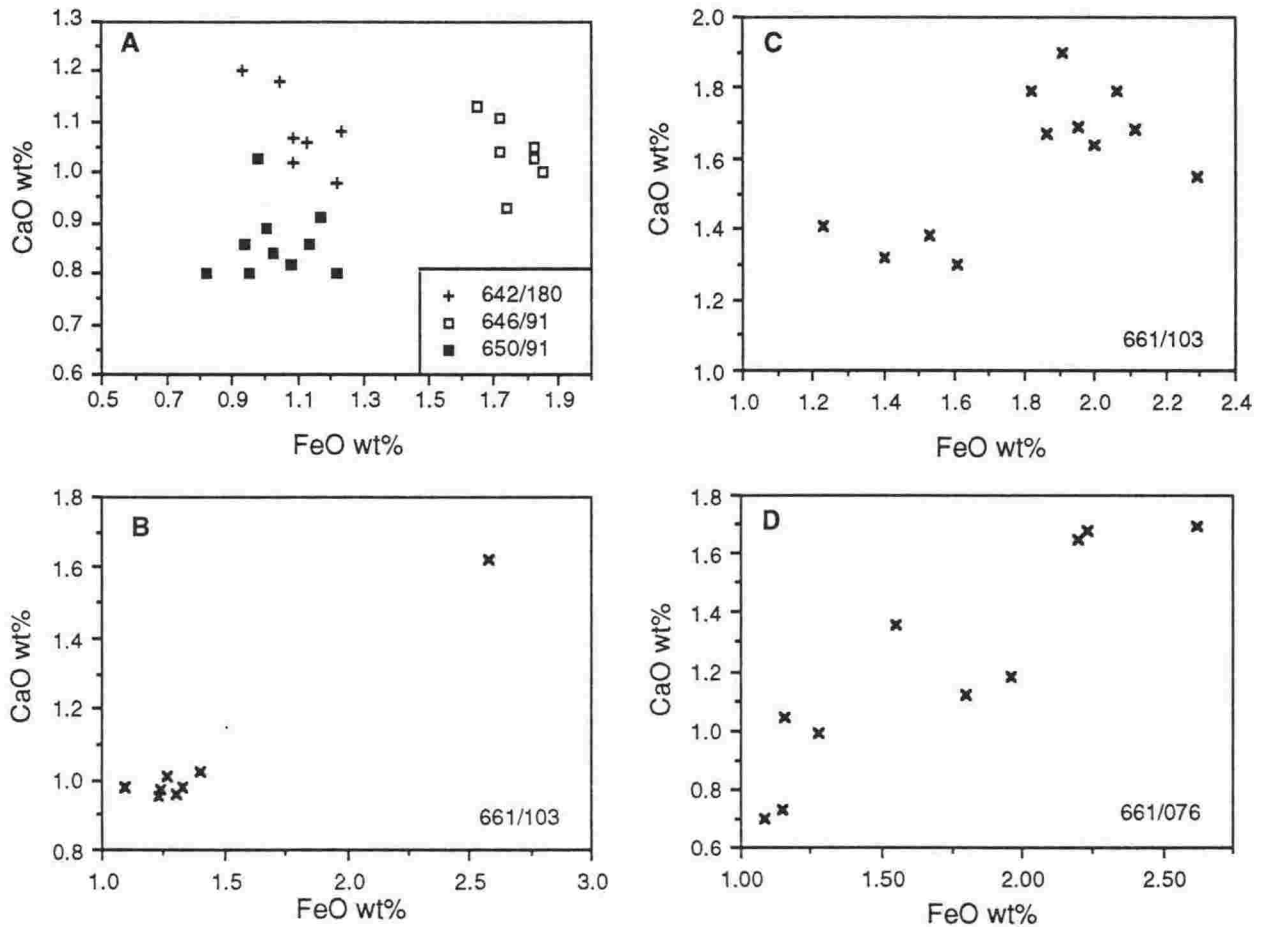
Fig. 9 Characteristics of tuffaceous horizons in Chatham Rise cores as shown by individual shard analyses. A, Three horizons, each consisting of a single, discrete, compositional population. B, Horizon consisting of a large population and containing a chemically anomalous shard. C, Horizon consisting of two compositional populations. D, Multiple populations or a near-continuum within a tuffaceous horizon.

which glass shards are most abundant. These horizons are not evident on X-ray radiographs of core slices, which only reveal textural and structural features of the sediments (e.g., cf. Fig. 4, 6).

Glass chemistry

Over 230 shards were analysed by electron microprobe from 26 tuffaceous horizons. All shards have calc-alkaline rhyolitic compositions, with SiO_2 content in the range 73.5–79.3 wt%, and total alkalis in the range 7.2–8.5 wt% (Table 1). Most have Na/K > 1. On Harker variation diagrams (Fig. 8), the shards form a unimodal grouping, indicating a single or closely related source provenance with similar petrogenetic origins. Their calc-alkaline composition and stratigraphic age indicate two possible source regions within New Zealand: Taupo Volcanic Zone (TVZ) (Cole 1979; Froggatt 1983; Wilson et al. 1984; Shane & Froggatt 1991) and the now-extinct Coromandel Volcanic Zone (CVZ) (Skinner 1986; Briggs & Fulton 1990). No evidence is seen for eruptive products from contemporary, intraplate basaltic volcanic centres such as at Timaru (Duggan & Reay 1986) and the Chatham Islands (Grindley et al. 1977). We cannot differentiate a TVZ source from a CVZ source on the basis of glass composition.

Only seven of the tuffaceous horizons examined have homogeneous chemical populations of shards indicative of single eruptive events. The rest are heterogeneous with two or more populations of glass mixed together (Fig. 9). The glass shards in the tuffaceous horizons can be grouped into four broad classes (Shane 1991): (1) single, homogeneous glass populations representing single eruptive events (Fig. 9A); (2) a major glass population with a few anomalous shards, probably reworked (Fig. 9B); (3) two discrete populations of glass shards inferred to represent separate eruptive events (Fig. 9C); and (4) multiple and indistinguishable glass populations that indicate mixing of two or more eruptive events (Fig. 9D). The distribution of these classes in cores is shown on Fig. 4, and implications of mixed glass populations are discussed in the section on Pliocene-Pleistocene tephra deposition on a current-sweet seafloor (below).

Because of the degree of mixing of different eruptive products in the cores, it is uncertain how many eruptive events are recorded. For Pleistocene-aged sediments, we have recognised five, chemically distinct horizons or zones, based on a dominant glass population within the samples. Three chemically distinct horizons occur in core U642 at (1) 0.31 m depth; (2) 1.31 m depth; and (3) 1.81 m depth. A fourth

chemically distinct horizon occurs at depths of 0.91 m and 1.11 m in core U646, and a fifth horizon occurs at 0.91 m in core U650. Because each horizon is chemically and stratigraphically different, five major eruptive events are recorded. In addition, a number of smaller eruptive events are recorded as anomalous shards within and between these horizons.

Correlations

Several authors have attempted to correlate Pleistocene tephra exposed in onshore sequences in New Zealand with deep-sea cores up to about 1000 km away in the Southwest Pacific, using magnetostratigraphy, biostratigraphy, fission-track ages, and more recently by chemical fingerprinting of glass shards (Watkins & Huang 1977; Froggatt 1983; Froggatt et al. 1986; Nelson et al. 1986; Shane & Froggatt 1991). Using the sequence stratigraphy established for the North Chatham Slope (Fig. 7), and comparing the glass chemistry of tuffaceous horizons in our cores with tephra in other deep-sea cores and in onshore sequences in New Zealand, we can make two tentative correlations. These are (1) the late Pleistocene core U650, 0.91 m depth, can be correlated with the widespread Mt Curl Tephra (referred to as Rangitawa Tephra by Kohn et al. in press), variously dated at 0.23–0.38 Ma (Froggatt et al. 1986) but which is probably close to 0.35 Ma old (Kohn et al. in press); and (2) the late Pleistocene core U642, 1.80 m depth, with the c. 0.27 Ma Layer E tephra of Ninkovich (1968) and Watkins & Huang (1977).

We compare glass compositions for correlation purposes using similarity coefficients (SC) (Borchardt et al. 1971), based on all oxides except Cl, which is often invariant. High values of SC (>0.92) are obtained for correlative samples. The compositions of tephras from elsewhere that were used for correlation purposes are shown in Table 2. An SC of 0.96 was obtained for the match between glass at 0.91 m in core U650 and the Mt Curl Tephra at its type section in the Manawatu–Wanganui area (Table 2). This tephra has a distinctive high K_2O content and Na/K < 1 compared to other late Pleistocene tephras (Froggatt et al. 1986). The Haweran biostratigraphic age of core U650 supports this chemical correlation. Mt Curl Tephra, the co-eruptive airfall equivalent of the Whakamaru Ignimbrite, has been recognised in Tasman Sea DSDP core

591 and Southwest Pacific cores (Watkins & Huang 1977; Froggatt 1983; Froggatt et al. 1986; Nelson et al. 1986). In the southwestern Pacific, the correlative of the Mt Curl Tephra is known as Layer D. We obtain an SC of 0.94 for comparison of Layer D in core RC 12–215.

Core U642 is inferred to be stratigraphically younger than U650 (Fig. 7). Glass shards in core U642 at a depth of 1.81 m represent a chemically distinct, single population, similar to Layer E in several deep-sea cores in the western Pacific, including RC12–215 (Table 2; SC = 0.95). An age of c. 0.27 Ma for Layer E (Ninkovich 1968) is consistent with the stratigraphic position of core U642. Froggatt (1983) suggested the correlation of Layer E to the Matahina Ignimbrite in the Bay of Plenty region of North Island. We obtained an SC of 0.93 for the comparison between glass at 1.81 m in core U642 and this ignimbrite.

DISCUSSION

A late Neogene, high-resolution, deep-sea sequence stratigraphy

The fortuitous exposure of many Pliocene–Pleistocene seismic sequences by severe late Quaternary current erosion enabled various sequences to be sampled using conventional piston-coring equipment. In other parts of the world, such high-resolution, deep-sea sequence analyses have been undertaken only by correlating seismic sequences to long drill cores (e.g., Feeley et al. 1990).

The stratigrapically upwards increase in seismic impedance defining the base of sequence 13 is inferred to represent an increase in terrigenous sedimentation. A similar increase in terrigenous sedimentation associated with changes in seismic impedance or sequence architecture have been recorded on the southern flank of the Chatham Rise at DSDP site 594 (Lewis et al. 1986; Nelson 1986) and on the South Island continental margin in the late Miocene (Wood et al. 1989). The late Miocene (c. 9–10 Ma) age of reflector LM coincides with the onset of significant tectonic shortening within the New Zealand plate-boundary zone and regional uplift (Walcott 1978).

Above reflector LM on the North Chatham Slope, the Pliocene–Pleistocene sequences are inferred to reflect paleoceanographic fluctuations resulting from global climate cycles, interacting with slow tectonic subsidence of the Mernoo Saddle. A glacio-eustatic control on the North Chatham Slope currents is inferred from: (1) a present postglacial phase of reduced current erosion, thought to be largely post-last glacial; (2) an inferred intensification of the currents during glaciations as a consequence of a number of factors, including increased constriction of flow through the Mernoo Saddle during low sealevel; and (3) a broad correlation between the periodicity of late Pleistocene sequences and established marine oxygen-isotope stages.

Table 2 Composition of tephras used in correlations to samples from Chatham Rise cores. Analyses presented as in Table 1. Grid references from the metric NZMS 260 map series.

	Layer E[1]		Matahina Ignimbrite[2]		Layer D[3]		Mt Curl Tephra[4]	
SiO_2	78.11	(.33)	77.38	(.45)	77.93	(.28)	78.09	(.30)
Al_2O_3	12.45	(.24)	12.54	(.27)	12.26	(.17)	12.33	(.21)
TiO_2	0.13	(.03)	0.12	(.02)	0.12	(.03)	0.14	(.03)
FeO	1.13	(.12)	1.07	(.07)	0.87	(.11)	1.01	(.08)
MgO	0.11	(.03)	0.11	(.02)	0.12	(.02)	0.12	(.02)
CaO	0.88	(.07)	0.88	(.05)	0.78	(.05)	0.79	(.04)
Na_2O	3.76	(.17)	3.91	(.15)	3.53	(.14)	3.30	(.16)
K_2O	3.37	(.18)	3.83	(.17)	4.38	(.18)	4.33	(.15)
Cl	–		0.18	(.02)	–		–	
H_2O	4.35	(.69)	5.04	(1.95)	4.38	(1.03)	4.55	(.13)
n	21		10		18		132	

[1]Core RC12–215, western Pacific lat. 35°28′, long. 167°53.5′ (Froggatt unpubl. data).
[2]State Highway 38, Murupara, V17/305993.
[3]Core RC12–215 (Froggatt et al. 1986).
[4]Mt Curl Road, Manawatu, S22/195345 (Froggatt et al. 1986).

Limitations on stratigraphic resolution

The resolution of the stratigraphy is presently limited by several factors. Six of the 13 seismic sequences recognised were not sampled (Fig. 7). In addition, the 1–3 m long cores represent only small sections of the c. 10–40 m thick sequences. Therefore, although the cores can be used to place the sequences into a broad biostratigraphic framework, they do not constrain the absolute lengths of time represented by

individual sequences and their intervening unconformities, nor do they constrain the short-term sedimentation rates. Furthermore, there is some uncertainty for certain cores as to the actual sequence penetrated, due to faulting near the core site (Fig. 2).

The maximum long-term sedimentation rates from lower slope areas of sediment drift accumulation are c. 70–110 mm/ka (270–430 m since c. 3.8 Ma). Considering (1) the late Quaternary rates of hemipelagic deposition on the eastern North Island lower continental slope (c. 100 mm/ka; Lewis 1980), (2) the Pliocene–Pleistocene rates at DSDP site 594, 300 km south of the investigated area (25–150 mm/ka; Kennett & von der Borch et al. 1986), and (3) the Pleistocene rates of abyssal pelagic sedimentation up to 1000 km east of North Island (<2 mm/ka; Watkins & Huang 1977), we suspect that hemipelagic sediments accumulating upslope of sediment drifts on the North Chatham Slope were deposited at short-term rates in the order of c. 50–150 mm/ka. This rate implies that individual cores (1.1–3.2 m long) represent between c. 7 and 64 ka of continuous sedimentation.

Apart from the two, tentative, late Pleistocene tephra correlations, the ages of the cores have been assigned exclusively on the basis of their calcareous nannofossil and foraminiferan biostratigraphy. Thus, they are tied to the New Zealand late Neogene microfossil zonations, which have been developed largely from onshore sequences and from the Tasman Sea DSDP core 284 (Beu et al. 1987; Edwards 1987).

We cannot discount the possibility of local anomalies in first and last appearances of significant taxa that might be due to unfavourable paleoenvironmental conditions in the region of subtropical convergence because, at the western end of the Chatham Rise, the modern surface-water circulation patterns, and interactions between cool subtropical and subantarctic water, are complex and variable, and the Subtropical Convergence Zone is not well defined (Heath 1976, 1985). For example, south of the Subtropical Convergence Zone at DSDP site 594, the planktic foraminifer *Globorotalia inflata* appears at the Gauss/Matuyama boundary in the adopted magnetostratigraphy, c. 1 Ma earlier than it does at DSDP site 593 (Hornibrook pers. comm. 1992). Also, *G. crassula* makes its first appearance at that site in the late Nukumaruan, whereas, elsewhere in the New Zealand region, it is recognised as a datum close to the base of the Nukumaruan Stage (2.40–2.15 Ma; Edwards 1987).

The effect of bottom currents, even in areas of modified hemipelagic sedimentation upslope of major seafloor scour and sediment drift accumulation, has been to produce low-diversity, corroded nannofloras with loss of solution-prone species. Bottom currents are also inferred to be responsible for reworking the small quantities of Oligocene and Miocene nannoflora into the Pliocene–Pleistocene sediments from nearby sources, probably on the upper flanks of Mernoo Bank (Herzer & Wood 1988).

Pliocene–Pleistocene rhyolitic tephra deposition on a current-swept seafloor

The rhyolitic tephra deposited on the North Chatham Slope is inferred to be the airfall product of eruptions from two, closely related source provences within the late Neogene, North Island, calc-alkaline arc. The upper, late Opitian (c. 4.0–3.6 Ma) part of sequence 13 (cores U652, U653, and U654) and the late Opoitian–Waipipian core U661 (Fig. 4) probably predate the onset of volcanism within the TVZ c. 2.3–2.0 Ma ago (Lowe et al. 1988; Grindley et al. 1988) and, hence, the

shards are inferred to be products of now-extinct rhyolitic centres (Fig. 1) on the Coromandel Peninsula (Nelson et al. 1986; Skinner 1986). The number of discrete eruptions recorded in the early Pliocene cores is uncertain because mixing of separate eruptive products is common (Fig. 9) and because the detailed stratigraphic relationships between the cores is not known (they may or may not be chronostratigraphically synchronous).

In contrast to the early Pliocene cores, the late Pliocene – late Pleistocene (c. 1.6–0.25 Ma) cores from sequences 10–6 (Fig. 7) contain the distal airfall products of at least five eruptions from the TVZ. These include possible co-eruptive correlatives of the late Pleistocene Whakamaru and Matahina Ignimbrites. Rare to very minor amounts of glass occur throughout the post-last-glacial age sequence 1 cores U645, U651, and U653 (Fig. 4, 7). Some of this glass in sequence 1 is reworked from older sequences, and some may be airfall sprinklings from TVZ eruptions.

Distances of 460–600 km between the volcanic source areas and the core sites imply that very explosive eruptions have occurred since the early Pliocene. As the present prevailing winds in the region are westerlies, the presence of glass shards at these distances to the south of the sources suggest the ejection of material high into the atmosphere (e.g., Nelson et al. 1986). Large, explosive, silicic eruptions are often associated with caldera formation. Such calderas are known from the TVZ (Wilson et al. 1984) and have recently been found in the CVZ (Briggs & Fulton 1990). Rock compositions from these areas are broadly similar to glasses found in the Chatham Rise cores. Thus, we consider the latter to be distal products of these large eruptions.

An important feature of volcanic glass occurrence on the North Chatham Slope is the absence of megascopic tephra in all cores. This is unusual for deep-sea cores from east of New Zealand spanning the interval from late early Pliocene to late Quaternary. For example, of the 17 tephras identified by Watkins & Huang (1977) in South Pacific cores, 8 are megascopic and include the 5 tephras recognised by Ninkovich (1968). Elsewhere, in DSDP Leg 90 cores from the Southwest Pacific and Tasman Sea, 15 late Cenozoic, silicic, megascopic tephras have been recorded (Nelson et al. 1986).

One explanation for the absence of megascopic tephra in cores from the North Chatham Slope is that the combined physical oceanographic and sedimentary processes made this region unfavourable for developing thick concentrations of ash on the seafloor, irrespective of the rates of airfall transport of glass to the area. The sediments are inferred to have accumulated at low rates, and bioturbation is extensive, producing predominantly homogeneous and mottled sedimentary textures. In addition, significant bottom-current activity is clear from the multiple, regional-scale erosion surfaces and sediment drifts evident in seismic profiles (Fig. 3), from the sedimentary textures in cores, and from the presence of corroded and reworked microflora. These combined processes have the effect of disseminating and reworking the glass shards into the terrigenous and biogenic components of the sediments, enabling multiple tephra deposits to be mixed. Furthermore, the northwest Chatham Rise slope lies due south of the inferred volcanic sources, which is probably not favourable for maximum fallout, considering the prevailing westerly winds. Some of the eruptions recorded may not have been of sufficient magnitude to produce visible ash at the site, although this clearly does not account for the microscopic occurrence of Mt Curl Tephra,

which is 100 mm thick at DSDP site 594 to the south (Fig. 1) (Froggatt et al. 1986).

CONCLUSIONS

1. The foraminiferan and nannofossil biostratigraphy of late Miocene – late Quaternary piston cores from the northwest Chatham Slope provides a framework for interpretation of high-resolution seismic stratigraphy.

2. A regional increase in the strength of seismic reflectors occurs at the base of sequence 13 (9–10 Ma). This reflects an increase in terrigenous sedimentation accompanying the onset of shortening across the Pacific and Australian plate boundary in the New Zealand region.

3. Pliocene–Pleistocene cores from 7 out of 13 unconformity-bound sequences consist predominantly of bioturbated, hemipelagic mudstone with minor but variable amounts of volcanic glass, and resedimented glauconitic sand. They exhibit the textural characteristics of sediments deposited at slow rates under the influence of variable bottom currents. The structures of cores, and inferred sedimentary processes, are consistent with seismic stratigraphic interpretations.

4. No megascopic tephra occur in any cores, but the relative down-core concentrations of glass indicate prominent fluctuations in the rate of tephra accumulation during the Pliocene–Pleistocene. Individual tuffaceous horizons may contain the airfall deposits of one or two eruptions, or of multiple eruptions mixed together. The physical oceanography, slow sedimentation, and extensive bioturbation in the region produced unfavourable conditions for preserving megascopic, Pliocene–Pleistocene tephra.

5. Early Pliocene (late Opoitian) glass shards originated from the now-extinct Coromandel Volcanic Zone, whereas Pleistocene ash, including probable co-eruptive correlatives of the Whakamaru Ignimbrite (Mt Curl Tephra; c. 0.35 Ma) and Matahina Ignimbrite (Layer E; c. 0.27 Ma) originated from the Taupo Volcanic Zone.

6. High-resolution, deep-sea sequence stratigraphic analysis is possible using conventional piston cores and high-frequency seismic profiles in favourable settings that preserve repeated episodes of current erosion and deposition.

ACKNOWLEDGMENTS

REFERENCES

Barnes, P. M. 1992: Mid-bathyal current scours and sediment drifts adjacent to the Hikurangi deep-sea turbidite channel, eastern New Zealand: evidence from echocharacter mapping. *Marine geology 106*: 169–187.

Beu, A. G.; Edwards, A. R.; Pillans, B. J. 1987: A review of New Zealand Pleistocene stratigraphy, with emphasis on the marine rocks. *In*: Itihara, M.; Kamei, T. *ed*. Proceedings of the first international colloquium on Quaternary stratigraphy of Asia and Pacific area, Osaka, 1986. Pp. 250–269.

Borchardt, G. A.; Havard, M. E.; Schmitt, R. A. 1971: Correlation of volcanic ash deposits by activation analysis of glass separates. *Quaternary research 1*: 247–260.

Briggs, R. M.; Fulton, B. W. J. 1990: Volcanism, structure and petrology of the Whiritoa–Whangamata coastal section, Coromandel Volcanic Zone, New Zealand: facies model evidence for the Tunaiti caldera. *New Zealand journal of geology and geophysics 33*: 623–633.

Carter, L.; Carter, R. M.; Griggs, G. B. 1982: Sedimentation in the Conway Trough, a deep near-shore marine basin at the junction of the Alpine transform and Hikurangi subduction plate boundary, New Zealand. *Sedimentology 29*: 475–497.

Cole, J. W. 1979: Structure, petrology, and genesis of Cenozoic volcanism, Taupo Volcanic Zone, New Zealand—a review. *New Zealand journal of geology and geophysics 22*: 631–657.

Cullen, D. J. 1980: Distribution, composition and age of submarine phosphorite on Chatham Rise, east of New Zealand. *Society of Economic Paleontologists and Mineralogists special publication 29*: 139–148.

Doyle, L. J.; Orrin, H. P.; Woo, C. C. 1979: Sedimentation on the eastern United States continental slope. *In*: Doyle, L. J.; Pilkey, O. H. *ed*. Geology of continental slopes. *Society of Economic Paleontologists and Mineralogists special publication 27*: 119–129.

Duggan, M. B.; Reay, A. 1986: The Timaru Basalt. *In*: Smith, I. E. M. *ed*. Late Cenozoic volcanism in New Zealand. *Royal Society of New Zealand bulletin 23*: 264–277.

Edwards, A. R. 1987: An integrated biostratigraphy, magnetostratigraphy and oxygen isotope stratigraphy of the late Cenozoic of New Zealand. *New Zealand Geological Survey record 23*: 80 p.

Edwards, A. R.; Hornibrook, N. de B.; Raine, J. I.; Scott, G. H.; Stevens, G. R.; Strong, C. P.; Wilson, G. J. 1988: A New Zealand Cretaceous–Cenozoic geological time scale. *New Zealand Geological Survey record 35*: 135–149.

Feeley, M. H.; Moore, T. C.; Loutit, T. S.; Bryant, W. R. 1990: Sequence stratigraphy of Mississippi Fan related to oxygen isotope sea-level index. *American Association of Petroleum Geologists bulletin 74*: 407–424.

Froggatt, P. C. 1983: Toward a comprehensive upper Quaternary tephra and ignimbrite stratigraphy in New Zealand using electron microprobe analysis of glass shards. *Quaternary research 19*: 188–200.

Froggatt, P. C.; Nelson, C. S.; Carter, L.; Griggs, G.; Black, K. P. 1986: An exceptionally large late Quaternary eruption from New Zealand. *Nature 319*: 578–582.

Gonthier, E. G.; Faugeres, J. C.; Stow, D. A. V. 1984: Contourite facies of the Faro Drift, Gulf of Cadiz. *In*: Stow, D. A. V.; Piper, D. J. W. *ed*. Fine-grained sediments: deep-water processes and facies. *Geological Society special publication 15*: 275–292.

Grindley, G. W.; Adams, C. J. D.; Lumb, J. T.; Watters, W. A. 1977: Paleomagnetism, K-Ar dating and tectonic interpretation of upper Cretaceous and Cenozoic volcanic rocks of the Chatham Islands, New Zealand. *New Zealand journal of geology and geophysics 20*: 425–468.

Grindley, G. W.; Oliver, P. J.; Seward, D. 1988: Stratigraphy, geochronology and paleomagnetism of ignimbrites in the Matahina Basin, Taupo Volcanic Zone. *Geological Society of New Zealand miscellaneous publication 41a*: 71.

Heath, R. A. 1976: Oceanic circulation in the head of the Hikurangi Trench, east coast, New Zealand. *New Zealand journal of marine and freshwater research 10*: 651–674.

————1985: A review of the physical oceanography of the seas around New Zealand — 1982. *New Zealand journal of marine and freshwater research 19*: 79–124.

Herzer, R. H. 1981: Late Quaternary stratigraphy and sedimentation of the Canterbury continental shelf, New Zealand. *New Zealand Oceanographic Institute memoir 89*: 71 p.

Herzer, R. H.; Wood, R. A. 1988: The geology and structure of Mernoo Bank and surrounding area, western Chatham Rise. *New Zealand Geological Survey record 29*.

Hornibrook, N. de B. 1982: Late Miocene to Pleistocene *Globorotalia* (Foraminiferida) from the DSDP leg 29, site 284, southwest Pacific. *New Zealand journal of geology and geophysics 25*: 83–99.

Hornibrook, N. de B.; Brazier, R. C,; Strong, C. P. 1989: Manual of New Zealand Permian to Pleistocene foraminiferal biostratigraphy. *New Zealand Geological Survey paleontological bulletin 56*: 175 p.

Kennett, J. P.; von der Borch, C. C. et al. 1986: Site 594: Chatham Rise. *Initial reports of the deep-sea drilling project XC part 1*: 653–744.

Kohn, B. P.; Pillans, B.; McGlone, M. S. in press: Zircon fission track age for middle Pleistocene Rangitawa Tephra, New Zealand: stratigraphic and paleoclimatic significance. *Palaeogeography, palaeoclimatology, palaeoecology.*

Lewis, K. B. 1980: Quaternary sedimentation on the Hikurangi oblique-subduction and transform margin, New Zealand. *In*: Ballance, P. F.; Reading, H. G. *ed.* Sedimentation in oblique-slip mobile zones. *International Association of Sedimentologists special publication 4*: 171–189.

Lewis, K. B.; Bennett, D. J.; Herzer, R. H.; von der Borch, C. C. 1986: Seismic stratigraphy and structure adjacent to an evolving plate boundary, western Chatham Rise, New Zealand. *In*: Kennett, J. P.; von der Borch, C. C. et al. *ed. Initial reports of the deep-sea drilling project XC part 2*: 1325-1327.

Lowe, D. J.; Briggs, R. M.; Keane, A. J.; Itaya, T. 1988: Age of the Kauroa Ash Formation, western North Island. *Geological Society of New Zealand miscellaneous publication 41a*: 95.

McDougall, J. C. 1982: Bounty sediments. *New Zealand Oceanographic Institute oceanic series 1:1 000 000.*

Nelson, C. S. 1986: Lithostratigraphy of deep-sea drilling project leg 90 drill sites in the southwest Pacific: an overview. *Initial reports of the deep-sea drilling project XC part 2*: 1471–1489.

Nelson, C. S.; Froggatt, P. C.; Gossan, G. J. 1986: Nature, chemistry, and origin of late Cenozoic megascopic tephras in leg 90 cores from the southwest Pacific. *Initial reports of the deep-sea drilling project XC part 2*: 1161–1171.

Ninkovich, D. 1968: Pleistocene volcanic eruptions in New Zealand recorded in deep sea sediments. *Earth and planetary science letters 4*: 89–102.

Scott, G. H.; Bishop, S.; Burt, B. J. 1990: Guide to some Neogene globorotalids (Foraminiferida) from New Zealand. *New Zealand Geological Survey paleontological bulletin 61*: 135 p.

Shane, P. A. R. 1991: Remobilised silicic tuffs in middle Pleistocene fluvial sediments, southern North Island, New Zealand. *New Zealand journal of geology and geophysics 34*: 489–499.

Shane, P. A. R.; Froggatt, P. C. 1991: Glass chemistry, paleomagnetism, and correlation of middle Pleistocene tuffs in southern North Island, New Zealand, and Western Pacific. *New Zealand journal of geology and geophysics 34*: 203–211.

Skinner, D. N. 1986: Neogene volcanism in the Hauraki Volcanic Region. *Royal Society of New Zealand bulletin 23*: 21–47.

Stow, D. A. V.; Holbrook, J. A. 1984: North Atlantic contourites: an overview. *In*: Stow, D. A. V.; Piper, D. J. W. *ed.* Fine-grained sediments: deep-water processes and facies. *Geological Society special publication 15*: 245–256.

Walcott, R. I. 1978: Present tectonics and late Cenozoic evolution of New Zealand. *Geophysical journal of the Royal Astronomical Society 52*: 137–164.

Walker, R. G.; Mutti, E. 1973: Turbidite facies and facies associations. *In*: Middleton, G. V.; Bouma, A. H. *ed.* Turbidites and deep-water sedimentation. Society of Economic Paleontologists and Mineralogists Pacific short course notes. Anaheim. Pp. 119–158.

Watkins, N. D.; Huang, T. C. 1977: Tephras in abyssal sediments east of the North Island, New Zealand: chronology, paleowind velocity, and paleoexplosivity. *New Zealand journal of geology and geophysics 20*: 179–198.

Wilson, C. J. N.; Rogan, A. M.; Smith, I. E. M. 1984: Caldera volcanoes of the Taupo Volcanic Zone, New Zealand. *Journal of geophysical research 89*: 8463–8484.

Wood, R. A.; Andrews, P. B.; Herzer, R. H. et al. 1989: Cretaceous and Cenozoic geology of the Chatham Rise region, South Island, New Zealand. *New Zealand Geological Survey basin studies 3*: 76 p.

Wright, I. C.; Ashby, J. N.; Hoskins, R. H. 1985: An age for the sudden disappearance of *Globorotalia dehiscens* in Mangapoike River Valley, New Zealand. *New Zealand Geological Survey record 9*: 102–104.